

EXPLORING CHEMICAL TRANSFORMATIONS MEDIATED BY SINGLE-ELECTRON
OXIDATION: HYDRODECARBOXYLATION, ALKENE-DIFUNCTIONALIZATION, AND
HOMOBENZYLIC C-H OXIDATION

Jeremy Dale Griffin

A dissertation submitted to the faculty of The University of North Carolina at Chapel Hill in
partial fulfillment of the requirements for the degree of Doctor of Philosophy in the Department
of Chemistry

Chapel Hill
2018

Approved by:

David A. Nicewicz

Jeffrey S. Johnson

Simon J. Meek

Jillian L. Dempsey

Alexander J. M. Miller

© 2018
Jeremy Dale Griffin
ALL RIGHTS RESERVED

ABSTRACT

Jeremy Dale Griffin: Exploring Chemical Transformations Mediated by Single-Electron Oxidation: Hydrodecarboxylation, Alkene-Difunctionalization, and Homobenzylic Oxidation
(Under the direction of David A. Nicewicz)

Inspired by nature, chemists have strived to promote chemical reactions using visible light. The field of photoredox catalysis has matured from the early stages of being a mere curiosity concerning mainly physical chemists to being a synthetically useful class of reactions. Although photoredox methodologies are not yet widely used in everyday experiments carried out by the average chemist, the use of these technologies are on the rise. This is in part due to their unique ability to enable new reaction manifolds not accessible by many polar reactions.

The Nicewicz lab has developed a suite of methodologies so far using *organic* photoredox catalysts. Three new methodologies will be described in the following chapters, preceded by a brief discussion on vital aspects of photochemistry. All of the methods described herein are hallmarked by the production of radical intermediates which undergo unique reactivity. A method for hydrodecarboxylation directly from carboxylic acid substrates is described, which is applicable to unactivated substrates. A new strategy for alkene difunctionalization enables the reversal of classic halofunctionalization reactions. Finally, a selective alkane C–H oxidation is in the process of being developed, which has so far been shown to be selective for homobenzylic C–H bonds. Along the way investigations in the reaction mechanisms of each of these methods will also be outlined.

ACKNOWLEDGEMENTS

When I started my studies at UNC-CH I knew *nothing* about organic chemistry and I knew even less about photoredox catalysis. I could not have made it this far without those who pushed me to be the best chemist and person that I could be. I have to thank Andrew Perkowski as the first mentor I had at UNC, and the person who was responsible for all of my bench training. He never made me feel like I didn't belong here because of my lack prior training, and did everything in his power to help me when I asked it of him. Nathan Romero may have the greatest intellects of anyone I have ever met. His relative knowledge about chemistry compared to my own, inspired me to learn everything that I could while at UNC. He inspired me to tackle difficult problems. Begrudgingly, I have to thank Cole Cruz and Cortney Cavanaugh (they will probably spend hours analyzing why I put Cole's name first). Ya'll have been a lot of fun. I thank all my homies in Nicewicz South, stay strong. I also thank Dave Nicewicz, he originally inspired to join his lab with his passion for the chemistry. I enjoyed being in the lab because he allowed me to grow as a chemist by giving me freedom to work on bad ideas.

I thank my mom, Jackie who gave me everything even when she had nothing. Finally, I would like to thank Lana, who is the reason that I get up in the morning (because she wakes the dog up and lets her jump on my face).

To my family:
“You win some, lose some, and wreck some”
-Dale Earnhardt

TABLE OF CONTENTS

LIST OF FIGURES.....	xiv
LIST OF TABLES	xix
LIST OF SCHEMES.....	xx
LIST OF CHARTS.....	xxi
LIST OF ABBREVIATIONS.....	xxii
CHAPTER 1: INTRODUCTION TO PHOTOREDOX CATALYSIS.....	1
1.1 A Brief Description of Photophysical Processes.....	2
1.2 Electron Transfer	5
1.2.1 Thermodynamics of Electron Transfer	5
1.2.2 Determining the Rate of Electron Transfer	7
1.3 Acridinium Photooxidants	9
1.4 Conclusions	12
References.....	13
CHAPTER 2: DEVELOPMENT AND MECHANISTIC INVESTIGATION OF A PHOTOREDOX SYSTEM FOR HYDRODECARBOXYLATION OF CARBOXYLIC ACIDS.....	15
2.1 Introduction.....	15

2.1.1 Importance of Carboxylic Acids as Functional Handles.....	15
2.1.2 Previous Strategies for decarboxylation.....	17
2.1.2.1 Kolbe and Non-Kolbe Electrolysis	17
2.1.2.2 Barton Decarboxylation.....	18
2.1.2.3 Transition Metal Catalyzed Decarboxylation	22
2.1.2.4 Decarboxylation via Photochemical Oxidation of Carboxylates.....	22
2.1.2.5 Decarboxylation of malonates	25
2.1.3 Rate of Decarboxylation of Acyloxy Radicals	26
2.1.4 Atom Economy and Efficiency Comparisons between Hydrodecarboxylation Methodologies.....	28
2.2 Developing a Catalytic Photoredox Method for Hydrodecarboxylation.....	31
2.2.1 Initial Optimization of an Activated Carboxylic Acid Substrate.....	33
2.2.2 Continuing Optimization: Extension to Tertiary Alkyl Substituted Carboxylic Acids	35
2.2.3 Continuing Optimization: Extension to Primary Alkyl Substituted Carboxylic Acids	37
2.2.4 Summary of Optimization	39
2.2.5 Exploring the Scope of the Photoredox Hydrodecarboxylation	40
2.3 Application Towards Malonic Acid Derivatives.....	42
2.3.1 Developing Conditions for the Double Decarboxylation of Malonic Acid Derivatives	43
2.3.2 Scope of Malonic Acid Hydrodecarboxylation	45
2.4 Investigation of Hydrodecarboxylation Mechanism	46

2.4.1 Initial Mechanistic Proposal	46
2.4.2 The Role of Trifluoroethanol.....	47
2.4.2.1 Is Trifluoroethanol a Hydrogen-atom Donor?	47
2.4.2.2 Effect of Trifluoroethanol on Catalyst Excited State	50
2.4.3 Kinetic Analysis of Hydrodecarboxylation.....	52
2.4.3.1 Kinetic Isotope Effect Experiments	52
2.4.3.2 Further Kinetic Analysis.....	55
2.4.4 Hydrodecarboxylation dependence on substrate identity.....	57
2.4.4.1 Substrate Competition Experiments.....	58
2.4.4.2 Pre-association complex between Mes-Acr-Ph ⁺ and Carboxylate salts.....	61
2.4.4.3 Importance of Back Electron Transfer	64
2.5 Conclusions	65
2.6 Experimental	66
2.6.1 General Methods and Materials.....	66
2.6.2 Catalyst Preparation	67
2.6.3 Substrate Preparation	68
2.6.4 Monoacid Decarboxylation Procedures and Characterization Data	75

2.6.5 Malonic acid derivative Decarboxylation Procedures and Characterization Data	83
2.6.6 Electrochemical Measurements	85
2.6.7 Procedures for Collecting Kinetic Data and Raw Initial Rates Data	87
2.6.8 Kinetic Isotope Effect	91
2.6.8.1 Synthesis of Deuterated Carboxylic Acid.....	91
2.6.8.2 Procedure for Collecting KIE Data	92
2.6.9 UV/vis and Fluorescence Emission Details.	93
2.6.10 NMR Titration Experimental Details.....	95
2.6.10.1 Synthesis of TBA hydrocinnamate:	95
2.6.10.2 NMR Titrations	95
2.6.11 NMR Spectra:	95
References.....	105
CHAPTER 3: REVERSAL OF ALKENE HALOFUNCTIONALIZATION REGIOSELECTIVITY BY MERGING ORGANIC PHOTOREDOX AND COPPER CATALYSIS.....	112
3.1 Introduction.....	112
3.1.1 Alkene Difunctionalization	112
3.1.2 Alkene Halofunctionalization Through Electrophilic Activation.....	115
3.1.2.1 Enantioselective Halofunctionalization Reactions.....	117
3.1.2.1.1 Chiral Halogenating Reagents.....	117
3.1.2.1.2 Controlling Attack of the Nucleophile and Halonium delivery simultaneously	119

3.1.2.2 Heteroatom-Halide 1,2-substitution in Natural Products	121
3.1.3 Anti-Markovnikov Alkene Hydrofunctionalization in the Nicewicz Lab	123
3.2 Developing a Strategy For Catalytic Reversal of Alkene Halofunctionalization	125
3.2.1 Early Design Strategy	126
3.2.2 Inspiration for Halofunctionalization from Polymer Chemistry	128
3.2.3 Optimization of Chlorolactonization Using A Copper co-catalyst.....	129
3.2.3.1 Origin of Undesired Chlorolactone Regioisomer	132
3.2.4 Scope of Chlorolactonization	134
3.2.5 Optimization of Conditions for Bromolactonization	136
3.2.6 Scope of Bromolactonization	138
3.2.7 Application toward other Halofunctionalization Reactions	139
3.3 Product identification: distinguishing regio- and diastereoisomers	140
3.3.1 Distinguishing Regioisomers.....	140
3.3.2 Distinguishing Trans and Cis Diastereomers	142
3.4 Mechanism of Photoredox/Copper Mediated Halofunctionalization	143
3.4.1 Initial Mechanistic Proposal	143
3.4.2 UV/vis analysis of Cu (I) Oxidation by NCP	145
3.4.3 Evaluation of a Potential Chain Propagation Mechanism.....	146
3.5 Conclusions	147
3.6 Experimental	148

3.6.1 General Methods and Materials.....	148
3.6.2 Photoreactor Setup.....	150
3.6.3 Catalyst Synthesis.....	151
3.6.4 Substrate Synthesis.....	152
3.6.5 Halofunctionalization Procedures and Characterization Data.....	160
3.6.5.1 Important Notes.....	160
3.6.5.2 General Procedure for Chlorofunctionalization:.....	161
3.6.5.3 General Procedure for Bromofunctionalization:.....	178
3.6.5.4 General Procedure for Polar Halofunctionalizations.....	192
3.6.6 Analytical Data for Epoxides and Furans from Section 3.3.2.....	193
3.6.7 UV/vis Spectroscopy.....	199
3.6.8 Quantum Yield Determination.....	202
3.6.9 NMR Spectra.....	203
References.....	267
CHAPTER 4: HYBRIDIZATION TRANSFER THROUGH CARBON-CARBON FRAMEWORK ENABLES SELECTIVE HOMOBENZYLIC OXIDATION	272
4.1 Introduction.....	272
4.1.1 Site Selective Oxidation by Enzymes.....	272
4.1.1.1 Mechanism of Cytochrome P450 C–H oxidation.....	273
4.1.2 Traditional sp ³ C–H Bond Oxidation.....	274

4.1.3 Modern Approaches for Oxidation of sp^3 Hybridized C–H Bonds	276
4.1.3.1 Directed Functionalization of Unactivated C–H Bonds	277
4.1.3.2 Non-Directed C–H Functionalizations	278
4.1.3.2.1 Iron Catalyzed	278
4.1.3.2.2 Reagent Based C–H oxidation	279
4.1.3.2.3 Electrochemical C–H Oxidation.....	280
4.1.3.3 Summary of Modern C–H Oxidation Strategies.....	281
4.2 Developing a Strategy for Selective Homobenzylic Oxidation	282
4.2.1 Optimization of Tetrahydronaphthalene Oxidation.....	286
4.2.2 Initial Optimization of Propylbenzene Oxidation.....	288
4.2.3 Evaluating Reaction Irreproducibility.....	291
4.2.4 Kinetic Analysis of Homobenzylic Oxidation.....	295
4.2.4.1 Reaction Progress Kinetic Analysis	296
4.2.4.2 Evaluation of other acids	299
4.3 Reaction Mechanism.....	301
4.3.1 Initial Mechanistic Proposal	301
4.3.2 Fluorescence Quenching	304
4.4 Conclusions	306
4.5 Experimental	307
4.5.1 General Methods and Materials.....	307

4.5.2 Photoreactor Setup	309
4.5.3 Catalyst Synthesis	310
4.5.3.1 Mes-(3,6- <i>t</i> Bu-Acr)-Ph ⁺ Synthesis	310
4.5.3.2 Cobaloxime Catalyst synthesis	310
4.5.4 Substrate Synthesis	313
4.5.5 Procedure for Homobenzylic Oxidation Reactions	318
4.5.6 Electrochemical Measurements	319
4.5.7 Inductively Coupled Plasma Mass Spectroscopy (ICP-MS).....	320
4.5.8 Procedures for Collecting Kinetic Data	320
4.5.9 Fluorescence Emission Details	321
4.5.10 Stopped-Flow Experiments	322
References.....	324

LIST OF FIGURES

Figure 1.1: Overlay of absorbance and steady-state emission spectra of a xanthylium dye.....	3
Figure 1.2: Generic cyclic voltammogram.....	6
Figure 1.3: Generic Representation of a time correlated fluorescence spectrum and Stern-Volmer plot	8
Figure 1.4: Redox potentials of common organic functional groups.....	11
Figure 1.5: Structures of acridinium photocatalyst with their respective redox properties.....	11
Figure 2.1: Selection of C-C and C-X bond forming reactions of Carboxylic acids and esters.	16
Figure 2.2: Kolbe and Non-Kolbe Electrolysis pathways.	17
Figure 2.3: Use of a carboxylic acid from the chiral pool allows for the synthesis of (-)-aurantioclavine after a Barton decarboxylation	19
Figure 2.4: Barton Decarboxylation Sequence.	19
Figure 2.5: Baran Hydrodecarboxylation using redox active esters.	20
Figure 2.6: Mechanism proposed by Kozłowski et al. for the palladium catalyzed hydrodecarboxylation of arenes.	22
Figure 2.7: Mechanism of the Minisci Reaction.....	22
Figure 2.8: Decarboxylation protocol using photogenerated phen ⁺ • developed by Hatanaka and co-workers.....	23
Figure 2.9: Reaction conditions for a typical Krapcho decarboxylation and mechanism.....	25
Figure 2.10: Values for k_{CO_2} determined by Pincock and coworkers	26
Figure 2.11: Reaction pathways for decomposition of 1-Naphthylmethyl alkanoates.	27
Figure 2.12: Thermodynamic favorability of electron transfer between excited state acridinium and carboxylate salts.....	32
Figure 2.13: Important properties of thiophenol.....	32

Figure 2.14: Comparison of the solvent and base requirements for benzylic, 3° alkyl, and 1° alkyl carboxylic acid substrates.....	39
Figure 2.15: Application of Previously Developed Reaction Conditions with Malonic Acid Derivatives.....	43
Figure 2.16: Summary of deuterium labeling experiments.....	48
Figure 2.17: Time-correlated Fluorescence Spectra of Mes-Acr-Ph ⁺ in TFE and MeOH.....	50
Figure 2.18: Steady-state Emission Spectra of Mes-Acr-Ph ⁺ in TFE and MeOH.....	51
Figure 2.19: To determine if H-atom transfer was rate limiting, initial rates were measured for decarboxylation	53
Figure 2.20: Competition isotope experiment through the in-situ formation of PhSH/PhSD.....	54
Figure 2.21: Rate dependence of carboxylate ion concentration	55
Figure 2.22: %Conversion versus time for the hydrodecarboxylation of 2,2-dimethyl-3-phenylpropanoic acid under the standard reaction conditions..	56
Figure 2.23: (top) oxidation potentials of the tetrabutylammonium salts of three representative carboxylic acids +.....	58
Figure 2.24: Substrate competition experiments in TFE and 9:1 MeOH:H ₂ O.....	59
Figure 2.25: Substrate competition experiments in TFE and 9:1 MeOH:H ₂ O.....	60
Figure 2.26: UV/vis absorption spectra of the catalyst before and after adding carboxylate salt.....	61
Figure 2.27: (top left) ¹ H and (top right) ¹⁹ F NMR spectra of Mes-Acr-Ph ⁺ BF ₄ ⁻ [25 mM] in CD ₃ OD.....	62
Figure 2.28: Cyclic voltammograms for (top left) TBA propanoate (top right) TBA isobutyrate (bottom left) TBA pivalate and (bottom right) hydrocinnamic acid	86
Figure 2.29: (left) Initial rate versus concentration of Mes-Acr-Ph ⁺ at low concentrations (right) -ln of initial rate versus -ln of initial concentration of Mes-Acr-Ph ⁺	88
Figure 2.30: Initial rates plot for various initial concentrations of Mes-Acr-Ph ⁺	90
Figure 2.31: UV-Vis spectrum of Mes-Acr-Ph (15 μM) before and after the Stern-Volmer quenching experiment. R-CO ² -K ⁺ =potassium hydrocinnamate.....	94
Figure 3.1: Major strategies for alkene difunctionalization.	113

Figure 3.2: Electrophilic halogenating reagents and mechanism of traditional halofunctionalization.....	115
Figure 3.3: Nucleophile assisted alkene activation as proposed by Borhan and coworkers.	116
Figure 3.4: Halonium ion intermediates can be transferred between alkenes, potentially eroding enantioselectivity.....	117
Figure 3.5: Enantiospecificity of a tosylate displacement reaction	118
Figure 3.6: Enantioselective Bromolactonization catalyzed by a bifunctional BINOL based catalyst.....	119
Figure 3.7: Enantioselective chlorolactonization of 1,1-disubstituted styrenes developed by Borhan et al.....	120
Figure 3.8: 1,2-Heteroatom-halide relationships are found in natural products.....	122
Figure 3.9: Mechanism of Anti-Markovnikov Hydrofunctionalization developed by the Nicewicz Lab.....	123
Figure 3.10: Anti-Markovnikov addition of carboxylic acids to alkenes.....	124
Figure 3.11: Atom Transfer from a benzene sulfonyl chloride and benzene sulfonic acid produce the same sulfonyl radical.....	126
Figure 3.12: Early attempts at halofunctionalization through radical cation intermediates and relevant bond dissociation energies.....	127
Figure 3.13: General Mechanism for an Atom Transfer Radical Polymerization (ATRP) and relevant rate constants	128
Figure 3.14: Comparison of ^1H NMR shifts between regioisomers 3.5 and 3.26.	140
Figure 3.15: Comparison of ^{13}C NMR shifts determined by HSQC for each regioisomer.....	141
Figure 3.16: Analysis of diastereomers by formation of the corresponding epoxide products...	142

Figure 3.17: UV/vis absorption spectra of the 0.5 mM [CuClphen] ₂ (red line) before and after adding <i>N</i> -chlorophthalimide.....	145
Figure 3.18: Proposed Mechanism of a chain Propagated chlorolactonization.....	146
Figure 3.19: Photoreactor setup used for halofunctionalization reactions.	150
Figure 3.20: (top left) UV/vis spectrum of 5 x 10 ⁻⁴ M solution of [CuBr/bpy] ₂	200
Figure 3.21: (top left) UV/vis spectrum of 5 x 10 ⁻⁴ M solution of [CuCl/Phen] ₂	201
Figure 3.22: Photoreactor setup used in the quantum yield determination studies.....	203
Figure 4.1: Enzymatic Oxidation of 11-deoxycortisol to cortisol.	272
Figure 4.2: Enzymes like cytochrome P450 can routinely catalyze C–H functionalization reactions using molecular oxygen as the terminal oxidant.	273
Figure 4.3: Selective Benzylic Oxidation Methods.	274
Figure 4.4: Tertiary selective C–H functionalization with DMDO and related reagents.....	275
Figure 4.5: Directed C–H insertion enables selective functionalization of traditional inert C–H bonds.	277
Figure 4.6: Selective functionalization remote from functional groups.....	278
Figure 4.7: Activated amide intermediates developed by the Alexanian lab.	279
Figure 4.8: Electrochemical oxidation unactivated C–H bonds mediated by quinuclidine	280
Figure 4.9: Mechanism for anti-Markovnikov styrene oxidation proposed by Aiwen Lei and co-workers.	283
Figure 4.10: Mechanism for dehydrogenation of tetrahydronaphthalene proposed by Kanai and co-workers.....	284
Figure 4.11: (left) Kinetic profile of propylbenzene oxidation under the standard conditions (red line) and the same excess experiment (blue line).	296
Figure 4.12: Instantaneous reaction rate plotted against [propylbenzene] [M].	297
Figure 4.13: Acids having p <i>K</i> _a values in the range of approximately -1–5 were screened as a comparison to nitric acid.	299

Figure 4.14: (left) Reaction profiles of propylbenzene oxidation when using 5 mol% HNO ₃ (red line) or DCA (blue line).....	300
Figure 4.15: (left) Time-resolved fluorescence spectra of Mes-(3,6- <i>t</i> Bu-Acr)-Ph+ (15 μM) with increasing concentration of LiNO ₃ (0-19 mM).....	304
Figure 4.16: (left) Time-resolved fluorescence spectra of Mes-(3,6- <i>t</i> Bu-Acr)-Ph+ (15 μM) with increasing concentration of BMS (0-19 mM).....	305
Figure 4.17: Combined Stern-Volmer plots for Mes-(3,6- <i>t</i> Bu-Acr)-Ph+ singlet excited state quenching.	305
Figure 4.18: Photoreactor setup used for screening small scale reactions.	309
Figure 4.19: Cyclic voltammograms for (left) Propylbenzene (right) Lithium Nitrate.	319
Figure 4.20: Synthesis of Mes-(3,6- <i>t</i> Bu-Acr)-Ph•	322
Figure 4.21: UV-vis spectrum of 50 μM [Co(dmgbF ₂) ₂ •2L], 50 μM Mes-(3,6- <i>t</i> Bu-Acr)-Ph• before and after mixing.....	323

LIST OF SCHEMES

Scheme 1.1: Photophysical and thermochemical properties of acridinium and its excited states..	9
Scheme 2.1: Ideal scenario for reduction of a carboxylic acid to an alkane	31
Scheme 2.2: Mechanistic Proposal for Hydrodecarboxylation.	46
Scheme 2.3: Back electron transfer (BET) could explain rate differences between substrates....	64
Scheme 3.1: General Plan for Reversing Halofunctionalization Selectivity.....	125
Scheme 3.2: Plausible mechanism for formation of undesired regioisomer in the absence of copper catalyst.....	133
Scheme 3.3: Mechanistic proposal for chlorolactonization catalyzed by Mes-Acr-Me ⁺ and CuCl ₂ /phen.....	143
Scheme 3.4: General Scheme for Synthesis of 1,2 disubstituted alkene substrates.....	152
Scheme 3.5: Synthesis of 7-((<i>tert</i> -butyldimethylsilyl)oxy)-2,2,5-trimethylhept-4-enoic acid....	154
Scheme 3.6: Synthesis of 2-(prop-1-en-2-yl)benzoic acid	156
Scheme 3.7: Synthesis of <i>tert</i> -butyl (<i>E</i>)-(2,2-dimethyl-5-phenylpent-4-en-1-yl)carbamate	157
Scheme 4.1: General plan for alkane oxidation.	285
Scheme 4.2: Phenol could act as a redox-mediator after oxidation by Mes-(3,6- <i>t</i> Bu-Acr)-Ph ⁺ .	293
Scheme 4.3: Proposed mechanism of alkane dehydrogenation.	301
Scheme 4.4: Proposed mechanism of styrene oxidation.	303
Scheme 4.5: Synthesis of butane-1,3-diyl dibenzene.....	313
Scheme 4.6: Synthesis of Estrone Methyl-ether	314
Scheme 4.7: Synthesis of (3,7-dimethyloctyl)benzene	315
Scheme 4.8: Synthesis of 3-phenylpropyl acetate	317
Scheme 4.9: Synthesis of methyl 3-phenylpropanoate	318

LIST OF TABLES

Table 2.1: Comparison of Atom Economy (AE) and Reaction Mass Efficiency (RME) between hydrodecarboxylation methodologies	29
Table 2.2: Optimization of Hydrodecarboxylation conditions (2,2-diphenyldecanoic acid).	34
Table 2.3: Optimization of Hydrodecarboxylation conditions (1,1-dimethylpropanoic acid).	36
Table 2.4: Optimization of Hydrodecarboxylation conditions (3-phenylpropanoic acid).	38
Table 2.5: Optimization of Hydrodecarboxylation conditions for malonic acid derivatives	44
Table 2.6: Initial rate data for hydrodecarboxylation at various initial carboxylate and catalyst concentrations.....	87
Table 2.7: Initial rate data for high catalyst concentrations (5-10 mol%) using two different lamp configurations.....	89
Table 2.8: Initial Rates of Hydrodecarboxylation of Proteo and Deutero 1,1-dimethyl propanoic acid.....	92
Table 3.1: Optimization of Chlorolactonization ((<i>E</i>)-2,2-dimethyl-5-phenylpent-4-enoic acid)	129
Table 3.2: Important Control Reactions	132
Table 3.3: Optimization of Bromolactonization.	136
Table 4.1: Optimization of homobenzylic oxidation of tetrahydronaphthalene	287
Table 4.2: Optimization of propylbenzene oxidation.....	289
Table 4.3: Optimization of propylbenzene oxidation, continued.	292
Table 4.4: Analysis of trace-metals using ICP/MS.....	294

LIST OF CHARTS

Chart 2.1: Scope of Photoredox Mediated Hydrodecarboxylation. ^a	41
Chart 2.2: Scope of Photoredox Mediated Hydrodecarboxylation of Malonic Acid Derivatives.....	45
Chart 3.1: Scope of photoredox/copper catalyzed chlorolactonization. ^a	134
Chart 3.2: Scope of photoredox/copper catalyzed bromolactonization. ^a	138
Chart 3.3: Scope of other nucleophiles for halofunctionalization of alkenes.....	139

LIST OF ABBREVIATIONS

ΔG	Gibbs free energy
^{13}C	Carbon NMR
^1H NMR	Proton Nuclear Magnetic Resonance Spectroscopy
A	Amperes
ATRP	Atom Transfer Radical Polymerization
BDE	bond dissociation energy
BET	Back electron transfer
bpy	2,2'-bipyridine
C	Celsius
C-C	Carbon-carbon bond
C-H	Carbon-hydrogen bond
C-O	Carbon-oxygen bond
C-X	Carbon-heteroatom bond
CO_2	Carbon dioxide
COSY	Homonuclear Correlation Spectroscopy
CT	Charge transfer
CV	Cyclic Voltammetry
$\text{d}_1\text{-TFE}$	Trifluoroethyl alcohol-OD
$\text{d}_2\text{-TFE}$	2,2,2-Trifluoroethyl-1,1- d_2 alcohol
DCA	Dichloroacetic acid
DCB	1,4-dicyanobenzene
DFT	Density functional theory

DMDO	Dimethyl dioxirane
e^-	Electron
$E_{0,0}$	Excited State energy
$E_{1/2}$	Half-wave potential
$E_{p/2}$	Half-peak potential
ESI	Electrospray ionization
ET	Electron Transfer
eV	Electronvolt
F	Faraday's constant
FID	Flame ionization detector
GC	Gas chromatography
HAT	Hydrogen atom transfer
HOMO	Highest Occupied Molecular Orbital
HRMS	High-Resolution Mass Spectroscopy
HSQC	Heteronuclear single quantum coherence
$h\nu$	Photon or energy of a photon
I	Fluorescence Intensity
IBX	o-Iodoxybenzoic acid
ICP/MS	Inductively Coupled Plasma tandem Mass Spectroscopy
IR	Infrared
ISC	intersystem crossing
K	Kelvin
K	Equilibrium constant

k	Rate constant
kcal	kilocalorie
k_{CO_2}	Rate constant for decarboxylation
k_{ET}	Rate constant for electron transfer
KIE	Kinetic isotope effect
LE	Locally Excited
LED	Light emitting diode
LRMS	Low-Resolution Mass Spectroscopy
LUMO	Lowest Unoccupied Molecular Orbital
Lut+Cl ⁻	2,6-lutidinium chloride
M	Molar
m/z	Mass per unit charge
MeOH	Methanol
mol	Mole
MS	Mass spectroscopy
MW	Molecular weight
N-O	Nitrogen-oxygen bond
NHPI	N-hydroxyphthalimide
nm	Nanometer
NMR	Nuclear Magnetic Resonance
ns	Nanoseconds
PDI	Polydispersity index
Phen	Phenanthrene

phen	1,10-phenanthroline
PhSH	Thiophenol
ppb	Parts per billion
ppm	Parts per million
ps	Picoseconds
RBF	Round bottom flask
RME	Reaction Mass Efficiency
RT	Room temperature
s	Seconds
S ₀	Singlet ground state
S ₁	First singlet excited state
SCE	Saturated Calomel Electrode
SET	Single electron transfer
S _N 2	Bimolecular nucleophilic substitution
T	Temperature
T ₁	First triplet excited state
TCSPC	Time-correlated single photon counting
TFDO	Methyl(trifluoromethyl)dioxirane
TFE	Trifluoroethanol
TPB	tert-Butyl peroxybenzoate
TS	Transition state
UV	Ultraviolet
UV/vis	Ultraviolet-visible absorption spectroscopy

V	Voltage
α	First carbon atom attached to functional group
β	Second carbon atom attached to functional group
δ	Fourth carbon-atom from a given functional group
ϵ	Molar extinction coefficient
λ	Wavelength
μs	Microsecond
τ	Excited State Lifetime
Y	Third carbon atom from a given functional group
Φ	Quantum yield

CHAPTER 1: INTRODUCTION TO PHOTOREDOX CATALYSIS

All of the work presented herein is concerning the use of photoredox catalysis. This chapter is not intended to be an extensive review of the literature regarding photoredox catalysis, but rather a summary of the mathematical and theoretical underpinnings of the field which are uncommon to other areas of organic chemistry and contextualize some of the discussions and experiments in later chapters. Photoredox catalysis is based upon single electron transfer (SET) processes, which have been an area of intense study because they represent a controlled manifold for producing radical intermediates. The development of a number of many photo-oxidants and reductants excited by visible light, some of which have been known for over 80 years,¹ have only been explored relatively recently for their ability to facilitate organic reactions.² Even more recently, the use of *organic* molecules excited by visible light has become an important branch of photoredox catalysis.³ Organic molecules which can both absorb visible light and participate in reversible redox events are relatively rare. However, the handful of organic photoredox catalysts which have been evaluated so far have often been able to provide reactivity inaccessible by classic metal-based photoredox catalysts.

Due to the relatively new development of this field, many operational challenges in running photoredox reactions still exist, such as lack of standardization with regards to irradiation source and scalability. However, the chemical community has recognized these issues and there has been a concerted effort to provide a means of standardization.⁴ Despite the remaining challenges,

photoredox reactions still have the opportunity to provide creative solutions to longstanding problems in chemistry.

1.1 A Brief Description of Photophysical Processes

Molecules that absorb light at a given wavelength can access several different electronically excited states. These excited states can be vastly different even within the same molecule. The ability for a molecule to act as a photoredox catalyst is based in its photophysical properties. Upon absorption of a photon of light, an electron from the ground state chromophore (S_0), in the highest occupied molecular orbital (HOMO) is promoted to the lowest unoccupied molecular orbital (LUMO). This forms the first singlet excited state (S_1), termed such because the overall spin of the ground state molecule is preserved.

The geometric positions of the S_1 state are typically necessarily very close to those of the S_0 directly after excitation. Initial excitation will likely lead to a vibrationally excited S_1 state, which more closely matches the geometry of the lowest vibrational mode of S_0 , according to the Franck-Condon principle.⁵ This quickly relaxes to the ground state vibrational mode of S_1 , resulting in the ground states of S_0 and S_1 having different geometries. Movement of nuclei, such as bond vibrations, occur on the order of picoseconds (10^{-12} s) whereas electronic transitions occur on the timescale of femtoseconds (10^{-15} s). Thus excitation is favored when the positions of the nuclei experience very little change between the respective vibrational modes. This also means that the likelihood of exciting a molecule to the lowest energy vibrational mode is more likely for geometrically similar S_0 and S_1 states. If the excitation results in production of a higher energy vibrational mode, thermal decay to the lowest vibrational state is the most likely outcome. This S_1 state has numerous potential fates: including returning to the S_0 state through fluorescence or

internal conversion, intersystem crossing to a triplet excited (T_1), or it can undergo bimolecular processes such as energy transfer or electron transfer.

Fluorescence from S_1 results in the reformation of S_0 with simultaneous release of a photon. This photon will be equal to or lower in energy than absorbed by S_0 , as a result of any energy lost to thermal relaxation between vibrational modes. Fluorescence can also occur to give various

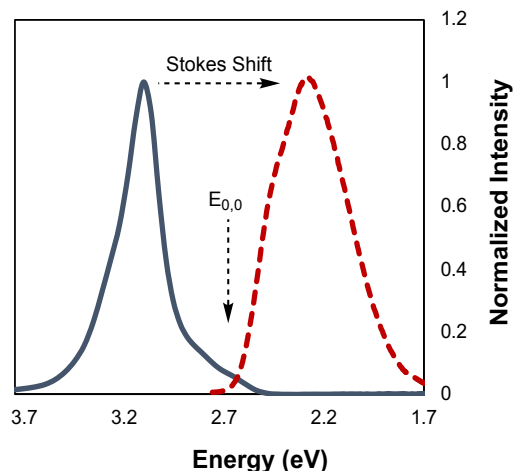


Figure 1.1: Overlay of absorbance and steady-state emission spectra of a xanthylium dye. The midpoint of the stokes shift is a good estimate of the excited state energy $E_{0,0}$. The value for $E_{0,0}$ for this particular molecule was found to be 2.63 eV. A very large Stokes shift was observed, potentially indicating a large geometrical change in the excited state.

vibrational states of S_0 , typically giving a net shift in λ_{\max} of the absorbance and fluorescence spectra known as the Stokes shift.⁶ The fluorescence and absorbance spectra often overlap in the middle point of the Stokes shift. This represents the point where S_1 emits a photon exactly equal to the energy difference between S_1 and S_0 lowest energy vibrational modes. Thus, the wavelength at which the absorbance and fluorescence spectra overlap is often used to estimate the excited state energy ($E_{0,0}$) (**Figure 1.1**).

Decay of S_1 occurs spontaneously can be described by an exponential function:

Equation 1.1.

$$N_t^* = N_0^* e^{-t/\tau}$$

Where N^* is the population of a excited state molecules. The excited state lifetime (τ) is an important property of excited state molecules, and describes the average time a population of molecules will stay in the excited state before decaying, and is equivalent to one over the decay constant ($1/k$). From this equation it can be derived that after one lifetime 36.8% of the excited state has decayed. Thus, multiple lifetimes have passed before the excited state has completely returned to the ground state. Excited state lifetimes are an important metric for comparing photoredox catalysts, as the amount of time that the excited state has to undergo productive chemistry is determined by the lifetime of that state. Importantly, the intensity of fluorescence (I) is directly proportional to the number of excited states, meaning that Equation 1.1 can be reformulated as:

Equation 1.2

$$I_t = I_0 e^{-t/\tau}$$

This means that the lifetime of excited state molecules can be determined by the decay in emission intensity versus time. Time-correlated single photon counting (TCSPC) is a time-resolved method for monitoring the fluorescence emission of an excited state.⁶ This technique was used to determine excited state lifetimes as shown in Chapters 2 and 4. Another important property of excited state molecules is the quantum yield of fluorescence (ϕ_F). Quantum yield is generally defined as follows:

$$\phi = \frac{\text{\# of molecules that undergo process X}}{\text{\# of photons absorbed}}$$

Thus, ϕ_F describes the number of excited state molecules which undergo fluorescence as opposed to undergoing other decay pathways. As shown in this equation quantum yield can be used to describe any process that involves the excited state in question. For example, a quantum yield of a reaction can be used to describe the efficiency of the excited state in catalyzing a certain reaction. This will be shown in context in Chapter 3.

As mentioned above, S_1 can also undergo intersystem-crossing (ISC) leading to the lowest energy triplet state (T_1). Since ISC is a forbidden transition the change in spin must occur concomitantly with a change in orbital angular momentum. This is a process called spin-orbit coupling and occurs when the S_1 state can interconvert with an orbital that has a different orbital angular momentum. The T_1 state decays back to S_0 through a process known as phosphorescence, which involves emission of a photon of lower energy than fluorescence due to the T_1 state being lower in energy than S_1 . Phosphorescence results in the electron returning to the HOMO, which also requires a forbidden spin flip. Thus T_1 states are typically much more long lived than S_1 states, meaning that while they are lower in energy they can often be more productive in photoinduced electron transfer processes.

1.2 Electron Transfer

1.2.1 Thermodynamics of Electron Transfer

Electron transfer is only one of several potentially productive ways an excited state can interact with a substrate (i.e. Energy Transfer). However, all of the chemistry discussed in the following chapters deals exclusively with electron transfer pathways. The favorability of a particular photoinduced electron transfer is described by the following equation:

Equation 1.3

$$\Delta G_{ET} = -F(E_{ox}(D^{+\bullet}/D) - E_{red}(A/A^{\bullet-})) - w - E_{0,0}$$

Conventionally the species undergoing oxidation is described by E_{ox} , and the species undergoing reduction is described by E_{red} . In this equation the redox potential of the excited state is described in two terms, one being the ground state redox potential and the other is the excited state energy $E_{0,0}$.

Since $E_{0,0}$ is the energy difference between excited state and the ground state (in their lowest energy vibrational states), the excited state redox potential can be determined by adding the ground state redox potential (E°) and $E_{0,0}$. This general principle will be used throughout in discussions of electron transfer.ⁱ Although, this equation tells us if an electron transfer event will be thermodynamically favorable, it cannot describe the rate of a particular electron transfer event. The equation which describes the rate of electron transfer was first formulated by Rudolph Marcus, however an experimental approach for determining the rate of photoinduced electron transfer will be discussed below.

As evidenced by the Equation 1.3, whether an electron transfer will occur spontaneously can be easily predicted. Cyclic voltammetry (CV) is an indispensable tool for determining redox values. Using CV allows for scanning electrochemical potential (volts, V) in a cell. If a suitable substrate is present, electron transfer can occur at the surface of the electrode when the appropriate

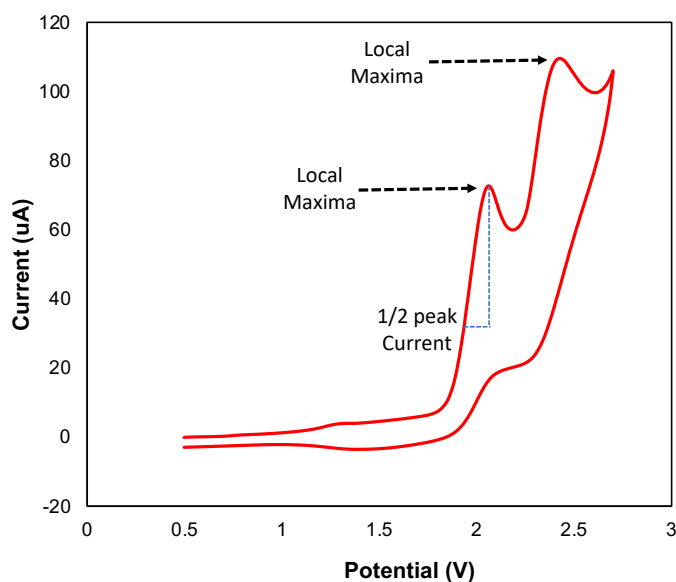


Figure 1.2: Generic cyclic voltammogram. This voltammogram has multiple local current maxima corresponding to oxidation events that occur at different potentials. The redox potential for an irreversible oxidation or reduction wave can be estimated by taking the potential at half of the peak current ($E_{p/2}$) for that feature.

ⁱ This equation will be used in a simplified form, excluding the work (w) term.

potential is reached. Current (Amps, A) can be measured as a function of potential. For reversible redox couples, the peak anodic current ($i_{p,a}$) is equal to the peak cathodic current ($i_{p,c}$). A simplified way of determining redox values is to average the potential at which $i_{p,a}$ and $i_{p,c}$ occur,⁷ and these values will be termed $E_{1/2}^{ox}$ or $E_{1/2}^{red}$ herein to signify that they correspond to reversible redox couples.

However, the vast majority of organic molecules do not have reversible redox couples, indicating that oxidized or reduced species are not stable (**Figure 1.2**). Redox values can be estimated for irreversible redox couples by taking the half-peak potential or the potential correlated with $i_p/2$.ⁱⁱ These redox values have been shown to be a good estimate of the true potential.⁸ However, to differentiate them from reversible redox couples they will be termed $E_{p/2}^{ox}$ or $E_{p/2}^{red}$ indicating that they were determined from half-peak potentials.

1.2.2 Determining the Rate of Electron Transfer

As discussed in Section 1.1 excited states experience exponential decay back to the corresponding ground states with lifetime τ . When an excited state molecule encounters another molecule a number of processes can deactivate the excited state including electron transfer. Molecules that can decrease the intensity of fluorescence bimolecularly are known as quenchers (Q). It is important to distinguish between two main types of quenching: 1) dynamic quenching occurs from the excited state of a molecule and includes electron transfer 2) static quenching occurs when the *ground state* is deactivated before absorption can occur. Since electron transfer is a dynamic quenching process, it results the excited state having an overall shorter lifetime.

ⁱⁱ This value can correspond to either a peak anodic current or peak cathodic current.

The Stern-Volmer relationship describes how increasing concentration of a Q molecule changes the excited state lifetime:

Equation 1.4

$$\frac{\tau_0}{\tau} = K_{SV}[Q] + 1 = k_q\tau_0[Q] + 1$$

K_{SV} is the Stern-Volmer constant and is equal to the rate constant of the bimolecular quenching (k_q) event multiplied by the unquenched lifetime (τ_0). This relationship allows for the measurement of the rate constant for a given quenching event, as excited state lifetime can be obtained from the

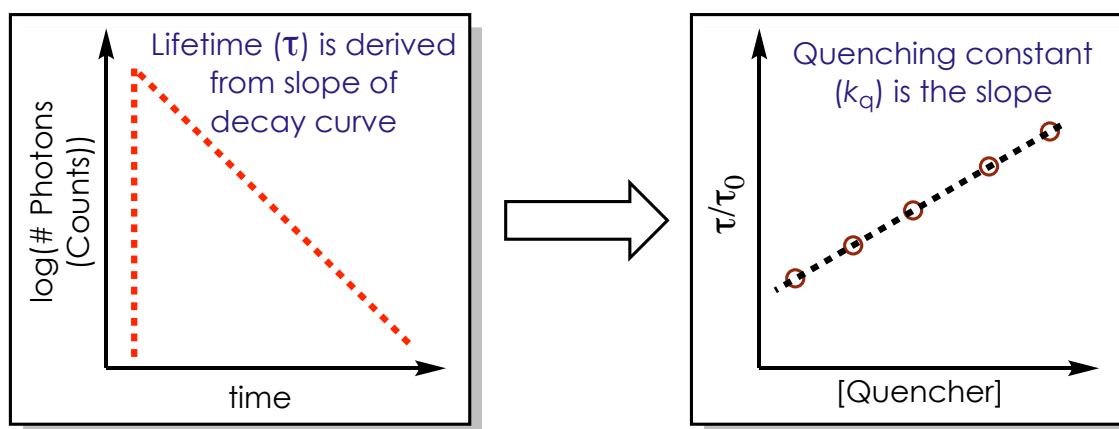


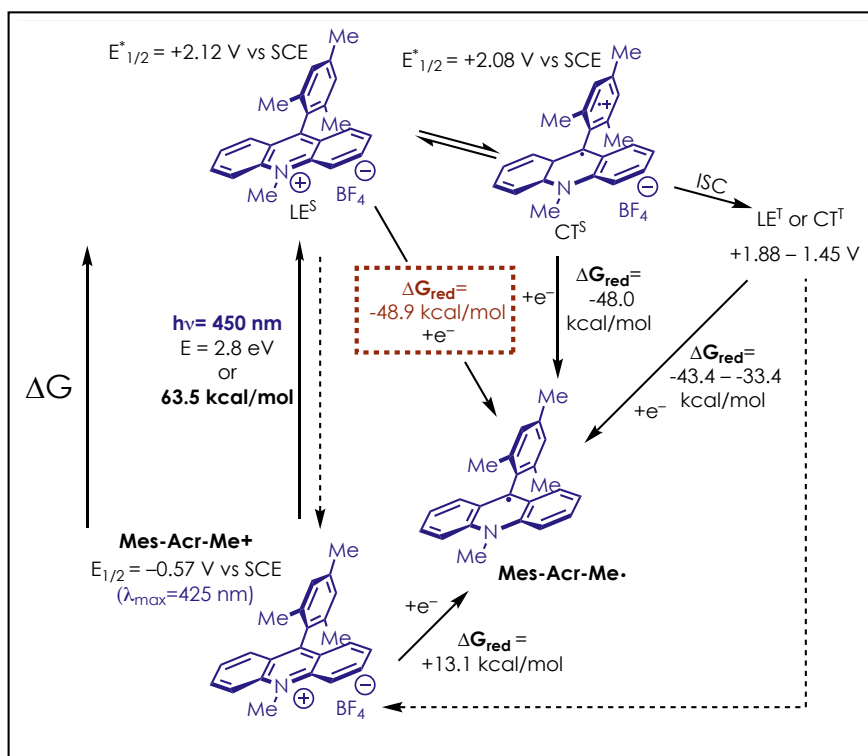
Figure 1.3: Generic representation of a time correlated fluorescence spectrum (right). The number of photon emitted by the fluorophore counted by the detector and plotted against time (typically in nanoseconds). Typically the data is plotted as the ln plot. If only one emitting species is present, the ln plot should be roughly a straight line corresponding to a monoexponential decay process. By fitting the curve to an exponential function, the excited state lifetime (τ) can be obtained. Determining τ at multiple concentrations of a quencher allows for generation of a Stern-Volmer plot (left) whose slope is $K_{SV} = k_q\tau_0$.

fluorescence intensity over time as described above in Equation 1.2. Since the Stern-Volmer relationship is a linear function plotting τ/τ_0 as a function of $[Q]$ allows for extraction of the K_{SV} from the slope of the line (**Figure 1.3**). k_q can also be obtained through using fluorescence intensity rather than lifetime, however this method cannot distinguish between dynamic and static quenching modes. Lifetime measurements on the other hand are not affected by ground-state quenching.

1.3 Acridinium Photooxidants

Acridiniums are some of the most potent visibly excited photooxidants currently known, as first reported by Fukuzumi.⁹ They are capable of photooxidation of a wide number of substrates not accessible by other common photocatalyst such as $\text{Ru}^{\text{II}}(\text{bpy})_3^{2+}$ and $\text{Ir}^{\text{III}}(\text{ppy})_3$ and its derivatives. $\text{Ru}^{\text{II}}(\text{bpy})_3^{2+}$ can act as either an oxidant or reductant in its excited state ($E_{1/2}^{\text{ox}} = -0.86 \text{ V vs SCE}$, $E_{1/2}^{\text{red}} = +0.77 \text{ V vs SCE}$).¹⁰ Since it has a relatively low excited state reduction potential, in order to access the more oxidizing Ru^{III} ($E_{1/2}^{\text{red}} = +1.29 \text{ V vs SCE}$) ground state

Scheme 1.1: Photophysical and thermochemical properties of acridinium and its excited states.



sacrificial oxidants are commonly employed.¹¹ $\text{Ir}^{\text{III}}(\text{ppy})_3$ on the other hand is a very poor excited state oxidant ($E_{1/2}^{\text{red}} = +0.31 \text{ V vs SCE}$), however some derivatives of this general structure are frequently used such as $\text{Ir}^{\text{III}}[\text{dF}(\text{CF}_3)\text{ppy}]_2(\text{dtbpy}))\text{PF}_6$ [$\text{dF}(\text{CF}_3)\text{ppy}$ = 2-(2,4-difluorophenyl)-5-fluoropyridine; dtbpy = 4,4'-ditertbutyl bipyridyl] have been more commonly employed as excited

state photooxidants.¹² While these are more oxidizing excited state species ($E_{1/2}^{red} = +1.21$ V vs SCE) they are still not capable of oxidizing many common functional groups.¹³ Due to the unique properties of acridinium photocatalysts to act as very strong excited state oxidants with the use of visible light, they were used exclusively in the work presented here.

Some of the relevant properties of acridinium photocatalysts are shown above in Scheme 1.1. Importantly, these organic photooxidants absorb in the visible region of the light spectrum, having a maximum absorption (λ_{max}) around 425 nm. However, they can also be excited with LED sources centered around 450 nm, which is the method typically employed by our lab. Reduction of acridinium in its ground state by one electron is uphill in energy ($E_{1/2}^{red} = -0.55$ V vs SCE). Thus, it would require fairly strong reductants to reduce acridinium in its ground state.

Upon excitation the S_1 state is reached termed here as the locally excited singlet state (LE^S) because the electronic transition is centered on the acridinium core.¹⁴ This excited state is now a powerful one-electron oxidant and single electron reduction of this excited state is favorable by nearly 50 kcal/mol. Reduction of acridinium in its excited state can occur from functional groups which are not typically regarded as reductants. The LE^S has been shown to be in thermal equilibrium with a slightly lower energy singlet state termed the charge transfer singlet state CT^S , and fluoresce occurs from both states to give a common lifetime.¹⁴ The CT^S state as implied by its name, involves the transfer of positive charge from the acridinium core to the pendant mesityl group in the 9-position. This CT^S is not present when less electron rich arenes are in the 9-positions such as xylyl.¹⁵ ISC is thought to occur from this state to reach lower energy triplet states. The identity of the triplet state has been a topic of debate in the literature and could be either a locally excited triplet state (LE^T) or charge transfer triplet state (CT^T). As opposed to some metal based photooxidants, the reduced form of acridinium (acridine radical) are only mildly reducing.

However, acridine radicals can still reduce even mild oxidants, allowing for regeneration of the ground state.

Though not a complete list, some substrates which can be considered as redox partners for excited state acridinium are shown in Figure 1.4. Some of the first substrates considered by our

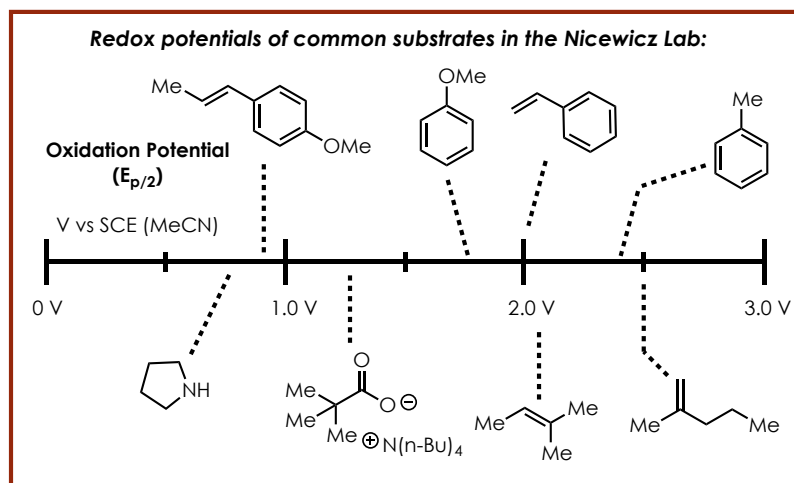


Figure 1.4: Redox potentials of common organic functional groups.

lab were alkenes.^{16,17} Only the most electron rich alkenes like anethole can oxidized by more commonly employed photooxidants such as $\text{Ru}(\text{bpy})_3^{2+}$. Excited state acridinium on the other hand is capable of undergoing SET with unsubstituted styrenes and trisubstituted alkenes. Even less electron rich alkenes such as 1,1-disubstituted alkenes have very high redox potentials and cannot undergo electron transfer with acridinium photooxidants.

The structures of the acridinium oxidants which will be referenced throughout the following chapters are shown in Figure 1.5, along with their relevant redox properties. The naming

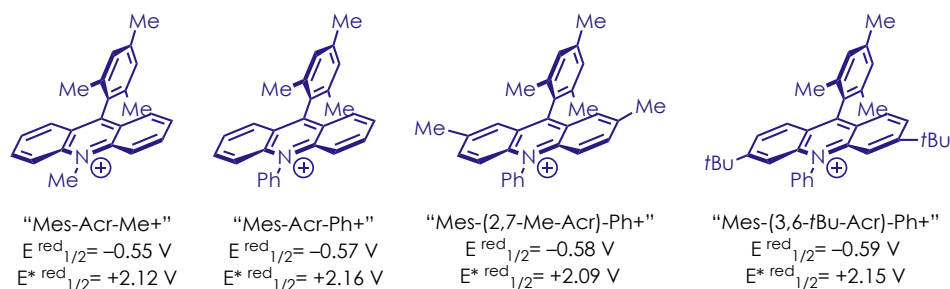


Figure 1.5: Structures of acridinium photocatalyst with their respective redox properties.

scheme of the acridinium catalysts shown in this figure reflects the positions of the substituents around the acridinium core. The catalysts will be named accordingly throughout the remaining chapters for clarity.

The structure of the favored acridinium catalyst has evolved over the course of our lab's history. Initially Mes-Acr-Me⁺ was used because of the relative ease of synthesis.^{18,19} However, this catalyst has been shown to be prone to demethylation and thus the more stable Mes-Acr-Ph⁺ was favored.²⁰ Eventually methodologies were developed which required the use of even stronger nucleophiles, and thus alkyl groups needed to be added to the acridinium core to block susceptible positions. While the 3 and 6 positions on the acridinium core are the most susceptible to nucleophilic or radical addition, derivatives with substitution at these positions are more difficult to synthesize. Mes-(2,7-Me-Acr)-Ph⁺ was found to sufficiently block these positions for some applications.²¹ Finally, the most robust acridinium catalyst used by our lab to date has been Mes-(3,6-*t*Bu-Acr)-Ph⁺, and has been used in more recent chemistry.^{22–25} Unfortunately, this catalyst currently requires a somewhat lengthy synthesis, but current work is underway address this. All of the catalysts shown in Figure 1.5 have a mesityl group located at the 9 position. This group has been shown to help block the otherwise susceptible position from nucleophilic attack.

1.4 Conclusions

Acridinium photooxidants are often uniquely able to participate in SET reactions that are not accessible by other ground state or excited state oxidants. Many unique tools are required for studying photoredox catalyzed reactions. The basic principles of many of the tools that will be used throughout the remaining chapters have been discussed.

REFERENCES

- (1) Burstall, F. H. 34. *J. Chem. Soc.* **1936**, 0 (0), 173.
- (2) Prier, C. K.; Rankic, D. A.; MacMillan, D. W. C. *Chem. Rev.* **2013**, 113 (7), 5322–5363.
- (3) Romero, N. A.; Nicewicz, D. A. *Chem. Rev.* **2016**, 116 (17), 10075–10166.
- (4) Le, C. “Chip”; Wismer, M. K.; Shi, Z.-C.; Zhang, R.; Conway, D. V.; Li, G.; Vachal, P.; Davies, I. W.; MacMillan, D. W. C. A. *ACS Cent. Sci.* **2017**, 3 (6), 647–653.
- (5) Anslyn, E. V.; Dougherty, D. A. *Modern Physical Organic Chemistry*; University Science, 2006.
- (6) Lakowicz, J. R. *Principles of Fluorescence Spectroscopy*, 3rd ed.; Lakowicz, J. R., Ed.; Springer US: Boston, MA, 2006.
- (7) Elgrishi, N.; Rountree, K. J.; McCarthy, B. D.; Rountree, E. S.; Eisenhart, T. T.; Dempsey, J. L. *J. Chem. Educ.* **2018**, 95 (2), 197–206.
- (8) Roth, H.; Romero, N.; Nicewicz, D. *Synlett* **2015**, 27 (5), 714–723.
- (9) Shunichi Fukuzumi, Hiroaki Kotani, Kei Ohkubo, Seiji Ogo, Nikolai V. Tkachenko, and; Helge Lemmetyinen, . *J. Am. Chem. Soc.*, **2004**, 126, (6), 1600-1601.
- (10) Kalyanasundaram, K. *Coord. Chem. Rev.* **1982**, 46, 159–244.
- (11) Ischay, M. A.; Lu, Z.; Yoon, T. P. [2+2] *J. Am. Chem. Soc.* **2010**, 132 (25), 8572–8574.
- (12) Zhang, X.; MacMillan, D. W. C. *J. Am. Chem. Soc.* **2017**, 139 (33), 11353–11356.
- (13) Michael S. Lowry; Jonas I. Goldsmith,; Jason D. Slinker,; Richard Rohl,; Robert A. Pascal, J.; George G. Malliaras, and; Bernhard, S. *Chem. Materials.*, **2005**, 17 (23), 5712-5719.
- (14) Andrew C. Benniston,; Anthony Harriman,; Peiyi Li,; James P. Rostron,; Hendrik J. van Ramesdonk,; Michiel M. Groeneveld,; Hong Zhang, and; Jan W. Verhoeven, *J. Am. Chem. Soc* **2005**, 127 (46), 16054–16064.
- (15) Romero, N. A.; Nicewicz, D. A. *J. Am. Chem. Soc.* **2014**, 136 (49), 17024–17035.
- (16) Margrey, K. A.; Nicewicz, D. A. A. *Acc. Chem. Res.* **2016**, 49 (9), 1997–2006.
- (17) Nicewicz, D. A.; Nguyen, T. M. *ACS Catal.* **2014**, 4 (1), 355–360.
- (18) Hamilton, D. S.; Nicewicz, D. A. *J. Am. Chem. Soc.* **2012**, 134 (45), 18577–18580.

- (19) Perkowski, A. J.; Nicewicz, D. A. *J. Am. Chem. Soc.* **2013**, *135* (28), 10334–10337.
- (20) Griffin, J. D.; Zeller, M. A.; Nicewicz, D. A. *J. Am. Chem. Soc.* **2015**, *137* (35), 11340–11348.
- (21) Wilger, D. J.; Grandjean, J.-M. M.; Lammert, T. R.; Nicewicz, D. A. *Nat. Chem.* **2014**, *6* (8), 720–726.
- (22) Romero, N. A.; Margrey, K. A.; Tay, N. E.; Nicewicz, D. A. *Science* **2015**, *349* (6254), 1326–1330.
- (23) McManus, J. B.; Nicewicz, D. A. *J. Am. Chem. Soc.* **2017**, *139* (8), 2880–2883.
- (24) Tay, N. E. S.; Nicewicz, D. A. *J. Am. Chem. Soc.* **2017**, *139* (45), 16100–16104.
- (25) Margrey, K. A.; Levens, A.; Nicewicz, D. A. *Angew. Chemie Int. Ed.* **2017**, *56* (49), 15644–15648.

CHAPTER 2: DEVELOPMENT AND MECHANISTIC INVESTIGATION OF A PHOTOREDOX SYSTEM FOR HYDRODECARBOXYLATION OF CARBOXYLIC ACIDSⁱ

2.1 Introduction

2.1.1 Importance of Carboxylic Acids as Functional Handles

Carboxylic acids and esters are some of the most commonly occurring functional groups in nature.¹ Synthetic chemists have utilized this abundant source of carbonyl compounds to carry out classic C-C bond forming reactions such as enolate alkylations and Michael additions, or C-X bond forming reactions such as α -oxidation reactions (**Figure 2.1, left**). Alkenes bearing electron withdrawing groups such as esters or carboxylic acids can be differentiated electronically from other alkenes within a molecule allowing for control over regioselectivity (**Figure 2.1, top right**).² Additionally, α,β -unsaturated carboxylic acids and esters are much more reactive than the corresponding unactivated alkenes toward cycloaddition reactions, such as the Diels-Alder reaction.³ Like other carbonyl containing compounds, carboxylic acids are Lewis-basic allowing them to coordinate Lewis or Brønsted-acids. Coordination with Lewis acids has been shown to enhance the rate of Diels-Alder cycloadditions, while simultaneously providing an avenue of inducing enantioselectivity⁴ (**Figure 2.1, bottom right**). Michael reactions can often be rendered enantioselective via the coordination

ⁱ The work presented in this chapter has previously been disclosed in a different form. See: Griffin, J. D.; Zeller, M. A.; Nicewicz, D. A. *J. Am. Chem. Soc.* **2015**, 137, (35), 11340-11348.

of a carboxylate containing nucleophile^{5,6} or electrophile. Additionally, the use of chiral auxiliaries has been a major strategy in order to induce enantioselectivity in both alkylation⁷ and Michael reactions⁸, the products of which are often chiral carboxylic acids.

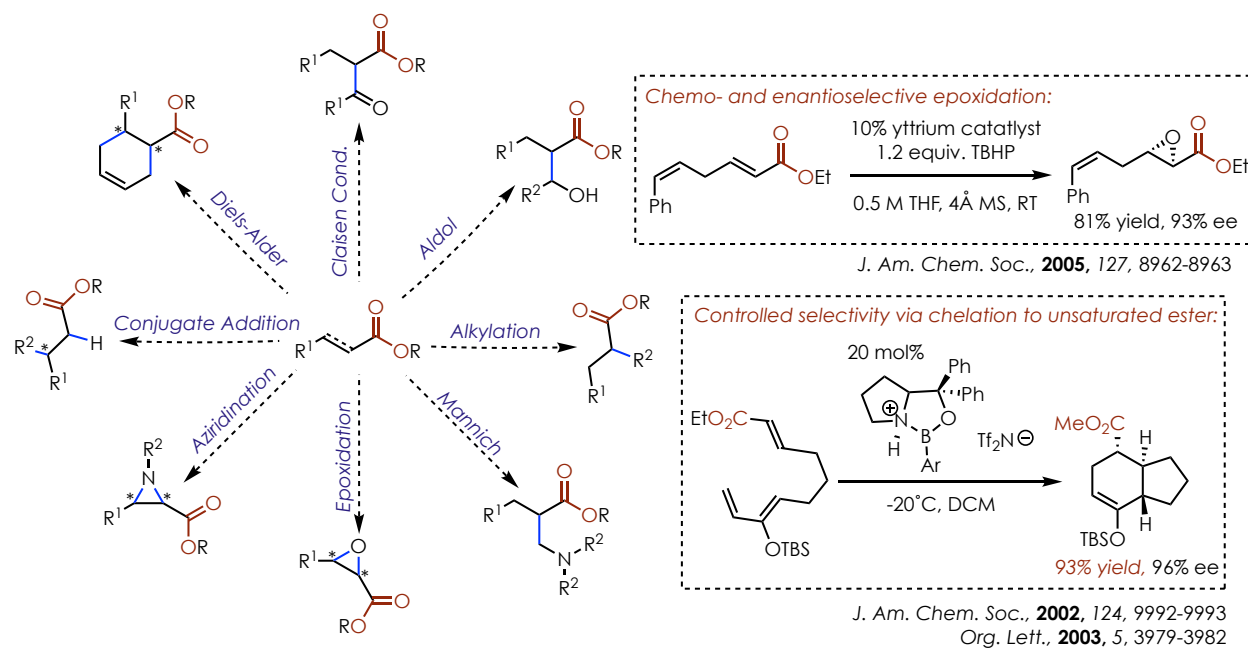


Figure 2.1: Selection of C-C and C-X bond forming reactions of Carboxylic acids and esters. Highlighting the usefulness of carboxylates for achieving chemo- and enantioselectivity

Malonates are used ubiquitously in the literature as nucleophiles in reactions not typically accessible by other carbon nucleophiles, such as the Tsuji-Trost allylation.⁹ Malonate enolates are more easily implemented as nucleophiles than other carbonyl enolates, because of their relatively low pK_a . Malonates are commonly used to accelerate the rate of intramolecular reactions, such as intramolecular Diels-Alder or metathesis reactions, through the Thorpe-Ingold effect.

2.1.2 Previous Strategies for decarboxylation

Though carboxylic acids are useful functional handles with a seemingly myriad number of strategies for installing or functionalizing them, they are not always a desired part of a downstream synthesis. The ability to remove carboxylic acids via hydrodecarboxylation could be viewed as a strategy for accessing the reactivity of carbonyl functional groups in a traceless manner. This could facilitate the assembly of complex molecular structures, while allowing for the use of classical disconnection strategies. Additionally, decarboxylation has been used as a strategy to generate useful radical intermediates. Thus, chemists have been interested in developing strategies for decarboxylation since the 18th century.

The synthetic utility of a malonic acid decarboxylation stems from the ability to use malonate as a source of “(-)CH₂(-)” synthon. This could be accomplished through the coupling of two electrophiles with malonate, followed by hydrolysis to the diacid and decarboxylation of both carboxylic acid components.

2.1.2.1 Kolbe and Non-Kolbe Electrolysis

In 1848 Hermann Kolbe developed an electrochemical methodology for decarboxylation of aliphatic carboxylates (**Figure 2.2, top**).^{10,11} In the electrochemical cell loss of an electron from

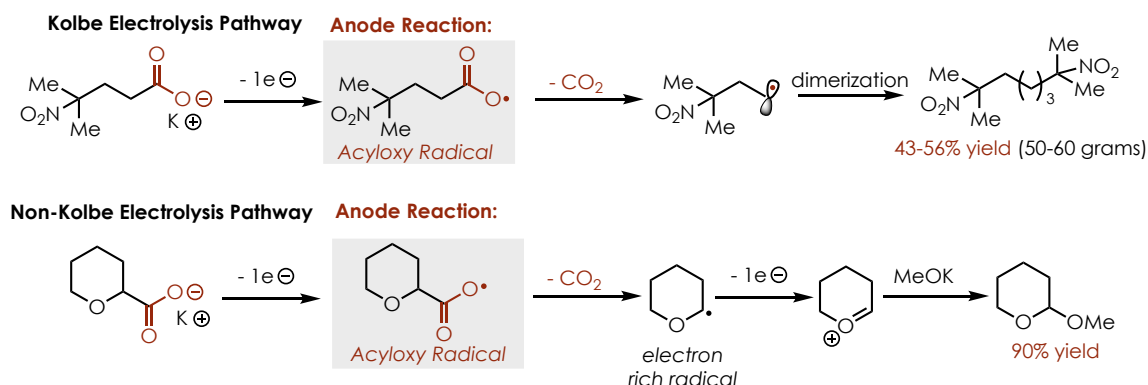


Figure 2.2: Kolbe and Non-Kolbe Electrolysis pathways.

the carboxylate results in the formation of an acyloxy radical.¹² This intermediate is proposed to rearrange, losing CO₂ and forming a more stable carbon-centered radical. These radicals can either recombine (Kolbe-Electrolysis) or undergo a second oxidation at the surface of the electrode (Non-Kolbe Electrolysis).¹³ The major determinant for selectivity between the two reaction pathways is based on the electronic nature of the carbon-centered radical and the electrode potential. Relatively electron poor radicals tend to undergo dimerization, while electron rich radicals tend to undergo secondary oxidation to form cationic intermediates that can be trapped with nucleophiles. In both Kolbe and Non-Kolbe reactivity reduction of protons, typically from solvent, occurs at the cathode, producing H₂.

The Kolbe electrolysis process has been shown to be very robust, and capable of being scaled to produce >50 grams of material on a simple lab scale setup (constant current of 3-5 A).¹⁴ Though the Kolbe electrolysis is a very reliable reaction, it represents a form of uncontrolled reactivity. The formation of highly reactive radicals are formed in high concentration at the surface of an electrode, which leads to radical-radical recombination. This precludes the radicals from engaging in more useful types of reactivity. Non-Kolbe electrolysis similarly provides uncontrolled reactivity, due to the over-oxidation of the substrate; although, this does allow for reactivity of the substrate with a secondary reactant.

2.1.2.2 Barton Decarboxylation

The Barton decarboxylation¹⁵⁻¹⁸ process has been one of the most utilized methods for excising a carboxylate functional group.¹⁹⁻²¹ This strategy has been employed in synthesis as a way to utilize the existing pool of chiral carboxylic acids, without including the carboxylic acid

functional group downstream in the synthesis. This was successfully demonstrated by Jia and coworkers in the enantioselective synthesis of (-)-aureantioclavine (**Figure 2.3**).²²

Decarboxylation in Total Synthesis: (-)-aureantioclavine:

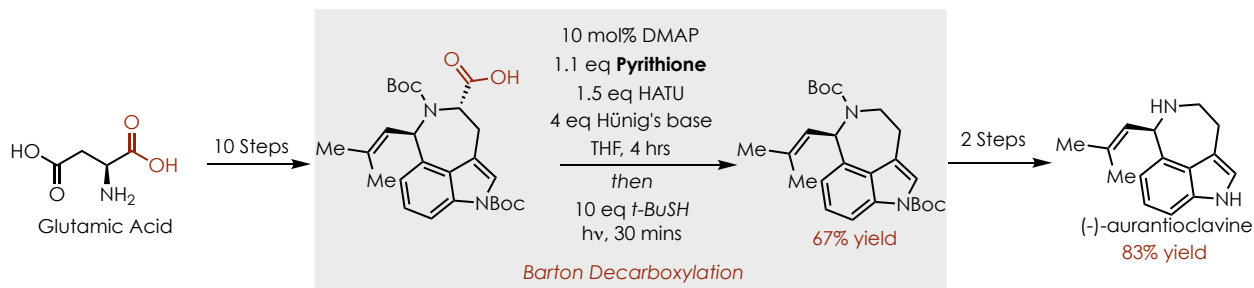


Figure 2.3: Use of a carboxylic acid from the chiral pool allows for the synthesis of (-)-aureantioclavine after a Barton decarboxylation

Akin to the Kolbe electrolysis the key step involves the production of an unstable acyloxy radical intermediate. In order to generate the acyloxy radical, the carboxylic acid substrate is first converted to the corresponding thiohydroxamate ester via the intermediacy of an acyl chloride or activated ester (Figure 2.4).

The weak N-O bond in the thiohydroxamate ester can be cleaved using a variety of conditions including UV light, heat, or the use of an appropriate radical initiator. Upon cleavage

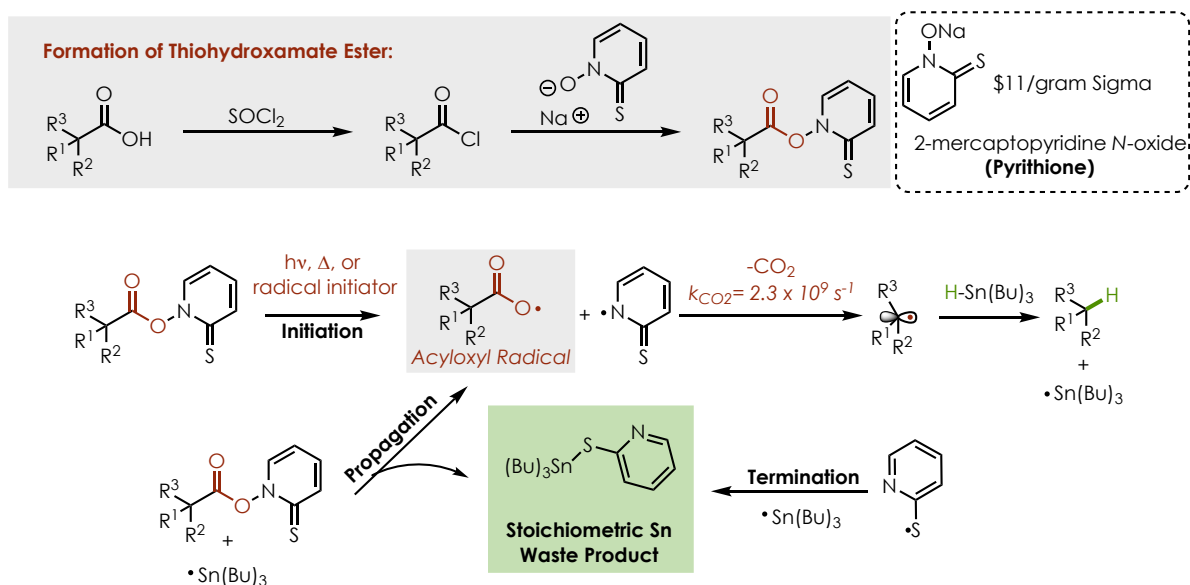


Figure 2.4: Barton Decarboxylation Sequence.

of the N-O bond and formation of the corresponding acyloxy radical, rapid CO₂ loss occurs forming a carbon centered radical which can be trapped with an appropriate H-atom donor or other radical trap. Since pre-activation of the substrate is required these reactions produce a large amount of potentially toxic waste. The original Barton protocol utilized a trialkyl stannane as H-atom donor, however modifications have been developed which employ thiols,^{23,24} silanes,²⁵ or chloroform.²⁶ All of these methodologies require superstoichiometric quantities of H-atom donor to produce significant quantities of products. The overall atom economy of the Barton decarboxylation is necessarily low due to the multi-stage process required to convert the carboxylate to the corresponding hydrocarbon product (vide infra, see 2.1.4).

Recently, interest has emerged in a new class of activated esters that can be employed in Barton-type decarboxylative processes. The Baran lab has been particularly active in this area, demonstrating that *N*-hydroxyphthalimide (NHPI) esters can participate in redox mediated

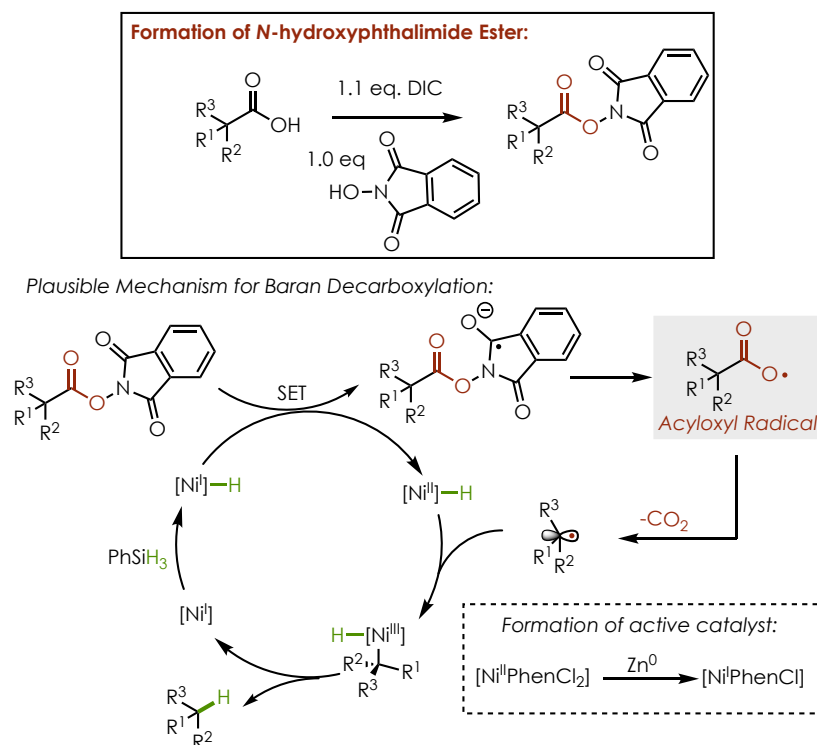


Figure 2.5: Baran Hydrodecarboxylation using redox activae esters.

cleavage of the weak N-O bond and ultimately lead to carbon-centered radical intermediates, in a similar process to the Barton decarboxylation.²⁷ The reduction of the redox esters is typically mediated by a nickel catalyst along with a stoichiometric reductant such as zinc. Although a mechanism for the reaction has not been proposed, alkyl radicals have been proposed to recombine with nickel (II) effectively oxidizing the metal center to nickel (III).^{28,29} Similarly to other nickel catalyzed reductions of NHPI esters, the reaction likely proceeds through the reduction of the activated ester from a low valent nickel species. Upon reduction, the NHPI ester likely fragments; it is unclear whether this proceeds through the intermediacy of an acyloxy radical.

Ultimately, a carbon centered radical is produced which can recombine with a Ni (II) hydride, forming an unstable Ni (III) intermediate which likely quickly reductively eliminates the reduced product (**Figure 2.5**). Phenylsilane was used as the hydride source in this case. It is also possible that a mechanism involving direct H-atom abstraction from the silane is operative as silanes have been shown to be competent H-atom donors in similar hydrodecarboxylation reactions.²⁵ Zinc metal was used presumably to form the active Ni catalyst or regenerate the Ni catalyst after reduction of the NHPI ester. Like the Barton decarboxylation this method suffers from low atom economy (*vide infra*, see 2.1.4).

NHPI esters have also been shown to participate in numerous coupling reactions to form new C-C bonds including alkylations,³⁰ alkenylations,³¹ arylations,³² and alkynylations.³³ Although, many useful transformations have been developed using this decarboxylative process, the overall atom-economy is very low, similarly to the Barton decarboxylation, and requires pre-activation of the carboxylic acid. Similarly, these redox active esters have been shown to undergo reaction with photoreductants by the Overman lab.^{34,35}

2.1.2.3 Transition Metal Catalyzed Decarboxylation

Hydrodecarboxylative and decarboxylative coupling³⁶ methodologies have been reported using a variety of transition metal catalysts. These processes require extremely high temperatures for alkyl substituted carboxylic acids,³⁷ thus this type of decarboxylation is typically limited to substrates with sp^2 or sp hybridization at the α -carbon. These reactions can be carried out with a variety of transition metals including Pd,^{37–41} Cu^{42–45}, Ag^{43,46,47}, and Rh⁴⁸. They likely do not

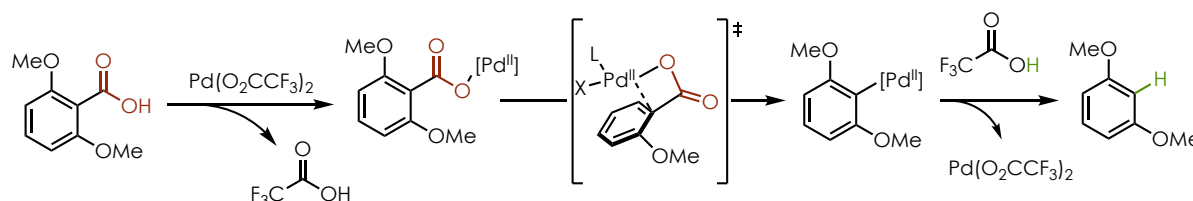


Figure 2.6: Mechanism proposed by Kozłowski et al for the palladium catalyzed hydrodecarboxylation of arenes.

proceed through the intermediacy of an acyloxy radical intermediate, but rather a concerted decarboxylative metalation transition state (**Figure 2.6**).⁴⁹

2.1.2.4 Decarboxylation via Photochemical Oxidation of Carboxylates

Single electron oxidation of a carboxylate was shown to be possible with ground state oxidants such as Ag(II) in the Minisci reaction (**Figure 2.7**).^{50,51} It is unclear whether oxidation of the carboxylate occurs through an inner sphere or outer sphere electron transfer, or in a concerted or step-wise decarboxylation, therefore a generalized mechanism is proposed in **Figure 2.7**. The Minisci reaction requires elevated temperatures and stoichiometric quantities of strong

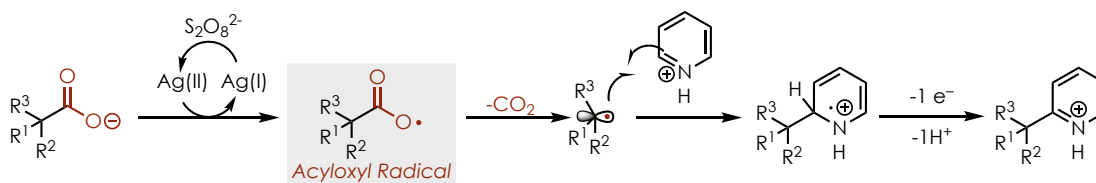


Figure 2.7: Mechanism of the Minisci Reaction.

oxidants such as persulfate in order to accomplish the reactivity. These conditions are useful for generating nucleophilic radicals that can add to radical acceptors such as pyridine. Due to the necessity for stoichiometric strong oxidants, a reductive decarboxylation would be difficult under these conditions, due to the oxidizable nature of most H-atom donors. Additionally, the use of harsh reaction conditions could limit functional group compatibility.

Recently there has been a resurgence of interest in decarboxylative processes involving direct oxidation of a carboxylate. Photooxidants have been found to be a superior alternative for reductive decarboxylation processes (hydrodecarboxylation). These methods accomplish

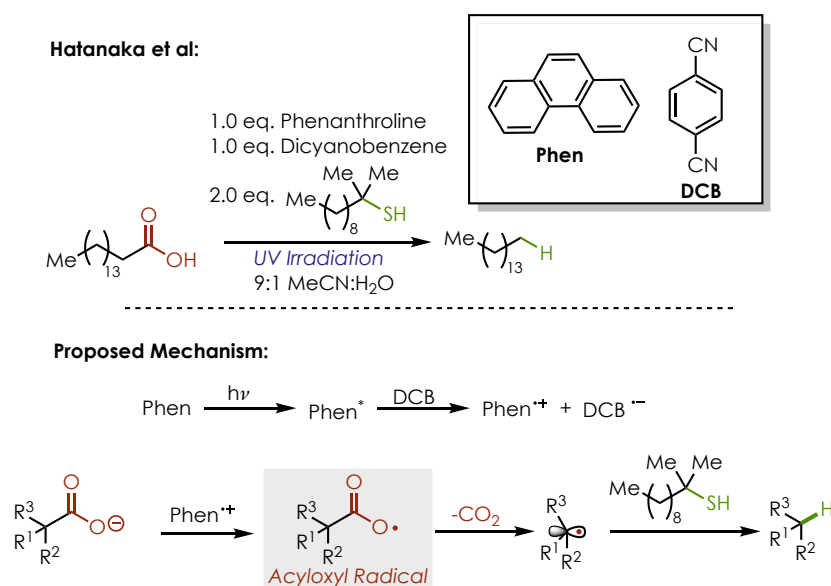


Figure 2.8: Decarboxylation protocol using photogenerated phen⁺• developed by Hatanaka and co-workers.

oxidation of carboxylates in a mild fashion, avoiding dimerization or over-oxidation which is problematic in uncontrolled radical formation processes (Miniski and Kolbe reactions). The use of stoichiometric photooxidants for hydrodecarboxylation is possible with both quinones⁵² and a dicyanobenzene/phenanthrene electron relay system.⁵³ However, poor yields are observed unless stoichiometric amounts of both photooxidant and H-atom donor are used.

The Hatanaka decarboxylation protocol (**Figure 2.8**) demonstrates that a photo-generated oxidant could be used to accomplish a hydrodecarboxylation. Excitation of phenanthrene (phen) with ultraviolet (UV) light produces a powerful photoreductant ($E_{1/2}^{ox} = -2.36$ V vs SCE, S_1 state)^{54,55} which can undergo an electron transfer (ET) with dicyanobenzene (DCB, $E_{1/2}^{red} = -1.46$ V vs SCE)⁵⁶ to produce the active oxidant phen⁺, along with DCB^{•-}. After deprotonation of the carboxylic acid starting material, phen⁺ ($E_{1/2}^{red} = +1.50$ V vs SCE)^{53,54ii} can undergo favorable ET with the carboxylate ion ($E_{p/2}^{ox} \sim +1.16$ V vs SCE)⁵⁷ⁱⁱⁱ forming an acyloxy radical intermediate and reforming phenanthrene. This electron transfer is thermodynamically favored, having a $\Delta G^\circ = -7.8$ kcal \cdot mol⁻¹. Upon formation of the acyloxy radical, loss of CO₂ occurs forming a more stabilized carbon-centered radical. This radical can then be trapped with the thiol H-atom donor to afford the reduced product. This protocol was shown to be relatively broad in nature; allowing for the hydrodecarboxylation of protected amino acid derivatives, as well as aliphatic carboxylic acids such as deoxycholic acid, a naturally occurring steroid. Due to the use of stoichiometric reagents to accomplish this methodology suffers from poor atom economy (vide infra, see 2.1.4); the use of UV light also limits the applicability of this method toward sensitive substrates and raises additional safety concerns.

Photochemical oxidation of carboxylates has become a very intense area of research in recent years. Coupling reactions, including addition to arenes,^{58–60} alkenes,^{61–64} and fluorinations,^{65–67} pioneered primarily by the MacMillan lab have been accomplished. These systems ultimately operated similarly to the system developed by our lab. Importantly, these coupling reactions utilize catalytic quantities of photooxidant. Additionally, Wallentin and

ⁱⁱ The oxidation potential of phenanthrene differs in the literature by as much as +270 mV vs SCE.

ⁱⁱⁱ The oxidation potential of carboxylate ions slightly depend on the substitution.

coworkers have disclosed a photoredox method for hydrodecarboxylation of amino acid derivatives as well as phenyl acetic acid derivatives.⁶⁸ This system was similar to the one concomitantly discovered to the system that will be discussed below.

2.1.2.5 Decarboxylation of malonates

Krapcho and coworkers developed conditions for the monodecarboxylation of malonates.⁶⁹ The original conditions reported by Krapcho called for the use of cyanide to carry out the dealkylation of a malonate ester. These conditions have been modified significantly in recent applications, such that simple salts such as sodium chloride can be used instead of highly toxic cyanide (**Figure 2.9**).⁷⁰ This type of decarboxylation is specific to malonates or other carboxylic esters bearing a pendant electron acceptor group such as a nitrile or carbonyl. Mechanistically this

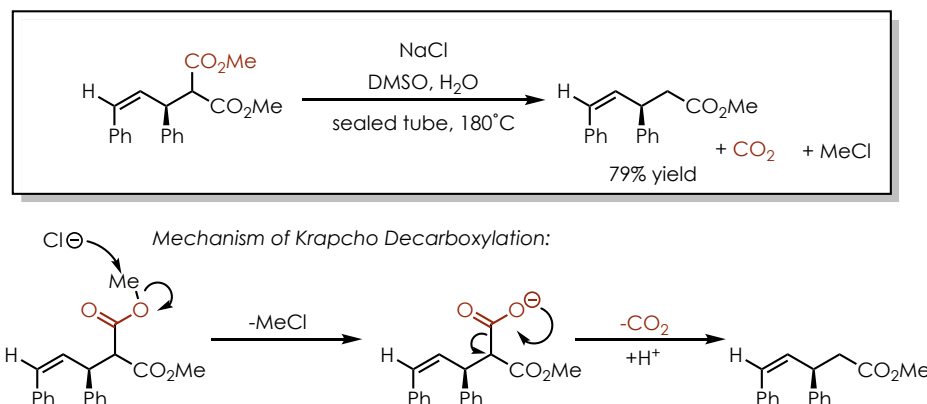


Figure 2.9: Reaction conditions for a typical Krapcho decarboxylation and mechanism.

type of decarboxylation is distinct from the radical hydrodecarboxylation reactions discussed above. Under very high reaction temperatures, a nucleophile such as chloride can undergo S_N2 attack on a methyl or ester, resulting in an unstable carboxylate intermediate (although it is not clear if this is a discrete intermediate or if decarboxylation occurs in a concerted fashion). The carboxylate intermediate rearranges to extrude CO₂ and results in an enolate which can presumably be protonated upon workup. This reaction while useful, requires harsh reaction conditions with

temperatures typically exceeding 160°C. Additionally, this reaction is not amendable to a second decarboxylation which would furnish the alkane product.

2.1.3 Rate of Decarboxylation of Acyloxy Radicals

Studies were undertaken by Pincock and co-workers to demonstrate that alkyl substituted acyloxy radicals decarboxylate with 1st order rate constants (k_{CO_2}) between $1.3 - 11 \times 10^9 s^{-1}$ (Figure 2.10).⁷¹ It is important to note that k_{CO_2} can be highly variable depending on substitution, with aryl substituted acyloxy radicals losing CO₂ on the order of $10^8 s^{-1}$.⁷² Some alkyl substituted

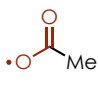
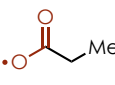
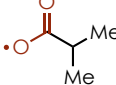
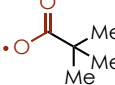
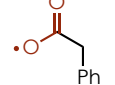
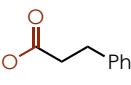
						
k_{CO_2}	$1.3 \times 10^9 s^{-1}$	$2.0 \times 10^9 s^{-1}$	$6.5 \times 10^9 s^{-1}$	$11 \times 10^9 s^{-1}$	$5.0 \times 10^9 s^{-1}$	$2.3 \times 10^9 s^{-1}$
Lifetime	770 ps	500 ps	150 ps	90 ps	200 ps	435 ps

Figure 2.10: Values for k_{CO_2} determined by Pincock and coworkers

acyloxy radicals were measured by Ryzhkov and co-workers to have k_{CO_2} values estimated to be on the order of $10^{12} s^{-1}$,⁷² approaching the limit for a barrierless monomolecular rate constant ($6.21 \times 10^{12} s^{-1}$).^{iv} Rate constants are generally consistent with the degree of the resulting radical stabilization; the formation of very unstable radicals results in significantly smaller k_{CO_2} although there are some anomalies which have much larger than expected rate constants. While there are some discrepancies in the lifetime of such unstable radicals, it has been generally agreed upon that they are very short lived intermediates, decomposing on orders approaching or faster than the diffusion limit.

^{iv} Calculated from the Eyring Equation: $k = \frac{\kappa k_B T}{h} e^{\frac{\Delta G^\ddagger}{RT}}$, where $\Delta G^\ddagger = 0$ for a barrierless reaction at 298.15 K.

These values were determined through the photoexcitation of corresponding naphthyl esters which have been shown to undergo homolytic cleavage (**Figure 2.11**).⁷³ Upon cleavage the radical intermediates could participate in two competing pathways. Decarboxylation from the acyloxy radical intermediate, leads to radical-radical recombination to form product **2** (**Figure 2.11**). Alternatively, the caged radical pair could undergo an electron transfer event, forming a carboxylate and benzylic cation. This could subsequently be trapped with the methanol solvent to form products **3** and **4** (**Figure 2.11**) Variation in the ester fragment, while holding the naphthyl fragment constant, was expected to produce change in the rate of decarboxylation (k_{CO_2}) but not for the rate of electron transfer (k_{ET}). Using the known value of k_{ET} for this process ($k_{ET} =$

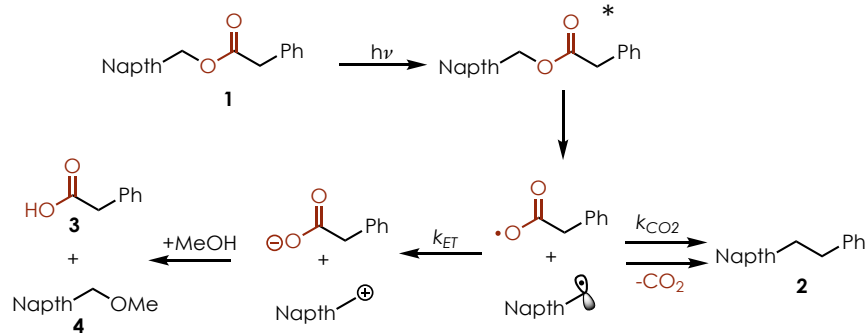


Figure 2.11: Reaction pathways for decomposition of 1-Naphthylmethyl alkanoates

$2.6 \times 10^{10} s^{-1}$),^{74,75} allowed for the determination of k_{CO_2} by studying product distributions. This work also demonstrates that ET between two caged radicals can be competitive with decarboxylation of an acyloxy radical, as product ratios were generally found to favor the electron transfer products (**3** and **4**, **Figure 2.11**). The implication for this on the hydrodecarboxylation developed by our lab will be discussed further in Section 2.4.4.3.

2.1.4 Atom Economy and Efficiency Comparisons between Hydrodecarboxylation Methodologies

Atom economy (**AE**) is an important metric for determining the efficiency of a chemical reaction. It is defined simply as: $\% \text{ Atom Economy} = \frac{\text{molecular mass of desired products}}{\text{molecular mass of all reactants}} \times 100\%$.^{76,77} Catalytic reagents are generally not included when determining % atom economy. Achieving high atom economy can reduce cost and the amount of waste generated by a chemical process. In order to get a better picture of the efficiency and “green-ness” of a reaction, Reaction Mass Efficiency (**RME**) can be used as a metric for the efficiency of a reaction. RME describes not only the atom economy but also the chemical yield and stoichiometry of all reagents used. It is defined as: $\text{RME} = \frac{\text{mass of product}}{\text{mass of all starting materials}}$.⁷⁷ While there are other measures, such as E-factor, which describe the total waste of a process, atom economy and reaction mass efficiency will be used as to compare hydrodecarboxylation methodologies as they represent unoptimized processes, and purification methods would likely be similar between substrates in most cases.

Hydrodecarboxylation processes have historically had very low atom economy because of the reduction of molecular weight compared to the starting materials, and the use of stoichiometric reagents to activate the carboxylate and deliver a single hydrogen-atom. Therefore, the development of a catalytic hydrodecarboxylation process would be very advantageous from an atom economy standpoint; particularly if no pre-activation of the substrate is required. An ideal hydrodecarboxylation could utilize an H-atom from the carboxylic substrate in order to form the reduced product and generate only CO₂ as a stoichiometric waste product.

Table 2.1: Comparison of Atom Economy (AE) and Reaction Mass Efficiency (RME) between hydrodecarboxylation methodologies

Method	Substrate	MW (g/mol)	% Yield	% AE ^v	RME ^{vi}	Reaction time
Barton ¹⁵	Stearic Acid	284.48	90%	35% (29%)	0.17 (0.14)	-
Barton ¹⁵	Cholic Acid ^{vii}	432.67	72%	47% (39%)	0.20 (0.18)	-
Hatanaka ⁵³	Palmitic Acid	256.43	82%	28%	0.22	6 h
Hatanaka ⁵³	Deoxycholic Acid	392.58	76%	46%	0.28	6 h
Baran ²⁷	Enoxolone	470.68	81%	54% (46%)	0.39 (0.33)	1 h
Baran ²⁷	Cholic Acid	408.58	45%	50% (42%)	0.20 (0.17)	1 h
Nicewicz ⁷⁸	Tridecanoic acid	214.35	49%	79%	0.29	48 h
Nicewicz ⁷⁸	Enoxolone	470.68	95%	91%	0.75	24 h

Table 2.1 shows a comparison of % AE and RME for a number of hydrodecarboxylation methodologies. Since larger substrates will inherently have larger maximum % AE and RME, two substrates were included for each methodology. Fatty acids and terpenoid substrates (typically steroidal) were a commonality between several hydrodecarboxylation methods, therefore they were used as a benchmark for comparison.^{viii} Due to the use of only catalytic reagents, the

^v First number indicates %AE for only the hydrodecarboxylation step, while in parentheses is indicated the combined %AE for the formation of the activated esters and hydrodecarboxylation steps.

^{vi} First number indicates RME for only the hydrodecarboxylation step, while in parentheses is indicated the combined RME for the formation of the activated esters and hydrodecarboxylation steps. Since yields were not available in all cases for the activation steps, RME was calculated assuming quantitative conversion from the corresponding carboxylic acid starting materials.

^{vii} Acetylated derivative of cholic acid.

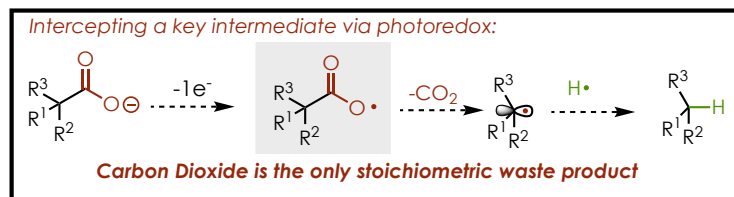
^{viii} Since the substrate scopes for each hydrodecarboxylation method were significantly different, substrates were chosen to show similar substrate types, including direct comparisons where applicable.

hydrodecarboxylation methodology developed by this lab (Nicewicz, **Table 2.1**) displays the highest possible atom economy for a hydrodecarboxylation (substrates have different % AE due to the differences in MW). Other methodologies rely on either a previous activation of the carboxylic acid (Barton and Baran, **Table 2.1**) or require several stoichiometric reagents (Hatanaka, **Table 2.1**). This drastically detracts from achieving high atom economy; atom economy; <50% was observed for all other methods and substrates.

Since generally high yields were achieved for other decarboxylation processes, RME was also used to compare efficiency of hydrodecarboxylation methods. Due to the particularly low yield for the decarboxylation of tridecanoic acid, a lower than average RME was determined, however this still compares favorably to other hydrodecarboxylation methods among fatty acid substrates. A high RME was found for the decarboxylation of naturally occurring steroid enoxolone, which was superior to RME for other hydrodecarboxylation methodologies among steroidal substrates. A direct comparison (enoxolone) could be made with Baran protocol which utilizes activated esters rather than decarboxylation directly from the carboxylic acid. Reaction time is another metric of efficiency that should be considered. Although the hydrodecarboxylation method developed by our lab compares favorably with respect to %AE and RME, reaction times for this reaction were observed to be much longer than other strategies (reasons for this will be discussed below, in Section 2.4.3.2).

2.2 Developing a Catalytic Photoredox Method for Hydrodecarboxylation

Having examined the previous body of literature regarding hydrodecarboxylation, we determined that a catalytic hydrodecarboxylation directly from the carboxylic acid would be useful to the chemical community. The Nicewicz lab has established a research program based on single electron oxidation reaction pathways, in order to facilitate unique reactivity such as anti-



Scheme 2.1: Ideal scenario for reduction of a carboxylic acid to an alkane

Markovnikov hydrofunctionalization of alkenes,^{79–87} and C-H^{88–90} and C-O⁹¹ functionalization of electron rich arenes. Taking inspiration from the works of Kolbe^{10,11} and Hatanaka⁵³ it seemed that it would be possible to extend a single electron oxidation strategy in order to accomplish hydrodecarboxylation, via the intermediacy of an acyloxy radical. Inspiration from the Barton decarboxylation^{15,17} as well as our own work, suggested that an H-atom donor such as thiophenol could be used to trap the resulting carbon-centered radical intermediate. An ideal hydrodecarboxylation would limit the production of stoichiometric waste to carbon dioxide (**Scheme 2.1**). If a strategy for hydrodecarboxylation could be developed, a stepwise double decarboxylation of malonic acid derivatives to give the corresponding alkanes could also be feasible under the same conditions. Although there are methods for decarboxylating malonates and malonic acid derivatives (see 2.1.2.5), there were no methods for removing both carboxylic acid moieties in a one pot procedure.

Carboxylic acids have been used in other contexts in the Nicewicz lab,^{79,81,84,87,92} indicating that the acid itself is not competitively oxidizable with various other functional groups. At the

onset of the project the oxidation potentials of carboxylic acids were determined to be higher than the solvent window for acetonitrile ($E_{p/2}^{\text{ox}} > 2.5\text{ V vs SCE}$), as opposed to their corresponding tetrabutylammonium carboxylates which were found to have oxidation potentials in the range of

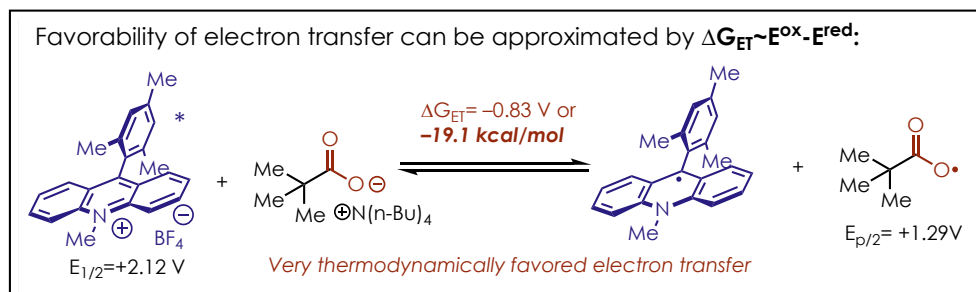


Figure 2.12: Thermodynamic favorability of electron transfer between excited state acridinium and carboxylate salts.

+1.3 V vs SCE. Mesityl acridinium catalysts have been shown to have excited state reduction potentials of above +2.0 V vs SCE,^{93,94} therefore the single electron oxidation of a carboxylate should be considerably thermodynamically favorable (**Figure 2.12**). Since it is apparent that carboxylates are the species capable of undergoing oxidation, not the carboxylic acids, solvent and base selection was hypothesized to be a major factor in determining the success of this strategy.

In order to get efficient reactivity an appropriate H-atom donor would need to be selected. The Nicewicz lab has shown that thiophenol (PhSH) is a superior H-atom donor to other H-atom donors with similar bond dissociation energies (BDE), indicating that PhSH has several important properties (Figure 2.13). Firstly, the BDE of PhSH is sufficiently low to allow for thermodynamically favored H-atom transfer.⁹⁵ Importantly for this work, PhSH has a pK_a of 6.62

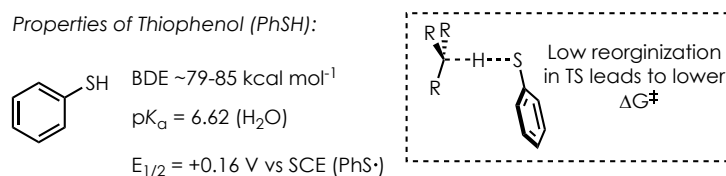


Figure 2.13: Important properties of thiophenol.

in water⁹⁶ indicating that the conjugate base, thiophenolate, could deprotonate an equivalent of carboxylic acid (acetic acid $pK_a = 4.76$ in H_2O)⁹⁶ starting material and reform the active H-atom donor. Phenylthiyl radical has been found to have relatively high reduction potentials ($E_{1/2}^{red} \text{ PhS} \bullet = +0.16 \text{ V vs SCE}$),⁹⁷ indicating that they can undergo efficient electron transfer with the reduced acridinium ($E_{1/2}^{ox} = \text{Mes-Acr-Me} \bullet -0.55 \text{ V vs SCE}$). A computational comparison of phenylmalononitrile, another potential H-atom donor, and PhSH shows that the reaction of a benzylic radical with PhSH has the lower barrier to the transition state (TS) for H-atom transfer. This indicates that PhSH has a relatively low amount of structural reorganization in the TS. This is reflected by the drastic increase in reaction rates compared with phenylmalononitrile which has a similar BDE.⁹⁴

2.2.1 Initial Optimization of an Activated Carboxylic Acid Substrate

Optimization began with an activated substrate, containing aryl groups alpha to the carboxylic acid group, which should stabilize the radical resulting from decarboxylation. At 5 mol% loading of the acridinium photooxidant (Mes-Acr-Me⁺), 20 mol% of thiophenol as a hydrogen atom donor, and 10 mol% of 2,6-lutidine as a base, a 46% ¹H NMR yield of the decarboxylated product was obtained (**Table 2.2, Entry 1**). The yield was increased to 72% after another 24 h, indicating that the catalysts were still active, albeit providing very slow reactivity (**Table 2.2, Entry 2**). Increasing the loading of base to 50 mol% provided quantitative conversion to the product after 24 h (**Table 2.2, Entry 3**), while using 1 equivalent hampered reactivity (**Table 2.2, Entry 4**). Increased base loading increases the concentration of carboxylate in solution, which leads to an increase in reaction rate. Although quantitative yield could be obtained under these

conditions, further optimization was carried out in order to reduce thiophenol loadings, with as little as 5 mol% giving

Table 2.2: Optimization of Hydrodecarboxylation conditions (2,2-diphenyldecanoic acid)^{ix}.

<div style="display: flex; align-items: center; justify-content: space-around;"> <div style="text-align: center;"> <p>5 mol% Mes-Acr-Me+ conditions [0.5 M], CHCl₃ 455 nm LEDs ambient temperature</p> </div> <div style="text-align: center;"> <p>Mes-Acr-Me+</p> </div> </div>				
Entry	H-atom donor	Base	Time	Yield
1	 20 mol% (PhSH)	 10 mol% (2,6-Lutidine)	24 h	49%
2	20 mol% PhSH	10 mol% 2,6-Lutidine	48 h	72%
3	20 mol% PhSH	50 mol% 2,6-Lutidine	24 h	quant.
4	20 mol% PhSH	1 equiv. 2,6-Lutidine	24 h	47%
5	10 mol% PhSH	50 mol% 2,6-Lutidine	24 h	quant
6	5 mol% PhSH	50 mol% 2,6-Lutidine	24 h	97%
7	none	50 mol% 2,6-Lutidine	24 h	7%
8	5 mol% PhSH	50 mol% 2,6-Lutidine	4 h	46%
9	5 mol% PhSH	50 mol% 2,6-Lutidine	8 h	75%
10	5 mol% PhSH	50 mol% 2,6-Lutidine	12 h	91%

^{ix} Conditions in bold are highlighted to show change in reaction conditions from previous entries in the table. Reactions carried out on a 0.5 mmol scale in N₂-sparged solvents [0.5M] at ambient temperature. Yields determined by ¹H NMR analysis of crude reactions.

nearly quantitative yields after 24 h (**Table 2.2, Entry 6**). Thiophenol was found to be necessary to achieve acceptable reactivity with only a small amount of the alkane product formed in its absence; this could have occurred through abstraction of a hydrogen-atom from solvent (**Table 2.2 Entry 7**). At this point reaction times could be lowered to 12 hours without much deleterious effect on reactivity (**Table 2.2, Entry 10**).

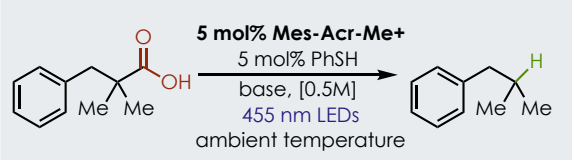
2.2.2 Continuing Optimization: Extension to Tertiary Alkyl Substituted Carboxylic Acids

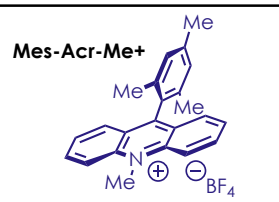
When the less activated 1,1-dimethylpropanoic acid was exposed to these reaction conditions, only a minimal amount of decarboxylated product was observed (the remaining mass balance was unreacted carboxylic acid substrate), even after extended reaction times (**Table 2.3, Entry 1**). Due to the hypothesis that ionization of the carboxylic acid would be of crucial importance, both solvent and base were screened because both were hypothesized to have an effect on carboxylate ion concentration in solution. Screening more polar solvents such as MeCN initially had a very minimal effect (**Table 2.3, Entry 2**). However, altering the base to sodium bicarbonate increased the yield slightly when using MeCN as solvent (**Table 2.3, Entry 3**), and significantly when using a 9:1 MeCN:H₂O mixture (**Table 2.3, Entry 4**).

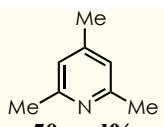
Since it was obvious more polar solvent conditions were beneficial for the reactivity, both MeOH and a 9:1 MeOH:H₂O mixture were screened as solvents, increasing the yield of decarboxylated product to nearly 70% in the latter case (**Table 2.3, Entry 6**). This indicates that increasing the equilibrium concentration of carboxylate relative to the carboxylic acid was important. The p*K*_a of carboxylic acids can be up to five units greater in methanol than in water (the p*K*_a of AcOH in H₂O is 4.76 vs 9.63 in MeOH), while the p*K*_a of protonated amines are similar in both solvents (triethylammonium is 10.75 in water and 10.78 in methanol).⁹⁸

Ionization of the carboxylate seemed to have the greatest effect on reactivity, therefore 15-crown-5 ether was added as an additive in an attempt to increase the extent of ionization of the carboxylate ion but led to a decrease in yield (**Table 2.3, Entry 8**). However, when using a

Table 2.3: Optimization of Hydrodecarboxylation conditions (1,1-dimethylpropanoic acid)^x.





Entry	Base	Solvent	Additive	Time	Yield
1	50 mol% (2,6-Lutidine)	CHCl ₃	none	48 h	5%
2	50 mol% 2,6-Lutidine	MeCN	none	48 h	7%
3	1 equiv. NaHCO₃	MeCN	none	48 h	14%
4	1 equiv. NaHCO ₃	9:1 MeCN:H₂O	none	48 h	30%
5	1 equiv. NaHCO ₃	MeOH	none	48 h	43%
6	1 equiv. NaHCO ₃	9:1 MeOH:H₂O	none	48 h	69%
7 ^{xi}	1 equiv. NaHCO ₃	9:1 MeOH:H ₂ O	10 mol% 15-crown-5	48 h	55%
8 ^{ix}	1 equiv. NaHCO ₃	9:1 MeOH:H ₂ O	10 mol% TBA BF₄	48 h	90%
9 ^{ix}	50 mol% (2,6-Lutidine)	9:1 MeOH:H ₂ O	none	48 h	70%
10 ^{ix}	 50 mol% (2,4,6-Collidine)	9:1 MeOH:H ₂ O	none	48 h	94%

^x Conditions in bold are highlighted to show change in reaction conditions from previous entries in the table. Reactions carried out on 0.3-0.5 mmol scale in N₂-sparged solvents at ambient temperature. Yields determined by ¹H NMR or GC/MS analysis of crude reactions.

^{xi} Reactions were carried out using Xylyl-Acr-Me⁺

catalytic quantity of tetrabutylammonium tetrafluoroborate (**TBA BF₄**), a major improvement in yield was observed (**Table 2.3, Entry 8**). It is likely that **TBA BF₄** is acting as phase transfer agent in order to increase the solubility of partially insoluble NaHCO₃. A rescreening of bases in the optimized solvent conditions showed 2,6-Lutidine ($pK_a = 6.75$ in H₂O)⁹⁹ behaved comparatively to NaHCO₃, but that the use of the more basic 2,4,6-trimethylpyridine (collidine, $pK_a = 7.4$ in H₂O)⁹⁹ gave good yields of decarboxylated product (**Table 2.3, Entry 10**).

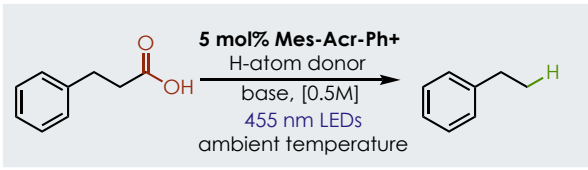
2.2.3 Continuing Optimization: Extension to Primary Alkyl Substituted Carboxylic Acids

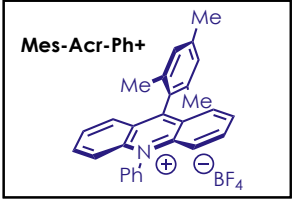
When these conditions were applied to the less stabilized, primary alkyl substituted hydrocinnamic acid, less than 4% of the desired product was obtained even after 72 hours of irradiation time (**Table 2.4, Entry 1**). Screening of various thiols, bases, and acridinium photocatalysts afforded very little increases in the efficiency of the reaction, although increasing the thiol loading to 20 mol% was found to be somewhat beneficial. We ultimately found it operationally more simple to use diphenyl disulfide (Ph₂S₂) in place of PhSH, with no apparent change in reactivity when using the same loading (same loading with respect to the active H-atom donor). Ph₂S₂ is a solid and did not require careful handling required by PhSH due to its disagreeable odor. Ph₂S₂ has been demonstrated to undergo homolysis under irradiation with 455 nm light, to form thiyl radicals⁹⁴ (This will be discussed further in Section 2.4.1). Appreciable gains in yield were not observed until other polar alcohol solvents were screened.

Members of our lab had found success using trifluoroethanol (TFE) as a cosolvent¹⁰⁰; we found that using TFE as the solvent increased the yields to around 40% after 48 hours and 69% after 72 h (**Table 2.4, Entry 2**) when using 2,4,6-collidine. This indicated that the reaction was proceeding at a somewhat constant, but very slow rate which is not typical for most reactions

because the amount of starting material decreasing over time generally decreases the rate of reaction (This will be discussed further in Section 2.4.3.2). This could be improved to nearly complete conversion by using *i*-Pr₂NEt; 20 mol% loading was found to be optimal (**Table 2.4, Entry 3**). Oxidizable amine bases are known to form aminium radical cations in similar

Table 2.4: Optimization of Hydrodecarboxylation conditions (3-phenylpropanoic acid)^{xii}.





Entry	H-atom donor	Base	Solvent	Additive	Time	Yield
1	5 mol% (PhSH)	1 equiv. NaHCO ₃	9:1 MeOH:H ₂ O	10 mol% TBA BF ₄	72 h	4%
2	10 mol% Ph ₂ S ₂	50 mol% 2,4,6-Collidine	CF₃CH₂OH	none	72 h	69%
3	10 mol% Ph ₂ S ₂	20 mol% (<i>i</i>-Pr₂NEt)	CF ₃ CH ₂ OH	none	72 h	95%
4	10 mol% Ph ₂ S ₂	20 mol% (<i>i</i> -Pr ₂ NEt)	9:1 MeOH:H₂O	none	72 h	14%
5	10 mol% Ph ₂ S ₂	20 mol% (<i>i</i> -Pr ₂ NEt)	CF ₃ CH ₂ OH	none	24 h	85%
6	none	20 mol% (<i>i</i> -Pr ₂ NEt)	CF ₃ CH ₂ OH	none	72 h	6%

photoredox systems^{101,102}; this indicates that *i*-Pr₂NEt is mostly protonated in solution, effectively insulating them from being oxidized.

When *i*-Pr₂NEt was used as base in 9:1 MeOH:H₂O, only 14% yield was obtained (**Table 2.4, Entry 4**) indicating that the major increase in conversion originates from the use of TFE as

^{xii} Conditions in bold are highlighted to show change in reaction conditions from previous entries in the table. Reactions carried out on a 0.3-0.5 mmol scale in N₂-sparged solvents at ambient temperature. Yields determined by ¹H NMR or GC/MS analysis of crude reactions.

solvent. The use of TFE as solvent also allowed for a drastic decrease in reaction rate, while still maintaining good yields (**Table 2.4, Entry 5**). Control experiments were carried out to show that Ph_2S_2 was necessary for reactivity, since it seemed feasible that TFE could act as a competent H-atom donor (this will be discussed further below in Section 2.4.2.1), however even after 72 h only a very low conversion to product was observed (**Table 2.4, Entry 6**).

2.2.4 Summary of Optimization

Figure 2.14 summarizes the conditions required for each substrate class. In general, activated substrates such as phenyl acetic acid derivatives could be efficiently reduced to the corresponding alkane product in a variety of solvent conditions, using weaker pyridine bases. Increasing alkyl substitution at the α -position led to greater reactivity in relatively non-polar solvents like CHCl_3 . Tertiary alkyl acids could be efficiently decarboxylated in very polar solvent mixtures like 9:1 $\text{MeOH}:\text{H}_2\text{O}$, while still using relatively weak bases.

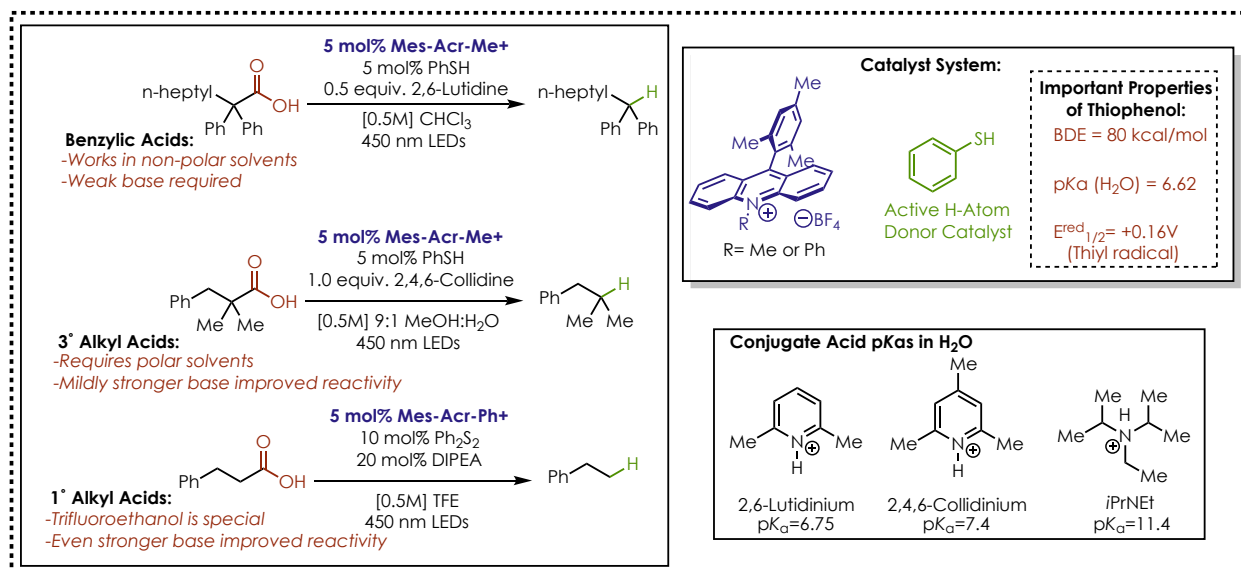


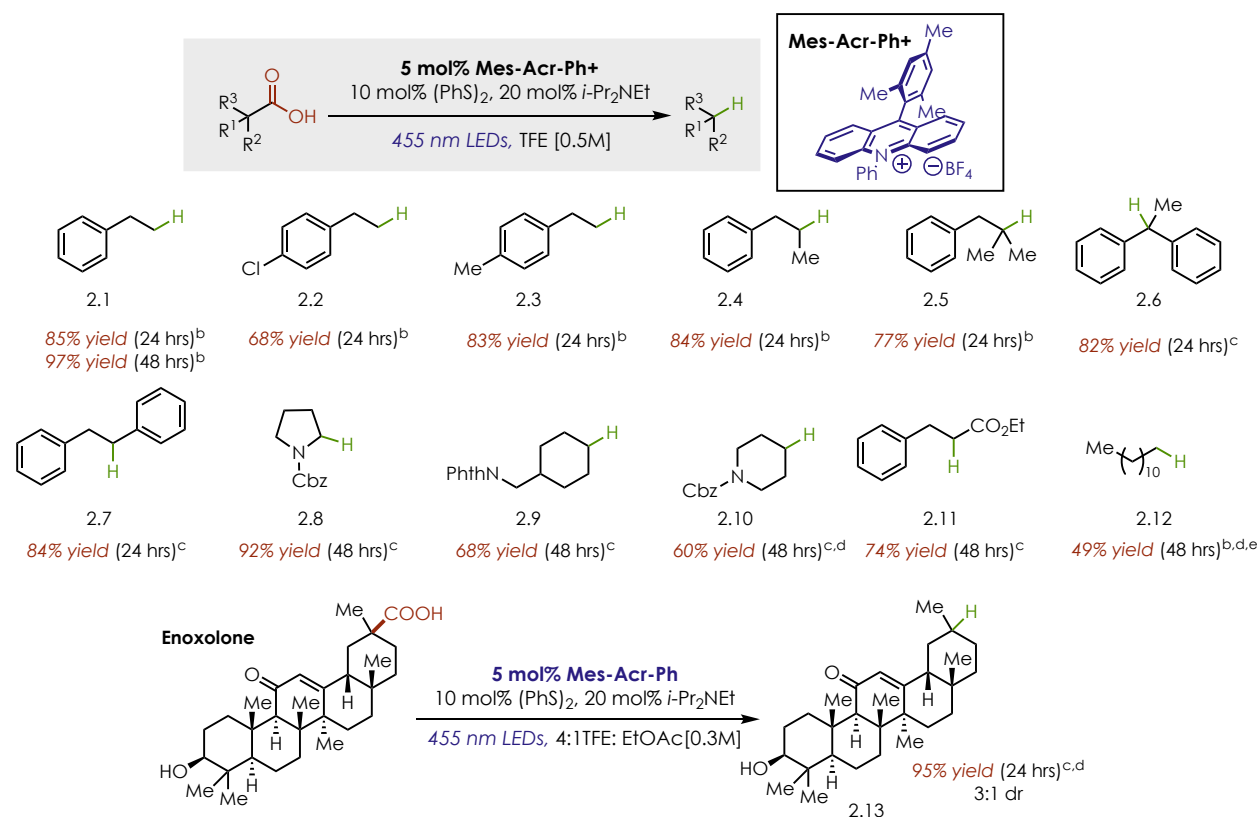
Figure 2.14: Comparison of the solvent and base requirements for benzylic, 3° alkyl, and 1° alkyl carboxylic acid substrates. The catalyst system proved to be generally effective across all substrate classes.

However, primary alkyl substrates uniquely were unreactive to a large degree in all solvent mixtures other than trifluoroethanol. Reactivity was improved for primary substituted acids using relatively strong bases such as Hünig's base. Mes-Acr-Ph⁺ was found to be more stable under a variety of reaction conditions than Mes-Acr-Me⁺ and was used in all cases. Lastly, although a variety of thiol and other potential hydrogen atom donors were screened thiophenol (or Ph₂S₂) was found to be the superior H-atom donor catalyst.

2.2.5 Exploring the Scope of the Photoredox Hydrodecarboxylation

With these optimized conditions, we decided to explore the scope of this reaction (**Chart 2.1**) Primary (2.1-2.3), secondary (2.4), tertiary (2.5) alkyl substituted carboxylic acids were all competent substrates. Variation of substrate electronics was tolerated well. Potentially reactive C-H bonds were well tolerated (benzylic C-H bonds in substrate 2.3). However, electron rich arenes, such as p- methoxyhydrocinnamic acid, were not viable substrates presumably due to competitive oxidation of the aromatic ring with the carboxylate functional group.

Chart 2.1: Scope of Photoredox Mediated Hydrodecarboxylation.^a



^aReactions carried out in N₂-sparged TFE [0.5M]. ^bYields for volatile compounds were determined by GC. ^cAverage of two isolated yields on >100 mg scale. ^d[0.3M] in 4:1 TFE:EtOAc. ^e 20 mol% Ph₂S₂

Carboxylic acid substrates bearing one (2.7) or two (2.6) aryl groups in the α position were also competent substrates. Protected amino acids (2.8) and other protected amine-containing substrates (2.9 and 2.10) were also tolerated using this method. Substrates bearing α- esters (2.11) could be efficiently decarboxylated under these conditions as well. Fatty acid tridecanoic acid initially gave only trace amounts of dodecane (2.11). Tridecanoic acid was only sparingly soluble in TFE; therefore, an additional solvent screen was conducted, and revealed that using 4:1 TFE/EtOAc [0.3 M] improved the reactivity substantially. Increasing disulfide loading from 10 to 20 mol % was also found to be optimal for this substrate. Remarkably, the highly functionalized natural product Enoxolone underwent hydrodecarboxylation in good yield as a mixture of

diastereomers (3:1), albeit with an extended reaction time (96 h, 85%). The increased reaction time required for this substrate is most likely due to the limited solubility of the substrate in TFE, even at lower concentrations. However, with the use of ethyl acetate as a co-solvent, the reaction time could be reduced to 24 h, with an improved yield. Using ethyl acetate as a co-solvent also improved reactivity for substrate 2.10, which also exhibited low solubility in TFE.

Overall, reactivity was found to independent of the substitution of the α -position in trifluoroethanol, with the exception of substrates bearing sp^2 or sp hybridization at the α -position. Even though electron transfer should be favorable in all cases for carboxylates, the scope of the reaction could be limited due to difficulty in forming ion pairs with Mes-Acr-Ph⁺ (See Section 2.4.4.2), or a fast back electron transfer (BET) that becomes competitive with loss of CO₂ from the acyloxy radical (this will be discussed further in Section 2.4.4.3). The current decarboxylation protocol was found to be relatively functional group tolerant, although some very electron rich groups such as amines needed to be protected.

2.3 Application Towards Malonic Acid Derivatives

Due to the seemingly privileged status of malonates as carbon nucleophiles, the extension of this method to malonic acids was undertaken. In a process similar to the hydrodecarboxylation described above, malonic acid derivatives could potentially undergo mono- or double-decarboxylation. Thus, a robust method would need to be developed which could maintain catalyst integrity over the course of the reaction as the relative concentration of carboxylate is increased for malonic acids. pK_a differences between malonic acids and other carboxylic acids also needed to be considered. The first pK_a of malonic acid is 2.83, while the second pK_a is 5.69 (H₂O). Since

the pK_a was predicted to be much higher in non-water solvents, the second deprotonation could potentially require stronger base.

2.3.1 Developing Conditions for the Double Decarboxylation of Malonic Acid Derivatives

The conditions previously developed for mono-acid decarboxylation were not effective when applied to benzyl malonic acid, only giving about 21% yield of the corresponding monodecarboxylation product, with none of the doubly-decarboxylated product observed. Considering that hydrodecarboxylation of the related malonate monoester was much more efficient

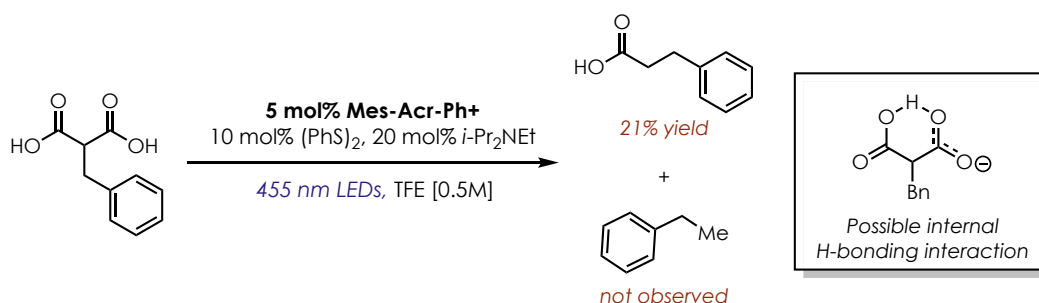
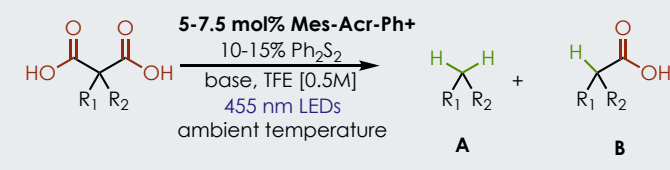
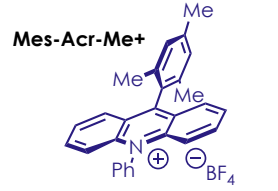


Figure 2.15: Application of Previously Developed Reaction Conditions with Malonic Acid Derivatives.

(See **Chart 2.1, 2.11**), it was reasonable that an internal hydrogen-bonding interaction could stabilize singly deprotonated malonic acids, and effectively shield them from oxidation (**Figure 2.15**). By raising the *i*-PrNEt loading to 1.0 equivalents and switching to a more reactive substrate (phenyl malonic acid) the doubly-decarboxylated product could be formed, with the remainder being starting material (**Table 2.5, Entry 1**). This could be improved further with an excess of *i*-PrNEt, to give 61% of toluene as the doubly-decarboxylated product, with the remaining mass balance made up of mono-decarboxylation product (**Table 2.5, Entry 2**). However, when attempting to apply these conditions to a less activated substrate, only mono-decarboxylation was observed in small quantities (**Table 2.5, Entry 3**). It seemed that the use of a stronger base could

be required, and when using 1.15 equivalents of potassium hydroxide as base, the corresponding doubly- decarboxylated product could be observed (**Table 2.5, Entry 4**).

Table 2.5: Optimization of Hydrodecarboxylation conditions for malonic acid derivatives^{xiii}

<div style="display: flex; align-items: center; justify-content: space-between;"> <div style="text-align: center;">  </div> <div style="text-align: center;">  </div> </div>					
Entry	R ₁	R ₂	Base	Time	Yield A/B
1	Ph	H	1 equiv. (<i>i</i> -Pr ₂ NEt)	48 h	45%/0%
2	Ph	H	1.2 equiv. (<i>i</i>-Pr₂NEt)	48 h	61%/39%
3	Bn	H	1.2 equiv. (<i>i</i> -Pr ₂ NEt)	72 h	0%/20%
4	Bn	H	1.15 equiv. KOH	72 h	8%/25%
5	Bn	Me	1.15 equiv. KOH	72 h	40%/60%
6 ^{xiv}	Bn	Me	1.15 equiv. KOH	72 h	55%/32%

Using a slightly more reactive substrate, appreciable yields of both mono and double-decarboxylation products were observed (**Table 2.5, Entry 5**), which could be improved when increasing the loading of both photocatalyst and Ph₂S₂ (**Table 2.5, Entry 6**). Ultimately, 1.0 equiv. of KO^{*t*}Bu was used instead of KOH, because it improved catalyst stability over long

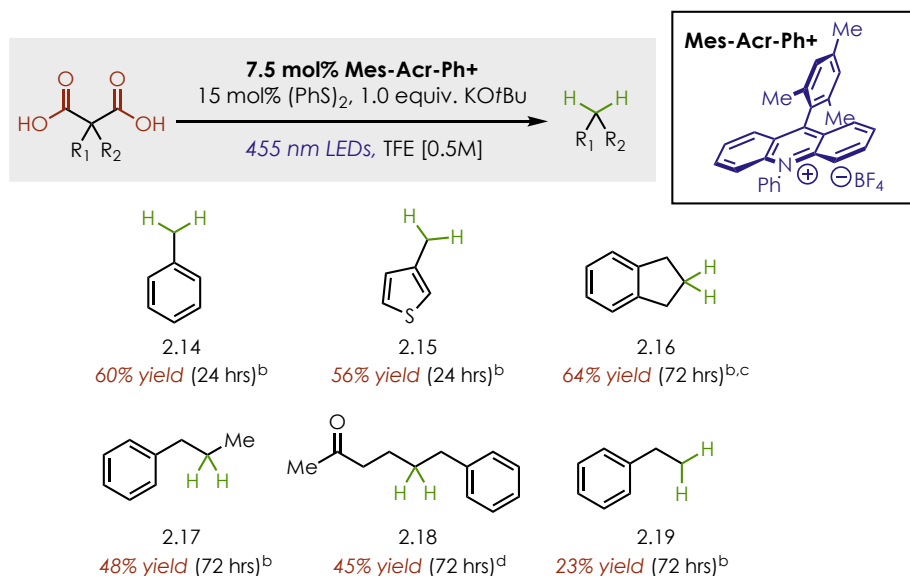
^{xiii} Conditions in bold are highlighted to show change in reaction conditions from previous entries in the table. Reactions carried out on a 0.3-0.5 mmol scale in N₂-sparged solvents at ambient temperature. Yields determined by ¹H NMR or GC/MS analysis of crude reactions.

^{xiv} Mes-Acr-Ph⁺ loading = 7.5 mol%; Ph₂S₂ loading = 15 mol%.

reaction times, and was easier to handle. Without the inclusion of photocatalyst no decarboxylated products were obtained, showing that thermal decomposition was not a viable mechanism.

2.3.2 Scope of Malonic Acid Hydrodecarboxylation

Chart 2.1: Scope of Photoredox Mediated Hydrodecarboxylation of Malonic Acid Derivatives^a



^aReactions carried out in N₂-sparged TFE [0.5M]. ^bYields for volatile compounds were determined by GC. ^cAverage of two isolated yields on >100 mg scale. ^dAverage of two isolated yields on >100 mg scale

Using the optimized conditions for malonic acid derivatives, we found that aryl substituted malonic acids underwent efficient hydrodecarboxylation, giving good yields after 24 hours. (**Chart 2.2, 2.14 and 2.15**). Dialkyl substituted malonic acids gave good yields, however very long reaction times were required to achieve acceptable yields (**Chart 2.2, 2.16-2.18**). Unfortunately, monoalkyl substituted substrates such as benzyl malonic acid gave poor yields even after extended reaction times (**Chart 2.2, 2.19**). Though yields for hydrodecarboxylation of malonic acids were generally lower, the remaining mass balance typically consisted of unreacted malonic acid and mono-decarboxylated products. This was encouraging because the unreacted carboxylic acids could hypothetically be re-subjected to the reaction conditions to improve the overall yield of the

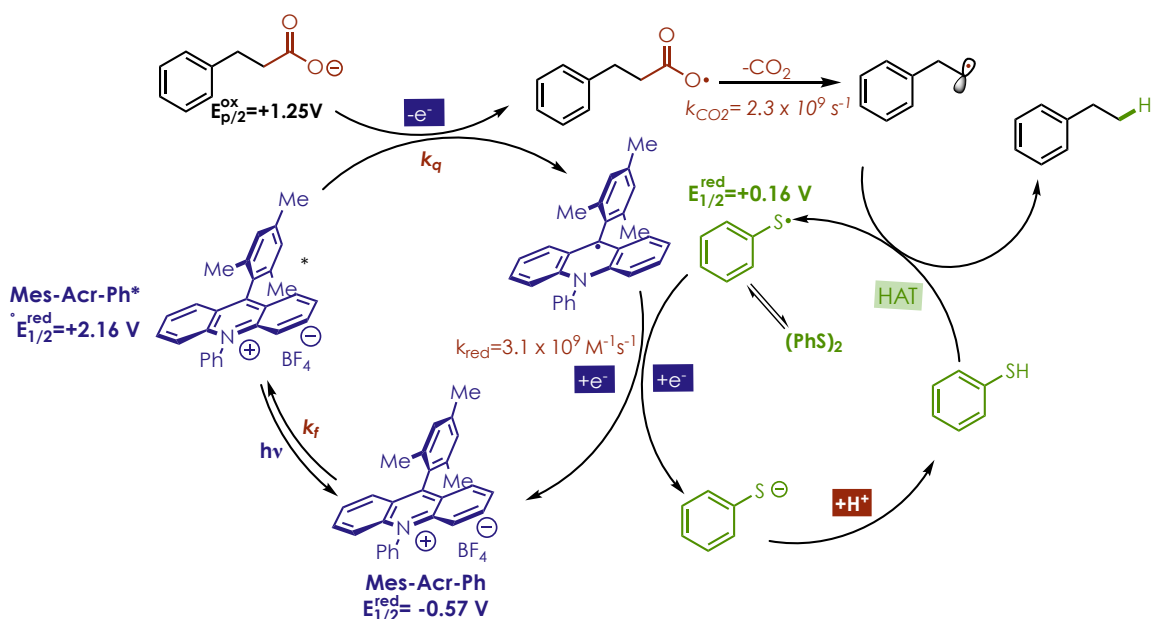
doubly decarboxylated products. The major obstacle seemed to be catalyst stability in the presence of strong bases such as KOH and KO^tBu.

2.4 Investigation of Hydrodecarboxylation Mechanism

2.4.1 Initial Mechanistic Proposal

Upon excitation with 450 nm light, Mes-Acr-Ph⁺ accesses a locally excited single state ($E_{1/2}^{\text{red}} = +2.16$ V vs SCE), which can undergo SET with the carboxylate forming an unstable acyloxy radical intermediate (**Scheme 2.2**). As mentioned above, Pincock and co-workers have measured rate constants for decomposition of these intermediates, typically on the order of 10^9 s⁻¹ for acids with sp³ hybridization at the α-position. Loss of CO₂ results in the formation of a carbon-centered radical which can subsequently be trapped with thiophenol to furnish the product. The thiyl radical formed subsequent to H-atom transfer can undergo reversible dimerization forming

Scheme 2.2: Mechanistic Proposal for Hydrodecarboxylation.



Ph₂S₂ which has been demonstrated to undergo rapid homolysis under irradiation with 455 nm LEDs. Thus, thiyl radical can enter the catalytic cycle either from H-atom transfer (from PhSH) or via homolysis of Ph₂S₂ without any perceivable effects on reactivity. The phenyl thiyl radical can also undergo SET with the reduced acridinium (Mes-Acr-Ph•). The bimolecular rate constants for this electron transfer have been determined by laser flash photolysis of Ph₂S₂ in the presence of an acridine radical ($\Delta G_{ET}^\circ = -16.4 \text{ kcal mol}^{-1}$). The thiolate, formed after thiyl radical reduction, could then deprotonate another equivalent of carboxylic acid regenerating the active H-atom donor, and thus the ultimate source of hydrogen atom incorporated in the product would come from the carboxylic acid starting material in an atom economical process.

2.4.2 The Role of Trifluoroethanol

Trifluoroethanol proved to uniquely provide large improvements in reactivity, however upon analysis of the proposed mechanism it was not immediately clear why this should be the case. Until TFE was identified as the superior solvent for this reaction, most positive improvements in reactivity were associated with increasing solvent polarity or strength of the base used. However, the improvement imparted by TFE could not be solely explained by polarity, as 9:1 MeOH:H₂O is the more polar solvent as evidenced by the dielectric constants of the two solvents ($\epsilon_{TFE} = 27.1 \text{ F/m}$; $\epsilon_{9:1 \text{ MeOH:H}_2\text{O}} = 36.8 \text{ F/m}$).^{103,104} Therefore, several studies were undertaken to uncover the origin of this unique solvent.

2.4.2.1 Is Trifluoroethanol a Hydrogen-atom Donor?

Due to the potentially weak C-H bonds, the potential for TFE to act as a H-atom donor was initially considered. This has been proposed as a potential role for alcohol solvents by our lab and

others, in radical based chemistry.¹⁰⁰ The BDE for TFE has been previously calculated to be 95 and 111 kcal/mol for the C–H and O–H bonds respectively.¹⁰⁵ Methanol has a similar C–H BDE of about 93 kcal/mol.¹⁰⁶ Thus, it seemed possible that alkyl radicals produced after loss of CO₂ could abstract C–H bond from TFE, but it was not clear why TFE would provide an advantage over MeOH since the BDE for the two solvents are very similar. Both of the solvents have much higher BDEs than thiophenol, however it seemed possible that TFE could trap the alkyl radical initially due to the relatively high concentration and then the resulting TFE radical could be trapped producing product. When no PhSH or Ph₂S₂ was added only trace amounts of product were detected by GC/MS even after 72 hours. This could indicate that TFE is not a H-atom donor in this system, but could also be interpreted to mean that the TFE radical is incapable of turning over the photocatalyst.

In order to determine if TFE could be acting as an intermediary H-atom donor, the hydrodecarboxylation of 2,2-dimethyl-3-phenylpropanoic acid was carried out in 2,2,2-trifluoroethanol-*d*₂ (*d*₂-TFE) and 2,2,2-trifluoroethanol-*d*₁ (*d*₁-TFE) (Figure 2.16). If *d*₂-TFE was used as solvent, no deuterium was incorporated in the product at full reaction conversion. Even

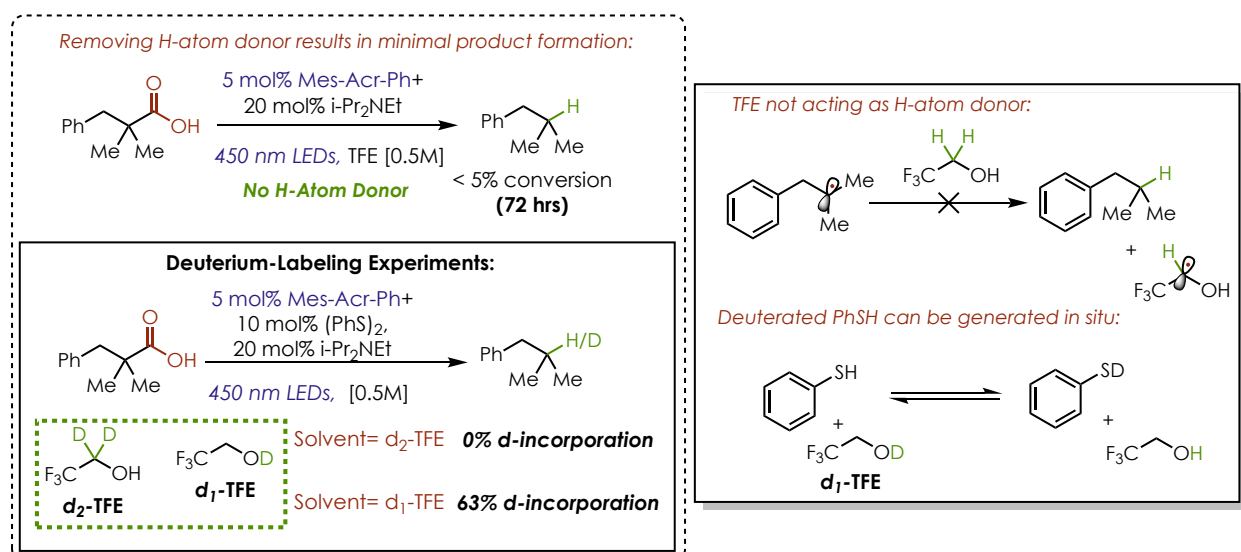


Figure 2.16: Summary of deuterium labeling experiments.

taking into account a significant kinetic isotope effect (KIE) this result makes it unlikely that TFE could be acting as an H-atom donor. When d_1 -TFE was used as solvent, 63% deuterium incorporation was observed in the product at the completion of the reaction. Since it is not likely that the O-H bond is the H-atom source (this H-atom transfer would be endothermic by ~ 14 kcal/mol), this is consistent with thiophenol acting as the sole H-atom donor. It is evident through this experiment that the acidic protons on the substrate, solvent, and PhSH are readily exchangeable, hence deuterium incorporation into the product. This also shows that the proton from the carboxylic acid starting material is incorporated in the final product, as less than 100% deuterium incorporation was observed.

2.4.2.2 Effect of Trifluoroethanol on Catalyst Excited State

Using time-correlated single photon counting (TCSEC) fluorescence spectroscopy, the fluorescence lifetime of Mes-Acr-Ph⁺ was measured in both TFE and MeOH. Fluorescence decay in TFE was mono-exponential with a lifetime of 10.8 ns, while in MeOH the fluorescence was bi-exponential, with lifetimes of 0.49 and 5.5 ns (**Figure 2.17**). The bi-exponential decay of fluorescence indicates two fluorescent excited state species, one of which is presumed to be the locally excited singlet (**LE^S**), however the identity of the second excited state is unclear. Mes-Acr-Ph⁺ exhibited significant static quenching in MeOH compared to TFE as evidenced by comparison of the steady-state emission spectra in both solvents (**Figure 2.18, top**); which shows that the

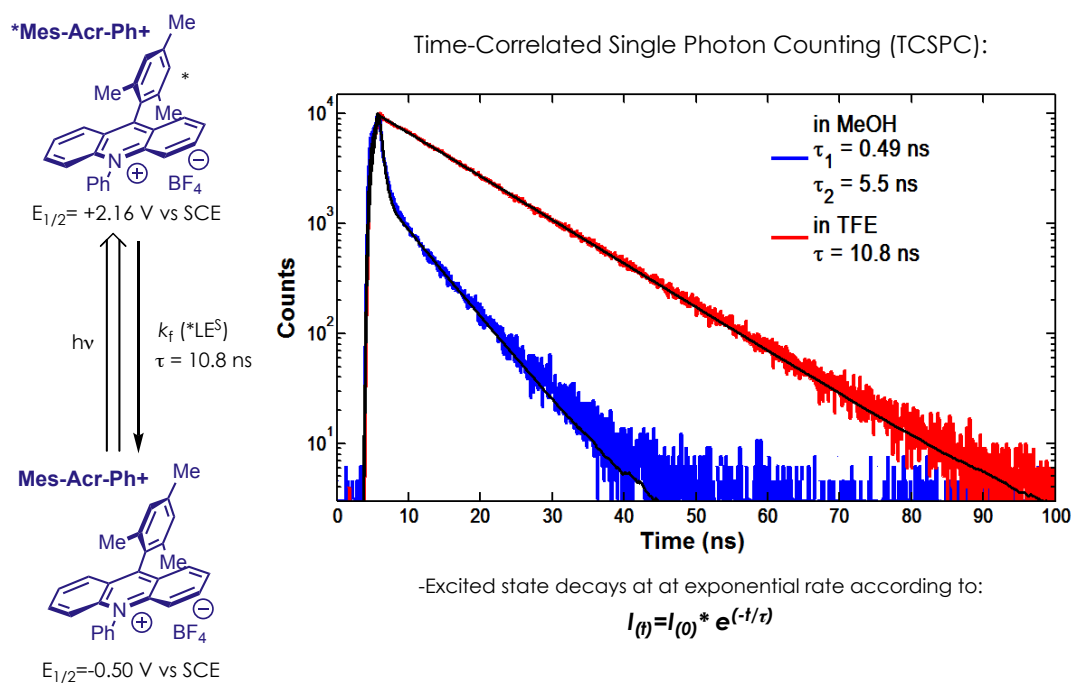


Figure 2.17: Time-correlated Fluorescence Spectra of Mes-Acr-Ph⁺ in TFE and MeOH. Mes-Acr-Ph⁺ has a mono-exponential decay in TFE, with a bi-exponential decay in MeOH indicating two emissive excited states in MeOH.

overall emission intensity is much lower in MeOH than in TFE. Furthermore the emission was significantly red-shifted in MeOH suggesting a higher population of the lower energy charge-transfer singlet state (CT^S) (**Figure 2.18, bottom**). This data prompted an investigation into the stability of Mes-Acr-Ph⁺ in MeOH:H₂O. Upon irradiating a solution of Mes-Acr-Ph⁺ in 9:1 MeOH:H₂O with 450 nm, significant decomposition of the catalyst occurred.

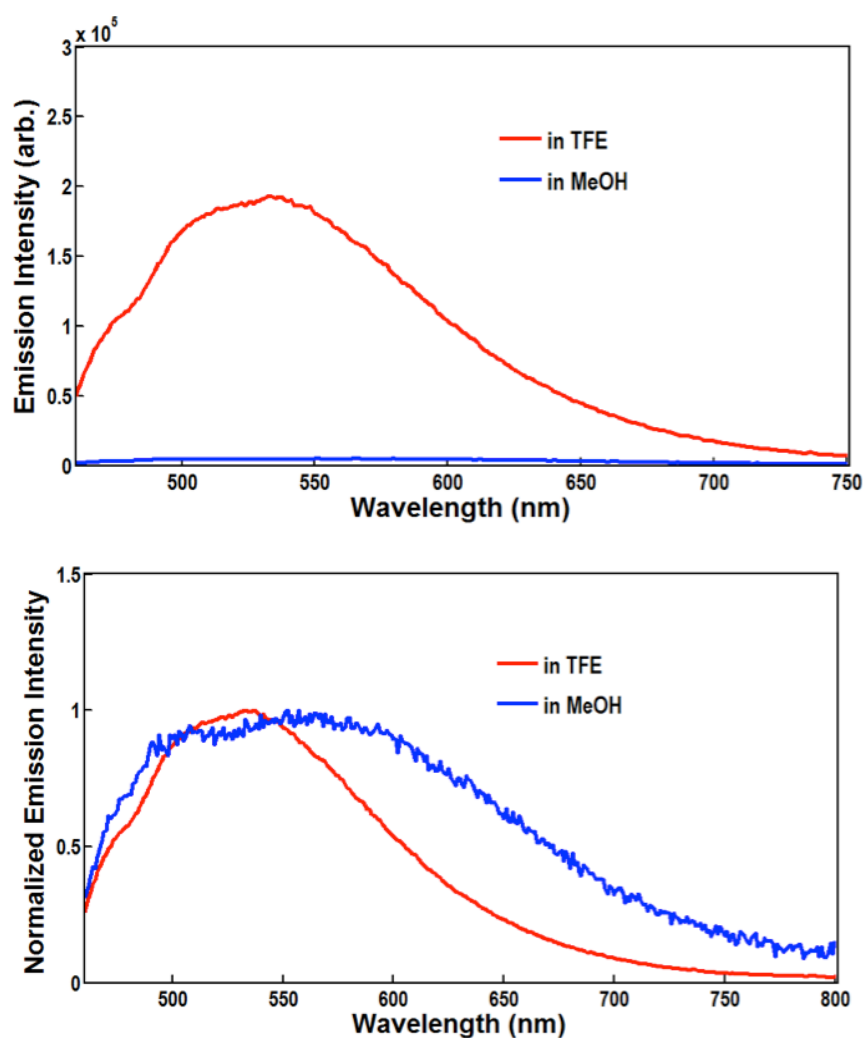


Figure 2.18: Steady-state Emission Spectra of Mes-Acr-Ph⁺ in TFE and MeOH. (top) Raw emission shows fluorescence intensity of Mes-Acr-Ph⁺ in MeOH is much lower than in TFE. (bottom) Normalized emission spectrum showing that the fluorescence emission is significantly red shifted in MeOH, indicating a higher population of Mes-Acr-Ph⁺ CT^S .

Together this data suggests that TFE is an ideal solvent for this system simply because it does not quench the LE^S of Mes-Acr-Ph⁺ (dynamic quenching), as longer excited state lifetimes were observed in TFE. TFE also has decreased nucleophilicity¹⁰⁷ compared to other alcoholic solvents which quench fluorescence through ground state interactions (static-quenching). Due to significant static and dynamic-quenching of fluorescence in MeOH, the steady-state concentration of excited state acridinium is far lower than in TFE. While Mes-Acr-Ph⁺ lifetime is not quenched in other solvents like CHCl₃, a polar protic solvent is necessary in order to deprotonate carboxylic acids using relatively weak bases.

2.4.3 Kinetic Analysis of Hydrodecarboxylation

Throughout the development of the hydrodecarboxylation protocol, the reactions were notably very slow; often requiring multiple days in order to obtain conversions above 50%. Therefore, an analysis of the reaction kinetics was carried out in order to potentially identify elementary steps which exerted rate limiting influence and the rate determining step (**RDS**).

2.4.3.1 Kinetic Isotope Effect Experiments

To determine if H-atom transfer could be rate limiting, the rate of hydrodecarboxylation was measured for 1,1-dimethylpropanoic acid under the optimized conditions and in a separate vessel the O-D analog was measured in *d*₁-TFE (**Figure 2.19**). Deuterium incorporation at all acidic/exchangeable positions should allow for the selective formation of deuterated-thiophenol (**PhSD**) in situ, and for the determination of a kinetic isotope effect (**KIE**). The incorporation of deuterium in the starting carboxylic acid was confirmed by IR spectroscopy via the lack of an O-H stretch and by ¹H NMR via the reduction of the intensity of the carboxylic acid proton (in very

dry CDCl₃). A deuterium incorporation of at least 80% was determined by NMR. The reaction rate was monitored by initial rates kinetics, with excellent mass balance observed over the course of

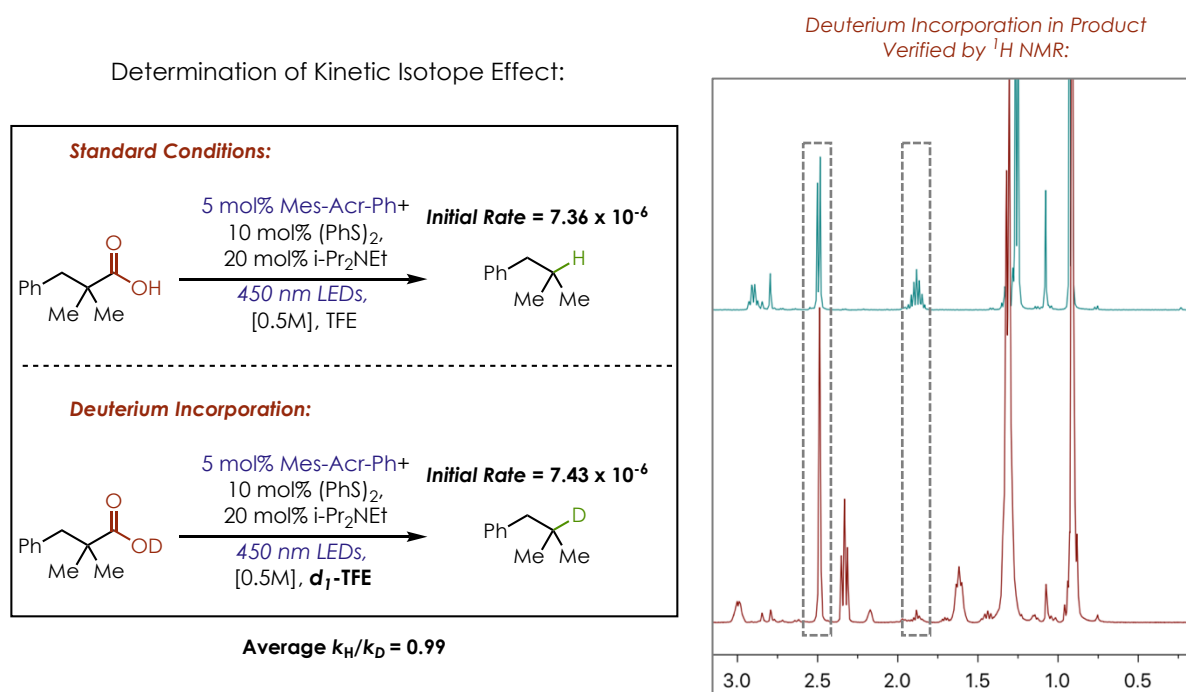


Figure 2.19: To determine if H-atom transfer was rate limiting, initial rates were measured for decarboxylation of 1,1-dimethylpropanoic acid under the standard reaction conditions, and for 2,2-dimethyl-3-phenylpropanoic acid-*d* using *d*₁-TFE. The top spectrum is a crude ¹H NMR run under normal conditions, while the bottom spectrum is the spectrum run under deuterium incorporation conditions. The overlay of the ¹H NMR spectra shows that deuterium was indeed incorporated into the product under these conditions. In the bottom spectrum the methylene signal is a singlet (2.49 ppm), while the methine signal is almost completely diminished (1.88 ppm). The bottom spectrum also shows methyl octanoate internal standard.

the reaction. A short induction period was found, likely due to the initially low solubility of Ph₂S₂ TFE, however this was not found to significantly affect the kinetics after multiple trials using the same conditions. The induction period could also be caused by slow formation of thiyl radical via homolysis of Ph₂S₂ when irradiated with 450 nm LEDs, thus a short period is required to establish an equilibrium. A KIE of nearly unity (0.99) was determined for the parallel reactions (**Figure 2.19**). Deuterium incorporation into the final product was ensured by ¹H NMR at complete reaction conversion. A KIE near one suggests that neither H-atom transfer or proton transfer is rate-

limiting. Dimerization of alkyl radicals was never observed during the optimization process; the reactions always provided excellent mass balance, consistent with the finding that H-atom transfer was not rate limiting.

A competition experiment was also carried out, in which a 1:1 mixture of proteo and deutero acid run in a mixture of 1:1 TFE:*d*₁-TFE. showed > 20:1 proton incorporation in the final product (**Figure 2.20**). This indicates that there is potentially a kinetic preference for HAT vs

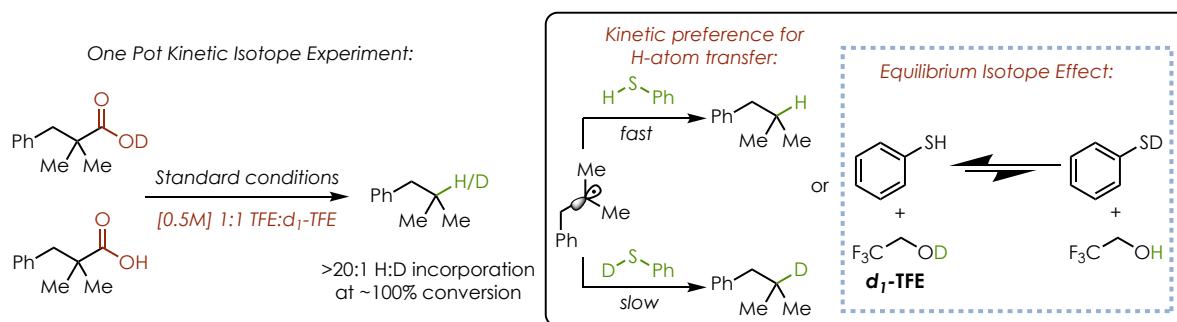


Figure 2.20: Competition isotope experiment through the in-situ formation of PhSH/PhSD. Although this experiment can't give information about the rate determining step, a significant KIE was observed. This could potentially be explained by (A) Kinetic preference for HAT over DAT or (B) via an equilibrium isotope effect in which PhSH is formed preferentially to PhSD.

deuterium atom-transfer (**DAT**) in this reaction; however, this experiment cannot give any information about the rate limiting step of the reaction. The large KIE observed in this experiment could also be a result of an equilibrium isotope effect in which PhSH is formed preferentially to PhSD, via deprotonation of the carboxylic acid or exchange with solvent. This could even be expected due to the relevant BDEs. While it is difficult to determine which factor, or both, is contributing to this competition experiment KIE, it is clear that H-atom transfer does not exert rate-limiting influence on this reaction from the separate initial rates measured in separate reaction vessels.

2.4.3.2 Further Kinetic Analysis

Further kinetic analysis of the reaction was undertaken in order to determine the RDS. The reaction was found to be first order with respect to carboxylate ion (**Figure 2.21, left**). Interestingly

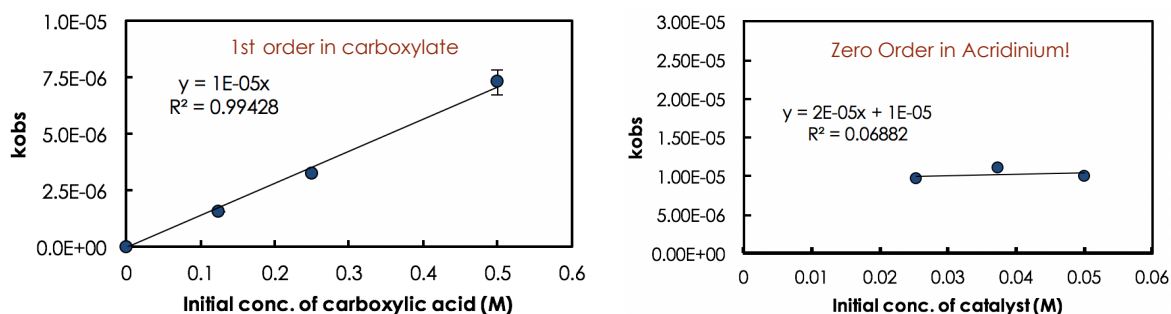


Figure 2.21: Rate dependence of carboxylate ion concentration (2,2-dimethyl-3-phenylpropanoic acid and *i*-Pr₂NEt were kept at a constant ratio) and Mes-Acr-Ph⁺. Mes-Acr-Ph⁺ was found to have zero-order dependence at high concentrations (>0.025 M, above 5 mol% catalyst loading) while having a fractional order dependence at lower concentrations (not shown).

the reaction was found to be zero-order with respect to Mes-Acr-Ph⁺ at higher loadings of catalyst (**Figure 2.21, right**), while at very low catalyst loadings a fractional order was found demonstrating saturation kinetics (See Section 2.6.7). This was suggestive of a light-limited reaction, as zero-order photocatalyst dependence would be expected for an optically saturated solution (all photons entering the solution are absorbed). Further investigation into this led to the

discovery that the reaction rate was very dependent on the photon flux; the reaction rate decreases drastically if only one LED flood lamp is used to irradiate the reaction vial (**Figure 2.22**). Although it was very difficult at this stage, due to the light source being used, to control exact photon flux Figure 2.22 shows a definite light dependence for this reaction. The dependence on light suggests that this method could be improved through the use of a flow methodology which could allow for a greater absorbance of light because of the increased surface area. Combined with the lack of KIE (See section 2.4.3.1) the data suggests that carboxylate oxidation or loss of carbon dioxide is potentially the rate limiting step for this reaction.

It is also of interest to note the magnitude of fluorescence quenching of the excited state. Although the k_q derived from Stern–Volmer experiments indicate a rapid rate of oxidation, the quenching efficiency is very low; for potassium hydrocinnamate (5 mM), only 2% of Mes-Acr-Ph⁺ fluorescence is quenched. This reflects that bimolecular quenching is competitive with fast

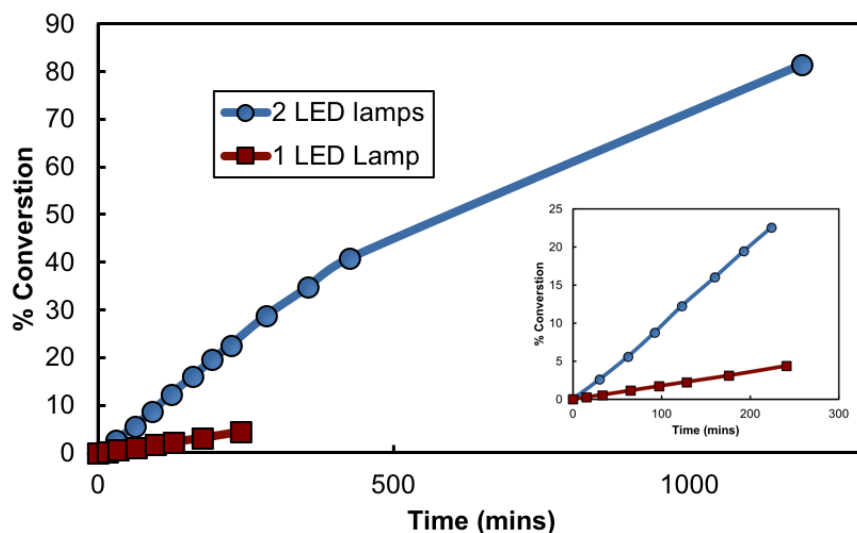


Figure 2.22: %Conversion versus time for the hydrodecarboxylation of 2,2-dimethyl-3-phenylpropanoic acid under the standard reaction conditions. (●) Irradiation using two 450 nm LED flood lamps. (■) Irradiation carried out using only one 450 nm LED flood lamp. Initial reaction rate is dramatically decreased when decreasing photon flux. Inset shows zoomed comparison of early rate of conversion.

decay of the excited state by fluorescence ($k_f = 9.3 \times 10^7 \text{ s}^{-1}$ in TFE) and is consistent with the light dependence shown in Figure 2.22. The very low quenching efficiency demonstrates that even though the rate constant for carboxylate oxidation is very large, it is still possible for RCOO[−] oxidation to be turnover limiting in the reaction.

2.4.4 Hydrodecarboxylation Dependence on Substrate Identity

During the development of this hydrodecarboxylation reaction, it became apparent that there were innate differences in reactivity based on the degree and type of substitution at the α -position of the carboxylic acid substrates. This was particularly apparent when investigating solvent systems other than TFE, such as methanol/water. As demonstrated in Section 2.2.3, primary carboxylic acid derivatives produced only small amounts of hydrodecarboxylation product, while tertiary substituted acids provided excellent conversion in this system (Section 2.2.2). It seemed plausible that substitution at the α -position could affect the substrate oxidation potential, possibly making carboxylate oxidation less thermodynamically favored for less substituted acids. However, measuring the half wave oxidation potentials of propionate (1°), isobutyrate (2°), and pivalate (3°) revealed that the oxidation potentials were nearly identical (**Figure 2.23, top**). The potentials were sufficiently low that electron transfer from carboxylate ion to Mes-Acr-Ph⁺ LE^S should be very thermodynamically favorable (ΔG_{ET}° are approximately −20 kcal/mol in each case).

Despite having very similar redox potentials, it still seemed reasonable that variation of substrate sterics/electronics could present differences in the kinetic barrier to electron transfer

Comparison of Half-Wave Oxidation Potential of Carboxylates:

Substrate:			
$E_{p/2}$:	+1.25 V	+1.31 V	+1.29 V

Comparison Rates of Quenching of Mes-Acr-Ph⁺ (LE^S):

Substrate:			
k_q ($M^{-1}s^{-1}$):	3.91×10^8	2.52×10^8	2.34×10^8

Figure 2.23: (top) oxidation potentials of the tetrabutylammonium salts of three representative carboxylic acids were measured in a 0.1 M solution of tetrabutylammonium hexafluorophosphate in MeCN. All potentials are reported vs SCE. (bottom) Bimolecular quenching constants measured for the potassium salt of each carboxylic acid with Mes-Acr-Ph⁺.

between substrates. Therefore, the rates of electron transfer (k_{ET}) were measured via Stern-Volmer analysis of fluorescence quenching for three carboxylates with varying alkyl substitution (**Figure 2.23, bottom**). The observed quenching constants indicate that only a small difference in k_{ET} exists between substrates, in TFE. Somewhat surprisingly, the 1° substituted carboxylate displayed the largest quenching constants, albeit by a small margin.

2.4.4.1 Substrate Competition Experiments

Competition experiments between substrates bearing differing amounts of α -substitution were carried out in TFE and 9:1 MeOH:H₂O (**Figure 2.24**). When using equimolar amounts of each substrate, the conversion for each substrate was fairly similar at ~30% conversion. The primary carboxylic acid had the highest rate of apparent conversion in TFE, although only by a narrow margin. In MeOH:H₂O the selectivity was reversed, however the more surprising result was that the overall rate of conversion was much slower than expected, as the reaction took almost 24 hours to reach 30% conversion. Additionally, the ratio of isobutylbenzene to ethylbenzene formed

during the experiment was much lower than expected based on previous results of optimization, with the 3° substituted acid only marginally outcompeting the other two acid substrates. This suggests that the presence of 1° (and potentially 2°) substituted carboxylic acids impede the

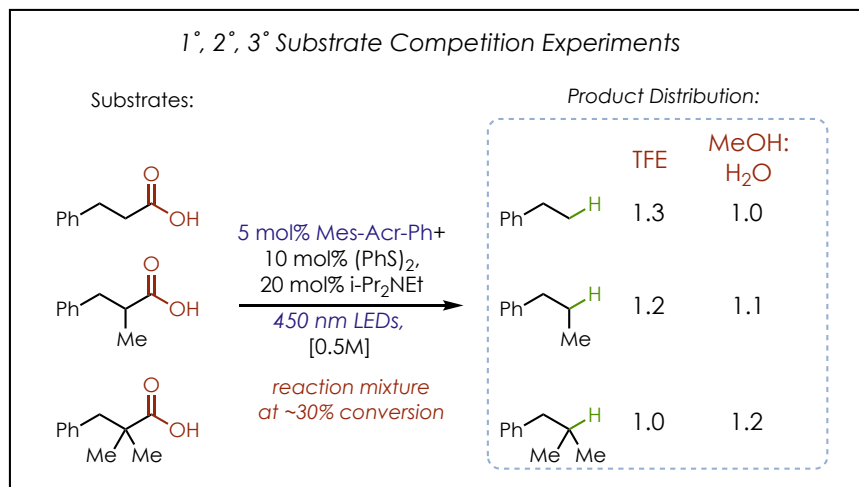


Figure 2.24: Substrate competition experiments in TFE and 9:1 MeOH:H₂O. Equimolar amounts (0.25 mmols) of each carboxylic acid were added to the same reaction vessel. All other reagents were added in their respective quantities relative to the total amount of carboxylic acid (0.75 mmol). The reactions were stopped at ~30% overall conversion in order to determine if a difference in the rate of hydrodecarboxylation. Yields were measured from crude ¹H NMR spectra.

reactivity of the 3° substituted acid. Since the rates of reaction of the individual substrates in the competition is similar, another explanation for the low reactivity of 1° carboxylic acids in this solvent system could be catalyst decomposition caused by either the primary carboxylate or primary radical formation. This is consistent with the similar values for k_q between carboxylate substrates.

While exploring the substrate scope, it was apparent there were differences in the rate of hydrodecarboxylation, even between two 1° alkyl substituted carboxylic acids. For example the decarboxylation of tridecanoic acid (**Chart 2.1, 2.12**) proceeded very slowly, which was initially attributed to low solubility. EtOAc could be used as a co-solvent to increase the solubility of the tridecanoic acid however the reaction rate remained exceptionally slow. To rule out the possibility

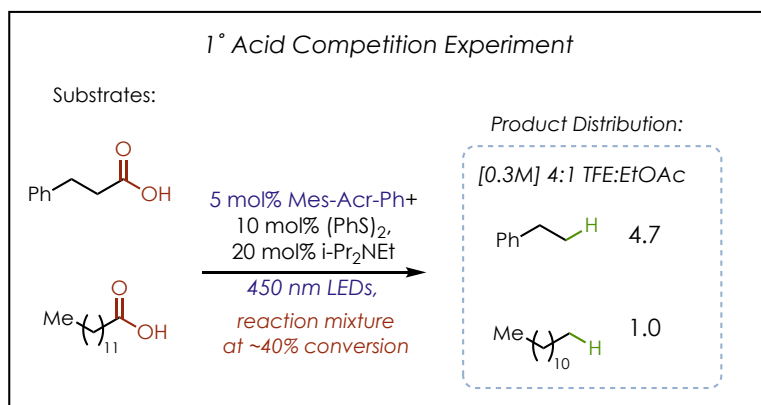


Figure 2.25: Substrate competition experiments in TFE and 9:1 MeOH:H₂O. Equimolar amounts (0.375 mmols) of each carboxylic acid were added to the same reaction vessel. All other reagents were added in their respective quantities relative to the total amount of carboxylic acid (0.75 mmol). The reactions were stopped at ~40% overall conversion in order to determine if a difference in the rate of hydrodecarboxylation. Yields were measured from crude ¹H NMR spectra.

that the addition of EtOAc changed the reaction conditions too significantly, a direct competition experiment was carried out between hydrocinnamic acid and tridecanoic acid (**Figure 2.25**). At ~40% overall conversion, the product ratios (4.7:1) reflected that tridecanoic acid indeed reacted at a much slower rate in TFE:EtOAc. A potential explanation for this will be discussed in the next Section (Section 2.4.4.2).

2.4.4.2 Pre-association complex between Mes-Acr-Ph⁺ and Carboxylate salts

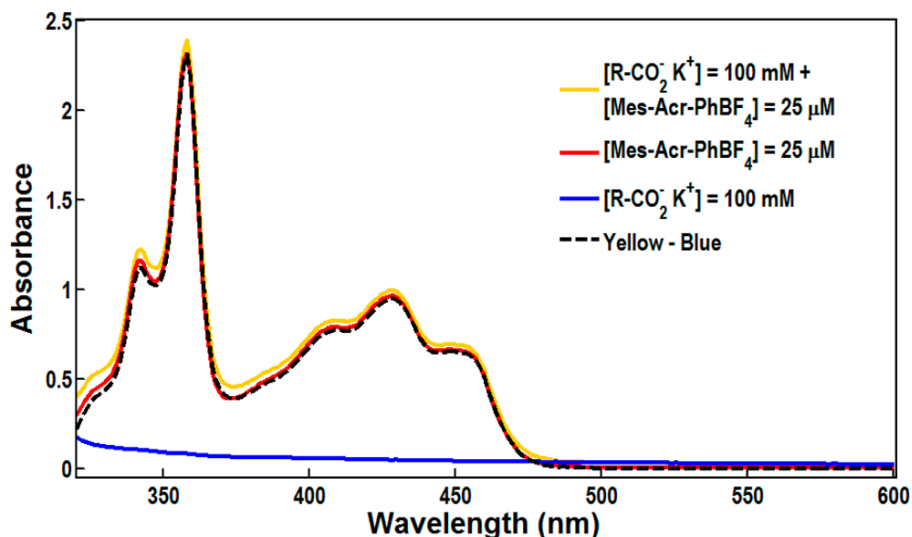


Figure 2.26: UV/vis absorption spectra of the catalyst before and after adding carboxylate salt. The red line shows Mes-Acr-Ph⁺ before the addition of carboxylate. The yellow line shows the absorption spectrum of the catalyst after adding the carboxylate. The blue line is the absorption spectrum of the carboxylate and the dashed black line is the subtraction of the carboxylate from the absorption spectrum of the catalyst with added quencher (yellow-blue).

The potential for the formation of a pre-association complex between Mes-Acr-Ph⁺ and carboxylate ions was intriguing because it could potentially explain anomalous rate differences between similar substrates. Initially, the possibility of a charge-transfer complex between Mes-Acr-Ph⁺ and potassium hydrocinnamate was explored. Previous ground state charge-transfer complexes have been uncovered between Mes-Acr-Ph⁺ and alkenes,⁹⁴ thus it seemed plausible that such an interaction could occur with carboxylate salts. The UV/vis spectrum of Mes-Acr-Ph⁺ was completely unchanged after the addition of 4,000 equivalents of the carboxylate salt (**Figure 2.26**). Thus formation of a ground state charge-transfer complex seemed unlikely. However, the absence of a charge-transfer complex does not preclude the formation of pre-association of Mes-Acr-Ph⁺ and the carboxylate salts.

^1H NMR spectra of Mes-Acr-Ph $^+$ show that the arene protons signals shift significantly upon increasing addition of tetrabutylammonium salt of 3-phenylpropanoic acid (primary carboxylate salt, structure shown in **Table 2.4**). The ^{19}F NMR peaks were found to broaden significantly as well, suggestive of a rapid exchange of BF_4^- and the carboxylate as counterions. Significant broadening at high concentrations prohibited determination of the saturation point of

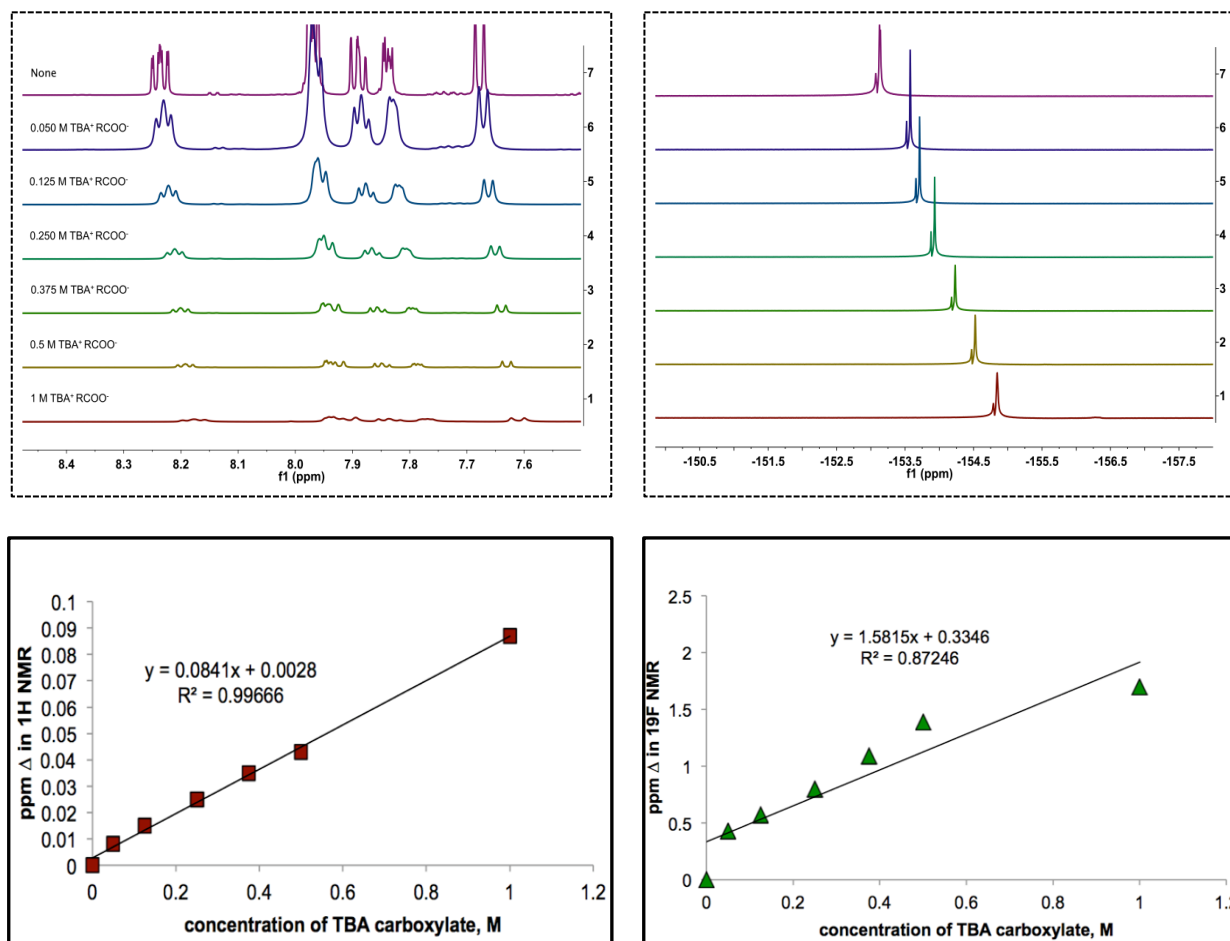


Figure 2.27: (top left) ^1H and **(top right)** ^{19}F NMR spectra of Mes-Acr-Ph $^+$ BF_4^- [25 mM] in CD_3OD . Residual methanol solvent peak was set to 3.31 ppm in each ^1H NMR. ^{19}F NMR spectra were spiked with 20 μL of TFE before taking ^{19}F NMRs and the corresponding peak was set to -78.82 ppm in each spectrum. TBA $^+$ RCOO $^-$ = tetrabutylammonium hydrocinnamate **(bottom left)** The change in shift of Mes-Acr-Ph $^+$ as a function of concentration of TBA hydrocinnamate. The most downfield peak on Mes-Acr-Ph $^+$ was used as a reference point to determine the ppm shift. **(bottom right)** The change in shift of BF_4^- counterion as a function of concentration of TBA hydrocinnamate. The larger signal corresponding the most abundant Boron isotope in BF_4^- was used as a reference point to determine ppm shift.

this titration; however the Δ ppm was found to be linear with substrate concentration in the concentration range measured for ^1H NMR shifts. (**Figure 2.27**). This data suggests that ion pairing between the catalyst and carboxylate salts could be an important interaction. Particular substrates that are better able to ion pair with Mes-Acr-Ph⁺ may undergo more facile electron transfer depending on the type of ion pair (contact, loose, solvent separated, or aggregated), temperature, and other factors.¹⁰⁸ Electron transfer rates between two ions can be affected by solvent; ion-pairs typically undergo faster electron transfer in non-polar solvents due to the formation of tighter pairs in these solvents.¹⁰⁹ Currently, it seems that since Mes-Acr-Ph⁺ and RCOO⁻ exist as ion pairs in solution, the steric hindrance around the carboxylate salt could potentially affect the K_A for the formation of this pair. Although, the k_q for the series of carboxylate salts suggests that there was very little difference in rate of electron transfer between substrates, the substrate with the least steric hindrance had a slight higher rate of electron transfer (see Figure 2.23). Other considerations include increase in reorganization necessary for larger carboxylate ions. These factors could potentially explain the rate differences between substrates even those containing similar α -substitution patterns, such as the substrates in the competition experiment in above in **Figure 2.25**.

Fukuzumi has demonstrated in a similar system that in an acetonitrile/water mixture there are significant differences in the ability of a series of primary, secondary, and tertiary alkyl substituted carboxylates to quench the photoexcited state of a 10-methyl acridinium catalyst via an electron transfer mechanism.¹¹⁰ This could potentially indicate a different mechanism in different solvent systems and highlights the importance of solvent in these systems. In early optimization of this reaction (**Table 2.2**) substrates bearing α -phenyl groups were found to efficiently decarboxylate in chloroform, whereas alkyl substituted carboxylic acids were sluggish

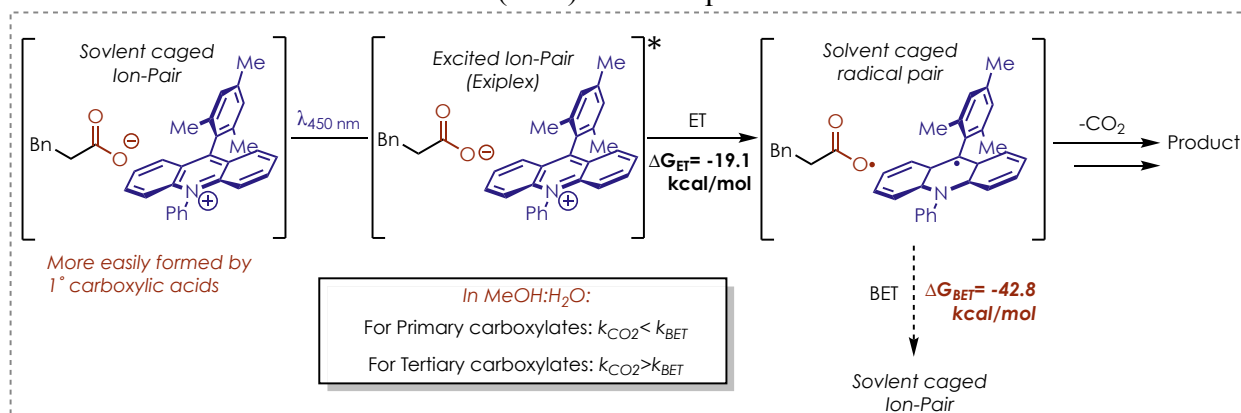
using this solvent. Wallentin et al. have also demonstrated the ability for an acridinium photooxidant to decarboxylate protected amino acids and phenyl acetic acid derivatives in dichloroethane, but alkyl-substituted acids were not possible.⁶⁸ These points make it clear that ion-pairing differences with Mes-Acr-Ph⁺ don't explain the differences in k_{ET} between when substrates have different α -substitution (in non-TFE solvents), therefore another explanation for this observation is needed. Further discussion will be provided in the next section (**Section 2.4.5**).

Additionally, the importance of ion pairs for this electron transfer could also offer another explanation for the requirement of TFE as solvent. Based on relevant solvent polarities dielectric constants, ($\epsilon_{TFE} = 27.1$ F/m; $\epsilon_{9:1\text{ MeOH:H}_2\text{O}} = 36.8$ F/m)^{103,104} TFE is less polar than 9:1 MeOH:H₂O. TFE is still polar enough to facilitate carboxylic acid deprotonation, but tighter ion pairs are expected to form in TFE with Mes-Acr-Ph⁺.

2.4.4.3 Importance of Back Electron Transfer

It is possible that a back electron transfer process occurring from the acridine radical (Mes-Acr-Ph•) to the acyloxy radical (RCOO•) is faster than CO₂ loss for primary carboxylic acids in

Scheme 2.3: Back electron transfer (BET) could explain rate differences



MeOH:H₂O, as this electron transfer is thermodynamically favorable and probably rapid (**Scheme 2.3**). This would suggest that for tertiary carboxylic acids, which have faster rates of

decarboxylation (See section 2.1.3), CO₂ loss is competitive with back electron transfer. This would manifest in observed rate differences between substrates even though the rates of electron transfer are similar for all substrates (See Figure 2.23).

However, the competition experiment shown in Figure 2.24 run in MeOH:H₂O seems to suggest that at early conversions the rate of product formation is similar for primary, secondary, and tertiary carboxylic acids. Also, the overall rate of conversion for the tertiary acid was slower than expected in the competition experiment. Since there is only a slight rate enhancement for the tertiary substrate in MeOH:H₂O, it seems plausible that catalyst decomposition is an issue with more reactive radical intermediates produced from primary carboxylic acids, consistent with a slower than expected rate for the tertiary acid in the competition experiment.

2.5 Conclusions

Carboxylates participate in a myriad of carbon-carbon and carbon-heteroatom bond forming reactions, thus the removal of a carboxylic acid functional group presents a unique opportunity to accomplish a traceless functionalization of organic molecules. A methodology for the hydrodecarboxylation of aliphatic carboxylic acids using a photoredox strategy was developed. This methodology was found to tolerate numerous functional groups, and additionally all degrees of substitution at the α -carbon were well tolerated. This method could also be used to reduce malonic acid derivatives directly to the corresponding alkanes. Mechanistic studies were used to provide a hypothesis for the role of a unique solvent effect; while kinetic analysis was used to demonstrate that the reaction was light limiting using LED flood lamps.

2.6 Experimental

2.6.1 General Methods and Materials

General Methods:

Infrared (IR) spectra were obtained using a Jasco 260 Plus Fourier transform infrared spectrometer. Proton and carbon magnetic resonance spectra (^1H NMR and ^{13}C NMR) were recorded on a Bruker model DRX 400 or a Bruker AVANCE III 600 CryoProbe (^1H NMR at 400 MHz or 600 MHz and ^{13}C NMR at 101 or 151 MHz) spectrometer with solvent resonance as the internal standard (^1H NMR: CDCl_3 at 7.26 ppm, and $(\text{CD}_3)_2\text{O}$ at 2.05 ppm; ^{13}C NMR: CDCl_3 at 77.0 ppm and $(\text{CD}_3)_2\text{O}$ at 206.26 ppm). ^1H NMR data are reported as follows: chemical shift, multiplicity (s = singlet, d = doublet, t = triplet, dd = doublet of doublets, ddt = doublet of doublet of triplets, ddd = doublet of doublet of doublets, dddd = doublet of doublet of doublet of doublets m = multiplet, brs = broad singlet), coupling constants (Hz), and integration. Mass spectra were obtained using a Micromass (now Waters Corporation, 34 Maple Street, Milford, MA 01757) Quattro-II, Triple Quadrupole Mass Spectrometer, with a Z-spray nano-Electrospray source design, in combination with a NanoMate (Advion 19 Brown Road, Ithaca, NY 14850) chip based electrospray sample introduction system and nozzle. Thin layer chromatography (TLC) was performed on SiliaPlate 250 μm thick silica gel plates provided by Silicycle. Visualization was accomplished with short wave UV light (254 nm), aqueous basic potassium permanganate solution, cerium ammonium molybdate solution followed by heating. Flash chromatography was performed using SiliaFlash P60 silica gel (40-63 μm) purchased from Silicycle. Irradiation of photochemical reactions was carried out using 2 15W PAR38 Royal Blue Aquarium LED floodlamps Model# 6851 purchased from Ecoxotic with borosilicate glass vials purchased from Fisher Scientific. Gas chromatography

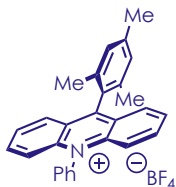
(GC) was performed on an Agilent 6850 series instrument equipped with a split-mode capillary injection system accompanied by an Agilent 5973 network mass spec detector (MSD) or Agilent 6850 Series II with flame ionization detector. GC yields were determined by standardization against pure compounds purchased from Sigma-Aldrich along with an internal standard. NMR yields were determined using hexamethyldisiloxane as an internal standard.

Materials:

Commercially available reagents were purchased from Sigma-Aldrich, Acros, Alfa Aesar, or TCI America, and used as received unless otherwise noted. Diethyl ether (Et₂O), dichloromethane (CH₂Cl₂), tetrahydrofuran (THF), toluene, and dimethylformamide (DMF) were dried by passing through activated alumina columns under nitrogen prior to use. 2,2,2-trifluoroethanol (TFE) was distilled from anhydrous potassium carbonate and sparged with nitrogen before use. Other common solvents and chemical reagents were purified by standard published methods. Diphenyl disulfide (Ph₂S₂), diisopropylethylamine (*i*-Pr₂NEt), 2,6-Lutidine, 2,4,6-trimethylpyridine (Collidine), hydrocinnamic acid, 2-methyl-3-phenylpropanoic acid, 3-(4-chlorophenyl)propanoic acid, 3-(*p*-tolyl)propanoic acid, ((benzyloxy)carbonyl)-L-proline, tridecanoic acid, Enoxolone, 1,3-dihydro-2H-indene-2,2-dicarboxylic acid, benzylmalonic acid, and phenylmalonic acid were all purchased from Sigma-Aldrich and used without further purification.

2.6.2 Catalyst Preparation

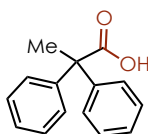
9-Mesityl-10-phenylacridinium tetrafluoroborate (Mes-Acr-Ph⁺):



Prepared according to methods previously reported by our lab.⁸³

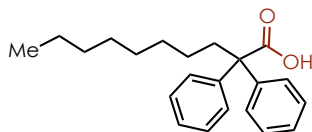
2.6.3 Substrate Preparation

2,2-diphenylpropanoic acid:



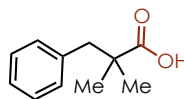
To a flame dried 250mL round bottom flask equipped with a stir bar was added 2.05 g (9.68 mmol) of biphenyl acetic acid. The flask was fitted with a septum and purged with nitrogen gas for 30 minutes before adding 100 mL of dry THF through the septum. The solution was cooled to -78°C; then 7.75 mL (2.5 M, 2.2 eq) of n-butyl lithium was carefully added through the septum and was allowed to stir for 40 minutes. 0.66 mL (10.56 mmol, 1.2 eq) of methyl iodide was added and the solution was allowed to warm to room temperature. This was allowed to stir overnight before HCl (3M) and water were used to quench the reaction. The solution was extracted x3 with ethyl acetate then x2 with DCM. This was dried with sodium sulfate then the solvent was removed under vacuum. The compound was purified via column chromatography (20:80 EtOAc:Hexanes) to give a white solid (1.46 g, 73% yield). Analytical data were in agreement with literature values¹¹¹ : ¹H NMR (400 MHz, CDCl₃) δ 11.51 (s, 1H), 7.59 – 6.88 (m, 10H), 1.97 (s, 3H).

2,2-diphenyldecanoic acid:



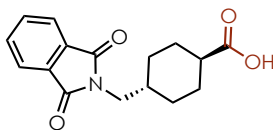
To a flame dried 250 mL round bottom flask equipped with a stir bar was added 2.62 g (12.34 mmol) of diphenyl acetic acid. The flask was fitted with a septum and purged with nitrogen gas for 30 minutes before adding 100mL of dry THF through the septum. The solution was cooled to -78°C ; then 11mL (2.5 M, 2.2 eq, 27.2 equiv.) of n-butyl lithium was carefully added through the septum and was allowed to stir for 40 minutes. 2.55 mL (14.8 mmol, 1.2 eq) of 1-bromooctane was added and the solution was allowed to warm to room temperature. This was allowed to stir overnight before HCl (3M) and water were used to quench the reaction. The solution was extracted x3 with DCM. This was dried with sodium sulfate then the solvent was removed under vacuum. The compound was purified via column chromatography (20:80 EtOAc:Hexanes) to give a white solid (1.46 g, 73% yield). Analytical data were in agreement with literature values : ^1H NMR (400 MHz, Chloroform-*d*) δ 7.33 (d, $J = 4.5$ Hz, 9H), 7.31 – 7.26 (m, 5H), 2.40 – 2.30 (m, 2H), 1.36 – 1.15 (m, 14H), 1.08 (s, 1H), 0.87 (t, $J = 7.0$ Hz, 3H).

2,2-dimethyl-3-phenylpropanoic acid:



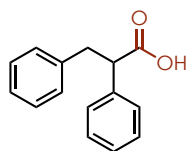
To a flame dried 250 mL round bottom flask equipped with a stir bar was added 100 mL dry THF. The solution was cooled to -78 °C, and n-BuLi (11.44mL, 2.5 M, 28.6 mmol, 1.1eq) was added. The solution was allowed to stir at -78 °C for about 30 mins after adding diisopropylamine (4 mL, 28.6 mmol, 1.1 eq). Methyl isobutyrate (2.96 mL, 26 mmol, 1.0 eq) was then added and then the solution was stirred an additional 30mins. Benzyl bromide (3.4 mL, 28.6 mmol, 1.1 eq) was added and the solution was allowed to warm up to room temperature. The solution was allowed to stir overnight before quenching with 3 M HCl and water. The aqueous layer was extracted x3 with DCM and dried with Na₂SO₄. The solvent was evaporated, which produced a slightly yellow oil. This was dissolved in 60 mL MeOH to which NaOH (5.2g, 5eq) was added. The solution was stirred at 60°C overnight before extracting the aqueous layer with diethyl ether to remove impurities, then acidifying the aqueous layer to a pH of 1 with 3M HCl. The aqueous layer was then extracted x3 with DCM which was dried over Na₂SO₄. The solvent was then evaporated and the product was purified via column chromatography (20:80 EtOAc:Hex), resulting in a white solid (2.56g, 56% yield). Analytical data were in agreement with literature values¹¹²: **¹H NMR** (400 MHz, CDCl₃) δ 7.35 – 7.23 (m, 3H), 7.23 – 7.16 (m, 2H), 2.93 (s, 2H), 1.24 (s, 6H).

trans-4-((1,3-dioxoisindolin-2-yl)methyl)cyclohexane-1-carboxylic acid:

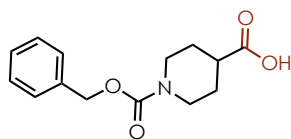


Prepared according to previously published literature procedure. Analytical data were in agreement with literature values.¹¹³

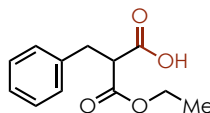
2,3-diphenylpropanoic acid:



To a flame dried 250mL RBF equipped with a stir bar was added 1.15g of NaH (60% w:w in mineral oil, 28.8 mmol 2eq) and 162 mg (1.44mmol, 0.1 eq) of potassium tertbutoxide. The flask was then fitted with a septum and purged with nitrogen. 75 mL of dry DMF was then added through the septum and the suspension was cooled to 0 °C. Next, 3.1 mL (3.4 g 14.4 mmol) diethyl phenyl malonate was added dropwise through the septum. This was allowed to stir for about 15 minutes, before adding 5.1 mL benzyl bromide (7.4g, 43.2 mmol, 3.0 eq) through the septum slowly. The solution was then heated to 70 °C and allowed to react approximately 30 h before quenching with water. The crude material was extracted with DCM three times. The organic layers were combined and dried with sodium sulfate. The solvent was removed via rotovap and high vacuum. The crude material was then dissolved in a 50:50 mixture (50 mL total volume) of ethanol and water. 10 eq of KOH was added to this mixture and gently refluxed for 15 h before removing from the heat and quenching with 3M HCl. The substrate decarboxylated upon acidic workup with 3M HCl at room temperature to give 2,3-diphenylpropanoic acid. This was then recrystallized from hexanes to give 1.8 g (56% yield) of the pure product. Analytical data were in agreement with literature values¹¹⁴: **¹H NMR:** (600 MHz, Chloroform-*d*) δ 10.26 (s, 1H), 7.45 – 6.99 (m, 10H), 3.90 (ddd, J = 8.7, 7.0, 1.9 Hz, 1H), 3.45 (ddd, J = 13.9, 8.5, 2.0 Hz, 1H), 3.07 (ddd, J = 13.8, 7.0, 1.9 Hz, 1H).

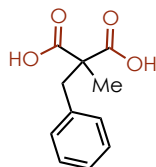
2-benzyl-3-ethoxy-3-oxopropanoic acid:

Prepared according to previously published literature procedure. Analytical data were in agreement with literature values.¹¹⁵

2-benzyl-2-methylmalonic acid:

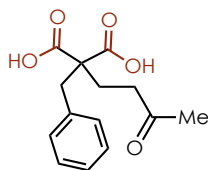
To a 250 mL round bottom flask was added 1.2 g (2.0 equivalents) of sodium hydride and 160 mg of potassium tertbutoxide (0.1 equivalents), followed by 75 mL of dry DMF. This was cooled to 0 °C before adding 3.4 mL of diethyl benzyl malonate slowly. This was allowed to react until Hydrogen evolution ceased, at which point 2.7 mL (3 equivalents) of methyl iodide was added to the solution. The solution was allowed to warm to room temperature, then heated to 70 °C for 24 hours while stirring. The reaction was quenched with H₂O and extracted x3 with DCM. The combined organic layers were washed with H₂O x3 and with a 5% solution of LiCl twice to remove DMF. The solvent was then evaporated in *vacuo*, giving an orange oil. This crude material was placed into a round bottom flask along with 5 equivalents of potassium hydroxide in 1:1 EtOH:H₂O and heated to reflux overnight. Ethanol was removed in *vacuo*, before diluting the reaction with H₂O and washing the aqueous layer with 10 mL diethyl ether. The pH of the aqueous layer was then brought to 2 and extracted with ethyl acetate x3. The organic layer was dried over sodium sulfate, and solvent removed, giving a brownish solid. The solid was then recrystallized from hexanes:EtOAc to give 1.9 grams of the product as a white solid (63%). Analytical data were in agreement with literature values.¹¹⁶

2-benzyl-2-methylmalonic acid:



To a 250 mL round bottom flask was added 1.2 g (2.0 equivalents) of sodium hydride and 160 mg of potassium tertbutoxide (0.1 equivalents), followed by 75 mL of dry DMF. This was cooled to 0 °C before adding 3.4 mL of diethyl benzyl malonate slowly. This was allowed to react until Hydrogen evolution ceased, at which point 2.7 mL (3 equivalents) of methyl iodide was added to the solution. The solution was allowed to warm to room temperature, then heated to 70 °C for 24 hours while stirring. The reaction was quenched with H₂O and extracted x3 with DCM. The combined organic layers were washed with H₂O x3 and with a 5% solution of LiCl twice to remove DMF. The solvent was then evaporated in *vacuo*, giving an orange oil. This crude material was placed into a round bottom flask along with 5 equivalents of potassium hydroxide in 1:1 EtOH:H₂O and heated to reflux overnight. Ethanol was removed in *vacuo*, before diluting the reaction with H₂O and washing the aqueous layer with 10 mL diethyl ether. The pH of the aqueous layer was then brought to 2 and extracted with ethyl acetate x3. The organic layer was dried over sodium sulfate, and solvent removed, giving a brownish solid. The solid was then recrystallized from hexanes:EtOAc to give 1.9 grams of the product as a white solid (63%). Analytical data were in agreement with literature values.¹¹⁷

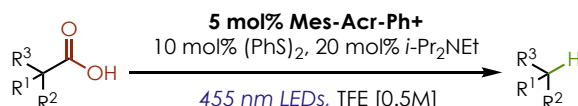
2-benzyl-2-(3-oxobutyl)malonic acid:



Diethyl 2-benzyl-2-(3-oxobutyl)malonate was prepared according to literature procedure.¹¹⁸ The ethyl ester was purified via column chromatography (3-5% acetone in hexanes). A 100 mL round bottom equipped with a stir bar and reflux condenser was charged with potassium hydroxide 85% (5.0 equiv) in H₂O (0.75 M). A solution of diethyl 2-benzyl-2-(3-oxobutyl)malonate (1.0 equiv) in EtOH (0.75 M) was then added and the reaction mixture was heated at reflux for 20 hours. The mixture was then removed from heat, brought to a pH of 3 with 3 M HCl, extracted with ethyl acetate and washed with brine. The organic layer was dried with Na₂SO₄, and the solvent was evaporated. The crude material was purified by recrystallization in Ethyl Acetate/Hexanes. **¹H NMR** (400 MHz, Acetone-*d*₆) δ 7.38 – 7.08 (m, 5H), 3.26 (s, 2H), 2.66 – 2.50 (m, 2H), 2.11 (s, 3H), 2.08 – 1.98 (m, 2H). **¹³C NMR** (101 MHz, Acetone-*d*₆) δ 206.84, 172.74, 137.27, 130.84, 129.01, 127.66, 58.21, 39.55, 39.00, 27.03.

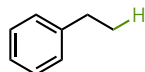
2.6.4 Monoacid Decarboxylation Procedures and Characterization Data

General Procedure for Hydrodecarboxylation of Monoacids:



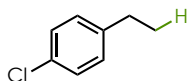
To a flame-dried one dram vial equipped with a magnetic stir bar was added the carboxylic acid substrate (1 equiv.), **Mes-Acr-Ph⁺** (5 mol%), and diphenyl disulfide (Ph₂S₂ 10 mol%). The vial was transferred into a nitrogen filled glovebox and N₂ sparged trifluoroethanol was added to achieve a concentration of 0.5 M with respect to acid substrate. *N,N*-diisopropylethylamine (*i*-Pr₂NEt, 20 mol%), was added, and the vial sealed with a Teflon coated septum screwcap. The reaction were removed from the glovebox and irradiated with two 450 nm lamps and stirred at ambient temperature from 24-96 hours. Upon completion, the solvent was removed in *vacuo* and the product was further purified by flash chromatography.

Ethylbenzene (2.1) :



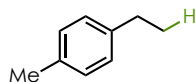
The compound was prepared according to the general procedure using 105.1 mg 3-phenylpropanoic acid (0.7 mmol), 15.4 mg diphenyl disulfide, 16.1 mg Mes-Acr-Ph⁺, 24 μ L *N,N*-diisopropylethylamine, and 1.4 mL trifluoroethanol. The mixture was allowed to react at ambient temperature under irradiation for 24 or 72 hours, at which time the reaction was washed with a solution of sodium hydroxide and extracted with DCM three times. The combined organic layer was dried over sodium sulfate. The reactions were then passed through a plug of silica into a vial containing internal standard before GC analysis.

1-Chloro-4-ethylbenzene (2.2):



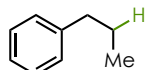
The compound was prepared according to the general procedure using 129.2 mg 3-(4-chlorophenyl)propanoic acid (0.7 mmol), 15.4 mg diphenyl disulfide, 16.1 mg Mes-Acr-Ph⁺, 24 μ L *N,N*-diisopropylethylamine, and 1.4 mL trifluoroethanol. The mixture was allowed to react at ambient temperature under irradiation for 24 hours, at which time the reaction was washed with a solution of sodium hydroxide and extracted with DCM three times. The combined organic layer was dried over sodium sulfate. The reactions were then passed through a plug of silica into a vial containing internal standard before GC analysis. **¹H NMR** (400 MHz, Chloroform-*d*) δ 7.29 – 7.21 (m, 2H), 7.16 – 7.09 (m, 2H), 2.62 (q, *J* = 7.6 Hz, 2H), 1.23 (t, *J* = 7.6 Hz, 4H), 0.89 (t, *J* = 7.0 Hz, 1H). **¹³C NMR** (101 MHz, Chloroform-*d*) δ 142.60, 131.21, 129.18, 128.33, 28.24, 15.52.

1-Ethyl-4-methylbenzene (2.3):



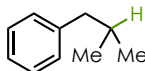
The compound was prepared according to the general procedure using 114.9 mg 3(*p*-tolyl)propanoic acid (0.7 mmol), 15.4 mg diphenyl disulfide, 16.1 mg Mes-Acr-Ph⁺, 24 μ L *N,N*-diisopropylethylamine, and 1.4 mL trifluoroethanol. The mixture was allowed to react at ambient temperature under irradiation for 24 hours, at which time the reaction was washed with a solution of sodium hydroxide and extracted with DCM three times. The combined organic layer was dried over sodium sulfate. The reactions were then passed through a plug of silica into a vial containing internal standard before GC analysis.

Propylbenzene (2.4):

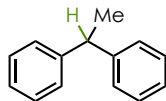


The compound was prepared according to the general procedure using , 114.9mg 2- methyl-3-phenylpropanoic acid (0.7 mmol), 15.3 mg diphenyl disulfide, 16.1 mg Mes-Acr-Ph⁺, 24 μ L *N,N*-diisopropylethylamine, and 1.4 mL trifluoroethanol. The mixture was allowed to react at ambient temperature under irradiation for 24 hours, at which time the reaction was washed with a solution of sodium hydroxide and extracted with DCM three times. The combined organic layer was dried over sodium sulfate. The reactions were then passed through a plug of silica into a vial containing internal standard before GC analysis.

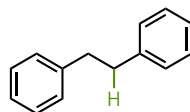
Isobutylbenzene (2.5):



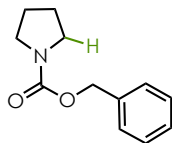
The compound was prepared according to the general procedure using 2,2- dimethyl-3-phenylpropanoic acid, 106.9mg (0.6 mmol), 13.1mg diphenyl disulfide, 13.8mg Mes-Acr- Ph⁺, 21 μ L *N,N*-diisopropylethylamine, and 1.2 mL trifluoroethanol. The mixture was allowed to react at ambient temperature under irradiation for 24 hours, at which time the reaction was washed with a solution of sodium hydroxide and extracted with DCM three times. The combined organic layer was dried over sodium sulfate. The reactions were then passed through a plug of silica into a vial containing internal standard before GC analysis. **¹H NMR** (600 MHz, Chloroform-*d*) δ 7.33 – 7.28 (m, 5H), 7.24 – 7.21 (m, 3H), 2.47 (d, *J* = 7.2 Hz, 2H), 1.87 (dt, *J* = 13.5, 6.8 Hz, 1H), 0.90 (d, *J* = 6.6 Hz, 7H). **¹³C NMR** (151 MHz, CDCl₃) δ 129.11, 129.07, 128.05, 127.50, 127.15, 125.60, 45.47, 30.25, 22.38.

Ethane-1,1-diyl dibenzene (2.6):

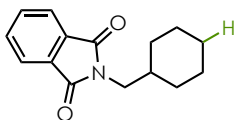
The compound was prepared according to the general procedure using 135.8mg 2,2-diphenylpropanoic acid (0.6 mmol), 13.1mg diphenyl disulfide, 13.8 mg Mes-Acr-Ph⁺, 21μL *N,N*-diisopropylethylamine, and 1.2 mL trifluoroethanol. The mixture was allowed to react at ambient temperature under irradiation for 24 hours, at which time the reaction mixture was diluted with dichloromethane, washed with 10% NaOH (aq), extracted with dichloromethane and dried over Na₂SO₄. The solvent was evaporated under reduced pressure and the crude residue was purified via silica column chromatography (pentanes). The product was isolated as a clear oil (83%). Analytical data were in agreement with literature values.¹¹⁹ **¹H NMR** (400 MHz, Chloroform-*d*) δ 7.38-7.22 (m, 9H), 7.22-7.16 (m, 1H), 4.18 (q, *J* = 7.2 Hz, 1H), 1.67 (d, *J* = 7.2 Hz, 3H). **¹³C NMR** (151 MHz, Chloroform-*d*) δ 146.38, 128.38, 127.65, 126.04, 44.80, 21.89.

1,2-diphenylethane (2.7):

The compound was prepared according to the general procedure using 135.8mg 2,3-diphenylpropanoic acid (0.6 mmol), 13.1mg diphenyl disulfide, 13.8 mg Mes-Acr-Ph⁺, 21μL *N,N*-diisopropylethylamine, and 1.2 mL trifluoroethanol. The mixture was allowed to react at ambient temperature under irradiation for 24 hours, at which time solvent was evaporated under reduced pressure and the crude residue was purified via silica column chromatography (pentanes). The product was isolated as a white solid (84%). Analytical data were in agreement with literature values.¹²⁰ **¹H NMR** (600 MHz, Chloroform-*d*) δ 7.32 – 7.23 (m, 5H), 7.22 – 7.15 (m, 5H), 2.93 (s, 4H). **¹³C NMR** (151 MHz, Chloroform-*d*) δ 141.77, 128.43, 128.31, 125.89, 37.94.

Benzyl pyrrolidine-1-carboxylate (2.8):

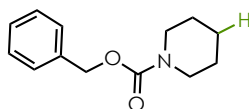
The compound was prepared according to the general procedure using 124.6 mg Z-L-proline (0.5 mmol), 11 mg diphenyl disulfide, 11.5 mg Mes-Acr-Ph⁺, 17.2 μ L *N,N*-diisopropylethylamine, and 1.0 mL trifluoroethanol. The mixture was allowed to react at ambient temperature under irradiation for 48 hours, at which time the reaction mixture was diluted with dichloromethane, washed with 10% NaOH (aq), extracted with dichloromethane and dried over Na₂SO₄. The solvent was evaporated under reduced pressure and the crude residue was purified via silica column chromatography (3% Acetone in Hexanes). The product was isolated as a white solid 88 mg (92%). Analytical data were in agreement with literature values.¹²¹ **¹H NMR** (400 MHz, Chloroform-*d*) δ 7.40 – 7.25 (m, 5H), 5.13 (s, 2H), 3.39 (dt, *J* = 13.6, 6.3 Hz, 4H), 1.85 (pd, *J* = 7.6, 4.8 Hz, 4H). **¹³C NMR** (101 MHz, CDCl₃) δ 154.78, 136.97, 128.21, 127.69, 127.67, 66.42, 46.09, 45.65, 25.59, 24.81.

2-(cyclohexylmethyl)isoindoline-1,3-dione (2.9):

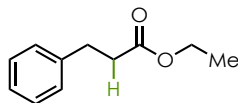
The compound was prepared according to the general procedure using 143.7mg trans-4-((1,3-dioxisoindolin-2-yl)methyl)cyclohexane-1-carboxylic acid (0.5 mmol), 11mg diphenyl disulfide, 11.5mg Mes-Acr-Ph⁺, 17.2 μ L *N,N*-diisopropylethylamine, and 1mL trifluoroethanol. The mixture was allowed to react at ambient temperature under irradiation for 48 hours, at which time the reaction was diluted with DCM and washed with 10% sodium hydroxide solution. The aqueous layer was washed with DCM three times. The combined organic layers were washed with brine

and dried over sodium sulfate. The reaction was purified by column chromatography using Acetone/hexanes (3% Acetone) as eluent to give the product as a white solid (68%). Analytical data were in agreement with literature values.¹²² **1H NMR** (400 MHz, Chloroform-*d*) δ 7.80 (dp, J = 7.2, 4.3 Hz, 2H), 7.67 (dp, J = 6.9, 4.2 Hz, 2H), 3.49 (d, J = 7.3 Hz, 2H), 1.77 (dtt, J = 10.9, 7.3, 3.4 Hz, 1H), 1.71-1.54 (m, 5H), 1.27-1.07 (m, 4H), 0.98 (tt, J = 11.8, 8.4, 6.5 Hz, 2H). **13C NMR** (101 MHz, Chloroform-*d*) δ 168.52 , 133.71 , 131.98 , 123.03 , 44.00 , 36.89 , 30.66 , 26.15 , 25.56 .

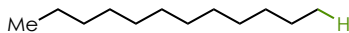
Benzyl piperidine-1-carboxylate (2.10):



The compound was prepared according to the general procedure using 131.6 mg 1-((benzyloxy)carbonyl)piperidine-4-carboxylic acid, 11 mg diphenyl disulfide, 11.5 mg Mes-Acr-Ph+, 17.2 μ L *N,N*-diisopropylethylamine, and 1.6mL 4:1 trifluoroethanol:EtOAc [0.3M]. The mixture was allowed to react at ambient temperature under irradiation for 48 hours, at which time the solvent was evaporated and the reaction was purified by column chromatography (3% Acetone in Hexanes). The yield was 65.7 mg (61%). **1H NMR** (400 MHz, CDCl₃) δ 7.33 (dd, J = 20,7, 4.4 Hz, 5H), 5.13 (s, 2H), 3.45 (t, J = 5.4 Hz, 4H), 1.68-1.44 (m, 6H). **13C NMR** (101 MHz, CDCl₃) δ 155.21, 136.91, 128.33, 127.76, 127.67, 66.77, 44.75, 25.58, 24.26.

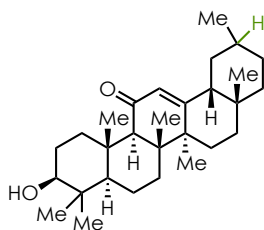
Ethyl 3-phenylpropanoate (2.11):

The compound was prepared according to the general procedure using 166.7 mg 2-benzyl-3-ethoxy-3-oxopropanoic acid, 16.4 mg diphenyl disulfide, 17 mg Mes-Acr-Ph⁺, 26 μ L *N,N*-diisopropylethylamine, and 1.5 mL trifluoroethanol. The mixture was allowed to react at ambient temperature under irradiation for 48 hours, at which time the solvent was evaporated and the reaction was purified by column chromatography (2% Acetone in Hexanes). The yield was 103 mg (77%). **¹H NMR** (400 MHz, Chloroform-*d*) δ 7.29 (t, J = 7.5 Hz, 2H), 7.25 – 7.16 (m, 3H), 4.13 (q, J = 7.1 Hz, 2H), 2.96 (t, J = 7.9 Hz, 2H), 2.63 (t, J = 7.8 Hz, 2H), 1.24 (t, J = 7.1 Hz, 3H). **¹³C NMR** (151 MHz, CDCl₃) δ 173.05, 140.68, 128.59, 128.42, 126.34, 77.37, 77.31, 77.16, 77.04, 76.95, 60.55, 36.08, 31.09, 14.34.

Dodecane (2.12):

The compound was prepared according to the general procedure using 129 mg tridecanoic acid, 26.4 mg diphenyl disulfide, 13.8 mg Mes-Acr-Ph⁺, 21 μ L *N,N*-diisopropylethylamine, 2.0 mL 4:1 TFE:EtOAc [0.3M]. The mixture was allowed to react at ambient temperature under irradiation for 48 hours, at which time the reaction mixture was passed through a plug of silica into a vial containing internal standard before GC/MS analysis. The yield was 51%.

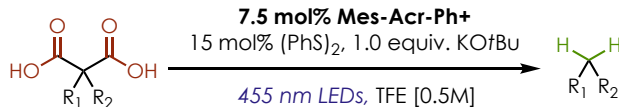
(4a*R*,6a*S*,6b*R*,8a*R*,10*S*,12a*S*,12b*R*,14b*R*)-10-hydroxy-2,4a,6a,6b,9,9,12a-heptamethyl-1,3,4,4a,5,6,6a,6b,7,8,8a,9,10,11,12,12a,12b,14b-octadecahydripicen-13(2*H*)-one (2.13):



The compound was prepared according to the general procedure using 141.2mg Enoxolone (0.3 mmol), 6.6mg diphenyl disulfide, 6.9mg Mes-Acr-Ph⁺, 10.5μL *N,N*-diisopropylethylamine, and 1 mL 4:1 TFE:EtOAc [0.3M]. The mixture was allowed to react at ambient temperature under irradiation for 24 hours, at which time the solvent was evaporated and the reaction was purified by column chromatography using EtOAc/hexanes (20% EtOAc) as eluent. The product was isolated as a white solid (83%) as a mixture of diastereomers (3:1). **¹H NMR Mixture:** ¹H NMR (400 MHz, Chloroform-*d*) δ 5.59 (d, *J* = 7.1 Hz, 1H), 3.22 (d, *J* = 8.8 Hz, 1H), 2.79 (dq, *J* = 13.5, 3.3 Hz, 1H), 2.34 (s, 1H), 2.17 (s, 1H), 2.01 (ddd, *J* = 16.9, 8.8, 3.2 Hz, 3H), 1.89 – 1.75 (m, 1H), 1.72 – 1.53 (m, 5H), 1.52 – 1.37 (m, 5H), 1.36 (d, *J* = 1.9 Hz, 3H), 1.33 – 1.21 (m, 3H), 1.19 (d, *J* = 4.4 Hz, 1H), 1.14 (d, *J* = 1.8 Hz, 6H), 1.00 (d, *J* = 1.2 Hz, 3H), 0.97 (dd, *J* = 7.3, 2.7 Hz, 2H), 0.88 (d, *J* = 6.3 Hz, 2H), 0.84 (d, *J* = 4.5 Hz, 3H), 0.81 (s, 3H), 0.70 (dd, *J* = 11.6, 1.9 Hz, 1H).

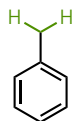
¹³C NMR Mixture (151 MHz, Chloroform-*d*) δ 200.38, 170.40, 127.99, 127.97, 78.78, 61.76, 61.25, 54.94, 54.92, 51.69, 45.44, 45.39, 45.36, 43.39, 43.33, 41.38, 40.82, 39.13, 37.74, 37.06, 34.29, 33.35, 32.81, 32.76, 32.40, 30.61, 28.93, 28.72, 28.09, 27.62, 27.32, 26.77, 26.64, 26.62, 26.50, 26.43, 23.33, 22.37, 18.70, 18.67, 17.49, 16.90, 16.37, 15.56. **Calculated** *m/z* for [M+H]⁺ = 427.36, [M+K]⁺=465.56. **Experimental** *m/z* for [M+H]⁺ = 427.56, [M+K]⁺=465.45 **IR** (Thin Film, cm⁻¹): 3053, 2951, 2867, 2359, 2306, 1652, 1265, 1208

2.6.5 Malonic acid derivative Decarboxylation Procedures and Characterization Data



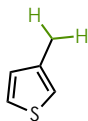
Potassium *tert*-butoxide (1 equiv) and the malonic acid (1 equiv) were dissolved in N₂ sparged trifluoroethanol (0.5M), under an N₂ atmosphere. This solution was transferred to a 2 dram vial equipped with a stir bar, diphenyl disulfide (15 mol%), and **Mes-Acr-Ph** (7.5 mol%). The vials were fitted with a Teflon screw cap and allowed to react under blue light irradiation for 24-72 hours at ambient temperature.

Toluene (2.14):



The compound was prepared according to the general procedure using 126.1 mg phenylmalonic acid (0.7 mmol), 79 mg of KOtBu, 23.1 mg diphenyl disulfide, 24.2 mg Mes-Acr-Ph⁺, and 1.4 mL TFE. The mixture was allowed to react at ambient temperature under irradiation for 24 hours, at which time the reaction was washed with a solution of sodium hydroxide and extracted with DCM three times. The organic layer was dried over sodium sulfate. The reactions were then passed through a plug of silica into a vial containing internal standard before GC analysis.

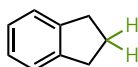
3-methylthiophene (2.15):



The compound was prepared according to the general procedure using 130.3 mg 2-(thiophen-3-yl)malonic acid (0.7 mmol), 79 mg of KOtBu, 23.1 mg diphenyl disulfide, 24.2 mg Mes-Acr-Ph⁺, and 1.4 mL TFE. The mixture was allowed to react at ambient temperature under irradiation for

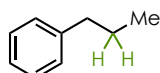
24 hours, at which time the reaction was washed with a solution of sodium hydroxide and extracted with DCM three times. The organic layer was dried over sodium sulfate. The reactions were then passed through a plug of silica into a vial containing internal standard before GC analysis.

2,3-dihydro-1*H*-indene (2.16):

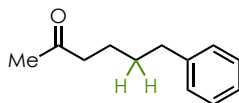


The compound was prepared according to the general procedure using 144.3 mg 1,3-dihydro-2*H*-indene-2,2-dicarboxylic acid (0.7 mmol), 22.9 mg diphenyl disulfide, 24.2 mg Mes- Acr-Ph⁺, and 1.4 mL of 0.57M solution KOH in TFE. The mixture was allowed to react at ambient temperature under irradiation for 72 hours, at which time the reaction was washed with a solution of sodium hydroxide and extracted with DCM three times. The organic layer was dried over sodium sulfate. The reactions were then passed through a plug of silica into a vial containing internal standard before GC analysis.

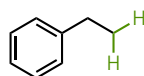
Propylbenzene (2.17):



The compound was prepared according to the general procedure using 145.7 mg 2- benzyl-2-methylmalonic acid, 23.1 mg diphenyl disulfide, 24.2 mg Mes-Acr-Ph⁺, 79 mg KO^tBu, and 1.4 mL trifluoroethanol. The mixture was allowed to react at ambient temperature under irradiation for 72 hours, at which time the reaction was washed with a 10% sodium hydroxide solution and extracted with dichloromethane. The organic layer was dried over sodium sulfate. The solution was then passed over a short plug of silica into a vial containing internal standard before GC analysis.

6-phenylhexan-2-one (2.18):

The compound was prepared according to the general procedure using 185 mg 2-benzyl-2-(3-oxobutyl)malonic acid, 79 mg KO^tBu, 24.2 mg Mes-Acr-Ph⁺, 23.1 mg diphenyl disulfide, and 1.4 mL trifluoroethanol. The reaction was allowed to react for 72 hours, upon which time the solvent was evaporated. The product was purified via column chromatography (3% acetone in hexanes). The yield was 57.7 mg (48%). **¹H NMR** (400 MHz, CDCl₃) δ 7.28 (dd, *J* = 8.5, 6.7 Hz, 2H), 7.18 (dd, *J* = 7.8, 5.6 Hz, 3H), 2.73 – 2.51 (m, 2H), 2.52 – 2.35 (m, 2H), 2.12 (s, 3H), 1.62 (p, *J* = 3.5 Hz, 4H). **¹³C NMR** (101 MHz, CDCl₃) δ 208.88, 142.09, 128.29, 128.22, 125.67, 43.47, 35.64, 30.86, 29.81, 23.37.

Ethylbenzene (2.19):

The compound was prepared according to the general procedure using 136.0 mg benzylmalonic acid (0.7 mmol), 79 mg of KO^tBu 23.1 mg diphenyl disulfide, 24.2 mg Mes-Acr-Ph⁺, and 1.4 mL TFE. The mixture was allowed to react at ambient temperature under irradiation for 72 hours, at which time the reaction was washed with a solution of sodium hydroxide and extracted with DCM three times. The organic layer was dried over sodium sulfate. The reactions were then passed through a plug of silica into a vial containing internal standard before GC analysis.

2.6.6 Electrochemical Measurements

Cyclic Voltammetry was performed using a Pine Instruments Wavenow potentiostat using a glassy carbon working electrode, Ag/AgCl in 3M NaCl reference electrode, and a platinum counter electrode. Measurements were taken by dissolving 0.05 mmols of sample in about 5 mL of a 0.1

M tetrabutylammonium hexafluorophosphate (TBAPF₆) solution in acetonitrile. The potential range scanned was typically 0.5 V and 2.5 V at a 100 mV/s. The potential range scanned for hydrocinnamic acid was between 0.5 V and 3.0 V. A background of the electrolyte solution was subtracted from each voltammogram. $E_{p/2}$ is given as the half-wave potential for irreversible oxidation, where the current is equal to one-half the peak current of the oxidation event. Carboxylate salts were made by reaction of the corresponding acid with 1 equivalent of TBA hydroxide in a solution of methanol. The solvent was then evaporated in *vacuo*. CV measurements were immediately taken once the salts were determined to be free of solvent. The oxidation potentials were based on the first oxidation wave a half peak potential and range from 1.25-1.31V vs SCE as seen below in Figure 2.28.

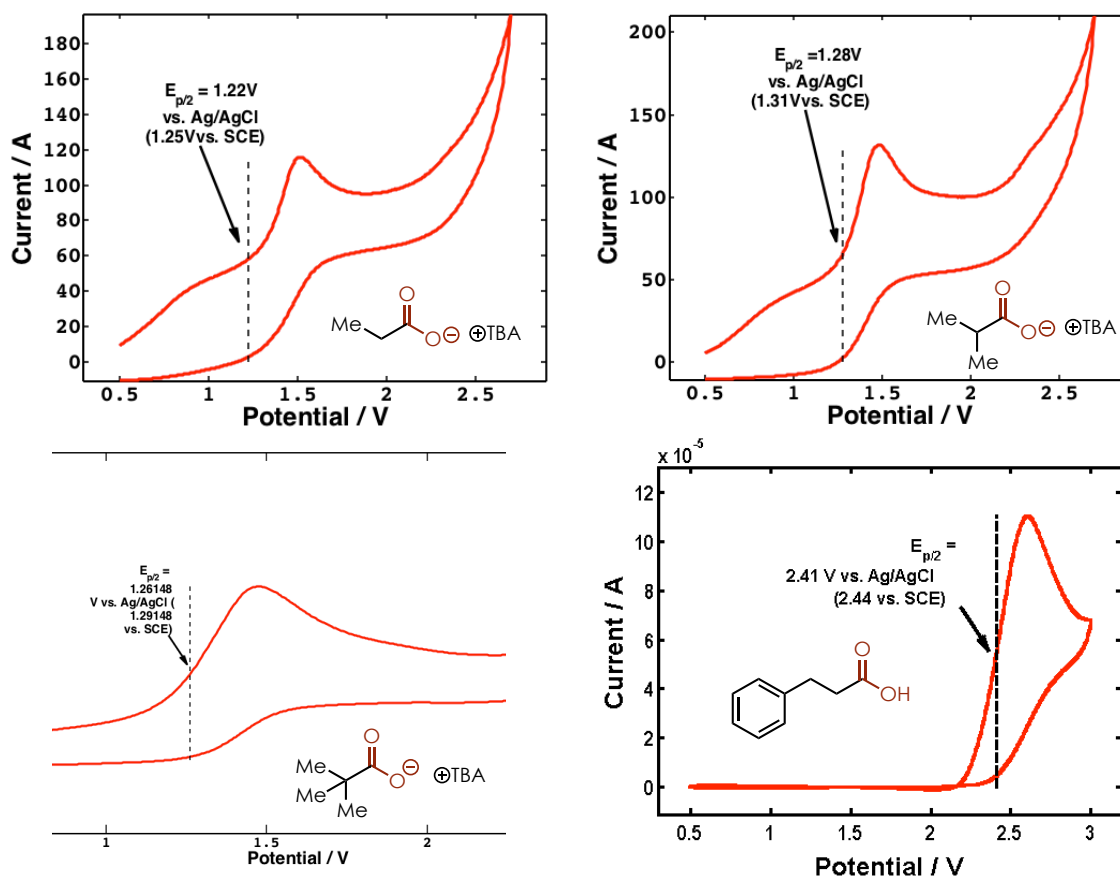


Figure 2.28: Cyclic voltammograms for (top left) TBA propanoate (top right) TBA isobutyrate (bottom left) TBA pivalate and (bottom right) hydrocinnamic acid

2.6.7 Procedures for Collecting Kinetic Data and Raw Initial Rates Data

Table 2.6: Initial rate data for hydrodecarboxylation at various initial carboxylate and catalyst concentrations

Entry	mmol Substrate	mmols <i>i</i> -Pr ₂ NEt	mmol Mes-Acr-Ph ⁺	Initial Rate (s ⁻¹)
1	0.75	0.15	0.038	7.53×10^{-6} ^{xv}
2	0.75	0.15	0.019	5.40×10^{-6}
3	0.75	0.15	0.0094	4.83×10^{-6}
4	0.375	0.075	0.038	3.30×10^{-6}
5	0.188	0.0376	0.038	1.60×10^{-6}
6 ^{xvi}	0.75	0.15	0.038	2.32×10^{-6}

Solid reagents 1,1 dimethyl 3-phenyl propanoic acid (0.188-0.75 mmols), diphenyl disulfide (0.075 mmols), and Mes-Acr-Ph⁺ catalyst (0.0094-0.038 mmols) were added to a reaction vial containing a stir bar. The vial was moved into a nitrogen-filled glovebox, where TFE (1.5 mL) and Diisopropylethylamine (0.0376-0.15 mmols) were added. Methyl octanoate (0.375 mmols) was also added as an internal standard. The vial was then sealed with a Teflon coated cap and removed from the glovebox. The cap was wrapped with PTFE tape and placed under nitrogen pressure. The samples were then irradiated with two 15W PAR38 Royal Blue Aquarium LED flood lamps Model# 6851 purchased from Ecoxotic. 15μL aliquots were removed from the solution via syringe through the septum cap at specific time points. Special care was taken to make sure the samples remained in the same spot in front of the lamp in each trial, and were not removed from the light

^{xv} Based on three trials. Average deviation was $5 \times 10^{-7} \text{ s}^{-1}$

^{xvi} Reaction carried out using a single 450 nm lamp rather than two.

at any time during the experiment. Methyl octanoate was added as an internal standard because it was non-oxidizable, soluble in TFE, and could be analyzed by GC (Agilent 6850 Series II, flame ionization detector). The GC response factor was determined using authentic isobutylbenzene purchased from Sigma-Aldrich. The conditions for each trial, as well as the calculated initial rates are given in Table 2.6.

Entries 1-3 show result of variation of catalyst concentration, and entries 1, 4, and 5 show the result of varying initial carboxylate concentration. Entry 6 shows the result of using one blue LED lamp to irradiate the reaction vessel. The initial rates were plotted against the initial concentration of carboxylate revealing a straight line that intercepts the origin as shown in **Section 2.4.3.2 (Figure 2.21)**. Initial rates were also plotted against initial concentration of acridinium catalyst, revealing a straight line not intercepting at the origin. The corresponding \ln plot suggests

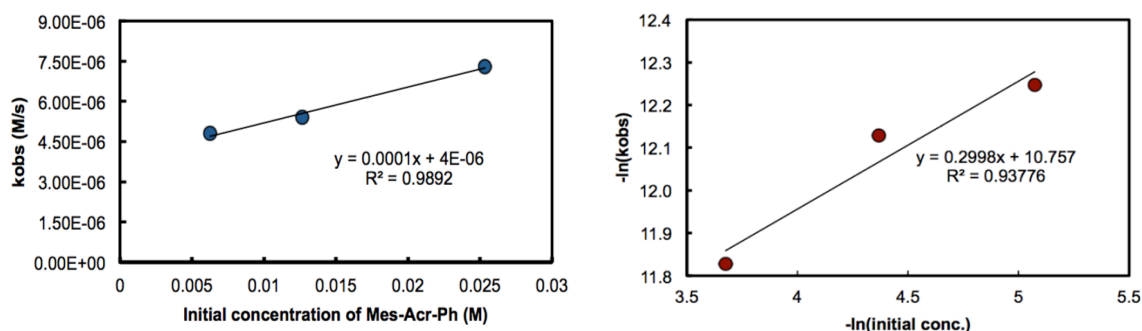


Figure 2.29: (left) Initial rate versus concentration of Mes-Acr-Ph⁺ at low concentrations (right) $-\ln$ of initial rate versus $-\ln$ of initial concentration of Mes-Acr-Ph⁺. Straight line not intercepting the origin and $-\ln$ plot suggest a fractional order with respect to the catalyst in the range between 1.25 and 5mol% catalyst loading.

a fractional order in catalyst concentration of 0.3 for low concentrations of Mes-Acr-Ph⁺, as shown in Figure 2.29.

Since other data suggested the reaction under study was light limiting, further kinetic analysis was performed to determine the order with respect to Mes-Acr-Ph⁺ at higher loadings of

the catalyst. Movement of the lamps from their original positions resulted in a change in the rate constants that were observed above. This further goes to demonstrate the light sensitivity of this reaction. Since it was difficult to replicate the exact lamp configuration used for the first kinetic studies two trials were performed, using different lamp configurations, to examine the effect of increased catalyst loading (7.5 and 10 mol% catalyst loading). The samples were irradiated with two 15W PAR38 Royal Blue Aquarium LED floodlamps Model# 6851 purchased from Ecoxotic (same as previous kinetic studies). The two lamp configurations differed only in their placement, as the lamps can be moved so that the reactions receive more or less direct irradiation.

Table 2.7: Initial rate data for high catalyst concentrations (5-10 mol%) using two different lamp configurations.

Entry	mmol Substrate	mmols <i>i</i> -Pr ₂ NEt	mmol Mes-Acr-Ph+	Initial Rate (s ⁻¹)
1	0.75	0.15	0.038	3.90×10^{-6}
2	0.75	0.15	0.056	3.80×10^{-6}
3	0.75	0.15	0.075	3.40×10^{-6}
4 ^{xvi}	0.75	0.15	0.038	9.60×10^{-6}
5 ^{xvi}	0.75	0.15	0.056	1.10×10^{-5}
6 ^{xvii}	0.75	0.15	0.075	1.00×10^{-5}

Other than lamp placement the reactions were performed exactly according to the method described above. Table 2.7 shows the results of these two trials. Entries 1-3 show the effect on the initial rate of changing catalyst loading in the range of 5-10 mol%. Entries 4-6 show rate constants obtained using a different lamp configuration. While in both cases the reaction appears to be zero order with respect to catalyst (for each lamp configuration the initial rates are within the error that

^{xvii} Using a different lamp configuration/placement.

was previously measured), dramatically different rate constants were obtained for each lamp configuration, highlighting the light sensitive nature of the reaction. A plot of measured initial

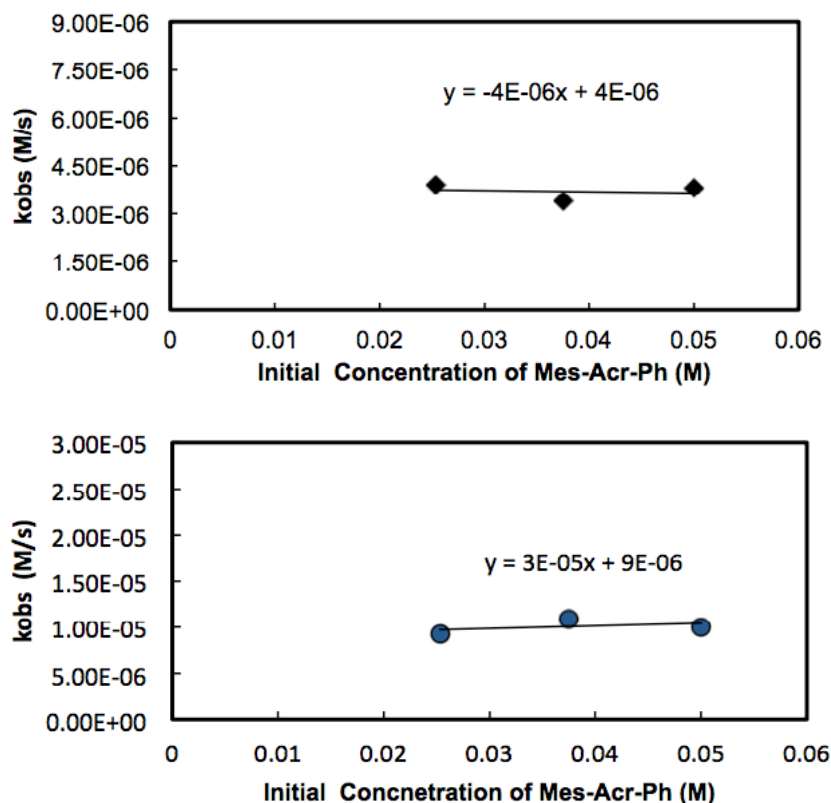
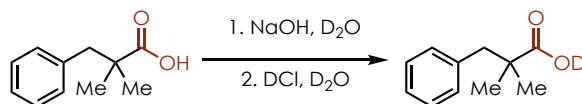


Figure 2.30: Initial rates plot for various initial concentrations of Mes-Acr-Ph⁺. The top and bottom graphs are a comparison of two different trials with different placements of the reaction vial in from of the LED lamps. Both show a zero-order dependence on Mes-Acr-Ph⁺ in this concentration range. **(top)** Corresponds to Entries 1-3 in Table 2.7. **(bottom)** corresponds to Entries 4-6 in Table 2.7.

rates shows that the reactions are close to zero order as the slopes are close to zero (Figure 2.30, top). This is also true for the second lamp configuration (Figure 2.30, bottom).

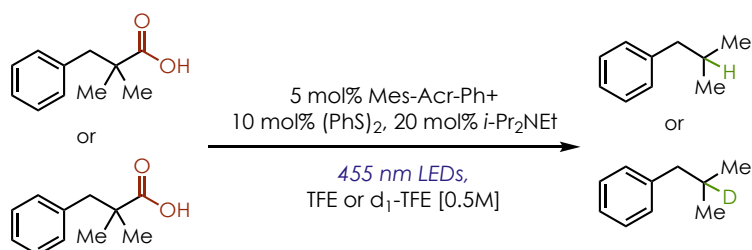
2.6.8 Kinetic Isotope Effect

2.6.8.1 Synthesis of Deuterated Carboxylic Acid



1,1 dimethyl 3-phenyl propanoic acid (2.8 mmols) was placed in an oven-dried 50 mL RBF, which was then sealed with a septum and Teflon tape. The flask was placed under nitrogen pressure, before adding 20 mL D₂O and 2.7g of a 30% w:w solution of NaOD through the septa. This was allowed to stir for about 30 minutes before slowly adding concentrated DCl through the septum until the solution reached a pH of 1. A white solid precipitated from solution, which was filtered and washed with copious amounts of D₂O. The resulting solid was dried under vacuum and stored in a desiccator until use. The incorporation of deuterium was confirmed by IR via the lack of an –OH stretch and by ¹H NMR via the reduction of the intensity of the carboxylic acid proton. NMR samples of both the proteo (for comparison) and deuterio acid were prepared using dry CDCl₃ in the glovebox, and sealed with a Teflon coated cap. A deuterium incorporation of around 80% can be estimated. Mass spectroscopy data could not be obtained due to the high rate of exchangeability of the carboxylic acid –OD bond. **¹H NMR** (400 MHz, Chloroform-*d*) δ 10.88 (s, 0.24H), 7.65 – 6.78 (m, 5H), 2.92 (s, 2H), 1.23 (s, 6H).

2.6.8.2 Procedure for Collecting KIE Data



Solid reagents 1,1 dimethyl 3-phenyl propanoic acid or 2,2-dimethyl-3-phenylpropanoic acid-*d* (0.75 mmols), diphenyl disulfide (0.075 mmols), and Mes-Acr-Ph⁺ (0.038 mmols) were added to a reaction vial containing a stir bar. The vial was moved into a nitrogen-filled glovebox, where TFE or d₁-TFE (1.5mL), Diisopropylethylamine (0.15 mmols), and methyl octanoate (0.375mmols) were added. The vial was then sealed with a Teflon coated cap and removed from the glovebox. The cap was wrapped with PTFE tape and placed under nitrogen pressure. The samples were then irradiated with two 15W PAR38 Royal Blue Aquarium LED floodlamps Model# 6851 purchased from Ecoxotic. 15μL aliquots were removed from the solution via syringe through the septum cap at specific time points. Special care was taken to make sure the samples remained in the same spot in front of the lamp in each trial, and were not removed from the light at any time during the experiment.

Table 2.8: Initial Rates of Hydrodecarboxylation of Proteo and Deutero 1,1-dimethyl propanoic acid

Entry	Initial Rate Proteo Acid (s ⁻¹)	Initial Rate Deutero Acid (s ⁻¹)	k _H /k _D
1	8.06 × 10 ⁻⁶	6.98 × 10 ⁻⁶	1.15
2	6.84 × 10 ⁻⁶	7.77 × 10 ⁻⁶	0.88
3	7.17 × 10 ⁻⁶	7.56 × 10 ⁻⁶	0.95

Methyl octanoate was added as an internal standard because it was non-oxidizable, soluble in TFE, and could be analyzed by GC (Agilent 6850 Series II, flame ionization detector). The GC response factor was determined using authentic isobutylbenzene purchased from Sigma-Aldrich. The rate data are given in Table 2.8. The kinetic isotope effect (KIE) was determined as an average of 3 trials to be 0.99 ± 0.11 .

2.6.9 UV/vis and Fluorescence Emission Details.

UV/vis analysis: UV-Vis spectra were taken on a Hewlett-Packard 8453 Chemstation spectrophotometer of both the Mes-Acr-Ph⁺ solutions as well as solutions containing only potassium hydrocinnamate (3- phenyl propanoate). To investigate the possibility of a donor-acceptor complex between the acridinium and carboxylate, six total solutions were prepared in TFE in which the total volume was 4.0 mL and the concentration of Mes-Acr-Ph was 2.5×10^{-6} M, while the concentration of potassium hydrocinnamate varied from 0 – 1.0×10^{-1} M.

Time Resolved Emission Spectra and Stern-Volmer Analysis (Time-Correlated Single Photon Counting) : Emission lifetime measurements were taken at ambient temperature using a Edinburgh FLS920 spectrometer and fit to single exponential or biexponential decay according to the methods previously described by our laboratory.⁹⁴ The fluorescence of Mes-Acr-Ph⁺ in TFE was observed as a single exponential decay, while the fluorescence of Mes-Acr- Ph⁺ in MeOH decayed by more complex kinetics and was fit to a biexponential decay model. The respective time constants and fluorescence spectra are given in Section 2.4.2.2 in Figures 2.17.

Stern-Volmer analysis on the quenching of fluorescence lifetime was carried out in TFE, where the concentration of Mes-Acr-Ph⁺ was 1.5×10^{-6} M. The quenching constant was determined with

carboxylate salt concentrations in the range of $0 - 1.0 \times 10^{-2}$ M. Bimolecular quenching constants, k_q were determined from the corresponding Stern-Volmer constant.¹²³ UV-Vis spectra of Mes-Acr-Ph⁺ were taken before and after the addition of the quencher to verify the stability of the catalyst; as shown below in Figure 2.31, at a large excess of quencher, the UV-vis spectrum is unchanged.

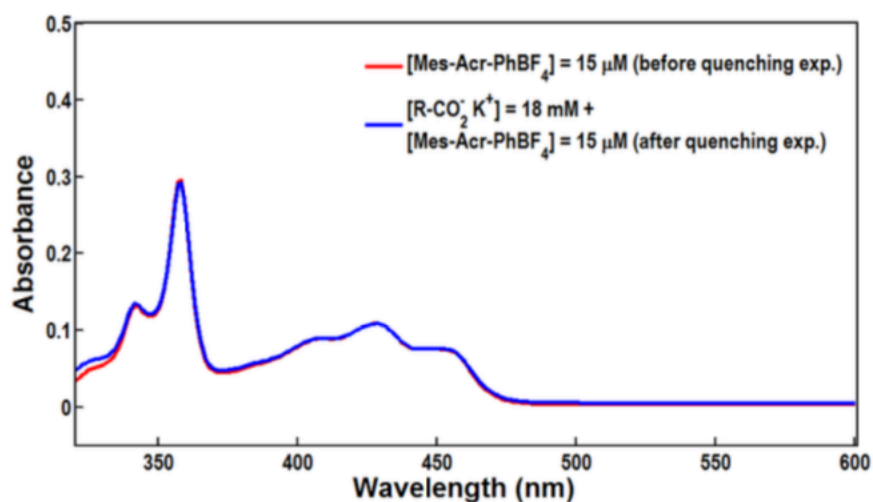


Figure 2.31: UV-Vis spectrum of Mes-Acr-Ph (15 μ M) before and after the Stern-Volmer quenching experiment. R-CO₂⁻K⁺=potassium hydrocinnamate

Steady-State Emission spectra: The fully corrected emission spectra of Mes-Acr-Ph⁺ were measured in both TFE and MeOH as previously disclosed by our laboratory and are shown in Section 2.4.2.2, Figure 2.18.⁹⁴ The maximum fluorescence intensity is 560 nm and 535 nm in MeOH and TFE, respectively. The relative fluorescence intensity was significantly greater in TFE than in MeOH, which is suggestive of competitive nonradiative decay pathways of the singlet excited state in MeOH.⁹³

2.6.10 NMR Titration Experimental Details

2.6.10.1 Synthesis of TBA hydrocinnamate:

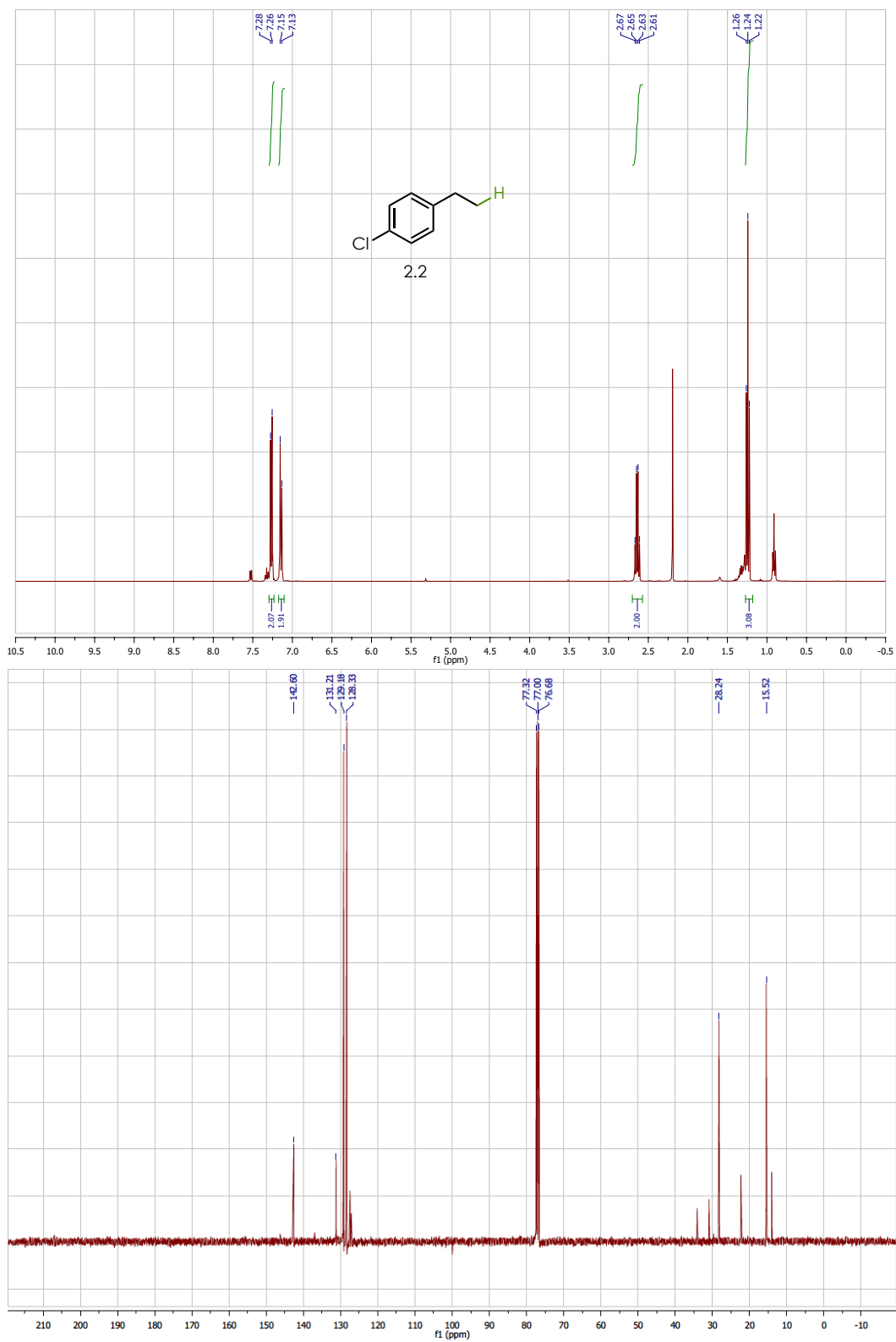
Tetrabutylammonium 3-phenyl propanoate was synthesized by reacting hydrocinnamic acid with 0.95 equivalents of tetrabutylammonium hydroxide in a solution of methanol (1M purchased from Fischer). The solvent was removed via rotovap and high vacuum and the resulting solid was washed with diethyl ether to remove the excess carboxylic acids. The resulting hygroscopic solid was dried under high vacuum and stored in a desiccator until use. ^1H NMR (600 MHz, Deuterium Oxide) δ 7.35 (ddd, J = 8.3, 7.2, 1.4 Hz, 2H), 7.32-7.28 (m, 2H), 7.28-7.22 (m, 1H), 3.20-3.09 (m, 8H), 2.88 (t, J = 7.8 Hz, 2H), 2.48 (ddd, J = 8.9, 7.2, 1.2 Hz, 2H), 1.61 (p, J = 7.8 Hz, 8H), 1.34 (h, J = 7.5 Hz, 8H), 0.93 (td, J = 7.4, 1.2 Hz, 12H).

2.6.10.2 NMR Titrations

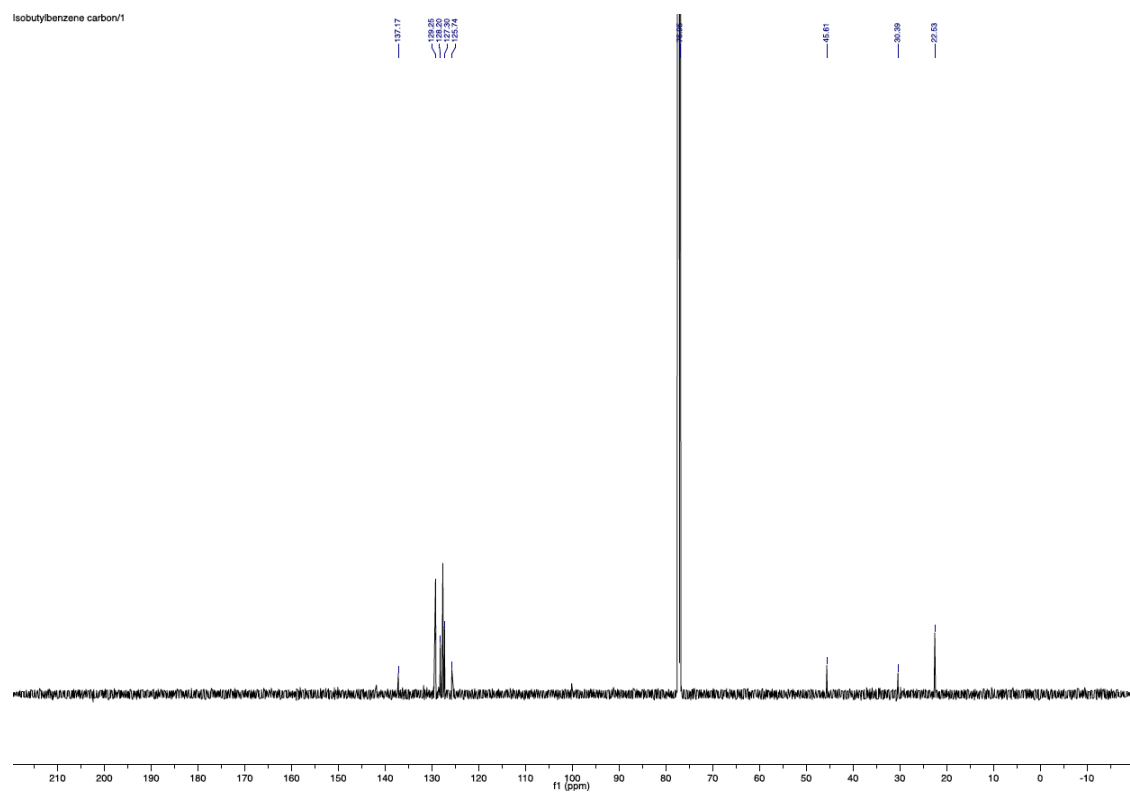
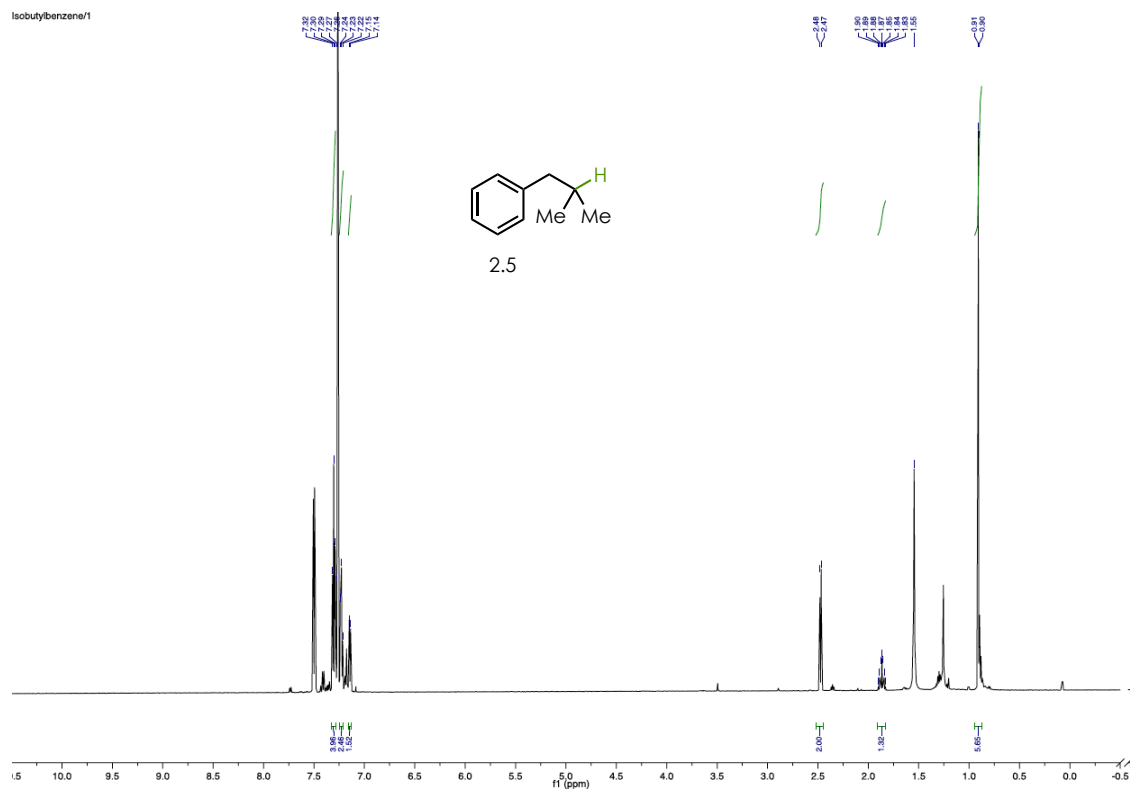
Stock solutions of Mes-Acr-Ph⁺ and tetrabutylammonium 3-phenyl propanoate were made in CD₃OD. Six solutions were made using these stock solutions where Mes-Acr-Ph⁺ was 25 mM in every case, with the concentration of TBA 3-phenyl propanoate at 0, 0.05, 0.125, 0.25, 0.375, and 0.5M in the six solutions. Additional CD₃OD was added to make each solution 0.75 mL in total volume. ^1H NMR were taken on a Bruker AVANCE III 600 CryoProbe (^1H NMR at 600 MHz). Each sample was then spiked with 20 μL of TFE before taking ^{19}F NMR on a Bruker model DRX 400 (^{19}F NMR at 376 MHz).

2.6.11 NMR Spectra:

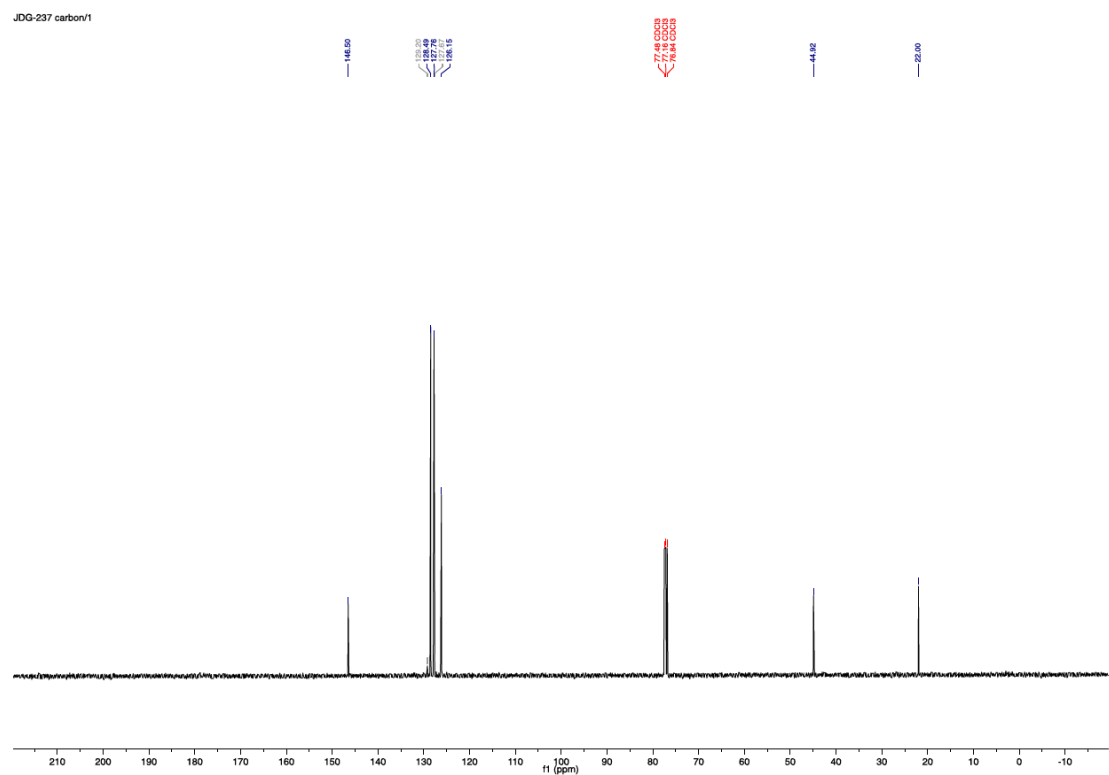
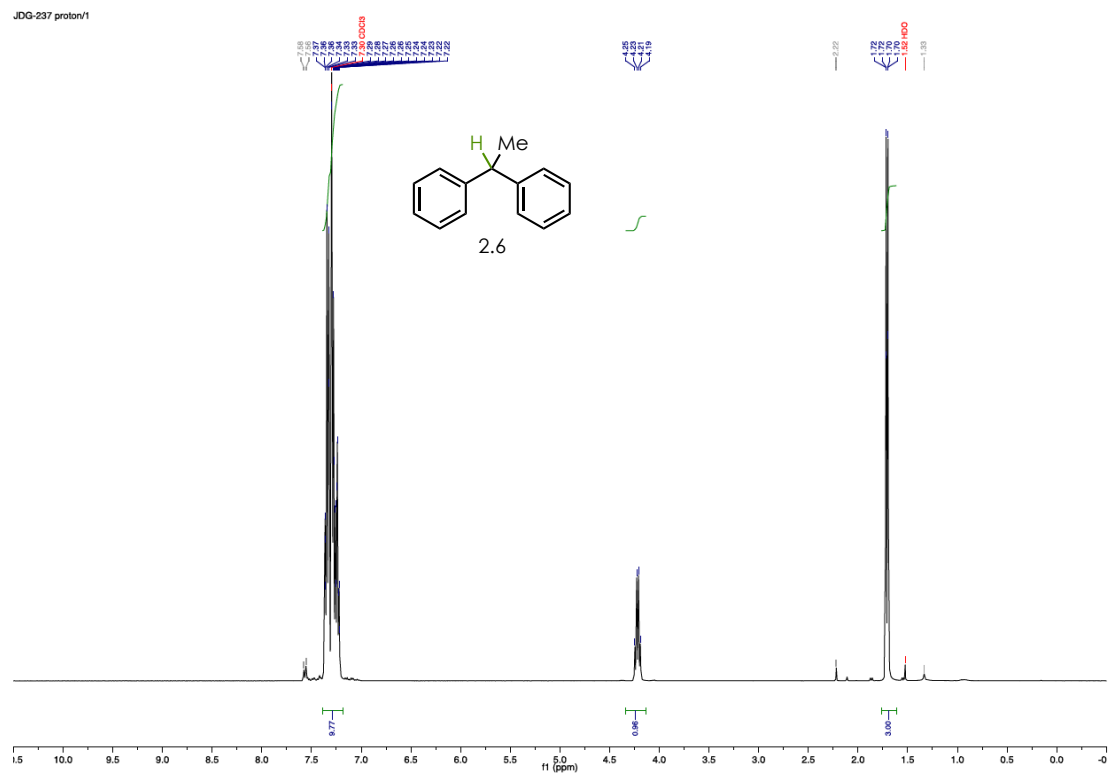
1-Chloro-4-ethylbenzene (2.2):



Isobutylbenzene (2.5):

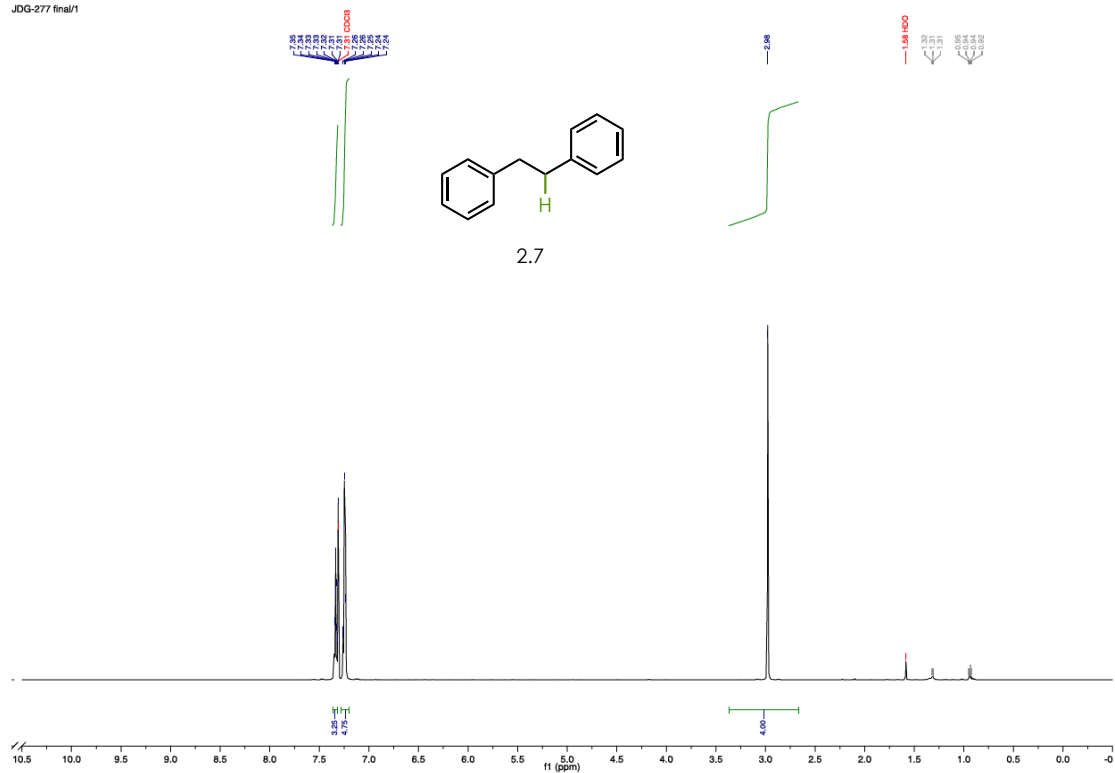


Ethane-1,1-diylidibenzene (2.6):

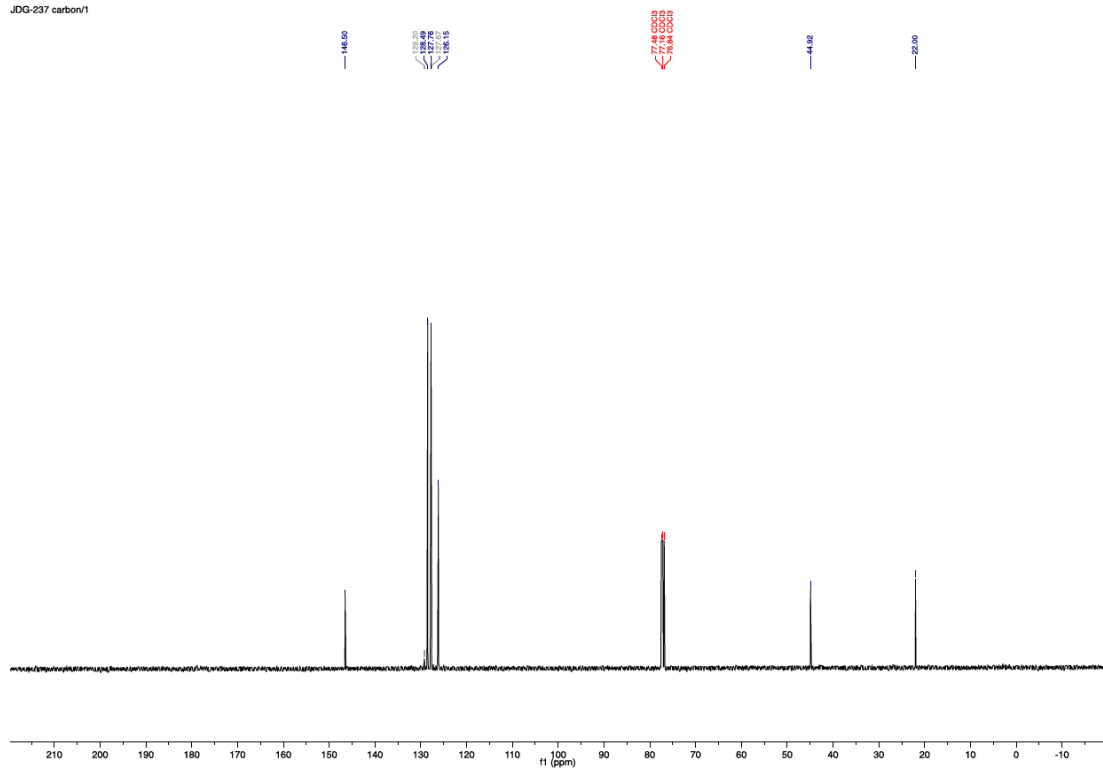


1,2-diphenylethane (2.7):

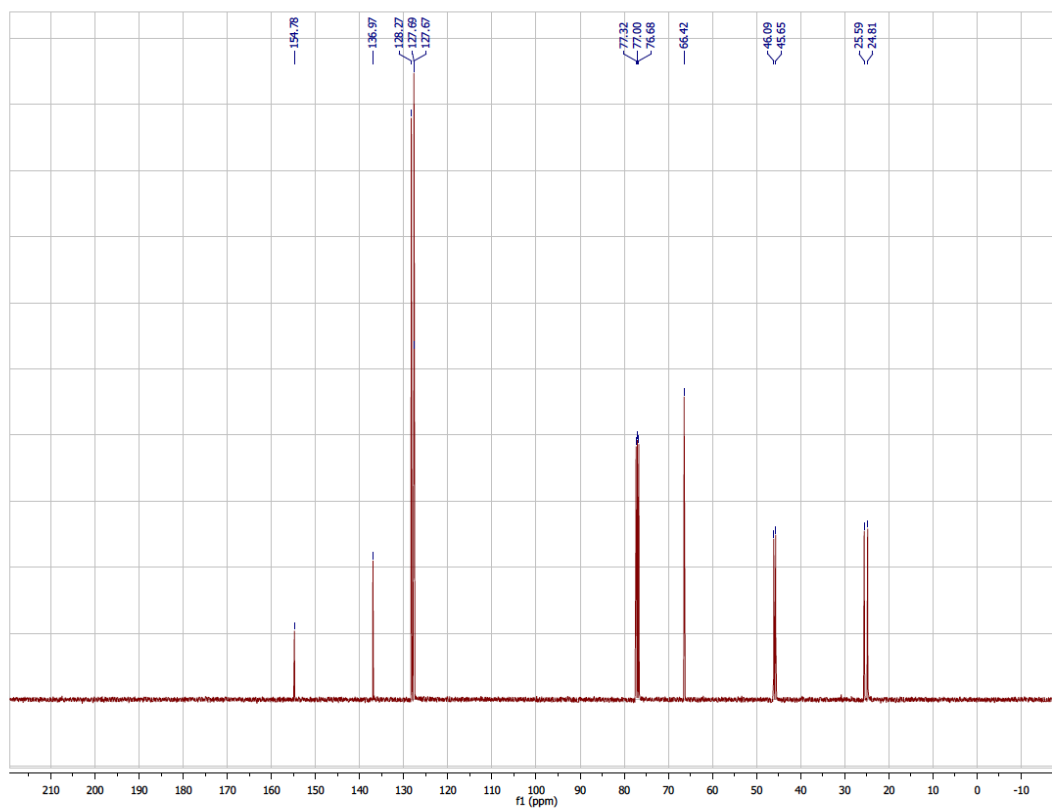
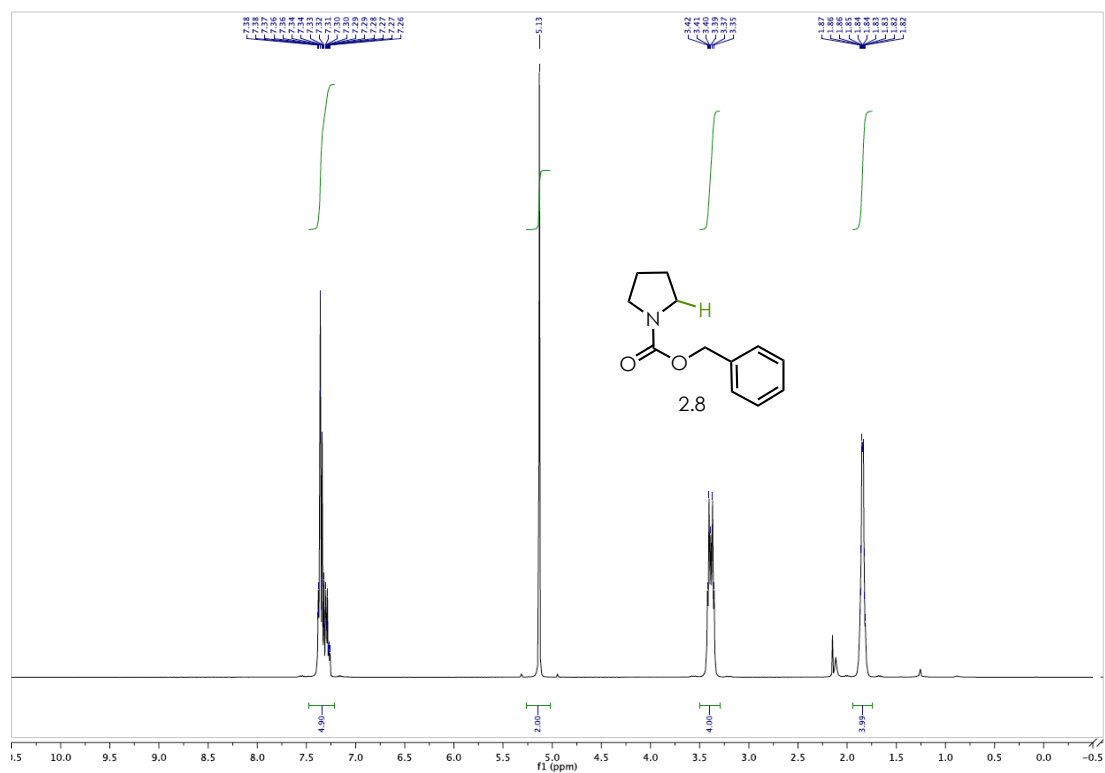
JDG-277 final/1



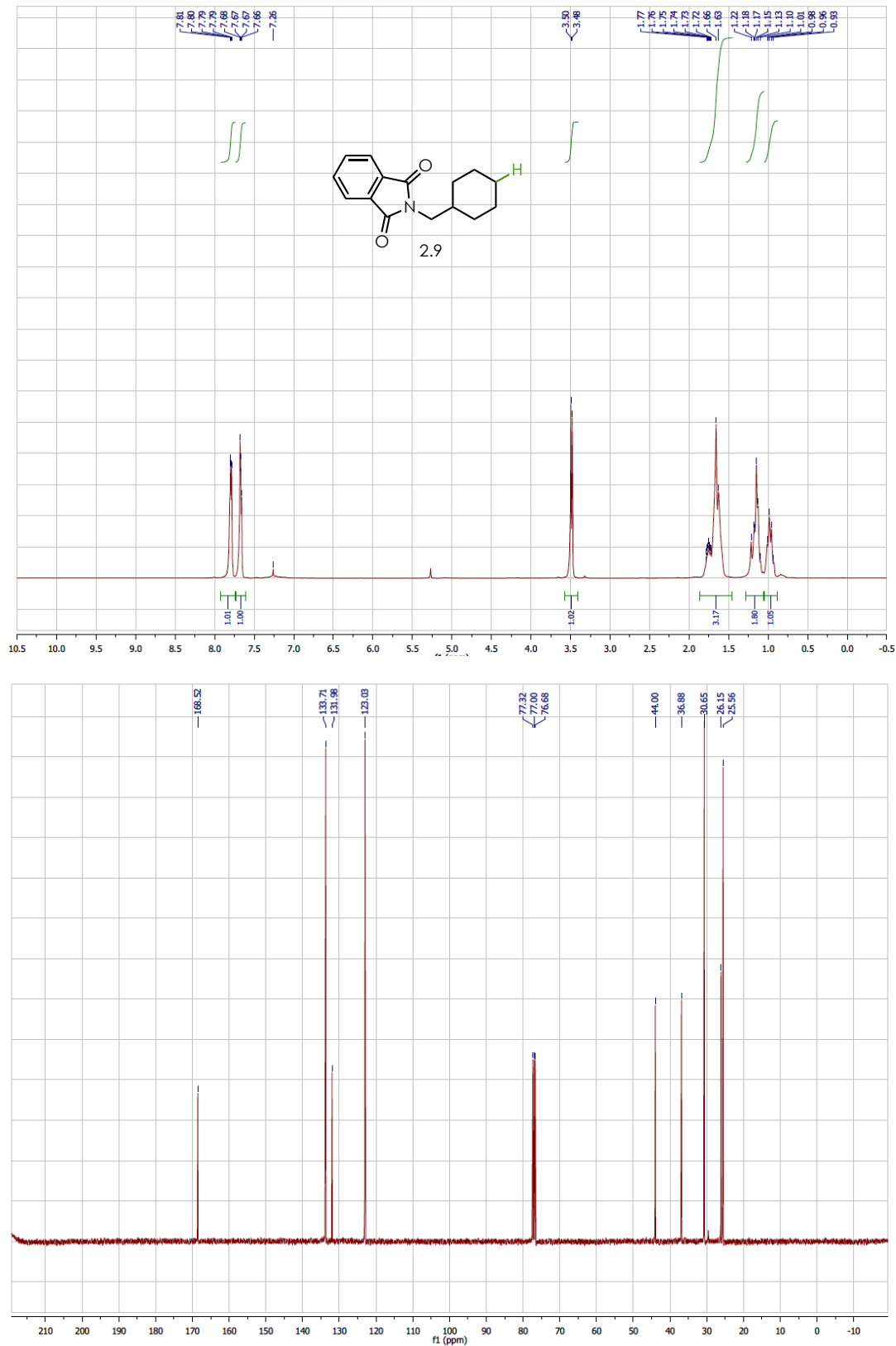
JDG-237 carbon/1



Benzyl pyrrolidine-1-carboxylate (2.8):

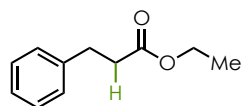


2-(cyclohexylmethyl)isoindoline -1,3-dione (2.9):

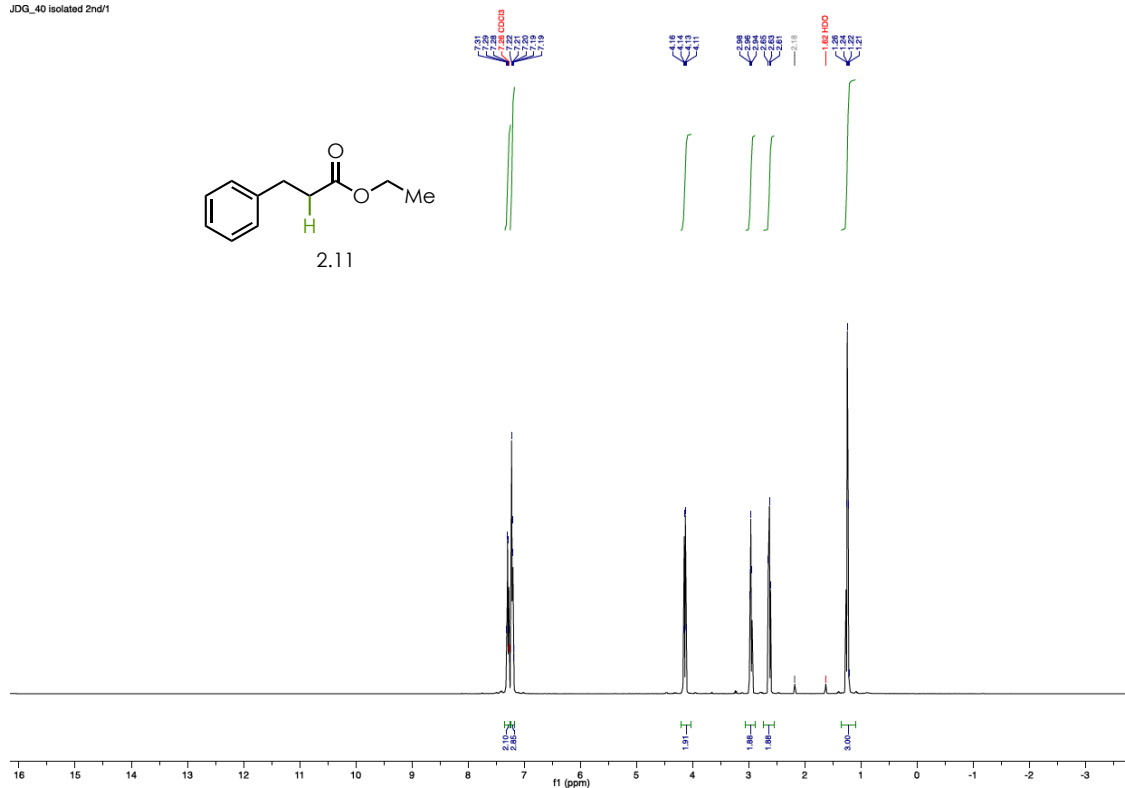


Ethyl 3-phenylpropanoate (2.11):

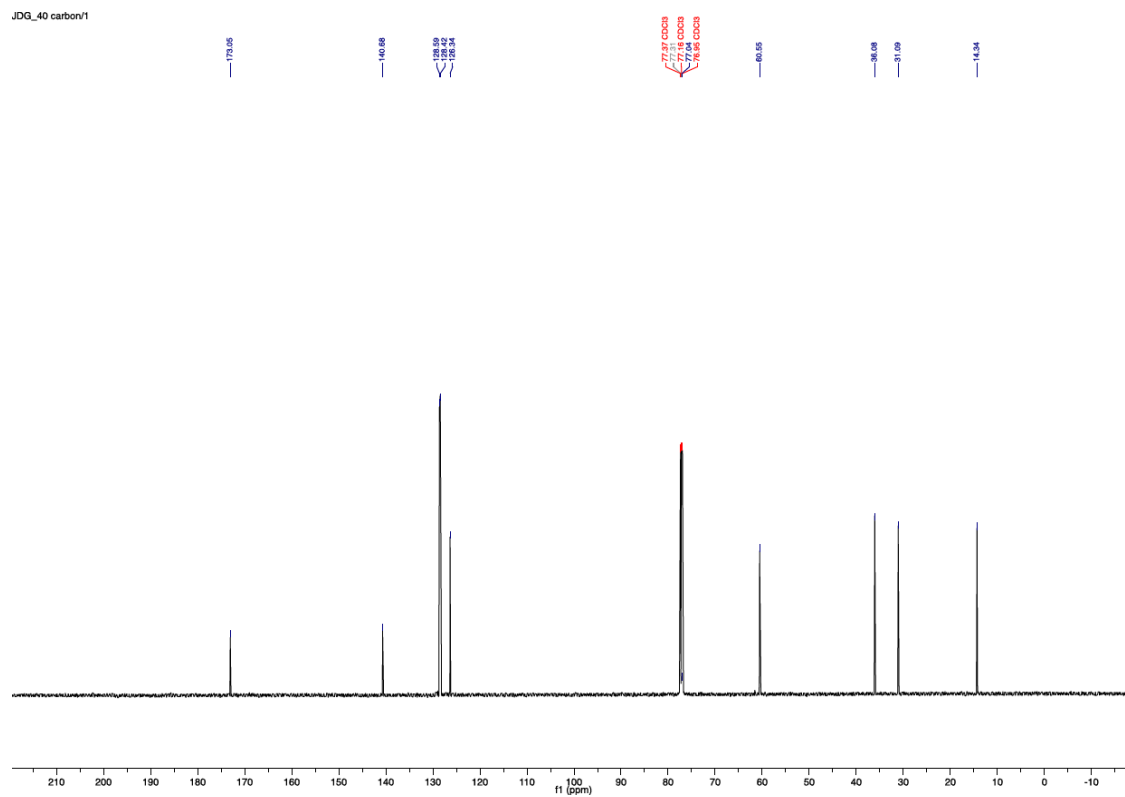
JDQ_40 isolated 2nd/1



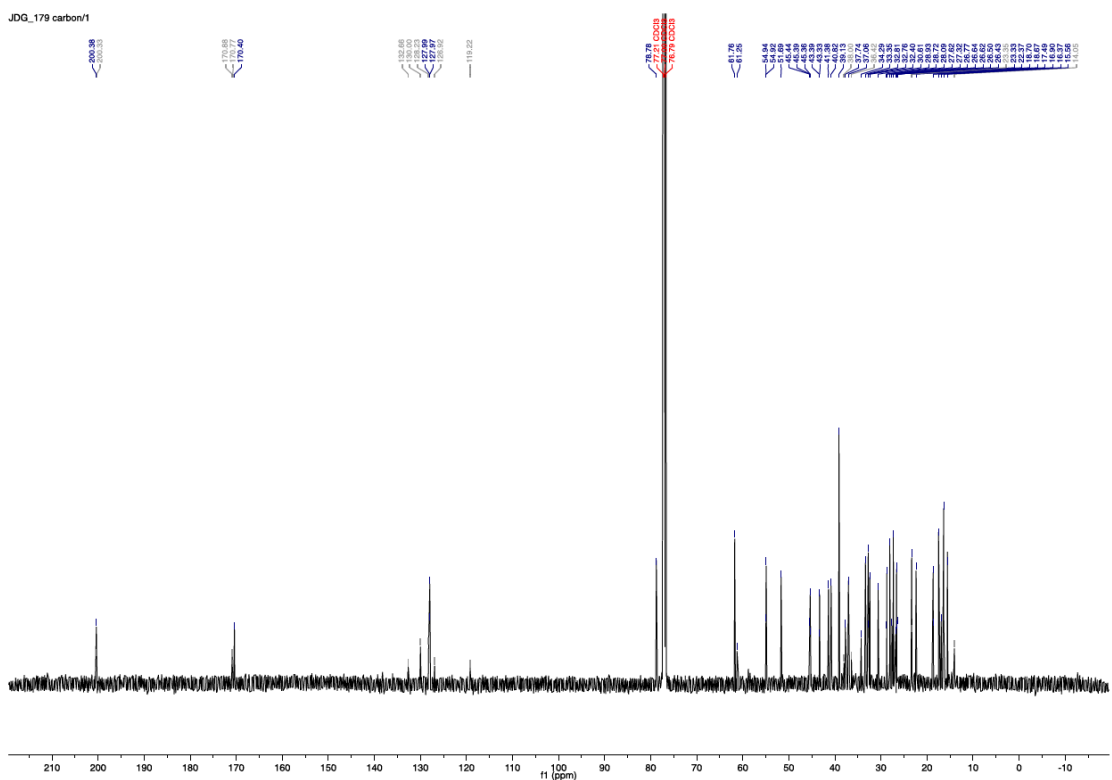
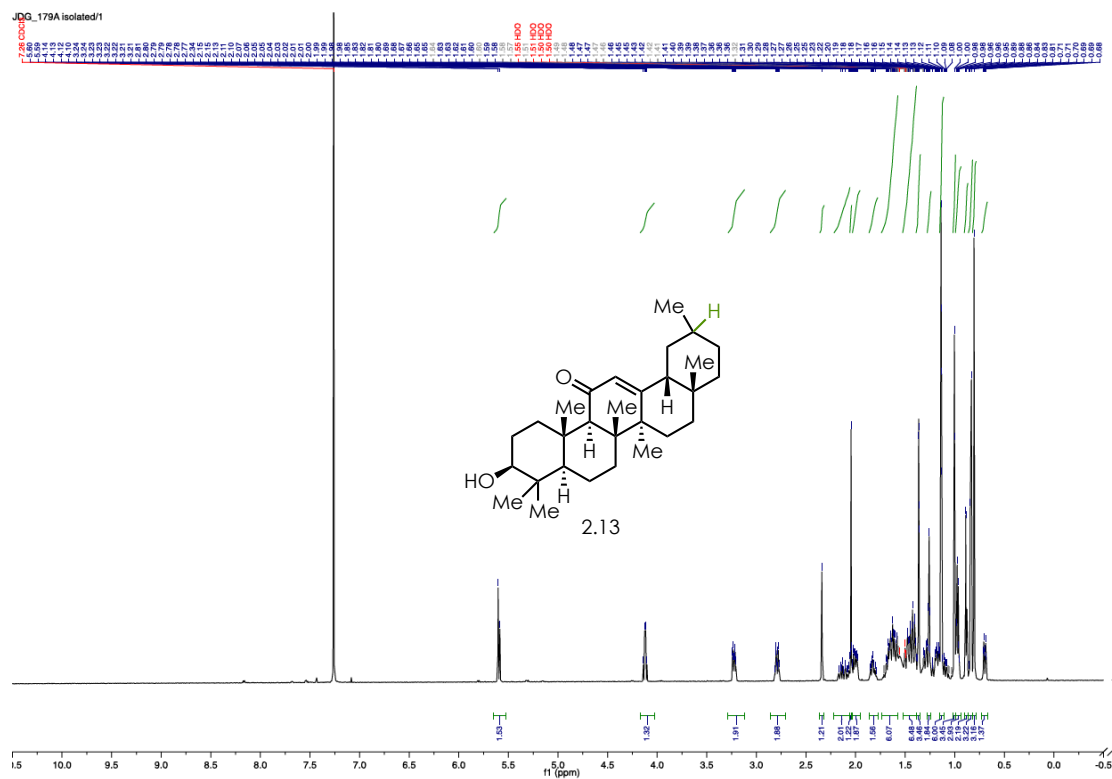
2.11



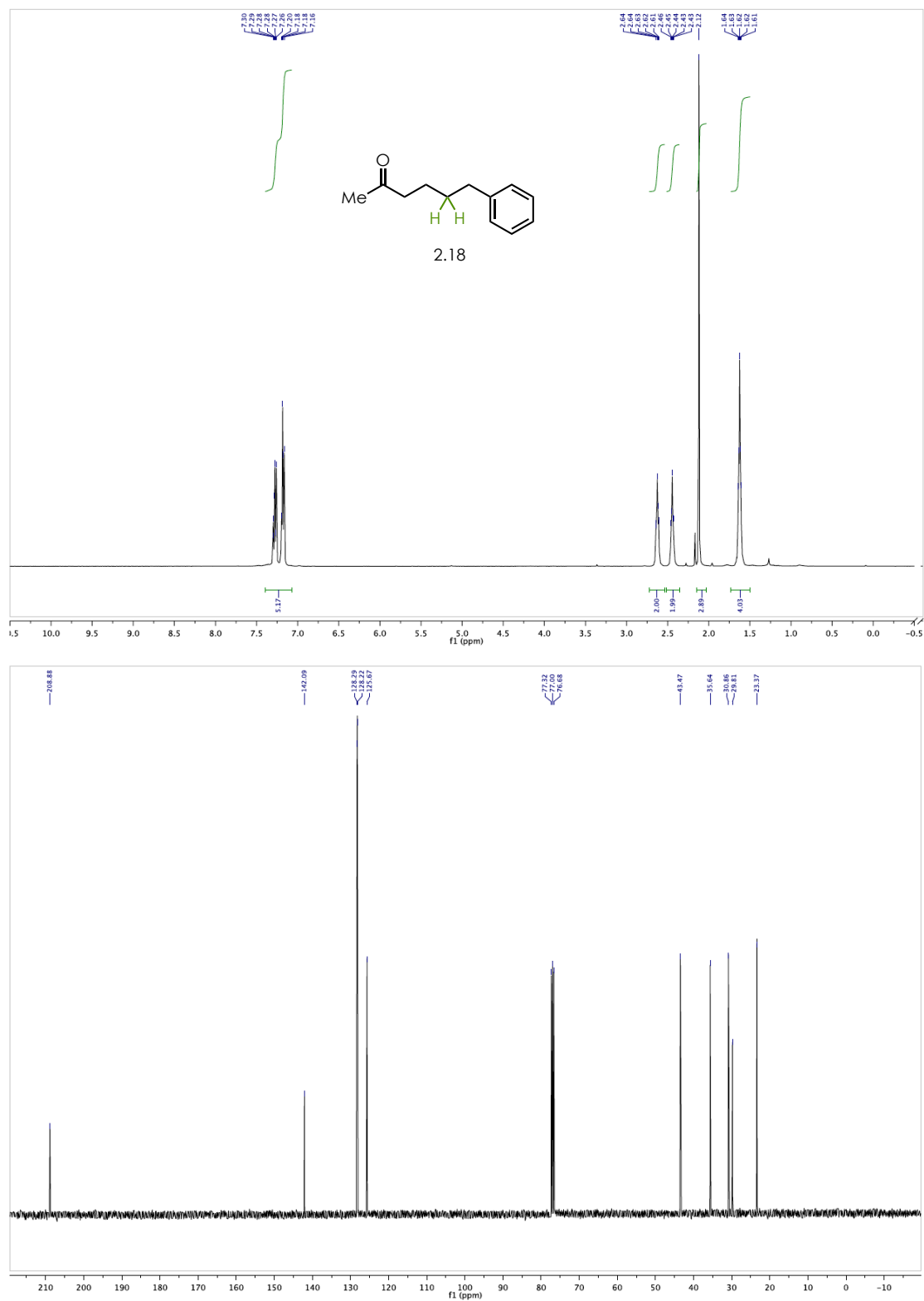
JDQ_40 carbon/1



(4*R*,6*aS*,6*bR*,8*aR*,10*S*,12*aS*,12*bR*,14*bR*)-10-hydroxy-2,4*a*,6*a*,6*b*,9,9,12*a*-heptamethyl-1,3,4,4*a*,5,6,6*a*,6*b*,7,8,8*a*,9,10,11,12,12*a*,12*b*,14*b*-octadecahydronicen-13(2*H*)-one (2.13):



6-phenylhexan-2-one (2.18):



REFERENCES

- (1) Scott, E.; Peter, F.; Sanders, J. *Appl. Microbiol. Biotechnol.* **2007**, 75 (4), 751–762.
- (2) Kakei, H.; Tsuji, R.; Ohshima, T.; Shibasaki, M. *J. Am. Chem. Soc.* **2005**, 127 (25), 8962–8963.
- (3) Kagan, H. B.; Riant, O. *Chem. Rev.* **1992**, 92 (5), 1007–1019.
- (4) Ryu, D. H.; Lee, T. W.; Corey, E. J. *J. Am. Chem. Soc.* **2002**, 124 (34), 9992–9993.
- (5) Zhang, F.-Y.; Corey, E. J. *Org. Lett.* **2000**, 2 (8), 1097–1100.
- (6) Shibasaki, M.; Sasai, H.; Arai, T. *Angew. Chemie Int. Ed. English* **1997**, 36 (12), 1236–1256.
- (7) M. Heravi, M.; Zadsirjan, V.; Farajpour, B. *RSC Adv.* **2016**, 6 (36), 30498–30551.
- (8) Oppolzer, W.; Pitteloud, R.; Bernardinelli, G.; Baettig, K. *Tetrahedron Lett.* **1983**, 24 (45), 4975–4978.
- (9) Trost, B. M.; Van Vranken, D. L. *Chem. Rev.* **1996**, 96 (1), 395–422.
- (10) Kolbe, H. Zersetzung *Ann. der Chemie und Pharm.* **1848**, 64 (3), 339–341.
- (11) Kolbe, H. Untersuchungen *Ann. der Chemie und Pharm.* **1849**, 69 (3), 257–294.
- (12) Vijh, A. K.; Conway, B. E. *Chem. Rev.* **1967**, 67 (6), 623–664.
- (13) Andrieux, C. P.; Gonzalez, F.; Savéant, J.-M. *J. Electroanal. Chem.* **2001**, 498 (1–2), 171–180.
- (14) Sharkey, W. H. Langkammerer, C. M. 2,7-Dimethyl-2,7-Dinitrooctane. *Org. Synth.* **1961**, 41, 24.
- (15) Barton, D. H. R.; Dowlatshahi, H. A.; Motherwell, W. B.; Villemin, D. *J. Chem. Soc. Chem. Commun.* **1980**, No. 15, 732–733.
- (16) Barton, D. H. R.; Crich, D.; Motherwell, W. B. *Tetrahedron Lett.* **1983**, 24 (45), 4979–4982.
- (17) Barton, D. H. R.; Crich, D.; Motherwell, W. B. *J. Chem. Soc. Chem. Commun.* **1983**, No. 17, 939–941.
- (18) Saraiva, M. F.; Couri, M. R. C.; Le Hyaric, M.; de Almeida, M. V. *Tetrahedron* **2009**, 65 (18), 3563–3572.

- (19) Ihara, M.; Suzuki, M.; Fukumoto, K.; Kametani, T.; Kabuto, C. *J. Am. Chem. Soc.* **1988**, *110* (6), 1963–1964.
- (20) Ling, T.; Poupon, E.; Rueden, E. J.; Theodorakis, E. *Org. Lett.* **2002**, *4* (5), 819–822.
- (21) Ito, H.; Takeguchi, S.; Kawagishi, T.; Iguchi, K. *Org. Lett.* **2006**, *8* (21), 4883–4885.
- (22) Xu, Z.; Hu, W.; Liu, Q.; Zhang, L.; Jia, Y. Total Synthesis of Clavicipitic Acid and Aurantioclavine: Stereochemistry of Clavicipitic Acid Revisited. *J. Org. Chem.* **2010**, *75* (22), 7626–7635.
- (23) Barton, D. H. R.; Zard, S. Z. *Pure Appl. Chem* **1986**, *58* (5), 675–684.
- (24) Fang, C.; Shanahan, C. S.; Paull, D. H.; Martin, S. F. *Angew. Chem. Int. Ed. Engl.* **2012**, *51* (42), 10596–10599.
- (25) Kazuya Yamaguchi; Yuji Kazuta; Hiroshi Abe; Akira Matsuda, A.; Shuto, S. *J. Org. Chem.* **2003**, *68* (24), 9255–9262.
- (26) Ho, J.; Zheng, J.; Meana-Pañeda, R.; Truhlar, D. G.; Ko, E. J.; Savage, G. P.; Williams, C. M.; Coote, M. L.; Tsanaktsidis, J. Chloroform as a Hydrogen Atom Donor in Barton Reductive Decarboxylation Reactions. *J. Org. Chem.* **2013**, *78* (13), 6677–6687.
- (27) Qin, T.; Malins, L. R.; Edwards, J. T.; Merchant, R. R.; Novak, A. J. E.; Zhong, J. Z.; Mills, R. B.; Yan, M.; Yuan, C.; Eastgate, M. D. . B. P. S. *Angew. Chemie Int. Ed.* **2017**, *56* (1), 260–265.
- (28) Noble, A.; McCarver, S. J.; MacMillan, D. W. C. *J. Am. Chem. Soc.* **2015**, *137* (2), 624–627.
- (29) Cornella, J.; Edwards, J. T.; Qin, T.; Kawamura, S.; Wang, J.; Pan, C.-M.; Gianatassio, R.; Schmidt, M.; Eastgate, M. D.; Baran, P. S. *J. Am. Chem. Soc.* **2016**, *138* (7), 2174–2177.
- (30) Qin, T.; Cornella, J.; Li, C.; Malins, L. R.; Edwards, J. T.; Kawamura, S.; Maxwell, B. D.; Eastgate, M. D.; Baran, P. S. *Science* **2016**, *352* (6287), 801–805.
- (31) Edwards, J. T.; Merchant, R. R.; McClymont, K. S.; Knouse, K. W.; Qin, T.; Malins, L. R.; Vokits, B.; Shaw, S. A.; Bao, D.-H.; Wei, F.-L.; et al. *Nature* **2017**, *545* (7653), 213–218.
- (32) Toriyama, F.; Cornella, J.; Wimmer, L.; Chen, T.-G.; Dixon, D. D.; Creech, G.; Baran, P. S. *J. Am. Chem. Soc* **2016**, *138* (35), 11132–11135.
- (33) Smith, J. M.; Qin, T.; Merchant, R. R.; Edwards, J. T.; Malins, L. R.; Liu, Z.; Che, G.; Shen, Z.; Shaw, S. A.; Eastgate, M. D.; et al. *Angew. Chemie Int. Ed.* **2017**, *56* (39), 11906–11910.
- (34) Lackner, G. L.; Quasdorf, K. W.; Overman, L. E. *J. Am. Chem. Soc.* **2013**, *135* (41), 15342–

15345.

- (35) Slutskyy, Y.; Overman, L. E. *Org. Lett.* **2016**, *18* (11), 2564–2567.
- (36) Rodríguez, N.; Goossen, L. J. *Chem. Soc. Rev.* **2011**, *40* (10), 5030–5048.
- (37) Matsubara, S.; Yokota, Y.; Oshima, K. *Org. Lett.* **2004**, *6* (12), 2071–2073.
- (38) Myers, A. G.; Tanaka, D.; Mannion, M. R. *J. Am. Chem. Soc.* **2002**, *124* (38), 11250–11251.
- (39) Tanaka, D.; Myers, A. G. *Org. Lett.* **2004**, *6* (3), 433–436.
- (40) Dickstein, J. S.; Mulrooney, C. A.; O'Brien, E. M.; Morgan, B. J.; Kozlowski, M. C. *Org. Lett.* **2007**, *9* (13), 2441–2444.
- (41) Cornella, J.; Righi, M.; Larrosa, I. *Angew. Chemie Int. Ed.* **2011**, *50* (40), 9429–9432.
- (42) Gooßen, L. J.; Thiel, W. R.; Rodríguez, N.; Linder, C.; Melzer, B. *Adv. Synth. Catal.* **2007**, *349* (14–15), 2241–2246.
- (43) Gooßen, L. J.; Rodríguez, N.; Linder, C.; Lange, P. P.; Fromm, A. *ChemCatChem* **2010**, *2* (4), 430–442.
- (44) Kolarovič, A.; Fáberová, Z. *J. Org. Chem.* **2009**, *74* (18), 7199–7202.
- (45) Gooßen, L. J.; Deng, G.; Levy, L. M. *Science* **2006**, *313* (5787), 662–664.
- (46) Gooßen, L. J.; Linder, C.; Rodríguez, N.; Lange, P. P.; Fromm, A. *Chem. Commun.* **2009**, No. 46, 7173–7175.
- (47) Wang, P.-F.; Wang, X.-Q.; Dai, J.-J.; Feng, Y.-S.; Xu, H.-J. *Org. Lett.* **2014**, *16* (17), 4586–4589.
- (48) Sun, Z.-M.; Zhang, J.; Zhao, P. *Org. Lett.* **2010**, *12* (5), 992–995.
- (49) Tanaka, D.; Romeril, S. P.; Myers, A. G. *J. Am. Chem. Soc.* **2005**, *127* (29), 10323–10333.
- (50) Anderson, J. M.; Kochi, J. K. *J. Am. Chem. Soc.* **1970**, *92* (6), 1651–1659.
- (51) Minisci, F.; Bernardi, R.; Bertini, F.; Galli, R.; Perchinnunzio, M. *Tetrahedron* **1971**, *27* (15), 3575–3579.
- (52) Davidson, R. S.; Steiner, P. R. *J. Chem. Soc.* **1971**, 0, 1682–1689.
- (53) Yoshimi, Y.; Itou, T.; Hatanaka, M. *Chem. Commun.* **2007**, 0 (48), 5244–5246.

- (54) Pac, C.; Nakasone, A.; Sakurai, H. *J. Am. Chem. Soc.* **1977**, *99* (17), 5806–5808.
- (55) Jones, W. E.; Fox, M. A. *J. Phys. Chem.* **1994**, *98* (19), 5095–5099.
- (56) Romero, N. A.; Nicewicz, D. A. *Chem. Rev.* **2016**, *116* (17), 10075–10166.
- (57) Galicia, M.; González, F. J.; González, F. J. *J. Electrochem. Soc.* **2002**, *149* (3), D46–D50.
- (58) Itou, T.; Yoshimi, Y.; Morita, T.; Tokunaga, Y.; Hatanaka, M. *Tetrahedron* **2009**, *65* (1), 263–269.
- (59) Zuo, Z.; Ahneman, D. T.; Chu, L.; Terrett, J. A.; Doyle, A. G.; MacMillan, D. W. C. *Science* **2014**, *345* (6195), 437–440.
- (60) Zuo, Z.; MacMillan, D. W. C. *J. Am. Chem. Soc.* **2014**, *136* (14), 5257–5260.
- (61) Yoshimi, Y.; Masuda, M.; Mizunashi, T.; Nishikawa, K.; Maeda, K.; Koshida, N.; Itou, T.; Morita, T.; Hatanaka, M. *Org. Lett.* **2009**, *11* (20), 4652–4655.
- (62) Yoshimi, Y.; Washida, S.; Okita, Y.; Nishikawa, K.; Maeda, K.; Hayashi, S.; Morita, T. *Tetrahedron Lett.* **2013**, *54* (32), 4324–4326.
- (63) Chu, L.; Ohta, C.; Zuo, Z.; MacMillan, D. W. C. *J. Am. Chem. Soc.* **2014**, *136* (31), 10886–10889.
- (64) Noble, A.; MacMillan, D. W. C. *J. Am. Chem. Soc.* **2014**, *136* (33), 11602–11605.
- (65) Rueda-Becerril, M.; Mahé, O.; Drouin, M.; Majewski, M. B.; West, J. G.; Wolf, M. O.; Sammis, G. M.; Paquin, J.-F. *J. Am. Chem. Soc.* **2014**, *136* (6), 2637–2641.
- (66) Ventre, S.; Petronijevic, F. R.; MacMillan, D. W. C. *J. Am. Chem. Soc.* **2015**, *137* (17), 5654–5657.
- (67) Wu, X.; Meng, C.; Yuan, X.; Jia, X.; Qian, X.; Ye, J. T. *Chem. Commun.* **2015**, *51* (59), 11864–11867.
- (68) Cassani, C.; Bergonzini, G.; Wallentin, C.-J. *Org. Lett.* **2014**, *16* (16), 4228–4231.
- (69) Krapcho, A. P.; Glynn, G. A.; Grenon, B. J. *Tetrahedron Lett.* **1967**, *8* (3), 215–217.
- (70) Dawson, G. J.; Williams, J. M.; Coote, S. J. *Tetrahedron: Asymmetry* **1995**, *6* (10), 2535–2546.
- (71) Hilborn, J. W.; Pincock, J. A. *J. Am. Chem. Soc.* **1991**, *113* (7), 2683–2686.
- (72) Fraind, A.; Turncliff, R.; Fox, T.; Sodano, J.; Ryzhkov, L. R. *J. Phys. Org. Chem.* **2011**, *24*

- (9), 809–820.
- (73) Givens, R. S.; Matuszewski, B.; Neywick, C. V. *J. Am. Chem. Soc.* **1974**, *96* (17), 5547–5552.
- (74) DeCosta, D. P.; Pincock, J. A. *J. Am. Chem. Soc.* **1989**, *111* (24), 8948–8950.
- (75) Falvey, D. E.; Schuster, G. B. *J. Am. Chem. Soc.* **1986**, *108* (23), 7419–7420.
- (76) Trost, B. M. *Angew. Chemie Int. Ed. English* **1995**, *34* (3), 259–281.
- (77) Dicks, A. P.; Hent, A. Atom Economy and Reaction Mass Efficiency. In *Green Chemistry Metrics*; Springer, 2015; pp 17–44.
- (78) Griffin, J. D.; Zeller, M. A.; Nicewicz, D. A. *J. Am. Chem. Soc.* **2015**, *137* (35), 11340–11348.
- (79) Hamilton, D. S.; Nicewicz, D. A. *J. Am. Chem. Soc.* **2012**, *134* (45), 18577–18580.
- (80) Grandjean, J.-M. M.; Nicewicz, D. A. *Angew. Chemie Int. Ed.* **2013**, *52* (14), 3967–3971.
- (81) Perkowski, A. J.; Nicewicz, D. A. *J. Am. Chem. Soc.* **2013**, *135* (28), 10334–10337.
- (82) Nguyen, T. M.; Nicewicz, D. A. *J. Am. Chem. Soc.* **2013**, *135* (26), 9588–9591.
- (83) Wilger, D. J.; Grandjean, J.-M. M.; Lammert, T. R.; Nicewicz, D. A. *Nat. Chem.* **2014**, *6* (8), 720–726.
- (84) Zeller, M. A.; Riener, M.; Nicewicz, D. A. *Org. Lett.* **2014**, *16* (18), 4810–4813.
- (85) Morse, P. D.; Nicewicz, D. A. *Chem. Sci.* **2015**, *6* (1), 270–274.
- (86) Gesmundo, N. J.; Grandjean, J.-M. M.; Nicewicz, D. A. *Org. Lett.* **2015**, *17* (5), 1316–1319.
- (87) Cavanaugh, C. L.; Nicewicz, D. A. *Org. Lett.* **2015**, *17* (24), 6082–6085.
- (88) Romero, N. A.; Margrey, K. A.; Tay, N. E.; Nicewicz, D. A. *Science* **2015**, *349* (6254), 1326–1330.
- (89) McManus, J. B.; Nicewicz, D. A. *J. Am. Chem. Soc.* **2017**, *139* (8), 2880–2883.
- (90) Margrey, K. A.; Levens, A.; Nicewicz, D. A. *Angew. Chemie Int. Ed.* **2017**, *56* (49), 15644–15648.
- (91) Tay, N. E. S.; Nicewicz, D. A. *J. Am. Chem. Soc.* **2017**, *139* (45), 16100–16104.

- (92) Griffin, J. D.; Cavanaugh, C. L.; Nicewicz, D. A. *Angew. Chemie Int. Ed.* **2017**, *56* (8), 2097–2100.
- (93) Andrew C. Benniston, ; Anthony Harriman, ; Peiyi Li,; James P. Rostron, ; Hendrik J. van Ramesdonk,; Michiel M. Groeneveld, ; Hong Zhang, and; Jan W. Verhoeven, . *J. Am. Chem. Soc* **2005**, *127* (46), 16054–16064.
- (94) Romero, N. A.; Nicewicz, D. A. *J. Am. Chem. Soc.* **2014**, *136* (49), 17024–17035.
- (95) Luo, Y.-R. *Handbook of Bond Dissociation Energies in Organic Compounds*; CRC Press, 2003.
- (96) Cox, B. G. High-Basicity Polar Aprotic Solvents. In *Acids and Bases*; Oxford University Press, 2013; pp 76–98.
- (97) Allan Godsk Larsen; Allan Hjarbæk Holm; Mark Roberson, A.; Daasbjerg, K. *J. Am. Chem. Soc* **2001**, *123* (8), 1723–1729.
- (98) Miguel, E. L. M.; Silva, P. L.; Pliego, J. R. *J. Phys. Chem. B* **2014**, *118* (21), 5730–5739.
- (99) Andon, R. J. L.; Cox, J. D.; Herington, E. F. G. *Trans. Faraday Soc.* **1954**, *50* (0), 918.
- (100) Wilger, D. J.; Gesmundo, N. J.; Nicewicz, D. A. *Chem. Sci.* **2013**, *4* (8), 3160–3165.
- (101) Prier, C. K.; Rankic, D. A.; MacMillan, D. W. C. *Chem. Rev.* **2013**, *113* (7), 5322–5363.
- (102) Narayanam, J. M. R.; Tucker, J. W.; Stephenson, C. R. J. *J. Am. Chem. Soc.* **2009**, *131* (25), 8756–8757.
- (103) Akerlof, G. *J. Am. Chem. Soc.* **1932**, *54* (11), 4125–4139.
- (104) Hong, D.-P.; Hoshino, M.; Kuboi, R.; Goto, Y. *J. Am. Chem. Soc.* **1999**, *121* (37), 8427–8433.
- (105) V. C. Papadimitriou; A. V. Prosser; Y. G. Lazarou, † and; Papagiannakopoulos, P. *Absolute J. Phys. Chem. A* **2003**, *107* (19), 3733–3740.
- (106) Jonathan S. Owen; Jay A. Labinger, and; Bercaw, J. E. *J. Am. Chem. Soc* **2006**, *128* (6), 2005–2016.
- (107) Schadt, F. L.; Bentley, T. W.; Schleyer, P. v. R. *J. Am. Chem. Soc.* **1976**, *98* (24), 7667–7675.
- (108) Marcus, R. A. *J. Phys. Chem. B* **1998**, *102* (49), 10071–10077.
- (109) Chatterjee, S.; Davis, P. D.; Gottschalk, P.; Kurz, M. E.; Sauerwein, B.; Yang, X.; Schuster,

- G. B. *J. Am. Chem. Soc.* **1990**, *112* (17), 6329–6338.
- (110) Suga, K.; Ohkubo, K.; Fukuzumi, S. *J. Phys. Chem. A* **2006**, *110* (11), 3860–3867.
- (111) Yang, M.; Jiang, X.; Shi, W.-J.; Zhu, Q.-L.; Shi, Z.-J. *Org. Lett.* **2013**, *15* (3), 690–693.
- (112) Beaulieu, L.-P. B.; Roman, D. S.; Vallée, F.; Charette, A. B. *Chem. Commun.* **2012**, 48 (66), 8249.
- (113) Singh, D.; Baruah, J. B. *Cryst. Growth Des.* **2012**, *12* (4), 2109–2121.
- (114) Zhu, S.-F.; Yu, Y.-B.; Li, S.; Wang, L.-X.; Zhou, Q.-L. *Angew. Chemie Int. Ed.* **2012**, *51* (35), 8872–8875.
- (115) Maligres, P. E.; Houpis, I.; Rossen, K.; Molina, A.; Sager, J.; Upadhyay, V.; Wells, K. M.; Reamer, R. A.; Lynch, J. E.; Askin, D.; . *Tetrahedron* **1997**, *53* (32), 10983–10992.
- (116) Neustadt, B. R.; Smith, E. M.; Nechuta, T. L.; Bronnenkant, A. A.; Haslanger, M. F.; Watkins, R. W.; Foster, C. J.; Sybertz, E. J. *J. Med. Chem.* **1994**, *37* (15), 2461–2476.
- (117) Moriuchi-Kawakami, T.; Kawata, K.; Nakamura, S.; Koyama, Y.; Shibutani, Y. *Tetrahedron* **2014**, *70* (52), 9805–9813.
- (118) Jason T. Brewer; Sean Parkin, A.; Grossman*, R. B. *Cryst. Growth Des.* **2004**, *4* (3), 591–594.
- (119) Tandiary, M. A.; Masui, Y.; Onaka, M. *Tetrahedron Lett.* **2014**, *55* (30), 4160–4162.
- (120) St. Denis, J. D.; Scully, C. C. G.; Lee, C. F.; Yudin, A. K. *Org. Lett.* **2014**, *16* (5), 1338–1341.
- (121) Sara J. Krivickas,; Emiliano Tamanini, †; Matthew H. Todd, , A.; Michael Watkinson, . *J. Org. Chem.* **2007**, *72* (22), 8280–8289.
- (122) Khedkar, M. V.; Shinde, A. R.; Sasaki, T.; Bhanage, B. M. *J. Mol. Catal. A Chem.* **2014**, *385*, 91–97.
- (123) Lakowicz, J. R. *Principles of Fluorescence Spectroscopy*, 3rd ed.; Lakowicz, J. R., Ed.; Springer US: Boston, MA, 2006.

CHAPTER 3: REVERSAL OF ALKENE HALOFUNCTIONALIZATION REGIOSELECTIVITY BY MERGING ORGANIC PHOTOREDOX AND COPPER CATALYSISⁱ

3.1 Introduction

3.1.1 Alkene Difunctionalization

Alkenes are attractive building blocks for synthesis because of their ease of synthesis and well defined reactivity patterns; they participate in a plethora of reaction pathways both polar and radical. The unsaturation present in alkenes also allows for the ability to build two C-X or C-C bonds simultaneously. This can lower the required number of steps in a sequence and increase molecular complexity rapidly. The Sharpless dihydroxylation has emerged as a uniquely successful example of alkene difunctionalization.¹ The use of this transformation in synthesis, despite the need for highly toxic osmium reagents, highlights the usefulness of transformations that rapidly build up molecular and stereo-complexity.² Seemingly inspired by the success of the Sharpless dihydroxylation, numerous reports of alkene difunctionalizations are continually developed, which can provide a wide array of new disconnections.

While there are many strategies to accomplish alkene difunctionalization, one of the major strategies hinges on a radical addition pathway; wherein a radical intermediate is trapped with an

ⁱ The work presented in this chapter has previously been disclosed in a different form. See: Griffin, J. D.; Cavanaugh, C. L.; Nicewicz, D. A. *Angew. Chemie. Int. Ed.* **2017**, 56, 2097-2100.

alkene radical acceptor (**Figure 3.1**, Radical Difunctionalization). Radical intermediates for these processes have been generated by single-electron reduction of an activated carbon-heteroatom or heteroatom-heteroatom bonds to form nitrogen,^{3–5} oxygen,⁶ sulfur,⁶ or carbon centered radicals.^{7,8}

Some of the most common radical intermediates used in these processes have been azido,⁹ trifluoromethyl,¹⁰ and sulfonamide radicals,¹¹ although examples of other radical intermediates have certainly been demonstrated. These reaction types often provide high selectivity, typically based on the degree of radical stability. The resulting radical following addition, often undergoes SET to form a cationic intermediate, which is ultimately trapped with a suitable nucleophile

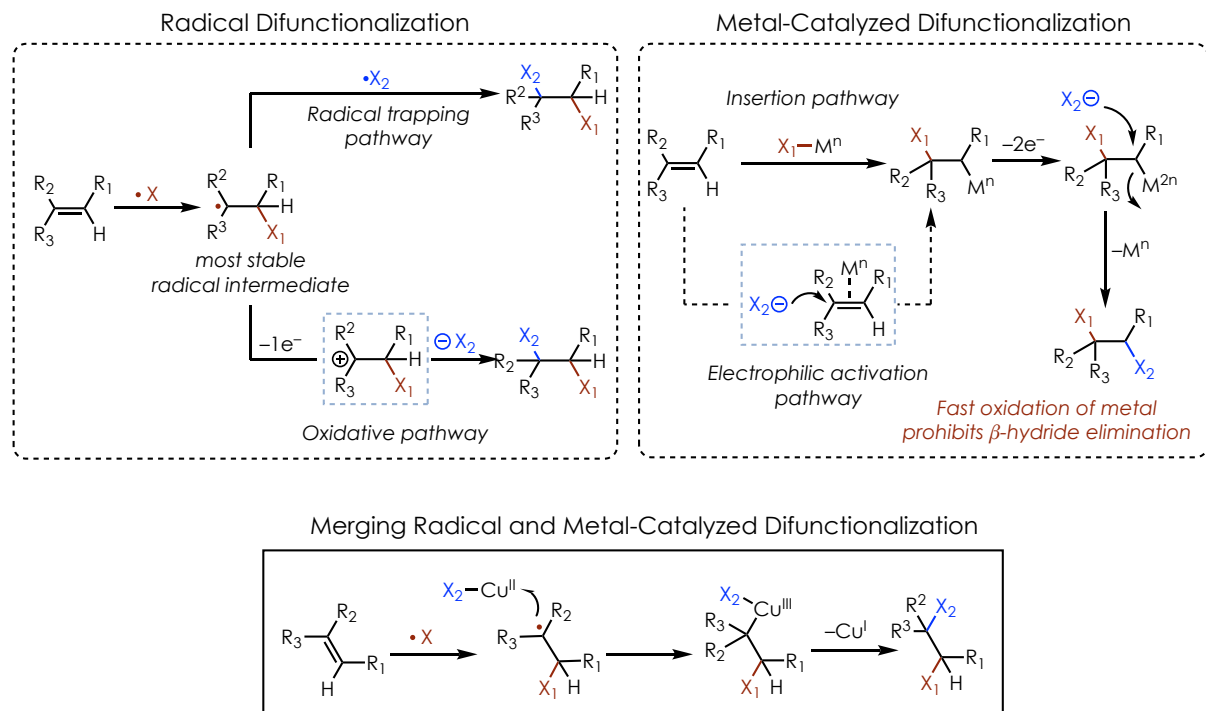


Figure 3.1: Major strategies for alkene difunctionalization.

allowing for differential functionalization of the alkene (See Oxidative pathway in **Figure 3.1**). Alternatively, radicals can undergo direct trapping with a radical-trapping agent to directly furnish the desired products (See Radical trapping pathway in **Figure 3.1**). Common radical trapping agents include oxygen, peroxides, or TEMPO (2,2,6,6-Tetramethyl-1-piperidinyloxy).

Another major strategy for alkene difunctionalization involves activation via nucleometalation (**Figure 3.1**, Metal Catalyzed Difunctionalization). This has most typically been accomplished using palladium based catalysts, wherein the nucleophile and palladium insert into the alkene simultaneously (See Insertion pathway in **Figure 3.1**).¹² The use of styrenes or dienes as the alkene component allows for regioselective nucleopalladation, due to the formation of the most stable Pd intermediate (Pd-allyl type complexes).¹³ The initial insertion also occurs with syn addition, allowing for diastereoselective and enantioselective transformations.^{14–16} Following nucleometalation, the resulting carbon-palladium intermediate can undergo numerous secondary functionalizations to create C-C,¹⁷ C-N,¹⁸ or C-O¹⁹ bonds. In order to avoid β -hydride elimination, fast oxidation of Pd(II) intermediates with strong oxidants to form Pd(IV) has been proposed.¹⁴ This highly unstable Pd(IV) intermediate can undergo either nucleophilic displacement (via S_N2) or reductive elimination to afford the net difunctionalized products. Metal based activations of alkenes have also commonly been described as electrophilic alkene activation when very electron poor metals are implicated.^{20,21} This involves precomplexation between the alkene species with the electrophilic metal center, which can activate it toward nucleophilic attack (See Electrophilic activation pathway in **Figure 3.1**). This activation pathway is not limited to electrophilic transition metals, as traditional alkene halofunctionalization also falls under this category, and will be discussed at length in the next section (**Section 3.1.2**).

A merger of these two strategies has been reported by the Buchwald⁶ and Liu groups (**Figure 3.1**, Merging Radical and Metal-Catalyzed Difunctionalization).^{22,23} Upon addition of a radical intermediate into an alkene, radical intermediates can be subsequently trapped by Cu(II) catalysts to form Cu(III) intermediates. These Cu(III) intermediates are proposed to undergo fast reductive elimination. These transformations were able to be rendered enantioselective using chiral

Bisoxazoline (BOX) ligands. A variety of radical precursors have so far been shown to be amendable to this strategy.

3.1.2 Alkene Halofunctionalization Through Electrophilic Activation

Halofunctionalization of alkenes are some of the oldest difunctionalization reactions in organic chemistry, the simplest of which are the halogen addition and halohydrin reactions.²⁴ They are a class of reactions signified by the activation of an alkene with electrophilic halogen sources. Originally elemental bromine was used to carry out these reactions, however a suite of more easily handled reagents, which can deliver chlorine, bromine, or iodine, have been since developed

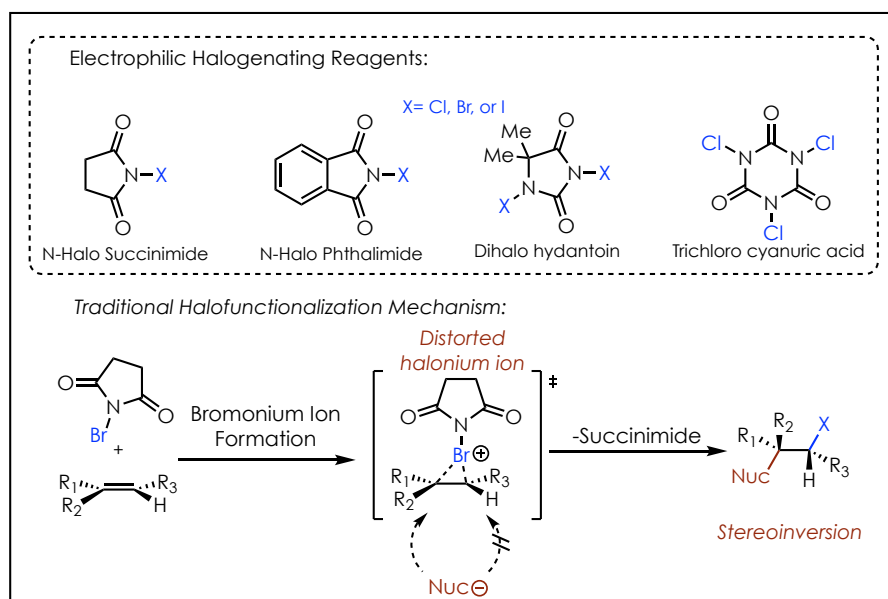


Figure 3.2: Electrophilic halogenating reagents and mechanism of traditional halofunctionalization.

(Figure 3.2). Like other difunctionalizations the rapid diversification of relatively easy to synthesize and cheap alkene functional groups makes this reaction highly useful. Electrophilic halogenations proceed through the formation of halonium ions, which form upon nucleophilic attack by an alkene at an electrophilic halogen source. Halonium ions can subsequently undergo

nucleophilic attack in a stereospecific fashion at the more substituted position, allowing for highly regio- and diastereoselective reactions. This selectivity arises from the distortion of the halonium ion such that the largest amount of positive charge is stabilized on the more electron rich carbon center.

In 2016 the Borhan group demonstrated that nucleophiles, such as tethered alcohols and carboxylic acids, can help to activate alkenes, increasing their reactivity with halogenating reagents.²⁵ In a series of styrene derivatives, the reactivity of the alkenes was observed to generally increase as the nucleophilicity of the tethered nucleophile increased (**Figure 3.3**). Since the RDS was determined to be formation of the chloronium ion, this finding was deemed to indicate nucleophile participation in the TS. This hypothesis was corroborated by DFT analysis of the TS, as well KIE, and NMR studies. Importantly, the NMR signals of 1,1-disubstituted alkenes were

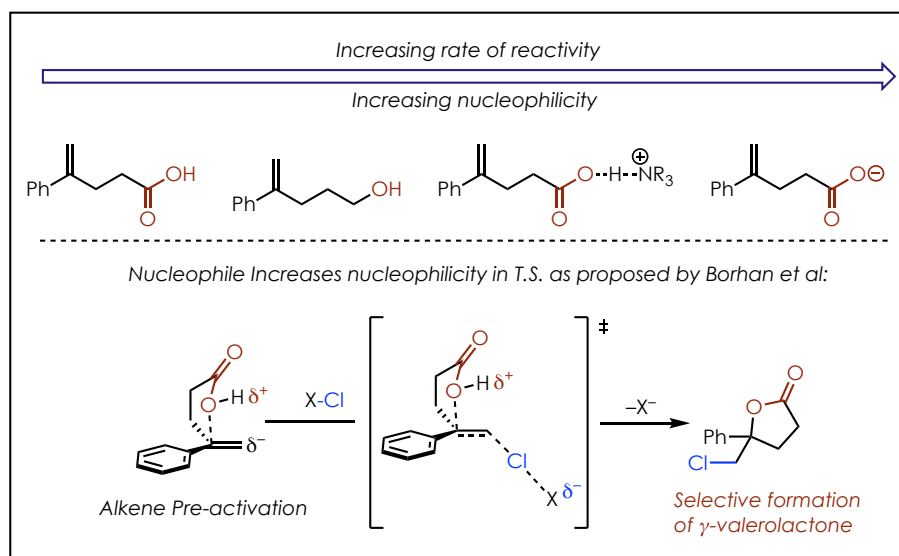


Figure 3.3: Nucleophile assisted alkene activation as proposed by Borhan and coworkers.

found to be significantly shifted upfield as the tethered group nucleophilicity increased. This suggested a ground state pre-activation complex. DFT analysis also predicted nucleophile participation in the TS. This is a significant finding as it illustrates that alkenes are often not

reactive enough on their own to undergo halofunctionalization, and must be activated with a tethered nucleophile. It is also of importance that this preactivation complex leads to the highly regioselective formation of the γ -valerolactone. This selectivity would also be expected for this substrate if a discreet halonium ion were formed as well due to the stabilization provided at the benzylic carbon atom.

3.1.2.1 Enantioselective Halofunctionalization Reactions

Recently, there have been many reports of enantioselective halofunctionalization reactions. These methodologies have all relied on leveraging the innate reactivity of alkenes with electrophilic halogen sources; therefore these methods provide the same regioselectivity as predicted by analysis of the corresponding halonium ion intermediates. A few examples of these methodology will be presented below, describing different strategies for enantioselective halofunctionalization. The examples found below also highlight the regioselectivity obtained from electrophilic methods, which will be important for comparing to the method developed by our lab in Section 3.2.

3.1.2.1.1 Chiral Halogenating Reagents

One of the first methods for rendering traditional halofunctionalization reactions enantioselective was through the in situ formation of a chiral electrophilic halogen source.²⁶ The

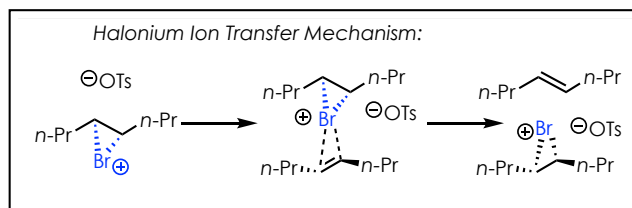


Figure 3.4: Halonium ion intermediates can be transferred between alkenes, potentially eroding enantioselectivity.

mode of enantioinduction of these reactions were proposed to be through formation of a halonium ion selectively on one of the two prochiral alkene faces.^{27,28} However, enantioselectivity was found to be low to moderate using this type of strategy. One potential complicating factor is the ability

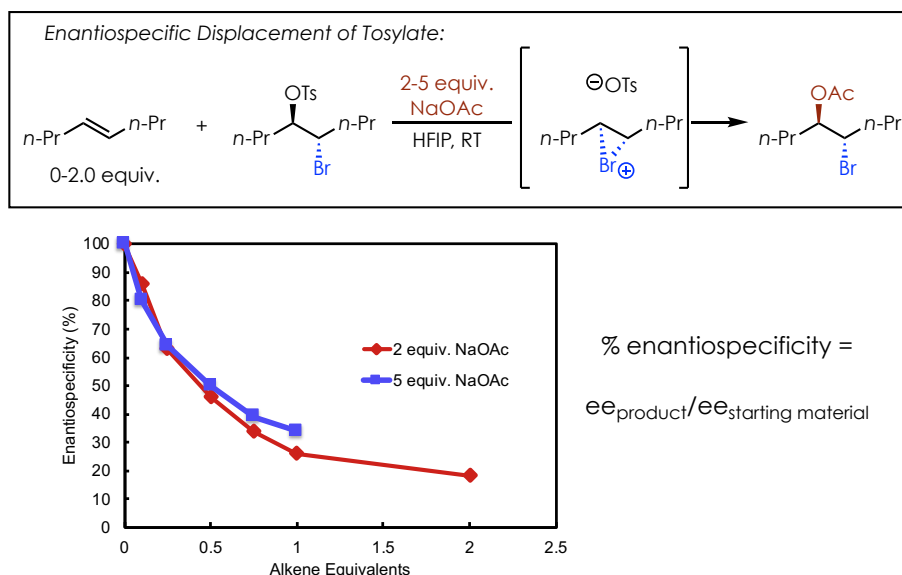


Figure 3.5: Enantiospecificity of a tosylate displacement reaction is significantly eroded as concentration of alkene increases as shown by Denmark and coworkers.

of halonium ion transfer between alkenes as first demonstrated by Brown et al.²⁹ The mechanism of halogen transfer between olefins was proposed to proceed through the intermediacy of a π -complex (**Figure 3.4**). More recently, Denmark and coworkers have shown that the enantiopurity of a chiral bromonium ion can be eroded in the presence of alkenes (**Figure 3.5**).³⁰ Even increasing equivalents of the acetate nucleophile did not greatly improve enantiospecificity at high alkene concentrations. This demonstrates that bromonium ion transfer is relatively facile; however the enantiospecificity of the analogous chloronium ion in this reaction was found to remain high even at high concentrations of alkene. Overall, these studies show that a more robust method is necessary in order to obtain high enantioselectivity in halofunctionalization reactions.

3.1.2.1.2 Controlling Attack of the Nucleophile and Halonium Delivery Simultaneously

Despite the problems associated with enantioselective halofunctionalization using stoichiometric chiral halogenating agents, many successful strategies have been developed using a catalyst controlled strategy. Of the enantioselective halofunctionalization methodologies developed so far, halolactonization has received the largest amount of attention. Chloro-,³¹ bromo-,³² and iodolactonizations³³ can all be carried out in a stereoselective fashion. However, other tethered nucleophiles^{34,35} as well as intermolecular variants³⁶ have also been explored in this chemistry as well.

In 2012, the Martin lab demonstrated that bromolactonization could be carried out with high enantio- and regioselectivity using a catalyst which controlled both the facial selectivity for bromonium ion formation as well as the approach of the tethered nucleophile (**Figure 3.6**).³² Using 2,4,4,6-tetrabromocyclohexadienone (TBCO) as the brominating reagent and a bifunctional catalyst derived from BINOL high regio-, diastereo-, and enantioselectivities could be obtained. This strategy leverages the innate regio- and diastereoselectivity of traditional

Martin et al 2012:

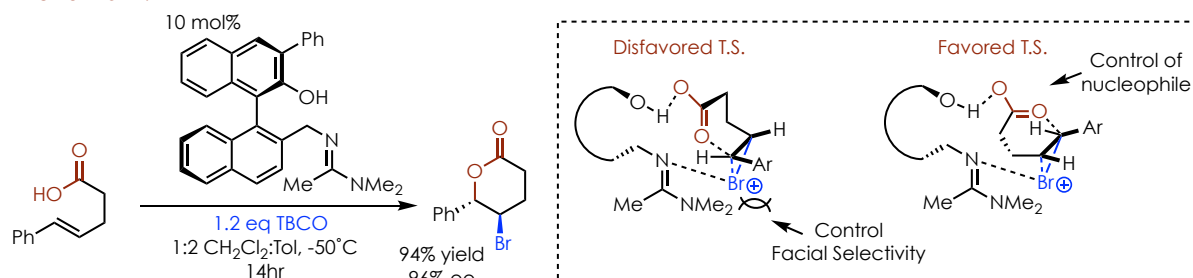


Figure 3.6: Enantioselective Bromolactonization catalyzed by a bifunctional BINOL based catalyst.

halofunctionalization reactions. This methodology favors the formation of δ -valerolactones due to the stabilization provided by the aryl group at the 5-position (This selectivity will be of note when discussing strategies for altering alkene regioselectivity in Section 3.2). The authors proposed a

dual function for the catalyst shown in Figure 3.6. Facial selectivity for bromonium ion formation is derived from steric repulsion of the large aromatic ring, while control of the nucleophile allows for fast trapping of the bromonium ion.

An example of enantioselective chlorolactonization of 1,1-disubstituted styrenes was reported in Borhan and coworkers in 2010 (**Figure 3.7**).³¹ Through the use of deuterium labeling studies, the authors were able to show that the mode of enantioinduction was the selective delivery

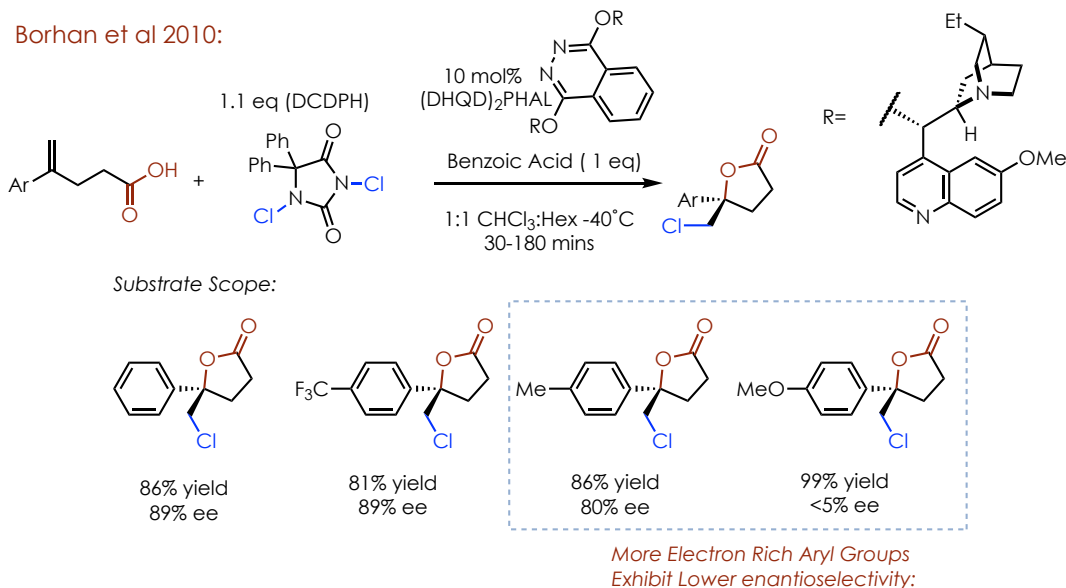


Figure 3.7: Enantioselective chlorolactonization of 1,1-disubstituted styrenes developed by Borhan et al.

of the chloronium ion.³⁷ ¹H NMR studies were also carried out, which suggested the existence of a hydrogen-bonding complex between the active catalyst (a cinchona alkaloid dimer) and the stoichiometric halogenating agent (1,3-dichloro-5,5-dimethyl hydantoin, DCDMH). This chiral H-bonded complex was proposed to be responsible for enantioselective chloronium ion formation. The enantioselectivity was found to be very good, except in the case of very electron rich styrenes. This finding is suggestive of a carbocation intermediate rather than a halonium ion or concerted addition of nucleophile and halogen which was later proposed by Borhan and coworkers (See above, Section 3.1.2). Again, the regioselectivity for these reactions follows the expected trends

for other halofunctionalization reactions. In this case it has been shown that 1,1-disubstituted styrene derivatives can be expected to form the γ -valerolactone product.

3.1.2.2 Heteroatom-Halide 1,2-substitution in Natural Products

Figure 3.8 shows some representative natural products which bear 1,2-heteroatom-halide relationships. Unsurprisingly, this motif is more common in marine natural products, although terrestrial organisms also produce halogenated natural products.³⁸ The various substitution patterns, ring sizes, and heteroatom/halogen combinations found in these natural products, highlight the utility of methodologies which could construct this motif in a single regioselective step. Installation of the halide 1,2-heteroatom-halide motif often occurs in a multi-stage fashion from alkenes. Alkenes are ideal starting materials for this installation of this subunit because they possess the correct carbon oxidation state and are easily and reliably synthesized. Some of the most common strategies for synthesizing this unique class of natural products have included the opening of epoxide intermediates with the corresponding halide.³⁹ This method allows for diastereocontrol and can be regiodivergent depending on the method used for epoxide opening, however a more efficient synthesis would be enabled by a direct regioselective difunctionalization of an alkene.

Medium size ether rings bearing bromide or chloride groups have been isolated from red algae of the genus *Laurencia*. Many of the *Laurencia* natural products have been synthesized previously by Crimmins,^{40,41} Overman,^{42,43} and others. The major strategy for installing the halogen and formation of the ether ring, involves multiple steps. The halogens were typically installed from the corresponding alcohol via the use of PBr₃ or SOCl₂ for this class of natural products. Virantmycin is unique among the natural products highlighted in Figure 3.8, as it does

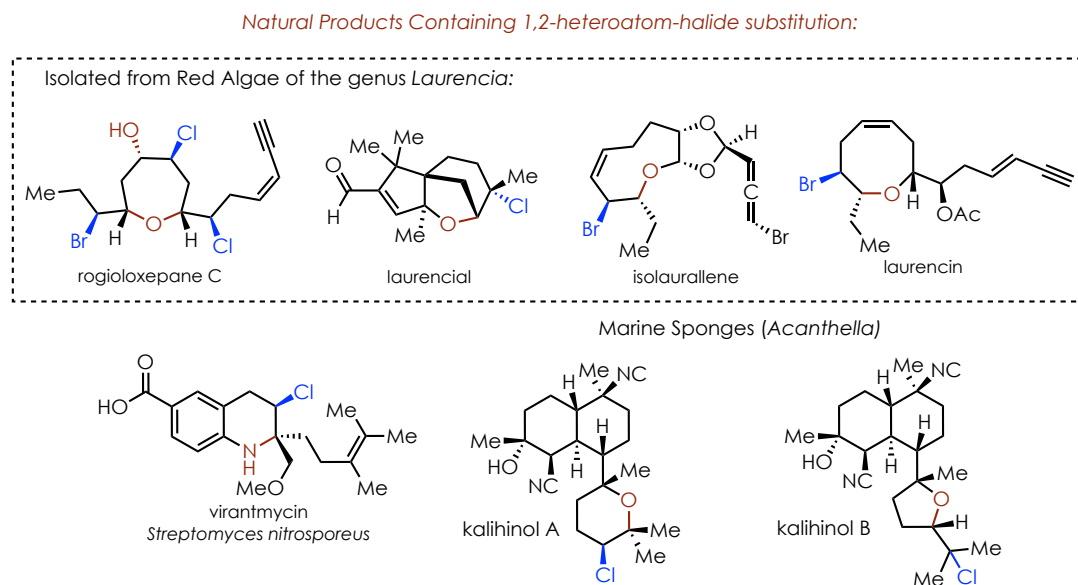


Figure 3.8: 1,2-Heteroatom-halide relationships are found in natural products.

not arise from a marine organism. The Corey⁴⁴ and Wulff⁴⁵ labs have accomplished total syntheses of virantmycin; again forming the heteroatom and halide bonds in separate steps. Finally, kalihinane diterpenoids are a class of natural products isolated from *Acanthella*, a genus of marine sponges. Over 50 natural products have been isolated from this family of natural products. Kalihinol A and B illustrate the importance of regioselective halofunctionalization methodologies, as these two natural products are constitutional isomers, in which the position of the chlorine and oxygen atoms are opposite. The Vanderwal⁴⁶ and Kawashima⁴⁷ labs have previously synthesized kalihinol A and B respectively.

3.1.3 Anti-Markovnikov Alkene Hydrofunctionalization in the Nicewicz Lab

Like traditional halofunctionalization reactions, alkene hydrofunctionalizations are known to proceed with very high regioselectivity due to stabilization of positive charge at the most substituted carbon of the alkene. For alkenes this is known as Markovnikov selectivity as it was

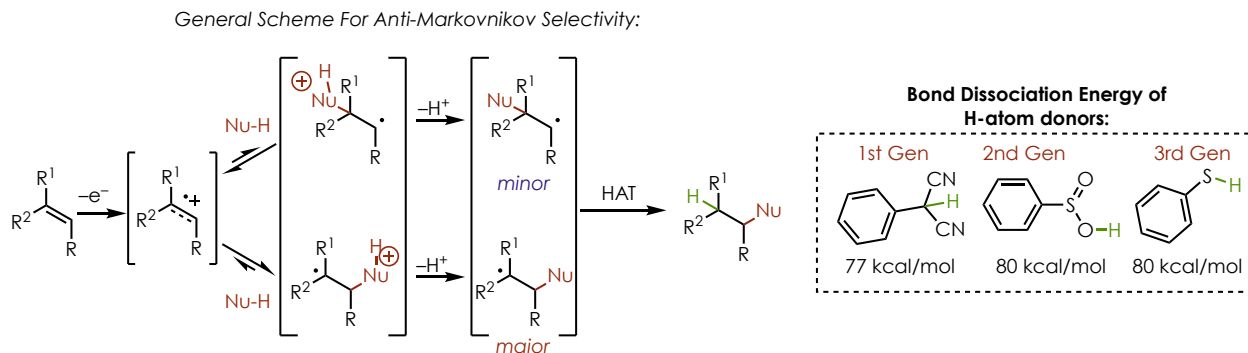


Figure 3.9: Mechanism of Anti-Markovnikov Hydrofunctionalization developed by the Nicewicz Lab.

first formulated as a general rule by Vladimir Markovnikov in 1865. Inspired by the original reports of Arnold⁴⁸ and Gassman,⁴⁹ which suggested that alkene cation radicals reacted with anti-Markovnikov selectivity, the Nicewicz lab has developed a general strategy for accomplishing anti-Markovnikov alkene hydrofunctionalization. Acridinium photooxidants which were originally reported by Fukuzumi and co-workers, are capable of oxidizing electron rich alkenes resulting in the formation of a cation-radical intermediate. As alluded to previously, nucleophilic attack occurs primarily at the least substituted carbon of the cation-radical (**Figure 3.9**). Following, irreversible deprotonation the more stable radical intermediate is formed at the more electron rich carbon. In order to afford hydrofunctionalization products, these radicals have been shown to undergo trapping with a series of redox active H-atom donors such as phenyl malononitrile, benzenesulfonic acid, and thiophenols. In 2012, Hamilton and Nicewicz published a methodology for the hydroetherification of alkenes with anti-Markovnikov selectivity.⁵⁰ They were also able to

show an example of an hydrolactonization with this methodology with a tethered carboxylic acid derivative as the nucleophile. Perkowski and Nicewicz later published an intermolecular variant of this reaction in which carboxylic acids such as acetic acid or benzoic acid could be used as nucleophiles.⁵¹ Both of these reports demonstrated that selectivity for nucleophile addition to the least substituted or electron rich position was obtained, typically as the sole product (**Figure 3.10**). This general reaction scheme has been found to be applicable to a number of different nucleophile reaction partners,^{52–55} including those which contain tethered unsaturation which can undergo subsequent radical cyclization (Polar-radical cycloaddition PRCC).^{56–59}

Some key aspects of this research that will become relevant in the following sections are:

- 1). The ability of alkene cation radicals to be trapped with carboxylic acid nucleophiles in an anti-Markovnikov fashion.
- 2). The use of a redox active co-catalyst that both traps the radical

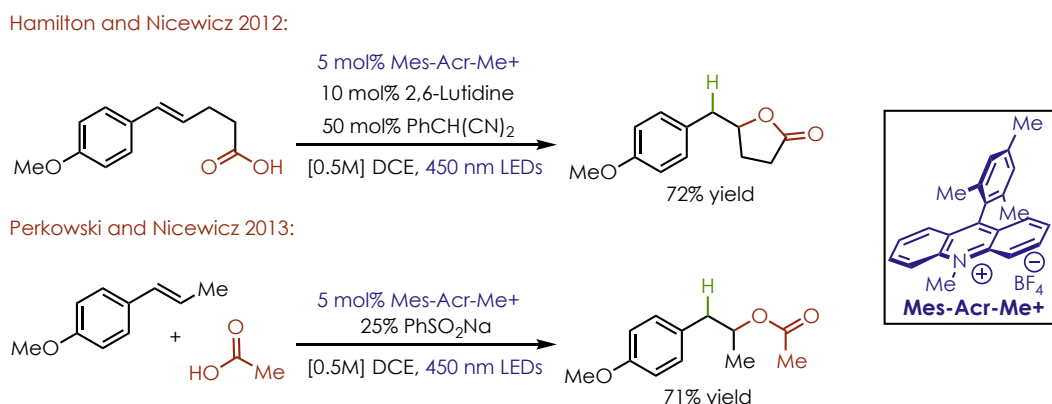
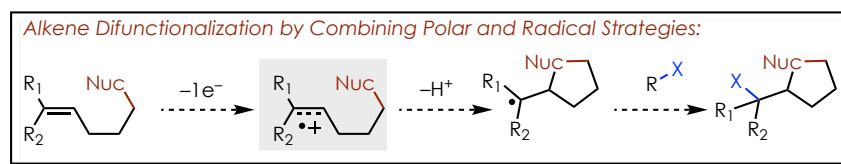


Figure 3.10: Anti-Markovnikov addition of carboxylic acids to alkenes.

intermediate, and is able to turn over the reduced acridinium catalyst. 3). The transformation is net-electron neutral, as the single electron removed from the alkene π -bond is ultimately returned to the substrate in the form of an H-atom.

3.2 Developing a Strategy For Catalytic Reversal of Alkene Halofunctionalization

As seen in the above discussions of previously developed halofunctionalization methodologies, very reliable selectivity can be obtained for the stereospecific addition of a nucleophile to a halonium ion (See Section 3.1.2). We believed that using a single-electron oxidation strategy, we could alter this innate selectivity and access traditionally inaccessible and often thermodynamically less favored isomer. Upon examining the mechanism of the previously developed anti-Markovnikov hydrofunctionalization chemistry (**Figure 3.9**, Section 3.1.3), it seemed possible to accomplish halofunctionalization by implementing a halogen-atom transfer



Scheme 3.3.1: General Plan for Reversing Halofunctionalization Selectivity

agent (**Scheme 3.1**). In the conceptual phase of reaction design, potentially problematic features were identified including: 1) Radical halogenating sources are typically the same as those employed in electrophilic alkene halofunctionalization, thus minimization of background reactions might be necessary 2) halogen-atom transfer from reagents such as *N*-bromosuccinimide is known to propagate chain-like reactivity, wherein the resulting nitrogen-centered radical abstracts a C-H bond from another substrate equivalent 3) Benzylic or tertiary halides may not be particularly stable. Additionally, in order to make this method catalytic with respect to the photooxidant the halogen transfer agent should also be able to regenerate the ground state photocatalyst through single electron oxidation. Thus, the dehalogenated reagent should be redox active.

3.2.1 Early Design Strategy

Initial attempts were made to carry out halofunctionalization using stoichiometric radical trapping agents. Carreira and coworkers reported that sulfonyl chlorides could act as chlorine atom transfer agents in 2008.⁶⁰ As shown above (Section 3.1.3), our lab had previously reported that benzene sulfinic acid was an active H-atom donor. We posited that since the same radical generated from H-atom transfer from benzene sulfinic acid would be generated upon abstraction of a chlorine atom from a sulfonyl chloride, this type of strategy would be amendable to our system (**Figure 3.11**). Importantly, this radical can undergo electron transfer with an acridine radical in order to regenerate the ground state acridinium photooxidant.⁵¹ Carboxylic acids were chosen as the initial

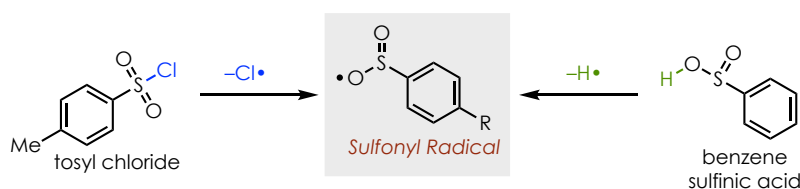


Figure 3.11: Atom Transfer from a benzene sulfonyl chloride and benzene sulfonic acid produce the same sulfonyl radical. This radical would be able to undergo favorable electron transfer with Mes-Acr-Me• to regenerate the ground state photo catalyst

nucleophile to be studied because halolactonization has been heavily documented in the literature to undergo reliable selectivity (See Section 3.1.2.1.2) and would be a good comparison for the ability of a new system which could alter the inherent regioselectivity.²⁶

Indeed, when 5-methyl-2,2-diphenylhex-4-enoic acid was used as a substrate along with 5 mol% of Mes-Acr-Me⁺, and 1.1 equivalents of tosyl chloride (**TsCl**) a very good yield of γ -chlorolactone product was isolated (**Figure 3.12**). However, upon attempting to extend this strategy to styrenyl substrates ((*E*)-2,2-dimethyl-5-phenylpent-4-enoic acid) using TsCl as the radical chlorine transfer reagent, none of the desired product could be observed by ¹H NMR with complete conversion of the starting materials to multiple unidentifiable products. Analysis of

BDEs reported in the literature showed that differences in bond strength between tertiary (~85 kcal/mol) and benzylic (~74 kcal/mol) C-Cl bonds could explain the differences in reactivity

Trapping Radicals with Halogen Transfer Reagents:

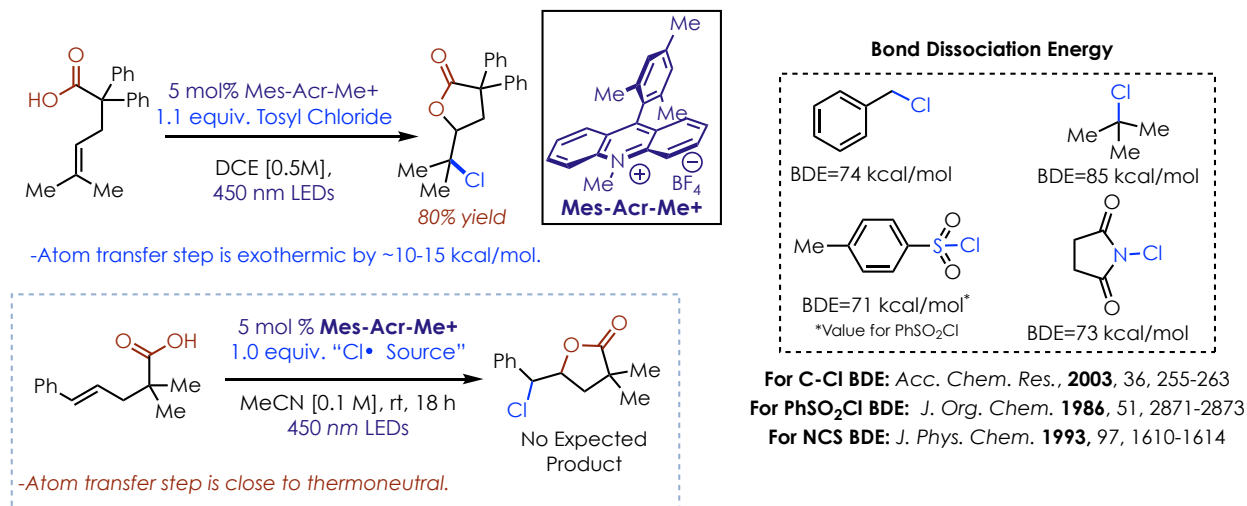


Figure 3.12: Early attempts at halofunctionalization through radical cation intermediates and relevant bond dissociation energies.

between the two substrates (**Figure 3.12**).⁶¹ While a chlorine atom transfer from TsCl (BDE = 71 kcal/mol)⁶² to a tertiary radical is favorable by 10-15 kcal/mol, transfer of a Cl• equivalent to a benzylic radical is approximately thermoneutral. This may also be exacerbated by the fact that the radical formed from (*E*)-2,2-dimethyl-5-phenylpent-4-enoic acid would be a secondary benzylic radical which could have an even weaker C-Cl BDE than benzyl chloride. Other radical atom transfer agents were screened in order to determine if a more appropriate BDE matching could be found, however other radical chlorinating agents have similar BDEs to sulfonyl chlorides (*N*-chlorosuccinimide has a BDE of 73 kcal/mol for example).⁶³

3.2.2 Inspiration for Halofunctionalization from Polymer Chemistry

After extensively screening radical transfer reagents without success, a new strategy was developed. Extensive literature searching revealed that there are very few known methods for transferring halogen atoms to a benzylic radical. Atom-Transfer Radical Polymerization (ATRP) is a strategy for obtaining very narrow polydispersity index (PDI) through a transiently formed radical.⁶⁴ This strategy has also been shown to be amendable to styrene polymerization. The mechanism of this unique polymerization proceeds through the abstraction of a benzylic halide

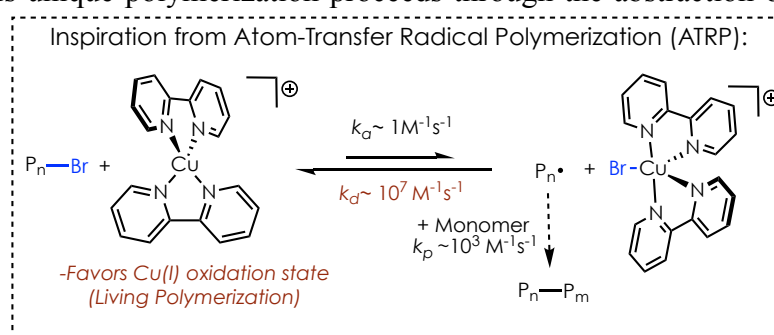


Figure 3.13: General Mechanism for an Atom Transfer Radical Polymerization (ATRP) and relevant rate constants

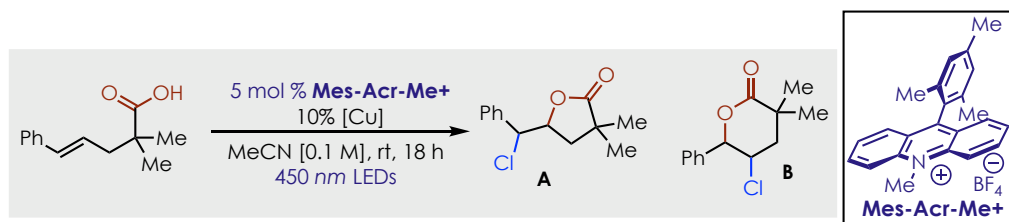
from the terminus of a propagating polymer chain, typically with a Cu(I) based catalyst. The benzylic radical can then undergo polymerization with the styrene monomer.

The key element of ATRP is the reversibility of the halogen-atom transfer from the Cu(II) halide complex (**Figure 3.13**). The equilibrium for this halogen-atom abstraction strongly favors the Cu(I) oxidation state. In the context of ATRP this means that very low concentrations of radical intermediates are present throughout the course of the reaction, and prevents deleterious side reactions such as radical-radical recombination (a type of chain termination). This type of polymerization is known as a ‘living polymerization’ because the polymer chains increase in length at roughly equal rates (the rates of chain propagation are slow compared to chain initiation),

and the polymer chains cannot terminate and remain active even after the monomer has been depleted.

3.2.3 Optimization of Chlorolactonization Using A Copper co-catalyst

Table 3.1: Optimization of Chlorolactonization ((*E*)-2,2-dimethyl-5-phenylpent-4-enoic acid)ⁱⁱ



Entry	Cu/Ligand	"Cl• Source"	A% Yield ⁱⁱⁱ (γ-lactone)	B% Yield ⁱⁱ (δ-lactone)	d.r. ^{iv}
1 ^v	CuCl ₂ /bpy	—	62%	—	1.5:1
2 ^{vi}	CuCl ₂ /bpy	1.0 equiv. Lut ⁺ Cl [−]	19%	—	2.6:1
3	CuCl ₂ /bpy	1.0 equiv NCP	90%	—	2.3:1
4	CuCl/bpy	1.0 equiv NCP	92%	—	2.4:1
5 ^{vii}	CuCl₂/phen	1.0 equiv NCP	85%	—	3.2:1
6 ^{viii}	CuCl ₂ /phen	1.0 equiv NCP	25%	12%	2.2:1

ⁱⁱ Reactions were carried out in N₂-sparged MeCN [0.1 M] under two LED lamps) for 18 h unless otherwise noted.

ⁱⁱⁱ Yield as determined by ¹H NMR spectroscopic analysis of the crude reaction mixture relative to the internal standard (Me₃Si)₂O.

^{iv} Diastereomeric ratio (d.r.) refers to the d.r. of product **A** only. Product **B** was only observed as one diastereomer, indicating that it was formed via a background electrophilic pathway.

^v Reaction was carried with 1 equivalent of CuCl₂ (and bpy when applicable) under air.

^{vi} Reaction was carried out with 20 mol% CuCl₂/bpy

^{vii} 2 hour reaction time.

^{viii} The reaction was carried out without Mes-Acr-Me⁺.

Since the oxidized catalyst is able to transfer a halogen atom to the propagating polystyrene radical (at the benzylic position), it seemed likely that a Cu(II) halide complex could also transfer a halogen-radical to afford a halofunctionalized product in our system. There are also a few examples of Cu(II) salts transfers halogen-atoms to organic radicals in an irreversible manner. Thus, chlorolactonization was again attempted with (*E*)-2,2-dimethyl-5-phenylpent-4-enoic acid using copper salts. The reaction was carried out initially utilizing an equivalent of CuCl₂, which gave a modest yield the desired regioisomer of 29% when applied to an all aliphatic substrate. When stoichiometric CuCl₂ was used along with 2,2'-bipyridine (**bpy**) as a ligand, the yield of the desired chlorolactone regioisomer **A** improved to 62%, without any of the undesired regioisomer formation (**Table 3.1, Entry 1**). Since this is a net-oxidative transformation, a second oxidant would be required in order to regenerate the ground state photocatalyst, therefore these reactions were also run in the presence of oxygen. The d.r. at this stage was only observed to be very mild. To confirm that this regioisomer would not be expected from traditional electrophilic chemistry, regioisomer **B** was also generated in an electrophilic manifold (See Section 3.6.5.5).

Since the use of stoichiometric metal salts is unattractive for a number of reasons, including solubility and potential contamination of the product, efforts were made toward using Cu in catalytic quantities. Initially, chloride salts such as 2,6-lutidinium chloride (**Lut⁺Cl⁻**) were considered as stoichiometric sources. Following chlorine-atom transfer to the substrate, an inactive CuCl species would be formed. In processes like the Wacker reaction, CuCl₂ can be regenerated in the presence of O₂ and an acid like HCl. However, **Lut⁺Cl⁻** only gave about one catalyst turnover (**Table 3.1, Entry 2**). Strong acids limit substrate compatibility, therefore other methods for turning over both the copper and acridinium catalysts were considered. The use of stoichiometric chlorinating reagents such as *N*-chlorosuccinimide (**NCS**) and *N*-chlorophthalimide (**NCP**) in the

presence of both catalysts afforded the desired regioisomer of the product, in 90% yield (**Table 3.1, Entry 3**). Since both of these reagents are two electrons oxidants, it was proposed that they were responsible for regenerating both catalysts. This was supported by the fact the CuCl could be used in place of CuCl₂ and the same results were obtained (**Table 3.1, Entry 4**). Ultimately, 1,10-phenanthroline was chosen as the ideal ligand because it gave both good yield and an improvement in diastereoselectivity, while also providing a much shorter reaction time of only 2 hours (**Table 3.1, Entry 5**). When Mes-Acr-Me⁺ was left out of the reaction both regioisomers were formed in low yield after 18 hour reaction times (**Table 3.1, Entry 6**). Almost no reactivity was observed after 2 hours indicating that Mes-Acr-Me⁺ was required.

3.2.3.1 Origin of Undesired Chlorolactone Regioisomer

Table 3.2: Important Control Reactions^{ix}

Entry	Catalyst	Irradiation	“Cl• Source”	B % Yield ^x (δ -lactone)
1	5 mol% Mes-Acr-Me ⁺	Yes	1.0 equiv NCS	50%
2	5 mol% Mes-Acr-Me ⁺	Yes	1.0 equiv NCP	30%
3	–	No	1.0 equiv NCP	–
4	–	No	1.0 equiv NCS	–
5	–	Yes	1.0 equiv NCP	–
6	5 mol% Mes-Acr-Me ⁺	No	1.0 equiv NCP	–
7	5 mol% TFA	No	1.0 equiv NCS	–
8	cat. CF₃SO₃H	No	1.0 equiv NCS	66%

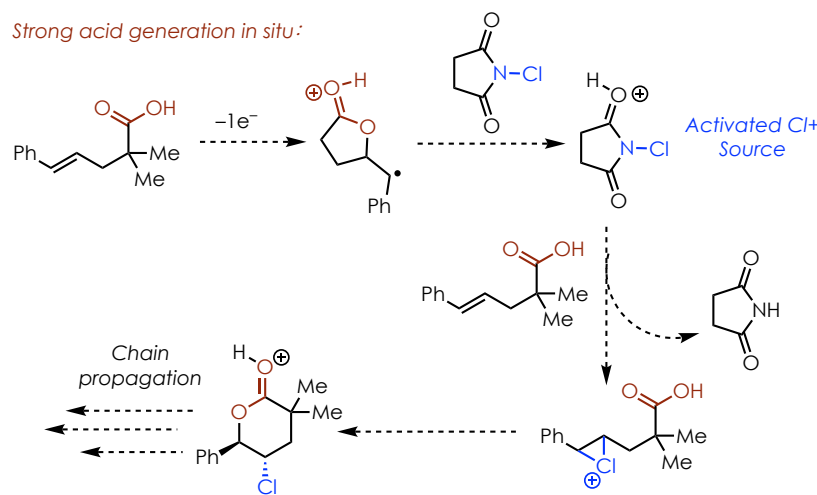
Interestingly, when CuCl₂ was left out of the reaction mixture, δ -lactone product **B** was the only observed product, which formed as a single diastereomer (**Table 3.2, Entries 1 and 2**). However, when both catalysts were not included, no reaction occurred with or without irradiation (**Table 3.2, Entries 3-5**), suggesting that Mes-Acr-Me⁺ plays a role in the formation of **B** as well. Additionally, when the catalyst was included but the reaction was not irradiated, no reaction occurred indicating that the reaction was proceeding through a single electron oxidation pathway

^{ix} Conditions in bold are highlighted to show change in reaction conditions from previous entries in the table. Reactions were carried out in N₂-sparged MeCN [0.1 M] under two LED lamps) for 18 h unless otherwise noted.

^x Yield as determined by ¹H NMR spectroscopic analysis of the crude reaction mixture relative to the internal standard (Me₃Si)₂O.

(**Table 3.2, Entries 6**). It seemed reasonable that under these conditions strong acid could have been formed through the initial oxidation of the alkene (**Scheme 3.2**). This could have the effect of activating the stoichiometric chlorinating reagents, which could then undergo electrophilic reactivity. To test this, reactions were carried out using a small quantities of acid. When the reaction was run with 5 mol% trifluoroacetic acid (TFA, $pK_a = -0.3$) no reaction occurred (**Table 3.2, Entry 7**), however when triflic acid (CF_3SO_3H , $pK_a = -14$) was used in the presence of substrate and NCS, and indeed product **B** was formed in 66% yield (**Table 3.2, Entry 8**). The pK_a of the cation-radical intermediate is most likely well below that of TFA. Thus, it seems possible that strong acid generated in situ could control reactivity in the absence of any Cu catalysts.

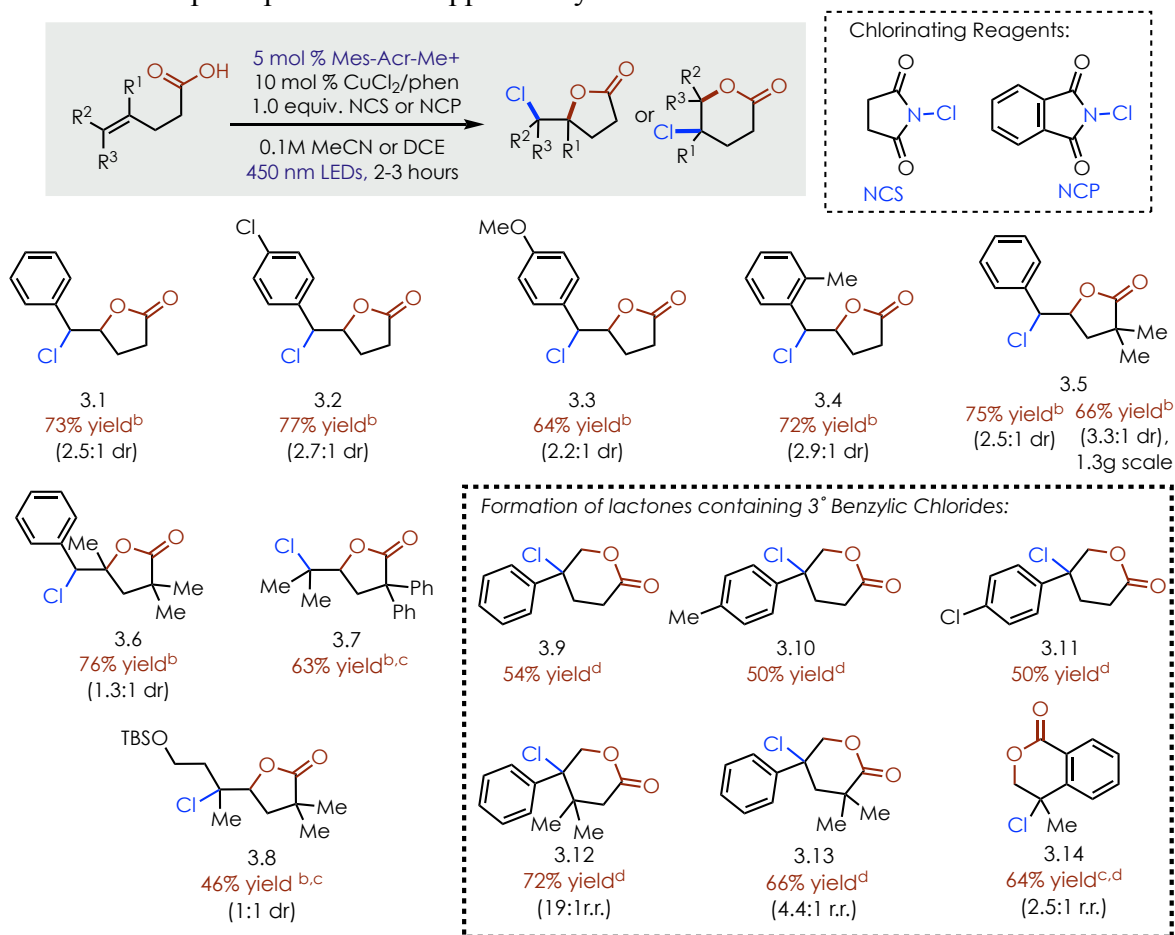
Scheme 3.3.2: Plausible mechanism for formation of undesired regioisomer in the absence of copper catalyst.



3.2.4 Scope of Chlorolactonization

The generality of the optimized conditions was examined for the chlorolactonization (**Chart 3.1**). Initially 1,2-disubstituted styrenes were evaluated; these substrates would be expected to give δ -lactones under electrophilic conditions (See Section 3.1.2.1.2, Figure 3.6), but give γ -lactones under these conditions. Varying substitution on the arene had very little effect on both yield and diastereoselectivity (3.1-3.4). Even electron rich styrenes could be tolerated with no background formation of δ -lactone products (3.3). As shown, previously in Section 3.2.3

Chart 3.1: Scope of photoredox/copper catalyzed chlorolactonization.^a



^a Products were isolated as single regioisomers except where noted. ^bCuCl₂/phen (10 mol%), NCP (1 equiv); ^c with AcOH (5.0 equiv) ^dCuCl₂/phen (10 mol%), NCS (1 equiv).

substitution at the carboxylic acid α -carbon was tolerated (3.5); this substrate could also be scaled

up to gram scale while maintaining good yield and diastereoselectivity in a simple batch setup (See Section 3.6.5.2). Trisubstituted styrenes were also shown to be capable of undergoing chlorolactonization under these conditions, however poor d.r. was observed (3.6).

The versatility of the chlorolactonization conditions was further demonstrated in the chlorofunctionalization of trisubstituted aliphatic alkenes (3.7 and 3.8). Under the originally optimized conditions, these substrates were highly prone to elimination of the chloride in situ, however when buffered with 5.0 equivalents of AcOH, the chlorolactone products could be isolated in synthetically useful quantities. Product 3.8 was isolated with the TBS (tert-butyldimethylsilyl) protected alcohol intact demonstrating the mildness of these conditions; although no diastereoselectivity was observed for this substrate.

1,1-disubstituted styrenes are prototypical substrates for enantioselective halofunctionalization methods; these substrates give γ -lactones under electrophilic conditions (See Section 3.1.2.1.2, Figure 3.7). However, with slight modifications to the optimized conditions, the less thermodynamically favored δ -lactone products could be formed (3.9-3.14).^{xi} Substrates bearing no substitution at the α - or β - positions led to the formation of only a single regioisomer in good yields, with mild variation of the arene electronics being tolerated (3.9-3.11). However, substitution at the β - carbonyl position led to a slight deterioration of regioselectivity, while substitution at the α - position began to favor the undesired regioisomer even more. This could indicate that background chlorolactonization is accelerated by a Thorpe-Ingold effect. Benzoic acids containing pendant unsaturation could also undergo chlorolactonization under these

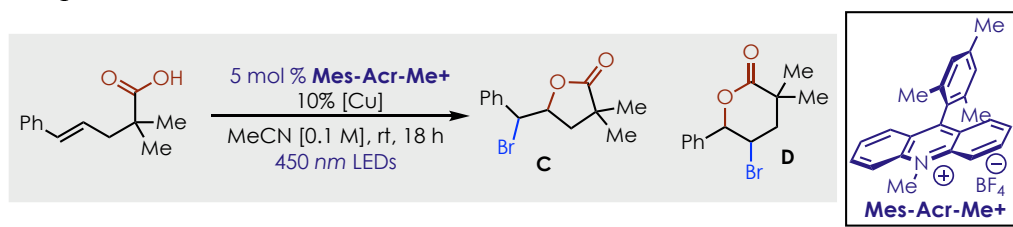
^{xi} These products were found to be unstable to silica gel, therefore NCS was used as the stoichiometric chlorinating agent because succinimide was more easily removed by filtration through a small silica plug.

conditions, although regioselectivity was particularly poor and the desired products were prone to elimination.

3.2.5 Optimization of Conditions for Bromolactonization

Conditions for bromolactonization were developed based on the optimal conditions for chlorolactonization. Potential radical bromine sources such as NBS (*N*-bromosuccinimide) and NBP (*N*-bromophthalimide) were found to be more prone to electrophilic type reactivity than their chlorine containing counterparts. When attempting to use these reagents to accomplish

Table 3.3: Optimization of Bromolactonization.^{xii}



Entry	Cu/Ligand	“Br• Source”	C% Yield ^{xiii} (γ-lactone)	D% Yield ^{xii} (δ-lactone)	d.r. ^{xiv}
1 ^{iv}	CuBr ₂ /bpy	1.0 equiv. NBS	29%	71%	2.5:1
2	CuBr ₂ /bpy	1.0 equiv. NBP	39%	61%	3.0:1
3	CuBr ₂ /bpy	1.0 equiv. DEBM	97%	3%	2.4:1
4 ^{xv}	CuBr ₂ /bpy	1.0 equiv. DEBM	—	—	—
5	—	1.0 equiv DEBM	—	—	—

^{xii} Reactions were carried out in N₂-sparged MeCN [0.1 M] under two LED lamps) for 18 h.

^{xiii} Yield as determined by ¹H NMR spectroscopic analysis of reaction mixtures relative to internal standard (Me₃Si)₂O.

^{xiv} Diastereomeric ratio (d.r.) refers to the d.r. of product **A** only. Product **B** was only observed as one diastereomer, indicating that it was formed via a background electrophilic pathway.

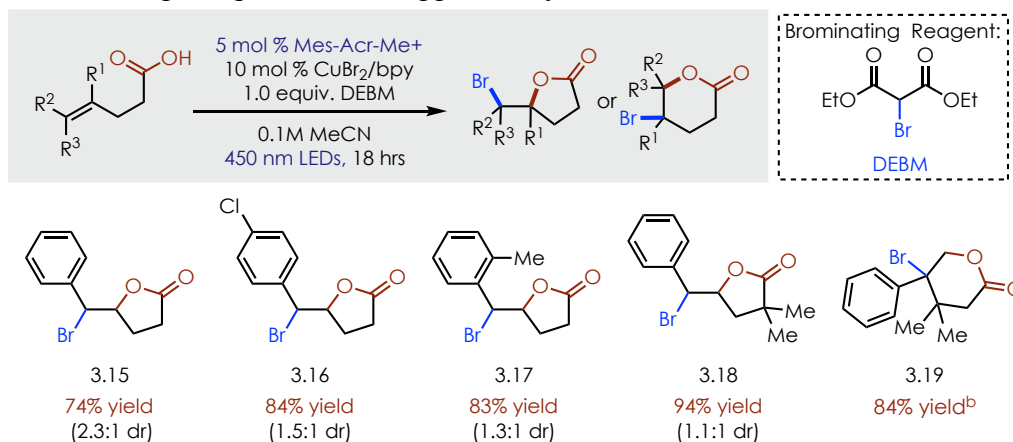
^{xv} The reaction was carried out without Mes-Acr-Me⁺

bromolactonization along with CuBr₂/bpy as a co-catalyst, low regioselectivity was observed (**Table 3.3, Entries 1 and 2**). This is due to uncatalyzed background electrophilic bromination (See Section 3.6.5.5, product 3.27). α -bromocarbonyl reagents have been shown to act as radical initiators in Cu^I catalyzed systems including ATRP, indicating that they can undergo oxidation of the metal center to a Cu^{II} halide complex.⁶⁴ Thus, diethylbromomalonate (DEBM) was screened for its ability to act as a less electrophilic stoichiometric bromine-atom donor. Indeed, when applied to the standard conditions, background reactivity was almost completely suppressed (**Table 3.3, Entry 3**). Importantly, when excluding either Mes-Acr-Me⁺ (**Table 3.3, Entry 4**), or CuBr₂/bpy (**Table 3.3, Entry 5**) no bromolactone products were observed, indicating that DEBM does not participate in background reactivity with the substrate. However, when CuBr₂/bpy was excluded from the reaction an additional product was observed by ¹H NMR. Further, analysis indicated that this product was the result of an anti-Markovnikov hydrolactonization product consistent with our previous work.⁵⁰ A potential mechanism for the formation of this byproduct involves DEBM acting as a hydrogen-atom donor.

3.2.6 Scope of Bromolactonization

Next, the scope of the bromolactonization was explored using these conditions (**Chart 3.2**). 1,2-disubstituted styrenes were found to be suitable substrates, however unlike the chlorolactonization only mildly electron rich styrenes were tolerated, this was exhibited by

Chart 3.2: Scope of photoredox/copper catalyzed bromolactonization.^a



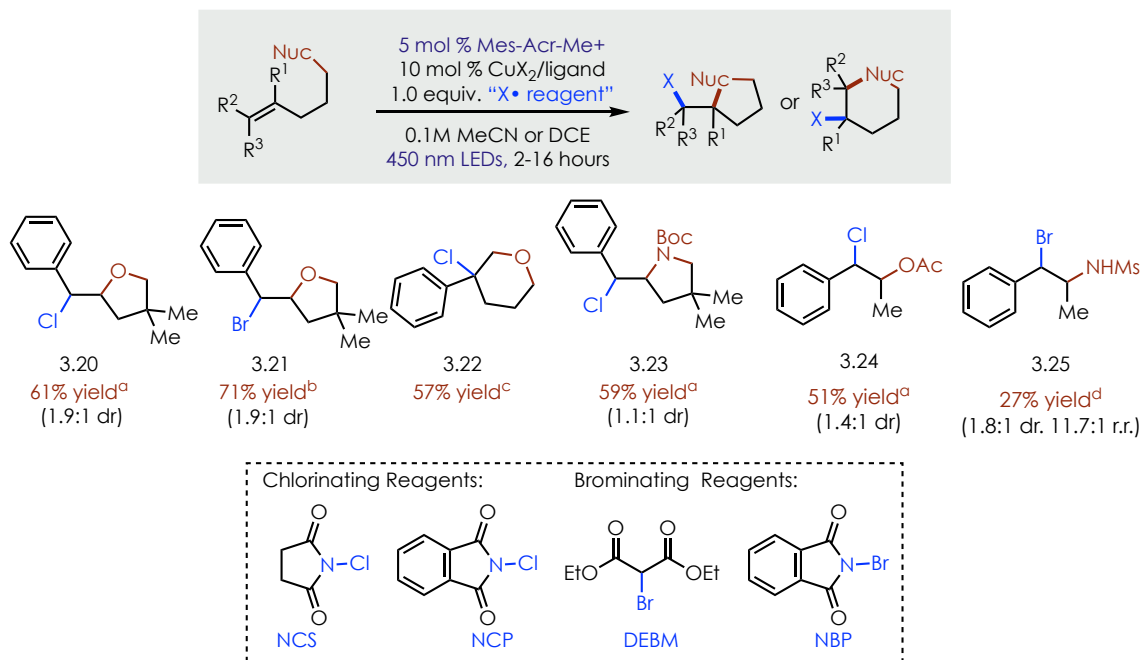
^a Products were isolated as single regioisomers except where noted.; ^b with 2,6-lutidine (10 mol%).

moderate variation of electronics on the arene ring (Entries 3.15-3.17). It is possible that electron rich substrates lead to very unstable benzylic bromides that decompose under the reaction conditions. Additionally, product 3.18 could be isolated in good yield as expected. Only the γ -lactone products were observed under the optimized reaction conditions when 1,2-disubstituted styrenes were used as substrates. Additionally, product 3.19 could be isolated as a single isomer, originating from a 1,1-disubstituted styrene. Other 1,1-disubstituted styrenes were not suitable substrates for bromolactonization; this could be potentially be due to elimination byproducts which are not possible for product 3.19.

3.2.7 Application toward other Halofunctionalization Reactions

To demonstrate the potential generality of this method, other halofunctionalization reactions were evaluated (**Chart 3.3**). Both Chloro- (3.20 and 3.22) and bromoetherification (3.21)

Chart 3.3: Scope of other nucleophiles for halofunctionalization of alkenes.



Products were isolated as single regioisomers except where noted. ^b $CuCl_2$ /phen (10 mol%), NCP (1 equiv); ^c $CuBr_2$ /bpy (10 mol%), DEBM (1 equiv); ^d $CuCl_2$ /phen (10 mol%), NCS (1 equiv); ^e $CuBr_2$ /phen (10 mol%), NBP (1 equiv)

could be accomplished using the standard conditions developed for the respective halolactonization reactions. These nucleophiles were found to favor the pyran regioisomers under electrophilic conditions (See Section 3.6.5.5, products 3.28). Protected amines could also undergo intramolecular chloroamination (3.23). Finally, intermolecular, three component couplings could be accomplished using acetic acid (3.24) or methanesulfonamide (3.25) as nucleophiles. Again, under electrophilic conditions the chloroacetoxylation reaction provided the opposite regioisomer (See Section 3.6.5.5, product 3.29), highlighting the utility of this method for reversing this inherent regioselectivity. These products were isolated in moderate to good yields despite being

largely unoptimized, and exhibited a reversal of regioselectivity based on expected selectivity for electrophilic halofunctionalization.

3.3 Product identification: distinguishing regio- and diastereoisomers

3.3.1 Distinguishing Regioisomers

Regioisomers of chlorofunctionalization could generally be distinguished by analysis of the ^1H NMR. However, NMR spectra for the regioisomers were often very similar, particularly for products derived from 1,2-disubstituted styrenes (Section 3.2.3.2, Chart 3.1, Entries 3.1-3.6, 3.15-3.18). To aid in future disambiguation between the regioisomers, the δ -lactone product was generated via reaction of the corresponding alkene under electrophilic conditions with dichlorodimethylhydantoin (3.26, See Section 3.6.5.5). The γ -lactone product (3.5) was generated via the chlorofunctionalization procedure described in detail in Section 3.6.5.2. Comparing the two regioisomers shows H_a in the product 3.26 is further downfield than H_a in the product 3.5. H_b in the δ -lactone product is further upfield than H_b in the γ -lactone product. The shifts of both H_a and H_b in each product match with the expected relative shifts.

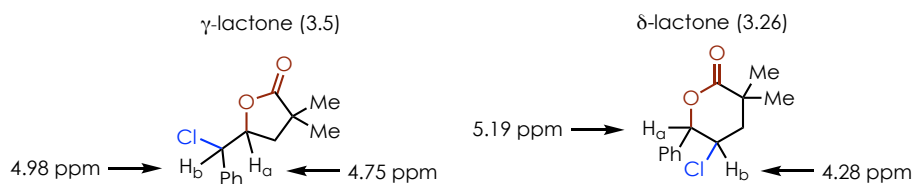


Figure 3.14: Comparison of ^1H NMR shifts between regioisomers 3.5 and 3.26.

HSQC data could be used as further evidence of which regioisomer is formed. Via HSQC C_a and C_b could be assigned for each product. As expected C_a is further downfield in 3.26, while C_b is further upfield, relative to the respective carbon shifts in product 3.5.

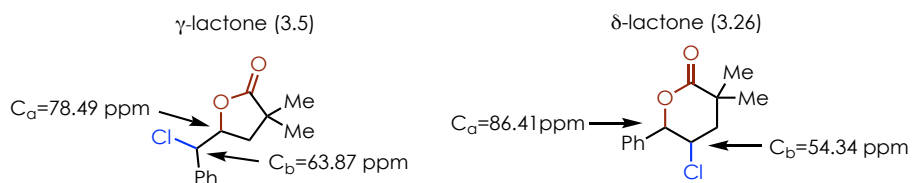


Figure 3.15: Comparison of ^{13}C NMR shifts determined by HSQC for each regioisomer.

These analyses could be extrapolated to products 3.1-3.5, 3.15-3.18, and 3.24. Analysis of HSQC data alone was sufficient for determining the regioisomer for products 3.7, 3.8, 3.20, and 3.21.^{xvi} Products derived from 1,1-disubstituted styrenes (3.9-3.14, 3.19, and 3.22), were compared to NMR spectra reported in the literature for their respective regioisomers and were found to be inconsistent with these products.^{25,31,65} HSQC is also consistent with these product assignments.^{xvii}

^{xvi} The relevant carbon shifts were more consistent with being adjacent to oxygen rather than a halogen

^{xvii} Quaternary carbons in the lactone are relatively upfield shifted.

3.3.2 Distinguishing Trans and Cis Diastereomers

To make a distinction between diastereomers of product 3.5 were separated (See Section 3.6.5.2). The major diastereomer was submitted to reductive conditions reported by Borhan and co-workers for reducing chlorolactones to their corresponding epoxy alcohol products.³⁷ When the major diastereomer was submitted to the reduction conditions, a mixture of the epoxide product, as well as a furan product, resulting from epoxide ring opening were obtained (**Figure 3.16, top**). These could be separated and characterized after column chromatography. It is important to note that a single epoxide was observed by crude ¹H NMR. This epoxide product exhibited a coupling

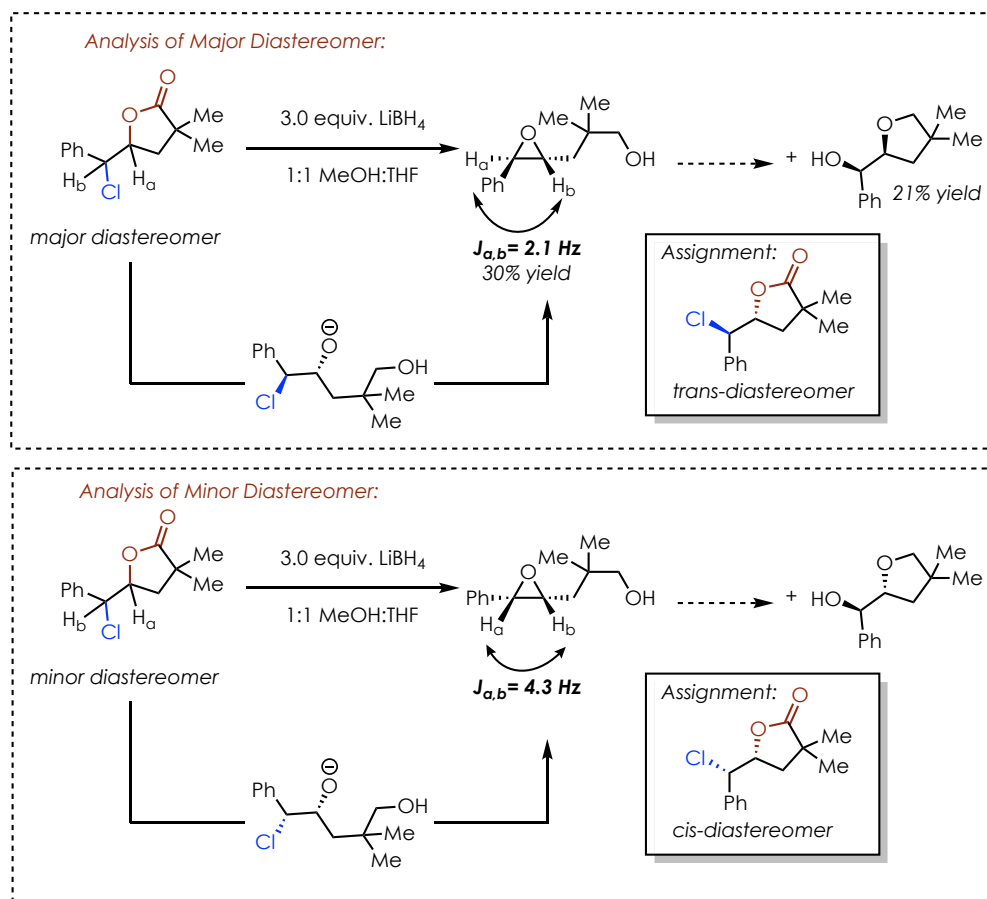


Figure 3.16: Analysis of diastereomers by formation of the corresponding epoxide products.

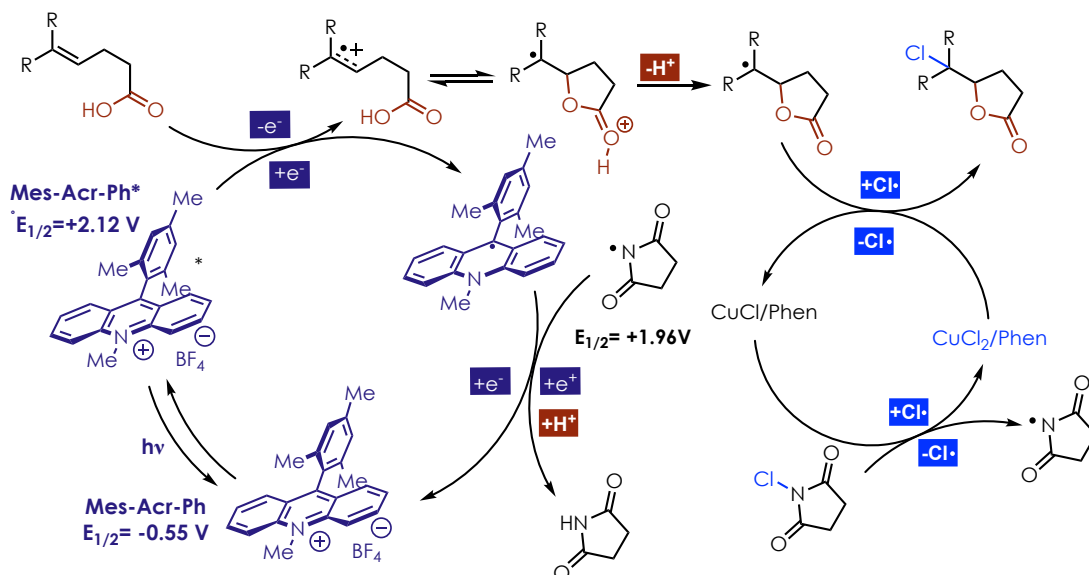
constant of 2.1 Hz between H_a and H_b . This small coupling constant is consistent with a trans-epoxide.^{xviii} Therefore, the major isomer was assigned as the trans-chlorolactone product.

The minor diastereomer was also submitted to the reduction conditions (**Figure 3.16, bottom**).^{xix} The cis epoxide as well as the corresponding furan were observed by crude NMR and the identities were confirmed by GC/MS. The cis epoxide was found to be unstable to silica gel resulting in the complete conversion to the corresponding furan. However, the epoxide was found to have a coupling constant of 4.3 Hz. This larger coupling constant is consistent with a cis epoxide. Therefore, the minor isomer was assigned as the cis-chlorolactone product.

3.4 Mechanism of Photoredox/Copper Mediated Halofunctionalization

3.4.1 Initial Mechanistic Proposal

Scheme 3.3.3: Mechanistic proposal for chlorolactonization catalyzed by Mes-Acr-Me⁺ and CuCl₂/phen



^{xviii} Full ¹H NMR spectral data included in Section 3.6.6

^{xix} The pure minor diastereomer could not be isolated in pure form. Therefore, a 2:1 mixture of minor:major diastereomers was submitted to the reaction conditions.

Upon excitation with 450 nm light, Mes-Acr-Me⁺ accesses a locally excited single state ($E_{1/2}^{red} = +2.12$ V vs SCE), which can undergo SET with the alkene^{xx} forming a reactive radical cation intermediate (**Scheme 3.3**). The cation radical undergoes fast nucleophilic trapping; after irreversible deprotonation an intermediate which forms the most stable radical. Two mechanisms are potentially possible for radical trapping the radical: 1.) outer sphere atom-transfer of the chlorine atom reducing Cu^{II} to Cu^I. 2.) Radical addition to CuCl₂ to form a very unstable Cu^{III} intermediate which undergoes reductive elimination to form the product and Cu^I.

However, based on the previous literature, including ATRP and other atom transfer radical addition (ATRA) reactions, an atom transfer mechanism seems more likely for this system.⁶⁶ Following formation of a Cu^I intermediate oxidation by NCS or NCP leads to regeneration of CuCl₂/phen and also a succinimide radical (**S•**). Importantly, this radical has been shown to have a very large reduction potential ($E_{1/2}^{red} = +1.96$ V vs SCE), thus **S•** could potentially directly oxidize many of the alkene substrates. This could potentially initiate a chain propagated mechanism, which will be explored below in Section 3.4.1.2. However, **S•** could also undergo electron transfer with Mes-Acr-Me• which would regenerate the photocatalyst, and following proton transfer from a substrate equivalent leads to the formation of succinimide, which is formed as a byproduct in the reaction.

^{xx} $E_{p/2}^{ox}$ values for styrenes used for this research likely span a range between approximately 1.2-1.9 V vs SCE based on values reported for similar substrates, while trisubstituted alkenes have $E_{p/2}^{ox}$ of approximately 2.0 V vs SCE.^{50,84}

3.4.2 UV/vis analysis of Cu (I) Oxidation by NCP

In order to determine if Cu^I oxidation by stoichiometric halogenating reagents to generate Cu^{II} species, UV/vis analysis of the relevant species was undertaken (**Figure 3.17**). Initially spectra of the independently generated Cu^I (red line) and Cu^{II} (yellow line) species were obtained, which were found to match the previously reported spectra.^{67,68} CuCl/phen exists as a dimer in solution

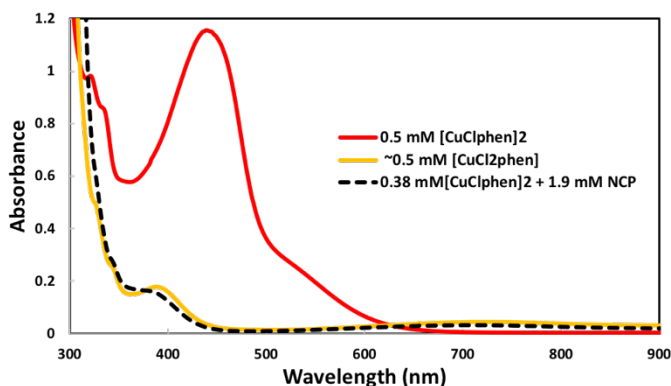


Figure 3.17: UV/vis absorption spectra of the 0.5 mM [CuClphen]₂ (red line) before and after adding *N*-chlorophthalimide (dashed black line). The yellow line shows a spectrum of ~0.5 mM [CuCl₂phen] which was independently synthesized for reference.

and has a strong absorbance centered around 439 nm, while [CuCl₂phen] is relatively weakly absorbing in this region but has characteristic local maxima at 388 nm and a broad absorbance at around 714 nm. NCP (at a final concentration of 1.9 mM) was added to the solution of 0.5 mM [CuClphen]₂; within 20 seconds the absorbance at 439 nm had completely bleached and a spectrum roughly matching the [CuCl₂phen] spectrum was obtained (See Section 3.6.7 for further details). The same analysis was performed with [CuBrbpy]₂. After mixing with DEBM the Cu^I absorbance at 424 nm was bleached while a spectrum similar to the independently synthesized [CuBr₂bpy] appeared (See 3.6.7 for further details). Both of these results seem to indicate that after halogen atom transfer occurs, Cu^I species are quickly oxidized in situ to Cu^{II}. Also, while both Cu^I species absorb strongly near the emission of the LED lamps ($\lambda_{max} = 450$ nm), this absorption is not likely to interfere because Cu^I is short lived. Both phthalimide and diethyl malonate were observed as

by-products in the crude reaction mixtures by ^1H NMR spectroscopy and GC–MS. This observation is consistent with the proposal of $\text{S}\cdot/\text{PhthN}\cdot$ reduction and subsequent protonation.

3.4.3 Evaluation of a Potential Chain Propagation Mechanism

In the mechanism proposed in Section 3.4.1, $\text{Mes-Acr-Me}\cdot$ is turned over by the succinimide ($\text{S}\cdot$) or phthalimide ($\text{PhthN}\cdot$), resetting the catalytic cycle. $\text{S}\cdot$ has been shown to undergo single-electron oxidation of $[\text{Ru}(\text{bpy})_3]^{2+}$ with rate constants on the order of $10^9 \text{M}^{-1}\text{s}^{-1}$ ⁶³ 5–6 orders of magnitude greater than that of C–H abstraction,⁶⁹ rearrangement,⁶³ or arene addition.⁷⁰ Thus, the potential for this radical to act as a one-electron oxidant has been established. However, $\text{S}\cdot$ has a very high reduction potential (+1.96 V vs SCE) and could potentially directly oxidize the alkene substrates, initiating a chain mechanism (**Figure 3.18**). To determine if chain propagation was occurring, the photochemical quantum yield for the reaction (Φ_{R}) was determined

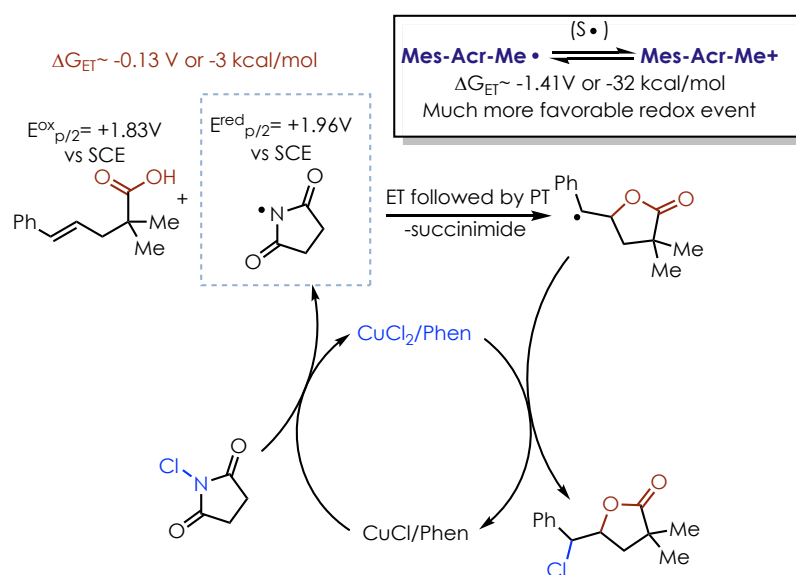


Figure 3.18: Proposed Mechanism of a chain Propagated chlorolactonization

to be 3.6% for the chlorolactonization reaction to form product 3.5.^{xxi} Under the reaction conditions solutions are optically dense (Mes-Acr-Me⁺ has an absorption >2 at 450 nm) indicating that all photons that enter solution are absorbed. Thus, a Φ_R of 3.6% indicates a very inefficient reaction in terms of photons absorbed vs moles of product formed. A very small Φ_R is more consistent with the mechanism proposed 3.4.1, as chain propagated reactions typically have very high quantum yields, often above 100%. However, a very inefficient chain propagation cannot be ruled out.

3.5 Conclusions

Halofunctionalization reactions have been long established to give reliable regioselectivity. The halide typically is formed at the least electron rich carbon, forming the more thermodynamically stable product. A methodology for the reversal of this innate regioselectivity has been developed using an organic photoredox and copper catalyzed strategy. This allowed the development of chloro- and bromolactonization reactions, which exhibited reliable regioselectivity for a host of substrates. Additionally, this strategy was shown to be amendable to other halofunctionalization reactions. Finally, a few key mechanistic steps were evaluated.

^{xxi}The photochemical quantum yield of reaction (Φ_R) is defined as such: $\Phi_R = \frac{\text{mols product}}{\text{mols photon}}$.

3.6 Experimental

3.6.1 General Methods and Materials

General Methods. Proton, carbon, Heteronuclear Single Quantum Coherence, and Correlated Spectroscopy (^1H NMR, ^{13}C NMR, HSQC, COSY, respectively) were recorded on a Bruker model DRX 400 or AVANCE III 600 CryoProbe spectrometer (^1H NMR at 400 MHz or 600 MHz, ^{13}C NMR at 100 MHz or 150 MHz respectively). Chemical shifts for proton NMR are reported in parts per million downfield from tetramethylsilane and are referenced to residual CHCl_3 in solution (CHCl_3 set to 7.26 ppm). Chemical shifts for ^{13}C NMR are reported in parts per million downfield from tetramethylsilane and are referenced to the carbon resonances of the solvent (CDCl_3 set to 77.00 ppm). NMR data are represented as follows: chemical shift, multiplicity (s = singlet, br s = broad singlet, d = doublet, dd = doublet of doublet, t = triplet, ddd = doublet of doublet of doublet, q = quartet, m = multiplet, etc.), coupling constants (Hz), and integration. High Resolution Mass Spectra (**HRMS**) were obtained using Thermo LTqFT mass spectrometer with electrospray ionization in positive mode. Low Resolution Mass Spectra (**LRMS**) were obtained using GC-MS (Agilent 6850 series GC equipped with Agilent 5973 network Electron Impact-MSD). Infrared (**IR**) spectra were obtained using a Jasco 260 Plus Fourier transform infrared spectrometer. Thin layer chromatography (TLC) was performed on SiliaPlate 250 μm thick silica gel plates purchased from Silicycle. Visualization was accomplished using fluorescence quenching, KMnO_4 stain, or ceric ammonium molybdate (CAM) stain followed by heating. Purification of the reaction products was carried out by chromatography using Siliaflash-P60 (40-63 μm) silica gel purchased from Silicycle. All reactions were carried out under an inert atmosphere of nitrogen in flame-dried

glassware with magnetic stirring unless otherwise noted. Reactions were carried out in standard borosilicate glass vials purchased from Fisher Scientific. Yield refers to isolated yield of analytically pure material unless otherwise noted. NMR yields were determined using hexamethyldisiloxane, $(\text{Me}_3\text{Si})_2\text{O}$, as an internal standard.

Materials. Commercially available reagents were purchased from Sigma Aldrich, Acros, Alfa Aesar, Fisher Scientific, or TCI, and used as received unless otherwise noted. Diethyl ether (Et_2O), dichloromethane (DCM), tetrahydrofuran (THF), toluene (PhMe), and dimethylformamide (DMF) were dried by passing through activated alumina columns under nitrogen prior to use. 1,2-dichloroethane (DCE) was purchased from Fischer and sparged with N_2 before being stored over activated 4Å molecular sieves in a glovebox. Acetonitrile (MeCN) was dried by passing through activated alumina column under nitrogen. MeCN was commonly stored in a glovebox after sparging with N_2 . Glacial acetic acid (AcOH) stored in the glovebox with 5% v/v acetic anhydride. Other common solvents such as chloroform (CHCl_3) were purified by standard published methods when necessary. Trans- β -methylstyrene was distilled over potassium hydroxide, sparged with N_2 , and stored in a glovebox freezer.

3.6.2 Photoreactor Setup

Reactions were irradiated using a photoreactor which consists of two Par38 Royal Blue Aquarium LED lamps (Model #6851) purchased from ecxotic. A standard magnetic stir plate was used as the support. Reaction efficacy can be impacted by the type of LED used. A fan was added above to cool the reaction and keep the temperature below 30 °C.

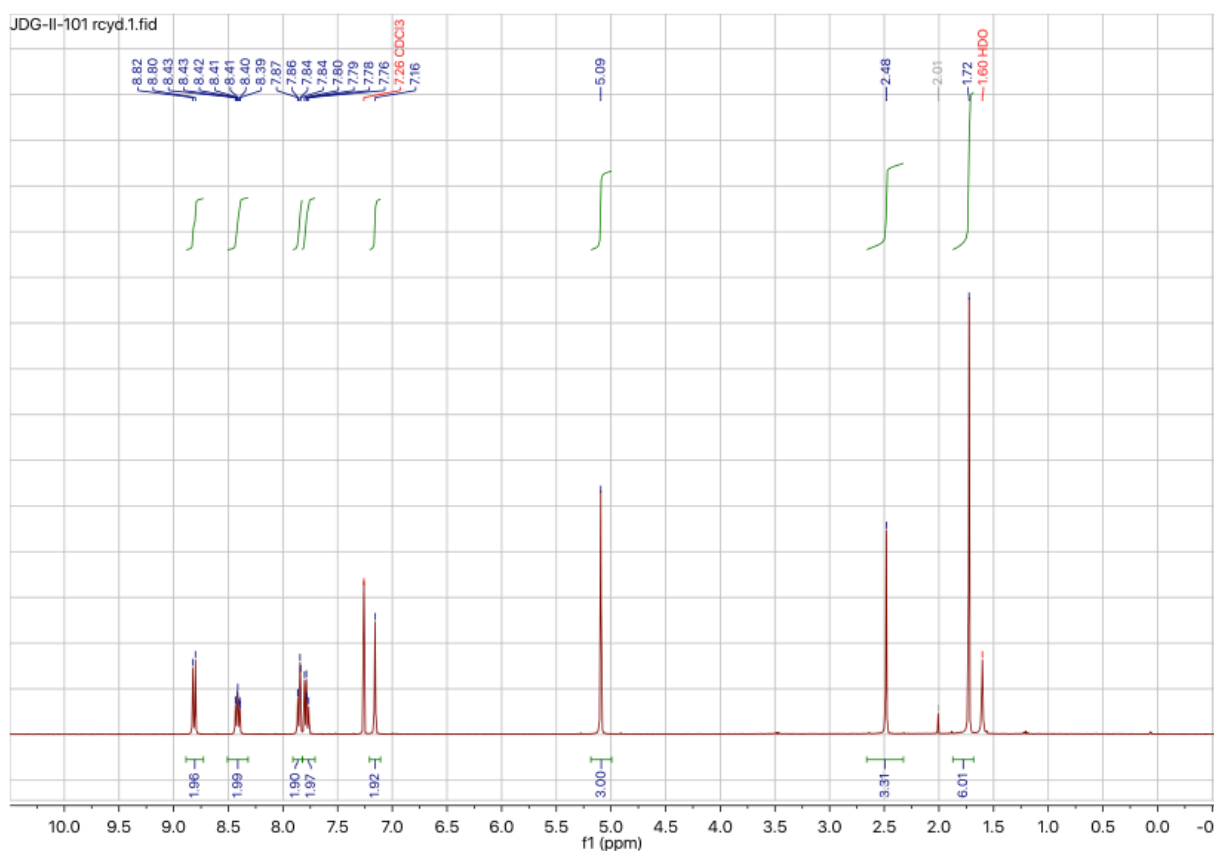


Figure 3.19: Photoreactor setup used for halofunctionalization reactions. Reaction vials were placed about 5 cm from the face of both lamps. Above a simple fan was used to cool the reaction.

3.6.3 Catalyst Synthesis

9-mesityl-10-methylacridin-10-ium tetrafluoroborate (**Mes-Acr-Me⁺**) was synthesized by the method of Fukuzumi et al.¹ Tetrafluoroboric acid (diethyl ether complex) was substituted for perchloric acid during the hydrolysis. The photocatalyst could be recrystallized by dissolving in a minimal amount of acetonitrile, then carefully layering on ether. Crystals form at the interface of the two solvents. The spectral data matched the values reported in the literature.⁷¹

¹H NMR (400 MHz, Chloroform-*d*) δ 8.81 (d, J = 9.2 Hz, 2H), 8.41 (ddd, J = 8.9, 6.6, 1.7 Hz, 2H), 7.85 (dd, J = 8.7, 1.6 Hz, 2H), 7.78 (dd, J = 8.7, 6.6 Hz, 2H), 7.16 (s, 2H), 5.09 (s, 3H), 2.48 (s, 3H), 1.72 (s, 6H).

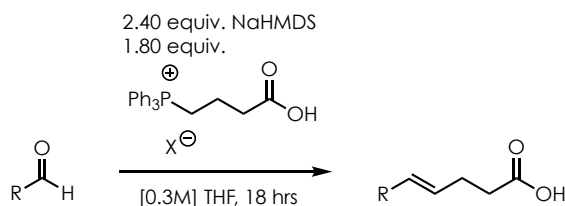


3.6.4 Substrate Synthesis

Pentenoic acid derivatives were prepared according to the following Wittig olefination procedure:

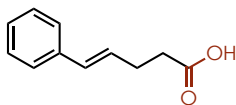
1.8 equivalents (relative to the necessary aldehyde precursor) 3-

Scheme 3.3.4: General Scheme for Synthesis of 1,2 disubstituted alkene substrates



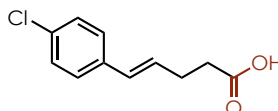
carboxypropyl)triphenylphosphonium bromide⁷² or chloride was weighed and dispensed into a flame-dried round bottom flask equipped with a magnetic stir bar. The flask was flushed with N_2 and THF was added to 0.3 M concentration. The solution was cooled to $0^{\circ}C$ before 2.4 equiv. Sodium hexamethyldisilazane (1.0 M in THF) was carefully added to the stirring solid. The contents were warmed to room temperature and stirred for 0.5 to 1 hour after which the solution was cooled to $-78^{\circ}C$ and 1 equiv. of the necessary aldehyde was added dropwise to the stirring ylide. The reaction stirred overnight while warming to room temperature. The reaction was quenched with H_2O , and diluted with equal amounts deionized H_2O and diethyl ether, and the aqueous phase was acidified to pH of 1 before extracting 3 times with ethyl acetate. The organics were combined and dried over Na_2SO_4 and concentrated under reduced pressure. Purification was accomplished via column chromatography (gradient: 2:1 Et_2O :Hexanes with 1% Acetic Acid by volume \rightarrow 1:1 Et_2O :Hexanes with 1% Acetic Acid by volume).

(*E*)-5-phenylpent-4-enoic acid:



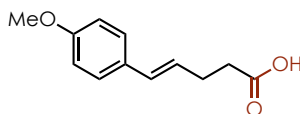
Obtained as the pure *E*-isomer in 65% isolated yield. Analytical data were in agreement with literature values.⁷³

(*E*)-5-(4-chlorophenyl)pent-4-enoic acid:



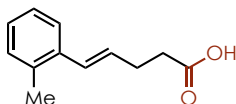
Obtained as a 6:1 mixture of *E*:*Z* isomers in an 89% isolated yield. Analytical data were in agreement with literature values.⁷³

(*E*)-5-(4-methoxyphenyl)pent-4-enoic acid:



Obtained as a 8:1 mixture of *E*:*Z* isomers in an 84% isolated yield. Analytical data matched were in agreement with literature values.⁷³

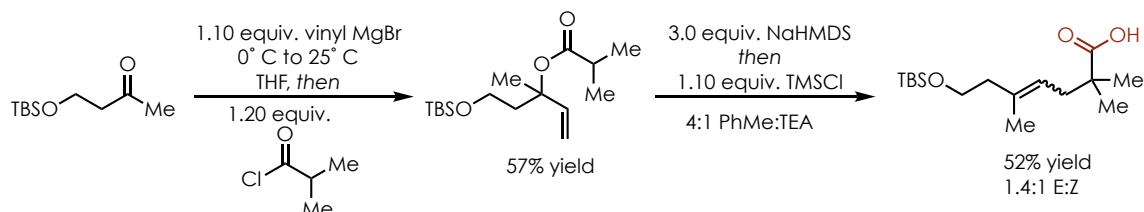
(*E*)-5-(*o*-tolyl)pent-4-enoic acid:



Obtained as a 1.9:1 mixture of *E*:*Z* isomers in an 93% isolated yield. Analytical data matched were in agreement with literature values.⁷³

7-((*tert*-butyldimethylsilyl)oxy)-2,2,5-trimethylhept-4-enoic acid:

Scheme 3.3.5: Synthesis of 7-((*tert*-butyldimethylsilyl)oxy)-2,2,5-trimethylhept-4-enoic



To a flame dried 250 mL round bottom flask containing 3.9 g of 4-((*tert*-butyldimethylsilyl)oxy)butan-2-one⁷⁴ was flushed with N₂ before adding 100 mL dry THF. The solution was cooled to 0°C before adding 21 mL vinyl magnesiumbromide solution (1 M in THF from Sigma) dropwise. This was allowed to stir for an additional hour while warming to room temperature, before 2.4 mL of isobutyryl chloride was added. The reaction was then stirred for 2 hours before the reaction was quenched with H₂O and then a saturated solution of ammonium chloride. The mixture was transferred to a separatory funnel where Et₂O was added. The phases were separated, and the aqueous layer was back extracted twice with Et₂O. The combined organics were dried over MgSO₄ and the solution was concentrated. 5-((*tert*-butyldimethylsilyl)oxy)-3-methylpent-1-en-3-yl isobutyrate was obtained cleanly after column chromatography to give 3.3 g (57% yield) of a clear oil.

¹H NMR: (400 MHz, Chloroform-*d*) δ 5.97 (dd, *J* = 17.5, 11.0 Hz, 1H), 5.19 – 5.06 (m, 2H), 3.68 (t, *J* = 7.3 Hz, 2H), 2.48 (hept, *J* = 7.0 Hz, 1H), 2.07 (tdd, *J* = 20.5, 13.9, 7.3 Hz, 2H), 1.55 (s, 3H), 1.14 (d, *J* = 7.0 Hz, 6H), 0.88 (s, 9H), 0.04 (s, 6H).

To a flame dried 250 mL round bottom flask was added 80 mL of dry toluene and 20 mL of freshly distilled triethylamine. Next, 3.3 g 5-((*tert*-butyldimethylsilyl)oxy)-3-methylpent-1-en-3-yl

isobutyrate was added in a solution of toluene and the solution was cooled to -78°C . 33 mL of a solution of NaHMDS in THF (1 M) was slowly added while stirring. This was stirred for 1 hour at -78°C before 1.5 mL of TMSCl was added, and the solution was allowed to warm to room temperature while stirring overnight. The reaction was quenched by adding H_2O and 3M HCl solution. The reaction mixture was transferred to a separatory funnel and the aqueous layer was brought to a pH of 1 then extracted with Et_2O three times. The combined organics were washed with H_2O and brine, before drying with MgSO_4 , filtered and concentrated to give a yellowish oil. The title compound was purified on column chromatography (15% EtOAc:Hexanes, 150 mL dry silica gel) to obtain 1.7 g (52% yield) of 7-((*tert*-butyldimethylsilyl)oxy)-2,2,5-trimethylhept-4-enoic acid (1.4:1 *E:Z*, yellowish oil).

^1H NMR: Mixture of *E:Z* isomers (400 MHz, Chloroform-*d*) δ 5.17 (t, $J = 6.7$ Hz, 1H *E/Z*), 3.70 – 3.55 (m, 2H *E/Z*), 2.27 (t, $J = 6.9$ Hz, 2H, *E/Z*), 2.22 (t, $J = 7.1$ Hz, 1H, *E/Z*), 2.17 (d, $J = 1.5$ Hz, 1H, *E/Z*), 1.73 (s, 3H *Z*), 1.63 (s, 3H *E*), 1.19 (s, 6H *E/Z*), 0.89 (s, 3H *Z*), 0.88 (s, 3H *E*), 0.05 (d, $J = 1.6$ Hz, 6H *Z*), 0.04 (d, $J = 1.6$ Hz, 6H *E*).

^{13}C NMR: (151 MHz, CDCl_3) δ 183.58, 183.45, 135.37, 134.99, 121.81, 121.43, 62.39, 61.72, 53.41, 43.31, 42.58, 42.32, 38.23, 38.20, 35.60, 25.96, 25.94, 24.65, 24.49, 24.26, 18.36, 18.31, 16.61, -5.30.

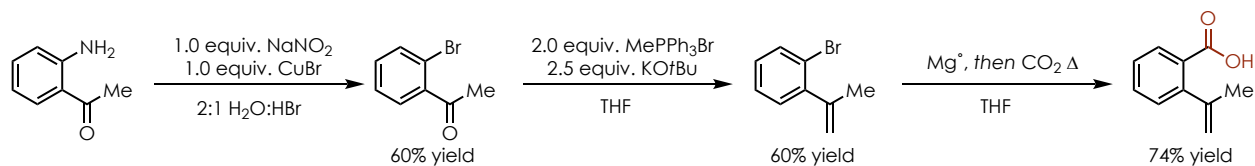
IR (thin film cm^{-1}): 3447, 2956, 2930, 2858, 1701, 1473, 1256, 1095

HRMS: m/z **calculated** for $\text{C}_{16}\text{H}_{32}\text{O}_3\text{Si}[\text{H}]^+$: 301.2193; **found**: 301.2193

NMR Spectra (^1H , ^{13}C): 185

2-(prop-1-en-2-yl)benzoic acid:

Scheme 3.6: Synthesis of 2-(prop-1-en-2-yl)benzoic acid



15 mL of 36% HBr and 35 mL of H_2O were added to a 250 mL round bottom flask, followed by 3 mL 1-(2-aminophenyl)ethan-1-one. The solution was cooled to 0°C before adding 1.7 g of NaNO_2 dissolved in H_2O dropwise. This was allowed to stir about 20 minutes after all of the NaNO_2 had been added. 3.6 g of CuBr was added, with N_2 bubbles forming immediately. This was stirred overnight before quenching the reaction with a saturated solution of NaHCO_3 . A precipitate formed which was filtered under vacuum. The mixture was then transferred to a separatory funnel and extracted 3 times with Et_2O . The organics were combined and dried over MgSO_4 , and concentrated giving a brownish oil. This was passed through a plug of silica to give 3.0 g of 1-(2-bromophenyl)ethan-1-one as a yellow oil (60% yield). No further purification was necessary. Characterization matched previous reports.⁷⁵

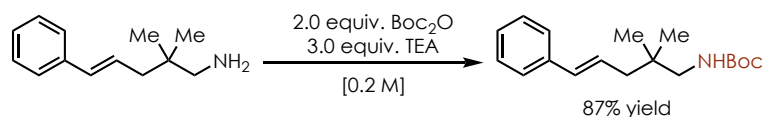
To a flame dried 250 mL round bottom flask was added 10.8 g of methyltriphenylphosphonium bromide and 4.2 g of KOtBu . The flask was then evacuated and refilled with N_2 before adding 150 mL of dry THF and stirring for 20 minutes. 3 g of 1-(2-bromophenyl)ethan-1-one was added and the solution was stirred overnight. The reaction was quenched with a saturated solution of ammonium chloride and the mixture was transferred to a separatory funnel. Et_2O was added and the two phases were separated. The aqueous layer was back extracted twice with Et_2O . The combined organics were dried with MgSO_4 , filtered, and concentrated. The product was purified

by dry loading the resulting material on celite and eluted from a short silica plug with hexanes. 1.8 g of 1-bromo-2-(prop-1-en-2-yl)benzene was obtained as a clear oil (60% yield). Characterization matched previous reports.⁷⁶

To a flame dried 100 mL round bottom flask was added 500 mg Mg° (2.0 eq) , and a small amount of I2. The flask was purged with N₂ before adding 25 mL dry THF, resulting in an orange solution. 1.8 g of 1-bromo-2-(prop-1-en-2-yl)benzene was added. After about ten minutes the orange color subsided; the solution was allowed to stir an addition 30 minutes before the solution was sparged with a balloon of CO₂ for about 5 minutes. The flask was kept under a balloon of CO₂ while stirring overnight. The reaction was then quenched with H₂O and transferred to a separatory funnel where more H₂O and Et₂O were added. The organic layer was removed before bringing the aqueous layer to a pH of 1 forming a white precipitate. The aqueous layer was extracted three times with Et₂O and the combined organics were dried with MgSO₄, filtered, and concentrated to give 1.1 g of 2-(prop-1-en-2-yl)benzoic acid (74% yield). No further purification was required. Characterization matched previous reports.⁵

***tert*-butyl (*E*)-(2,2-dimethyl-5-phenylpent-4-en-1-yl)carbamate:**

Scheme 3.3.7: Synthesis of *tert*-butyl (*E*)-(2,2-dimethyl-5-phenylpent-4-en-1-



To a flame dried 100 mL round bottom flask was added 1 gram of (*E*)-2,2-dimethyl-5-phenylpent-4-en-1-amine⁷⁷ and 2.3 grams of di-*tert*-butyl dicarbonate. The flask was flushed with N₂ before adding 25 mL of dry DCM and 2.2 mL of freshly distilled triethylamine. The reaction was allowed to stir overnight before removing DCM and most triethylamine under vacuum. The crude material

was then purified on silica gel (20% EtOAc:Hexanes) to give the product as a white solid 1.4 grams, 87% yield.

¹H NMR:(400 MHz,) δ 7.38 – 7.33 (m, 2H), 7.30 (dd, J = 8.5, 6.7 Hz, 2H), 7.23 – 7.17 (m, 1H), 6.39 (d, J = 15.7 Hz, 1H), 6.24 (dt, J = 15.4, 7.5 Hz, 1H), 4.59 (s, 1H), 3.01 (d, J = 6.5 Hz, 2H), 2.12 (dd, J = 7.5, 1.2 Hz, 2H), 1.45 (s, 9H), 0.92 (s, 6H).

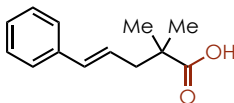
¹³C NMR: (151 MHz, CDCl₃) δ 156.19, 137.56, 132.54, 128.48, 127.01, 126.73, 126.04, 79.07, 50.49, 43.48, 35.46, 28.41, 24.84.

IR (thinfilm cm⁻¹): 3379, 2965, 2929, 1702, 1510, 1365, 1245, 1171, 967, 736

HRMS: m/z **calculated** for C₁₈H₂₇NO₂[Na]⁺: 312.1934; **found**: 312.1932

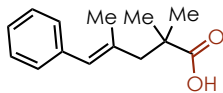
NMR Spectra (¹H, ¹³C): 186

(*E*)-2,2-dimethyl-5-phenylpent-4-enoic acid:



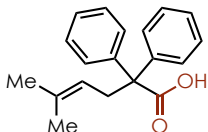
Prepared according to a previously reported literature procedure.⁵⁰

(*E*)-2,2,4-trimethyl-5-phenylpent-4-enoic acid:



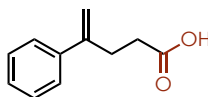
Prepared according to a previously reported literature procedure.

5-methyl-2,2-diphenylhex-4-enoic acid:



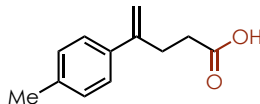
Prepared according to a previously reported literature procedure.⁵⁰

4-phenylpent-4-enoic acid:



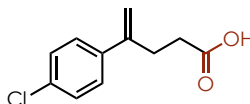
Prepared according to a previously reported literature procedure.⁷⁸

4-(*p*-tolyl)pent-4-enoic acid:



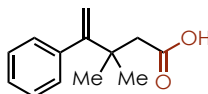
Prepared according to a previously reported literature procedure.⁷⁹

4-(4-chlorophenyl)pent-4-enoic acid:



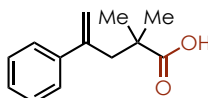
Prepared according to a previously reported literature procedure.⁷⁹

3,3-dimethyl-4-phenylpent-4-enoic acid:



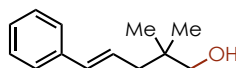
Prepared according to a previously reported literature procedure.⁵⁰

2,2-dimethyl-4-phenylpent-4-enoic acid:



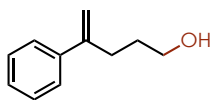
Prepared according to a previously reported literature procedure.⁸⁰

(*E*)-2,2-dimethyl-5-phenylpent-4-en-1-ol



Prepared according to a previously reported literature procedure.⁵⁰

4-phenylpent-4-en-1-ol:



Prepared according to a previously reported literature procedure.⁷⁸

3.6.5 Halofunctionalization Procedures and Characterization Data

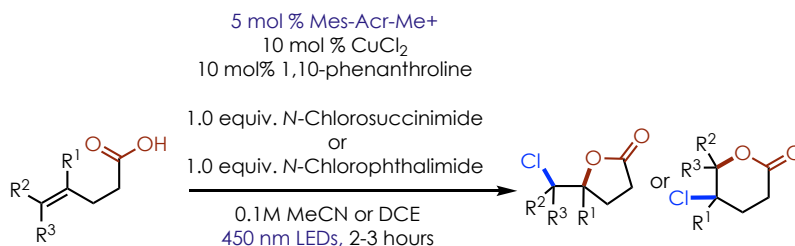
3.6.5.1 Important Notes

Note: NCP and NCS were purchased from Sigma and stored in a desiccator away from light. This was found to be particularly important for avoiding background reactivity, most likely through formation of Cl_2 . Copper (II) sources as well as ligands were stored in the desiccator as well to avoid absorption of H_2O .

Note: Products **3.9**, **3.10**, and **3.22** were found to decompose upon standing. Characterization data for these compounds was collected after preparing fresh samples. It was also noted that compounds **3.11**, **3.12**, **3.13**, **3.14**, and **3.19** were slightly less prone to decomposition, but still experienced some degree of decomposition upon standing.

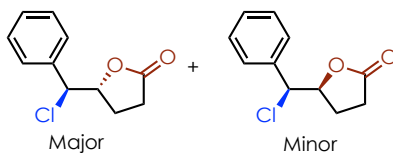
Note: Under the normal conditions products **3.7** and **3.8** were isolated with significant quantities of a new alkene product which was suspected to arise from chloride elimination. Using acetic acid as a buffer was found to alleviate this issue, and increased the yield of the desired chlorolactone.

3.6.5.2 General Procedure for Chlorofunctionalization:



The carboxylic acid substrate, N-Chlorophthalimide (**NCP**, 1.0 eq) or N-Chlorosuccinimide (**NCS**, 1.0 eq), CuCl₂ (0.1 eq), 1,10-phenanthroline, (0.1 eq) and acridinium photoredox catalyst (0.05 eq) were weighed and dispensed into a flame dried vial (2-dram) equipped with a stir bar and Teflon-coated septum cap. The vial was moved to a nitrogen filled glovebox where solvent was dispensed by syringe (MeCN or DCE to 0.1 M). Where noted acetic acid was added to the vial as well. The vial was then sealed and removed from the glovebox and the reaction vial was sealed with electrical tape. The reactions were irradiated (2x455 nm blue LED lamps) and stirred until completion. Reaction progress was monitored by GC/MS. Upon completion, the crude reactions were passed through a silica plug to remove CuCl₂ before NMR analysis.

5-(chloro(phenyl)methyl)dihydrofuran-2(3H)-one (3.1):



The average yield for the title compound was 75% (2 trials) at the 0.5 mmol scale, generated using **General Procedure for Chlorofunctionalization** using 88 mg of the starting carboxylic acid (0.1M in MeCN), 90.8 mg NCP, 10 mg Mes-Acr-Me⁺, 6.7 mg CuCl₂, 9 mg of 1,10-phenanthroline, and an irradiation time of 2 hours. The average diastomeric ratio was 3.1:1. The products were isolated by column chromatography on silica gel (20 mL dry silica, 2 cm column, 15% EtOAc/hexanes) as a low melting white solid.

Analytical data for **3.1**:

¹H NMR Major/minor diastereomers: ¹H NMR (600 MHz, Chloroform-*d*) δ 7.47 – 7.33 (m, 10H-5 major, 5 minor), 5.05 (d, *J* = 5.7 Hz, 1H-major), 4.98 (d, *J* = 5.1 Hz, 1H-minor), 4.92 – 4.88 (m, 1H-minor), 4.88 – 4.84 (m, 1H-major), 2.53 (m 3H-2 major, 1 minor), 2.47 – 2.39 (m, 1H-minor), 2.39 – 2.32 (m, 1H-major), 2.29 (dddd, *J* = 13.4, 12.5, 5.6, 3.9 Hz, 1H-major), 2.25 – 2.19 (m, 1H-minor), 2.15 – 2.07 (m, 1H-minor).

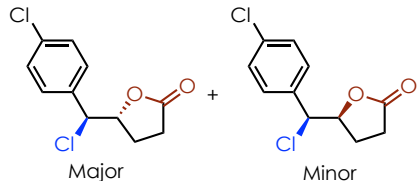
¹³C NMR Major/minor diastereomers: (151 MHz, CDCl₃) δ 176.19 (minor), 176.16 (major), 136.28 (major), 136.04 (minor), 129.13 (minor), 129.04 (major), 128.82 (major), 128.80 (minor), 127.94 (minor), 127.70 (major), 81.93 (major), 81.90 (minor), 64.03 (major), 63.60 (minor), 28.27 (major), 28.05 (minor), 24.53 (minor), 24.18 (major).

IR (thin film, cm⁻¹): 1778, 1455, 1175, 1028, 919, 701

HRMS *m/z* **calculated** for C₁₁H₁₁ClO₂ [H]⁺: 211.0520 and 213.0491; **found**: 211.0520 and 213.0491

NMR Spectra (¹H, ¹³C, HSQC, COSY): 187-188

5-(chloro(4-chlorophenyl)methyl)dihydrofuran-2(3H)-one (3.2):



The average yield for the title compound was 72% (2 trials) at the 0.5 mmol scale, generated using **General Procedure for Chlorofunctionalizations** using 105 mg of the starting carboxylic acid (0.1M in MeCN), 90.8 mg NCP, 10 mg Mes-Acr-Me⁺, 6.7mg CuCl₂, 9mg of 1,10-phenanthroline, and an irradiation time of 2 hours. The average diastereomeric ratio was 2.7:1. The products were isolated by column chromatography on silica gel (25 mL dry silica, 2 cm column, 10% EtOAc/hexanes) as a low melting white solid.

Analytical data for **3.2**:

¹H NMR Major/minor diastereomers:(600 MHz, Chloroform-*d*) δ 7.39 (m, 8H-4 major, 4 minor), 5.00-4.98 (m, 2H-1 major, 1 minor), 4.89 (ddd, *J* = 7.7, 6.2, 4.6 Hz, 1H-minor), 4.83 (td, *J* = 7.1, 6.2 Hz, 1H-major), 2.59 – 2.55 (m, 2H-major), 2.54 – 2.45 (m, 1H-minor), 2.45 – 2.40 (m, 1H-major), 2.40 – 2.35 (m, 1H-minor), 2.33 – 2.23 (m, 2H-1 major, 1 minor), 2.14 (dddd, *J* = 13.6, 10.2, 7.7, 6.2 Hz, 1H-minor).

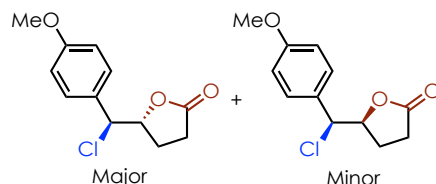
¹³C NMR Major/minor diastereomers:(151 MHz, CDCl₃) δ 175.99 (minor), 175.87 (major), 135.09 (minor), 135.00 (major), 134.96 (major), 134.73 (minor), 129.35 (minor), 129.09 (major), 129.02 (major), 128.97 (minor), 81.70 (major), 81.49 (minor), 63.14 (major), 62.91 (minor), 28.22 (major), 27.97 (minor), 24.52 (major), 24.45 (minor).

IR (thin film cm⁻¹): 2925, 1779, 1493, 1174, 1091, 1015, 916

HRMS *m/z* calculated for C₁₁H₁₀Cl₂O₂ [H]⁺: 245.0131 and 247.0101; found: 245.0131 and 247.0101

NMR Spectra (¹H, ¹³C, HSQC, COSY): 189-190

5-(chloro(4-methoxyphenyl)methyl)dihydrofuran-2(3*H*)-one (3.3):



The average yield for the title compound was 64% (2 trials) at the 0.5 mmol scale, generated using **General Procedure for Chlorofunctionalizations** using 103 mg of the starting carboxylic acid (0.1M in DCE), 90.8 mg NCP, 10 mg Mes-Acr-Me⁺, 6.7mg CuCl₂, 9 mg of 1,10-phenanthroline, and an irradiation time of 2 hours. The average diastereomeric ratio was 2.2:1. To separate from phthalimide, after the 2 hour reaction time the reaction was transferred to a separatory funnel and washed with a 10% NaOH solution and H₂O. The aqueous layer was back-extracted twice with DCM. The combined organics were dried and concentrated giving a dark brown oil. The products were isolated by column chromatography on silica gel (25 mL dry silica, 2 cm column, 20% EtOAc/hexanes) as a low melting white solid.

Analytical data for **3.3**:

¹H NMR Major/minor diastereomers:(600 MHz, Chloroform-*d*) δ 7.38 – 7.35 (m, 2H-minor), 7.35 – 7.32 (m, 2H-major), 6.93 – 6.87 (m, 4H-2 major, 2 minor), 5.00 (d, *J* = 5.8 Hz, 1H-major), 4.94 (d, *J* = 5.2 Hz, 1H- minor), 4.87 (ddd, *J* = 7.6, 6.2, 5.2 Hz, 1H-minor), 4.84 (ddd, *J* = 7.3, 6.6, 5.8 Hz, 1H-major), 3.81 (s, 6H-3 major, 3 minor), 2.54 – 2.48 (m, 2H-major), 2.45 – 2.42 (m, 1H-minor), 2.42 – 2.34 (m, 1H-major), 2.32 – 2.25 (m, 2H-1 major, 1 minor), 2.24 – 2.16 (m, 1H-minor), 2.09 (dddd, *J* = 13.6, 10.2, 7.6, 6.2 Hz, 1H-minor).

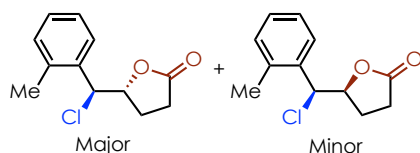
¹³C NMR Major/minor diastereomers:(151 MHz, CDCl₃) δ 176.27 (minor), 176.20 (major), 160.04 (minor), 159.98 (major), 129.21 (minor), 129.01 (major), 128.36 (major), 128.08 (minor), 114.13 (major), 114.10 (minor), 82.09 (minor), 82.04 (major), 63.86 (major), 63.43 (minor), 55.33 (major), 55.32 (minor), 28.28 (major), 28.08 (minor), 24.53 (minor), 24.42 (major).

IR (thin film cm^{-1}): 2936, 2839, 1778, 1611, 1514, 1252, 1177, 1029, 836

HRMS m/z **calculated** for $\text{C}_{12}\text{H}_{13}\text{ClO}_3$ $[\text{H}]^+$: 241.0626 and 243.0596; **found**: 241.0625 and 243.0596

NMR Spectra (^1H , ^{13}C , HSQC, COSY): 191-192

5-(chloro(*o*-tolyl)methyl)dihydrofuran-2(3*H*)-one (3.4):



The average yield for the title compound was 72% (2 trials) at the 0.5 mmol scale, generated using **General Procedure for Chlorofunctionalizations** using 95 mg of the starting carboxylic acid (0.1M in MeCN), 90.8 mg NCP, 10 mg Mes-Acr-Me⁺, 6.7mg CuCl_2 , 9mg of 1,10-phenanthroline, and an irradiation time of 2 hours. The average diastereomeric ratio was 2.9:1. The products were isolated by column chromatography on silica gel (25 mL dry silica, 2 cm column, 10% EtOAc/hexanes) as a colorless oil.

Analytical data for **3.4**:

^1H NMR Major/minor diastereomers: (600 MHz, Chloroform-*d*) δ 7.61 – 7.54 (m, 1H-minor), 7.51 (dd, $J = 7.3, 1.9$ Hz, 1H-major), 7.31 – 7.22 (m, 4H-2 major, 2 minor), 7.20 – 7.17 (m, 2H- 1 major, 1 minor), 5.32 (d, $J = 6.2$ Hz, 1H-major), 5.21 (d, $J = 5.7$ Hz, 1H-minor), 4.98 (ddd, $J = 7.5, 6.9, 5.7$ Hz, 1H-minor), 4.87 (td, $J = 7.0, 6.2$ Hz, 1H-major), 2.65 (ddd, $J = 17.9, 9.8, 5.4$ Hz, 1H-major), 2.57 (ddd, $J = 18.1, 9.7, 8.9$ Hz, 1H-major), 2.53 – 2.44 (m, 2H-minor), 2.44 – 2.35 (m, 8H-5 major, 3 minor), 2.30 – 2.21 (m, 1H-1 minor), 2.06 (dddd, $J = 13.4, 9.8, 8.4, 6.7$ Hz, 1H-1minor).

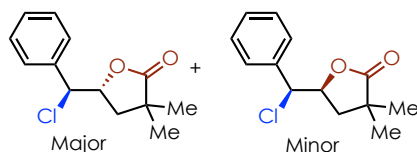
¹³C NMR Major/minor diastereomers:(151 MHz, CDCl₃) δ 175.94 (major), 175.80 (minor), 135.51(major), 135.44 (minor), 134.62 (minor), 134.60 (major), 130.64 (minor), 130.55 (major), 128.75 (minor), 128.59 (major), 127.78 (minor), 127.05 (major), 126.56 (minor), 126.43 (major), 81.76 (minor), 80.80 (major), 60.17 (major), 59.79 (minor), 28.19 (major), 28.02 (minor), 25.06 (minor), 24.32 (major), 19.32 (minor), 19.12 (major).

IR (thin film cm⁻¹): 2919.7, 1784, 1460, 1169, 917, 734

HRMS *m/z* **calculated** for C₁₂H₁₃ClO₂ [H]⁺: 225.0677 and 227.0647; **found**: 225.0676 and 227.0647

NMR Spectra (¹H, ¹³C, HSQC, COSY): 193-194

5-(chloro(phenyl)methyl)-3,3-dimethyldihydrofuran-2(3*H*)-one (3.5):



The average yield for the title compound was 75% (2 trials) at the 0.5 mmol scale, generated using **General Procedure for Chlorofunctionalizations** using 102 mg of the starting carboxylic acid (0.1M in MeCN), 90.8 mg NCP, 10 mg Mes-Acr-Me⁺, 6.7mg CuCl₂, 9 mg of 1,10-phenanthroline, and an irradiation time of 2 hours. The average diastereomeric ratio was 3.1:1. The products were isolated by column chromatography on silica gel (25 mL dry silica, 2 cm column, 10% EtOAc/hexanes) as a white solid.

The reaction was performed on 2.0 gram scale (8.38 mmol). 1.7 g of the starting carboxylic acid, 1.5 g of NCP (1.0 eq), 167 mg of Mes-Acr-Me⁺ (0.05 eq), 112.5 mg CuCl₂ (0.1 eq), and 151 mg 1,10-phenanthroline (0.1 eq) to a 100 mL round bottom flask (flame dried) equipped with a Teflon stir bar. The flask was fitted with a septum and evacuated and then refilled with N₂ three times. 80 mL of dry MeCN (0.1M) was sparged with N₂ for 15 minutes and then transferred to the flask

containing solid reagents via cannula. The flask was irradiated with two 455 nm blue LED lamps from either side, while cooling with a fan. After 3 hours TLC revealed the reaction had reached full conversion. Solvent was then removed in vacuo. The crude material was loaded onto celite and purified on column chromatography (4.5 cm column, 200 mL dry silica, gradient solvent system 3%→5%→7.5%→10% EtOAc in Hexanes). Gradient column conditions were used in order to separate a small amount of undesired regioisomer as well the diastereomers. The combined yield of both diastereomers was 66%, 1.3 g, with 3.3:1 d.r. Diastereomers were only partially separated under these conditions. All fractions containing the minor diastereomer contained some of the major diastereomer.

Analytical data for **3.5**:

¹H NMR Major/minor diastereomers: (400 MHz, Chloroform-*d*) δ 7.39 (m, 10H-5major, 5 minor), 4.98 (d, *J* = 6.6 Hz, 1H-major), 4.87 (d, *J* = 6.4 Hz, 1H-minor), 4.84 – 4.78 (m, 1H-minor), 4.75 (dt, *J* = 9.4, 6.4 Hz, 1H- major), 2.29 – 2.08 (m, 2H-major), 1.87 (qd, *J* = 13.0, 7.9 Hz, 2H-minor), 1.29 (s, 3H-major), 1.26 (s, 3H- major), 1.24 (s, 3H-minor), 1.19 (s, 3H-minor).

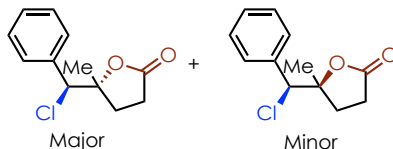
¹³C NMR Major/minor diastereomers: (151 MHz, CDCl₃) δ 180.83 (major), 180.69 (minor), 136.75 (major), 136.41(minor), 129.16 (minor), 129.03 (major), 128.84 (minor), 128.75 (major), 127.91 (minor), 127.73 (major), 79.02 (minor), 78.49 (major), 63.87 (minor/major), 40.47 (minor), 40.39 (minor), 40.31 (major), 40.14 (major), 24.90 (major), 24.77 (minor), 24.71 (major), 24.66 (minor).

IR (thin film cm⁻¹) 2969, 2360, 1774, 1455, 1205, 1119, 1035, 915, 699, 667

HRMS *m/z* **calculated** for C₁₃H₁₅ClO₂ [H]⁺: 239.0833 and 241.0804; **found**: 239.0833 and 241.0803

NMR Spectra (¹H, ¹³C, HSQC, COSY): 195-196

5-(chloro(phenyl)methyl)-3,3,5-trimethyldihydrofuran-2(3H)-one (3.6):



The average yield for the title compound was 76% (2 trials) at the 0.5 mmol scale, generated using **General Procedure for Chlorofunctionalizations** using 109 mg of the starting carboxylic acid (0.1M in MeCN), 90.8 mg NCP, 10 mg Mes-Acr-Me⁺, 6.7mg CuCl₂, 9mg of 1,10-phenanthroline, and an irradiation time of 2 hours. The average diastereomeric ratio was 1.3:1. The products were isolated by column chromatography on silica gel (25 mL dry silica, 2 cm column, 10% EtOAc/hexanes) as a colorless oil.

Analytical data for **3.6**:

¹H NMR Major/minor diastereomers: (600 MHz, Chloroform-*d*) δ 7.51 – 7.30 (m, 10H, 5 major, 5 minor), 4.94 (s, 1H-minor), 4.84 (s, 1H-major), 2.60 (d, *J* = 13.4 Hz, 1H-minor), 2.51 (d, *J* = 13.5 Hz, 1H-major), 1.93 (t, *J* = 13.8 Hz, 2H-1 major, 1 minor), 1.47 (s, 3H-minor), 1.46 (s, 3H-major), 1.33 (s, 3H-minor), 1.32 (s, 3H-major), 1.15 (s, 3H-minor), 1.07 (s, 3H-major).

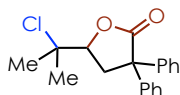
¹³C NMR Major/minor diastereomers:(151 MHz, CDCl₃) δ 181.53, 181.30, 136.44, 136.22, 129.01, 128.96, 128.85, 128.70, 128.45, 128.27, 83.74, 83.34, 68.95, 68.91, 44.69, 44.16, 40.73, 40.41, 28.60, 28.29, 27.46, 26.29, 26.08, 25.64.

IR (thin film cm⁻¹): 2974, 1773, 1455, 1236, 1093, 962, 755, 701

HRMS *m/z* **calculated** for C₁₄H₁₇ClO₂ [H]⁺: 253.0990 and 255.0960; **found**: 253.0988 and 255.0959

NMR Spectra (¹H, ¹³C, HSQC, COSY): 197-198

5-(2-chloropropan-2-yl)-3,3-diphenyldihydrofuran-2(3H)-one (3.7):



The average yield for the title compound was 63% (2 trials) at the 0.5 mmol scale, generated using **General Procedure for Chlorofunctionalizations** using 140 mg of the starting carboxylic acid (0.1M in DCE), 90.8 mg NCP, 10 mg Mes-Acr-Me⁺, 6.7mg CuCl₂, 9mg of 1,10-phenanthroline, 150μL of 95:5 Acetic acid:Acetic anhydride, and an irradiation time of 3 hours. The products were isolated by column chromatography on silica gel (25 mL dry silica, 2 cm column, 5% EtOAc/hexanes) as a white crystalline solid.

Analytical data for **3.7**:

¹H NMR (400 MHz, Chloroform-*d*) δ 7.59 – 7.12 (m, 10H), 4.30 (dd, *J* = 10.6, 5.2 Hz, 1H), 3.09 (dd, *J* = 13.2, 5.2 Hz, 1H), 2.96 (dd, *J* = 13.2, 10.6 Hz, 1H), 1.68 (s, 3H), 1.62 (s, 3H).

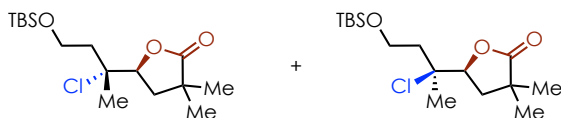
¹³C NMR (151 MHz, CDCl₃) δ 176.41, 141.92, 139.17, 129.04, 128.44, 127.95, 127.71, 127.34, 127.32, 81.88, 68.18, 58.35, 39.38, 29.18, 27.88.

IR (thin film cm⁻¹): 3060, 2979, 1770, 1496, 1447, 1170, 698

HRMS *m/z* **calculated** for C₁₉H₁₉ClO₂ [H]⁺: 315.1146 and 317.1117; **found**: 315.1145 and 317.1116

NMR Spectra (¹H, ¹³C, HSQC, COSY): 199-200

5-(4-((*tert*-butyldimethylsilyl)oxy)-2-chlorobutan-2-yl)-3,3-dimethyldihydrofuran-2(3H)-one (3.8):



The average yield for the title compound was 47% (2 trials) at the 0.5 mmol scale, generated using **General Procedure for Chlorofunctionalizations** using 150 mg of the starting carboxylic acid

as a mixture of alkene isomers (0.1M in DCE), 90.8 mg NCP, 10 mg Mes-Acr-Me⁺, 6.7mg CuCl₂, 9mg of 1,10-phenanthroline, 150μL of 95:5 Acetic acid:Acetic anhydride, and an irradiation time of 3 hours. The average diastereoisomeric ratio was 1.1:1. The products were isolated by column chromatography on silica gel (25 mL dry silica, 2 cm column, 5% EtOAc/hexanes), diastereomers could be separated on silica gel and thus were characterized separately. Both appeared as clear viscous oils.

Analytical data for **3.8-major**:

¹H NMR (600 MHz, Chloroform-*d*) δ 4.59 (t, *J* = 8.1 Hz, 1H), 3.84 (dd, *J* = 6.8, 5.7 Hz, 2H), 2.15 (d, *J* = 8.1 Hz, 2H), 2.01 (td, *J* = 6.3, 5.8, 4.7 Hz, 2H), 1.65 (s, 3H), 1.31 (s, 3H), 1.28 (s, 3H), 0.89 (s, 9H), 0.06 (d, *J* = 0.8 Hz, 6H).

¹³C NMR (151 MHz, CDCl₃) δ 181.25, 80.94, 71.94, 59.22, 43.22, 40.33, 38.65, 25.88, 25.43, 25.42, 24.69, 18.19, -5.44, -5.47.

IR (thin film cm⁻¹): 2956, 2930, 2857, 1780, 1463, 1255, 1122, 835, 778

HRMS *m/z* **calculated** for C₂₆H₃₅ClO₃Si[H]⁺: 335.1804 and 337.1774; **found**: 335.1802 and 337.1772

NMR Spectra (¹H, ¹³C, HSQC, COSY): 201-202

Analytical data for **3.8-minor**:

¹H NMR (600 MHz, Chloroform-*d*) δ 4.54 (dd, *J* = 9.5, 6.7 Hz, 1H), 3.90 – 3.84 (m, 2H), 2.23 – 2.04 (m, 4H), 1.54 (s, 3H), 1.31 (s, 3H), 1.29 (s, 3H), 0.89 (s, 9H), 0.06 (d, *J* = 1.4 Hz, 6H).

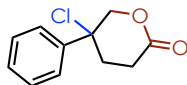
¹³C NMR (151 MHz, CDCl₃) δ 181.08, 81.15, 72.16, 59.52, 42.78, 40.33, 38.53, 25.87, 25.56, 25.33, 24.65, 18.18, -5.42, -5.45.

IR (thin film cm⁻¹): 2956, 2930, 2857, 1780, 1463, 1255, 1101, 835, 778

HRMS m/z calculated for $C_{26}H_{35}ClO_3Si[H]^+$: 335.1804 and 337.1774; **found**: 335.1802 and 337.1773

NMR Spectra (1H , ^{13}C , HSQC, COSY): 203-204

5-chloro-5-phenyltetrahydro-2H-pyran-2-one (3.9):



The average yield for the title compound was 54% (2 trials) at the 0.5 mmol scale, generated using **General Procedure for Chlorofunctionalizations** using 88.4 mg of the starting carboxylic acid (0.1M in DCE), 67 mg NCS, 10 mg Mes-Acr-Me⁺, 6.7mg CuCl₂, 9mg of 1,10-phenanthroline, and an irradiation time of 2 hours. After the reaction, the contents were transferred to a separatory funnel and diluted with DCM. The organic layer was washed with H₂O to remove succinimide. The aqueous layer was extracted twice more with DCM. All organics were combined and dried over Na₂SO₄. The organics were passed through a small plug of silica to remove any remaining Cu or acridinium impurities. After removing the solvent in vacuo the title compound was found to be clean by NMR.

Analytical data for **3.9**:

1H NMR: (600 MHz, Chloroform-*d*) δ 7.58 – 7.54 (m, 2H), 7.46 – 7.42 (m, 2H), 7.41 – 7.37 (m, 1H), 4.68 (dd, J = 12.4, 2.6 Hz, 1H), 4.62 (dd, J = 12.3, 0.6 Hz, 1H), 3.08 – 2.98 (m, 1H), 2.76 – 2.67 (m, 2H), 2.66 – 2.59 (m, 1H).

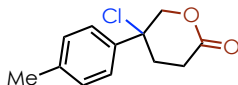
^{13}C NMR: (151 MHz, CDCl₃) δ 168.32, 139.10, 129.19, 129.00, 125.79, 76.92, 66.05, 34.04, 27.58.

IR (thin film cm⁻¹): 2932, 1744, 1447, 1399, 1263, 1186, 1089, 753

HRMS m/z **calculated** for $C_{11}H_{11}ClO_2$ $[H]^+$: 211.0520 and 213.0491; **found**: 211.0520 and 213.0491

NMR Spectra (1H , ^{13}C , HSQC, COSY): 205-206

5-chloro-5-(*p*-tolyl)tetrahydro-2*H*-pyran-2-one (3.10):



The average yield for the title compound was 50% (2 trials) at the 0.5 mmol scale, generated using **General Procedure for Chlorofunctionalizations** using 95 mg of the starting carboxylic acid (0.1M in DCE), 67 mg NCS, 10 mg Mes-Acr-Me⁺, 6.7mg CuCl₂, 9mg of 1,10-phenanthroline, and an irradiation time of 2 hours. After the reaction, the contents were transferred to a separatory funnel and diluted with DCM. The organic layer was washed with H₂O to remove succinimide. The aqueous layer was extracted twice more with DCM. All organics were combined and dried over Na₂SO₄. The organics were passed through a small plug of silica to remove any remaining Cu or acridinium impurities. After removing the solvent in vacuo the title compound was found to be clean by NMR.

Analytical data for **3.10**:

1H NMR: (600 MHz, Chloroform-*d*) δ 7.44 (d, J = 8.3 Hz, 2H), 7.24 (d, J = 8.1 Hz, 2H), 4.67 (dd, J = 12.3, 2.5 Hz, 1H), 4.60 (d, J = 12.4 Hz, 1H), 3.06 – 2.97 (m, 1H), 2.71 (dt, J = 7.1, 3.7 Hz, 1H), 2.68 (q, J = 7.4, 6.6 Hz, 1H), 2.65 – 2.59 (m, 1H), 2.37 (s, 3H).

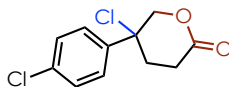
^{13}C NMR: (151 MHz, CDCl₃) δ 168.32, 139.28, 136.21, 129.66, 125.69, 76.82, 66.05, 34.11, 27.64, 21.05.

IR (thin film cm⁻¹): 1775, 1740, 1644, 1180, 818, 736

HRMS *m/z* **calculated** for C₁₂H₁₃ClO₂ [H]⁺: 225.0677 and 227.0647; **found**: 225.0677 and 227.0648

NMR Spectra (¹H, ¹³C, HSQC, COSY): 207-208

5-chloro-5-(4-chlorophenyl)tetrahydro-2H-pyran-2-one (3.11):



The average yield for the title compound was 57% (2 trials) at the 0.5 mmol scale, generated using **General Procedure for Chlorofunctionalizations** using 105 mg of the starting carboxylic acid (0.1M in DCE), 67 mg NCS, 10 mg Mes-Acr-Me⁺, 6.7mg CuCl₂, 9mg of 1,10-phenanthroline, and an irradiation time of 2 hours. After the reaction, the contents were transferred to a separatory funnel and diluted with DCM. The organic layer was washed with H₂O to remove succinimide. The aqueous layer was extracted twice more with DCM. All organics were combined and dried over Na₂SO₄. The organics were passed through a small plug of silica to remove any remaining Cu or acridinium impurities. After removing the solvent in vacuo the title compound was found to be clean by NMR.

Analytical data for **3.11**:

¹H NMR: (600 MHz, Chloroform-*d*) δ 7.50 (d, *J* = 8.7 Hz, 2H), 7.41 (d, *J* = 8.7 Hz, 2H), 4.65 (dd, *J* = 12.4, 2.4 Hz, 1H), 4.60 (d, *J* = 12.3 Hz, 1H), 3.01 (ddd, *J* = 19.6, 9.5, 7.3 Hz, 1H), 2.72 – 2.64 (m, 2H), 2.61 (dt, *J* = 13.8, 7.0, 3.4 Hz, 1H).

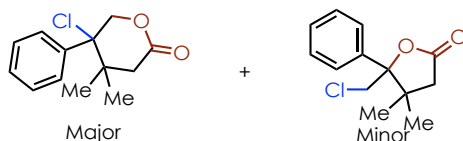
¹³C NMR: (151 MHz, CDCl₃) δ 167.92, 137.75, 135.28, 129.21, 127.32, 76.63, 65.40, 34.27, 27.53.

IR (thin film cm⁻¹): 1745, 1495, 1401, 1186, 1086, 1013, 811, 578

HRMS m/z **calculated** for $C_{11}H_{10}Cl_2O_2$ $[H]^+$: 245.0131 and 247.0101; **found**: 245.0131 and 247.0101

NMR Spectra (1H , ^{13}C , HSQC, COSY): 209-210

5-chloro-4,4-dimethyl-5-phenyltetrahydro-2H-pyran-2-one (3.12):



The average yield for the title compound was 72% (2 trials) at the 0.5 mmol scale, generated using **General Procedure for Chlorofunctionalizations** using 102 mg of the starting carboxylic acid (0.1M in DCE), 90.8 mg NCP, 10 mg Mes-Acr-Me⁺, 6.7mg $CuCl_2$, 9mg of 1,10-phenanthroline, and an irradiation time of 2 hours. The average regioisomeric ratio was 19:1. The products were isolated by column chromatography on silica gel (25 mL dry silica, 2 cm column, 10% EtOAc/hexanes) as a white solid.

Analytical data for **3.12**:

1H NMR Major/minor regioisomers: (600 MHz, Chloroform- d) δ 7.73 – 7.49 (m, 4H-2 major, 2 minor), 7.49 – 7.35 (m, 6H-3 major, 3 minor), 5.24 (d, J = 12.5 Hz, 1H-major), 4.70 (d, J = 12.4 Hz, 1H-major), 4.10 (d, J = 12.4 Hz, 1H-minor), 3.97 (d, J = 12.4 Hz, 1H-minor), 3.01 (d, 1H-minor), 2.83 (d, J = 18.0 Hz, 1H-major), 2.38 (d, J = 18.1 Hz, 2H-1 major, 1 minor), 1.46 (s, 3H-minor), 1.19 (s, 3H-major), 1.06 (s, 3H-major), 0.70 (s, 3H- minor).

^{13}C NMR Major/minor regioisomers: (151 MHz, $CDCl_3$) δ 174.69 (minor), 169.08 (major), 137.66 (minor), 137.21 (major), 128.67 (major), 128.58 (minor), 128.41 (minor), 128.26 (minor), 128.05 (major), 127.96 (major), 124.49 (minor), 90.92 (minor), 75.46 (major), 74.48 (major),

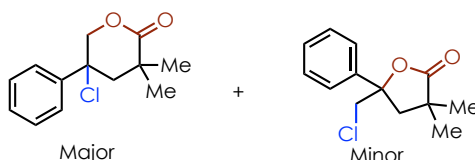
49.26 (minor), 44.87 (minor), 42.57 (major), 39.40 (major), 28.11 (minor), 25.11 (major), 24.85 (major), 22.20 (minor).

IR (thin film cm^{-1}): 2977, 1744, 1445, 1251, 1213, 1068, 701, 641

HRMS m/z **calculated** for $\text{C}_{13}\text{H}_{15}\text{ClO}_2$ $[\text{H}]^+$: 239.0833 and 241.0804; **found**: 239.0832 and 241.0803

NMR Spectra (^1H , ^{13}C , HSQC, COSY): 211-212

5-chloro-3,3-dimethyl-5-phenyltetrahydro-2H-pyran-2-one (3.13):



The average yield for the both regioisomers was 66% (2 trials) at the 0.5 mmol scale, generated using **General Procedure for Chlorofunctionalizations** using 102 mg of the starting carboxylic acid (0.1M in DCE), 67 mg NCS, 10 mg Mes-Acr-Me⁺, 6.7mg CuCl_2 , 9mg of 1,10-phenanthroline, and an irradiation time of 2 hours. After the reaction, the contents were transferred to a separatory funnel and diluted with DCM. The organic layer was washed with H_2O to remove succinimide. The aqueous layer was extracted twice more with DCM. All organics were combined and dried over Na_2SO_4 . The organics were passed through a small plug of silica to remove any remaining Cu or acridinium impurities. After removing the solvent in vacuo the title compounds were isolated as a mixture of regioisomers (4.4:1). The major regioisomer could be isolated by column chromatography on silica gel (15 mL dry silica, 2 cm column, 5% EtOAc/hexanes) as a white solid.

Analytical data for **3.13**:

¹H NMR Major regioisomer:(600 MHz, Chloroform-*d*) δ 7.59 – 7.50 (m, 2H), 7.42 (td, *J* = 7.3, 6.3, 1.4 Hz, 2H), 7.39 – 7.35 (m, 1H), 4.77 (d, *J* = 11.8 Hz, 1H), 4.69 (dd, *J* = 11.9, 1.9 Hz, 1H), 2.67 – 2.60 (m, 2H), 1.50 (s, 3H), 1.19 (s, 3H).

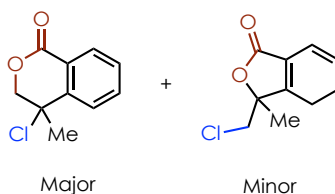
¹³C NMR Major regioisomer:¹³C NMR (151 MHz, CDCl₃) δ 175.61, 139.57, 129.05, 128.93, 125.87, 75.05, 66.57, 50.43, 37.98, 30.16, 30.05.

IR (thin film cm⁻¹): 2977, 2359, 1739, 1447, 1389, 1134, 1064, 762, 697

HRMS *m/z* **calculated** for C₁₃H₁₅ClO₂ [H]⁺:239.0833 and 241.0804; **found**: 239.0832 and 241.0803

NMR Spectra (¹H, ¹³C, HSQC, COSY): 213-214

4-chloro-4-methylisochroman-1-one (3.14):



The average yield for the both regioisomers was 64% (2 trials) at the 0.5 mmol scale, generated using **General Procedure for Chlorofunctionalizations** using 81.1 mg of the starting carboxylic acid (0.1M in DCE), 67 mg NCS, 10 mg Mes-Acr-Me⁺, 6.7mg CuCl₂, 9mg of 1,10-phenanthroline, and 150μL of 95:5 Acetic acid:Acetic anhydride an irradiation time of 2 hours. After the reaction, the contents were transferred to a separatory funnel and diluted with DCM. The organic layer was washed with H₂O to remove succinimide. The aqueous layer was extracted twice more with DCM. All organics were combined and dried over Na₂SO₄. The average regioisomeric ratio was 2.5:1. Purified on column chromatography on silica gel (25 mL dry silica, 2 cm column, 10% EtOAc:Hexanes).

Analytical data for **3.14**:

¹H NMR Major/minor regioisomers (600 MHz, Chloroform-*d*) δ 8.13 (dd, *J* = 7.8, 1.4 Hz, 1H-major), 7.91 (dt, *J* = 7.7, 1.0 Hz, 1H-minor), 7.72 – 7.64 (m, 4H-2 major, 2 minor), 7.58 (td, *J* = 7.5, 1.0 Hz, 1H-minor), 7.51 (td, *J* = 7.5, 1.5 Hz, 1H-major), 4.62 (d, *J* = 11.7 Hz, 1H-major), 4.49 (d, *J* = 11.6 Hz, 1H-major), 3.91 – 3.75 (m, 2H-minor), 1.99 (s, 3H-major), 1.78 (s, 3H-minor).

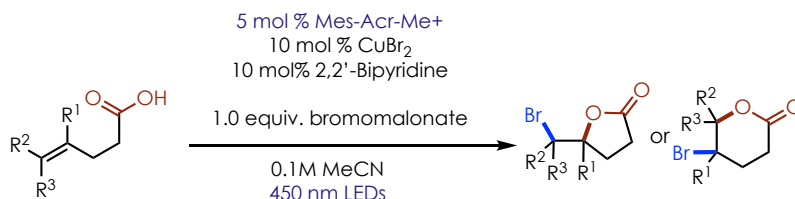
¹³C NMR Major/minor regioisomers (151 MHz, CDCl₃) δ 163.54 (major), 150.76 (minor), 143.22 (major/minor), 134.57 (major), 134.28 (minor), 130.78 (major), 129.80 (minor), 129.38 (major), 126.25 (minor), 125.93 (minor), 124.48 (major), 122.91 (major), 121.59 (minor), 85.16 (minor), 75.83 (major), 61.54 (major), 49.51 (minor), 27.64 (major), 23.51 (minor).

IR (thin film cm⁻¹): 2926, 1768, 1735, 1604, 1464, 1281, 1247, 1102, 765

HRMS *m/z* **calculated** for C₁₀H₉ClO₂ [H]⁺: 197.0364 and 199.0334; **found**: 197.0363 and 199.0334

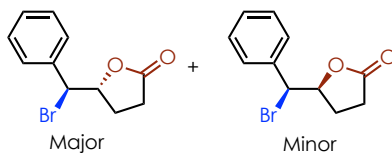
NMR Spectra (¹H, ¹³C, HSQC, COSY): 215-216

3.6.5.3 General Procedure for Bromofunctionalization:



The carboxylic acid substrate (1.0 eq), diethyl bromomalonate (1.0 eq), CuBr₂ (0.1 eq), 2,2'-bipyridine, (0.1 eq) and acridinium photoredox catalyst (0.05 eq) were weighed and dispensed into a flame dried vial (2-dram) equipped with a stir bar and Teflon-coated septum cap. The vial was moved to a nitrogen filled glovebox where solvent was dispensed by syringe (MeCN to 0.1 M). When noted, 2,6-lutidine (0.1 eq) was added to the vial as well. The vial was then sealed and removed from the glovebox and the reaction vial was sealed with electrical tape. The reactions were irradiated (2x455 nm blue LED lamps) and stirred until completion. Reaction progress was monitored by GC/MS. Upon completion, the crude reactions were concentrated then passed through a silica plug to remove CuBr₂ before NMR analysis.

5-(bromo(phenyl)methyl)dihydrofuran-2(3H)-one (3.15):



The average yield for the title compound was 74% (2 trials) at the 0.5 mmol scale, generated using **General Procedure for Bromofunctionalization** using 88 mg of the starting carboxylic acid (0.1M in MeCN), 85 μ L diethyl bromomalonate, 10 mg Mes-Acr-Me⁺, 11.2 mg CuBr₂, 7.8 mg 2,2'-bipyridine, and an irradiation time of 16 hours. The average diastereomeric ratio was 2.3:1. The products were isolated by silica gel (40 mL dry silica, 2.5 cm column, 10% EtOAc/hexanes then 30% EtOAc/hexanes) as a white solid.

Analytical data for **3.15**:

¹H NMR Major/minor diastereomers: (600 MHz, Chloroform-*d*) δ 7.45 (dd, J = 8.0, 1.4 Hz, 2H-minor), 7.44 – 7.40 (m, 2H-major), 7.39 – 7.30 (m, 6H-3 major, 3 minor), 5.01 (d, J = 6.9 Hz, 1H-major), 4.99 (d, J = 5.5 Hz, 1H-minor), 4.95 – 4.88 (m, 2H-1 major, 1 minor), 2.57 – 2.43 (m, 4H-3 major, 1 minor), 2.41 (dd, J = 10.0, 5.3 Hz, 1H-minor), 2.31 – 2.19 (m, 2H-1 major, 1 minor), 2.05 (dddd, J = 13.4, 10.1, 8.3, 6.8 Hz, 1H-minor).

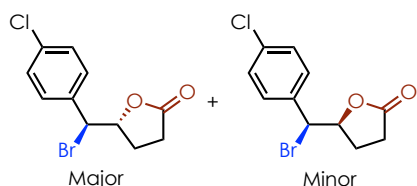
¹³C NMR Major/minor diastereomers: (151 MHz, Chloroform-*d*) δ 176.12 (major), 176.06 (minor) 137.08 (major), 136.87 (minor), 129.18 (minor), 129.12 (major), 128.93 (minor), 128.90 (major), 128.46 (minor), 128.30 (major), 82.03 (minor), 81.70 (major), 55.48 (major), 55.24 (minor), 28.63 (major), 28.40 (minor), 26.42 (major), 25.73 (minor).

IR (thin film, cm⁻¹): 1778, 1636, 1170, 1022, 911, 699

HRMS m/z **calculated** for C₁₁H₁₁BrO₂ [H]⁺: 255.0015 and 256.9995; **found**: 255.0014 and 256.9994

NMR Spectra (¹H, ¹³C, HSQC, COSY): 217-218

5-(bromo(4-chlorophenyl)methyl)dihydrofuran-2(3H)-one (3.16):



The average yield for the title compound was 84% (2 trials) at the 0.5 mmol scale, generated using **General Procedure for Bromofunctionalization** using 105 mg of the starting carboxylic acid (0.1M in MeCN), 85 μ L diethyl bromomalonate, 10 mg Mes-Acr-Me⁺, 11.2 mg CuBr₂, 7.8 mg 2,2'-bipyridine, and an irradiation time of 16 hours. The average diastereomeric ratio was 1.5:1. The products were isolated by silica gel (40 mL dry silica, 2.5 cm column, 10% EtOAc/hexanes then 30% EtOAc/hexanes) as a clear oil.

Analytical data for **3.16**:

¹H NMR Major/minor diastereomers: (600 MHz, Chloroform-*d*) δ 7.43 – 7.38 (m, 2H-1 major, 1 minor), 7.38 – 7.30 (m, 6 H-3 major, 3 minor), (d, *J* = , 1H-minor), 4.93 (d, *J* = 7.4 Hz, 1H-major), 4.91 – 4.82 (m, 2H-1 major, 1 minor), 2.58 – 2.45 (m, 5H-3 major, 2 minor), 2.31 – 2.24 (m, 1H-minor), 2.24 – 2.16 (m, 1H-major), 2.05 (ddq, *J* = 8.5, 5.0, 1.8 Hz, 1H-minor).

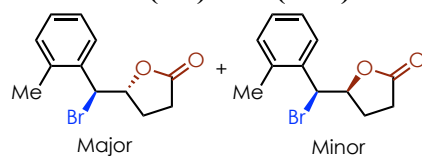
¹³C NMR Major/minor diastereomers: (151 MHz, Chloroform-*d*) δ 175.94 (minor), 175.92 (major), 135.80 (major), 135.66 (minor), 135.05(minor), 134.96 (major), 129.87 (major), 129.65 (minor), 129.09 (major/minor), 81.61 (minor), 81.50 (major), 54.48 (minor), 54.20 (major), 28.62 (major), 28.31 (minor), 26.63 (major), 25.76 (minor).

IR (thin film cm⁻¹): 1777, 1492, 1168, 1014, 915, 836

HRMS *m/z* **calculated** for C₁₁H₁₀ClBrO₂ [H]⁺:288.9625 and 290.9605; **found**: 288.9625 and 290.9605

NMR Spectra (¹H, ¹³C, HSQC, COSY): 219-220

5-(bromo(*o*-tolyl)methyl)dihydrofuran-2(3*H*)-one (3.17):



The average yield for the title compound was 83% (2 trials) at the 0.5 mmol scale, generated using **General Procedure for Bromofunctionalization** using 95 mg of the starting carboxylic acid (0.1M in MeCN), 85 μ L diethyl bromomalonate, 10 mg Mes-Acr-Me⁺, 11.2 mg CuBr₂, 7.8 mg 2,2'-bipyridine, and an irradiation time of 16 hours. The average diastereomeric ratio was 1.6:1. The products were isolated by silica gel (40 mL dry silica, 2.5 cm column, 10% EtOAc/hexanes then 30% EtOAc/hexanes) as a white solid.

Analytical data for **3.17**:

¹H NMR Major/minor diastereomers: (600 MHz, Chloroform-*d*) δ 7.59 – 7.53 (m, 1H-minor), 7.50 (dd, J = 7.4, 1.7 Hz, 1H-major), 7.26 – 7.19 (m, 4H-2 major, 2 minor), 7.19 – 7.14 (m, 2H-1 major, 1 minor), 5.26 (d, J = 7.7 Hz, 1H-major), 5.22 (d, J = 6.3 Hz, 1H-minor), 5.01 (dq, J = 16.4, 7.3 Hz, 2H-1 major, 1 minor), 2.68 – 2.51 (m, 5H- 3 major, 2 minor), 2.39 (d, J = 3.2 Hz, 6H-3 major, 3 minor), 2.36 – 2.23 (m, 2H-1 major, 1 minor), 1.94 (dtd, J = 13.3, 9.4, 7.4 Hz, 1H-minor).

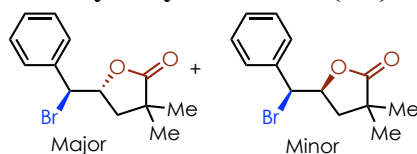
¹³C NMR Major/minor diastereomers: (151 MHz, Chloroform-*d*) δ 176.04 (major), 175.79 (minor), 135.92 (major), 135.62 (minor), 135.58 (minor), 135.50 (major), 130.88 (minor), 130.80 (major), 128.95 (minor), 128.83 (major), 128.22 (minor), 127.63 (major), 126.88 (minor), 126.67 (major), 82.00 (minor), 80.76 (major), 51.91 (major), 51.42 (minor), 28.68 (major), 28.51 (minor), 26.98 (major), 26.35 (minor), 19.44 (minor), 19.31 (major).

IR (thin film cm⁻¹): 1777, 1174, 1022, 916, 728, 657

HRMS m/z **calculated** for C₁₂H₁₃BrO₂ [H]⁺: 269.0172 and 271.0151; **found**: 269.0171 and 271.0150

NMR Spectra (¹H, ¹³C, HSQC, COSY): 221-222

5-(bromo(phenyl)methyl)-3,3-dimethyldihydrofuran-2(3H)-one (3.18):



The average yield for the title compound was 94% (2 trials) at the 0.5 mmol scale, generated using **General Procedure for Bromofunctionalization** using 102 mg of the starting carboxylic acid (0.1M in MeCN), 85 μ L diethyl bromomalonate, 10 mg Mes-Acr-Me⁺, 11.2 mg CuBr₂, 7.8 mg 2,2'-bipyridine, and an irradiation time of 16 hours. The average diastereomeric ratio was 2.1:1. The products were isolated by silica gel (3 mL dry silica, 2 cm column, DCM) as a white solid.

Analytical data for **3.18**:

¹H NMR Major/minor diastereomers: (600 MHz, Chloroform-*d*) δ 7.47 – 7.40 (m, 4H-2 major, 2 minor), 7.40 – 7.30 (m, 6H-3 major, 3 minor), 4.94 (d, J = 7.7 Hz, 1H-major), 4.90 (d, J = 6.8 Hz, 1H-minor), 4.84 (dtd, J = 9.5, 7.9, 6.1 Hz, 2H-1 major, 1 minor), 2.41 (dd, J = 13.0, 6.1 Hz, 1H-major), 2.09 (dd, J = 13.0, 9.6 Hz, 1H- major), 1.95 (dd, J = 13.0, 6.2 Hz, 1H-minor), 1.81 (dd, J = 13.1, 9.7 Hz, 1H-minor), 1.29 (d, J = 4.9 Hz, 6H- major), 1.25 (s, 3H-minor), 1.22 (s, 3H-minor).

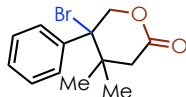
¹³C NMR Major/minor diastereomers: (151 MHz, Chloroform-*d*) δ 180.83 (major), 180.49 (minor), 137.40 (major), 137.07 (minor), 129.12 (minor), 129.03 (major), 128.90 (minor), 128.78 (major), 128.24 (minor), 128.19 (major), 78.92 (minor), 78.15 (major), 55.52 (major), 55.02 (minor), 42.25 (major), 41.48 (minor), 40.66 (minor), 40.64 (major), 24.80 (major), 24.74 (minor), 24.68 (major/minor).

IR (thin film cm⁻¹): 2969, 2360, 1774, 1455, 1205, 1119, 1035, 915, 699, 667

HRMS m/z **calculated** for C₁₃H₁₅BrO₂ [H]⁺: 283.0328 and 285.0308; **found**: 283.0327 and 285.0306

NMR Spectra (¹H, ¹³C, HSQC, COSY): 223-224

5-bromo-4,4-dimethyl-5-phenyltetrahydro-2H-pyran-2-one (3.19):



The average yield for the title compound was 84% (2 trials) at the 0.5 mmol scale, generated using **General Procedure for Bromofunctionalization** using 102 mg of the starting carboxylic acid (0.1M in MeCN), 85 μ L diethyl bromomalonate, 10 mg Mes-Acr-Me⁺, 11.2 mg CuBr₂, 7.8 mg 2,2'-bipyridine, 6 μ L 2,6-lutidine, and an irradiation time of 16 hours. The products were isolated by silica gel (40 mL dry silica, 2.5 cm column, 10% EtOAc/hexanes) as an off-white solid.

Analytical data for **3.19**:

¹H NMR : (600 MHz, Chloroform-*d*) δ 7.59 (dd, *J* = 8.0, 1.7 Hz, 2H), 7.40 – 7.31 (m, 3H), 5.23 (d, *J* = 12.5 Hz, 1H), 4.92 (d, *J* = 12.5 Hz, 1H), 2.73 (d, *J* = 18.0 Hz, 1H), 2.35 (d, *J* = 18.0 Hz, 1H), 1.34 (s, 3H), 1.09 (s, 3H).

¹³C NMR: (151 MHz, Chloroform-*d*) δ 168.98, 138.41, 128.97, 128.72, 127.93, 75.08, 73.01, 42.98, 39.78, 27.04, 24.63.

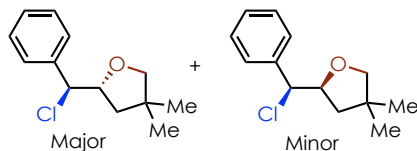
IR (thin film cm⁻¹): 2972, 1744, 1444, 1250, 1067, 701

HRMS *m/z* **calculated** for C₁₃H₁₅BrO₂ [H]⁺: 283.0328 and 285.0308; **found**: 283.0324 and 285.0307

NMR Spectra (¹H, ¹³C, HSQC, COSY): 225-226

3.1.1.1 Procedure and Characterization of other Halofunctionalizations

2-chloro(phenyl)methyl)-4,4-dimethyltetrahydrofuran (3.20):



The average yield for the title compound was 61% (2 trials) at the 0.5 mmol scale, generated using **General Procedure for Chlorofunctionalizations** using 95.1 mg of the starting alcohol (0.1M in MeCN), 90.8 mg NCP, 10 mg Mes-Acr-Me⁺, 6.7mg CuCl₂, 9mg of 1,10-phenanthroline, and an irradiation time of 2 hours. The average diastereomeric ratio was 1.9:1. The products were isolated by column chromatography on silica gel (25 mL dry silica, 2 cm column, 5% EtOAc/hexanes) as a colorless oil.

Analytical data for **3.20**:

¹H NMR Major/minor diastereomers: (600 MHz, Chloroform-*d*) δ 7.45 – 7.39 (m, 4H-2 major, 2 minor), 7.38 – 7.34 (m, 4H-2 major, 2 minor), 7.34 – 7.29 (m, 2H-1 major, 1 minor), 4.86 (d, *J* = 7.0 Hz, 1H-major), 4.78 (d, *J* = 7.5 Hz-1H, minor), 4.55 – 4.40 (m, 2H-1 major, 1 minor), 3.60 – 3.54 (m, 3H-1 major, 2 minor), 3.51 (d, 1H, *J* = 8.3 Hz-major), 1.92 (dd, *J* = 12.6, 6.8 Hz, 1H-major), 1.83 (dd, *J* = 12.6, 9.0 Hz, 1H-major), 1.51 (dd, *J* = 12.6, 6.7 Hz, 1H-minor), 1.42 (dd, 12.6, 9.4 Hz, 1H-minor), 1.11 (s, 3H-major), 1.09 (s, 3H-major), 1.06 (s, 3H- minor), 1.04 (s, 3H-minor).

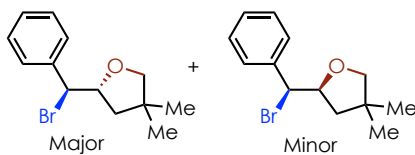
¹³C NMR Major/minor diastereomers: (151 MHz, CDCl₃) δ 138.94 (major), 138.74 (minor), 128.57 (major), 128.53 (minor), 128.49 (major), 128.42 (minor), 127.80 (minor), 127.72 (major), 82.86 (minor), 82.46 (major), 80.79 (major), 80.54 (minor), 66.43 (minor), 65.88 (major), 44.50 (minor), 44.16 (major), 40.03 (minor), 39.81 (major), 26.30 (major), 26.23 (minor), 25.79 (minor), 25.55 (major).

IR (thin film cm^{-1}): 2959, 2869, 1726, 1496, 1453, 1368, 1062, 698

HRMS m/z **calculated** for $\text{C}_{13}\text{H}_{17}\text{ClO}$ $[\text{H}]^+$: 225.1041, and 227.1011; **found**: 225.1040, and 227.1014

NMR Spectra (^1H , ^{13}C , HSQC, COSY): 227-228

2-bromo(phenyl)methyl)-4,4-dimethyltetrahydrofuran (3.21):



The average yield for the title compound was 71% (2 trials) at the 0.5 mmol scale, generated using **General Procedure for Bromofunctionalization** using 95.1 mg of the starting alcohol (0.1M in MeCN), 85 μL diethyl bromomalonate, 10 mg Mes-Acr-Me $^+$, 11.2 mg CuBr_2 , 7.8 mg 2,2'-bipyridine, and an irradiation time of 16 hours. The average diastereomeric ratio was 1.9:1. The products were isolated by silica gel (40 mL dry silica, 2.5 cm column, 10% EtOAc/hexanes, 20% EtOAc/hexanes, then 30% EtOAc/hexanes) as a colorless oil.

Analytical data for **3.21**:

^1H NMR Major/minor diastereomers: (600 MHz, Chloroform- d) δ 7.43 (dd, $J = 11.3, 7.5$ Hz, 4H-2 major, 2 minor), 7.39 – 7.32 (m, 4H-2 major, 2 minor), 7.29 (q, $J = 7.0, 6.1$ Hz, 2H-1 major, 1 minor), 4.90 (d, $J = 7.9$ Hz, 1H-major), 4.87 (d, $J = 7.8$ Hz, 1H-minor), 4.59 (qd, $J = 9.0, 6.8$ Hz, 2H-1 major, 1 minor), 3.61 (d, $J = 2.4$ Hz, 2H-minor), 3.59 – 3.51 (m, 2H-major), 2.07 (dd, $J = 12.6, 6.4$ Hz, 1H-major), 1.79 (dd, $J = 12.6, 8.9$ Hz, 1H-major), 1.59 – 1.55 (m, 1H-minor), 1.39 (dd, $J = 12.6, 9.2$ Hz, 1H-minor), 1.11 (s, 6H-major), 1.08 (s, 3H- minor), 1.06 (s, 3H-minor).

^{13}C NMR Major/minor diastereomers: (151 MHz, Chloroform- d) δ 139.50 (major), 139.37 (minor), 128.66 (minor), 128.58 (major), 128.52 (minor), 128.45 (major), 128.16 (major), 128.08

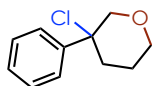
(minor), 82.71 (minor), 82.01 (major), 80.87 (major), 80.47 (minor), 58.47 (minor), 58.06 (major), 46.08 (major), 45.30 (minor), 40.27 (minor), 39.95 (major), 26.32 (minor/major), 25.95 (minor), 25.59 (major).

IR (thin film cm^{-1}): 3031, 2959, 2868, 1496, 1454, 1368, 1059, 697, 664

HRMS m/z **calculated** for $\text{C}_{13}\text{H}_{17}\text{BrO}$ $[\text{H}]^+$: 269.0536, and 271.0515; **found**: 269.0535, and 271.0514

NMR Spectra (^1H , ^{13}C , HSQC, COSY): 229-230

3-chloro-3-phenyltetrahydro-2H-pyran (3.22):



The average yield for the title compound was 57% (2 trials) at the 0.5 mmol scale, generated using **General Procedure for Chlorofunctionalizations** using 81 mg of the starting alcohol (0.1M in DCE), 67 mg NCS, 10 mg Mes-Acr-Me⁺, 6.7mg CuCl_2 , 9mg of 1,10-phenanthroline, and an irradiation time of 2 hours. After the reaction, the contents were transferred to a separatory funnel and diluted with DCM. The organic layer was washed with H_2O to remove succinimide. The aqueous layer was extracted twice more with DCM. All organics were combined and dried over Na_2SO_4 . The organics were passed through a small plug of silica to remove any remaining Cu or acridinium impurities. After removing the solvent in vacuo the title compound was obtained as a single regioisomer. The product was found to be volatile, therefore the use of high vacuum was avoided.

Analytical data for **3.22**:

^1H NMR (600 MHz, Chloroform- d) δ 7.61 – 7.56 (m, 2H), 7.39 (dd, J = 8.4, 6.9 Hz, 2H), 7.35 – 7.29 (m, 1H), 4.06 (dd, J = 12.2, 1.6 Hz, 1H), 3.99 (d, J = 12.3 Hz, 1H), 3.91 (dt, J = 11.5, 4.7 Hz,

1H), 3.62 (ddd, $J = 11.7, 8.6, 3.3$ Hz, 1H), 2.45 (dd, $J = 9.2, 4.2$ Hz, 1H), 2.41 (dddd, $J = 13.8, 6.8, 3.0, 2.0$ Hz, 1H), 2.09 (tq, $J = 8.9, 4.4$ Hz, 1H), 1.64 – 1.58 (m, 1H).

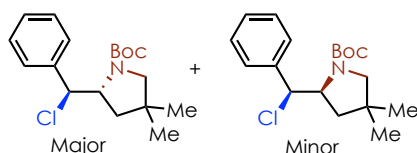
^{13}C NMR (151 MHz, CDCl_3) δ 142.02, 128.47, 128.16, 126.31, 76.16, 69.25, 67.99, 37.94, 23.20.

IR (thin film cm^{-1}): 2958, 2852, 1723, 1685, 1493, 1447, 1099, 1030, 755, 698, 587

LRMS m/z calculated for $\text{C}_{11}\text{H}_{13}\text{ClO}^+$: 196.06 and 198.06, **found**: 196.10 and 198.05

NMR Spectra (^1H , ^{13}C , HSQC, COSY): 231-232

tert-butyl 2-(chloro(phenyl)methyl)-4,4-dimethylpyrrolidine-1-carboxylate (**3.23**):



The average yield for the title compound was 59% (2 trials) at the 0.5 mmol scale, generated using **General Procedure for Chlorofunctionalizations** using 144.7 mg of the starting amine (0.1M in DCE), 90.8 mg NCP, 10 mg Mes-Acr-Me $^+$, 6.7mg CuCl_2 , 9mg of 1,10-phenanthroline, and an irradiation time of 3 hours. The average diastereomeric ratio was 1.2:1. The products were isolated by column chromatography on silica gel (40 mL dry silica, 2.5 cm column, 10% EtOAc/hexanes) as a colorless oil.

Analytical data for **3.23**:

^1H NMR Major/minor diastereomers: (600 MHz, Chloroform- d) δ 7.44 (d, $J = 7.3$ Hz, 2H-1 major, 1 minor), 7.36 – 7.26 (m, 8H-4 major, 4 minor), 6.04 (d, $J = 3.0$ Hz, 1H-major), 5.75 (d, $J = 3.1$ Hz, 1H-minor), 4.21 (ddd, $J = 9.9, 7.3, 3.0$ Hz, 1H-major), 4.17 – 4.08 (m, 1H-minor), 3.52 (dd, $J = 10.5, 1.9$ Hz, 1H-minor), 3.35 (dd, $J = 10.5, 1.8$ Hz, 1H-major), 3.08 (dd, $J = 12.7, 10.5$ Hz, 2H-1 major, 1 minor), 2.03 (ddd, $J = 22.0, 12.6, 9.3$ Hz, 2H-1 major, 1 minor), 1.56 (s, 9H-minor),

1.50 (s, 9H-major), 1.36 – 1.29 (m, 2H-1 major, 1 minor), 1.10 (d, $J = 8.3$ Hz, 6H-minor), 0.90 (s, 6H-major).

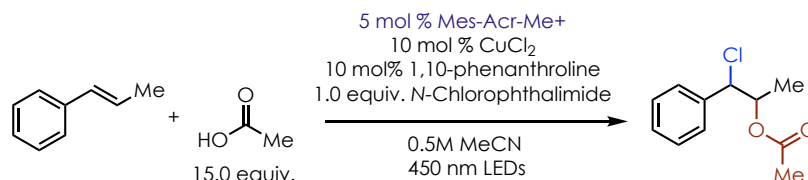
^{13}C NMR Major/minor diastereomers: (151 MHz, Chloroform-*d*) δ 155.09 (major), 154.42 (minor), 138.59 (major), 138.53 (minor), 128.43 (minor), 128.27 (major), 128.03 (minor), 127.85 (major), 127.24 (major), 127.01 (minor), 80.00 (minor), 79.63 (major), 65.63 (minor), 64.57 (major), 63.01 (minor), 62.94 (major), 60.45 (major), 59.52 (minor), 39.61 (minor), 38.72 (major), 36.91 (major), 36.68 (minor), 28.62 (minor), 28.56 (major), 26.50 (major), 26.48 (minor), 25.48 (major), 25.43 (minor).

IR (thin film cm^{-1}): 2960, 2871, 1690, 1452, 1401, 1366, 1253, 1164, 1104, 950, 699

HRMS m/z **calculated** for $\text{C}_{18}\text{H}_{26}\text{ClNO}_2$ $[\text{H}]^+$: 324.1725, and 326.1695; **found**: 324.1724 and 326.1694

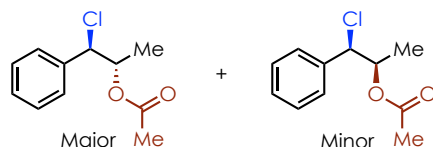
NMR Spectra (^1H , ^{13}C , HSQC, COSY): 233-234

Procedure for photoredox/copper mediated intermolecular chloroacetoxylation



91 mg *N*-chlorophthalimide (**NCP**, 1.0 eq), 7 mg CuCl_2 (0.1 eq), 9 mg 1,10-phenanthroline (0.1 eq), 10 mg Mes-Acr-Me⁺ (0.05 eq), were weighed and dispensed into a flame dried vial (1-dram) equipped with a stir bar and Teflon-coated septum cap. The vial was moved to a nitrogen filled glovebox where 65 μL β -methylstyrene, 429 μL glacial acetic acid (AcOH , 15.0 eq) with 5% v/v acetic anhydride, and solvent (MeCN 0.5 M) were dispensed by syringe. The vial was then sealed and removed from the glovebox and the reaction vial was sealed with electrical tape. The reactions were irradiated (2x455 nm blue LED lamps) and stirred for 2 hours. Upon completion, the crude reactions were passed through a silica plug to remove CuCl_2 before NMR analysis.

1-chloro-1-phenylpropan-2-yl acetate (**3.24**):



The average yield for the title compound was 51% (2 trials) at the 0.5 mmol scale. The average diastereomeric ratio was 1.4:1. The products were isolated by column chromatography on silica gel (10 mL dry silica, 1.0 cm column, 5% EtOAc/hexanes) as a colorless oil.

Analytical data for **3.25**:

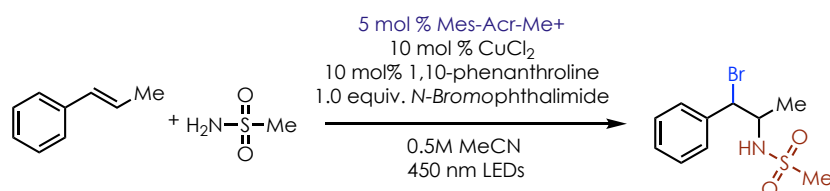
¹H NMR (400 MHz, Chloroform-*d*) δ 7.44 – 7.29 (m, 10H- 5 major, 5 minor), 5.38 – 5.24 (m, 2H-1 major, 1 minor), 4.98 (d, J = 5.7 Hz, 1H-major), 4.84 (d, J = 7.5 Hz, 1H-minor), 2.10 (s, 2H-minor), 1.97 (s, 3H-major), 1.32 (d, J = 6.3 Hz, 3H-major), 1.14 (d, J = 6.4 Hz, 3H-minor).

¹³C NMR (151 MHz, Chloroform-*d*) δ 170.19 (minor), 170.02 (major), 137.87 (minor), 137.61 (major), 128.79 (minor), 128.65 (major), 128.47 (minor), 128.38 (major), 127.82 (major/minor), 73.19 (minor), 73.05 (major), 65.25 (minor), 64.89 (major), 21.09 (minor), 20.97 (major), 17.55 (minor), 16.01 (major).

IR (thin film cm⁻¹): 3033, 2989, 2938, 1742, 1495, 1454, 1372, 1238, 1059, 959, 699, 603

HRMS *m/z* **calculated** for C₁₁H₁₃ClO₂ [H]⁺: 213.0677, and 215.0647; **found**: 213.0679 and 215.0649 **NMR Spectra (¹H, ¹³C, HSQC, COSY): 235-236**

Procedure for photoredox/copper mediated intermolecular bromoamination



48 mg methanesulfonamide, 113 mg *N*-bromophthalimide (NBP, 1.0 eq), 11 mg CuBr₂ (0.1 eq), 9. mg 1,10- phenanthroline (0.1 eq), 10 mg Mes-Acr-Me⁺ (0.05 eq), were weighed and dispensed into a flame dried vial (2-dram) equipped with a stir bar and Teflon-coated septum cap. The vial was moved to a nitrogen filled glovebox where 65 μL β-methylstyrene and solvent (DCE 0.1 M) were dispensed by syringe. The vial was then sealed and removed from the glovebox and the reaction vial was sealed with electrical tape. The reactions were irradiated (2x455 nm blue LED lamps) and stirred for 3 hours. Upon completion, the crude reactions were passed through a silica plug to remove CuBr₂ before NMR analysis.

The average yield for the title compound was 27% (2 trials) at the 0.5 mmol scale. The average diastereomeric ratio was 1.8:1. The average regioisomeric ratio was 11.7:1. The products were

isolated by column chromatography on silica gel (60 mL dry silica, 2.5 cm column, 10% EtOAc/hexanes then 30% EtOAc/hexanes) as a colorless oil.

Analytical data for **3.25**:

¹H NMR Major/minor diastereomers (minor regioisomer noted for observable peaks): (600 MHz, Chloroform-*d*) δ 7.44 (ddd, $J = 7.6, 3.2, 1.9$ Hz, 4H- 2 major, 2 minor), 7.39 – 7.34 (m, 4H- 2 major, 2 minor), 7.34 – 7.28 (m, 2H- 1 major, 1 minor), 5.39 (d, $J = 8.8$ Hz, 1H-minor regioisomer), 5.13 (d, $J = 5.0$ Hz, 1H-major), 4.99 (d, $J = 5.5$ Hz, 1H-minor), 4.65 (dd, $J = 8.8, 4.4$ Hz, 1H-minor regioisomer), 4.60 (d, $J = 9.0$ Hz, 1H-minor), 4.56 (d, $J = 9.2$ Hz, 1H-major), 3.94 – 3.83 (m, 2H- 1 major, 1 minor), 2.82 (s, 3H-major), 2.71 (s, 3H-minor), 2.67 (s, 3H- minor regioisomer), 1.58 (d, $J = 6.9$ Hz, 3H- minor regioisomer), 1.35 (dd, $J = 8.7, 6.6$ Hz, 6H-3 major, 3 minor).

¹³C NMR Major/minor diastereomers:(151 MHz, Chloroform-*d*) δ 138.07 (minor), 137.90 (major), 128.84 (minor), 128.69 (major), 128.66 (minor), 128.64 (major), 128.49 (major), 128.39 (minor), 60.64 (major), 59.59 (minor), 56.27 (minor), 55.86 (major), 42.08 (major), 41.49 (minor), 21.48 (minor), 19.06 (major).

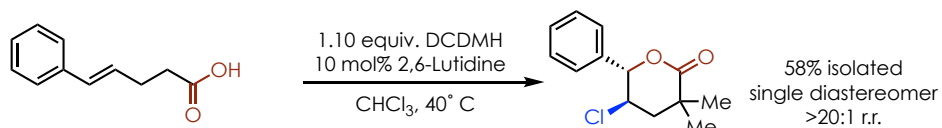
IR (thin film cm^{-1}): 3281, 2927, 1452, 1319, 1149, 993, 755, 700

HRMS m/z **calculated** for $\text{C}_{10}\text{H}_{14}\text{BrNO}_2\text{S}$ [K⁺]: 329.9560 and 331.9540; **found**: 329.9560 and 331.9540

NMR Spectra (¹H, ¹³C, HSQC, COSY): 237-238

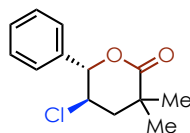
3.6.5.4 General Procedure for Polar Halofunctionalizations

Polar Chlorofunctionalization Method



The carboxylic acid substrate (1.0 eq, 102 mg) and Dichlorodimethyl hydantoin (DCDMH, 1.1 eq, 108 mg) were weighed and dispensed into a flame dried vial (2-dram) equipped with a stir bar and Teflon-coated septum cap. The vial was moved to a nitrogen filled glovebox where solvent was dispensed by syringe (CHCl_3 to 0.1 M), and 6 μL of 2,6-Lutidine was added via syringe. The vial was then sealed and removed from the glovebox and the reaction vial was sealed with electrical tape. The reaction was then heated at 40°C with a heating block for 24 h. CHCl_3 was then removed in vacuo and NMR analysis revealed the reaction had reached full conversion. The compound could be partially purified on column chromatography (10% EtOAc:Hex) however the product coeluted with monochlorodimethyl hydantoin. This impurity could be removed by bringing the sample up in DCM and washing with 10% sodium hydroxide solution. The isolated yield for the sole trial was 58%, however the purification was not optimized.

5-chloro-3,3-dimethyl-6-phenyltetrahydro-2H-pyran-2-one (3.26):



Analytical Data for **3.26**:

$^1\text{H NMR}$ (400 MHz, Chloroform- d) $^1\text{H NMR}$ 7.64 – 7.33 (m, 5H), 5.19 (d, $J = 9.8$ Hz, 1H), 4.28 (ddd, $J = 11.1, 9.8, 4.8$ Hz, 1H), 2.49 – 2.21 (m, 2H), 1.46 (s, 3H), 1.43 (s, 3H).

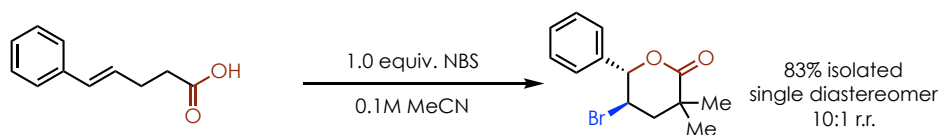
^{13}C NMR (151 MHz, CDCl_3) δ 175.10, 136.45, 129.27, 128.52, 127.19, 86.41, 54.34, 44.76, 39.70, 28.19, 27.70.

IR (thin film cm^{-1}): 3035, 2982, 2931, 2872, 1731, 1459, 1388, 1236, 1129, 1000, 842, 716, 642

HRMS m/z calculated for $\text{C}_{13}\text{H}_{15}\text{ClO}_2$ $[\text{H}]^+$: 239.0833 and 241.0804; found: 239.0832 and 241.0803

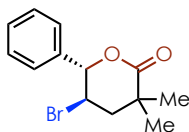
NMR Spectra (^1H , ^{13}C , HSQC, COSY): 239-240

Polar Bromofunctionalization Method



The carboxylic acid substrate (1.0 eq, 102 mg) and *N*-bromosuccinimide (1.0 eq, 89 mg) were weighed and dispensed into a flame dried vial (2-dram) equipped with a stir bar and Teflon-coated septum cap. The vial was moved to a nitrogen filled glovebox where solvent was dispensed by syringe (MeCN to 0.1 M). The vial was then sealed and removed from the glovebox and the reaction vial was sealed with electrical tape. The reaction was stirred in the dark overnight. The product was isolated via column chromatography (40 mL dry silica, 2.5 cm column, 10% EtOAc/hexanes) as white solid. The regioisomers were inseparable and resulted in a single isolated yield of 83% 10:1 r.r.

5-bromo-3,3-dimethyl-6-phenyltetrahydro-2H-pyran-2-one (3.27)



Analytical data for **3.27**:

¹H NMR Major/minor regioisomers: (600 MHz, Chloroform-*d*) δ 7.44 – 7.36 (m, 10H-5 major, 5 minor), 5.30 (d, J = 10.4 Hz, 1H-major), 4.94 (d, J = 7.7 Hz, 1H-minor), 4.87 – 4.77 (m, 1H-minor), 4.37 (td, J = 10.2, 6.3 Hz, 1H-major), 2.45 – 2.38 (m, 3H-2 major, 1 minor), 2.09 (dd, J = 13.0, 9.7 Hz, 1H-minor), 1.47 (s, 3H- major), 1.42 (s, 3H-major), 1.29 (d, J = 5.1 Hz, 6H-minor).

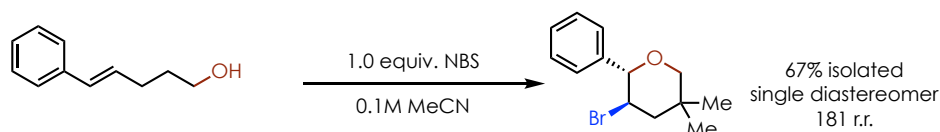
¹³C NMR Major/minor regioisomers: (151 MHz, Chloroform-*d*) δ 180.83 (minor), 175.11 (major), 137.42 (minor), 136.75 (major), 129.35 (major), 129.05 (minor) 128.80 (minor), 128.51 (major), 128.20 (minor), 127.34 (major), 86.83 (major), 78.17 (minor), 55.53 (minor), 45.83 (major), 45.18 (major), 42.30 (minor) 40.71 (major), 40.66 (minor), 27.99 (major), 27.50 (major), 24.81(minor), 24.70 (minor).

IR (thin film cm⁻¹): 1725, 1459, 1387, 1210, 1130, 984, 706

HRMS m/z **calculated** for C₁₃H₁₅BrO₂ [H]⁺: 283.0328 and 285.0308; **found**: 283.0327 and 285.0306

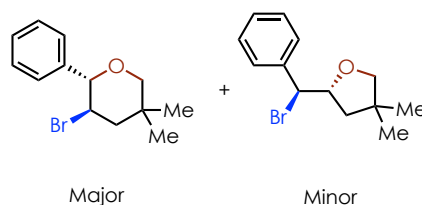
NMR Spectra (¹H, ¹³C, HSQC, COSY): 241-242

Procedure for Polar Bromoetherification:



The alcohol substrate (1.0 eq, 95 mg) and *N*-bromosuccinimide (**NBS**, 1.0 eq, 89 mg) were weighed and dispensed into a flame dried vial (2-dram) equipped with a stir bar and Teflon-coated septum cap. The vial was moved to a nitrogen filled glovebox where solvent was dispensed by syringe (MeCN to 0.1 M). The vial was then sealed and removed from the glovebox and the reaction vial was sealed with electrical tape. The reaction was stirred in the dark overnight. The product was isolated via column chromatography (40 mL dry silica, 2.5 cm column, 10% EtOAc) colorless oil. The regioisomers were inseparable and resulted in a single isolated yield of 67% 8:1 r.r.

3-bromo-5,5-dimethyl-2-phenyltetrahydro-2*H*-pyran (**3.28**)



Analytical data for **3.38**

¹H NMR Major/minor regioisomers: (600 MHz, Chloroform-*d*) 7.50 – 7.43 (m, 4H-2 major, 2 minor), 7.43 – 7.34 (m, 6H-3 major, 3 minor), 4.94 (d, *J* = 7.9 Hz, 1H-minor), 4.64 (ddd, *J* = 8.9, 7.9, 6.4 Hz, 1H-minor), 4.33 – 4.21 (m, 2H-major), 3.69 (dd, *J* = 11.3, 2.6 Hz, 1H-major), 3.62 – 3.56 (m, 2H-minor), 3.45 (d, *J* = 11.2 Hz, 1H-major), 2.40 – 2.28 (m, 1H-major), 2.10 (ddd, *J* = 12.6, 6.4, 0.9 Hz, 1H-minor), 2.06 – 1.96 (m, 1H-major), 1.83 (dd, *J* = 12.6, 8.9 Hz, 1H-minor), 1.26 (s, 3H-major), 1.15 (d, *J* = 1.9 Hz, 6H-minor), 0.97 (s, 3H-major).

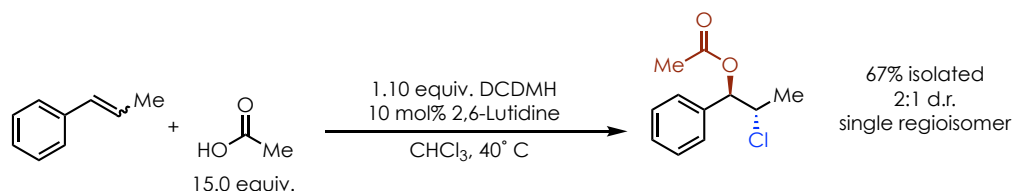
¹³C NMR Major/minor regioisomers: (151 MHz, Chloroform-*d*) δ 139.32 (minor), 139.25 (major), 128.48 (minor), 128.41 (major), 128.36 (minor), 128.14 (major), 128.10 (minor), 127.45 (major), 85.47 (major), 81.93 (minor), 80.75 (minor), 78.26 (major), 58.00 (minor), 50.61 (major), 49.08 (major), 45.99 (minor), 39.75 (minor), 34.99 (major), 26.43 (major), 26.26 (minor), 25.52 (minor), 23.56 (major).

IR (thin film cm⁻¹): 2956, 2866, 1646, 1455, 1368, 1277, 1078, 791, 756, 698

HRMS *m/z* **calculated** for C₁₃H₁₇BrO [H⁺]: 269.0536 and 271.0515; **found** 269.0536 and 271.0515

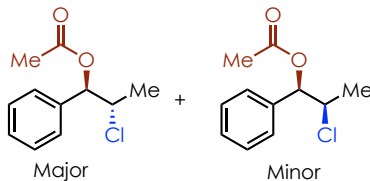
NMR Spectra (¹H, ¹³C, HSQC, COSY): 243-244

Procedure for Polar Chloroacetoxylation



Dichlorodimethyl hydantoin (DCDMH, 1.1 eq, 108 mg) was weighed and dispensed into a flame dried vial (1- dram) equipped with a stir bar and Teflon-coated septum cap. The vial was moved to a nitrogen filled glovebox where solvent was dispensed by syringe (CHCl₃ to 0.5 M). This was followed by the addition of 430 μL (15 eq) of acetic acid, and 6 μL of 2,6-Lutidine (0.1 eq). Finally, 65 μL of trans-beta methyl styrene was added (single alkene isomer). The vial was then sealed and removed from the glovebox and the reaction vial was sealed with electrical tape. The reaction was then heated at 40 °C with a heating block for 24 h. CHCl₃ and acetic acid were then removed in vacuo and NMR analysis revealed the reaction had reached full conversion. The product was isolated on silica gel (20 mL dry silica, 2cm column, 10% EtOAc:Hexanes) as a mixture of diastereomers (80% yield, 2:1 d.r.).

2-chloro-1-phenylpropyl acetate (3.29):



Analytical data for **3.29**:

^1H NMR (600 MHz, Chloroform-*d*) δ 7.39 – 7.31 (m, 10H-5 major, 5 minor), 5.91 (d, J = 5.2 Hz, 1H-major), 5.79 (d, J = 7.6 Hz, 1H-minor), 4.33 – 4.24 (m, 2H-1 major, 1 minor), 2.15 (s, 3H-major), 2.13 (s, 3H-minor), 1.47 (d, J = 6.7 Hz, 3H-major), 1.35 (d, J = 6.7 Hz, 3H-minor).

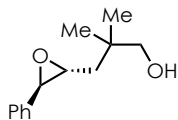
^{13}C NMR (151 MHz, CDCl_3) δ 169.76 (minor), 169.73 (major), 137.01 (minor), 136.71 (major), 128.73 (minor), 128.55 (major), 128.48 (minor), 128.30 (major), 127.29 (minor), 127.19 (major), 79.11 (minor), 78.12 (major), 58.87 (major), 58.53 (minor), 21.33 (minor), 20.99 (major/minor), 19.99 (major).

IR (thin film cm^{-1}): 2983, 1746, 1454, 1372, 1228, 1029, 758, 703, 623

HRMS m/z **calculated** for $\text{C}_{11}\text{H}_{13}\text{ClO}_2$ $[\text{H}]^+$: 213.0677 and 215.0647; **found**: 213.0677

NMR Spectra (^1H , ^{13}C , HSQC, COSY): 245-246

3.6.6 Analytical Data for Epoxides and Furans from Section 3.3.2

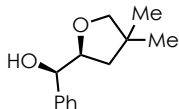


Analytical data for **trans-epoxide**:

¹H NMR (400 MHz, Chloroform-*d*) δ 7.50 – 7.25 (m, 5H), 3.65 (d, J = 2.1 Hz, 1H), 3.54 (d, J = 11.1 Hz, 1H), 1.77 (dd, J = 14.4, 4.0 Hz, 1H), 3.39 (d, J = 11.1 Hz, 1H), 3.05 (ddd, J = 7.9, 4.0, 2.1 Hz, 1H), 2.03 (broad, 1.59 (dd, J = 14.3, 7.9 Hz, 1H), 1.04 (d, J = 3.5 Hz, 6H).

NMR Spectra (¹H): 247

Analytical data for **cis-furan product**:



¹H NMR (400 MHz, Chloroform-*d*) δ 7.43 – 7.29 (m, 5H), 4.97 (d, J = 2.7 3.9 Hz, 1H), 3.57 (d, J = 1.4 Hz, 2H), 1.78 (dd, J = 12.3, 9.9 Hz, 1H), 1.32 (d, J = 6.3 Hz, 1H), 1.06 (d, J = 12.8 Hz, 6H).

NMR Spectra (¹H): 247

3.6.7 UV/vis Spectroscopy

UV/vis spectra were taken on a Hewlett-Packard 8453 Chemstation absorption spectrometer.

[CuCl/Phen]₂: A solution of [CuCl/Phen]₂ was prepared by weighing equimolar amounts of CuCl and 1,10-phenanthroline into a vial (0.05 mmol). In a glovebox, 10 mL MeCN (N₂ sparged) was added to give a 5×10^{-4} M solution of the complex. 350 μ L of this solution was transferred to a 2-dram vial and then diluted to 3.5 mL total volume, giving a 5×10^{-4} M solution of [CuCl/Phen]₂. 3 mL of this solution was transferred to a quartz cuvette and a UV/vis spectrum was obtained.

CuCl₂/Phen: A saturated solution of CuCl₂/Phen was prepared by weighing equimolar amounts of CuCl₂ and 1,10-phenanthroline into a vial (0.05 mmol). In a glovebox 10 mL MeCN (N₂ sparged) was added to give a saturated solution of unknown concentration of CuCl₂/Phen (due to the low solubility of CuCl₂/Phen). 350 μ L of this solution was transferred to a 2-dram vial and then diluted to 3.5 mL total solution volume of CuCl₂/Phen. 3mL of this solution was transferred to a quartz cuvette and a UV/vis spectrum was obtained.

[CuCl/Phen]₂ + NCP: To the cuvette containing [CuCl/Phen]₂ discussed above, was added 1 mL of 7.5×10^{-3} M solution of NCP in MeCN (5 eq relative to Cu⁺). The solution immediately lost its orange color and became a light blue solution. Adjusted concentrations of Cu⁺ and NCP were 3.75×10^{-4} M and 1.875×10^{-3} M respectively. A UV/vis spectrum was recorded immediately after mixing the solution. Solutions of [CuBr/Bpy]₂, CuBr₂/Bpy, and DEBM were made analogously to their counterparts as described above.

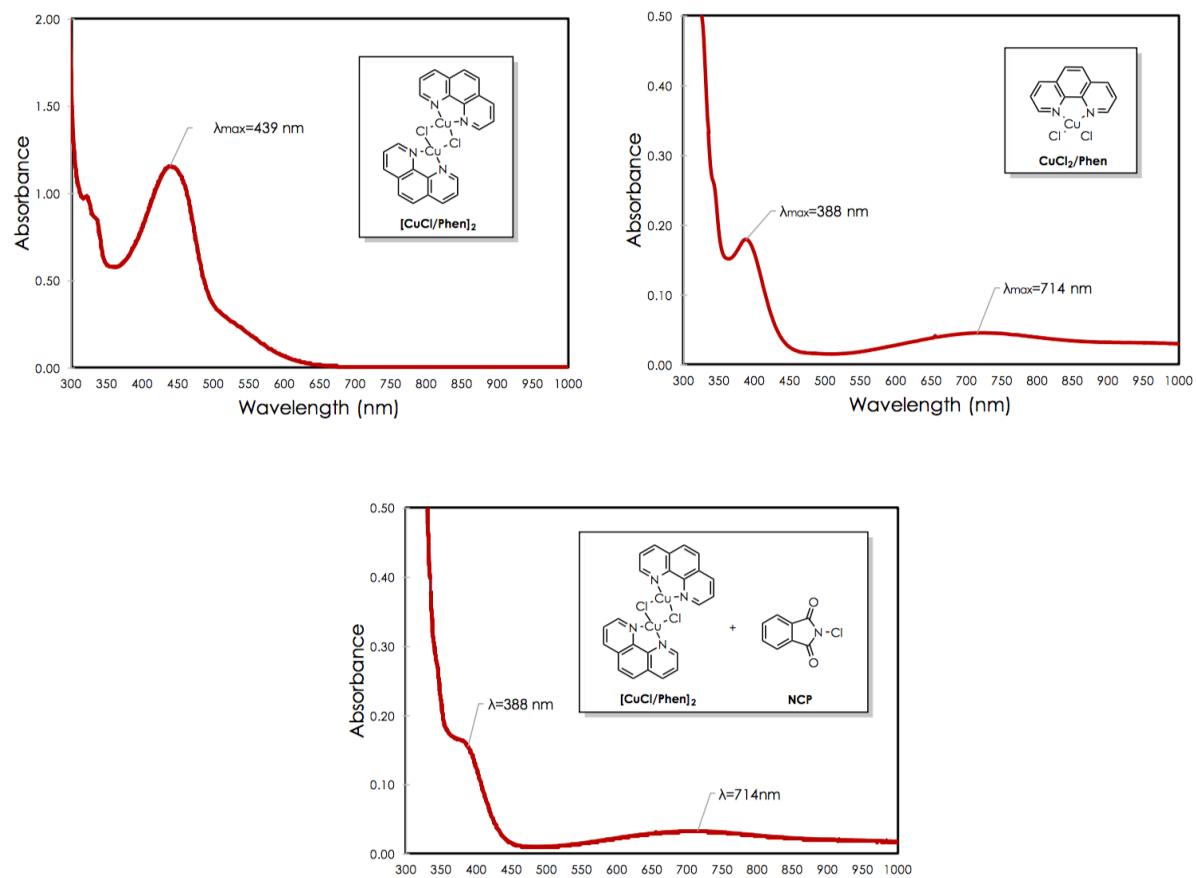


Figure 3.20: (top left) UV/vis spectrum of 5×10^{-4} M solution of $[\text{CuBr/bpy}]_2$ (top right) UV/vis spectrum of saturated solution of CuBr_2/bpy (bottom) UV/vis spectrum after reaction of $[\text{CuBr/bpy}]_2$ with diethylbromomalonate (DEBM).

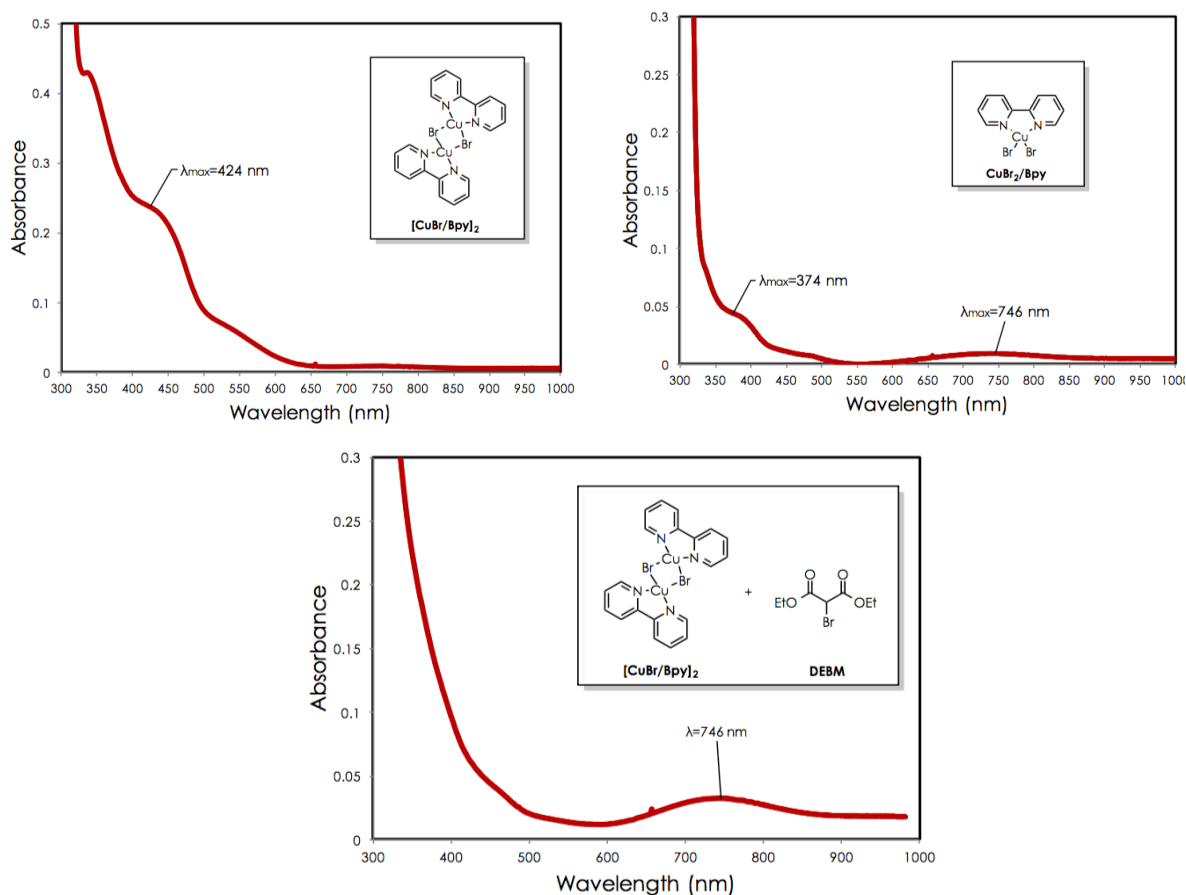
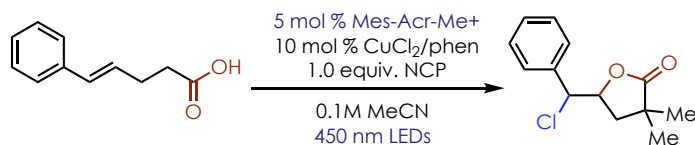


Figure 3.21: (top left) UV/vis spectrum of 5 x 10⁻⁴ M solution of [CuCl/Phen]₂ (top right) UV/vis spectrum of saturated solution of CuCl₂/Phen (bottom) UV/vis spectrum after reaction of [CuCl/Phen]₂ with N-Chlorophthalimide (NCP).

Upon the addition of the respective halogenating reagents to each Cu⁺ complex, the characteristic absorbance (439 nm for [CuCl/Phen]₂ and 424 nm for [CuBr/Bpy]₂) immediately disappeared. In both cases new features were observed which closely correspond with those observed in the UV/vis spectrum of the independently synthesized Cu²⁺ complexes. This is sufficient evidence to support the oxidation of the Cu⁺ metal center. Unfortunately, due to the very low solubility of both Cu²⁺ complexes quantitative data could not be recorded and the present data cannot be used to determine whether CuCl₂/Phen or CuBr₂/Bpy are the sole products of the oxidation. While at least some amount of Cu²⁺ does seem to be forming, it is still feasible that a Cu(III) intermediate could be formed under these conditions as well.

3.6.8 Quantum Yield Determination



The photochemical quantum yield was determined for the reaction above. In the dark, Potassium Ferrioxalate trihydrate (K₂Fe(C₂O₄)₃) was freshly prepared via the previously reported method.⁸¹ Purification was achieved via 3 recrystallizations, before making a 0.15 M solution in H₂O. 1.1 mL of the solution was irradiated for 30 seconds using a single blue LED (a second trial was conducted with irradiation for 15 seconds). After irradiation the sample was again kept in the dark, and 0.5 mL of the irradiated sample was transferred to a 25 mL volumetric flask. A solution of buffered 1,10 phenanthroline was prepared as previously described in the literature;⁸² 5 mL of the solution was transferred to the 25 mL volumetric flask. H₂O was added to the flask up to the mark, and the resulting solution was allowed to stir 20 minutes at room temperature. Finally, 250 μ L of the solution was transferred to a quartz cuvette, and diluted to 2.75 mL total volume with H₂O.

The mols of tris-phenanthroline-Fe²⁺ complex ($\epsilon_{510\text{ nm}} = 11,110\text{ M}^{-1}\text{ cm}^{-1}$)⁸³ was determined by UV/vis. The photon flux was then determined using the absolute quantum yield of **0.85** at 457.9 nm, for the photolysis of (K₂Fe(C₂O₄)₃). The average photon flux (two trials) was determined to be $1.50 \times 10^{-6}\text{ mol photons s}^{-1}$ after two trials (std. dev. = $5 \times 10^{-8}\text{ mol photons s}^{-1}$). The quantum yield of the reaction ($\Phi_R = \text{mol product/mol photons}$) was then determined by stopping the reaction at known time points at close to the reaction completion. Three trials were performed at ~60, 88,

and 94% conversion. The average quantum yield of the reaction for the three trials was 3.6% (std. dev.=0.32%).

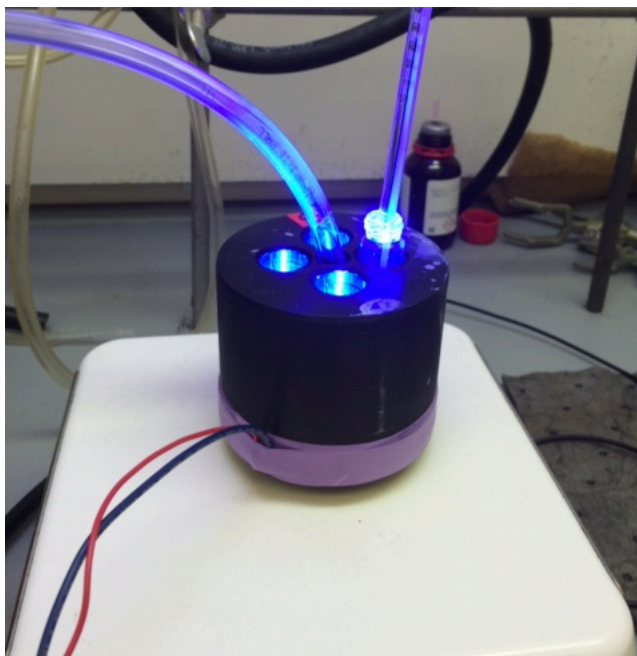
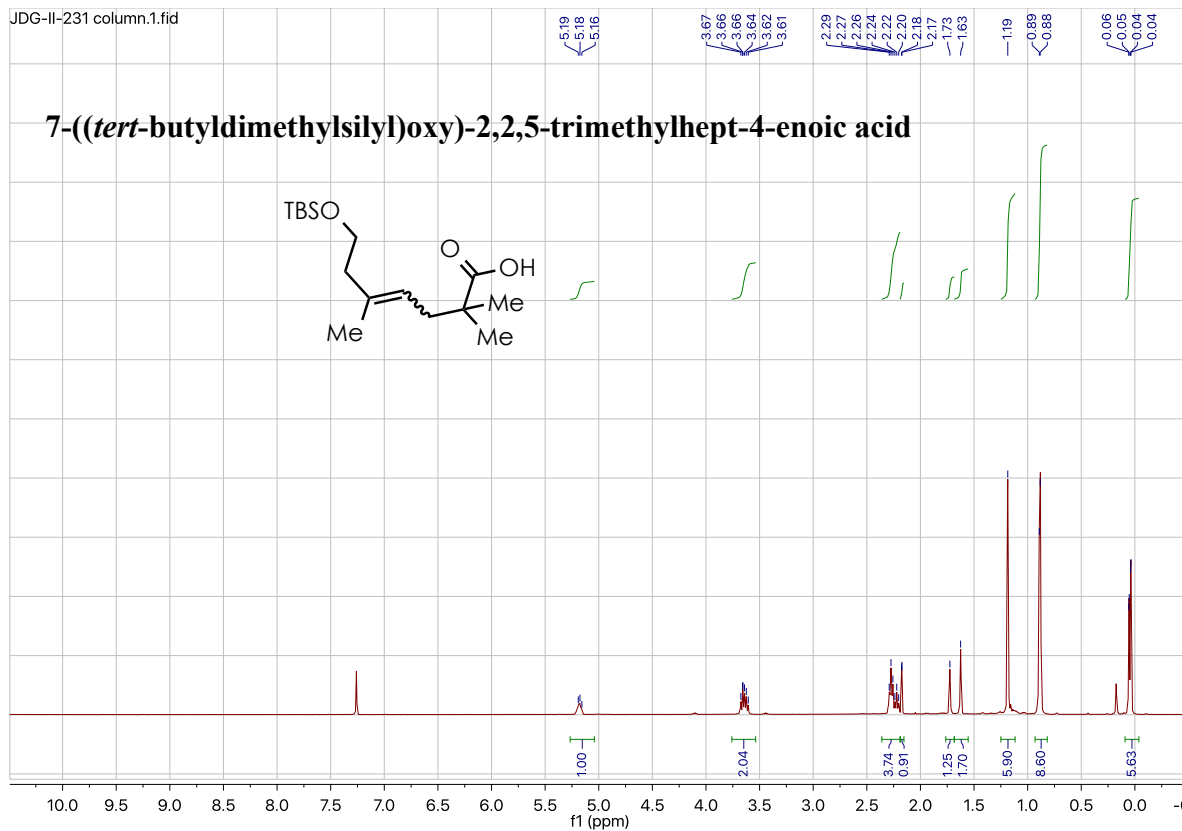
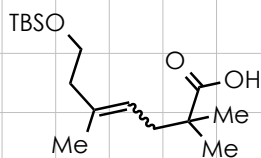


Figure 3.22: Photoreactor setup used in the quantum yield determination studies. This photoreactor allows for irradiation using a single 450 nm LED to ensure consistent photon flux. Individual reaction vials (1-dram) can be placed into the LED slots. The same slot was used for photon flux measurements, and quantum yield determination. The reactor is cooled by flowing air through the reactor and out a heat sink mounted on the bottom. Reactor temperature was maintained at 34 °C throughout the reactions. Stirring is accomplished by setting the reactor on a standard stir plate. CREE XT-E Royal Blue LEDs were used pre-soldered to MCPCB (metal core printed circuit board); purchased from www.rapidled.com (<http://www.rapidled.com/cree-xt-e-royal-blue-led/>)

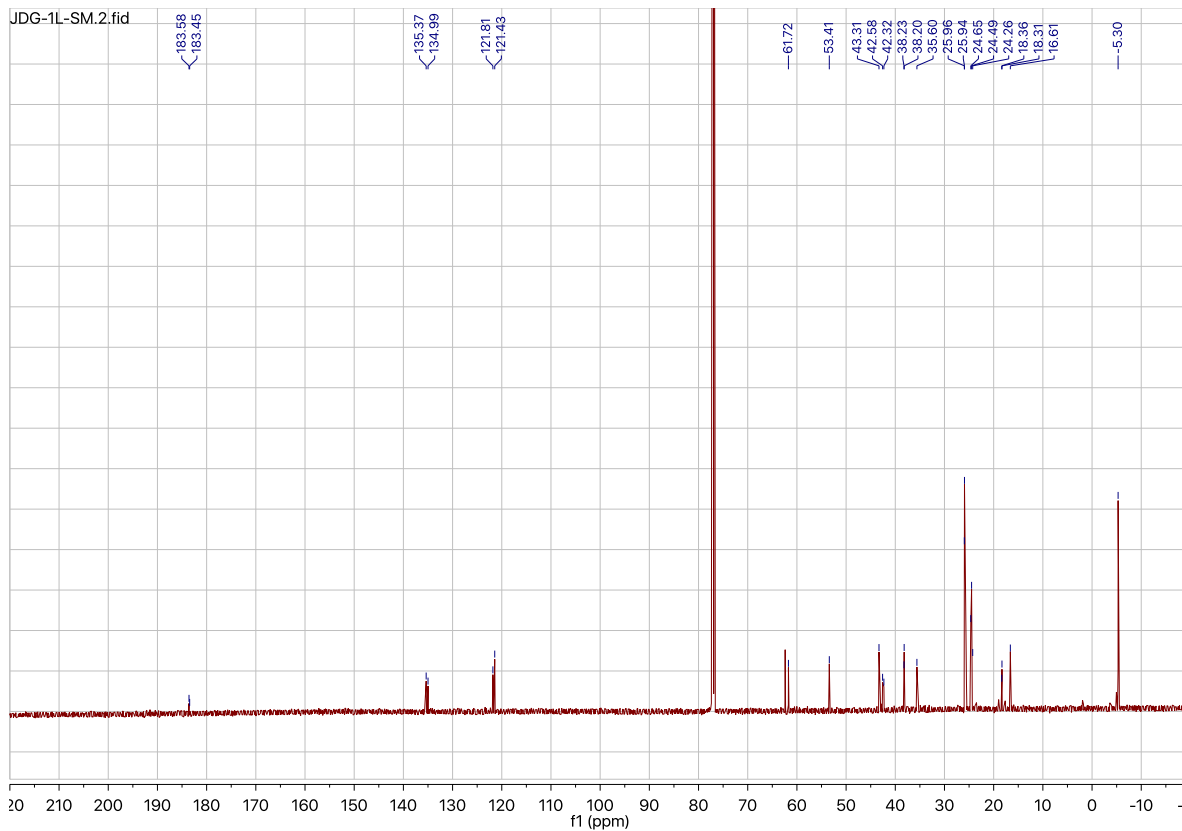
3.6.9 NMR Spectra

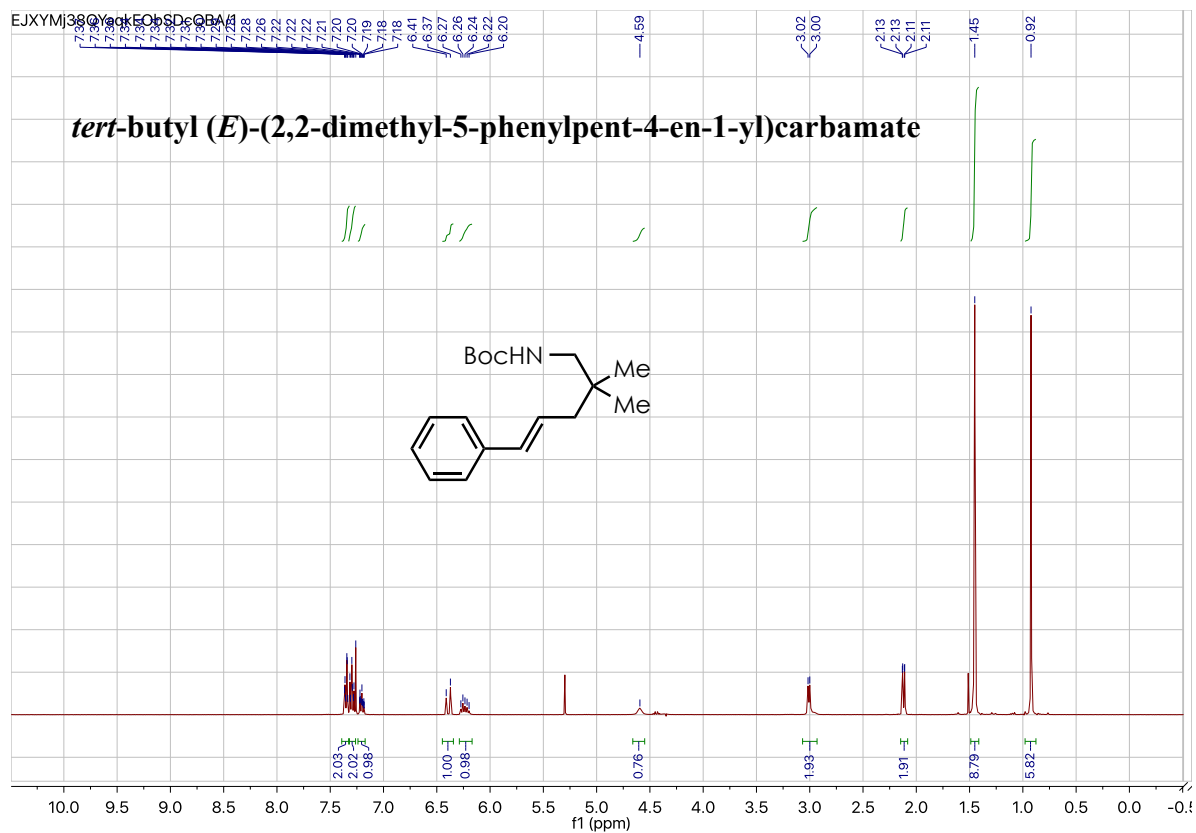
JDG-II-231 column.1.fid

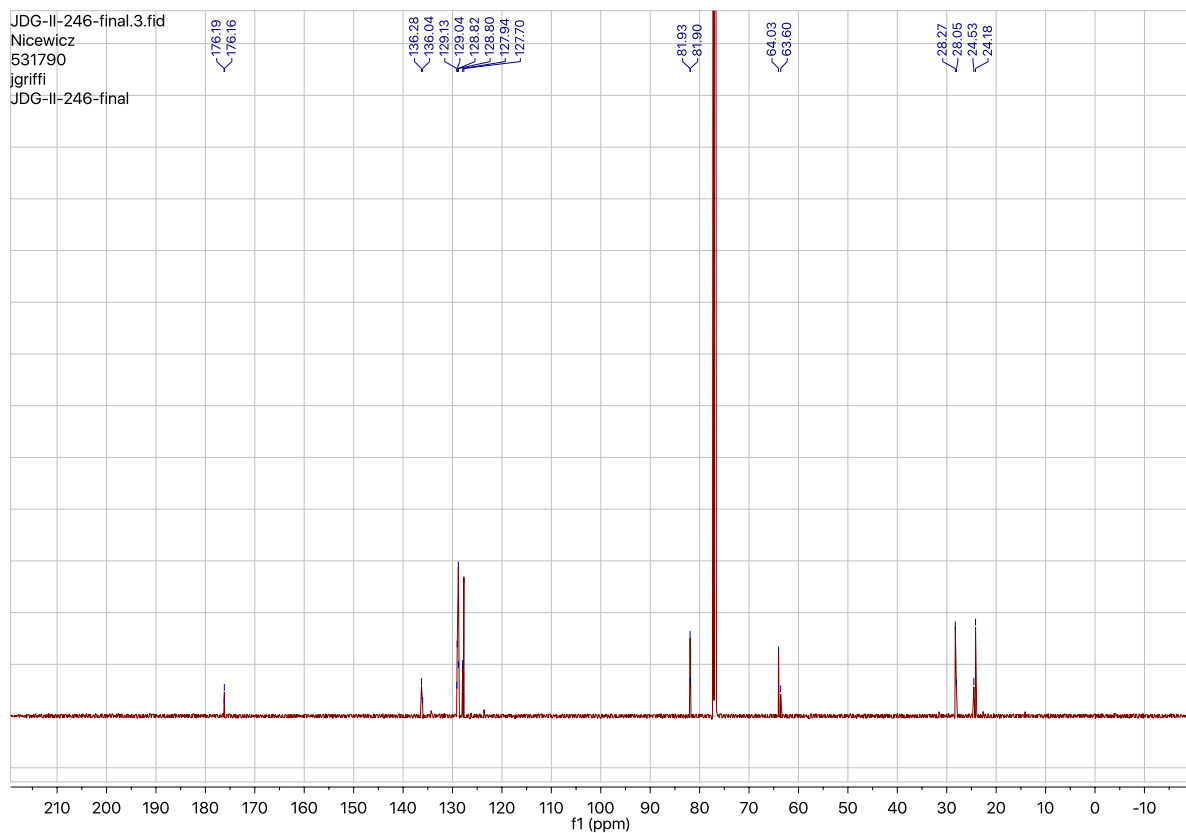
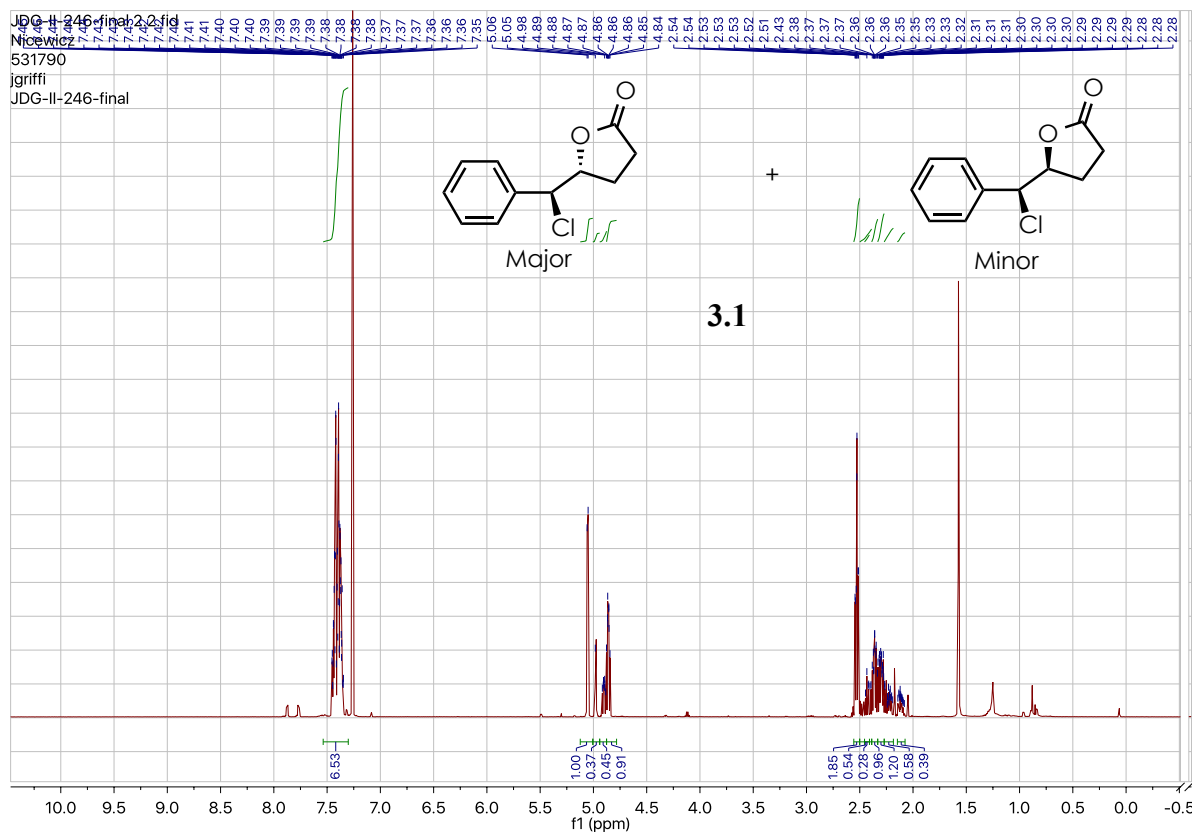
7-((*tert*-butyldimethylsilyl)oxy)-2,2,5-trimethylhept-4-enoic acid

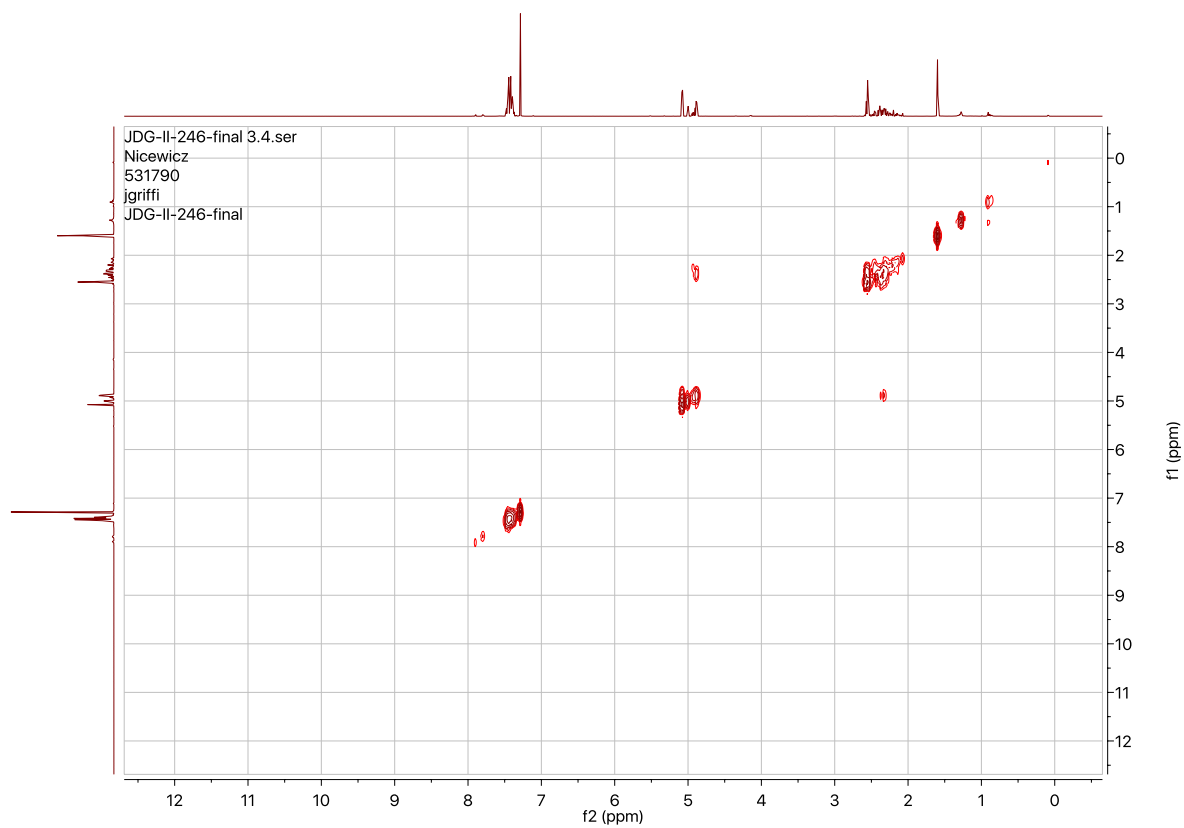
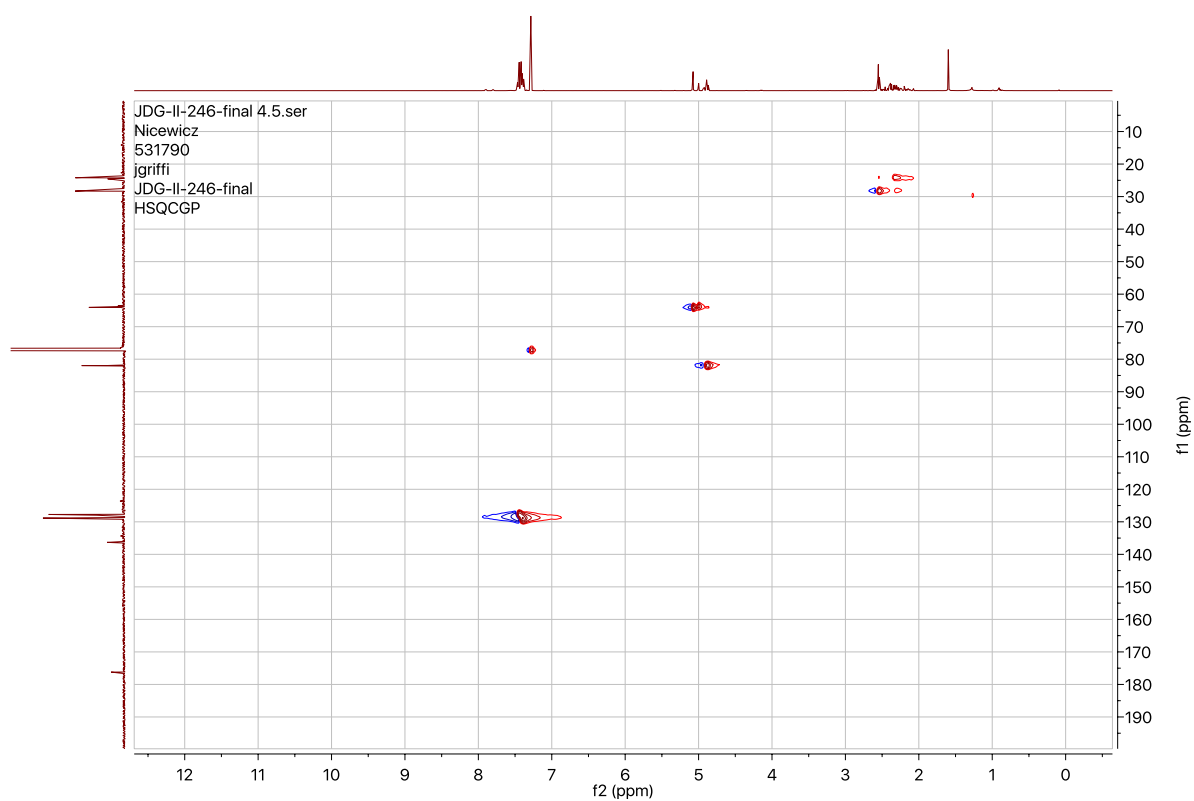


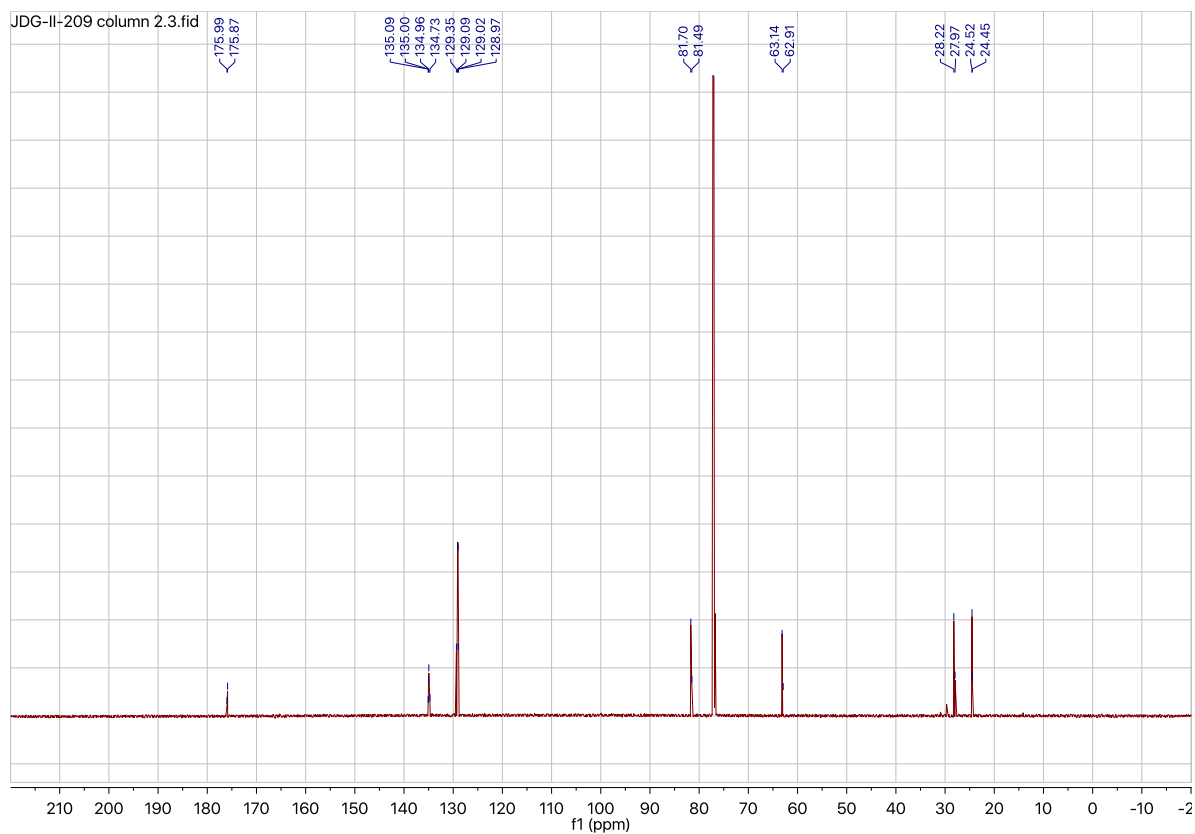
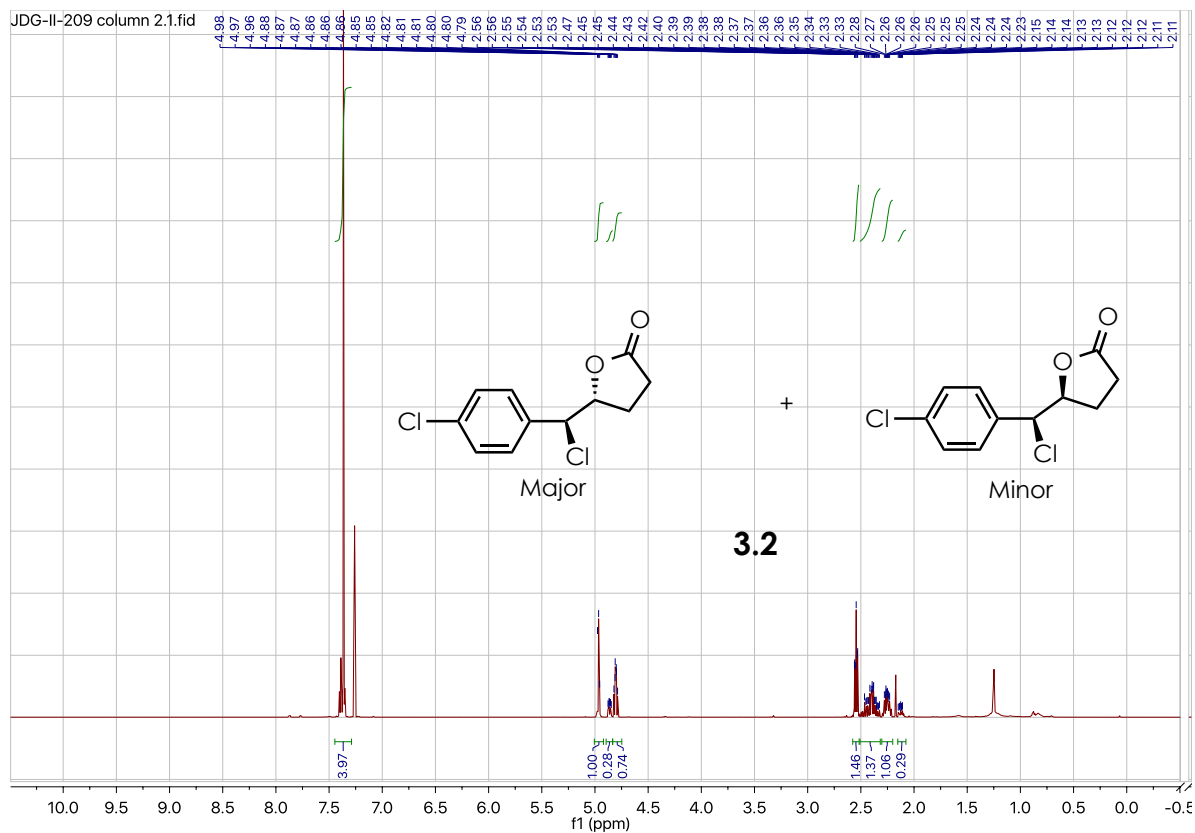
JDG-1L-SM.2.fid

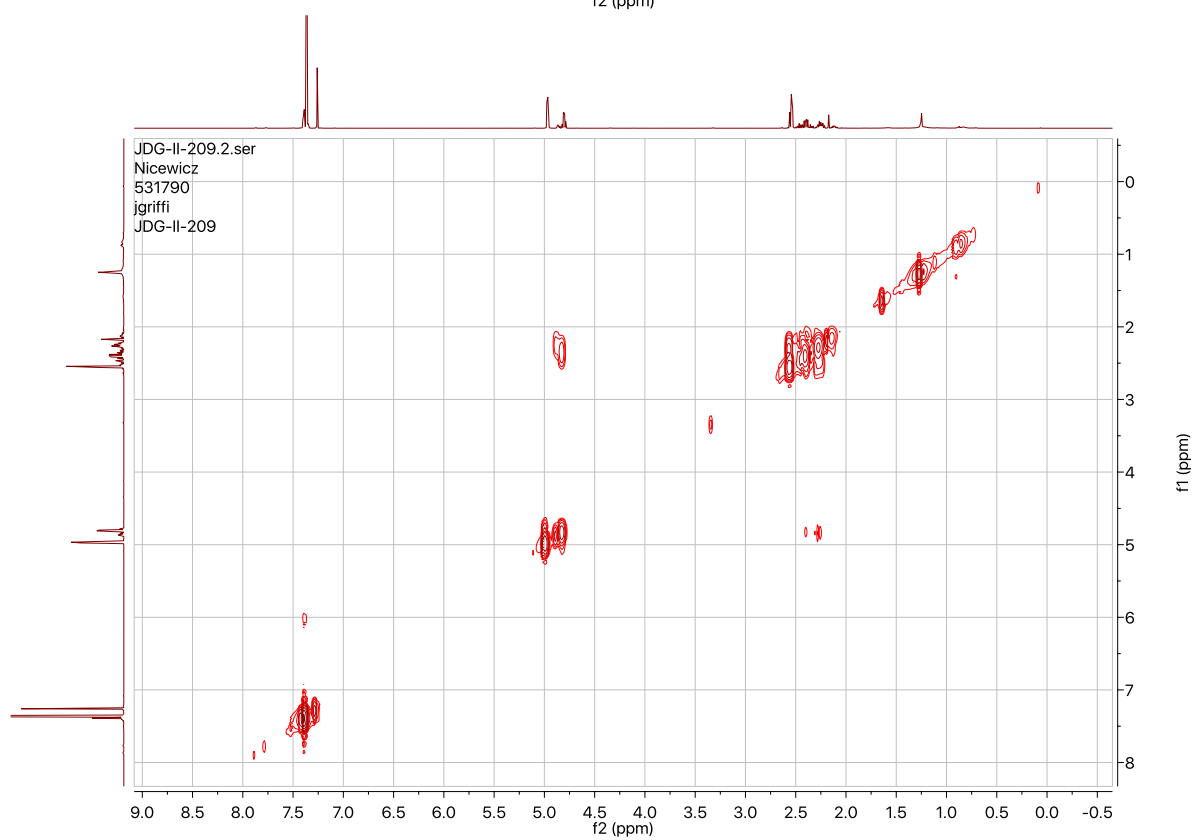
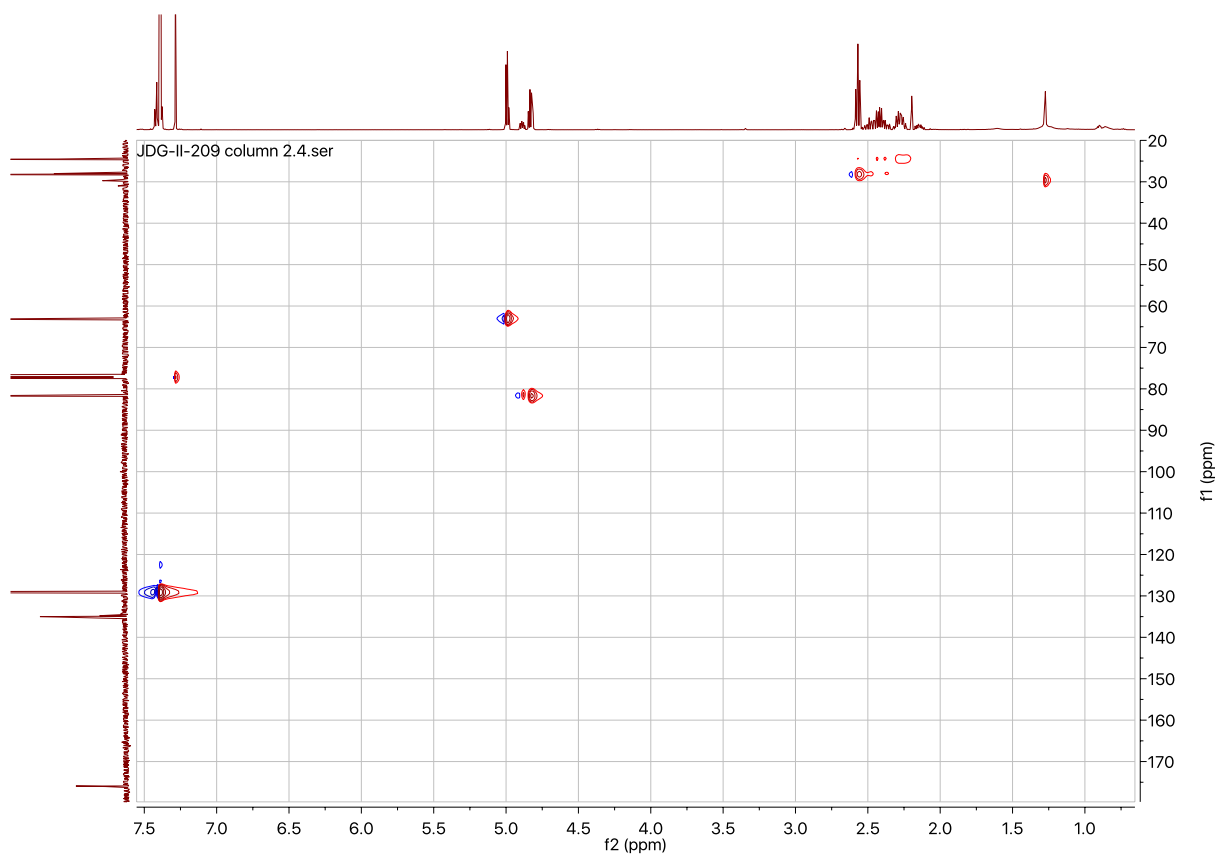


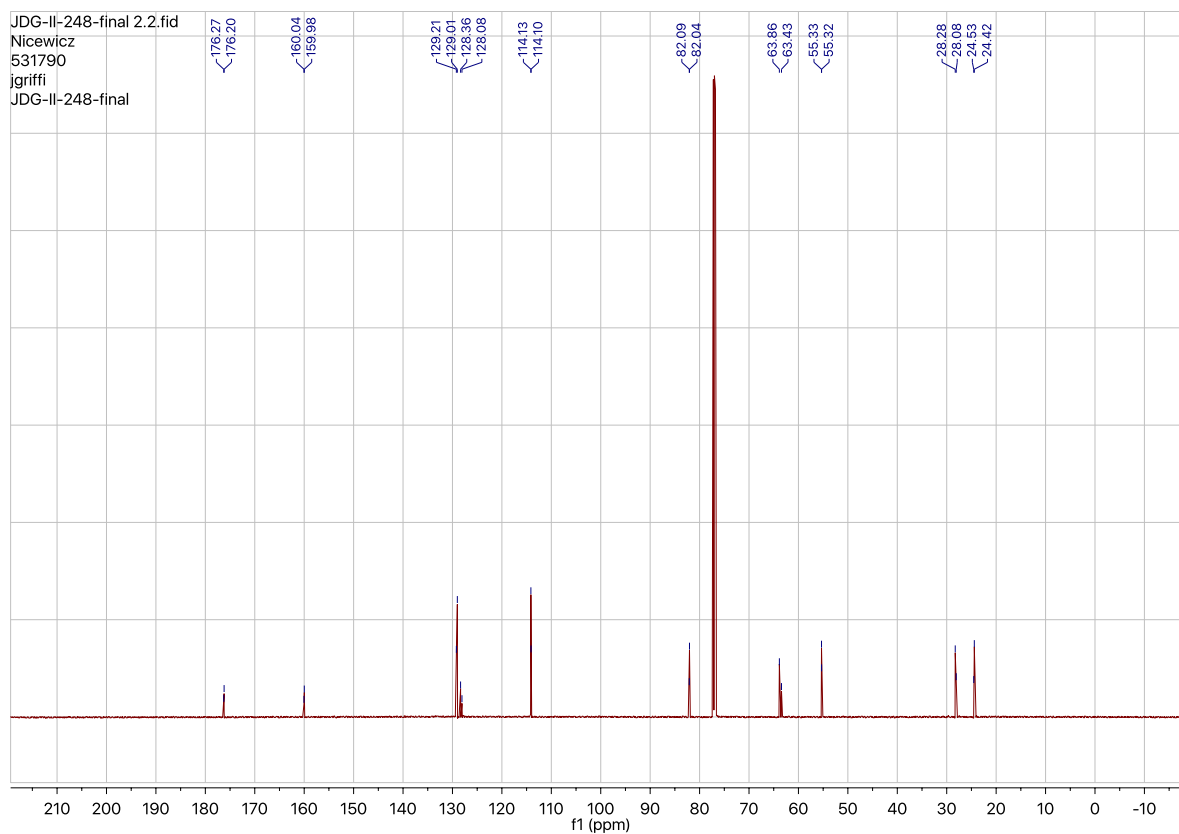
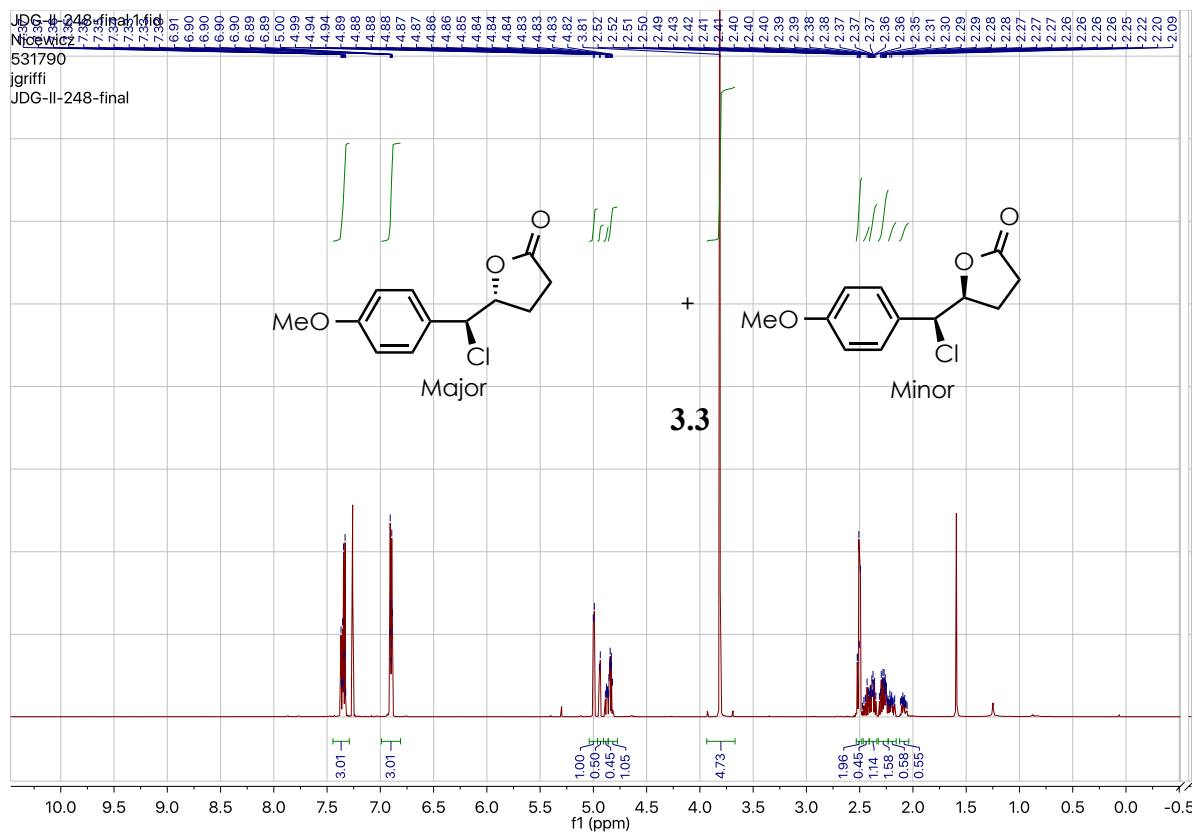


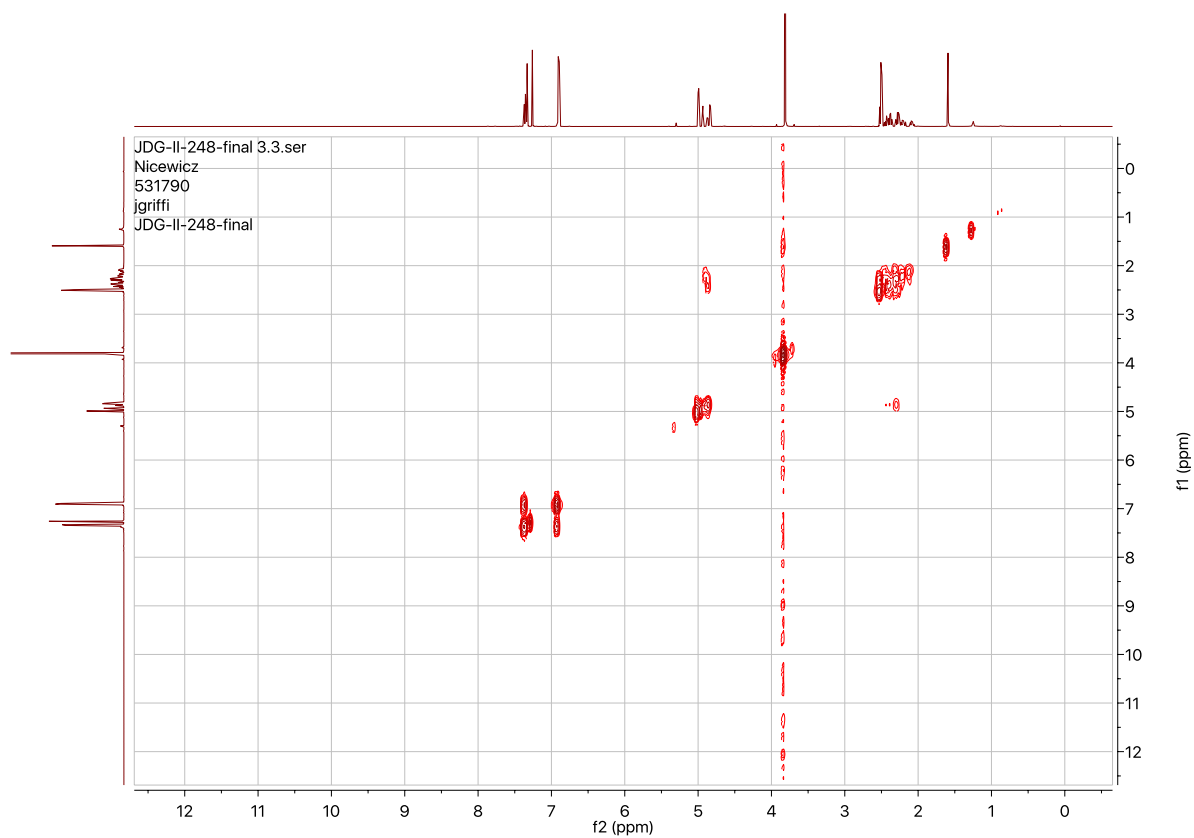
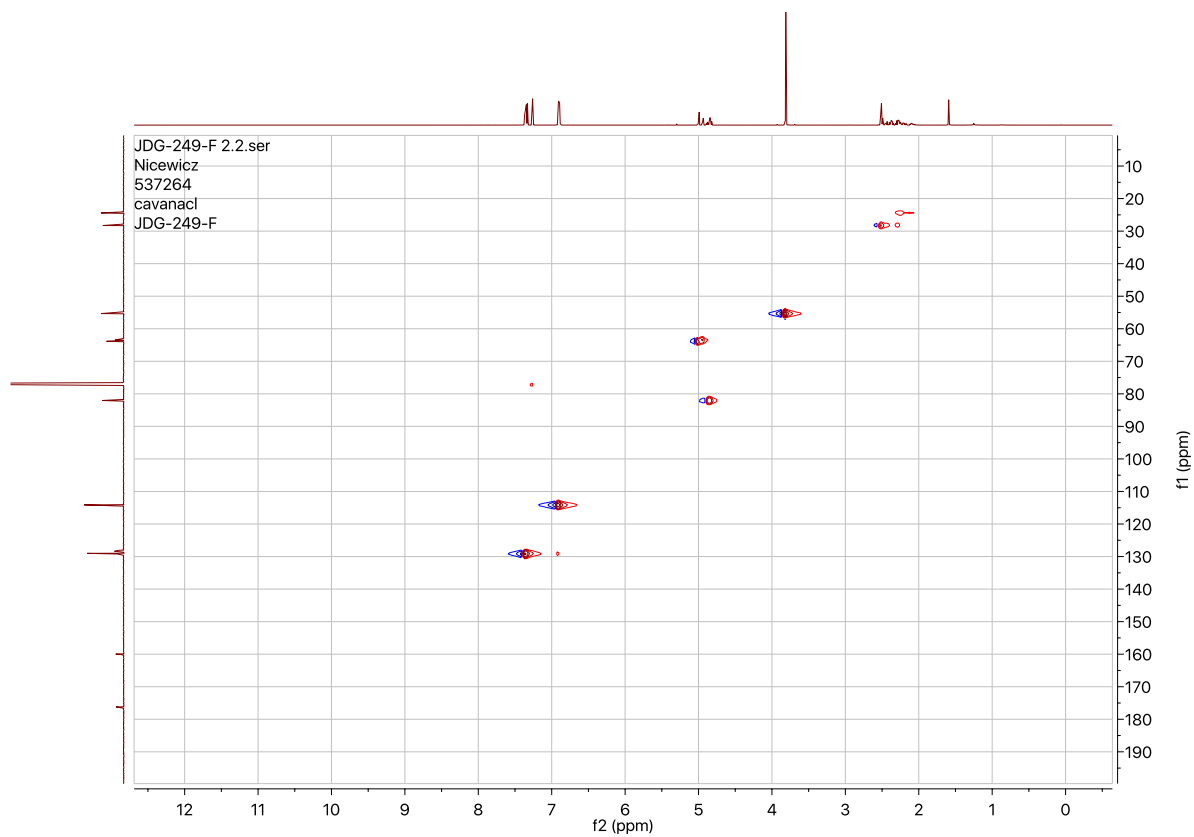


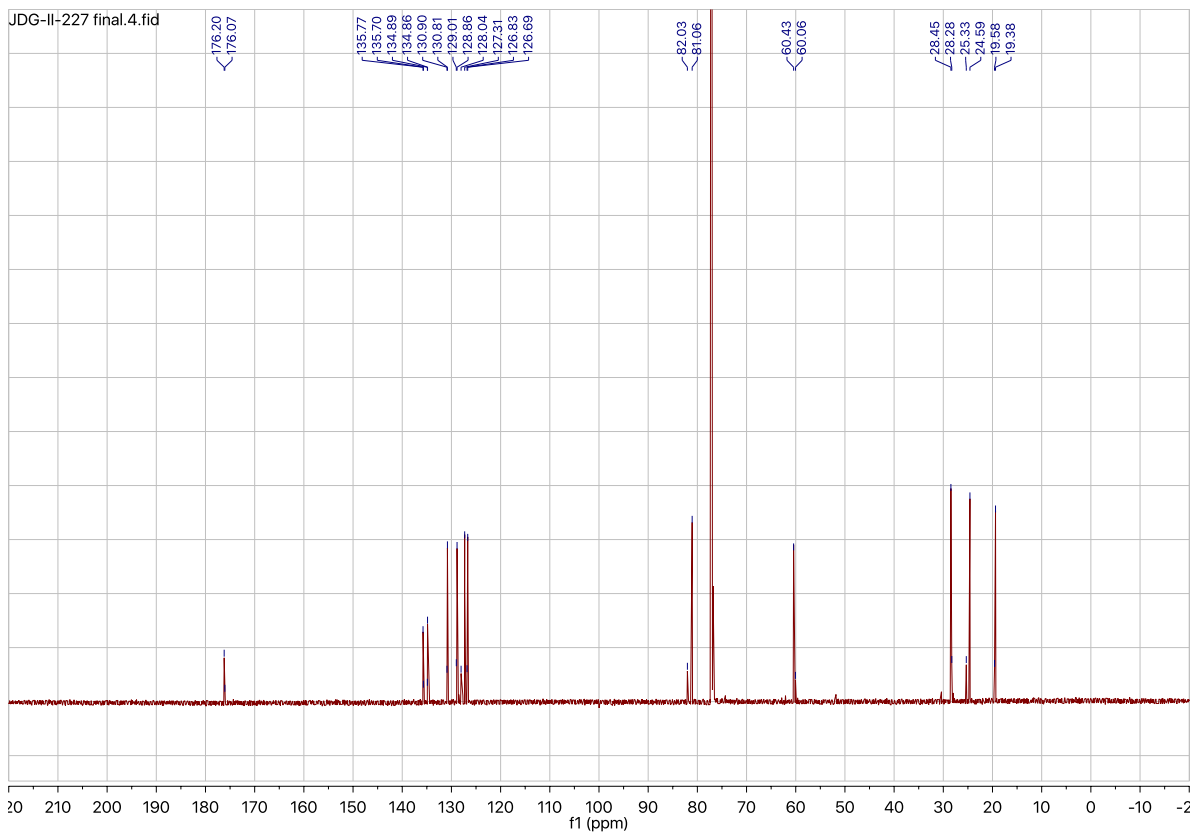
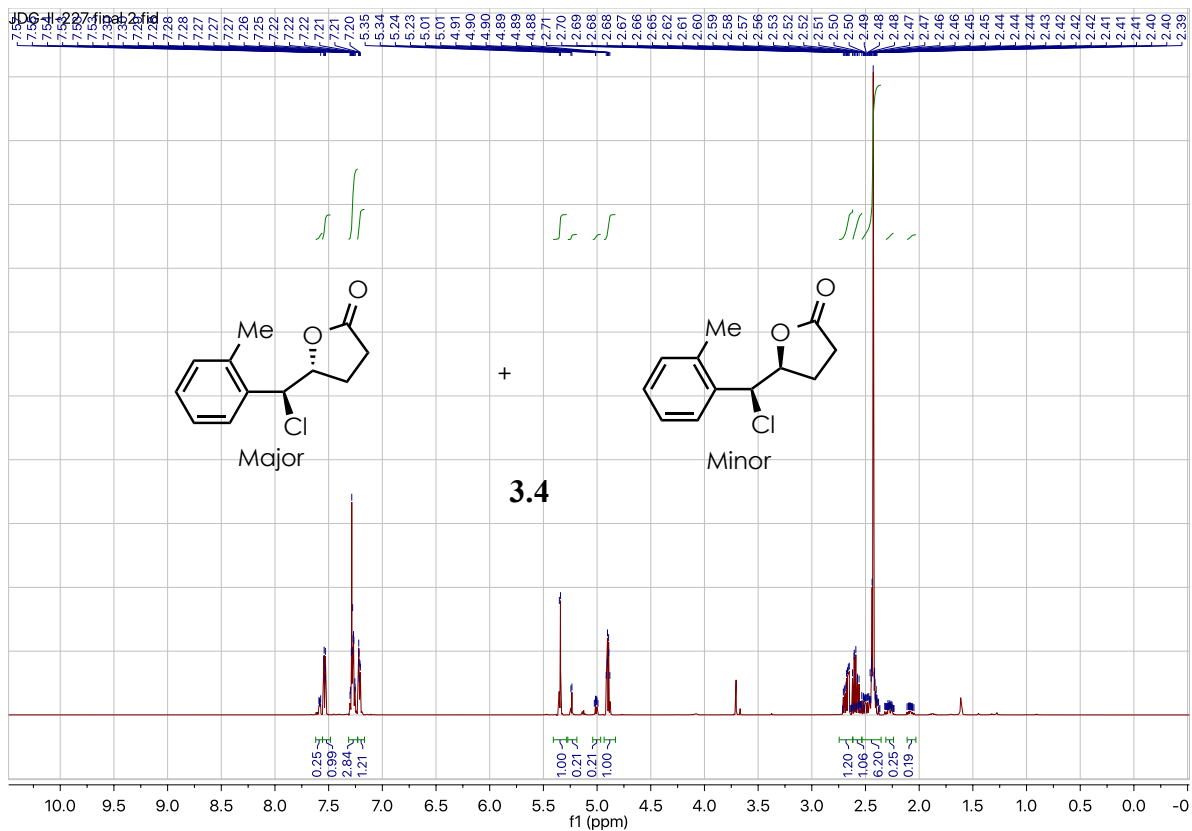


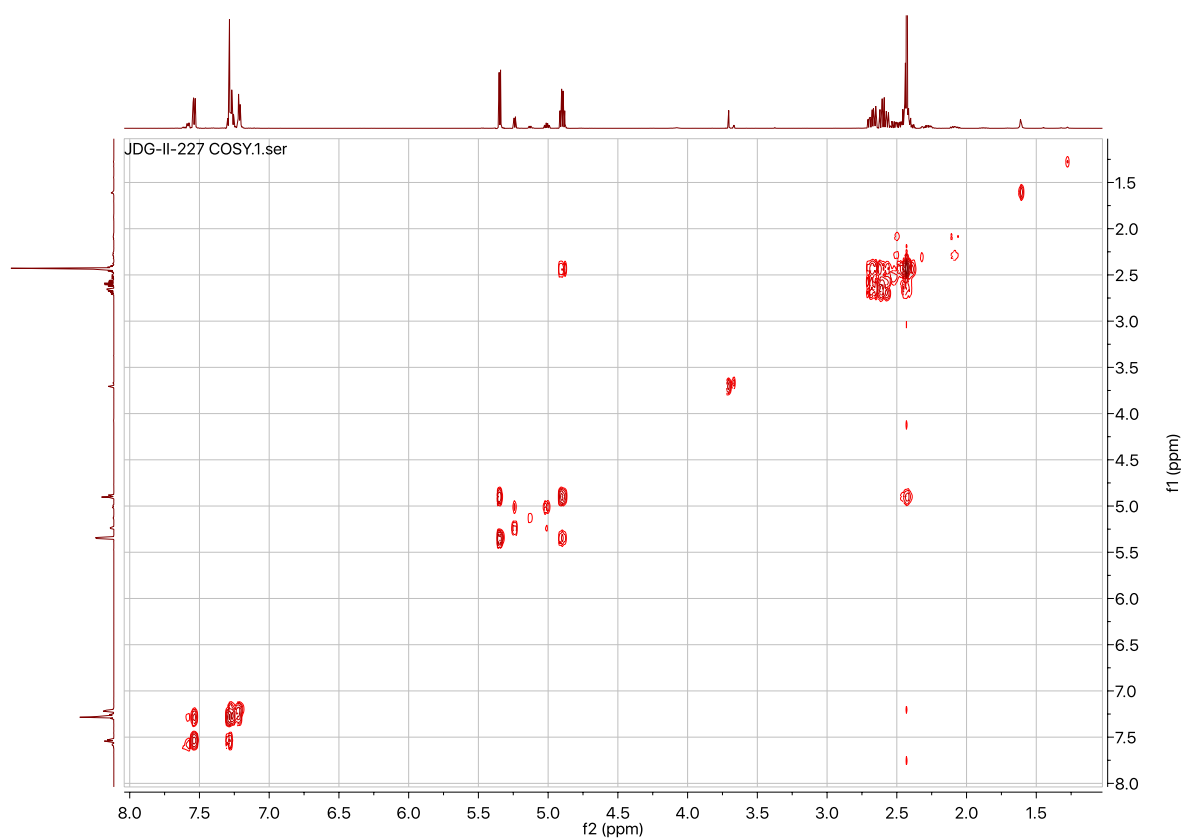
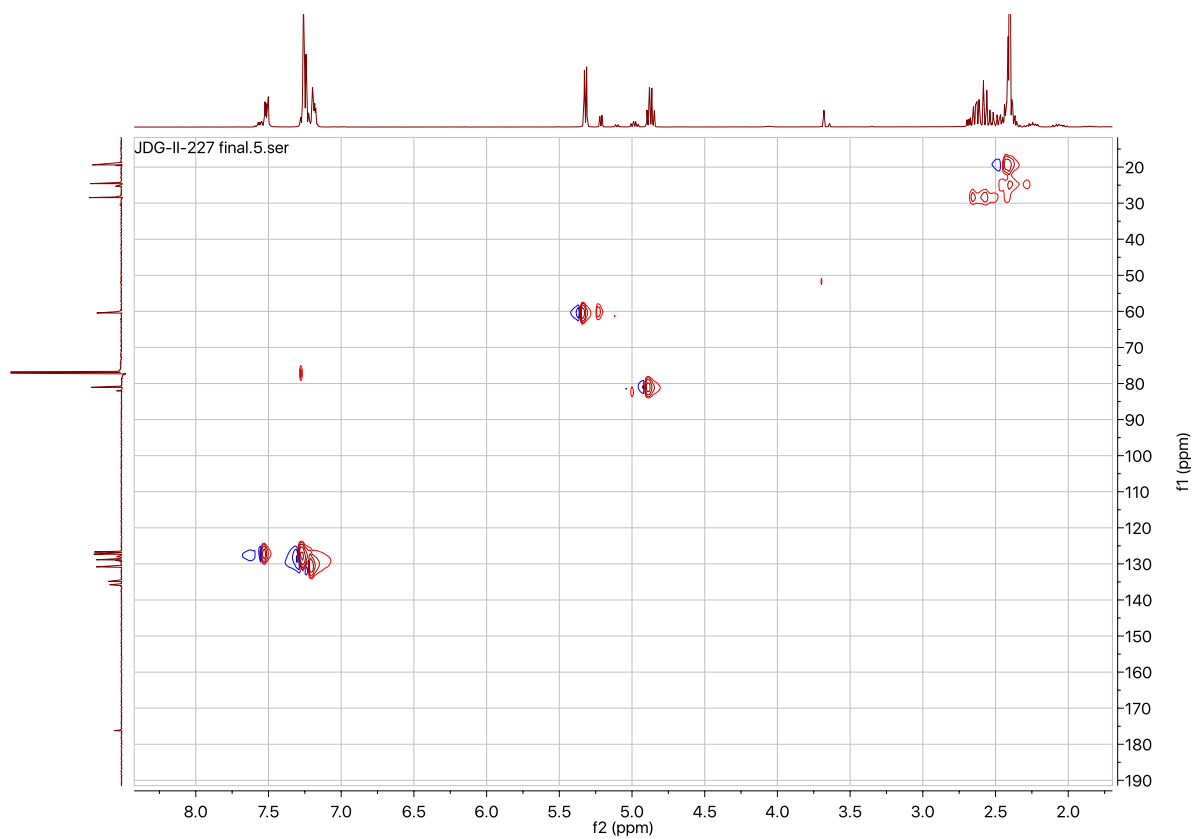


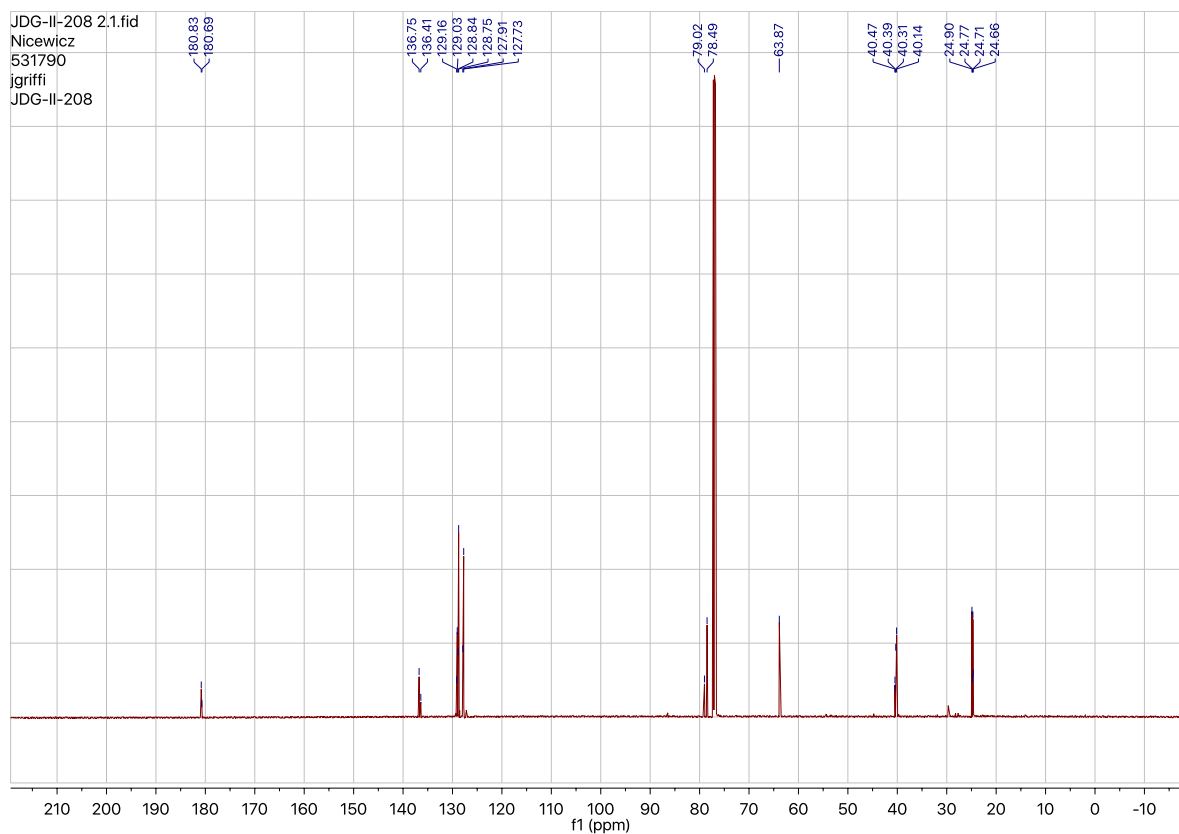
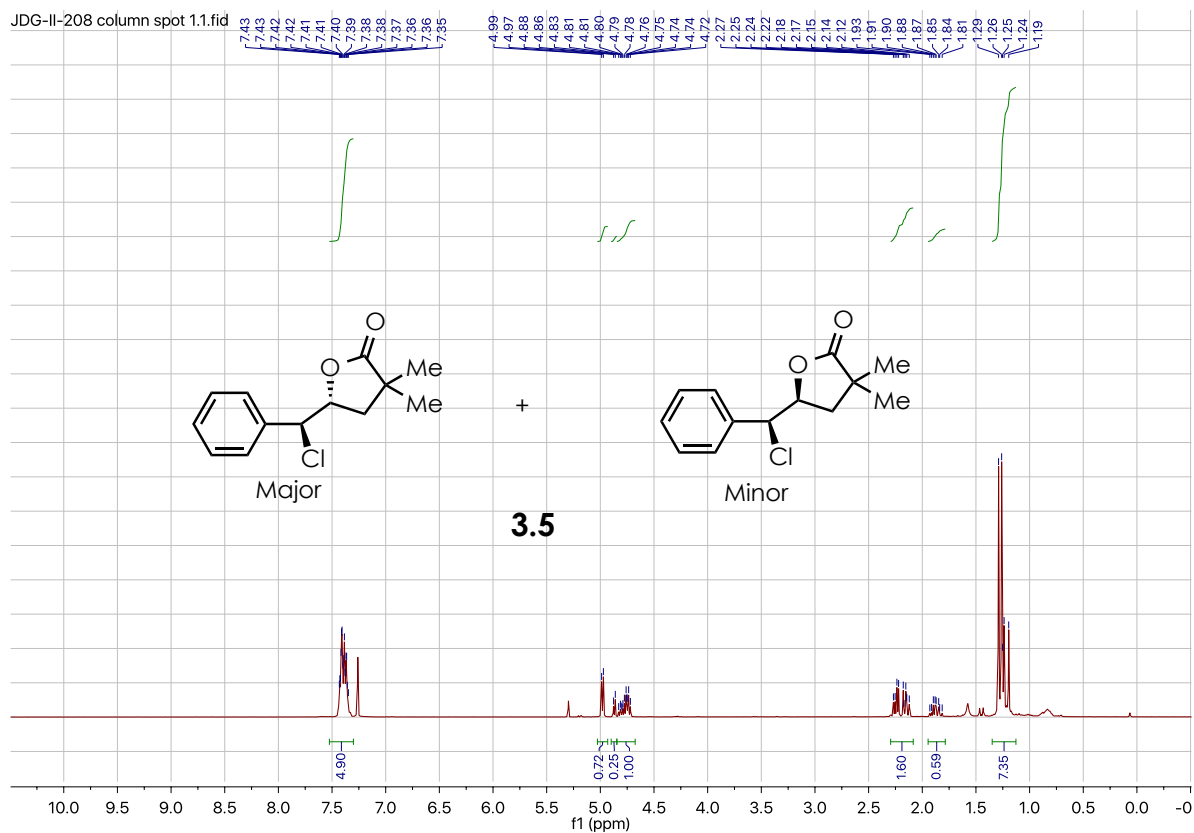


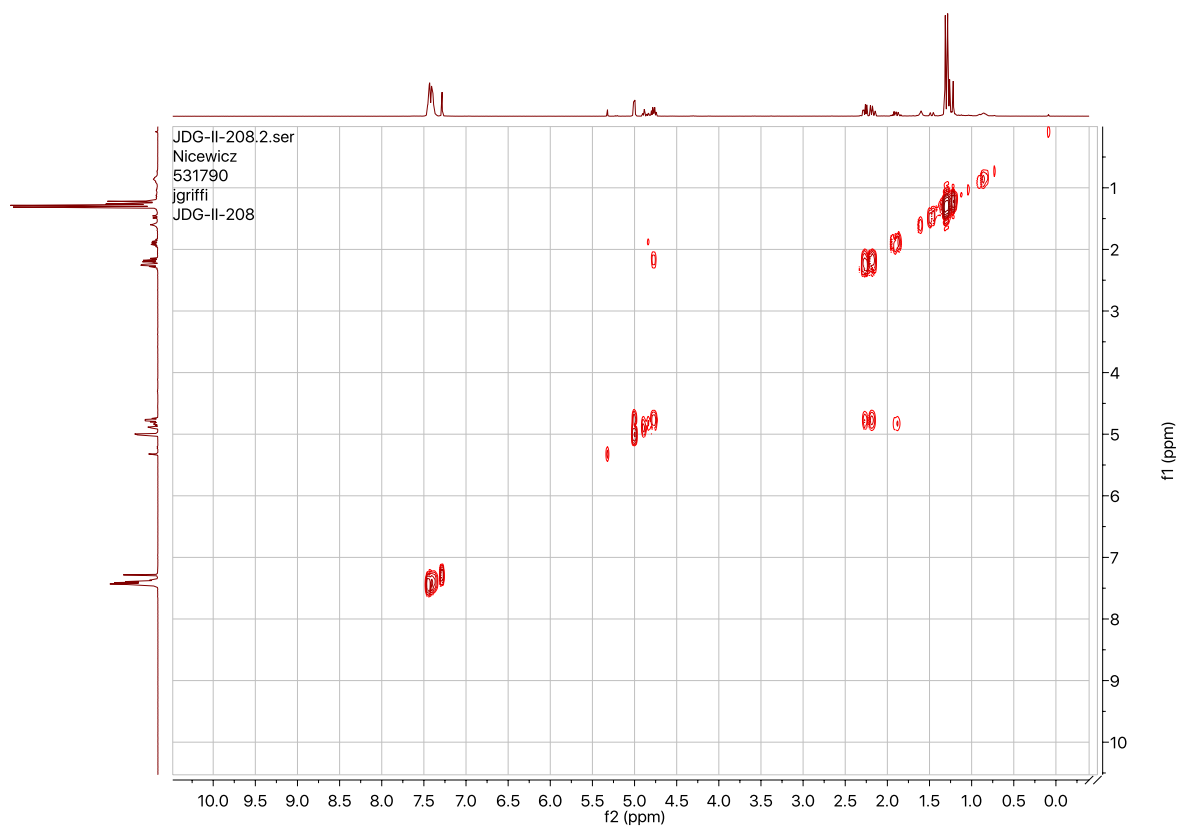
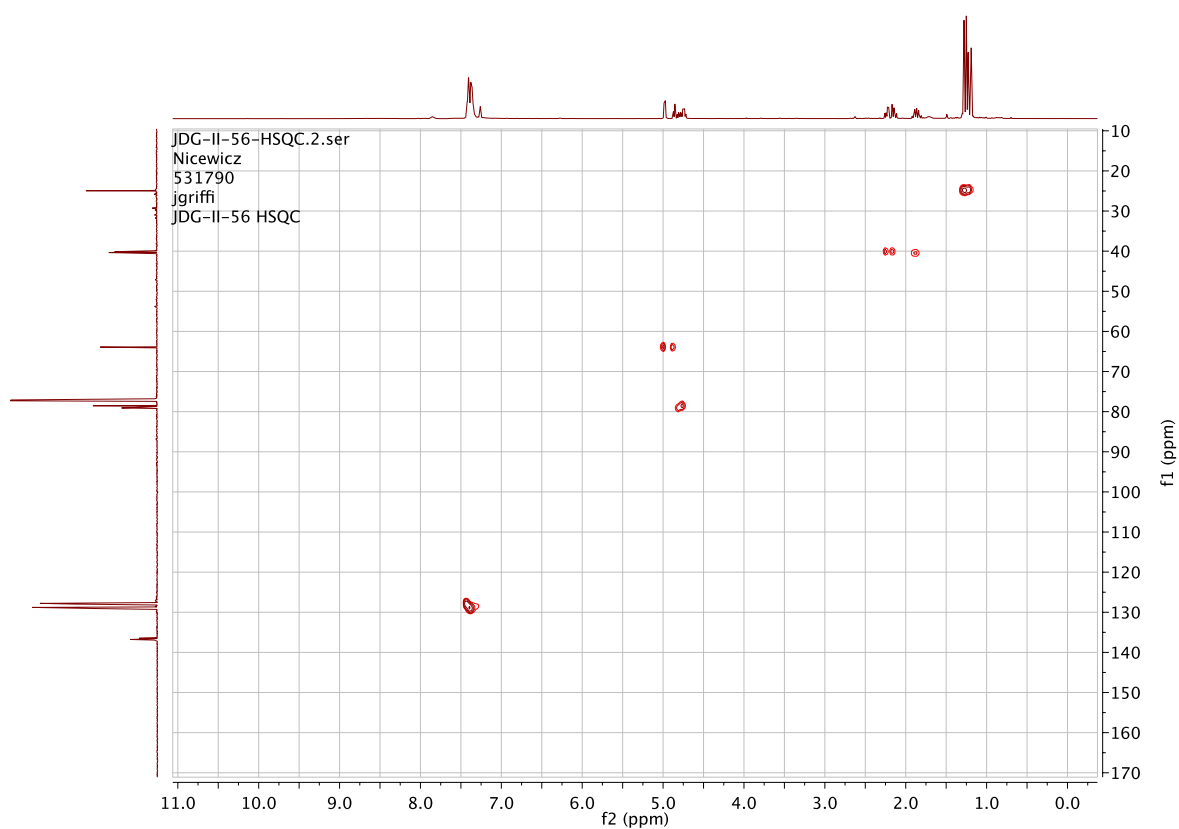


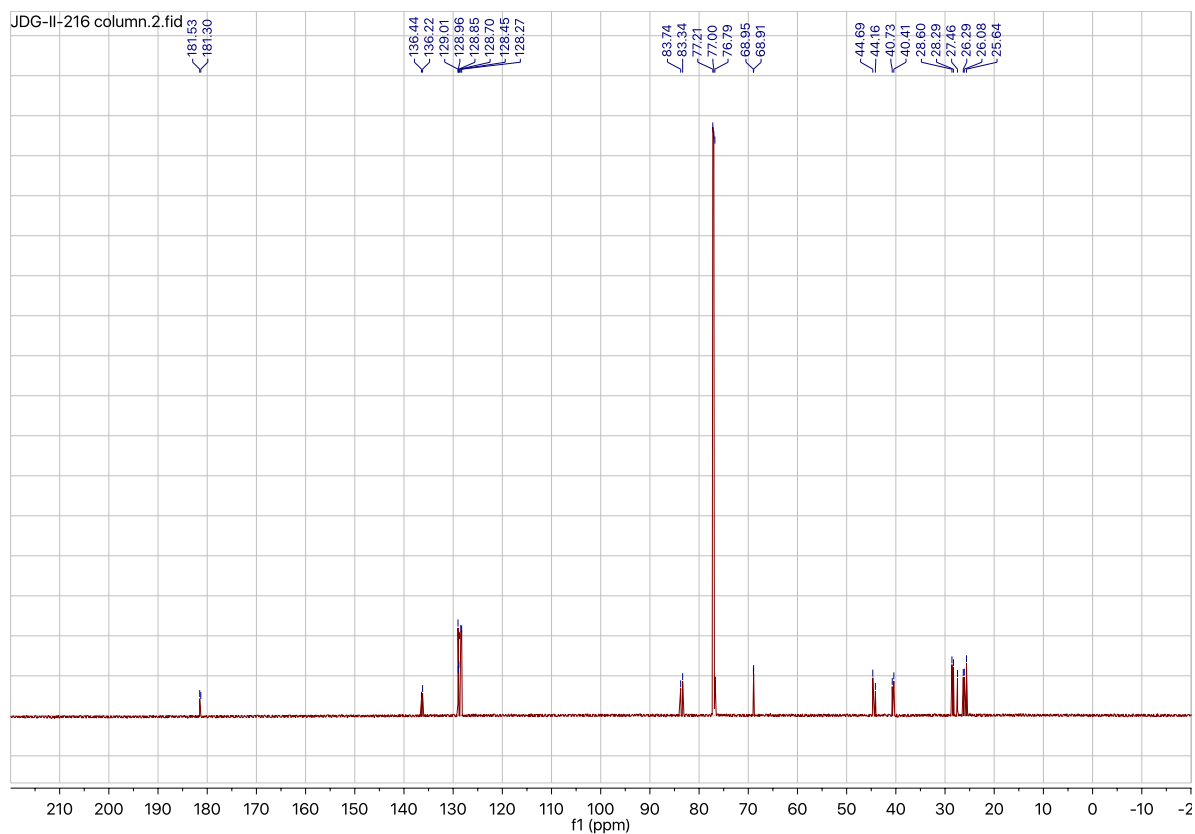
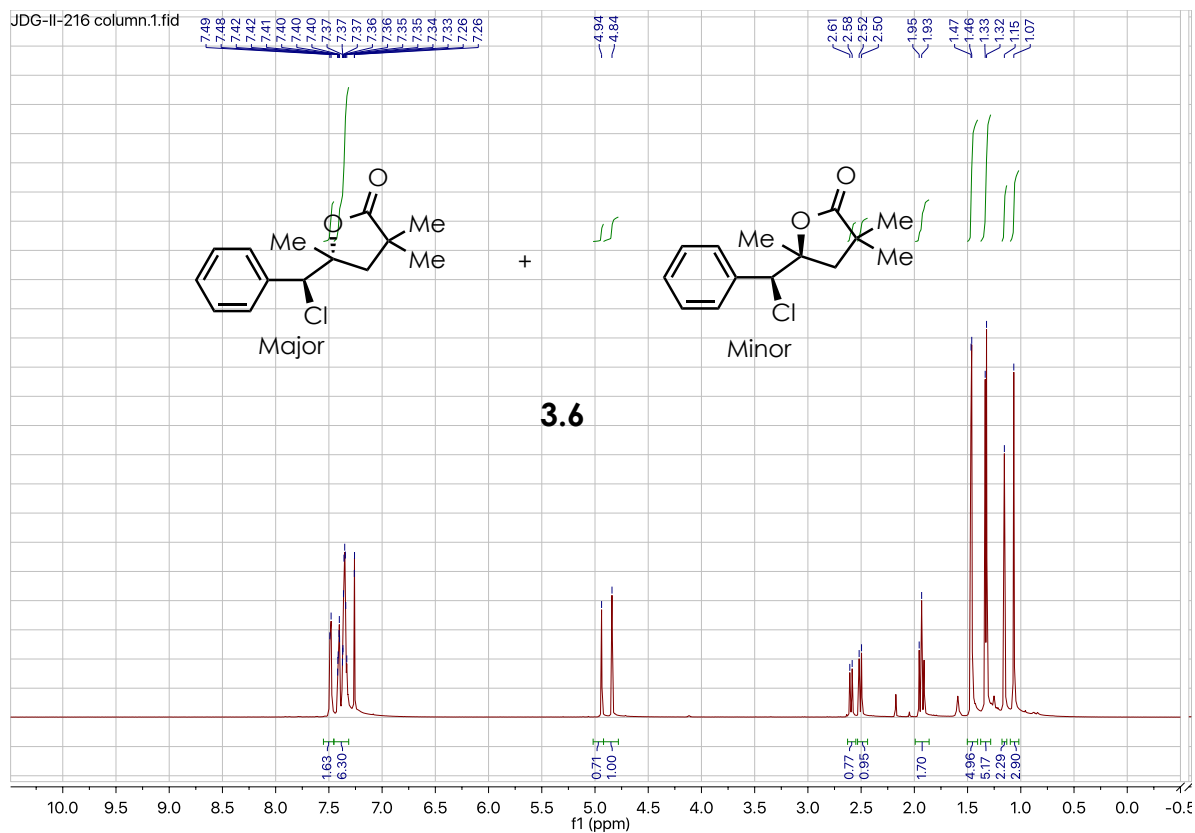


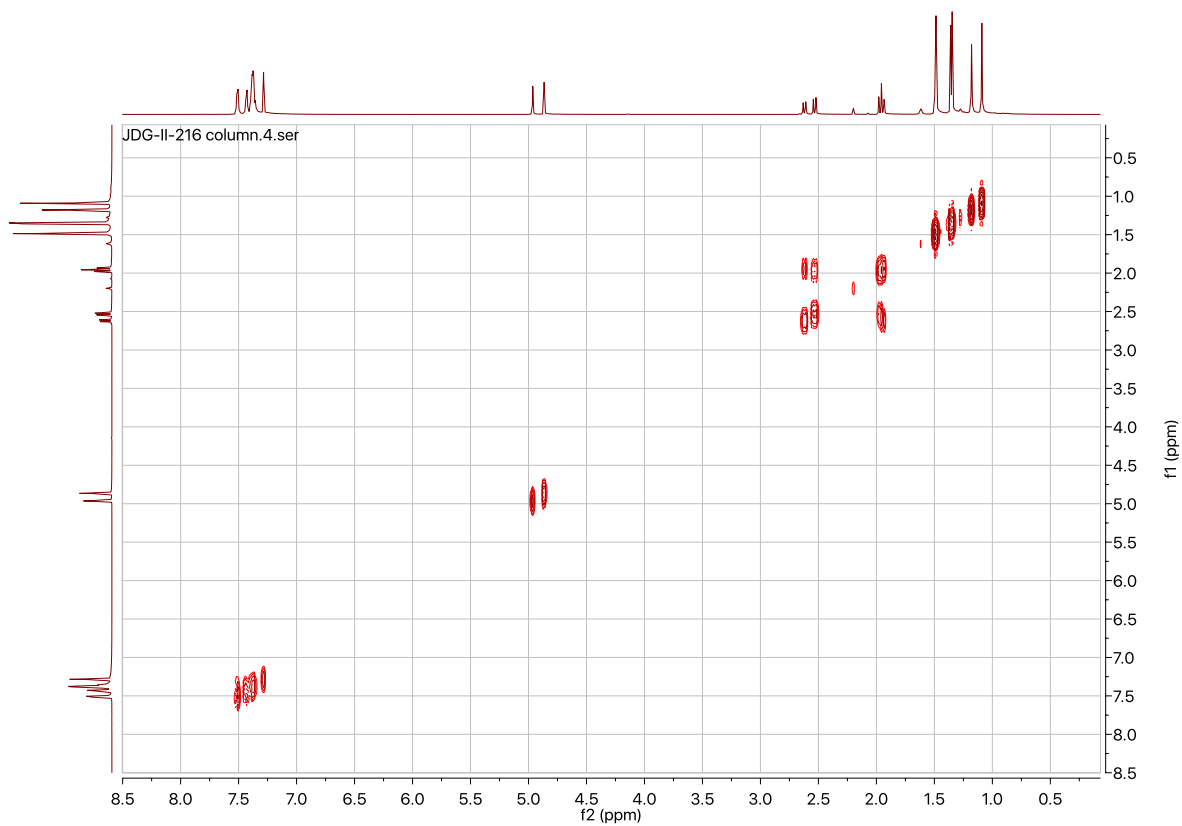
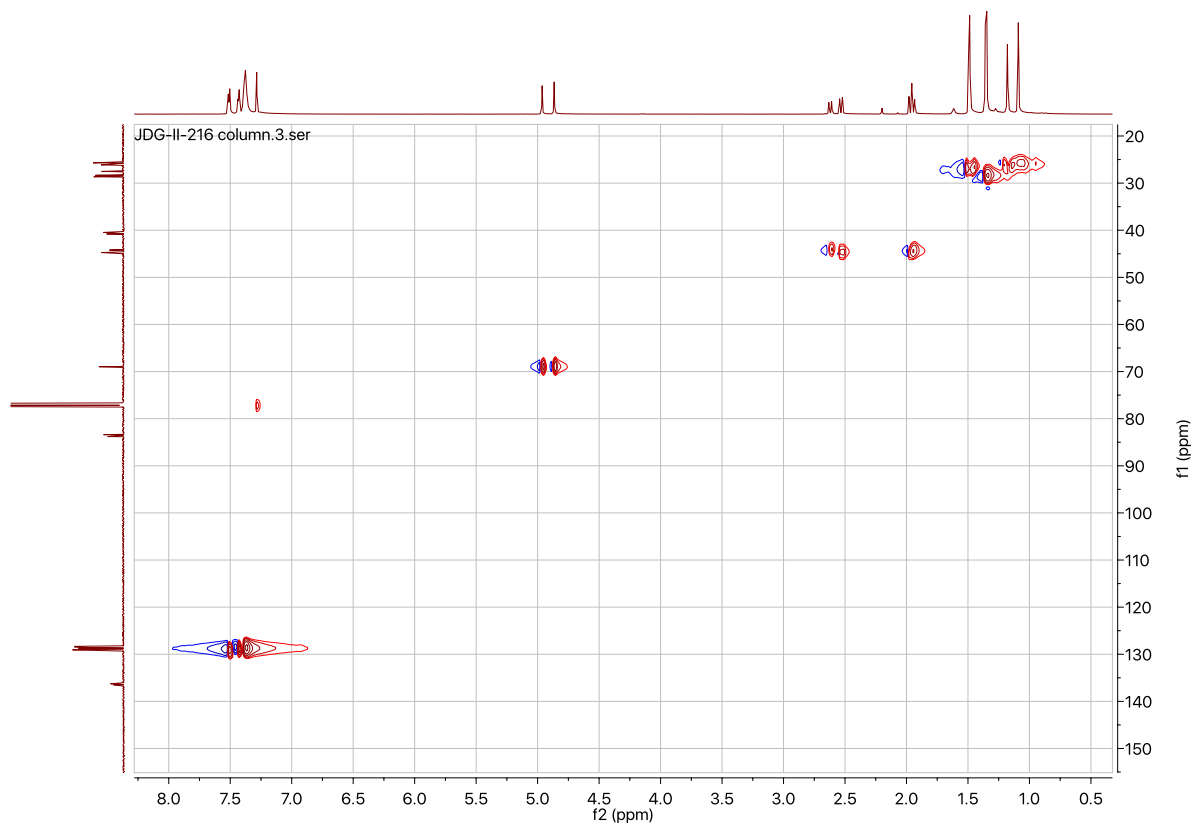


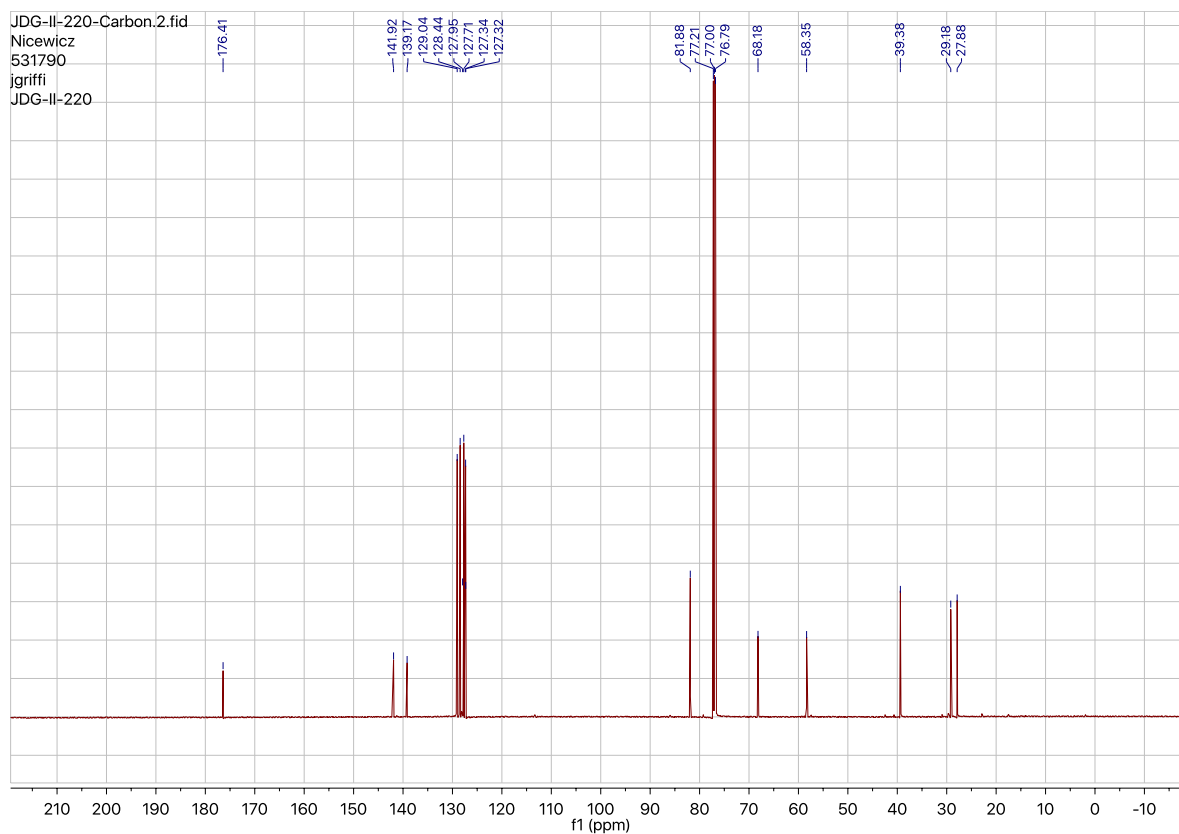
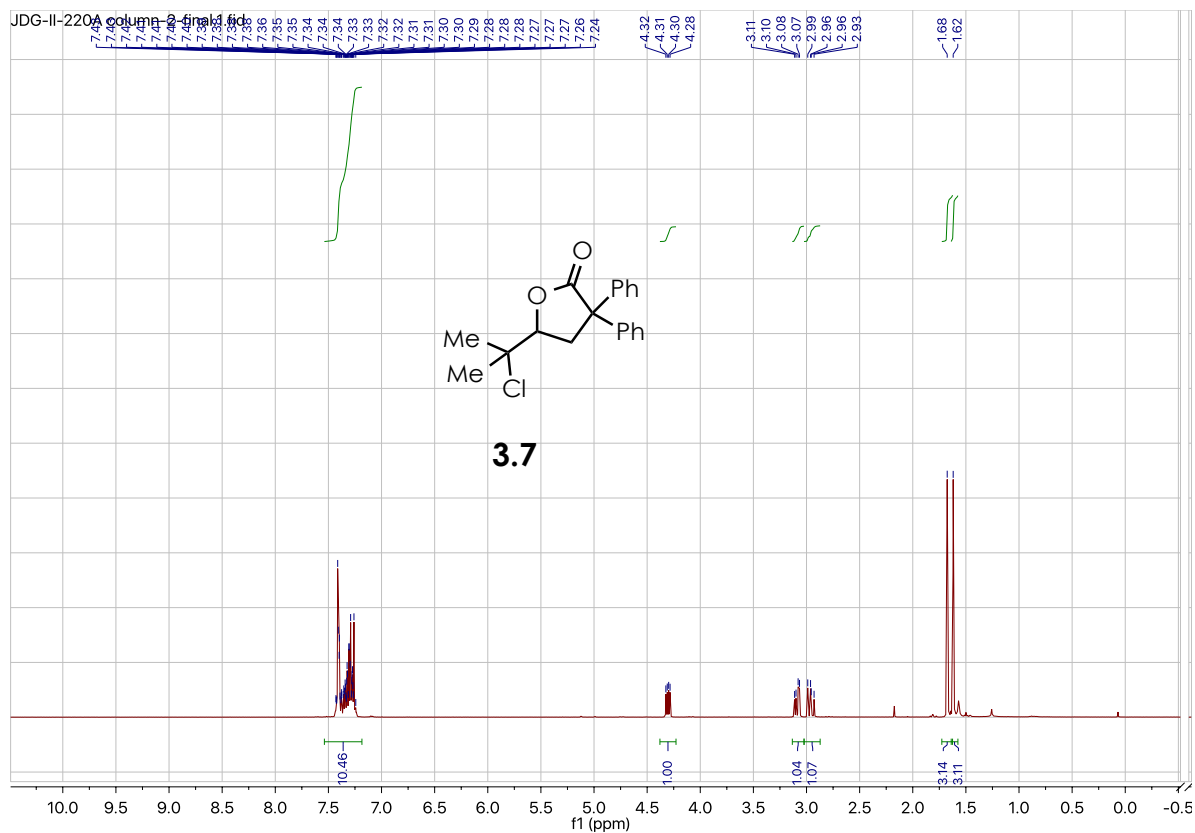


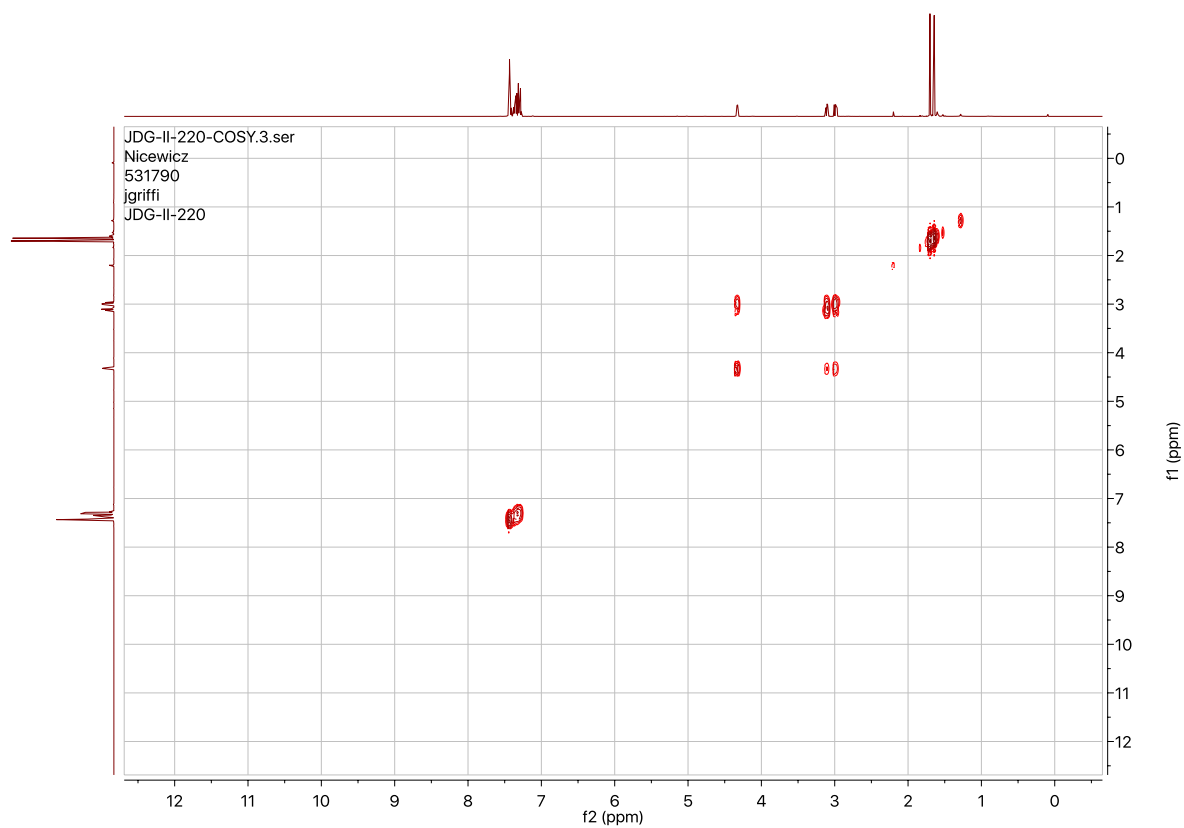
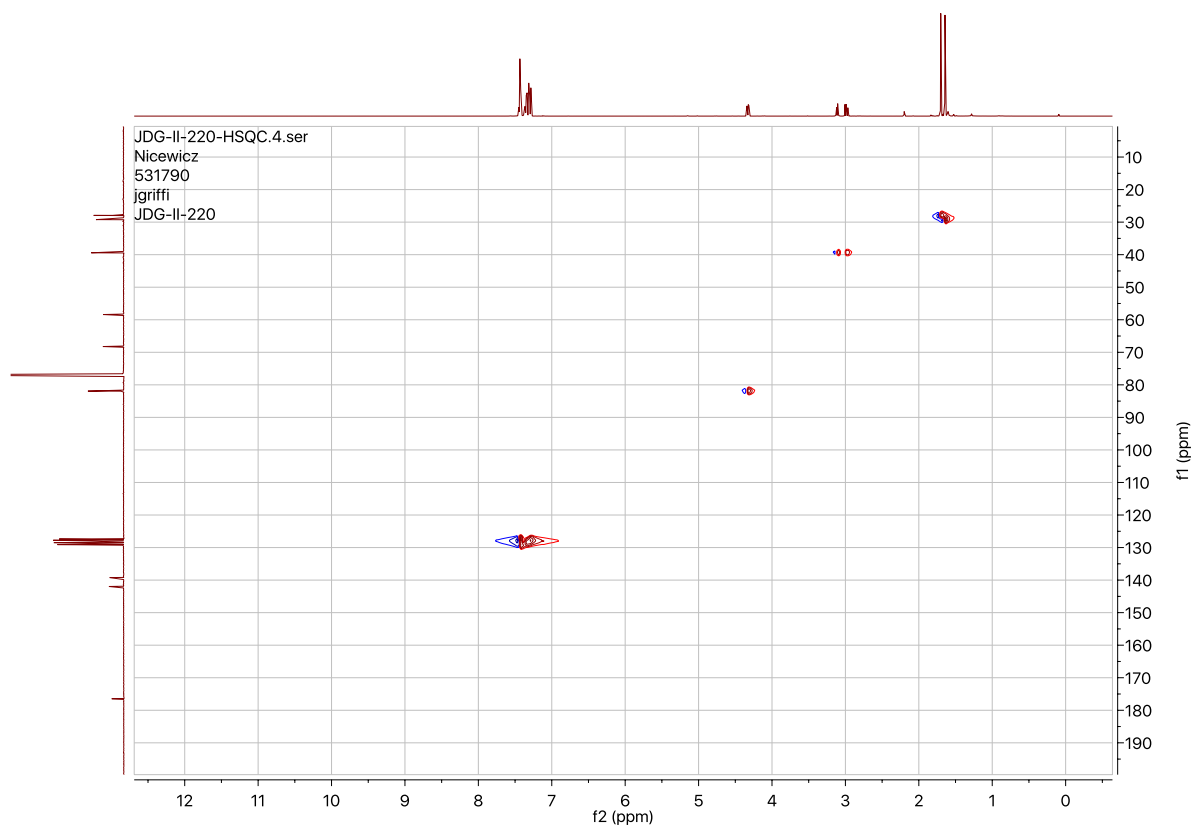


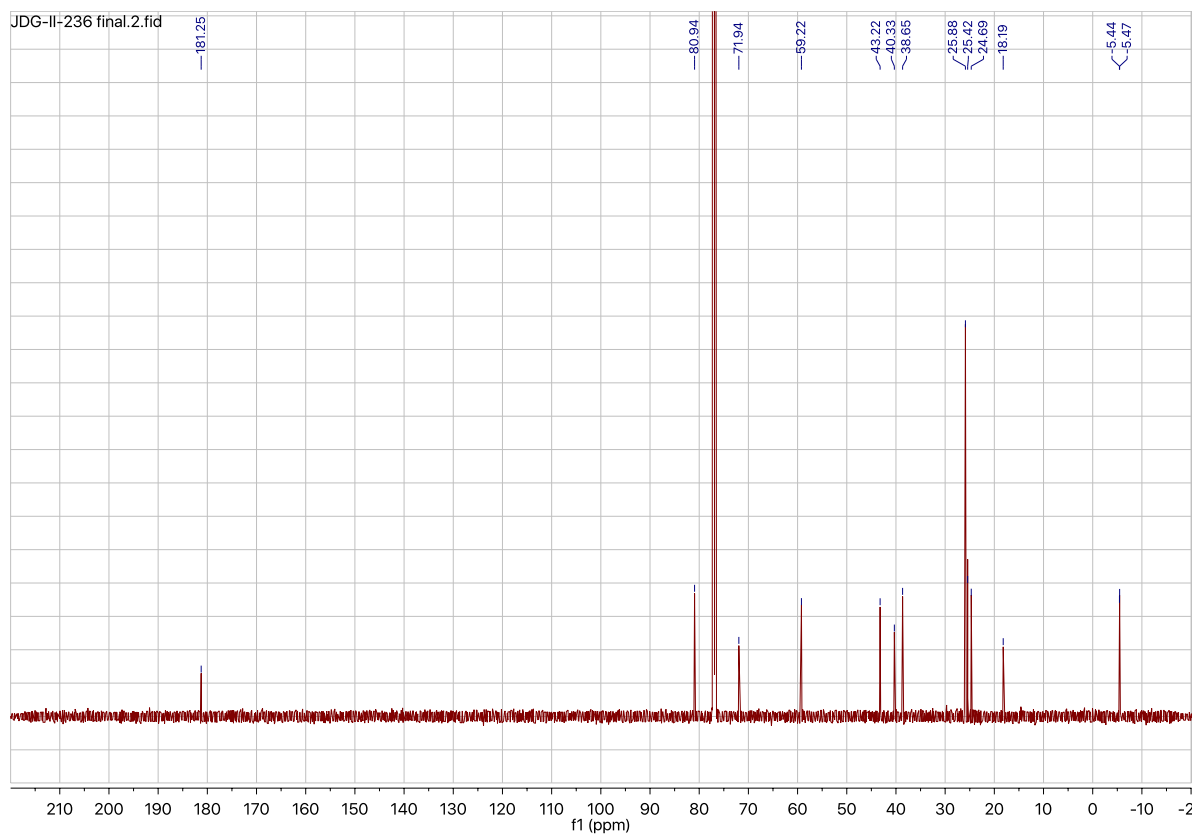
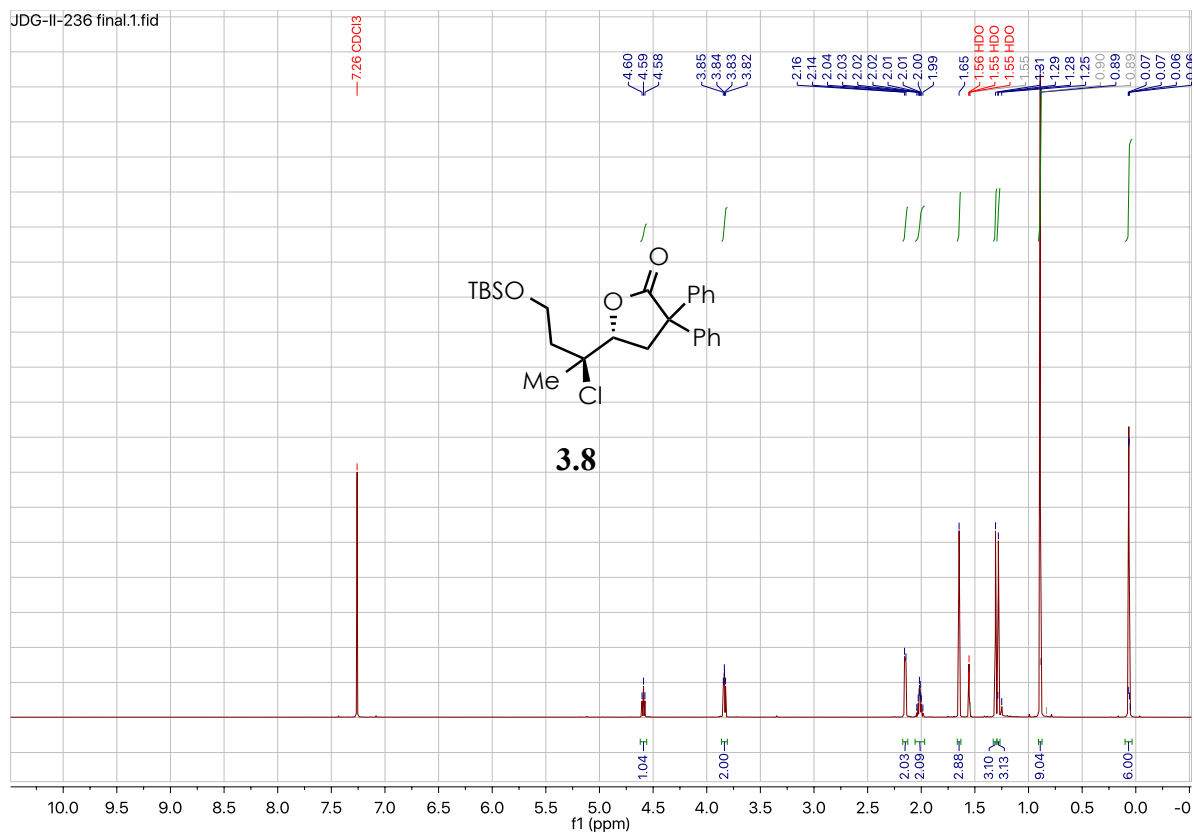


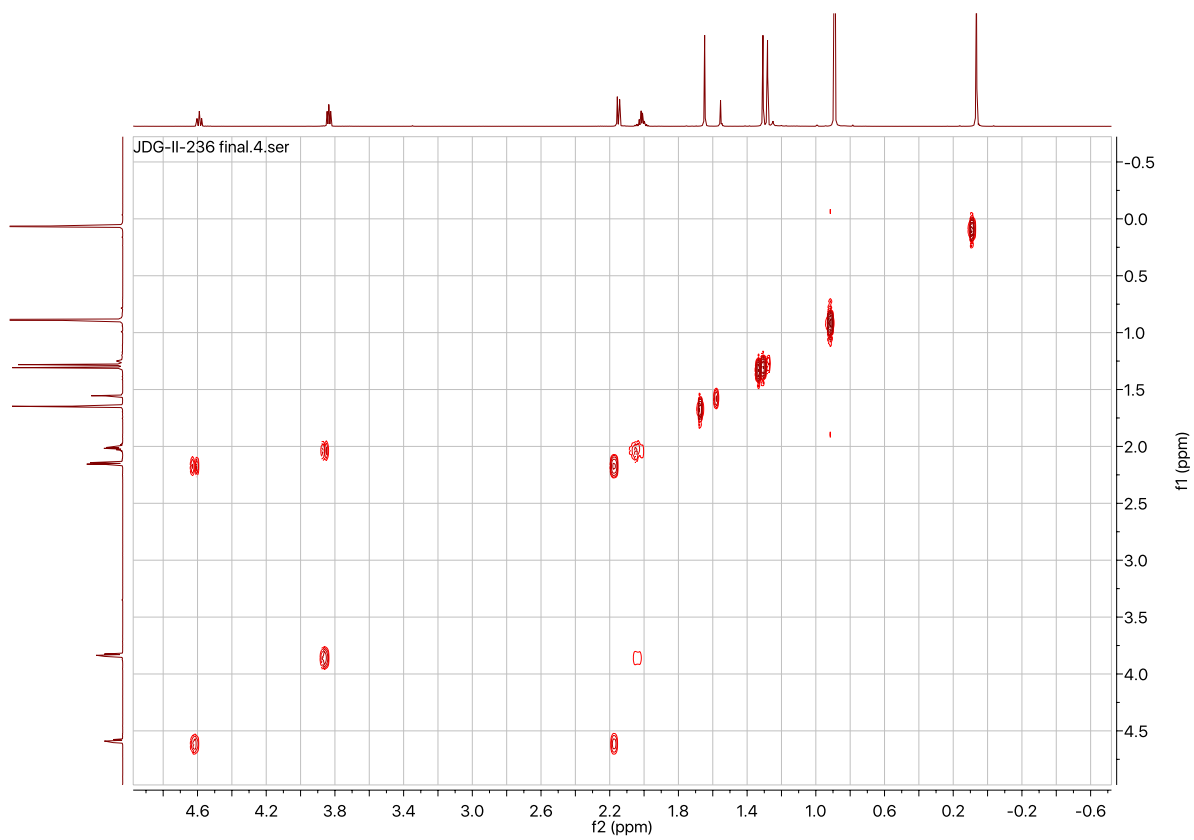
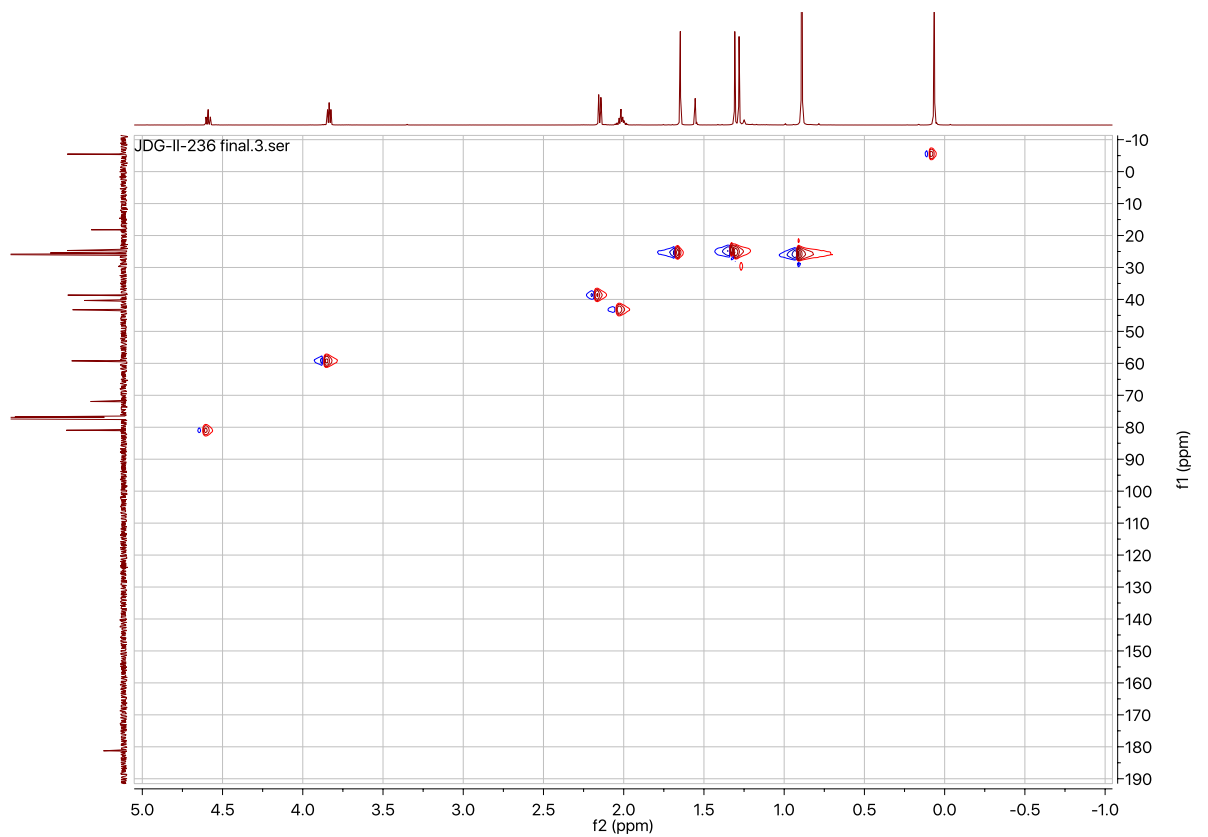




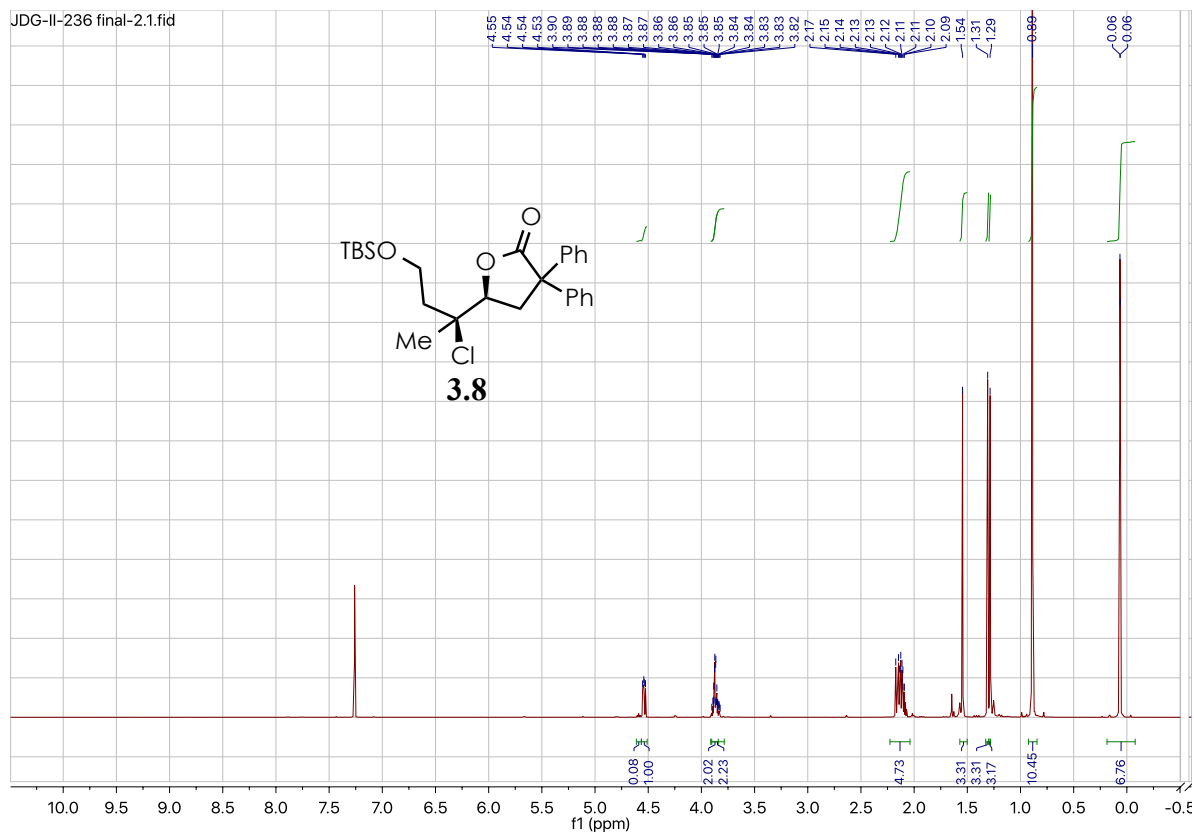




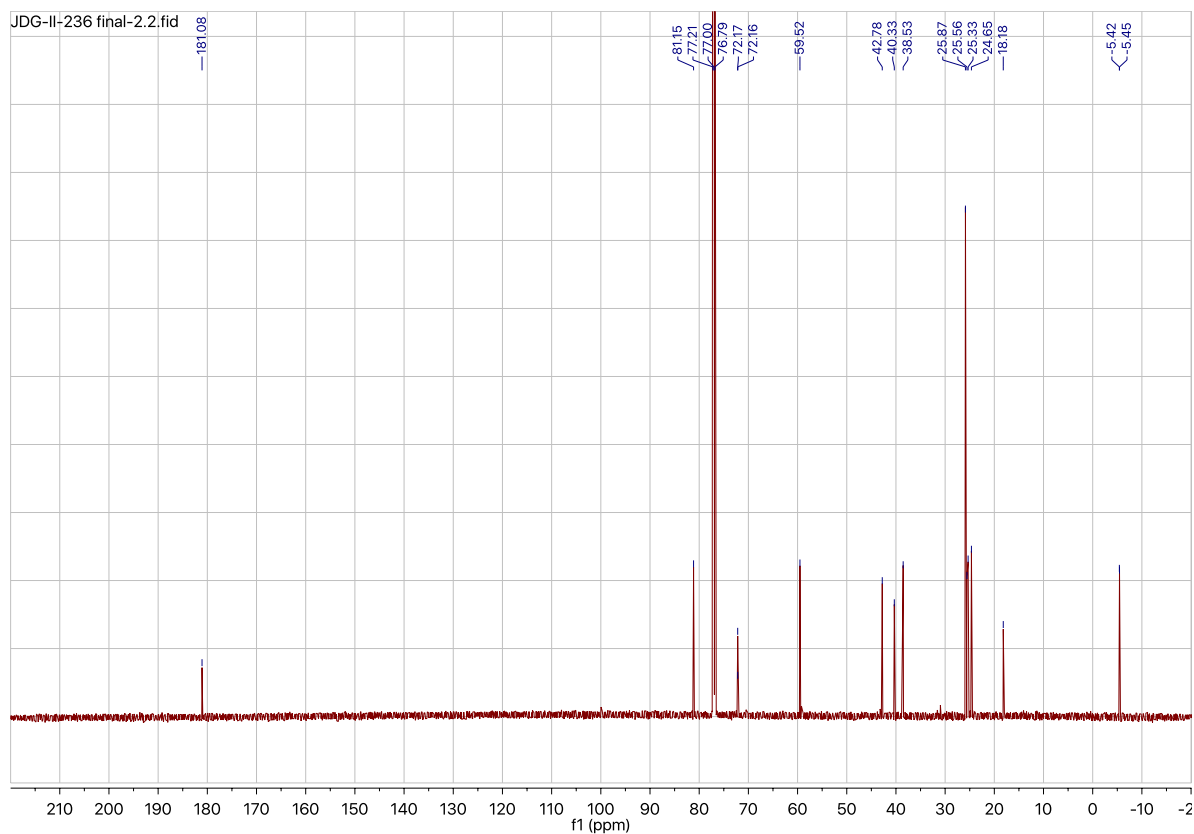


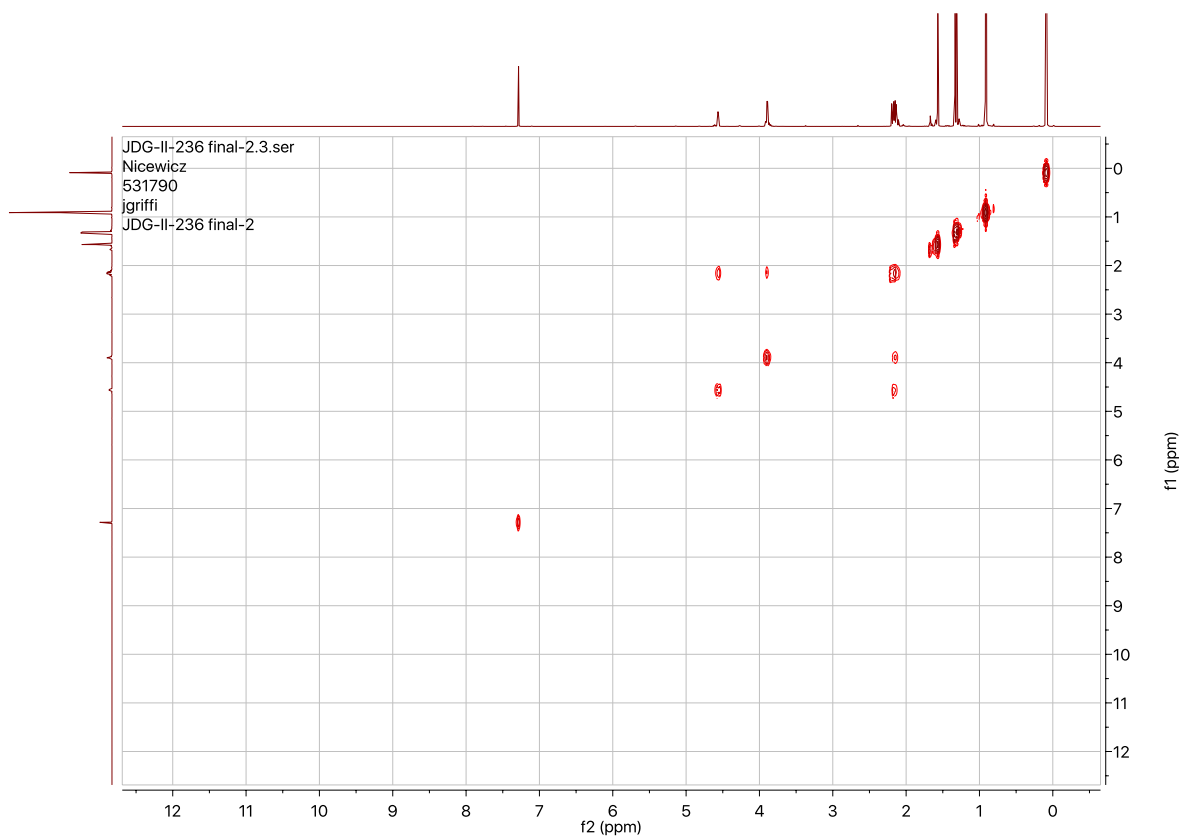
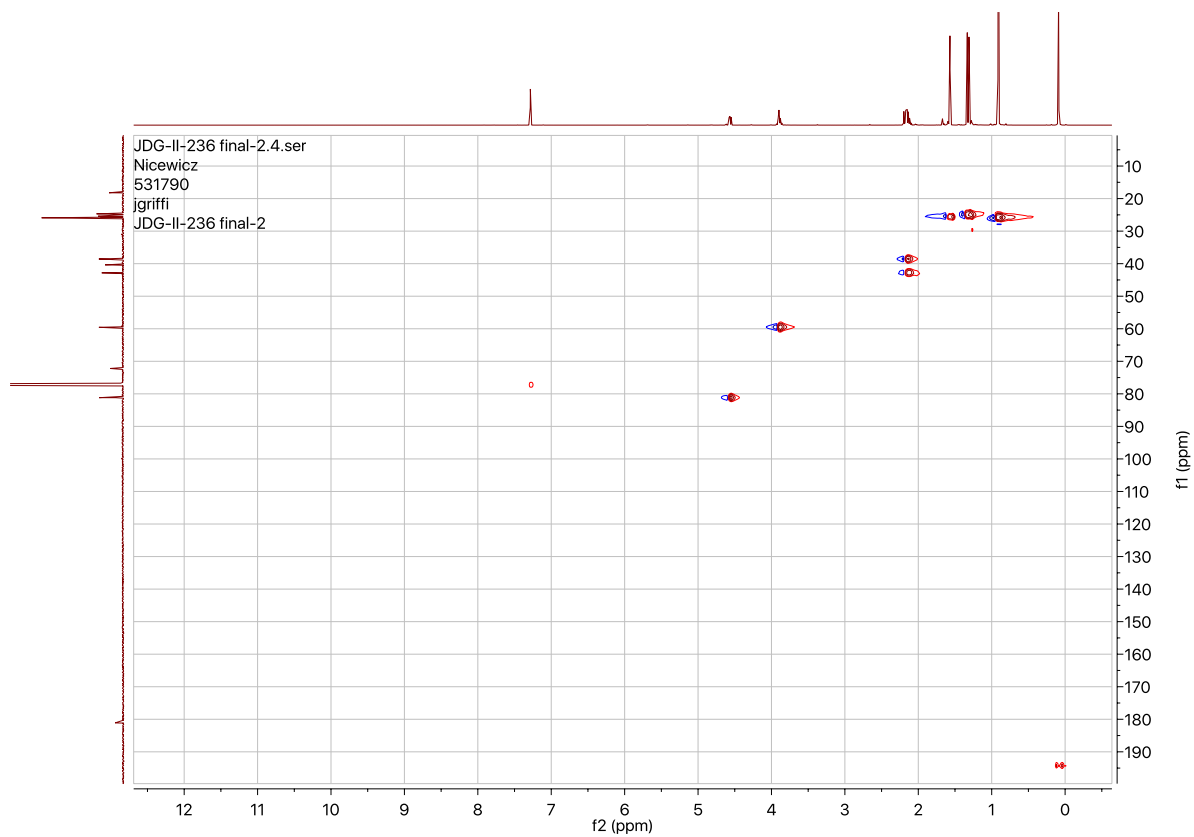


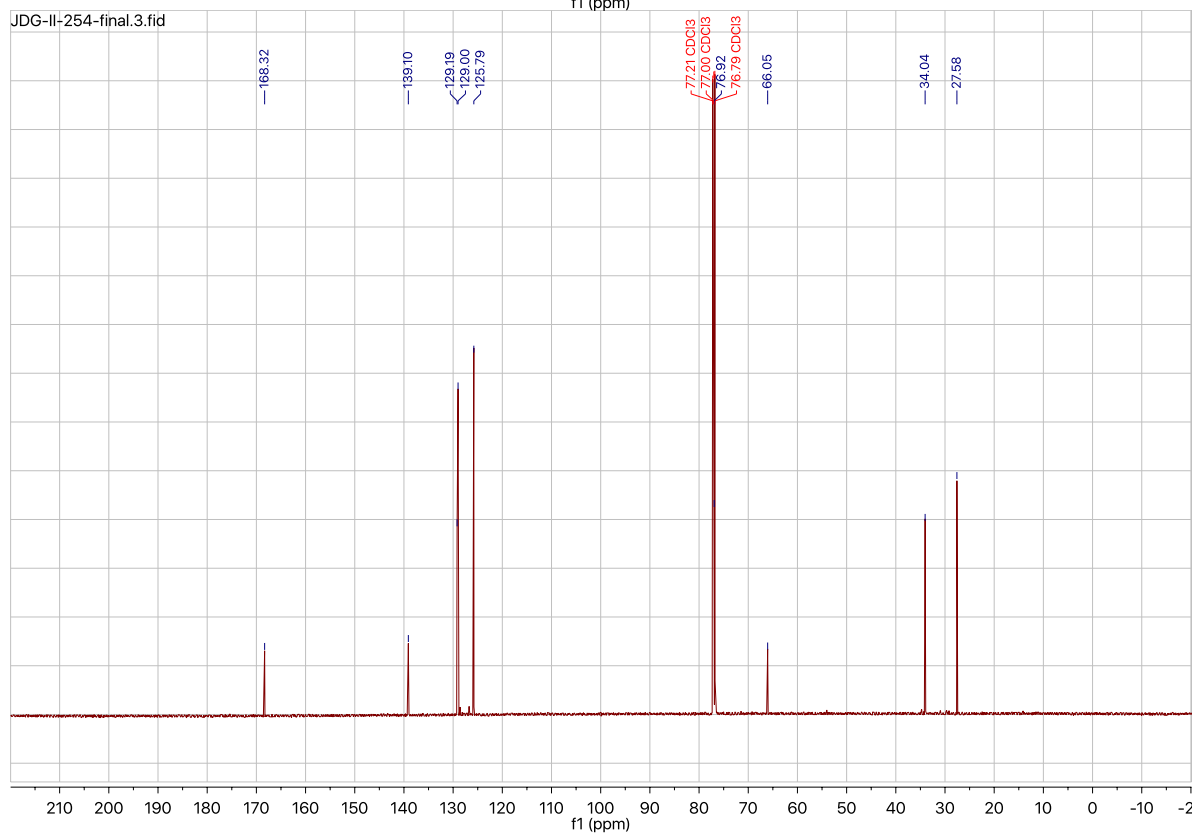
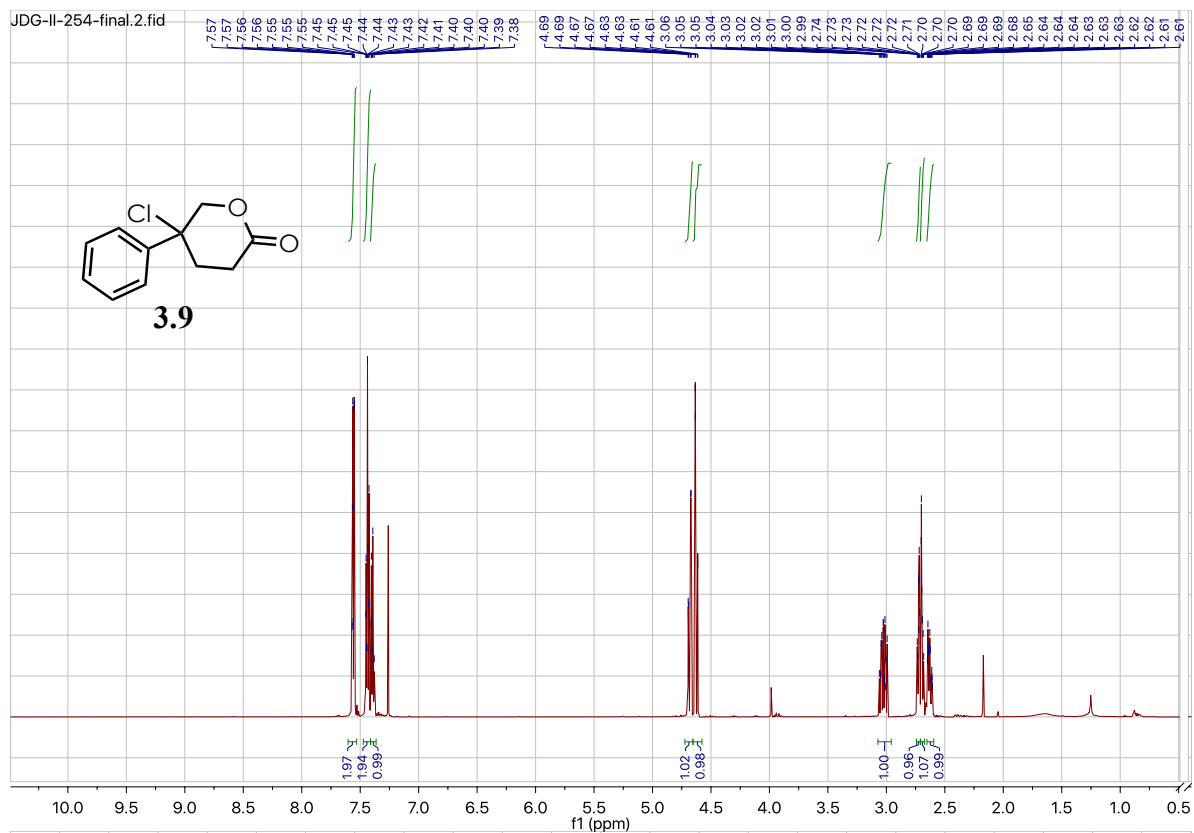
JDG-II-236 final-2.1.fid

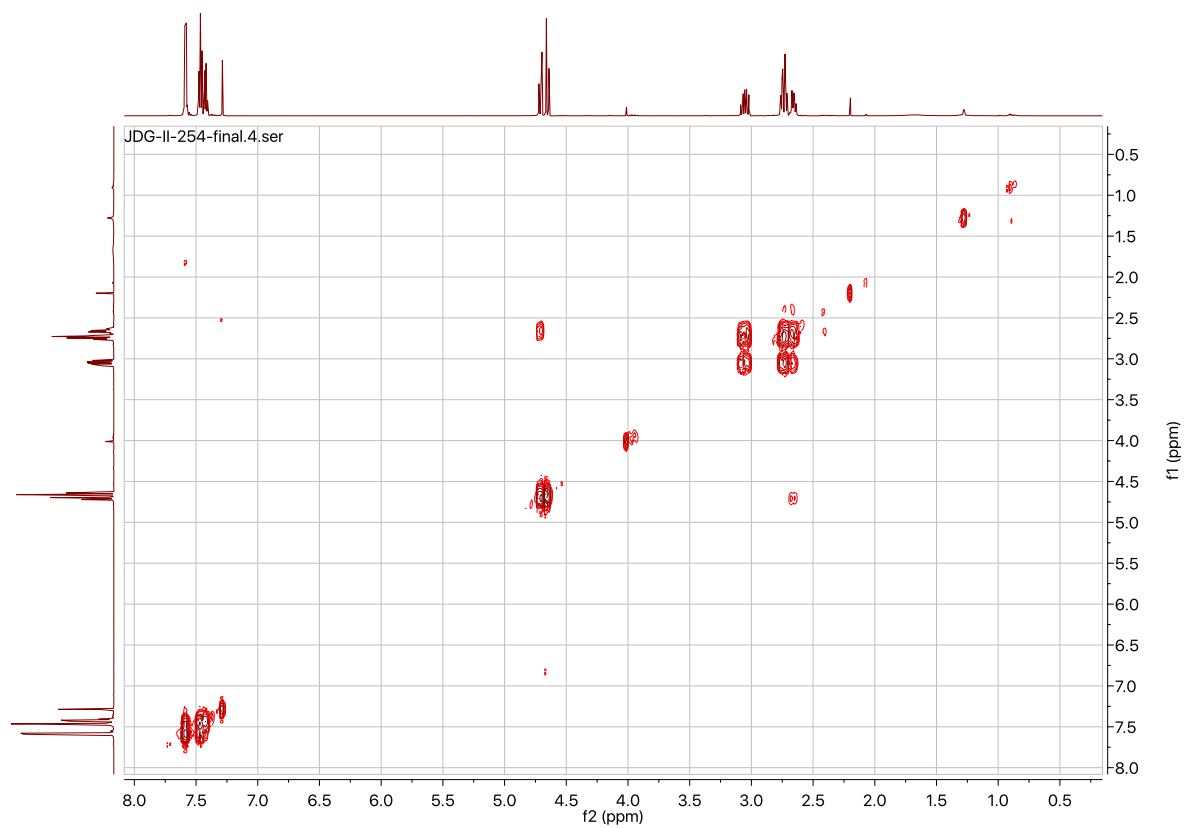
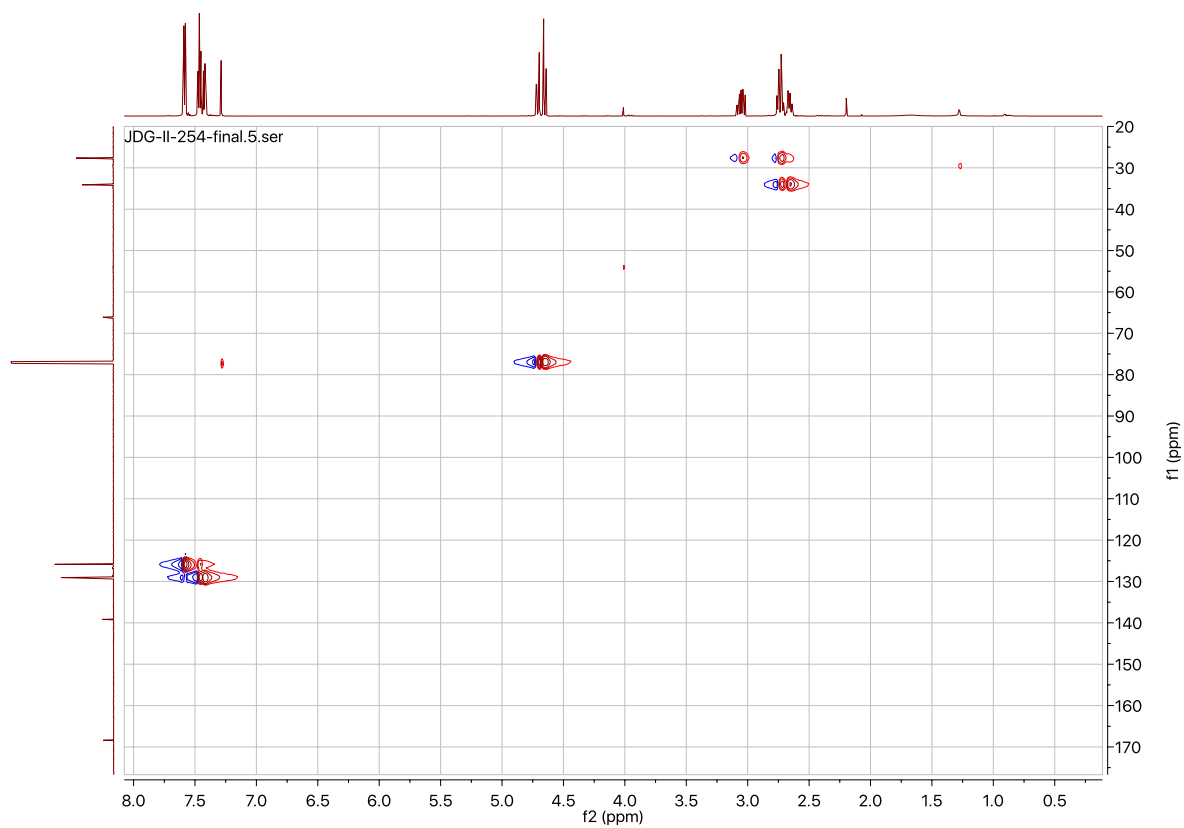


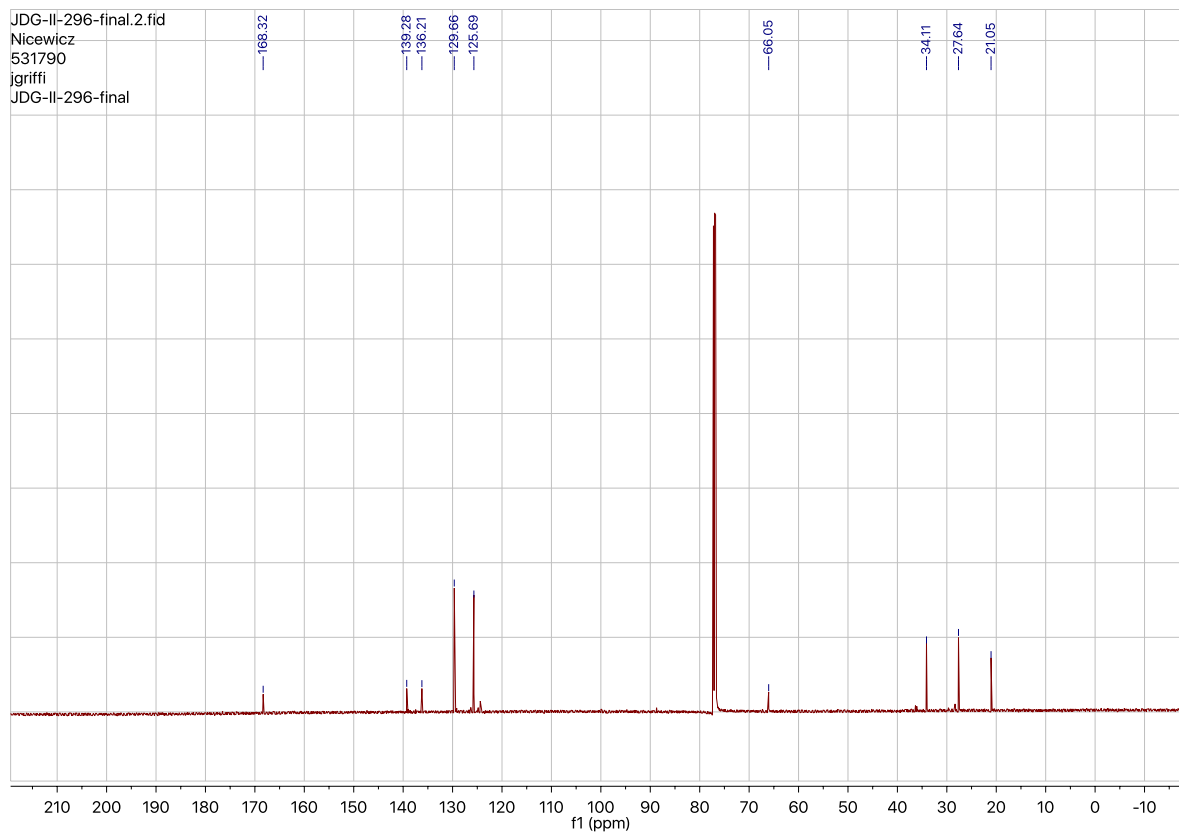
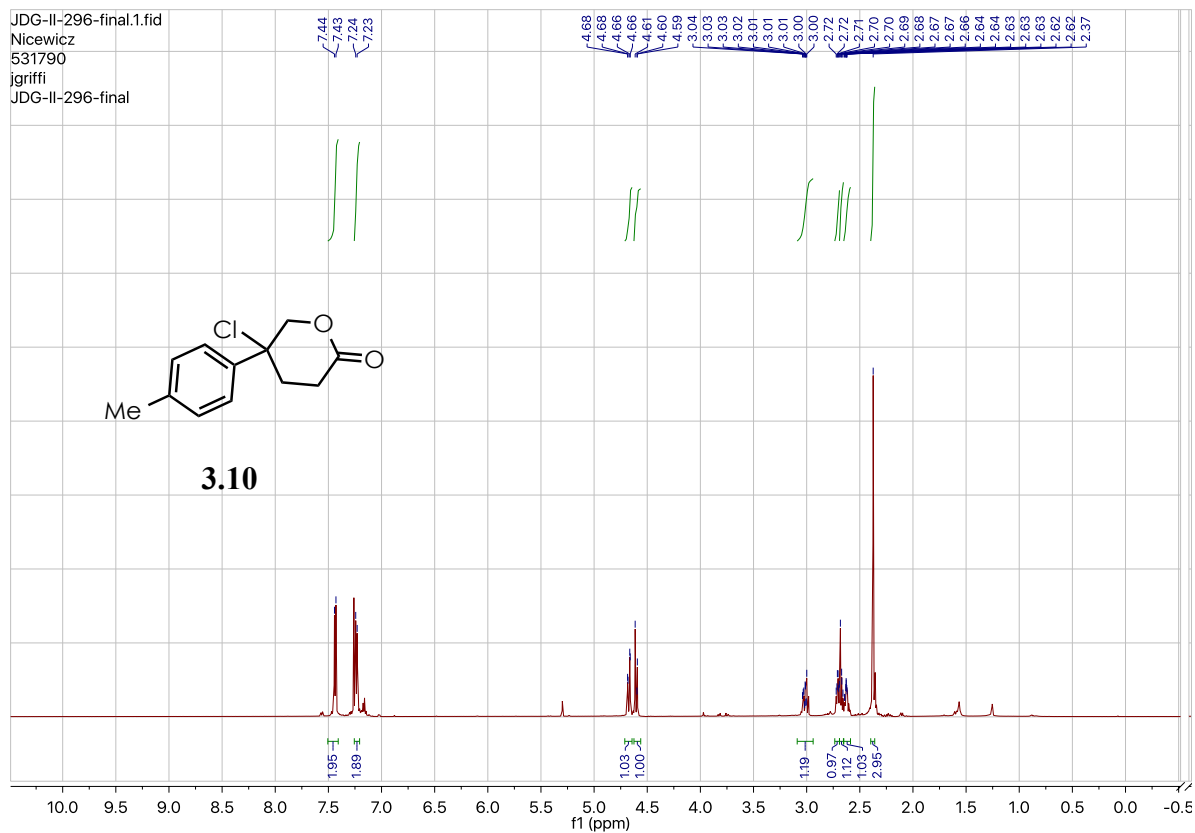
JDG-II-236 final-2.2.fid

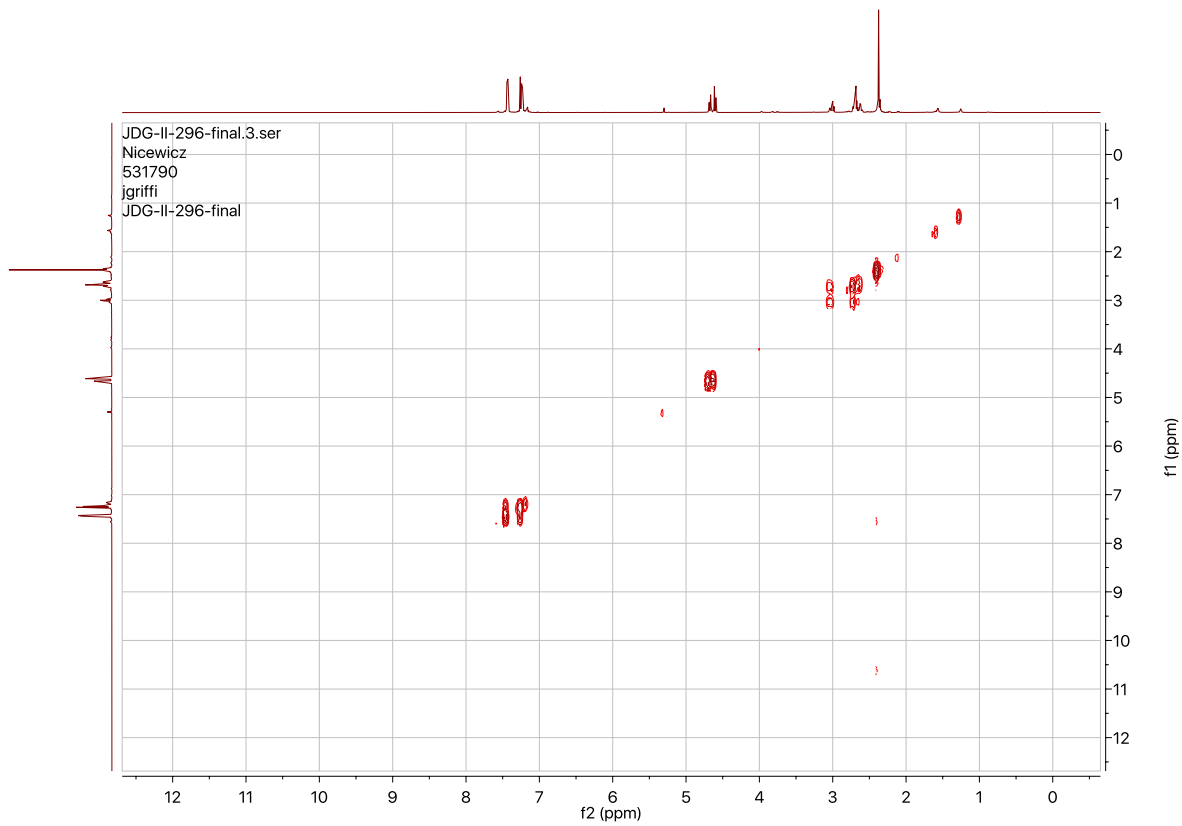
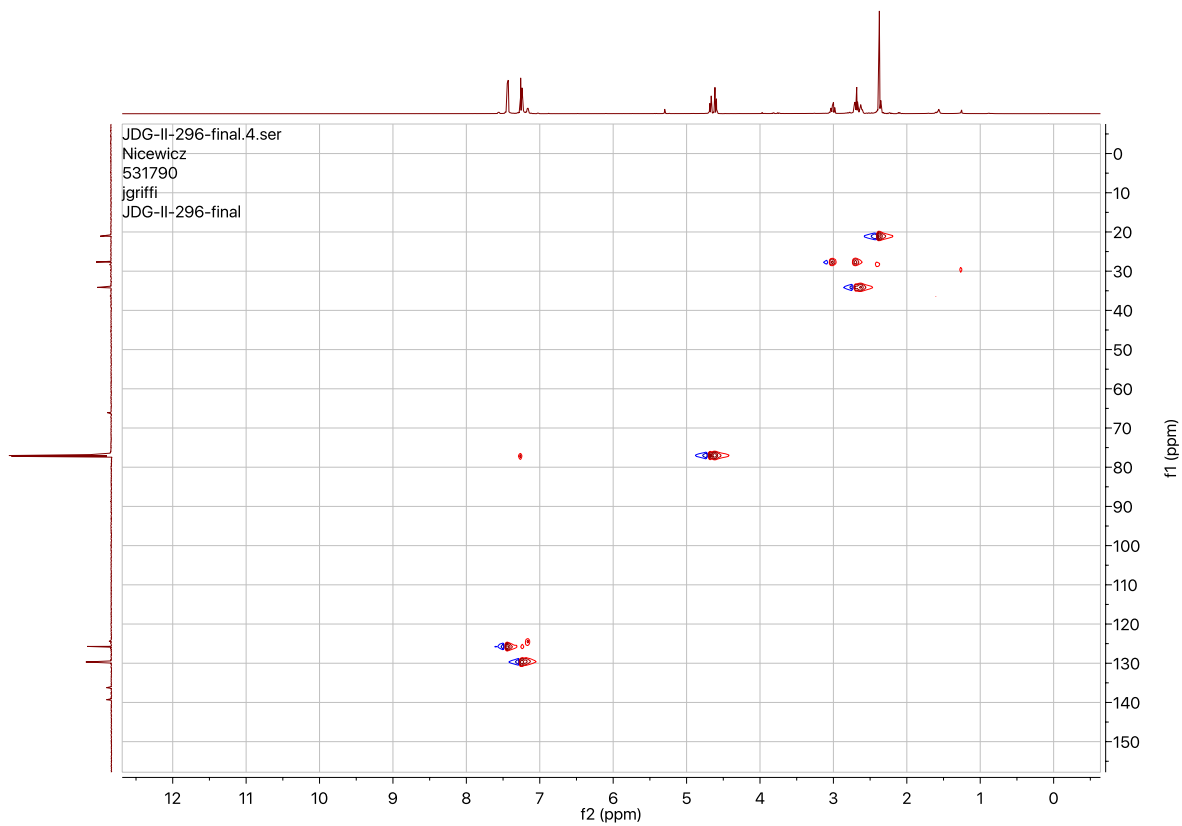


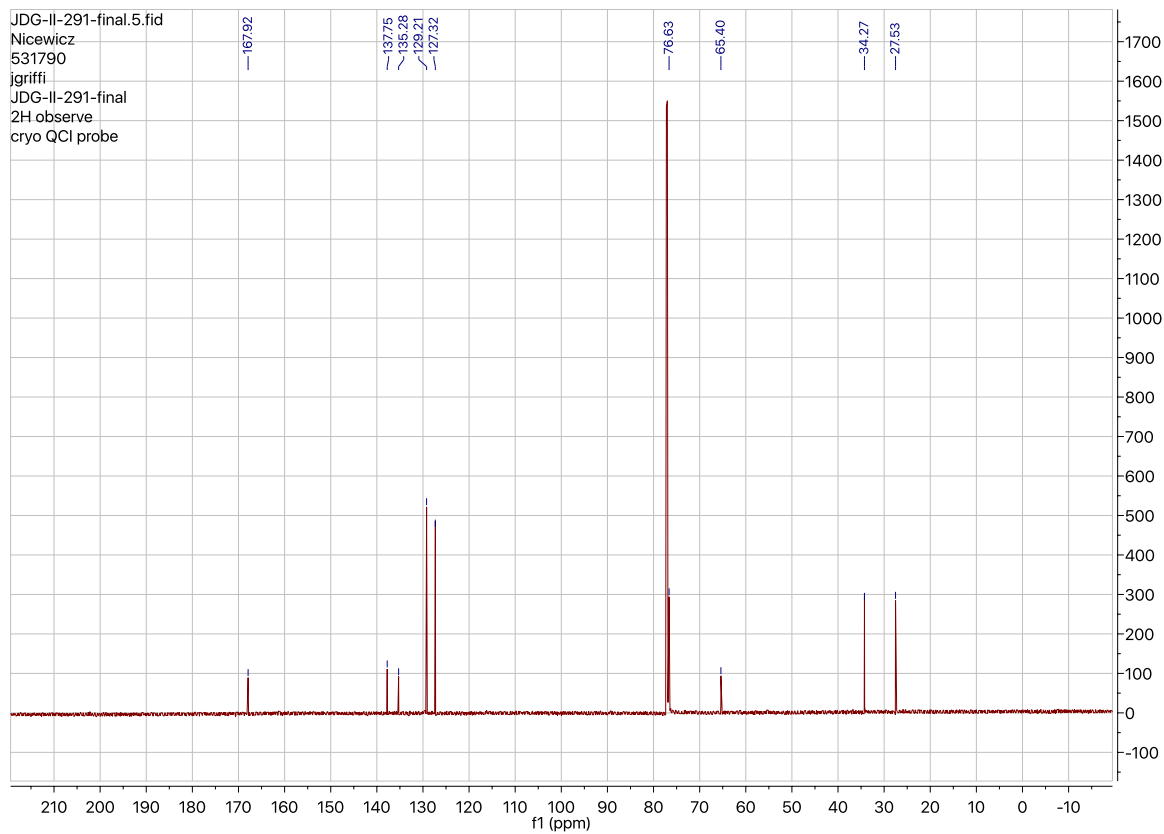
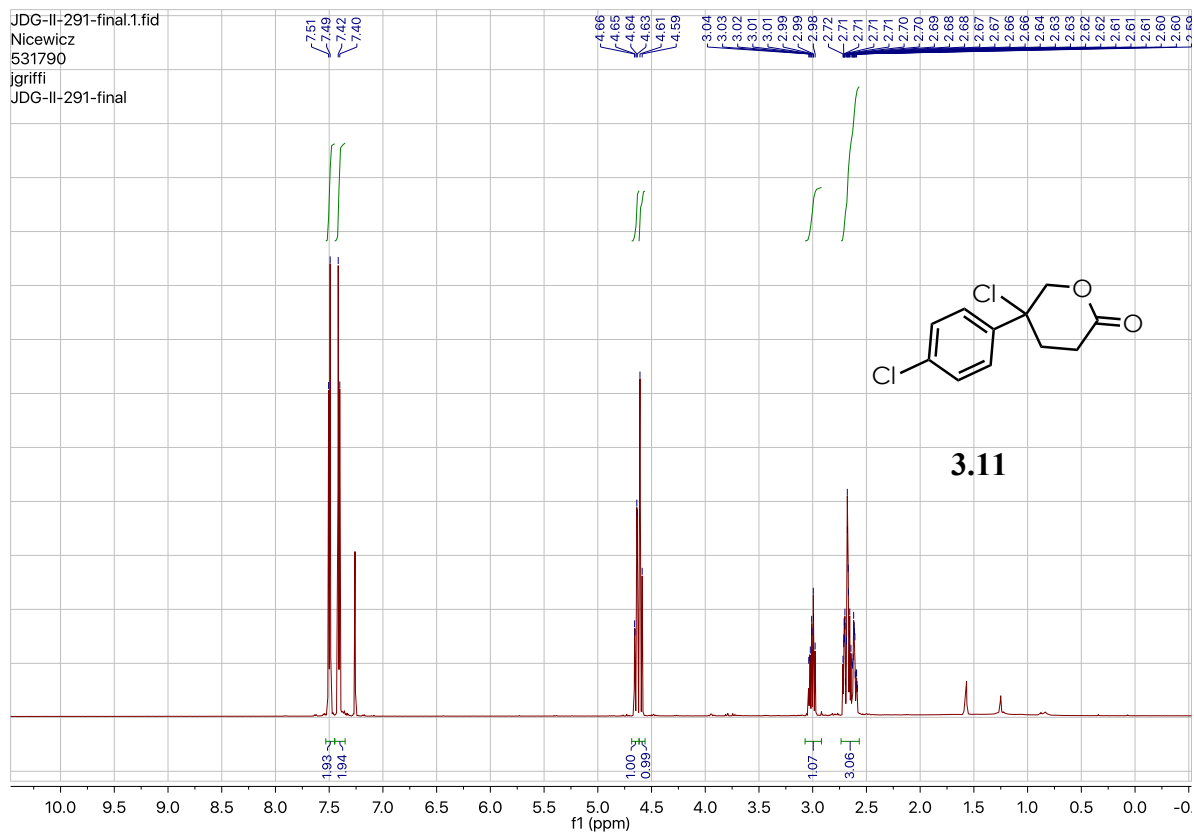


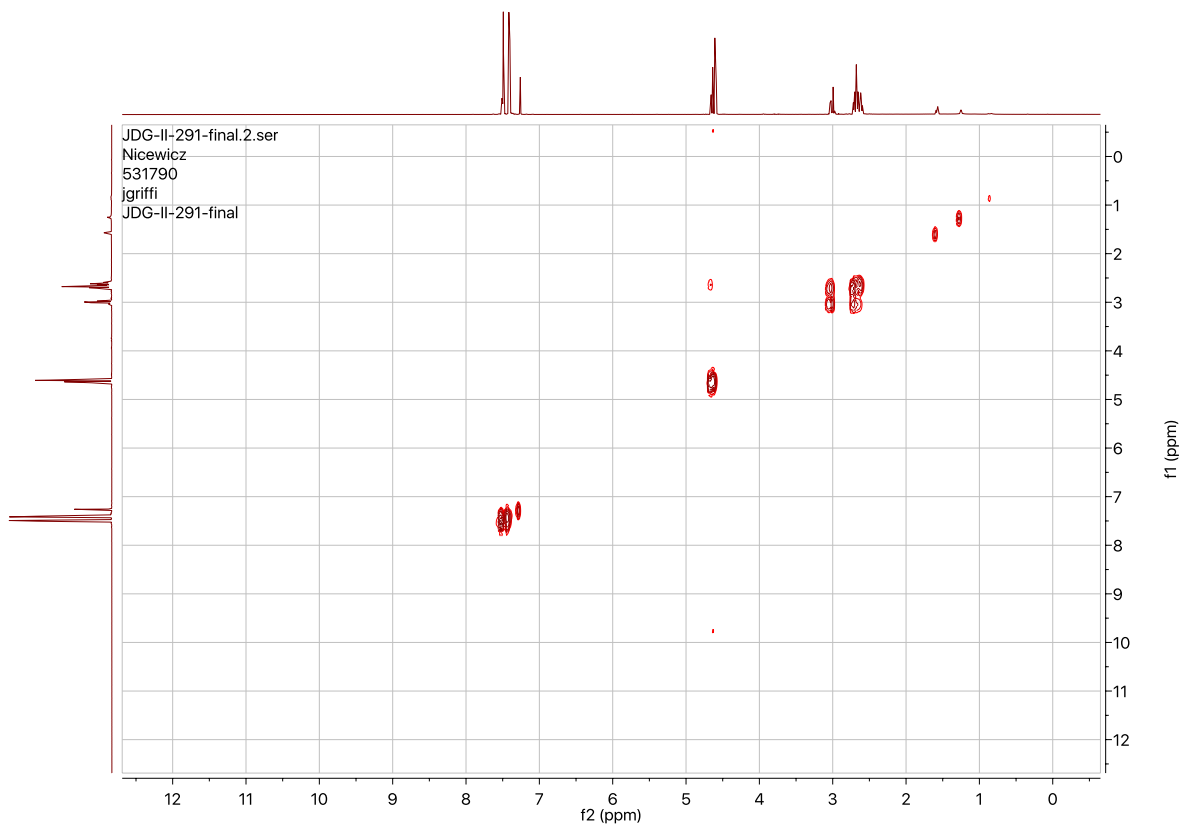
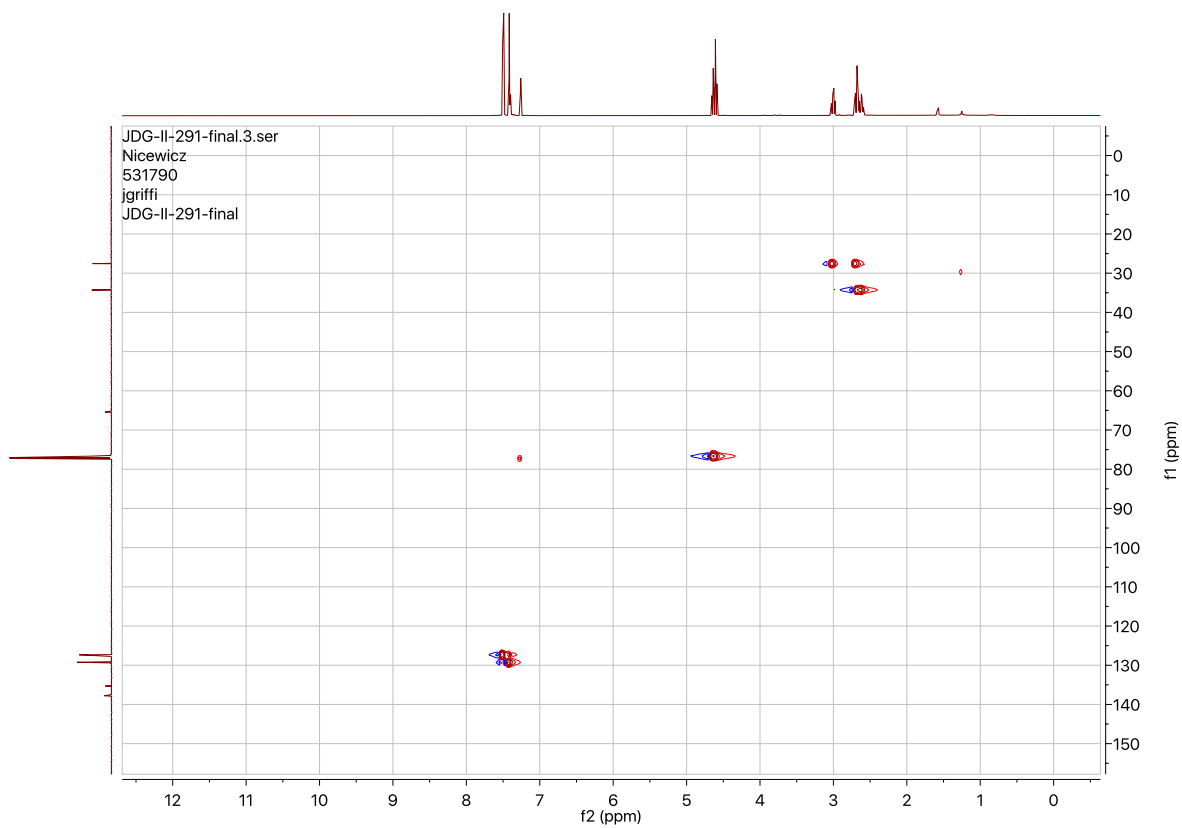


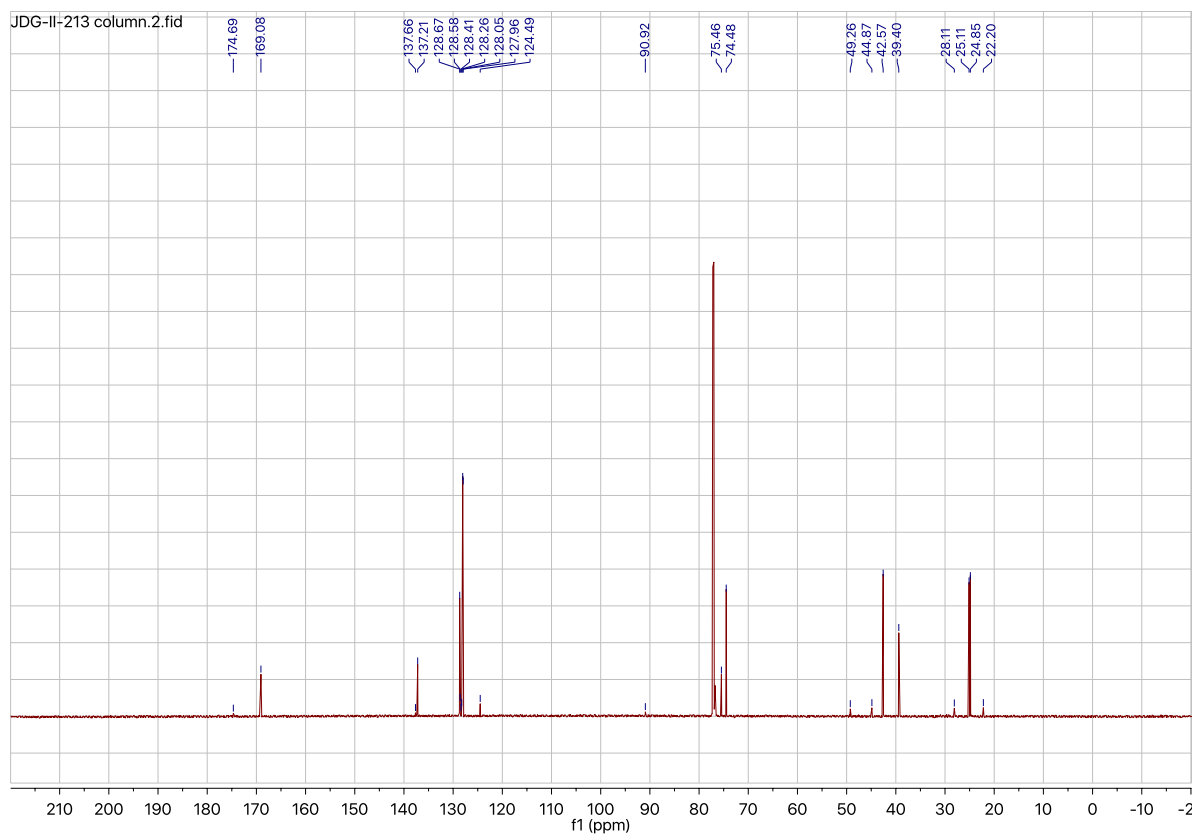
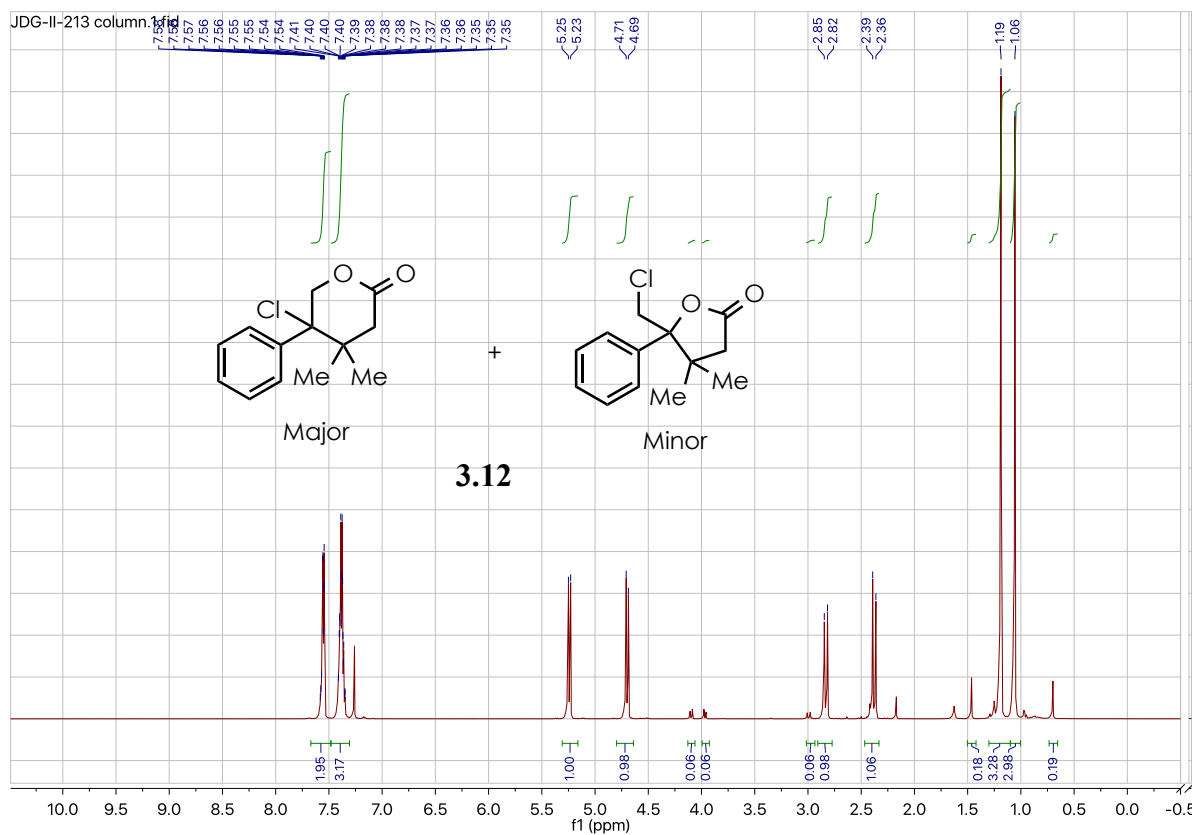


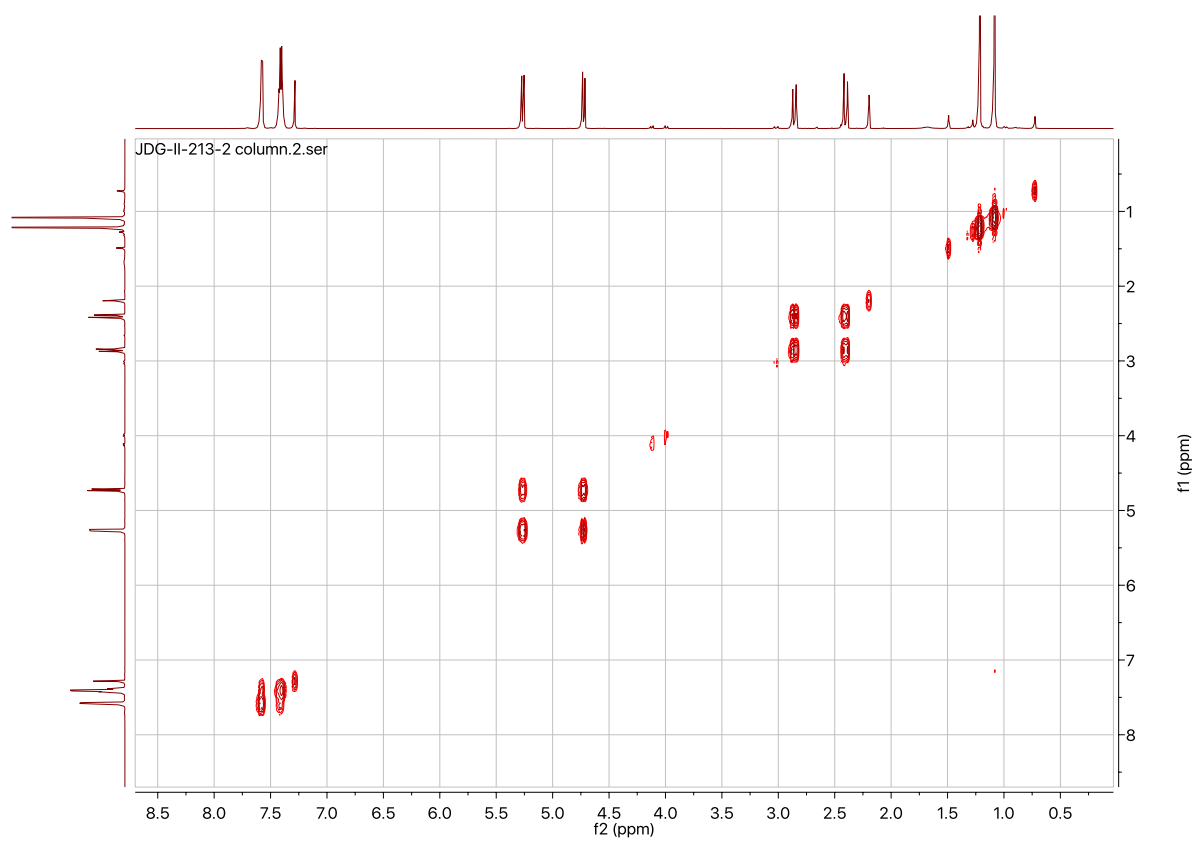
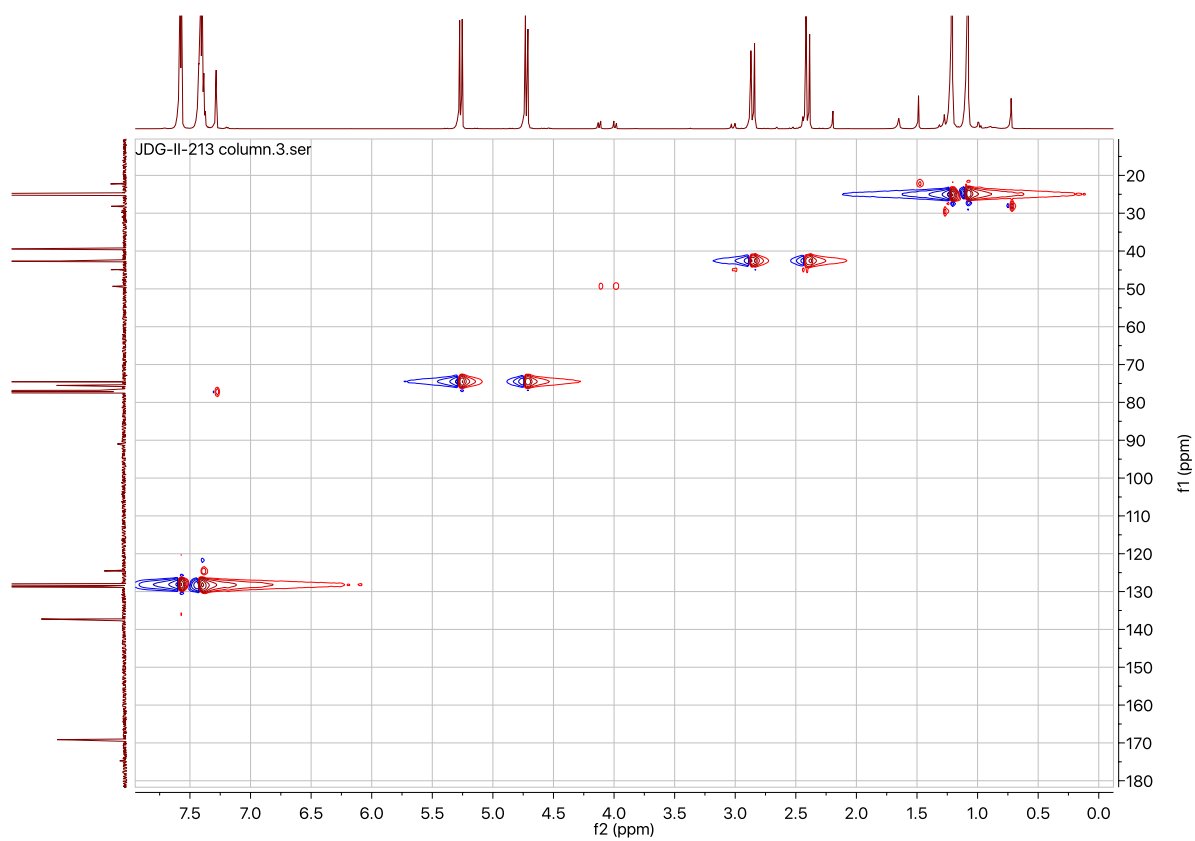


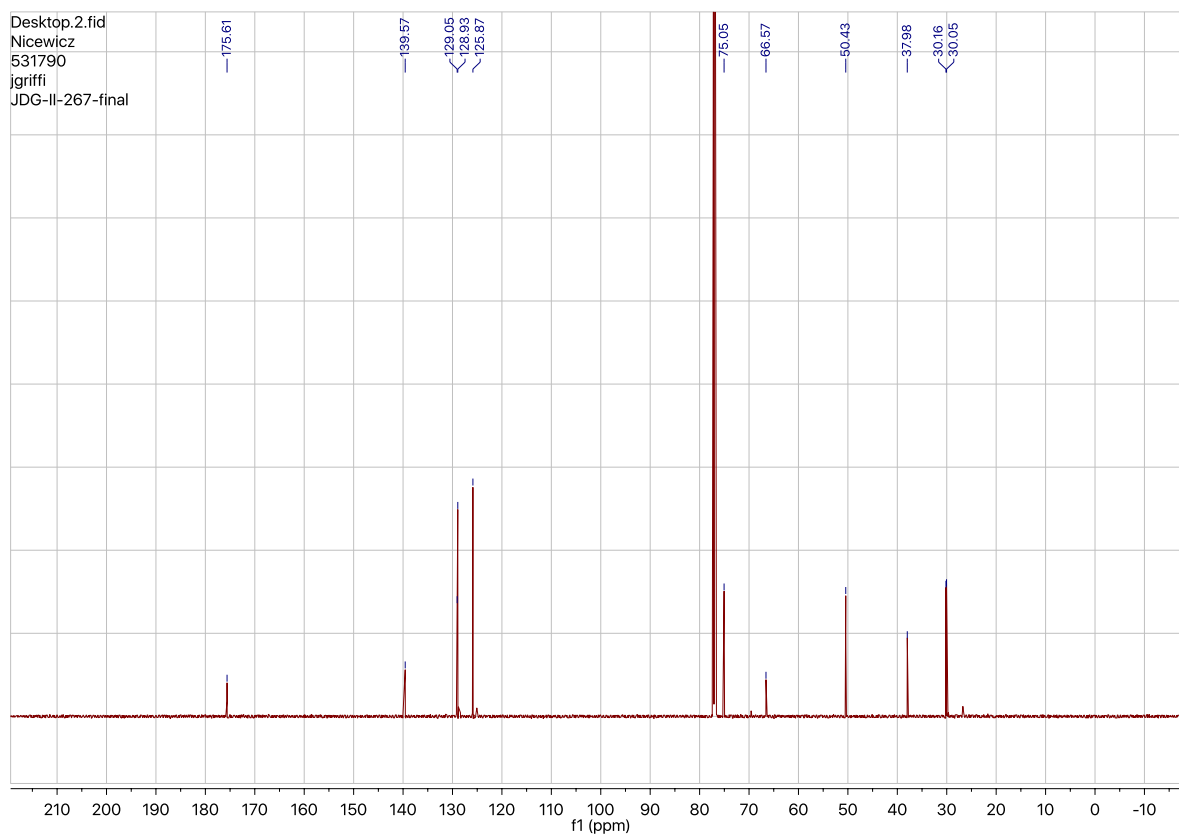
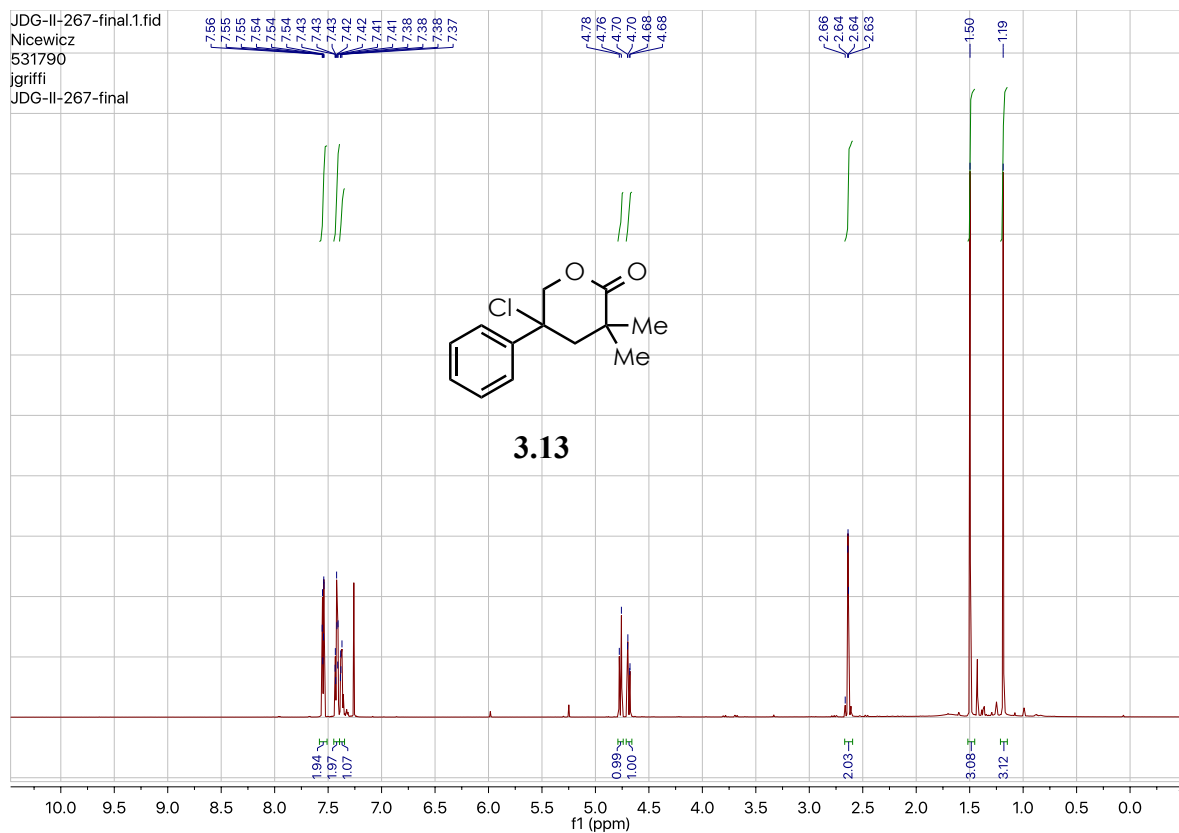


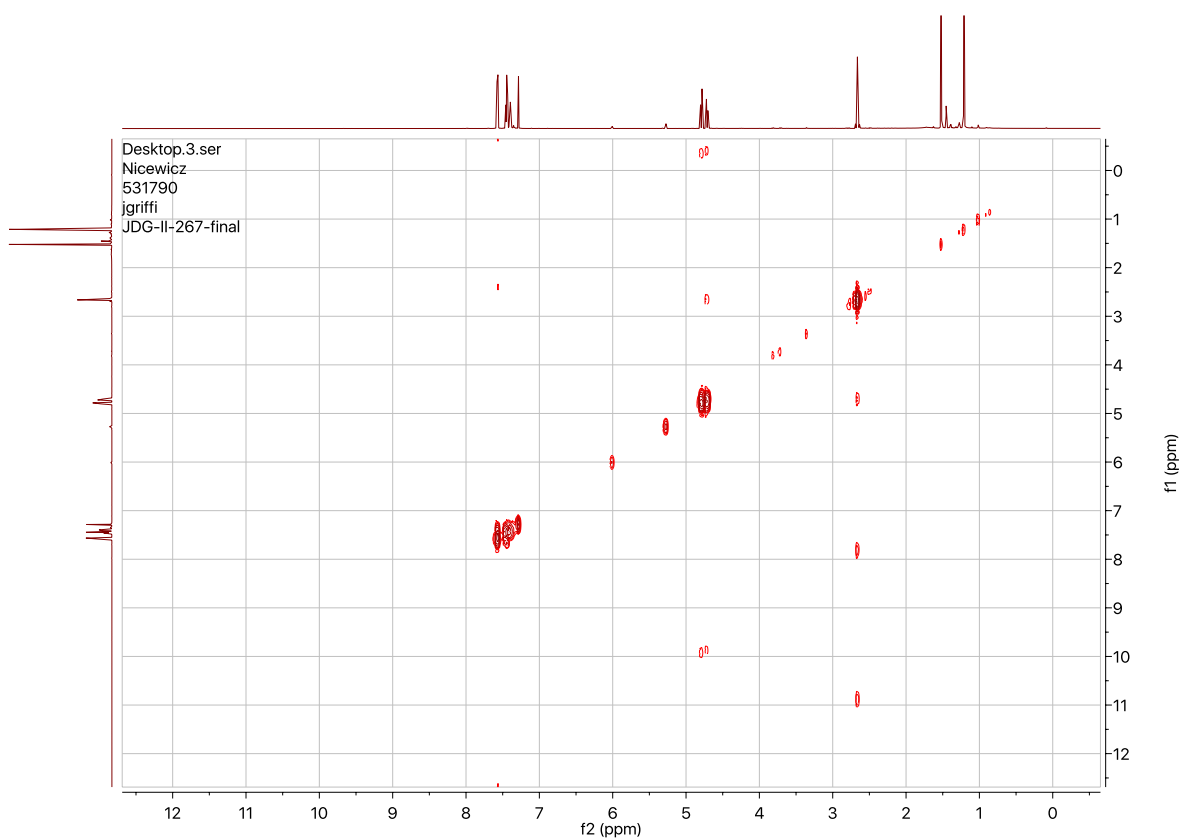
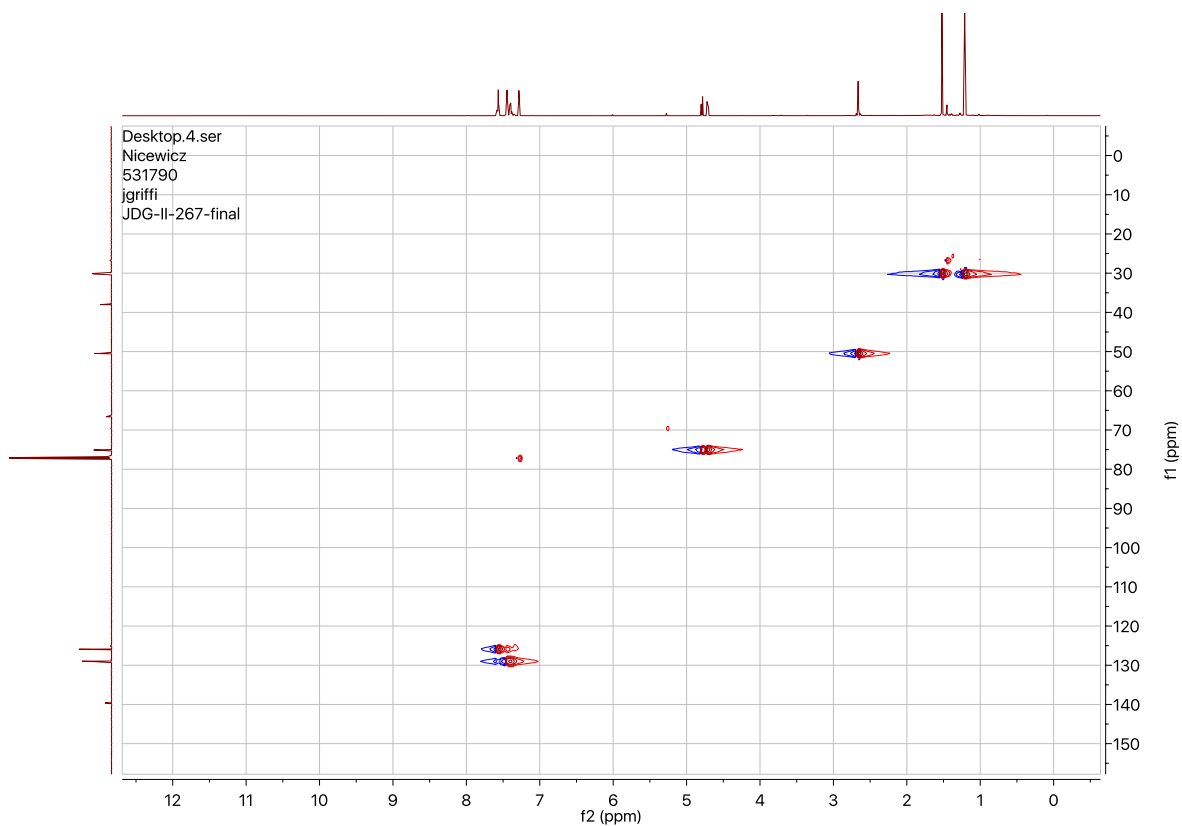


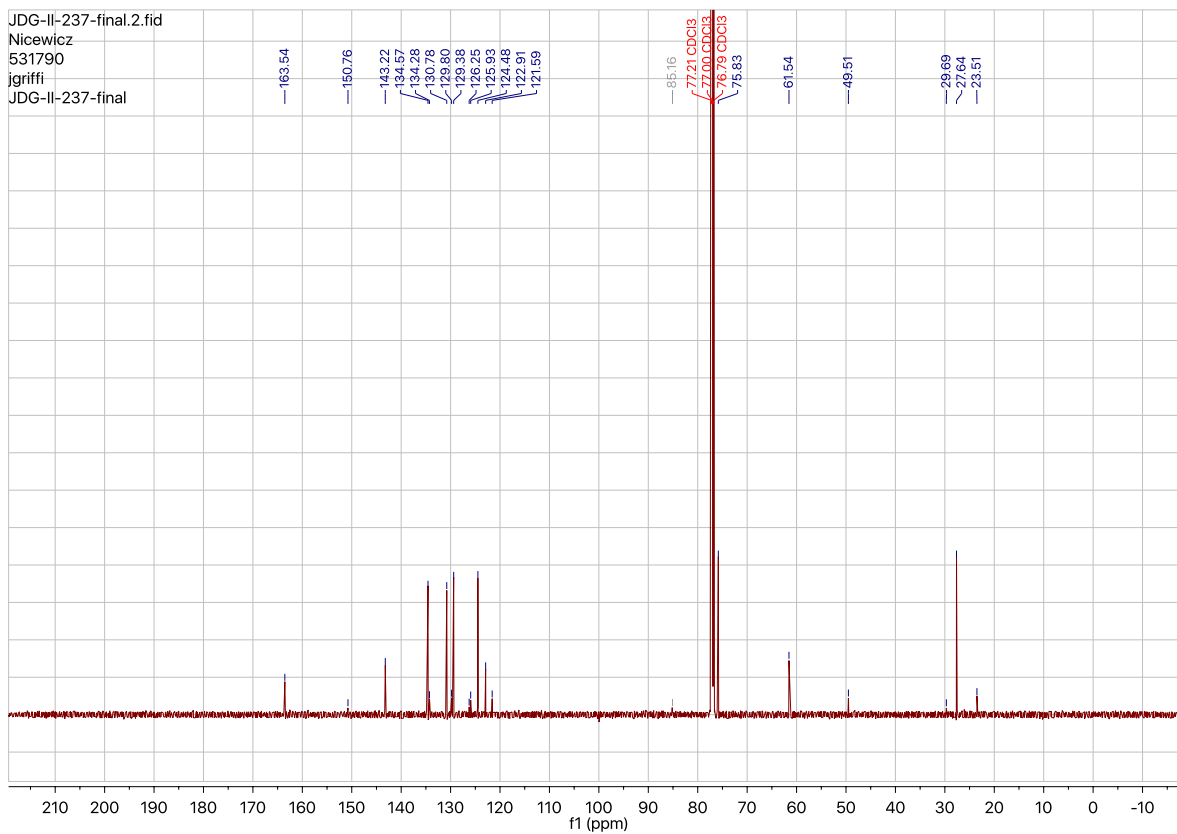
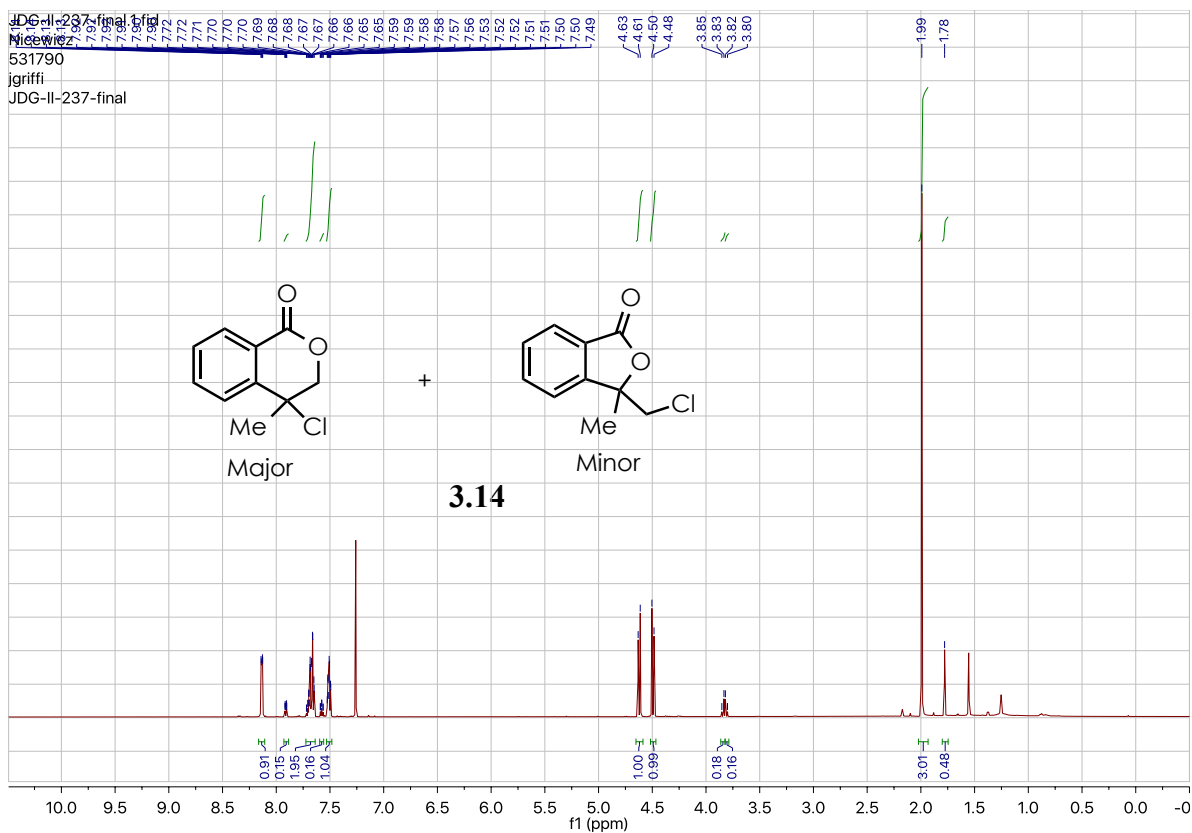


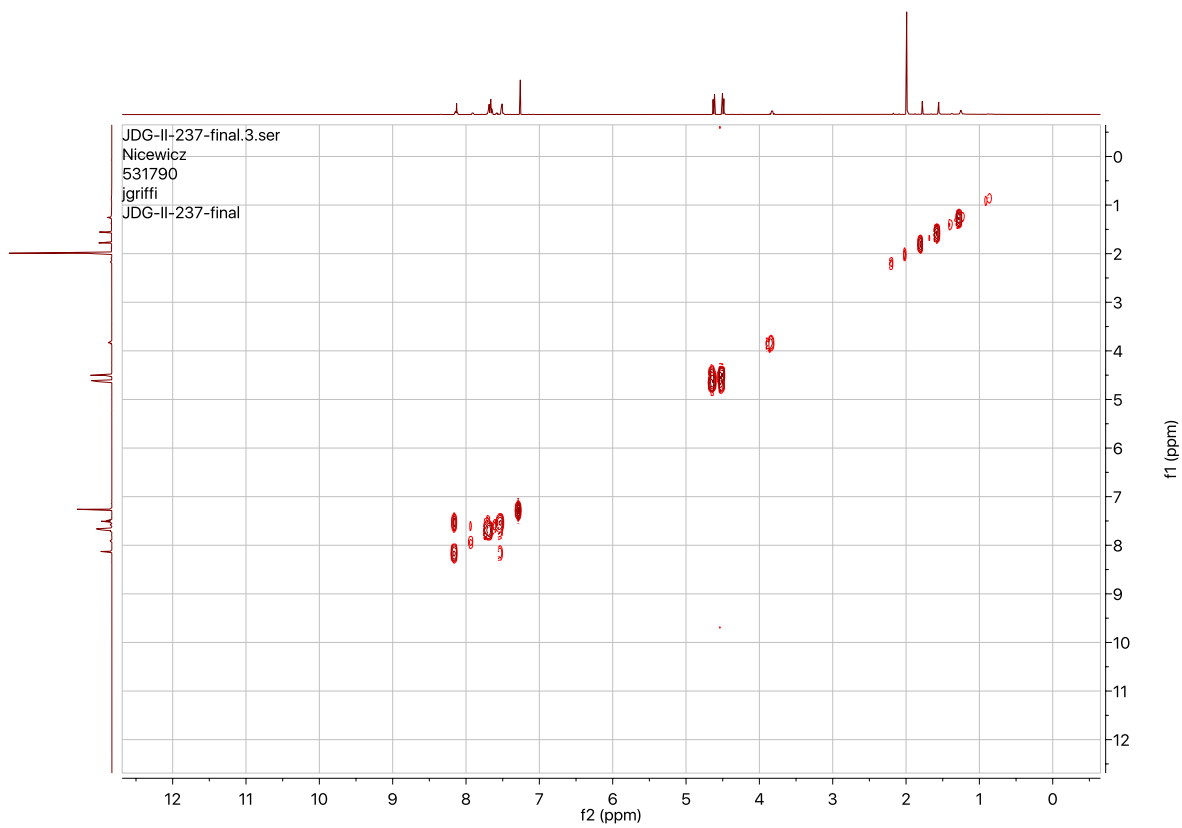
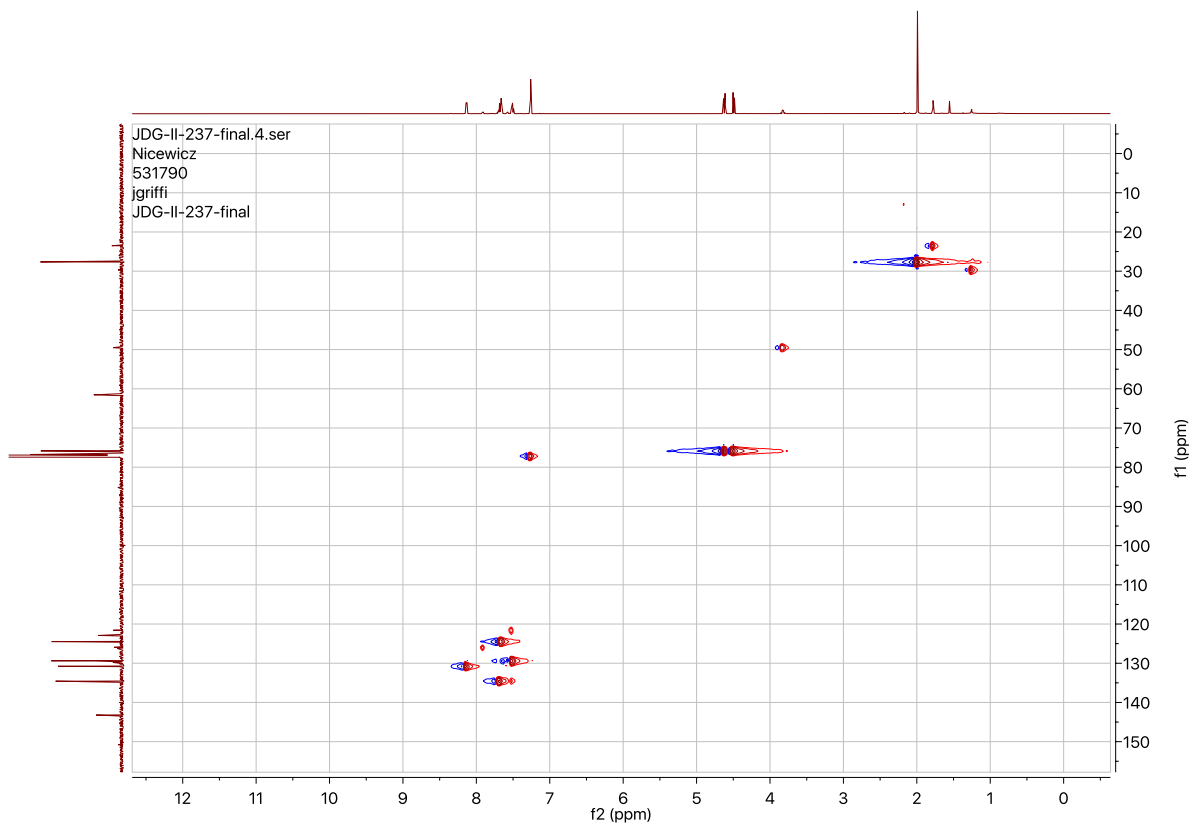








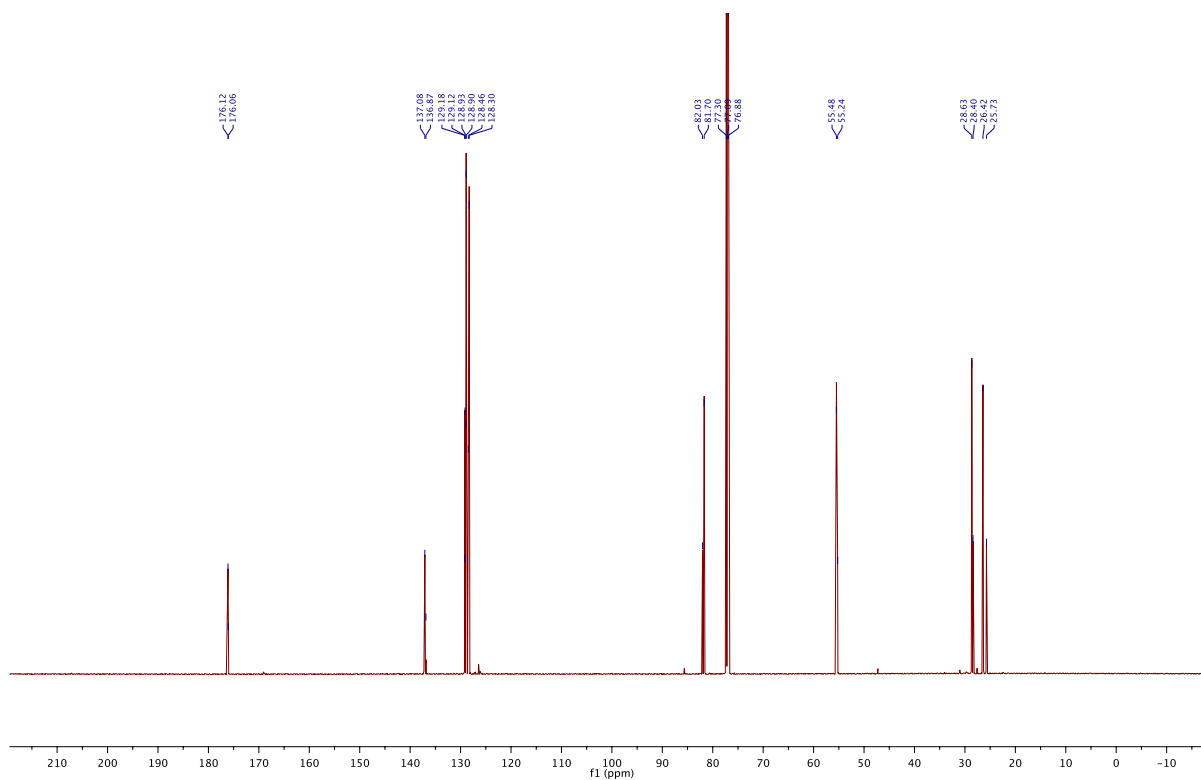
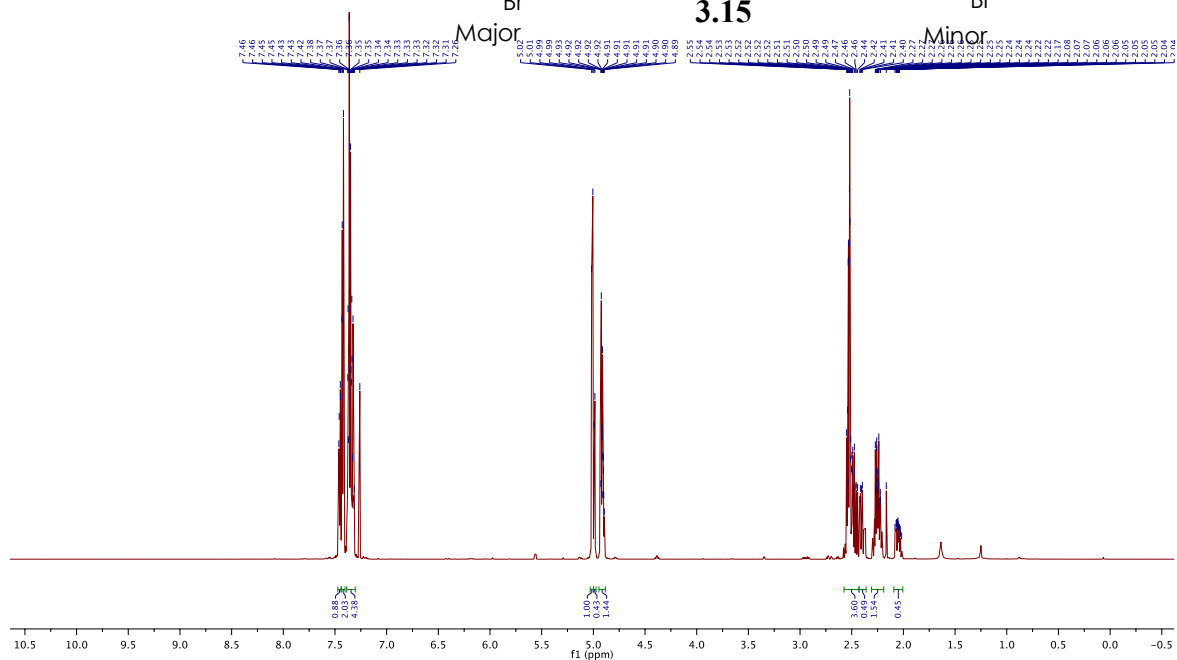


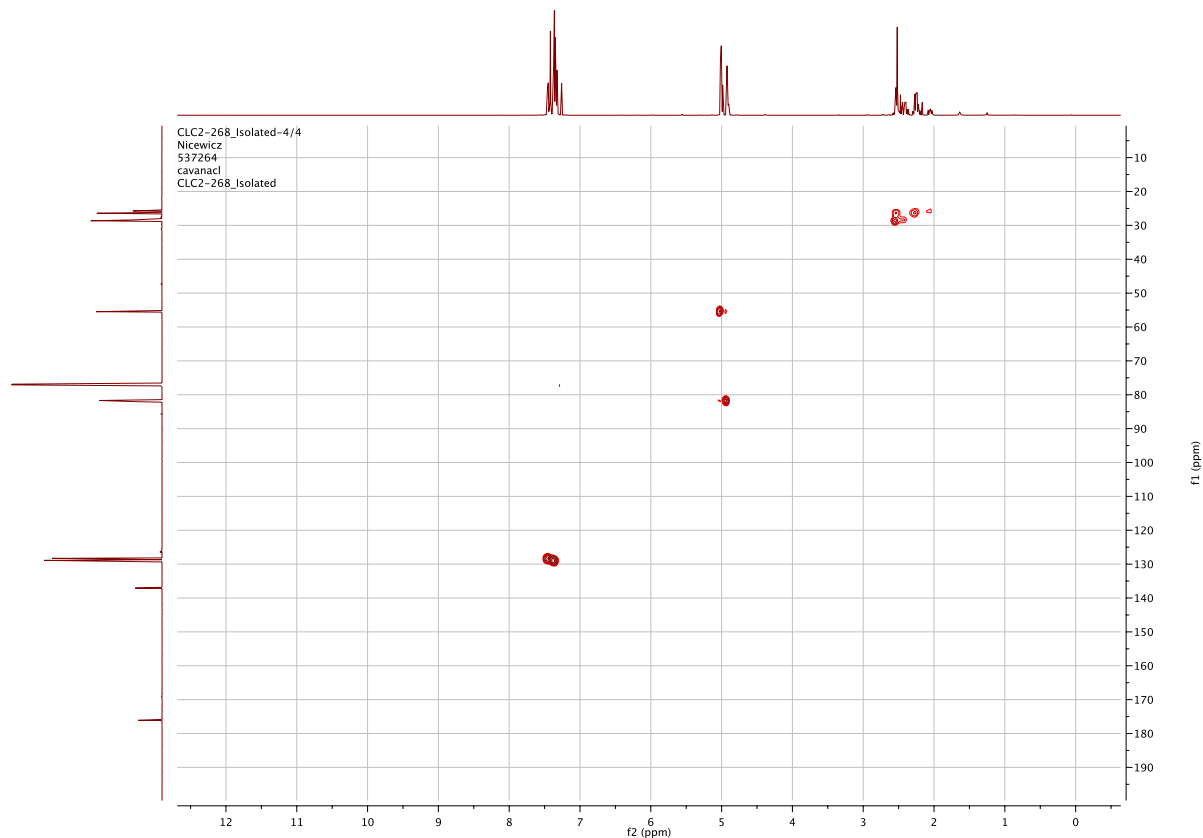


$+$

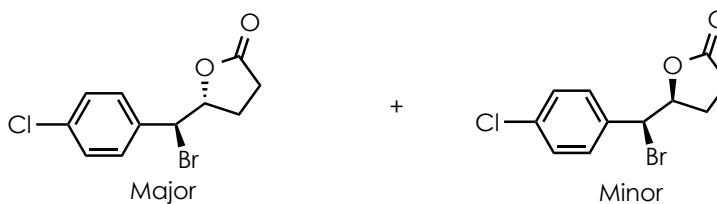
3.15

Minor

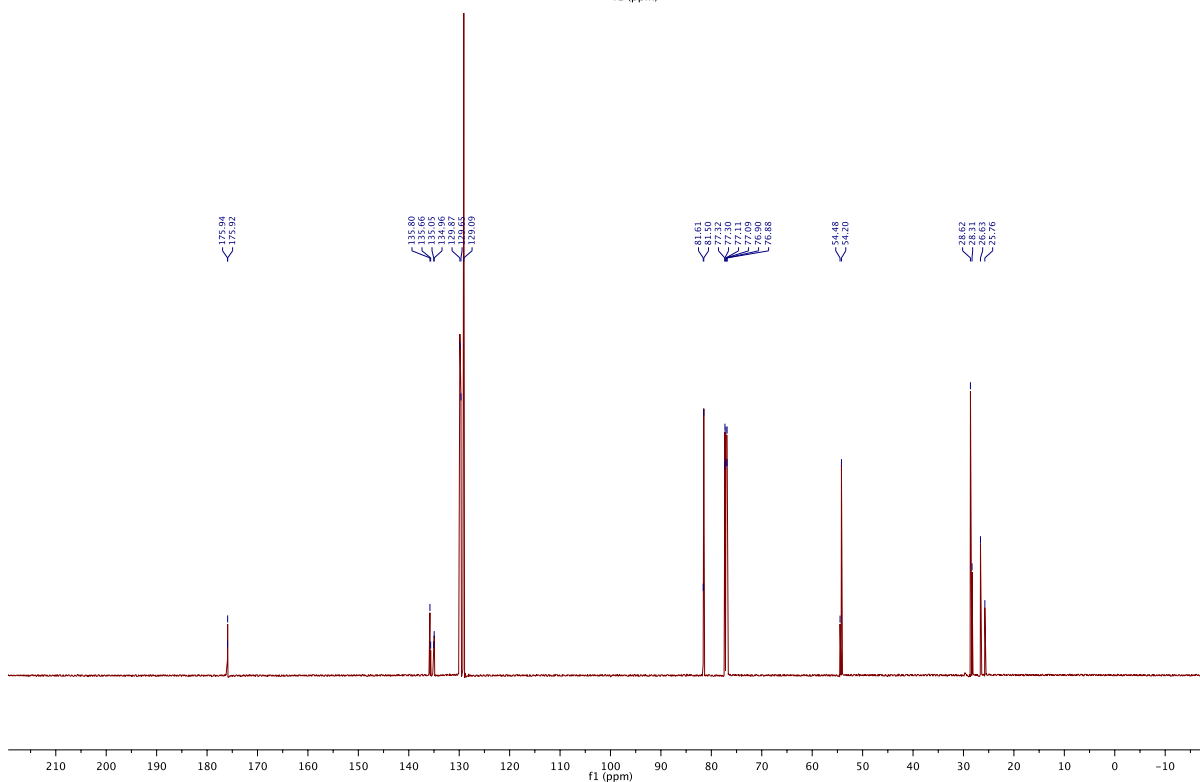
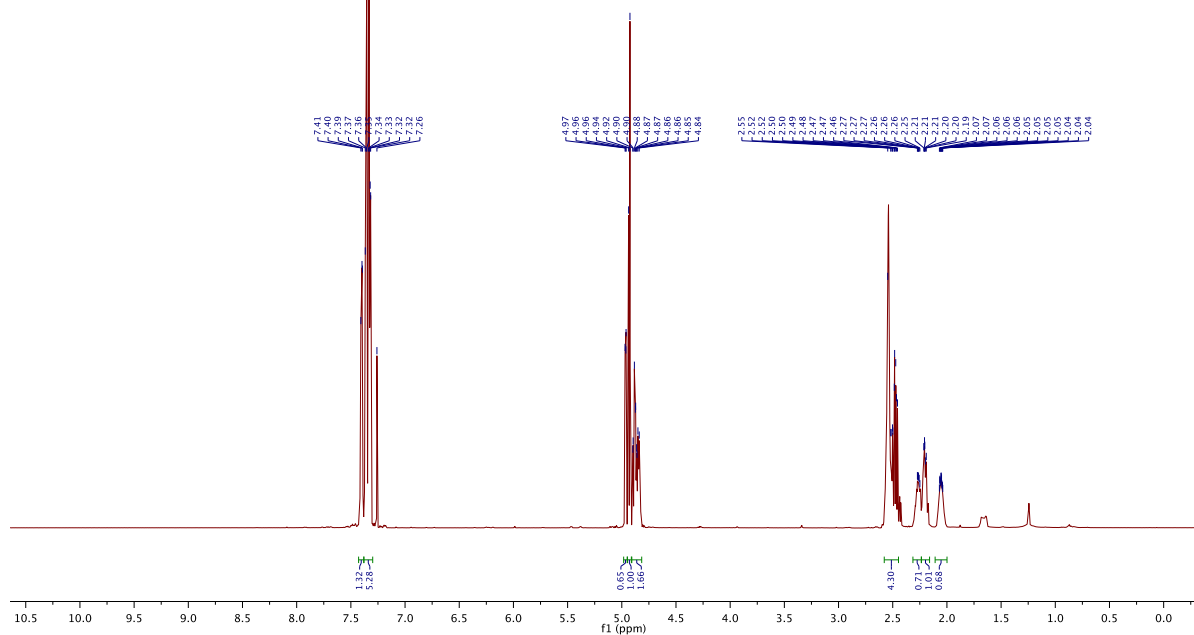


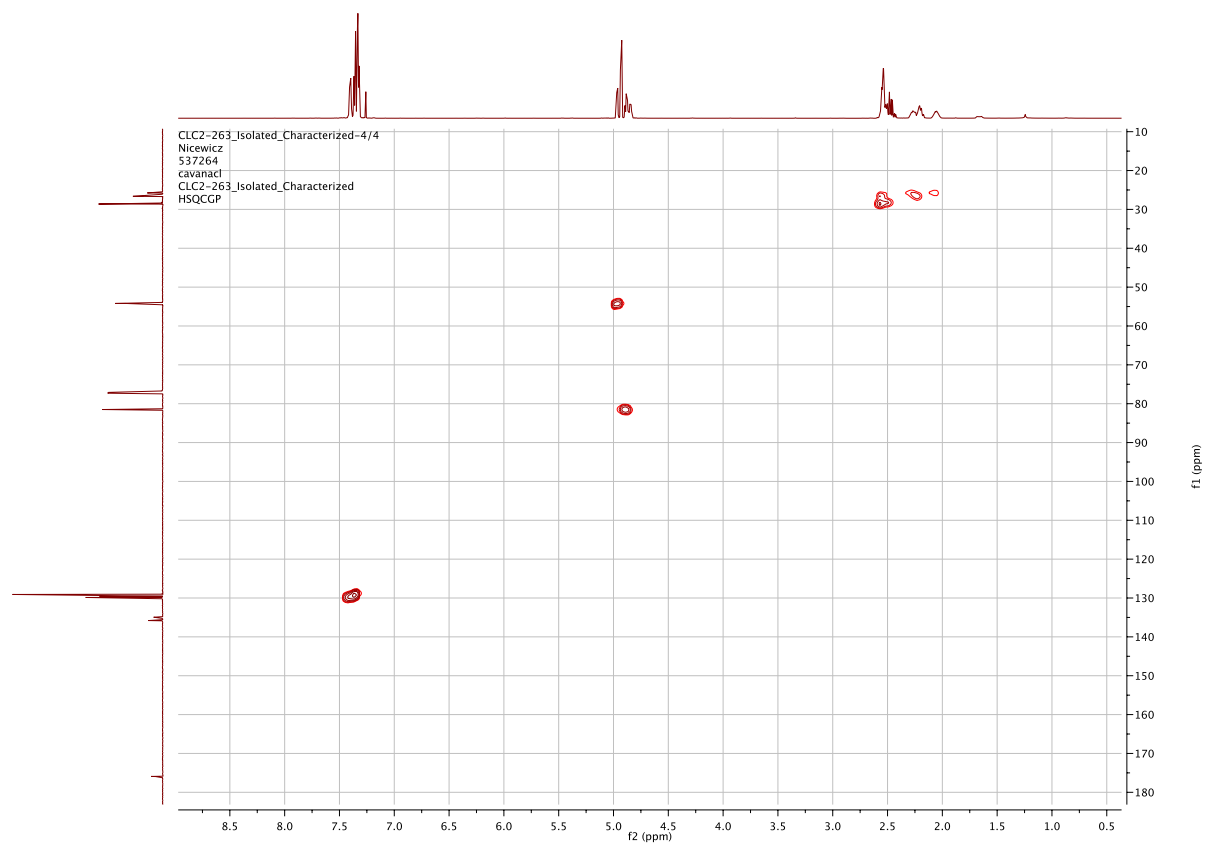


CLC2-263_Isolated_Characterized/1
 Nicewicz
 537264
 cavanaci
 CLC2-263_Isolated_Characterized

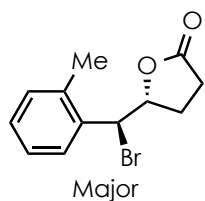


3.16

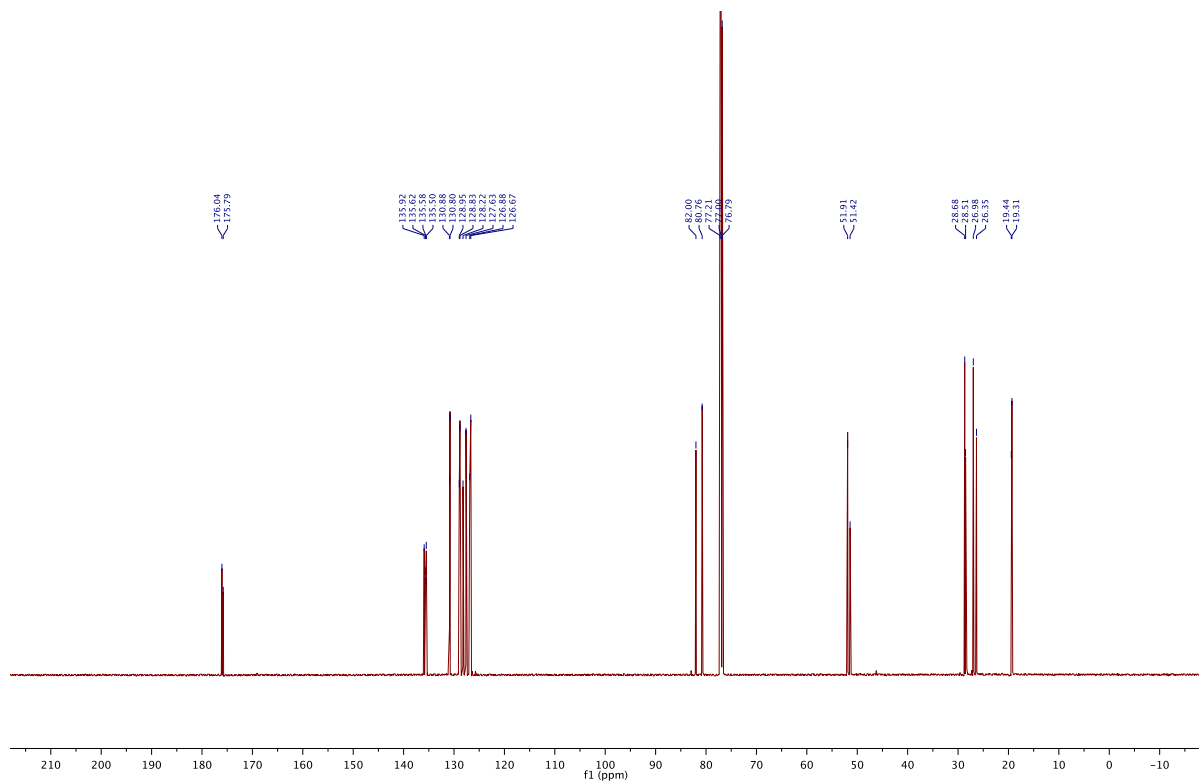
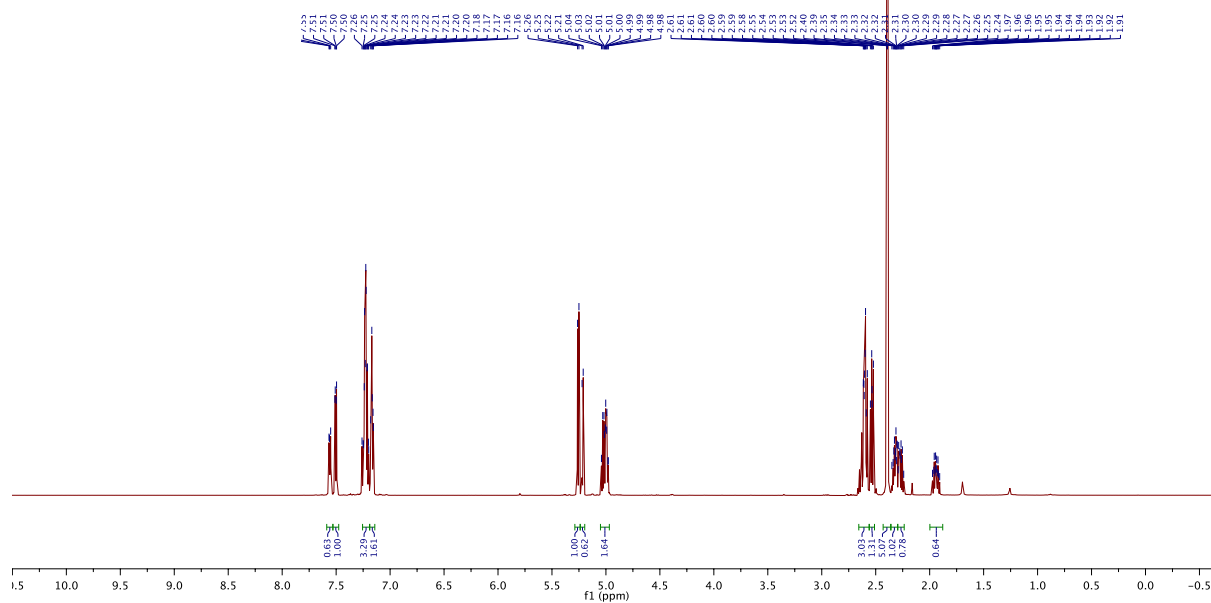
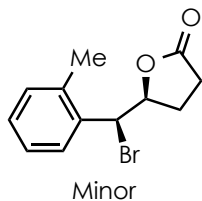


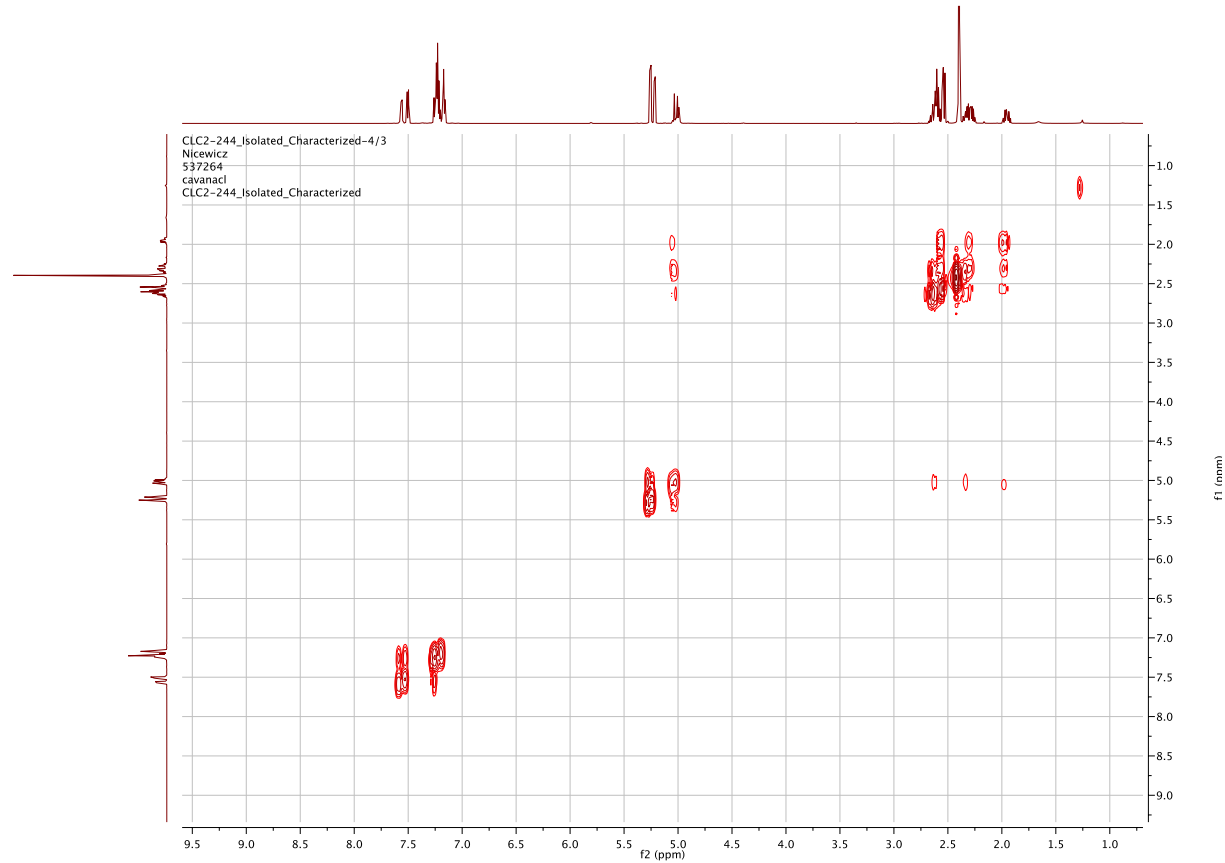
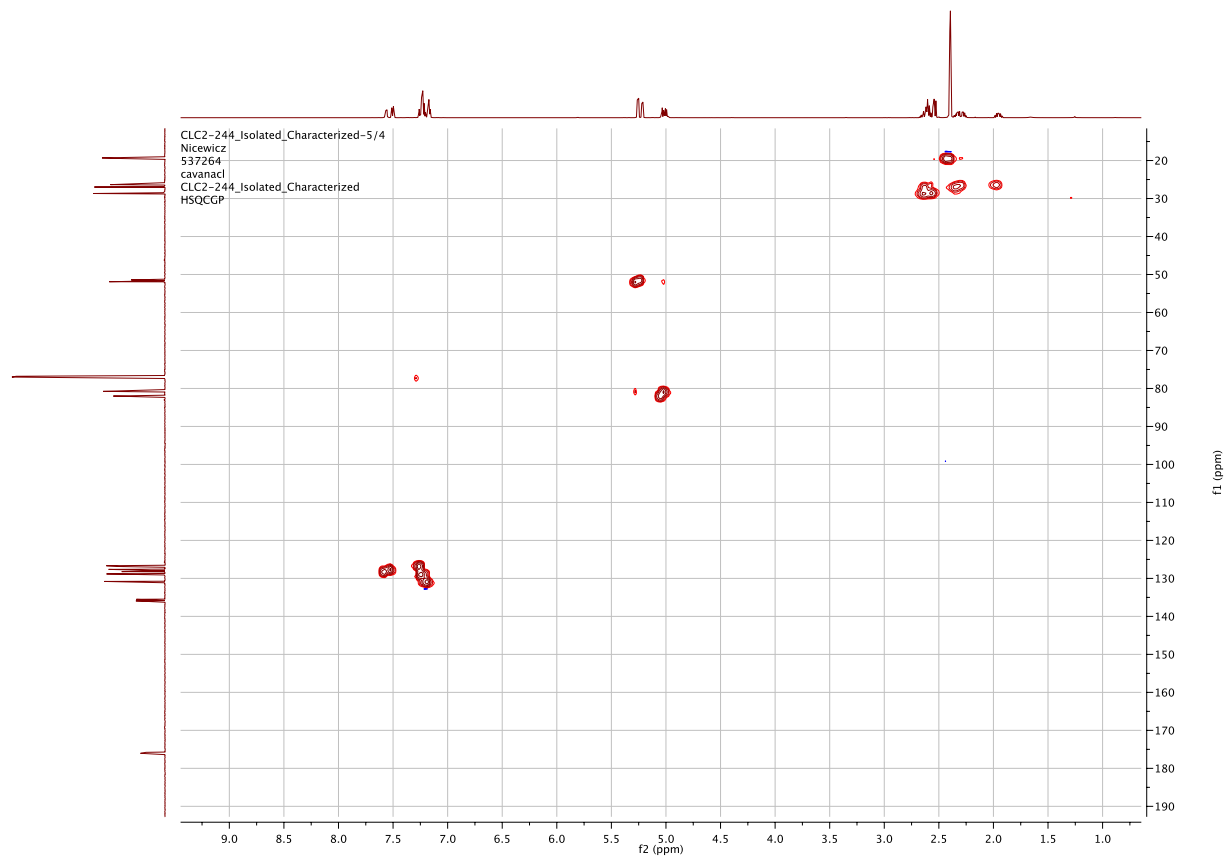


2-250_Isolated/1
 wicz
 264
 inactl
 2-250_Isolated

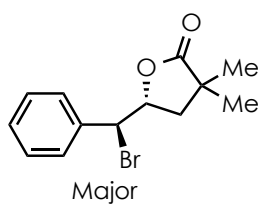


3.17



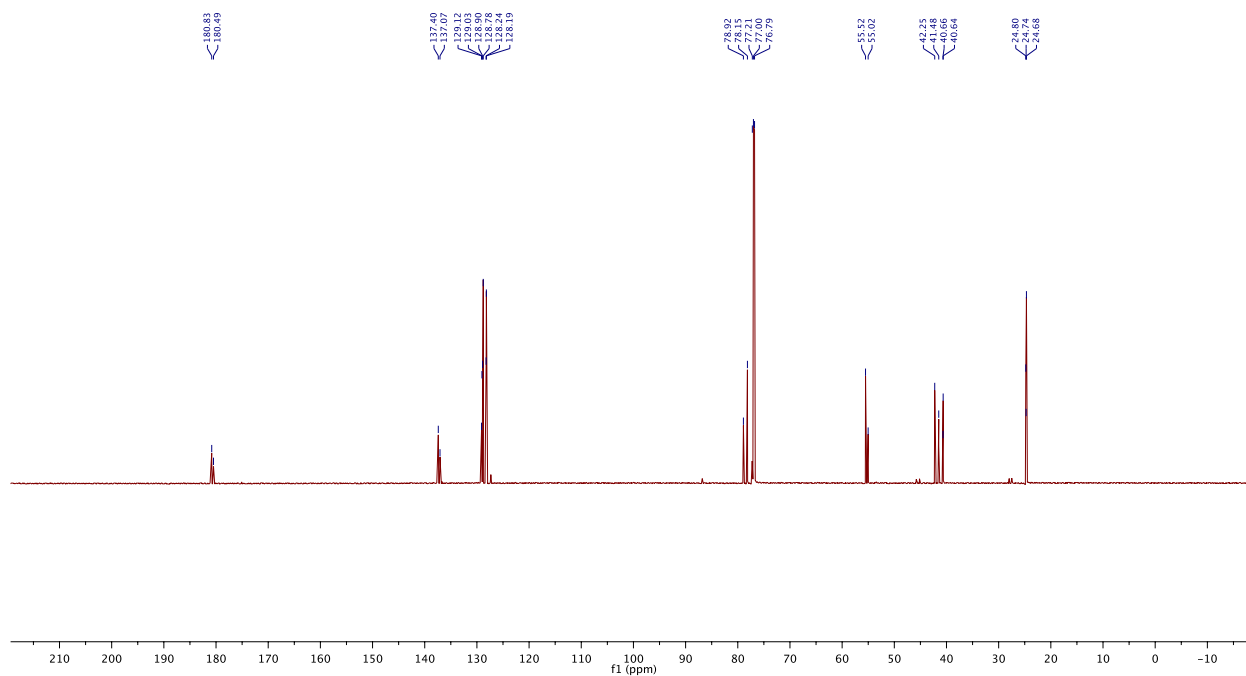
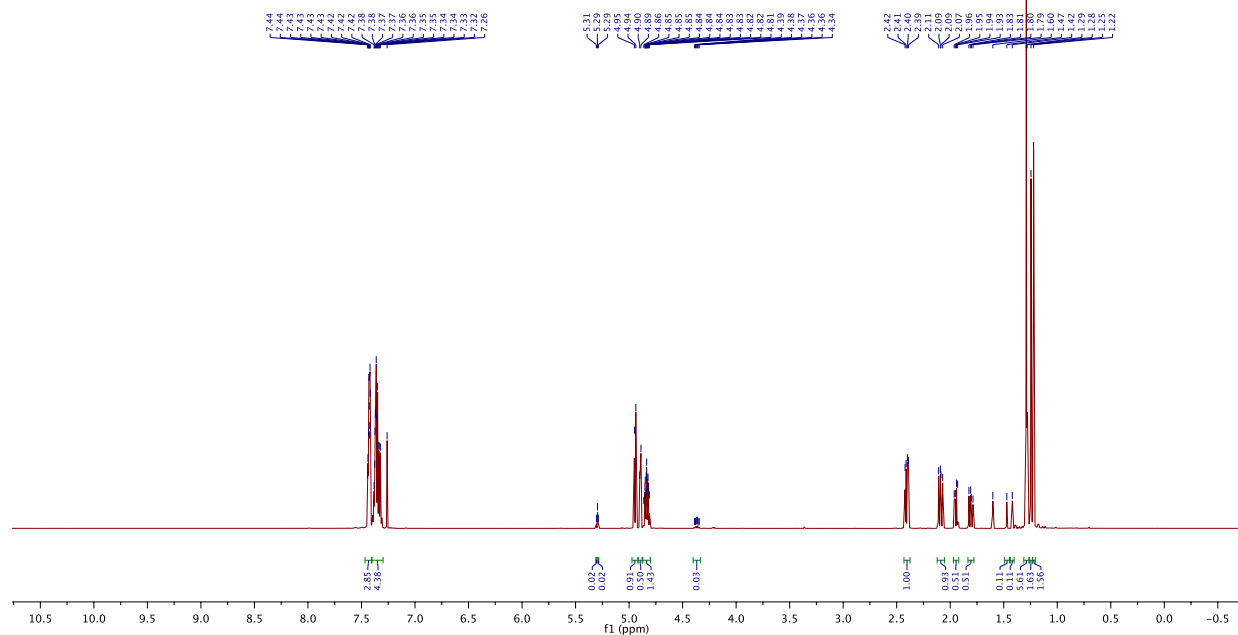
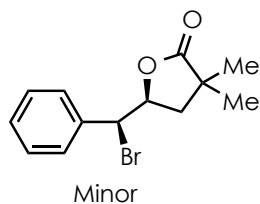


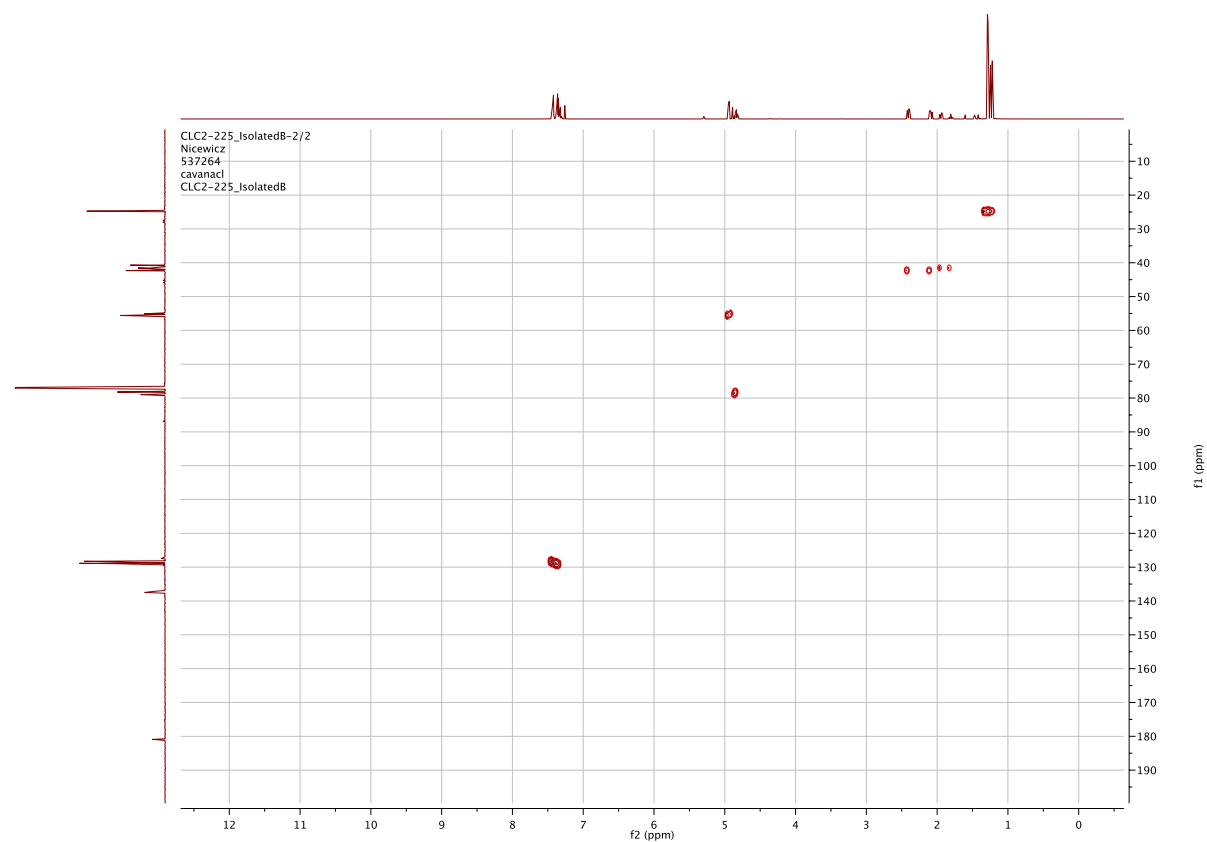
CLC2-225_IsolatedB/1
 Nicewicz
 537264
 cavanac1
 CLC2-225_IsolatedB



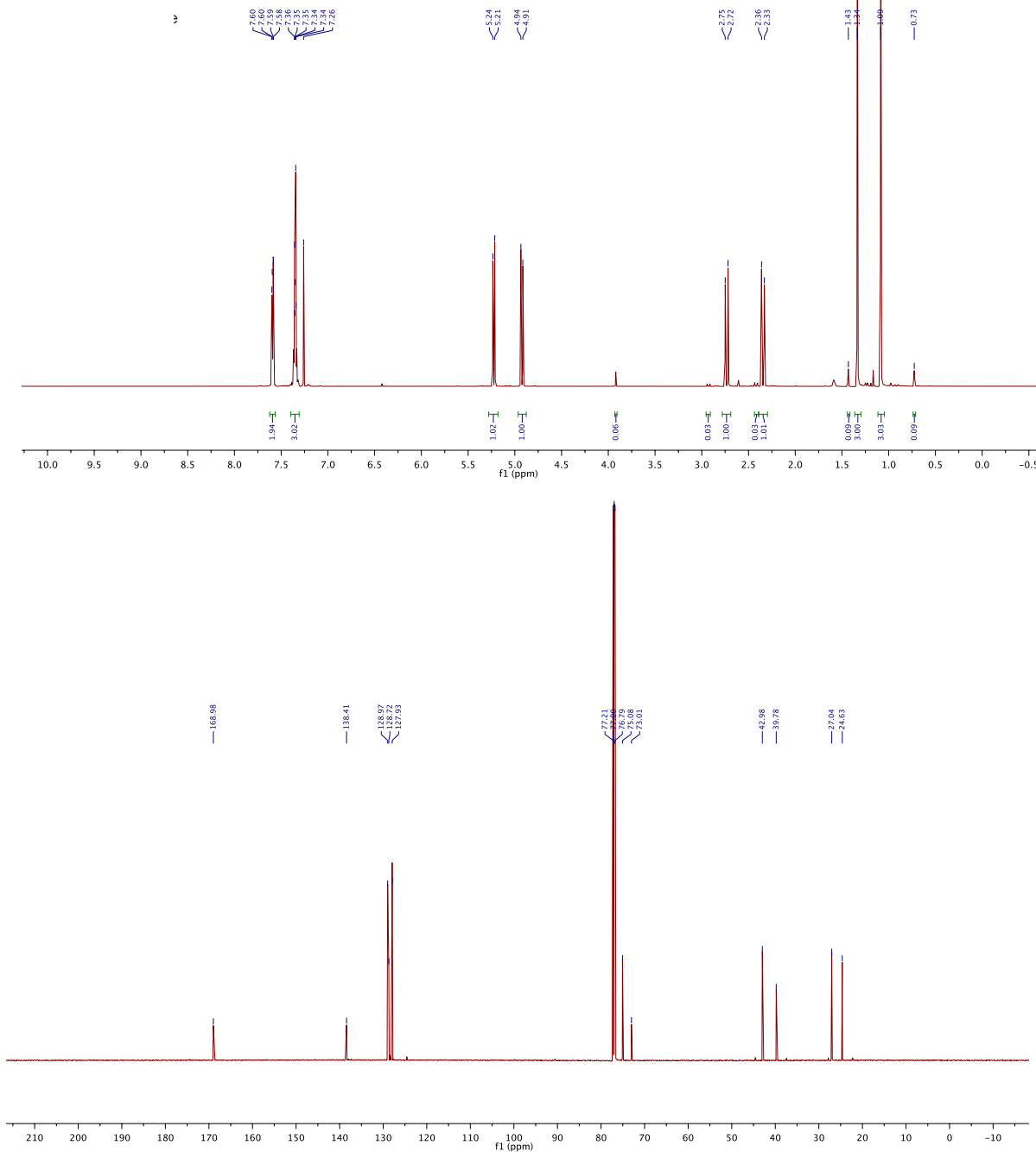
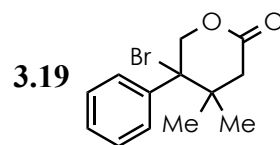
+

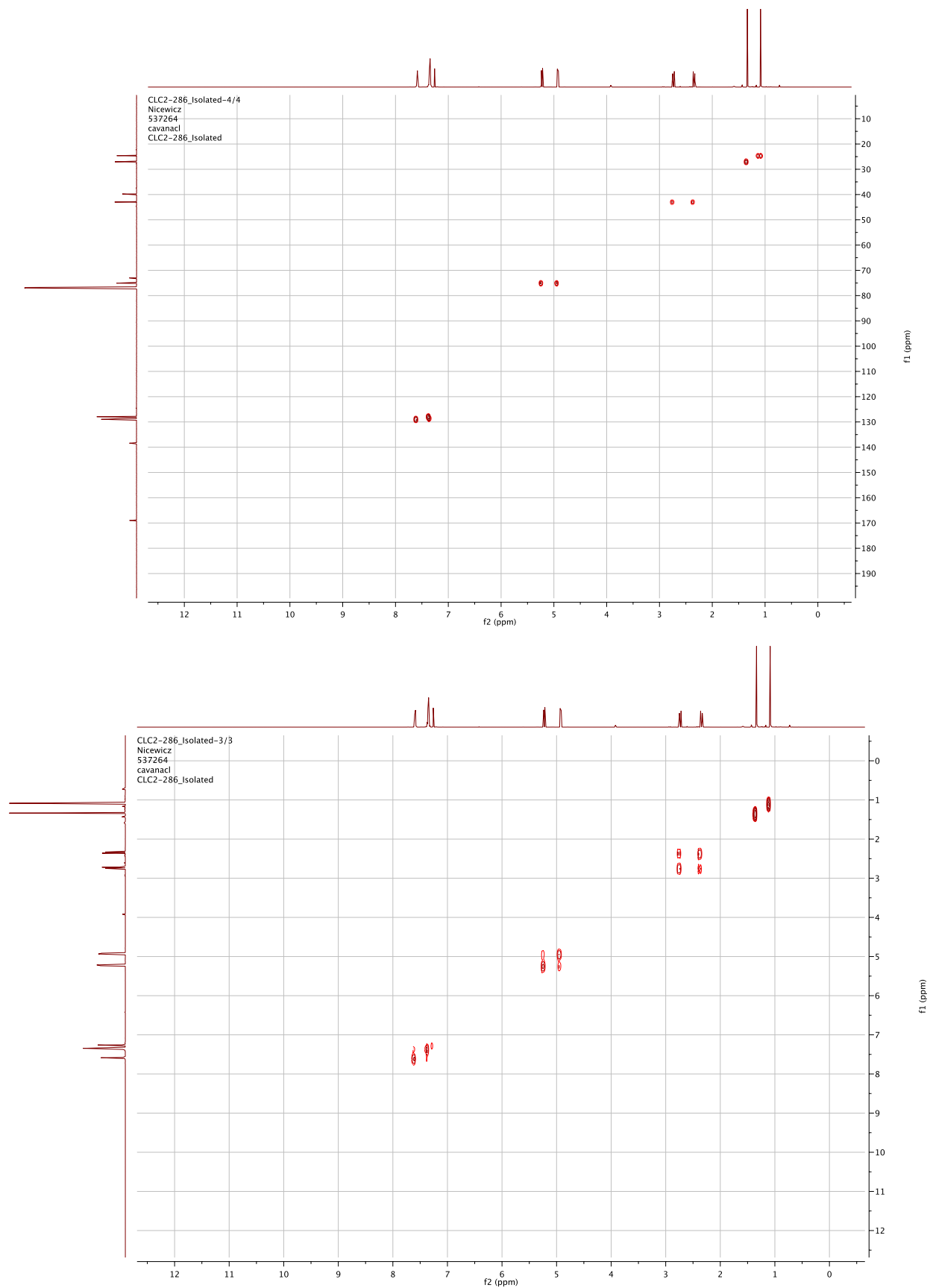
3.18

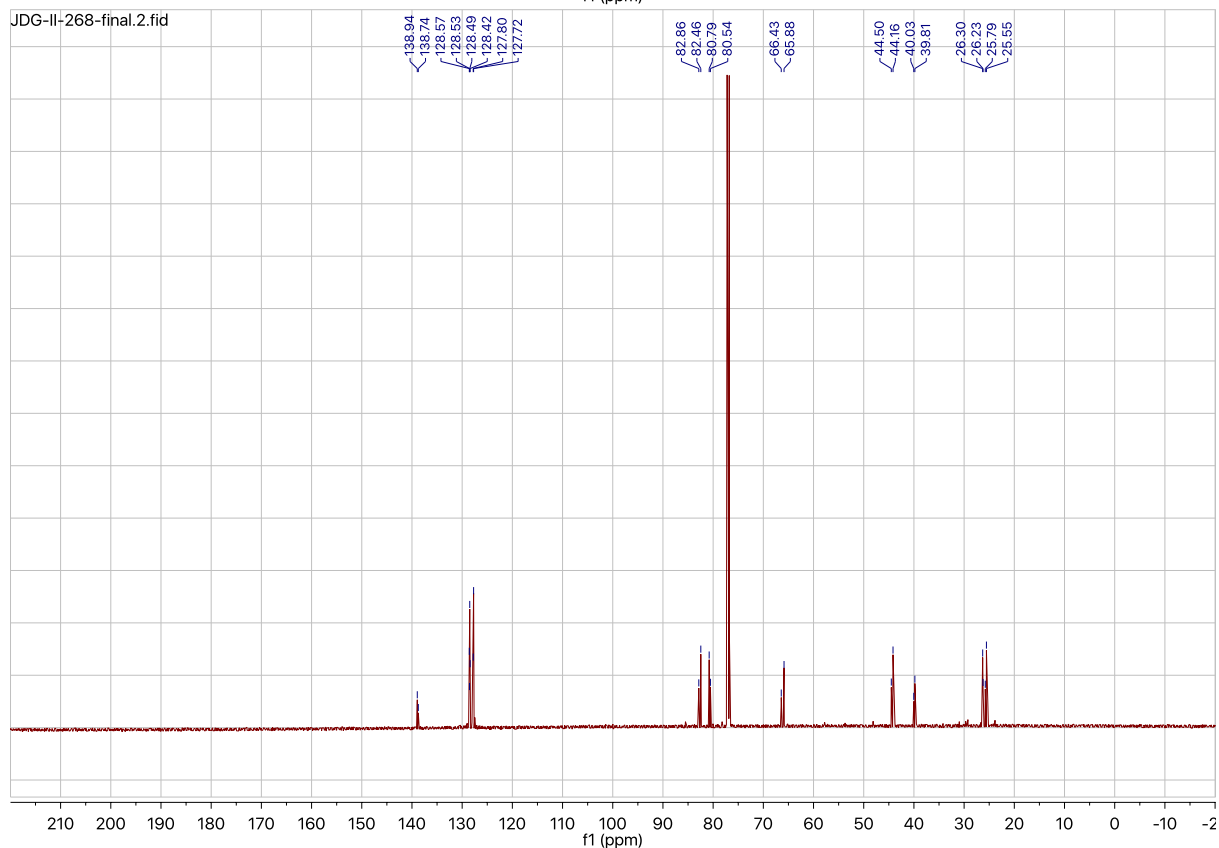
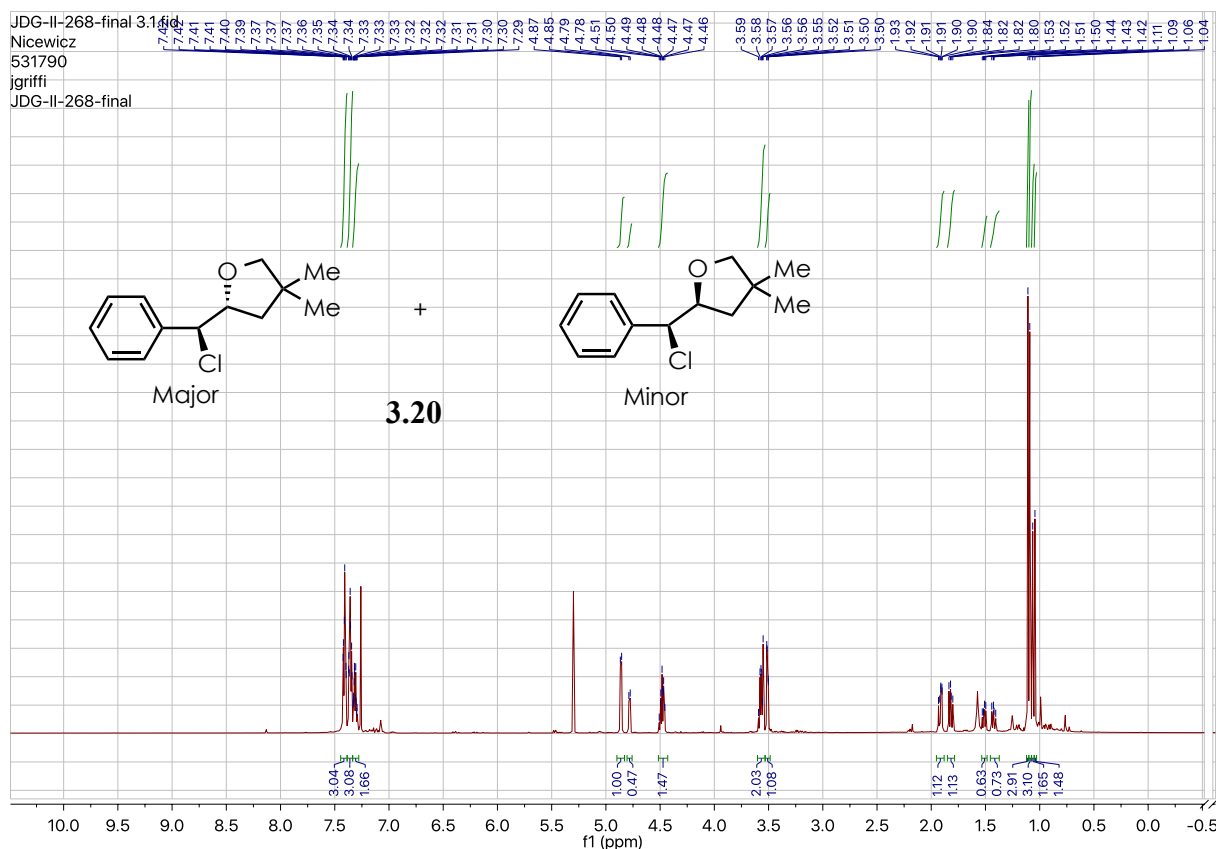


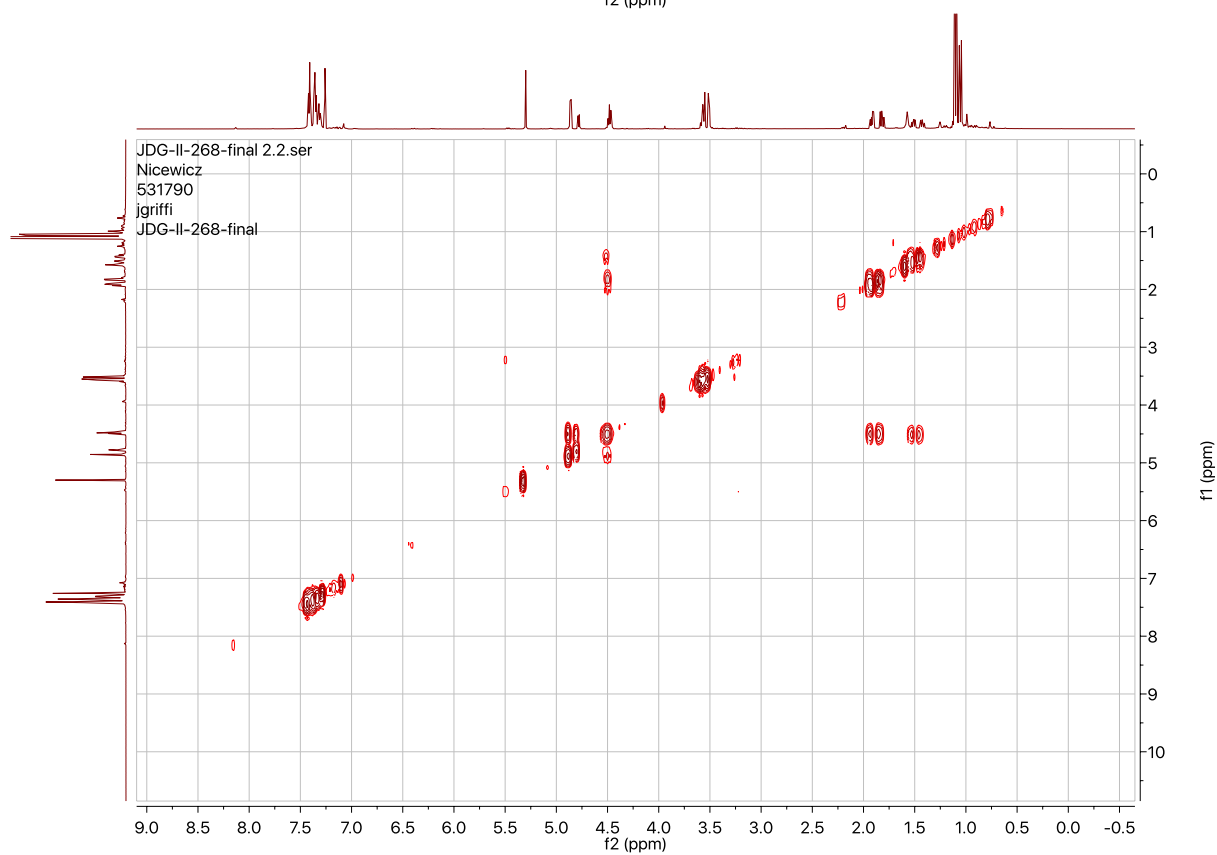
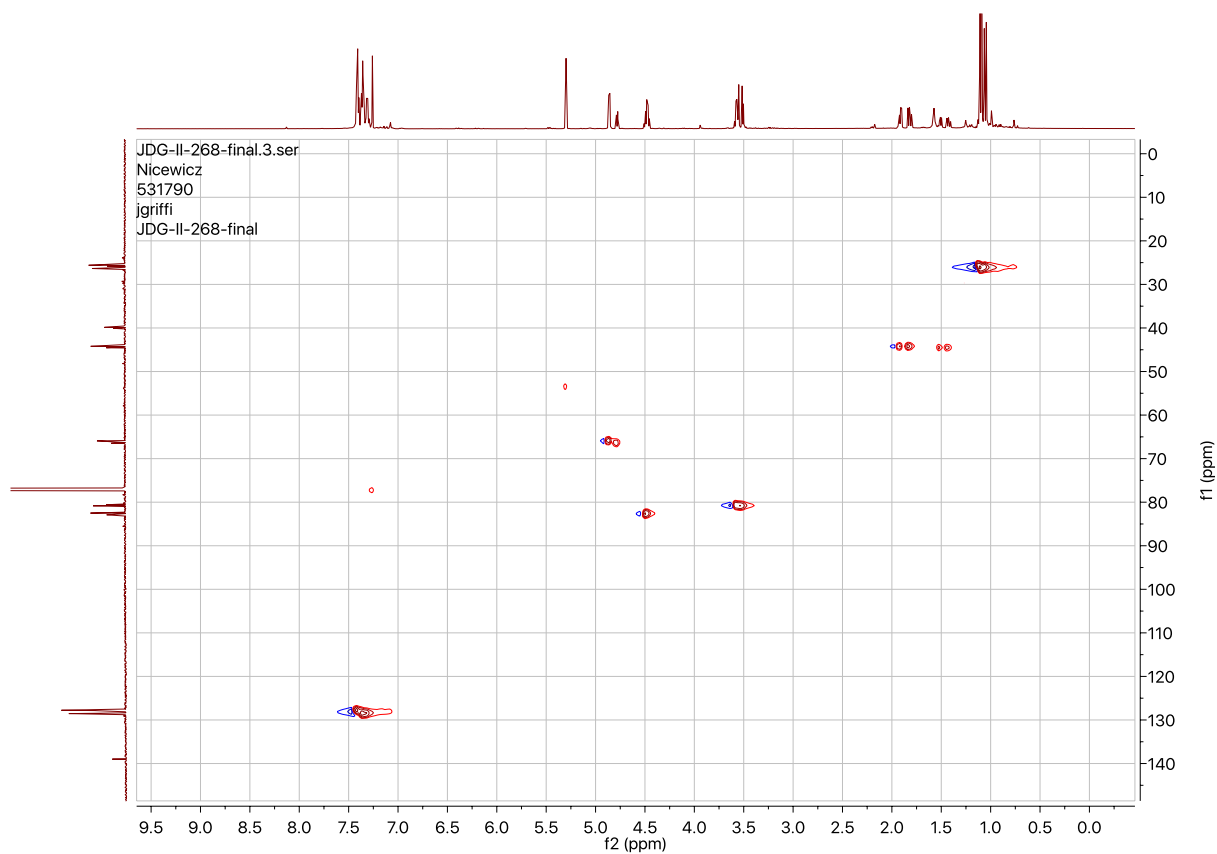


86_isolated/1
z
.
.
86_isolated

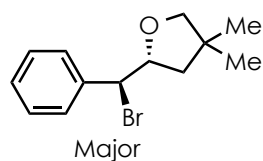




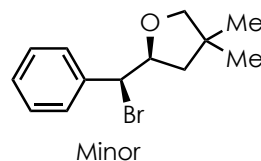




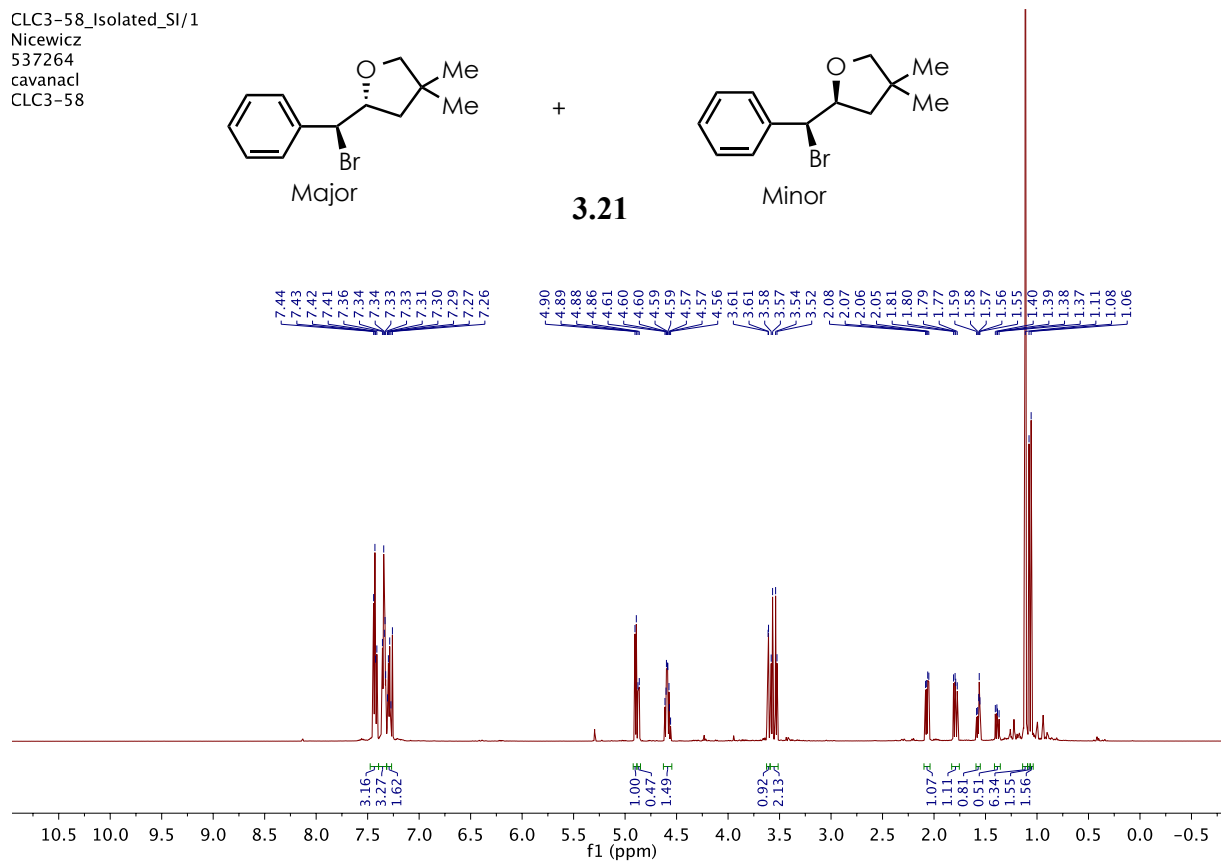
CLC3-58_Isolated_SI/1
 Nicewicz
 537264
 cavanacI
 CLC3-58



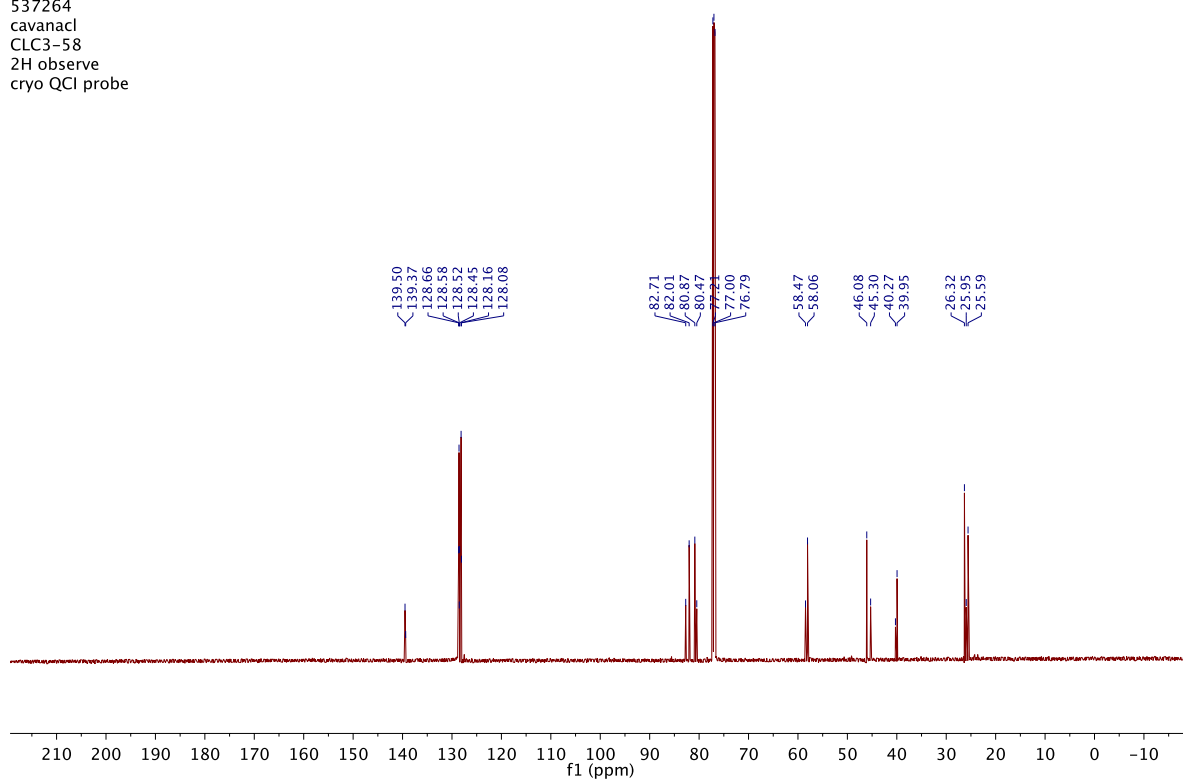
+

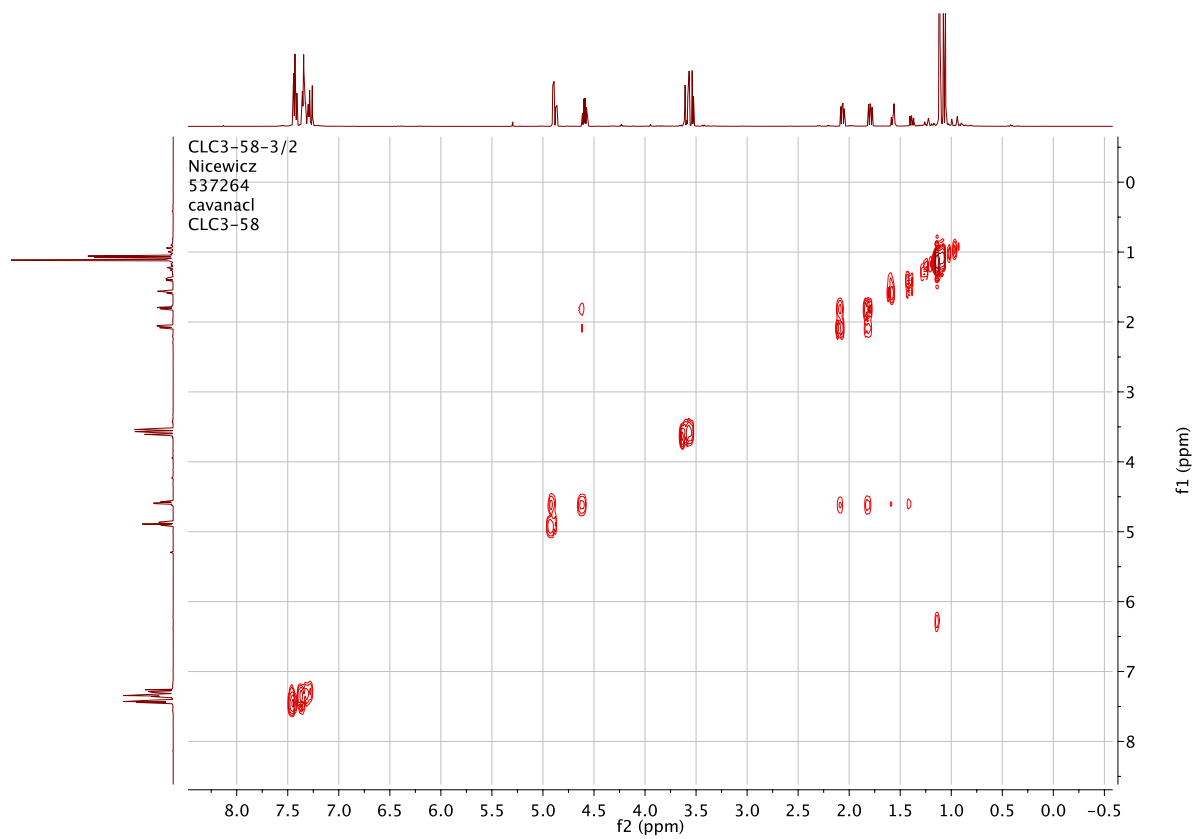
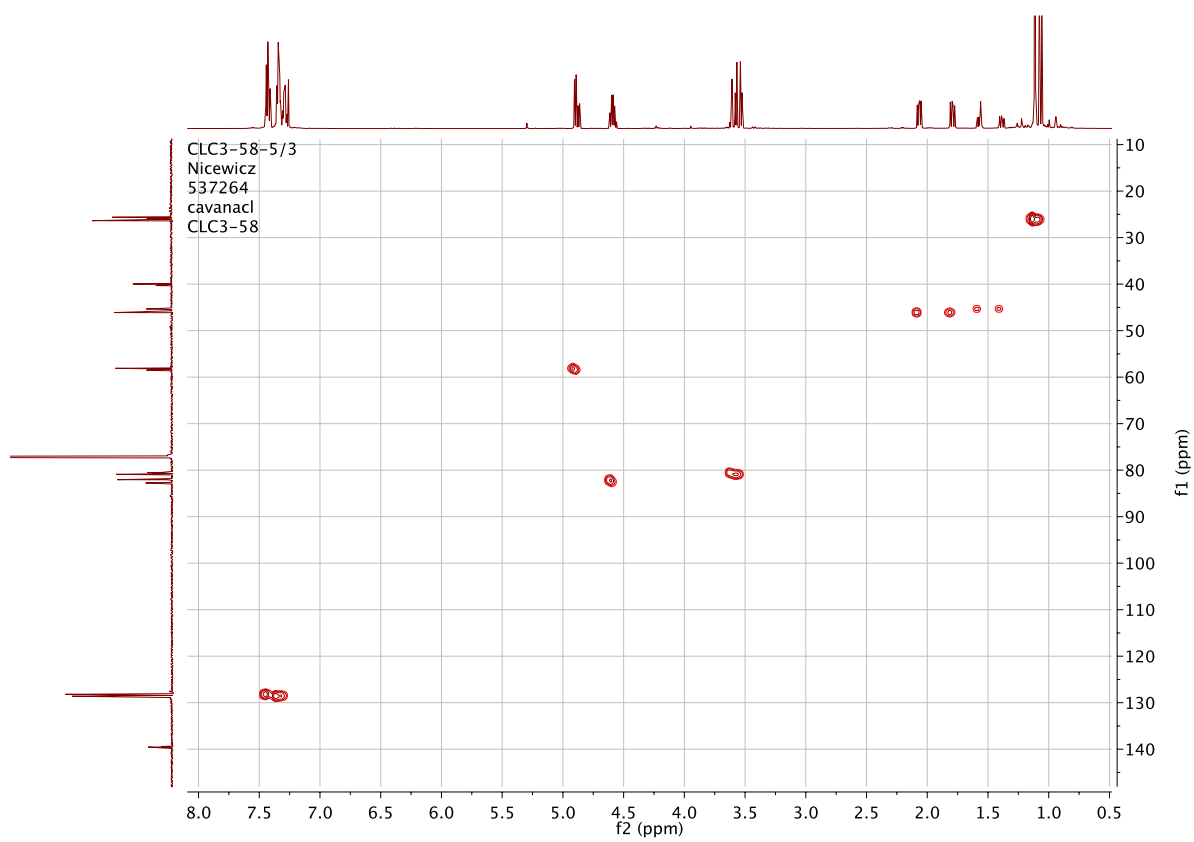


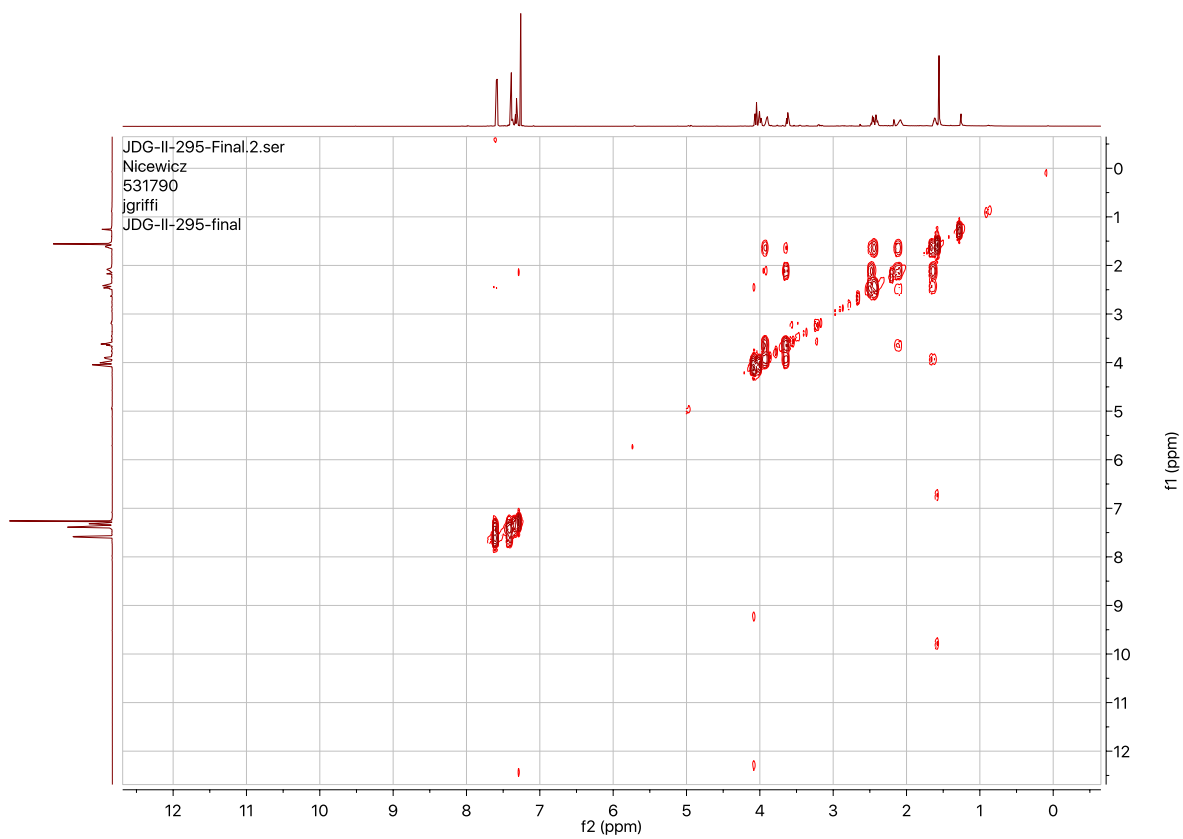
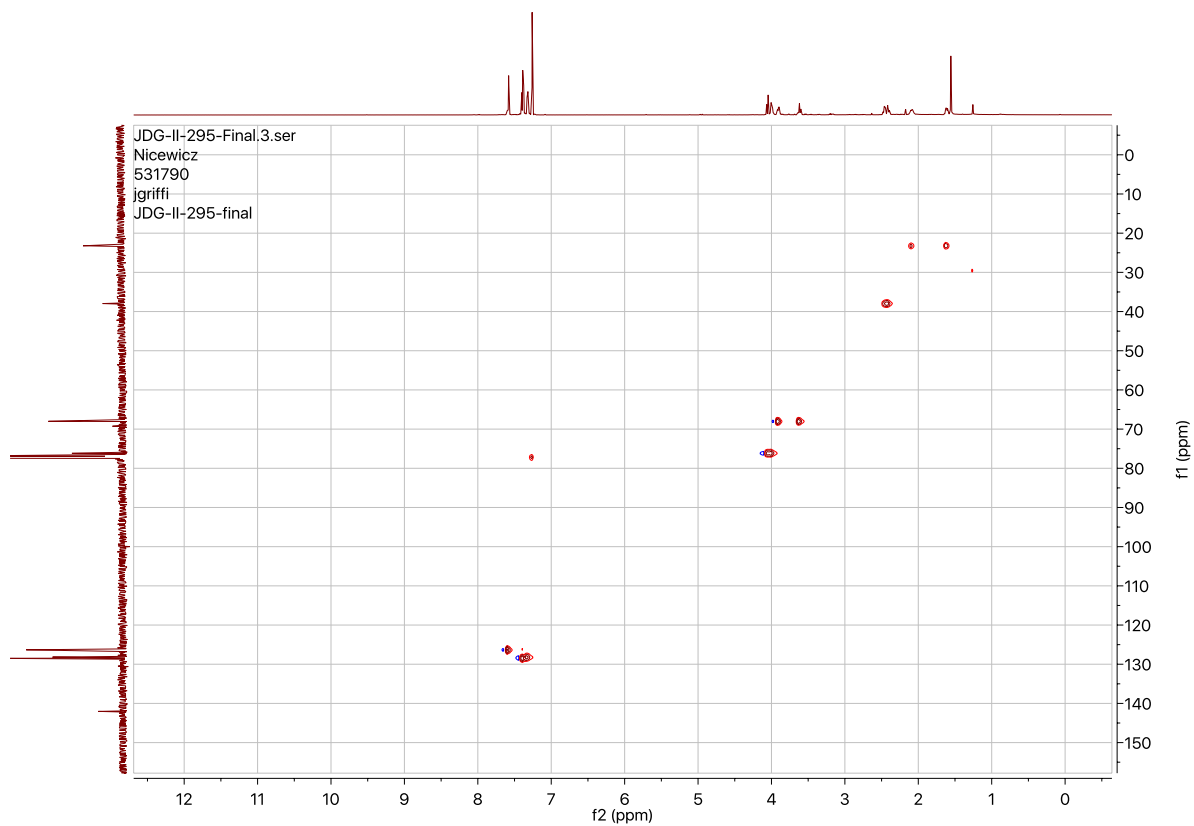
3.21



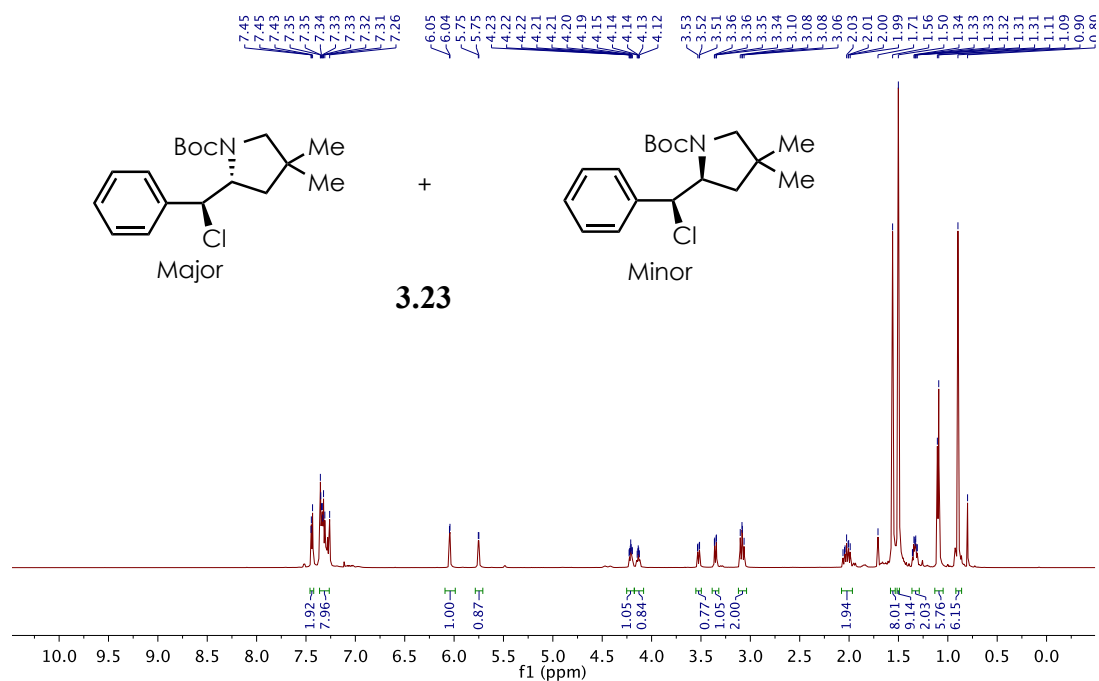
CLC3-58-6/5
 Nicewicz
 537264
 cavanacI
 CLC3-58
 2H observe
 cryo QCI probe



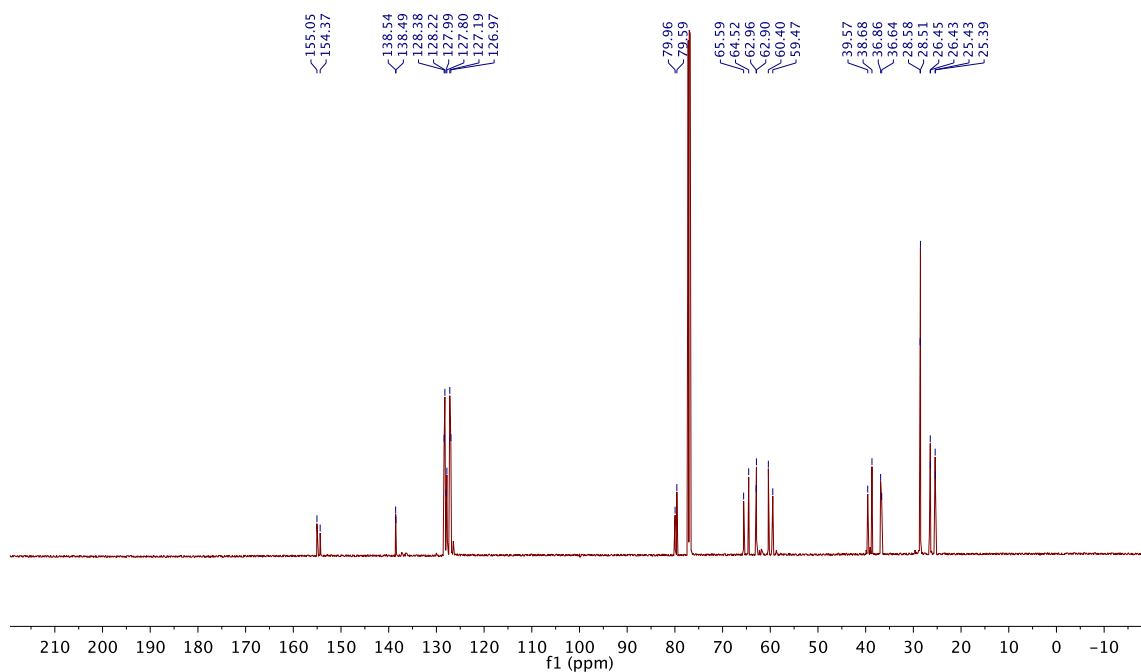


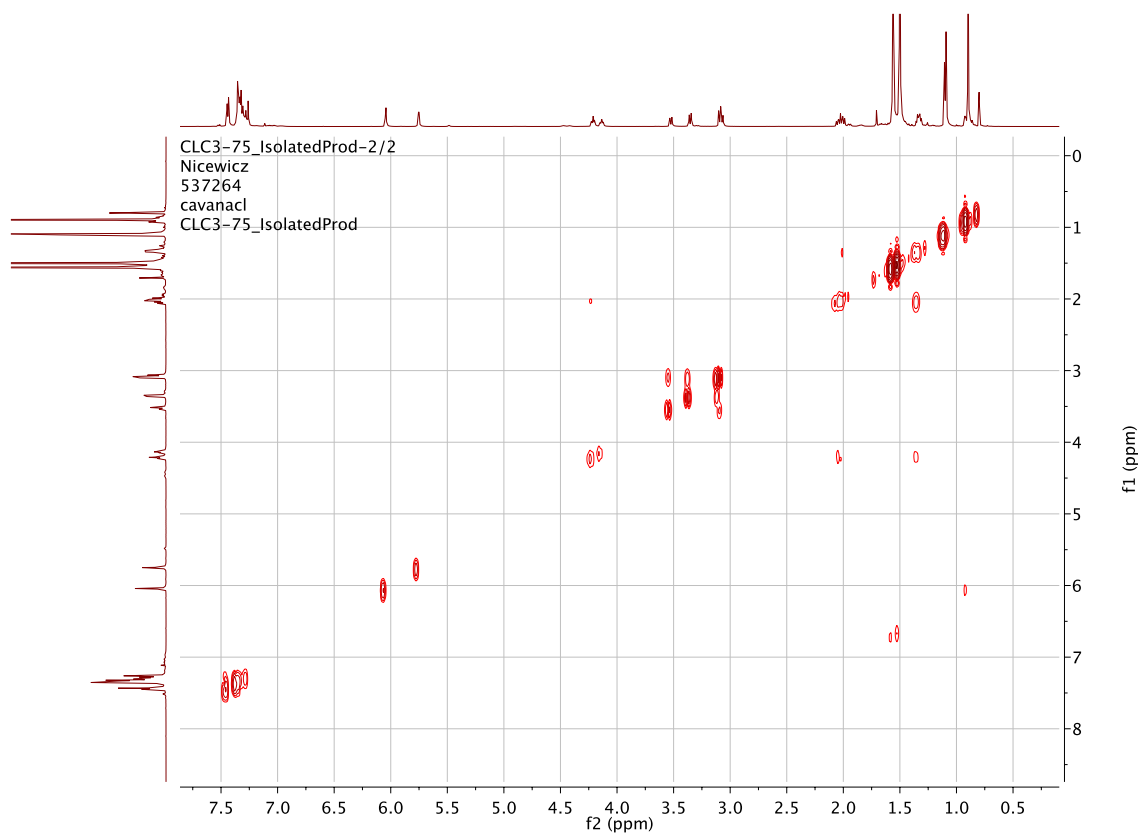
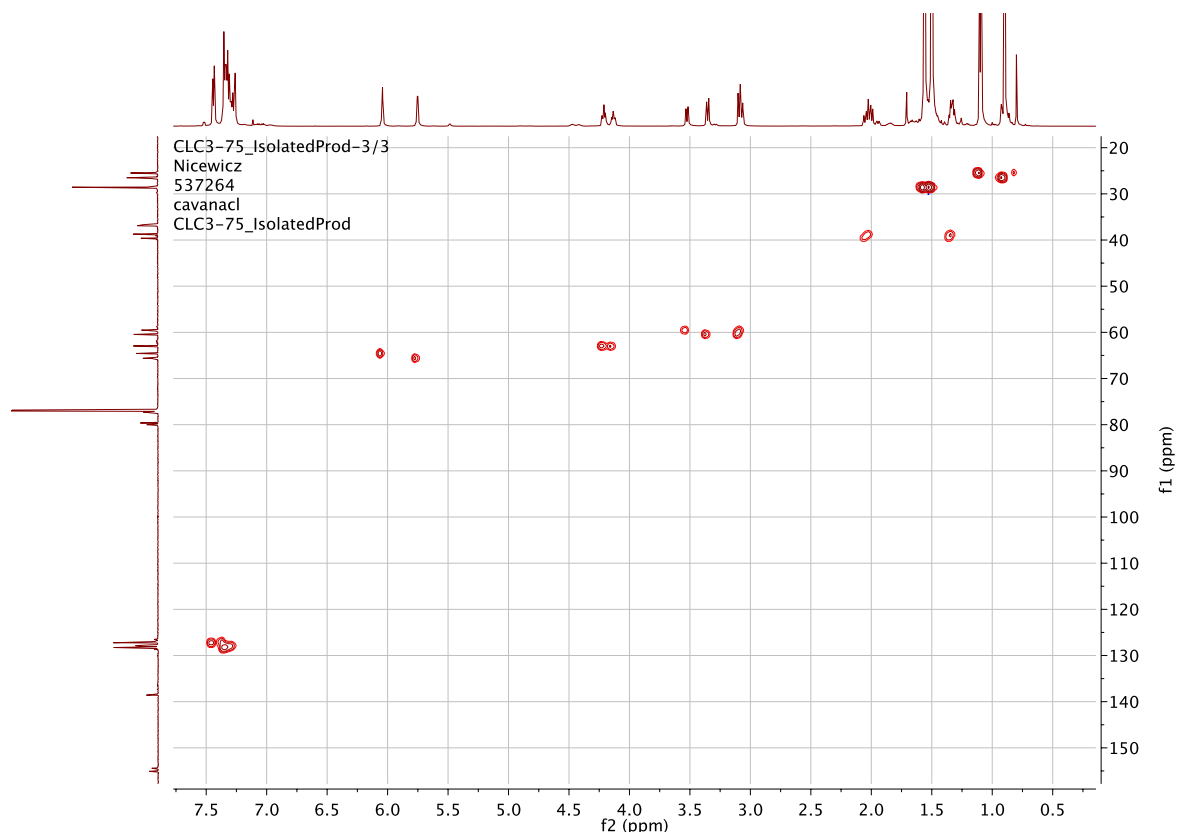


CLC3-75_IsolatedProd/1
 Nicewicz
 537264
 cavanacl
 CLC3-75_IsolatedProd

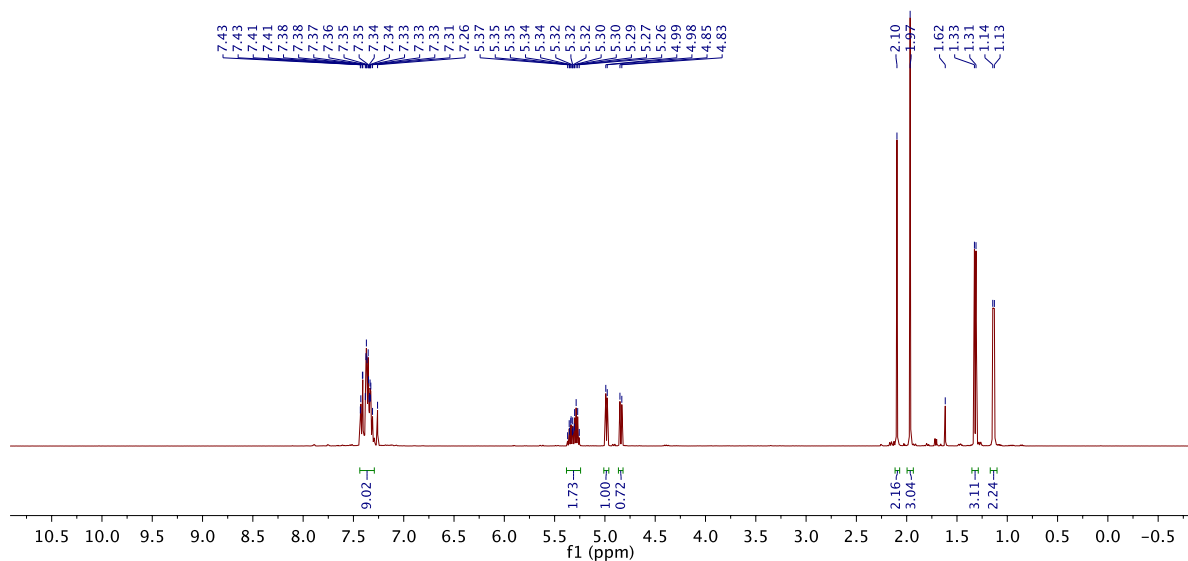


CLC3-75_IsolatedProd-4/4
 Nicewicz
 537264
 cavanacl
 CLC3-75_IsolatedProd
 2H observe
 cryo QCI probe

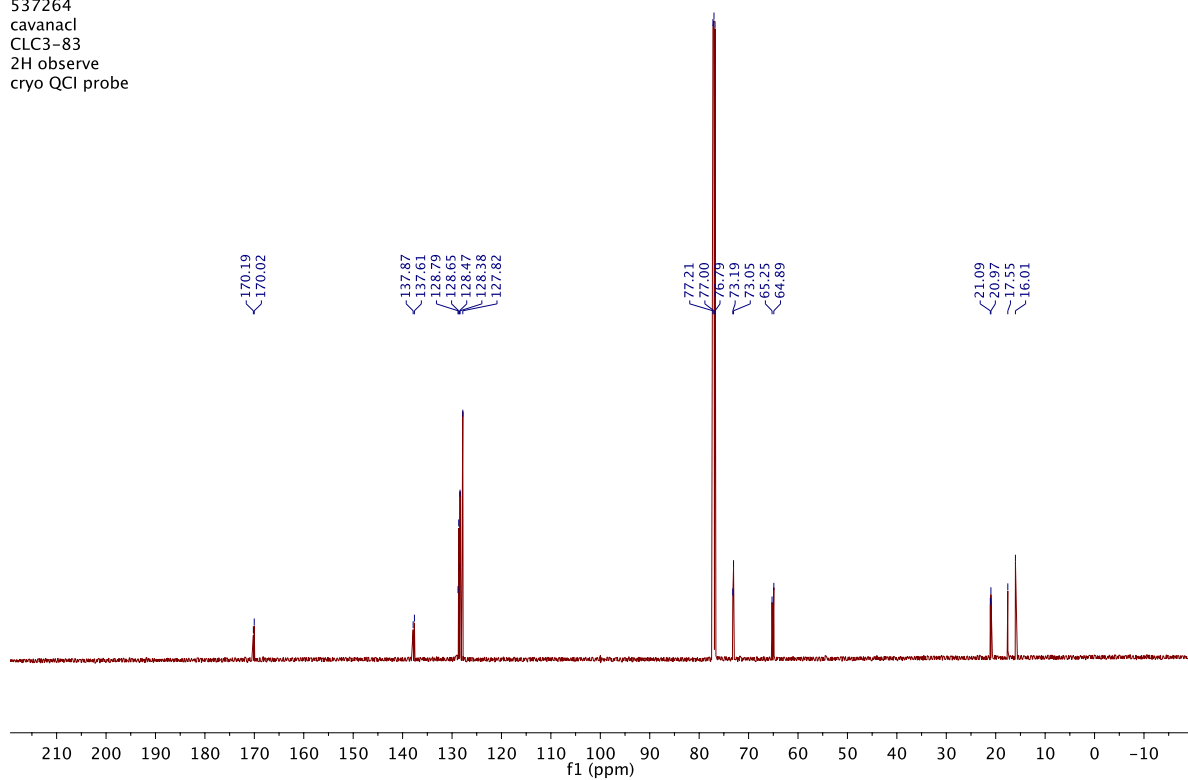


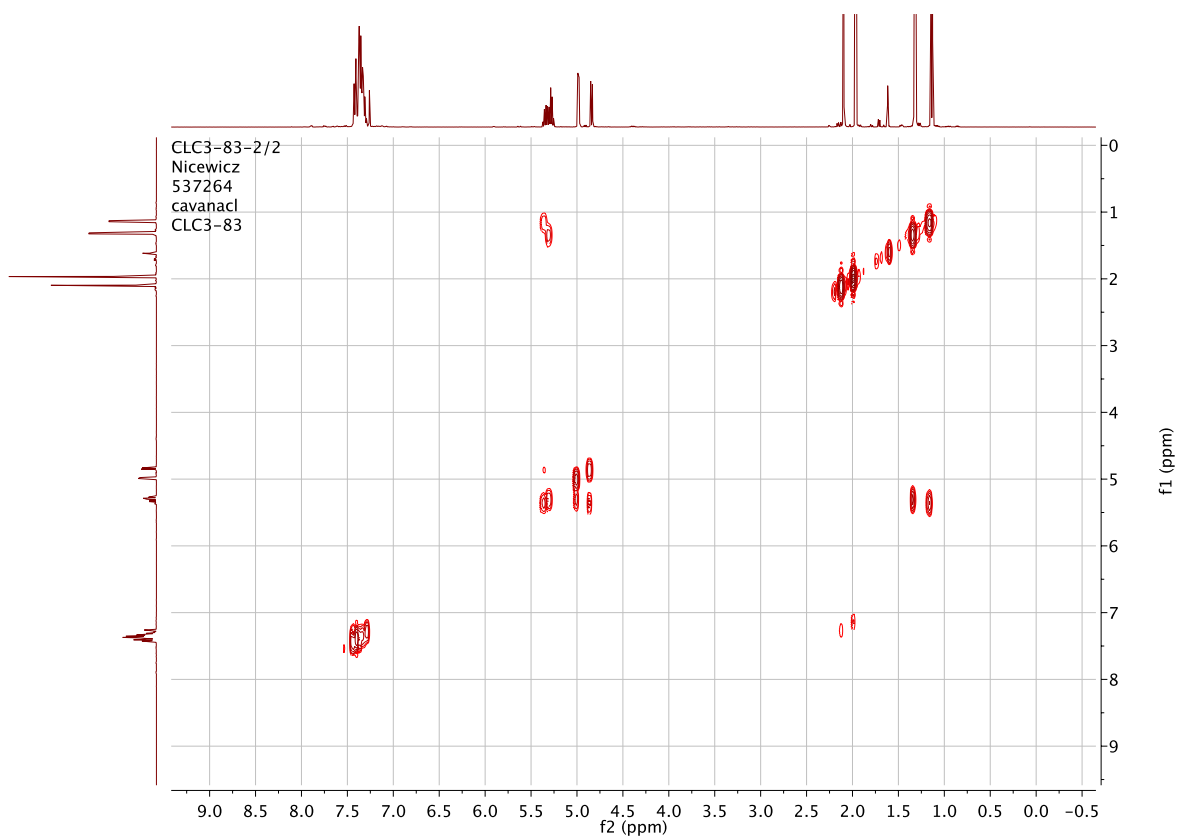
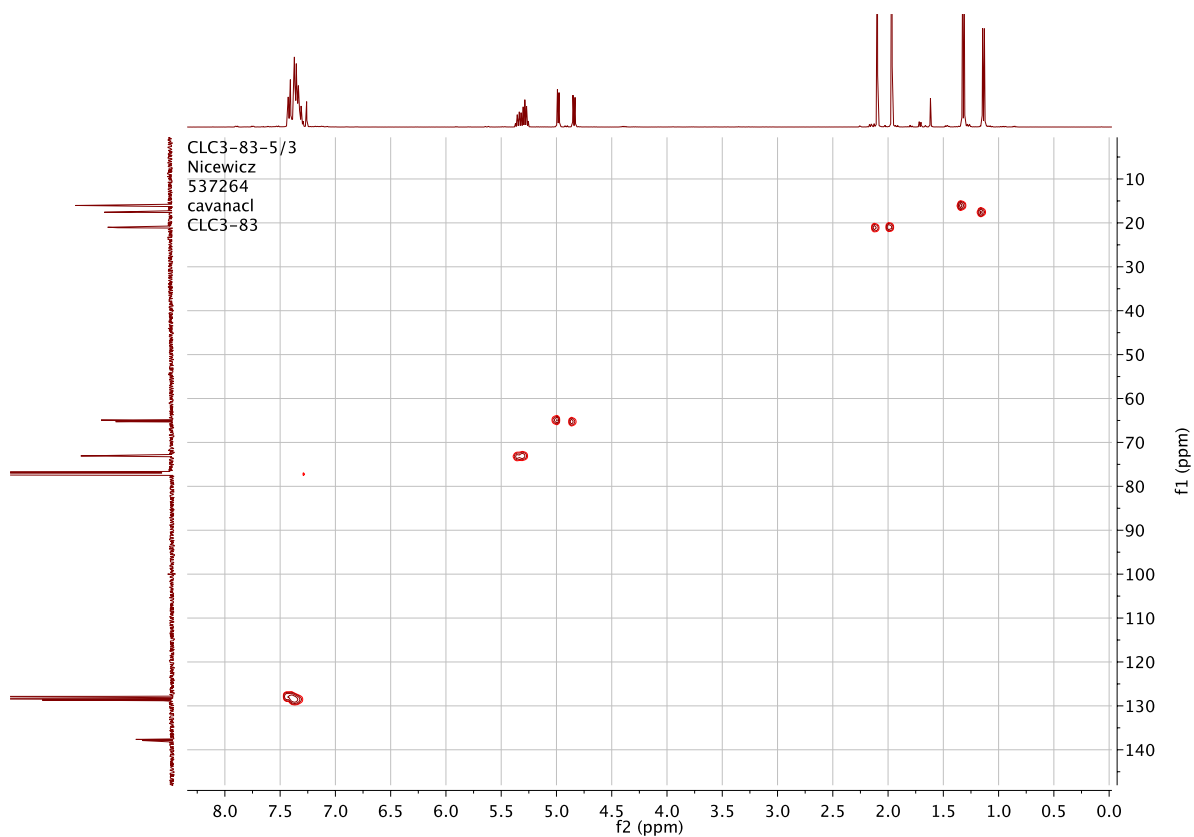


CLC3-83_Isolated/1
CLC3-83_Isolated

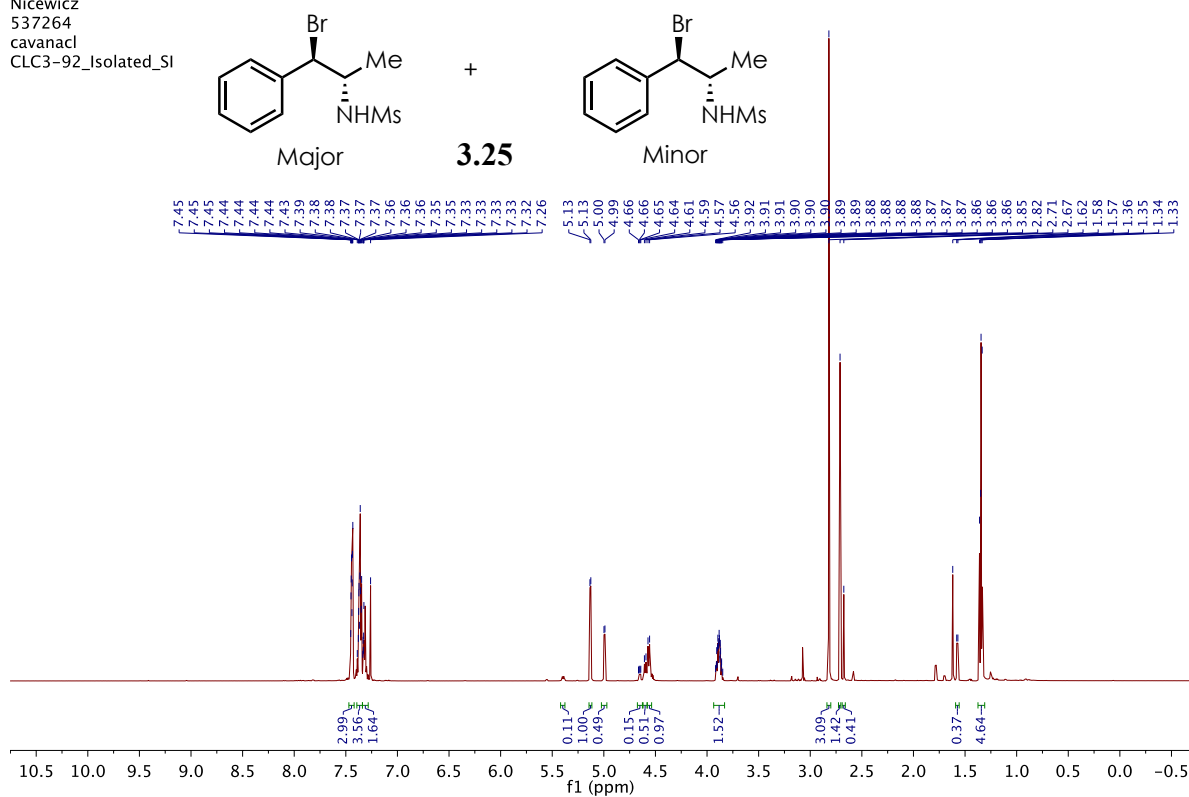


CLC3-83-4/5
Nicewicz
537264
cavanacI
CLC3-83
2H observe
cryo QCI probe

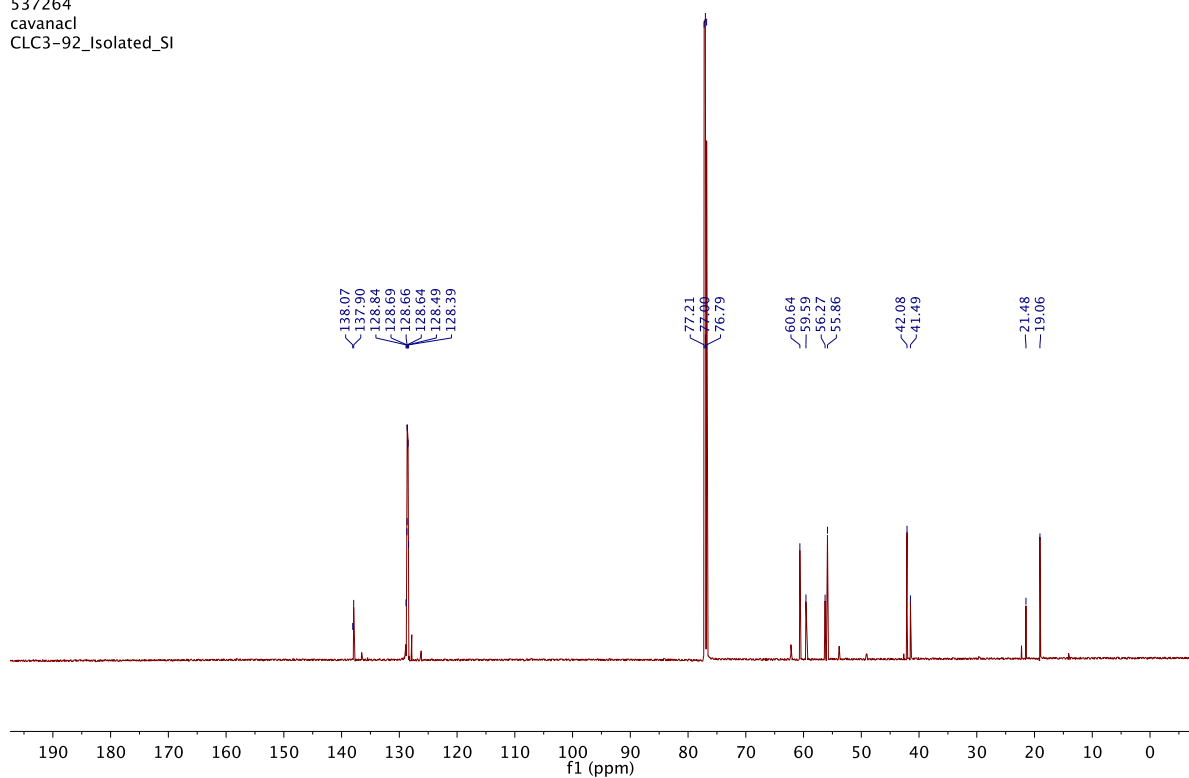


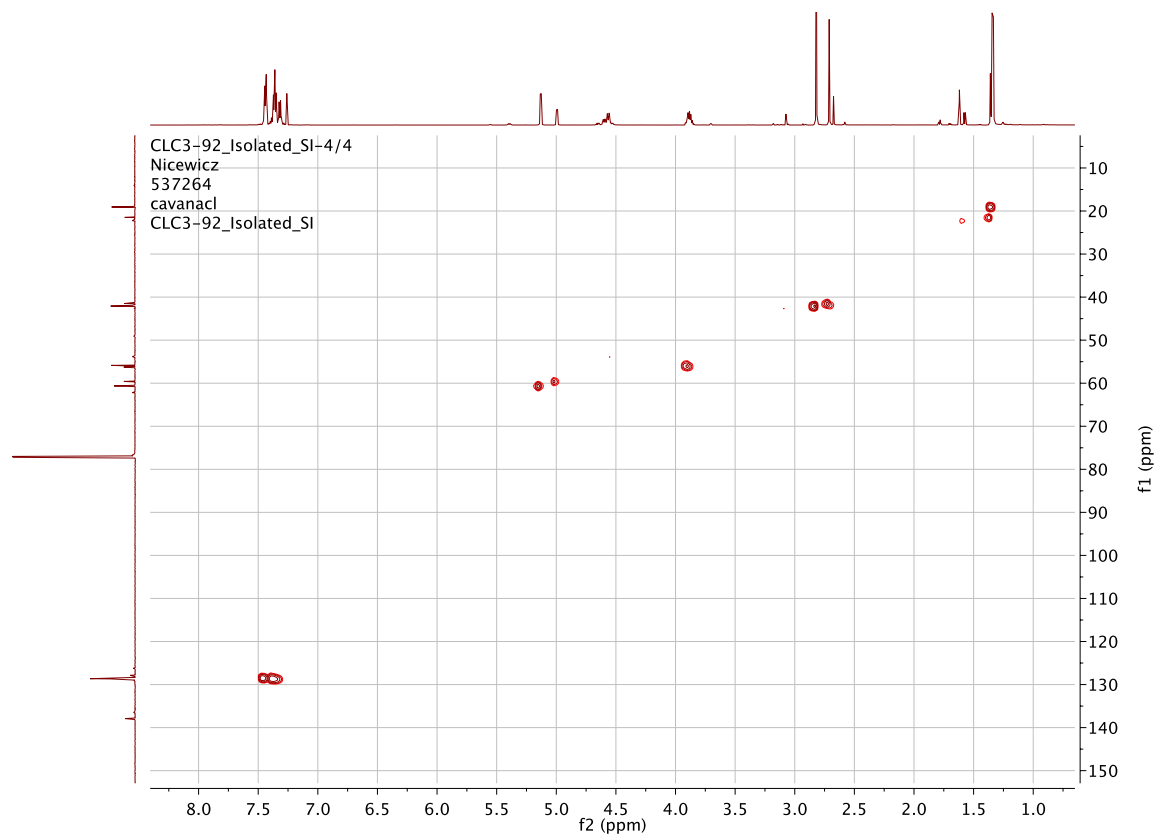
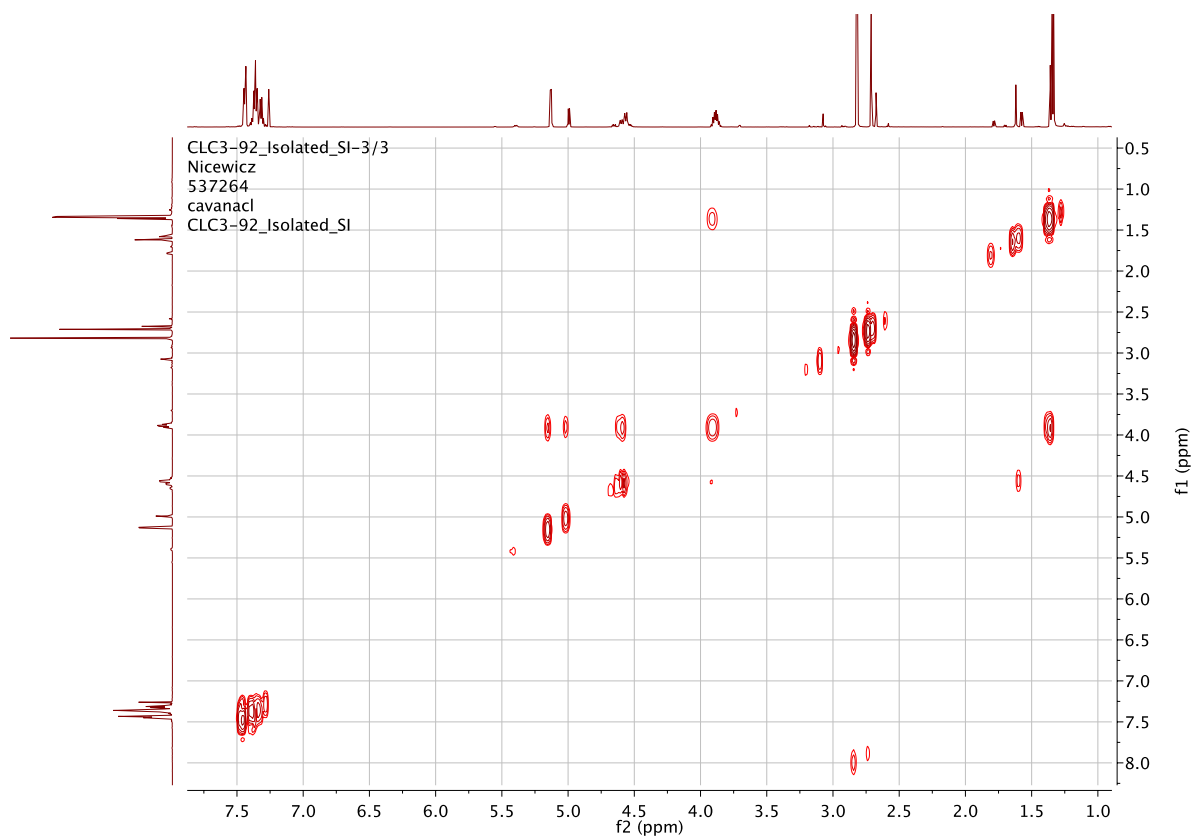


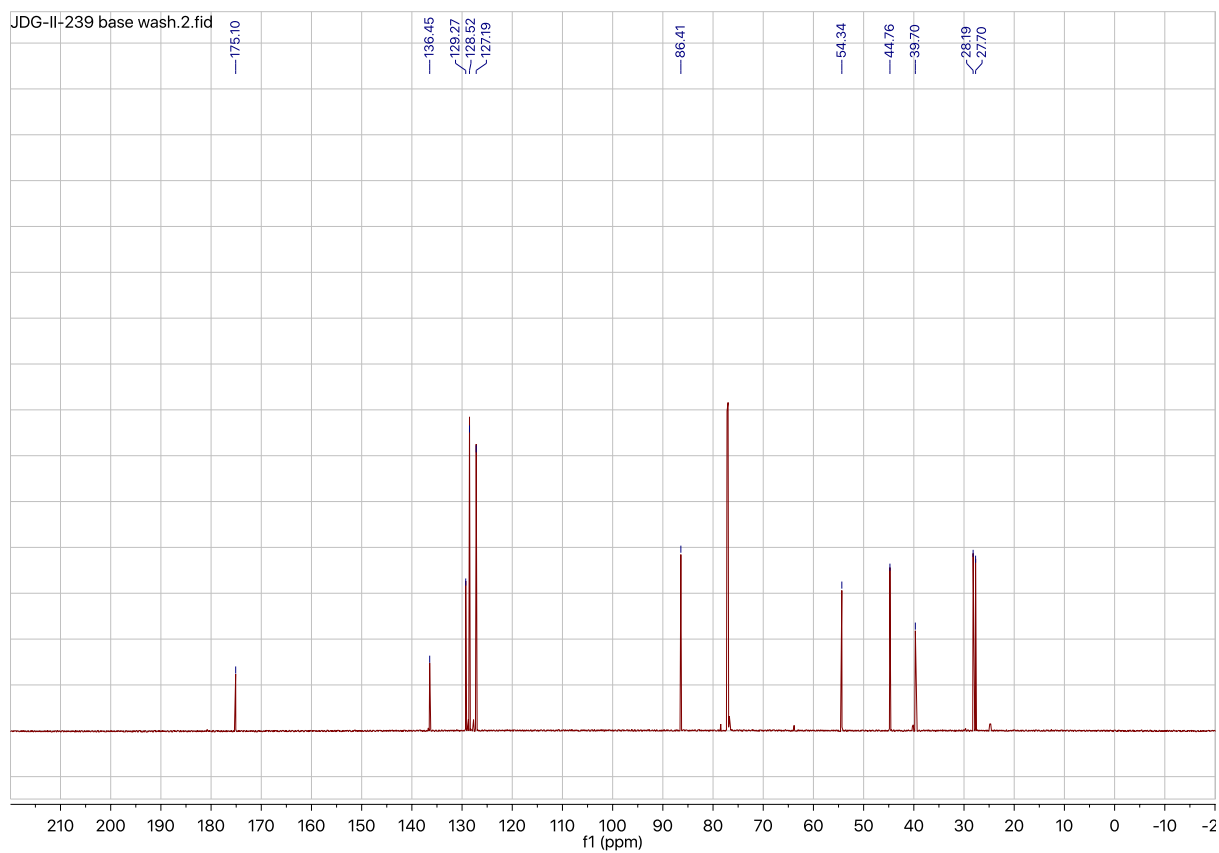
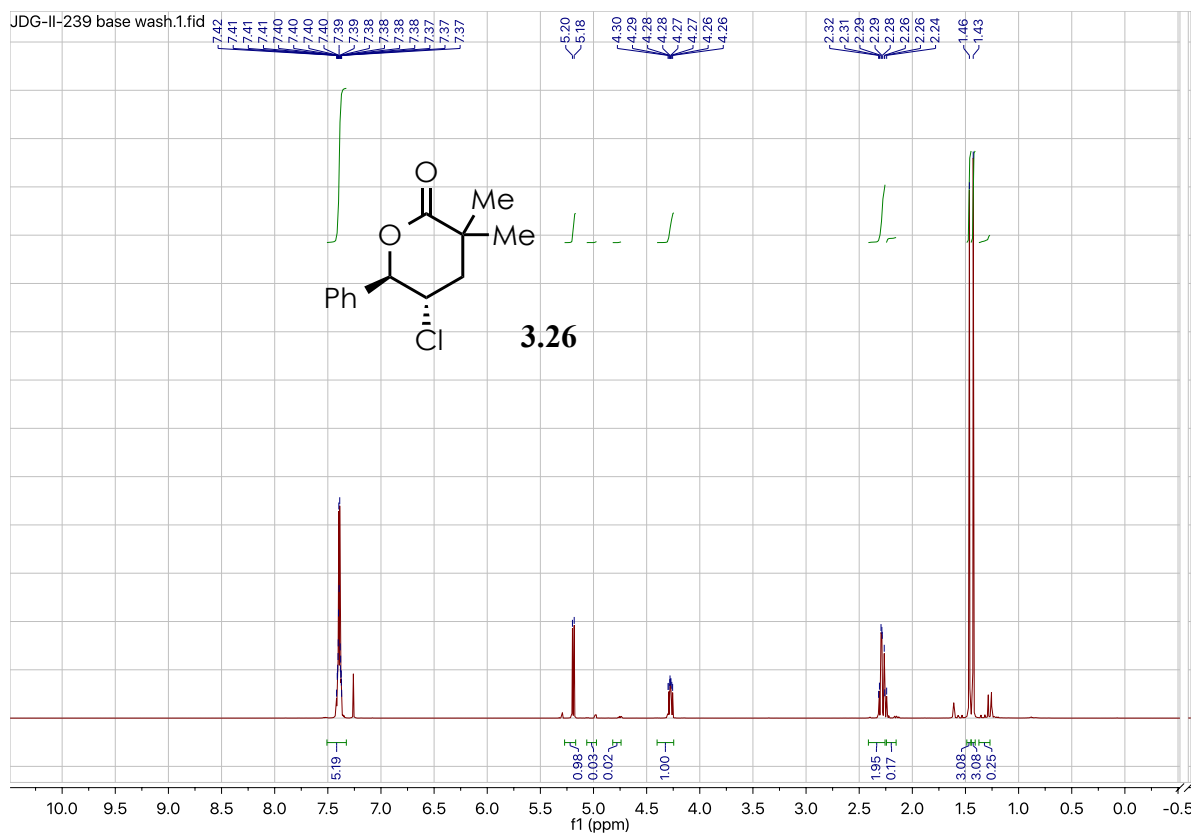
CLC3-92_Isolated_SI/1
 Nicewicz
 537264
 cavanac1
 CLC3-92_Isolated_SI

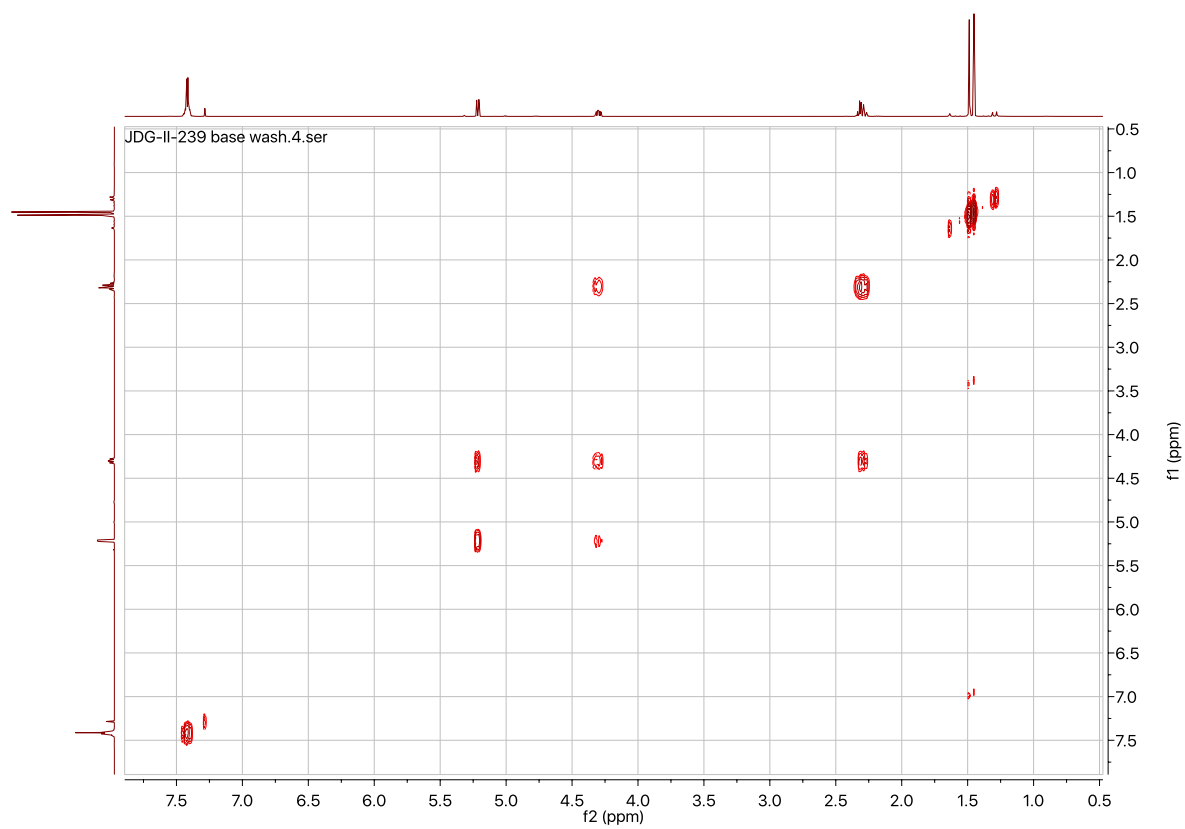
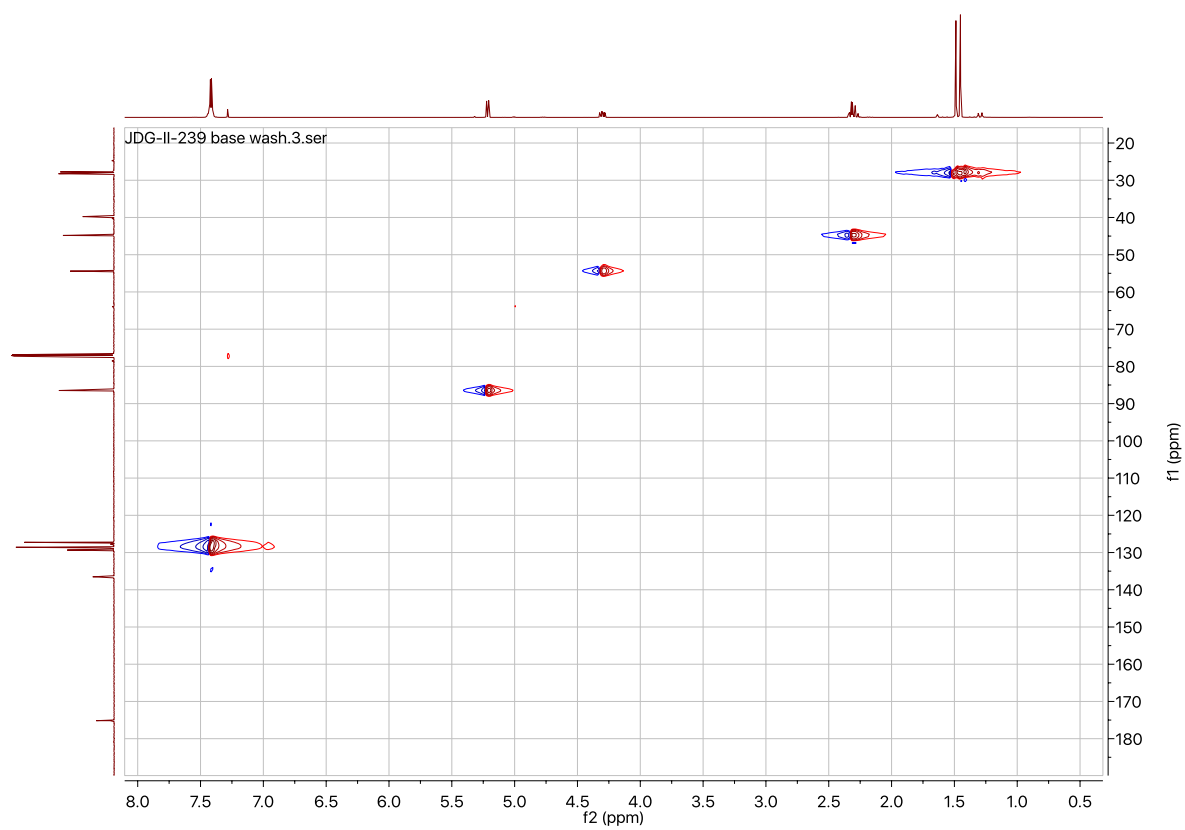


CLC3-92_Isolated_SI-2/2
 Nicewicz
 537264
 cavanac1
 CLC3-92_Isolated_SI

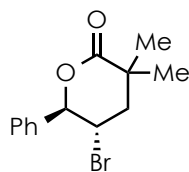




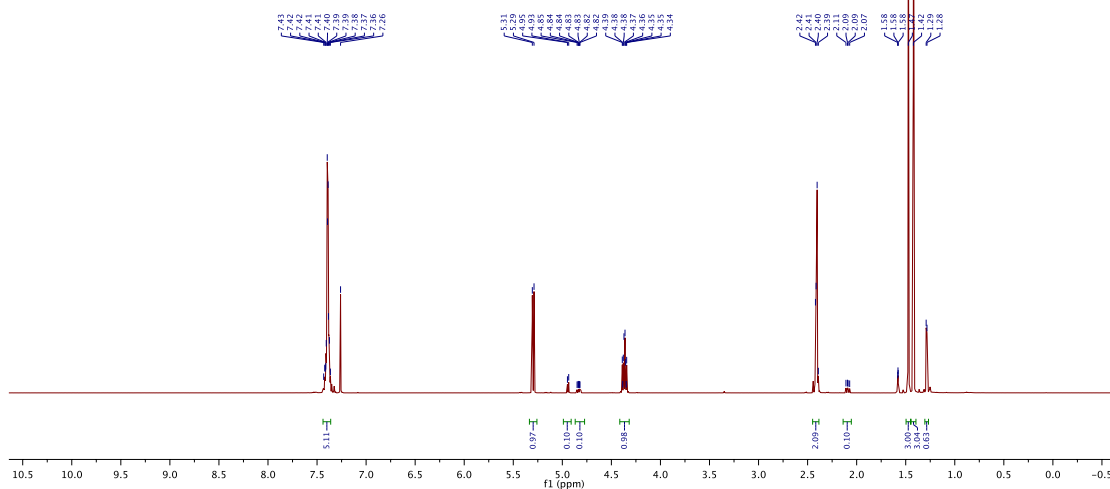




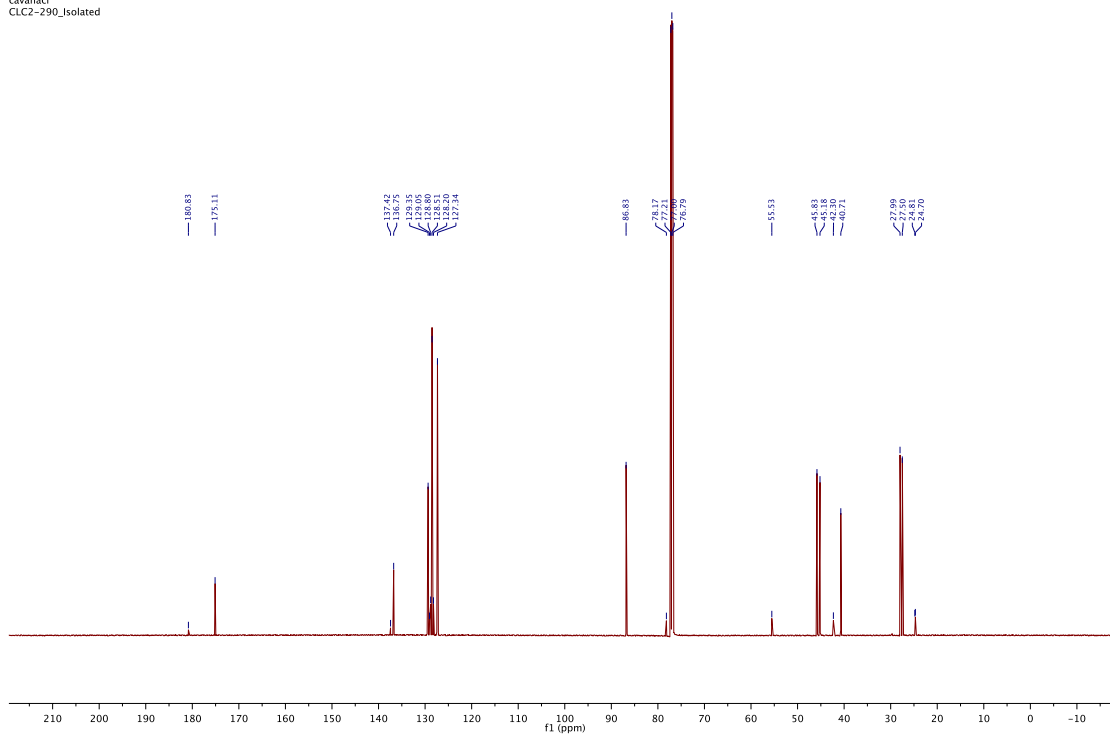
CLC2-290_Isolated/1
 Nicewicz
 537264
 cavanaci
 CLC2-290_Isolated

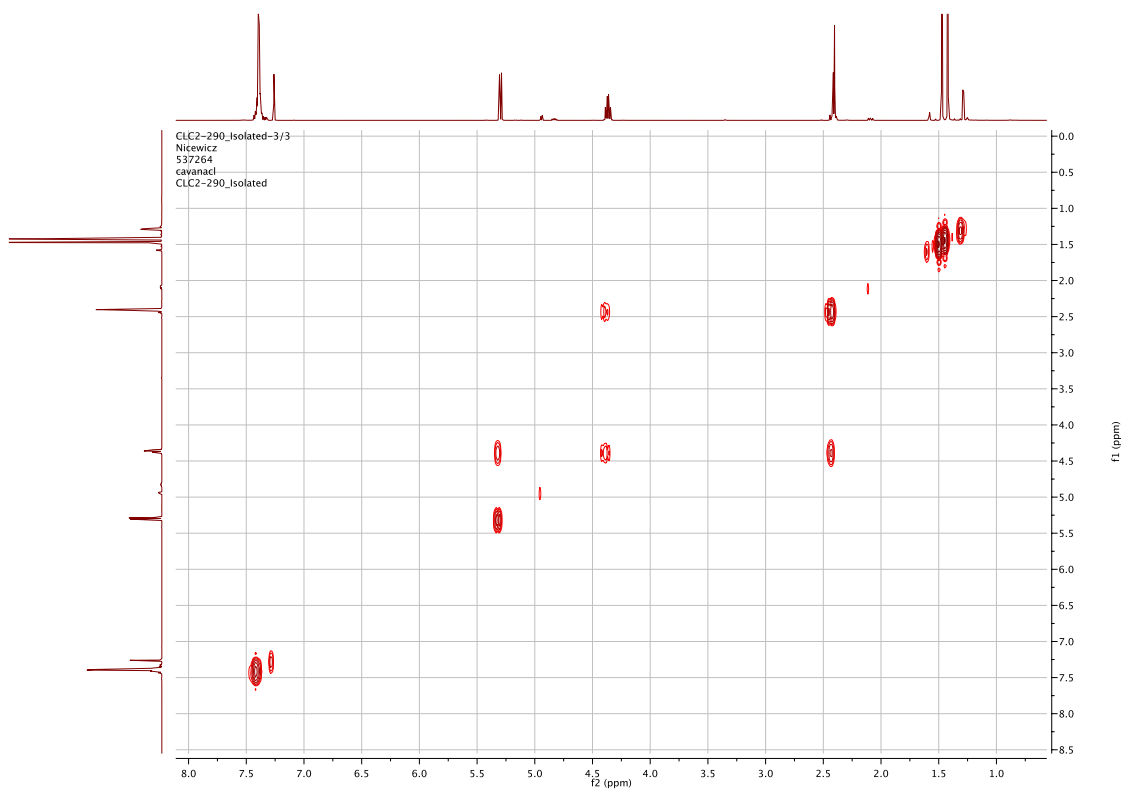
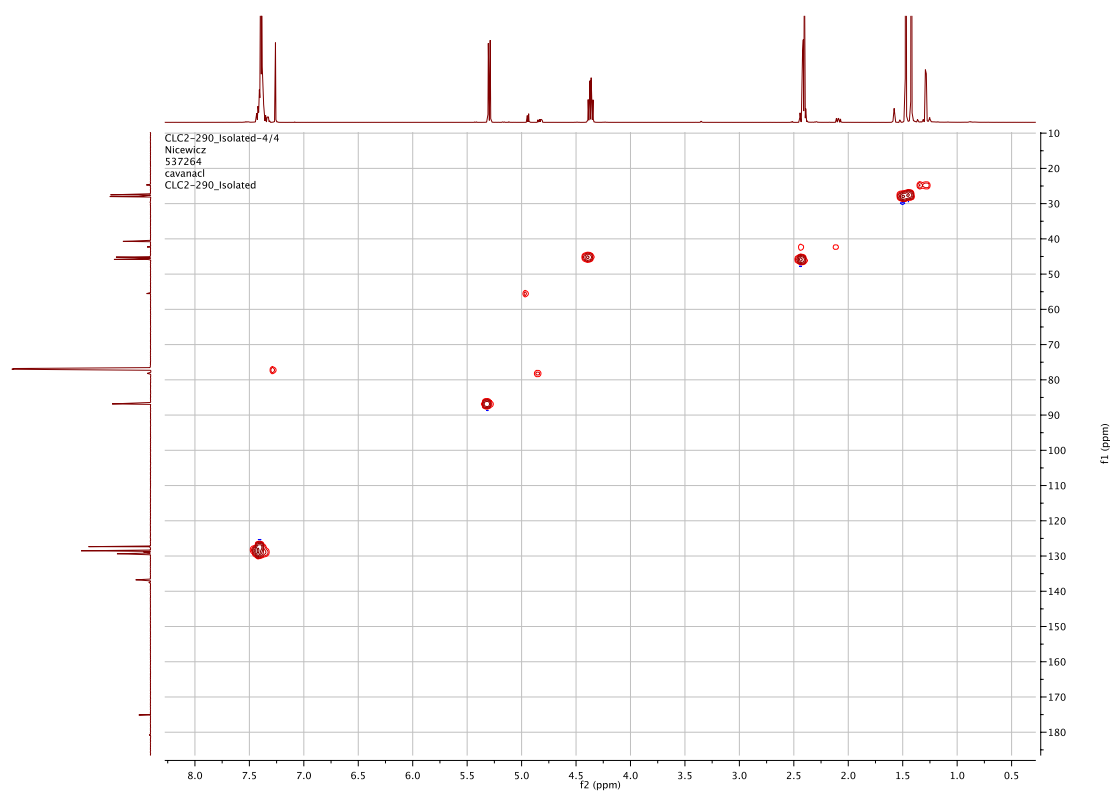


3.27

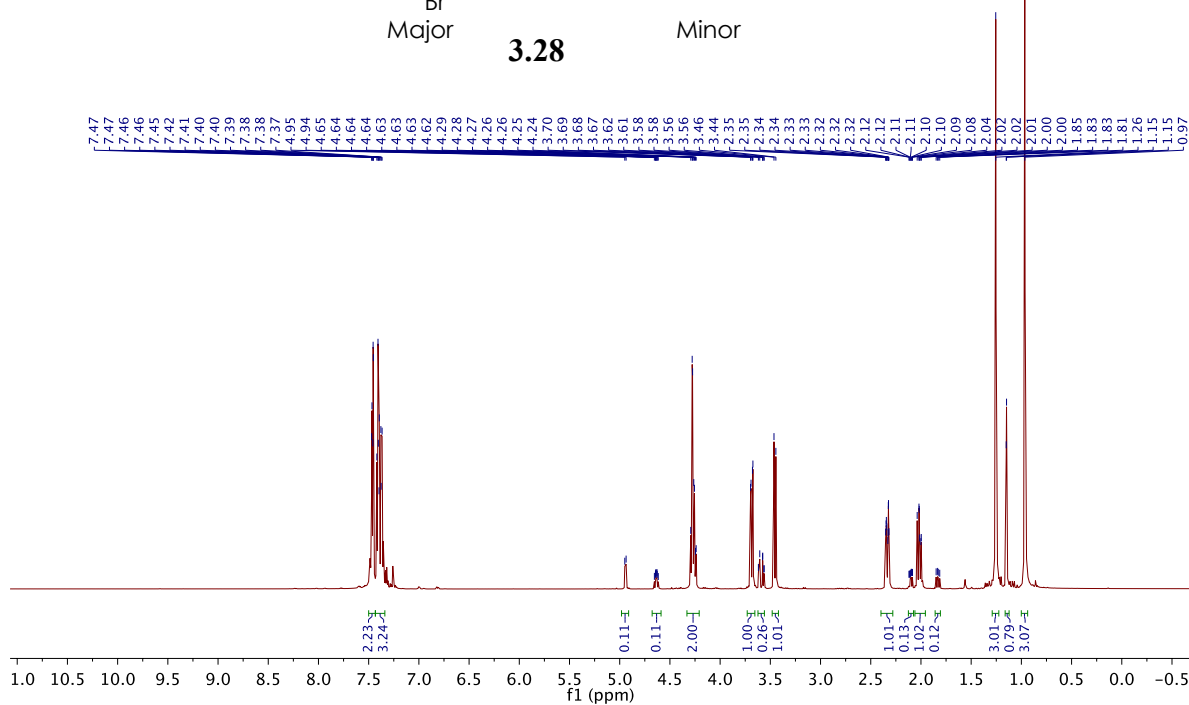
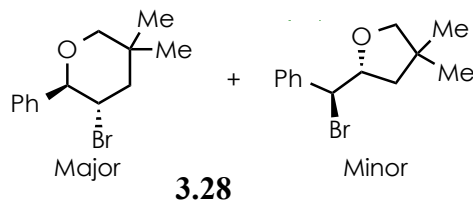


CLC2-290_Isolated-2/2
 Nicewicz
 537264
 cavanaci
 CLC2-290_Isolated

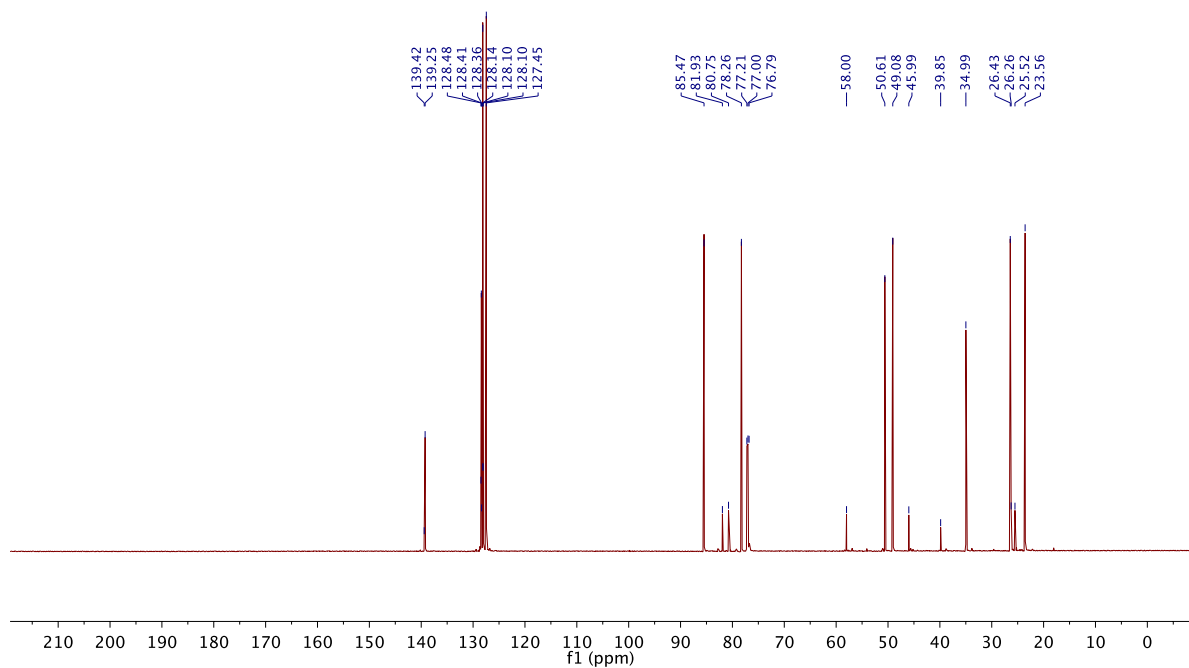


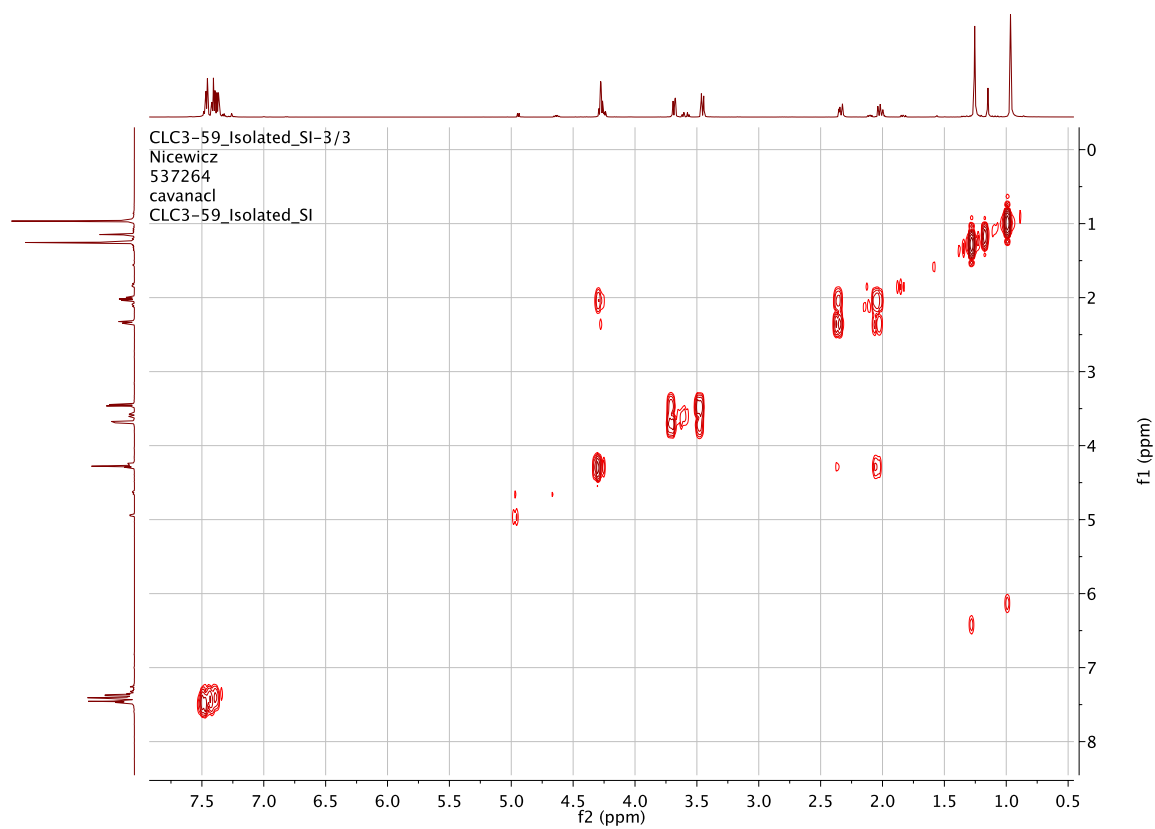
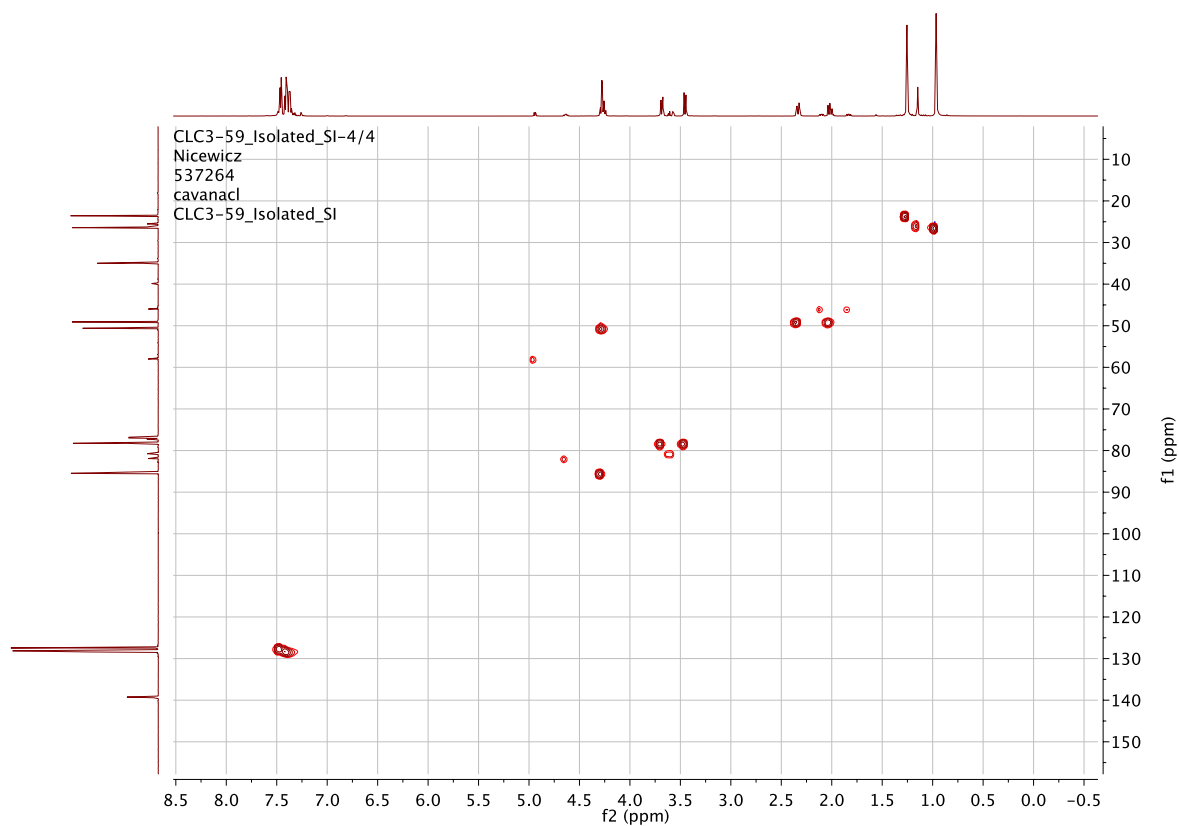


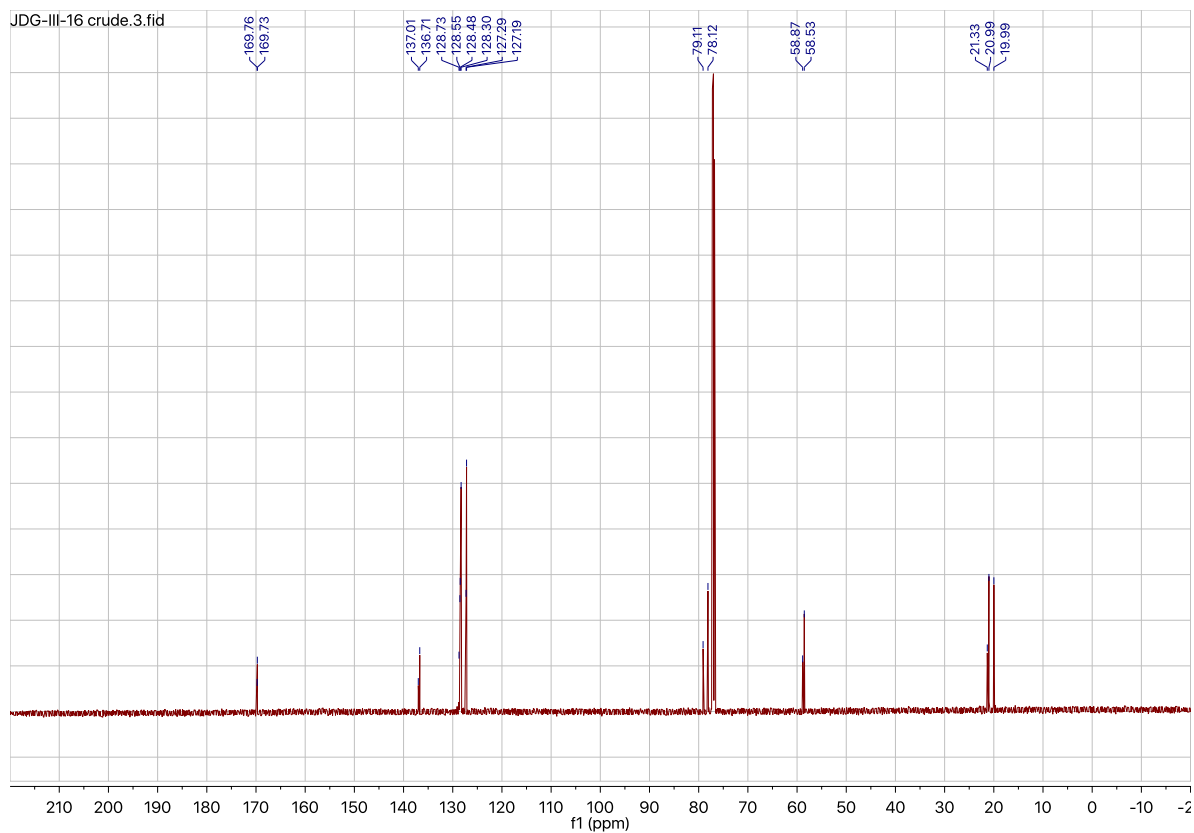
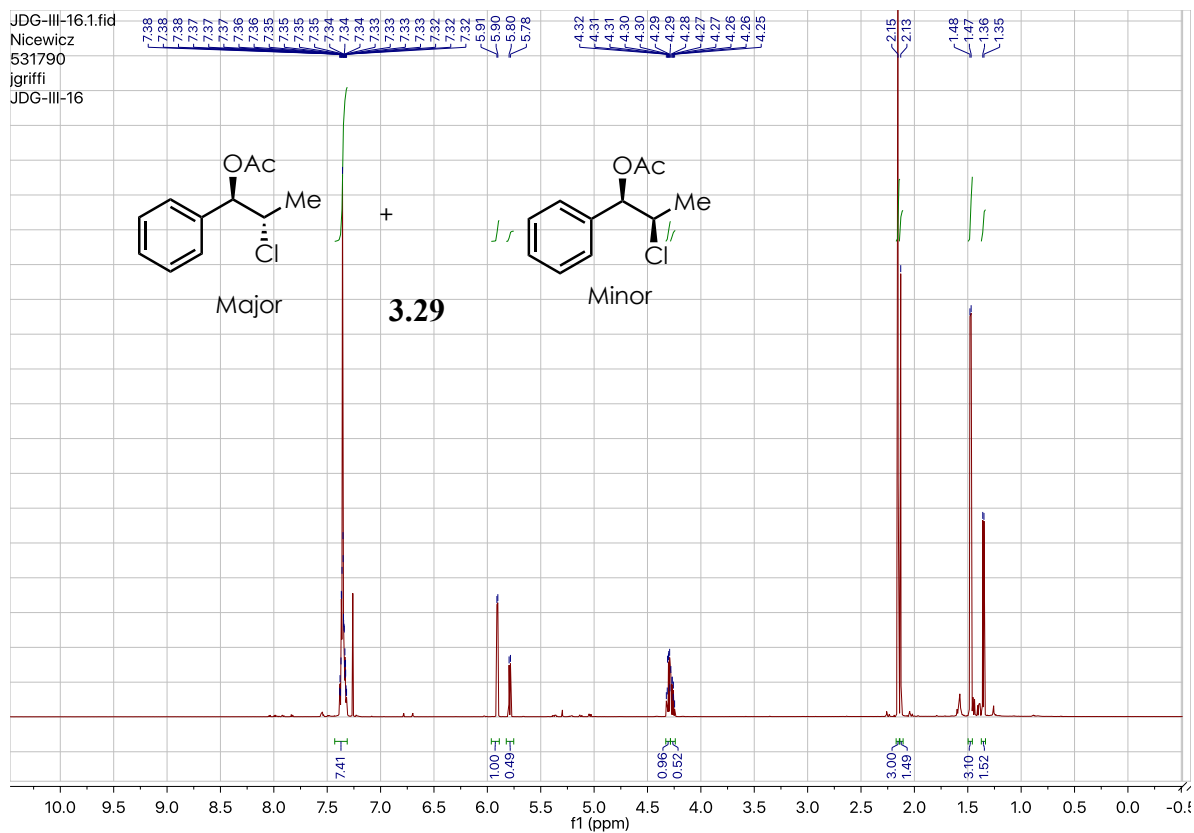
CLC3-59_Isolated_SI-2/1
 Nicewicz
 537264
 cavanacI
 CLC3-59_Isolated_SI

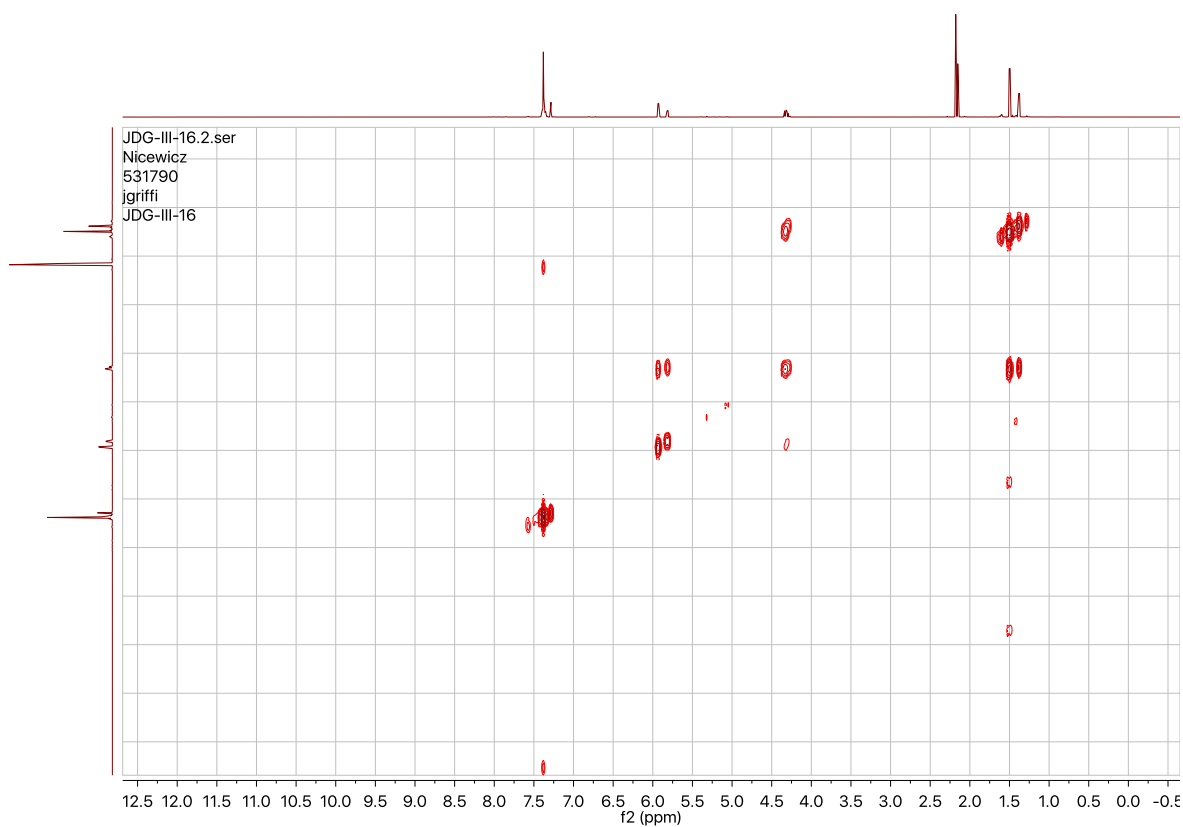
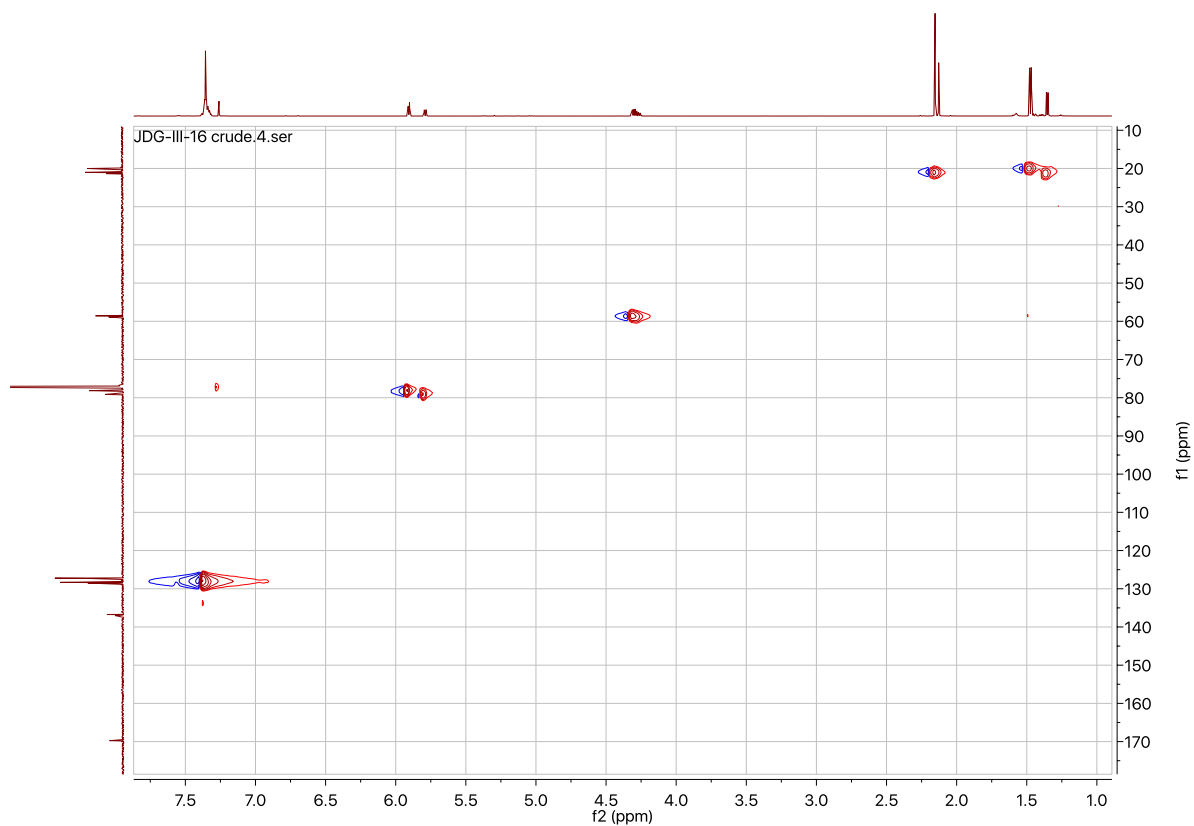


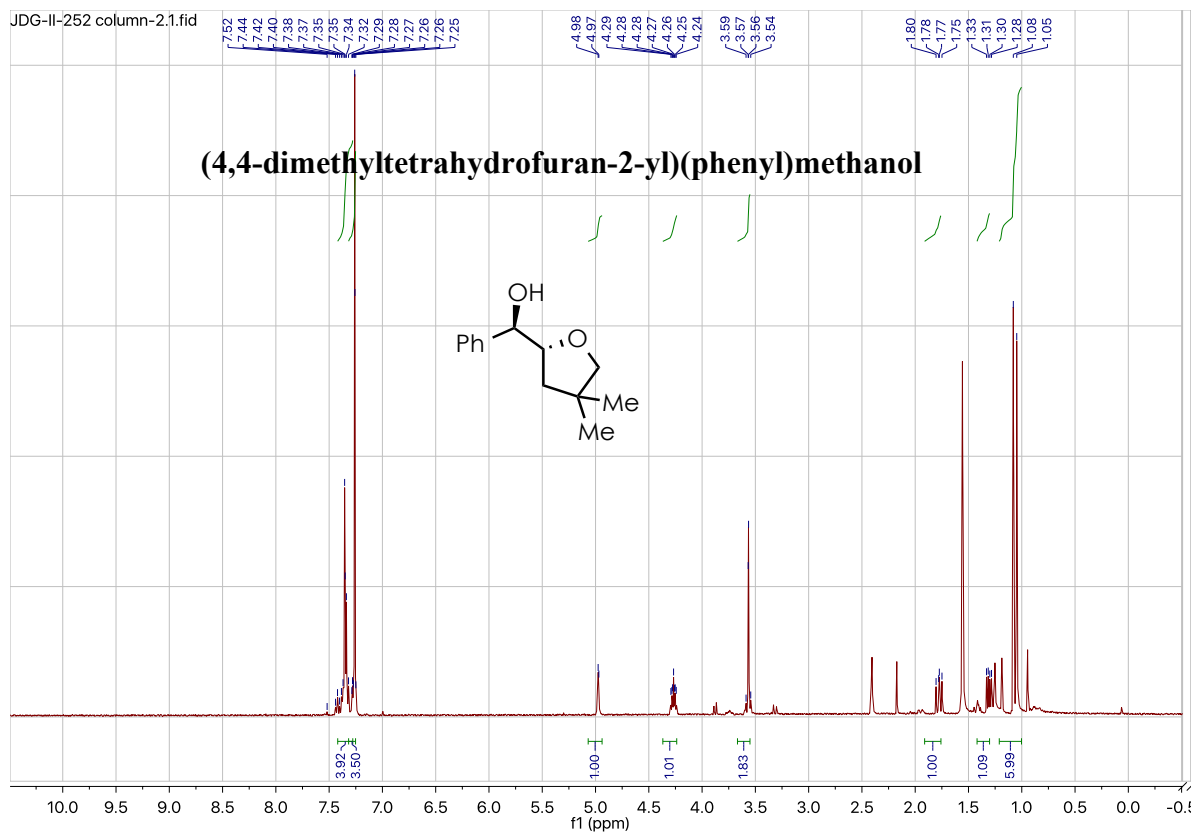
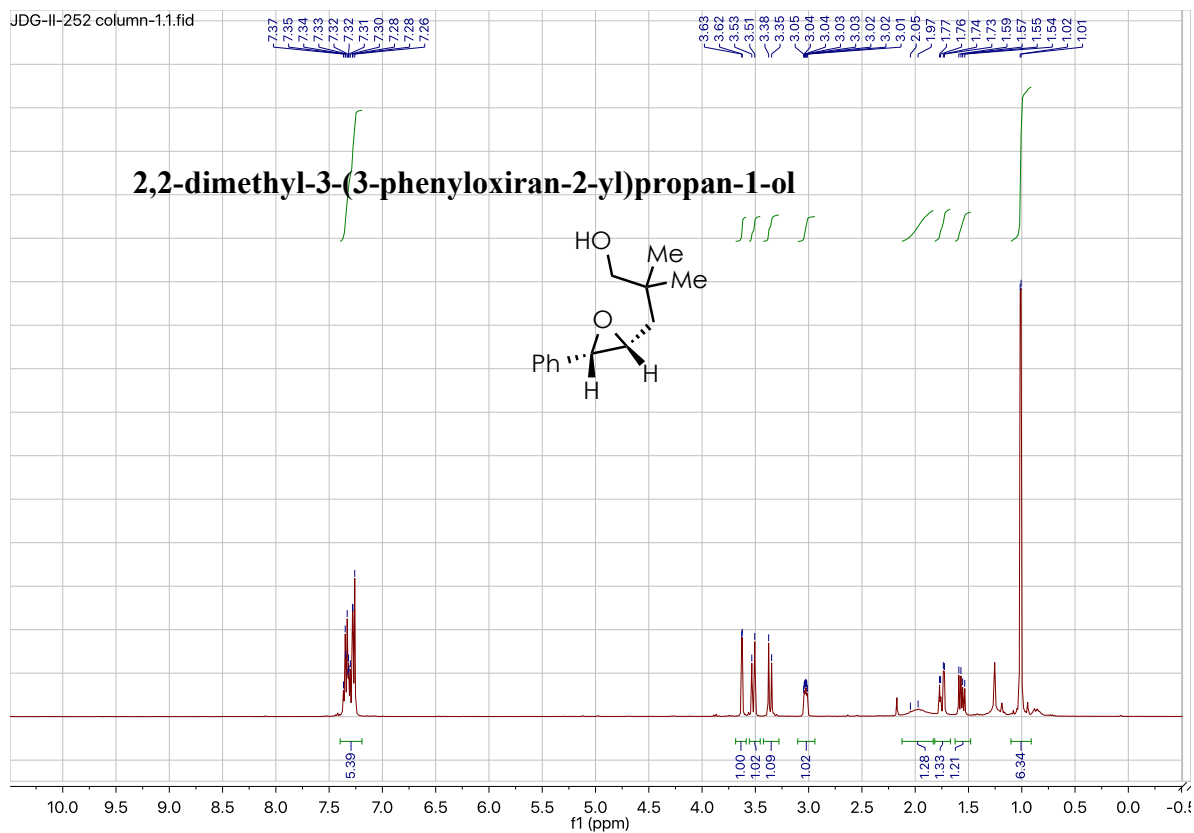
CLC3-59_Isolated_SI/2
 Nicewicz
 537264
 cavanacI
 CLC3-59_Isolated_SI











REFERENCES

- (1) Kolb, H. C.; VanNieuwenhze, M. S.; Sharpless, K. B. *Chem. Rev.* **1994**, *94* (8), 2483–2547.
- (2) Heravi, M. M.; Zadsirjan, V.; Esfandyari, M.; Lashaki, T. B. *Tetrahedron: Asymmetry* **2017**, *28* (8), 987–1043.
- (3) Zhang, B.; Studer, A. *Org. Lett.* **2014**, *16* (6), 1790–1793.
- (4) Li, Y.; Hartmann, M.; Daniliuc, C. G.; Studer, A. R. *Chem. Commun.* **2015**, *51* (26), 5706–5709.
- (5) Hemric, B. N.; Shen, K.; Wang, Q. *J. Am. Chem. Soc.* **2016**, *138* (18), 5813–5816.
- (6) Zhu, R.; Buchwald, S. L. *J. Am. Chem. Soc.* **2015**, *137* (25), 8069–8077.
- (7) Li, Y.; Studer, A. *Angew. Chemie Int. Ed.* **2012**, *51* (33), 8221–8224.
- (8) Yasu, Y.; Koike, T.; Akita, M. *Angew. Chemie Int. Ed.* **2012**, *51* (38), 9567–9571.
- (9) Zhang, B.; Studer, A. *Org. Lett.* **2013**, *15* (17), 4548–4551.
- (10) Zhu, R.; Buchwald, S. L. *J. Am. Chem. Soc.* **2012**, *134* (30), 12462–12465.
- (11) Zhang, H.; Pu, W.; Xiong, T.; Li, Y.; Zhou, X.; Sun, K.; Liu, Q.; Zhang, Q. *Angew. Chemie Int. Ed.* **2013**, *52* (9), 2529–2533.
- (12) Jensen, K. H.; Sigman, M. S. *Org. Biomol. Chem.* **2008**, *6* (22), 4083.
- (13) Haifeng Du; Baoguo Zhao, A.; Shi, Y. A F. *J. Am. Chem. Soc.* **2007**, *129* (4), 762–763.
- (14) Desai, L. V.; Sanford, M. S. *Angew. Chemie Int. Ed.* **2007**, *46* (30), 5737–5740.
- (15) And, M. J. S.; Sigman*, M. S. *J. Am. Chem. Soc.* **2006**, *128* (5), 1460–1461.
- (16) and, Y. Z.; Sigman*, M. S. *J. Am. Chem. Soc.* **2007**, *129* (11), 3076–3077.
- (17) Shibasaki, M.; Sasai, H.; Arai, T. *Angew. Chemie Int. Ed. English* **1997**, *36* (12), 1236–1256.
- (18) and, G. L.; Stahl*, S. S. *J. Am. Chem. Soc.* **2006**, *128* (22), 7179–7181.
- (19) Erik J. Alexanian; Chulbom Lee, A.; Sorensen, E. J. *J. Am. Chem. Soc.* **2005**, *127* (21), 7690–7691.
- (20) Chianese, A. R.; Lee, S. J.; Gagné, M. R. *Angew. Chemie Int. Ed.* **2007**, *46* (22), 4042–

4059.

- (21) Yang Li; Datong Song, and; Dong, V. M.. *J. Am. Chem. Soc* **2008**, *130* (10), 2962–2964.
- (22) Wang, F.; Wang, D.; Wan, X.; Wu, L.; Chen, P.; Liu, G. *J. Am. Chem. Soc.* **2016**, *138* (48), 15547–15550.
- (23) Wang, D.; Wang, F.; Chen, P.; Lin, Z.; Liu, G. *Angew. Chemie* **2017**, *129* (8), 2086–2090.
- (24) Smith, M.; March, J. *March's Advanced Organic Chemistry : Reactions, Mechanisms, and Structure.*; Wiley-Interscience, 2007.
- (25) Ashtekar, K. D.; Vetticatt, M.; Yousefi, R.; Jackson, J. E.; Borhan, B.. *J. Am. Chem. Soc.* **2016**, *138* (26), 8114–8119.
- (26) Denmark, S. E.; Kuester, W. E.; Burk, M. T. *Angew. Chemie Int. Ed.* **2012**, *51* (44), 10938–10953.
- (27) Grossman, R. B.; Trupp, R. J. *Can. J. Chem.* **1998**, *76* (9), 1233–1237.
- (28) Haas, J.; Piguel, S.; Wirth, T. *Org. Lett.* **2002**, *4* (2), 297–300.
- (29) Brown, R. S.; Nagorski, R. W.; Bennet, A. J.; McClung, R. E. D.; Aarts, G. H. M.; Klobukowski, M.; McDonald, R.; Santarsiero, B. D. *J. Am. Chem. Soc.* **1994**, *116* (6), 2448–2456.
- (30) Denmark, S. E.; Burk, M. T.; Hoover, A. J. O. *J. Am. Chem. Soc.* **2010**, *132* (4), 1232–1233.
- (31) Whitehead, D. C.; Yousefi, R.; Jaganathan, A.; Borhan, B. *J. Am. Chem. Soc.* **2010**, *132* (10), 3298–3300.
- (32) Paull, D. H.; Fang, C.; Donald, J. R.; Pansick, A. D.; Martin, S. F. *J. Am. Chem. Soc.* **2012**, *134* (27), 11128–11131.
- (33) Dobish, M. C.; Johnston, J. N. *J. Am. Chem. Soc.* **2012**, *134* (14), 6068–6071.
- (34) Huang, D.; Liu, X.; Li, L.; Cai, Y.; Liu, W.; Shi, Y. *J. Am. Chem. Soc.* **2013**, *135* (22), 8101–8104.
- (35) Chen, F.; Tan, C. K.; Yeung, Y.-Y. *J. Am. Chem. Soc.* **2013**, *135* (4), 1232–1235.
- (36) Li, L.; Su, C.; Liu, X.; Tian, H.; Shi, Y. *Org. Lett.* **2014**, *16* (14), 3728–3731.
- (37) Yousefi, R.; Ashtekar, K. D.; Whitehead, D. C.; Jackson, J. E.; Borhan, B. *J. Am. Chem. Soc.* **2013**, *135* (39), 14524–14527.

- (38) Gribble*, G. W. *Acc. Chem. Res.* **1998**, *31* (3), 141–152.
- (39) Chung, W.; Vanderwal, C. D. *Angew. Chemie Int. Ed.* **2016**, *55* (14), 4396–4434.
- (40) and, M. T. C.; Emmitte, K. A. *Org. Lett.* **1999**, *1* (12), 2029–2032.
- (41) And, M. T. C.; Emmitte, K. A. *J. Am. Chem. Soc.* **2001**, *123* (7), 1533–1534.
- (42) Overman, L. E.; Thompson, A. S. *J. Am. Chem. Soc.* **1988**, *110* (7), 2248–2256.
- (43) Bratz, M.; Bullock, W. H.; Overman, L. E.; Takemoto, T. T. *J. Am. Chem. Soc.* **1995**, *117* (22), 5958–5966.
- (44) and, H. S.; Corey, E. J. *Org. Lett.* **1999**, *1* (5), 823–824.
- (45) Back, T. G.; Wulff, J. E. *Angew. Chemie Int. Ed.* **2004**, *43* (47), 6493–6496.
- (46) Daub, M. E.; Prudhomme, J.; Le Roch, K.; Vanderwal, C. D. *J. Am. Chem. Soc.* **2015**, *137* (15), 4912–4915.
- (47) Miyaoka, H.; Abe, Y.; Sekiya, N.; Mitome, H.; Kawashima, E. *Chem. Commun.* **2012**, *48* (6), 901–903.
- (48) Neunteufel, R. A.; Arnold, D. R. *J. Am. Chem. Soc.* **1973**, *95* (12), 4080–4081.
- (49) Gassman, P. G.; Bottorff, K. J. *J. Am. Chem. Soc.* **1987**, *109* (24), 7547–7548.
- (50) Hamilton, D. S.; Nicewicz, D. A. *J. Am. Chem. Soc.* **2012**, *134* (45), 18577–18580.
- (51) Perkowski, A. J.; Nicewicz, D. A. *J. Am. Chem. Soc.* **2013**, *135* (28), 10334–10337.
- (52) Nguyen, T. M.; Nicewicz, D. A. *J. Am. Chem. Soc.* **2013**, *135* (26), 9588–9591.
- (53) Nguyen, T. M.; Manohar, N.; Nicewicz, D. A. *Angew. Chemie Int. Ed.* **2014**, *53* (24), 6198–6201.
- (54) Wilger, D. J.; Grandjean, J.-M. M.; Lammert, T. R.; Nicewicz, D. A. *Nat. Chem.* **2014**, *6* (8), 720–726.
- (55) Morse, P. D.; Nicewicz, D. A. *Chem. Sci.* **2015**, *6* (1), 270–274.
- (56) Grandjean, J.-M. M.; Nicewicz, D. A. *Angew. Chemie Int. Ed.* **2013**, *52* (14), 3967–3971.
- (57) Zeller, M. A.; Riener, M.; Nicewicz, D. A. *Org. Lett.* **2014**, *16* (18), 4810–4813.
- (58) Gesmundo, N. J.; Grandjean, J.-M. M.; Nicewicz, D. A. *Org. Lett.* **2015**, *17* (5), 1316–1319.

- (59) Cavanaugh, C. L.; Nicewicz, D. A. *Org. Lett.* **2015**, *17* (24), 6082–6085.
- (60) Gaspar, B.; Carreira, E. M. *Angew. Chemie Int. Ed.* **2008**, *47* (31), 5758–5760.
- (61) Stephen J. Blanksby, and; G. Barney Ellison, . *Acc. Chem. Res.* **2003**, *36* (4), 255–263.
- (62) Chatgililoglu, C. A. *J. Org. Chem.* **1986**, *51* (15), 2871–2873.
- (63) Lind, J.; Jonsson, M.; Eriksen, T. E.; Merenyi, G.; Eberson, L. *J. Phys. Chem.* **1993**, *97* (8), 1610–1614.
- (64) Matyjaszewski, K.; Xia, J. *Chem. Rev.* **2001**, *101* (9), 2921–2990.
- (65) Han, X.; Dong, C.; Zhou, H.-B. *Adv. Synth. Catal.* **2014**, *356* (6), 1275–1280.
- (66) Pintauer, T.; Matyjaszewski, K. A. *Chem. Soc. Rev.* **2008**, *37* (6), 1087.
- (67) Kitagawa, S.; Munakata, M. *Inorg. Chem.* **1981**, *20* (7), 2261–2267.
- (68) Majumdar, P.; Ghosh, A. K.; Falvello, L. R.; Peng, S.-M.; Goswami, S. S. *Inorg. Chem.* **1998**, *37* (7), 1651–1654.
- (69) Walling, C.; El-Taliawi, G. M.; Zhao, C. *J. Am. Chem. Soc.* **1983**, *105* (15), 5119–5124.
- (70) Chow, Y. L.; Zhao, D. C. *J. Org. Chem.* **1989**, *54* (3), 530–534.
- (71) Hiroaki Kotani; Kei Ohkubo, A.; Fukuzumi*, S. *J. Am. Chem. Soc* **2004**, *126* (49), 15999–16006.
- (72) Wube, A. A.; Hüfner, A.; Thomaschitz, C.; Blunder, M.; Kollroser, M.; Bauer, R.; Bucar, F. *Bioorg. Med. Chem.* **2011**, *19* (1), 567–579.
- (73) Tan, C. K.; Zhou, L.; Yeung, Y.-Y. *Org. Lett.* **2011**, *13* (10), 2738–2741.
- (74) Khrizman, A.; Cheng, H. Y.; Moyna, G. S. *J. Label. Compd. Radiopharm.* **2011**, *54* (8), 401–407.
- (75) Cabrero-Antonino, J. R.; Leyva-Pérez, A.; Corma, A. *Chem. - A Eur. J.* **2012**, *18* (35), 11107–11114.
- (76) Maity, S.; Zheng, N. A *Angew. Chem. Int. Ed. Engl.* **2012**, *51* (38), 9562–9566.
- (77) Denis V. Gribkov; Kai C. Hultsch, * and; Hampel, F. *J. Am. Chem. Soc* **2006**, *128* (11), 3748–3759.
- (78) and, A. T.; Hartwig*, J. F.. *J. Am. Chem. Soc* **2006**, *128* (18), 6042–6043.

- (79) Geary, G. C.; Hope, E. G.; Stuart, A. M.. *Angew. Chemie Int. Ed.* **2015**, 54 (49), 14911–14914.
- (80) Gorin, C. F.; Beh, E. S.; Bui, Q. M.; Dick, G. R.; Kanan, M. W. *J. Am. Chem. Soc.* **2013**, 135 (30), 11257–11265.
- (81) Johnson, R. C. *J. Chem. Educ.* **1970**, 47 (10), 702.
- (82) Kirk, A. D.; Namasivayam, C. *Anal. Chem.* **1983**, 55 (14), 2428–2429.
- (83) Demas, J. N.; Bowman, W. D.; Zalewski, E. F.; Velapoldi, R. A. *J. Phys. Chem.* **1981**, 85 (19), 2766–2771.
- (84) Roth, H.; Romero, N.; Nicewicz, D. *Synlett* **2015**, 27 (5), 714–723.

CHAPTER 4: HYBRIDIZATION TRANSFER THROUGH CARBON-CARBON FRAMEWORK ENABLES SELECTIVE HOMOBENZYLIC OXIDATION

4.1 Introduction

4.1.1 Site Selective Oxidation by Enzymes

One of the long standing challenges of organic chemistry is to achieve selective functionalization of complex organic molecules. Nature routinely accomplishes site selective reactions such C–H oxidations on very complex substrates. Cytochrome P450 are heme containing proteins which are present in every known lifeform. Although these enzymes are known to catalyze a number of different reactions including epoxidation, oxidation of alcohols, aromatics, and

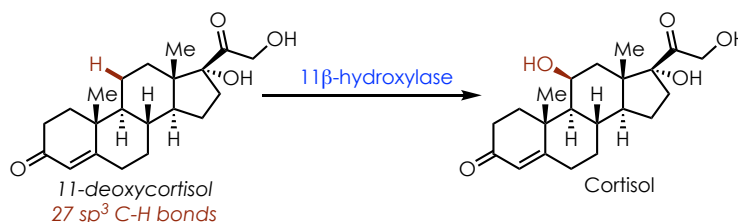


Figure 4.1: Enzymatic Oxidation of 11-deoxycortisol to cortisol.

amines; their ability to achieve C–H oxidation (both sp^2 and sp^3 C–H oxidation) will be discussed here.¹ At least 12,000 P450 enzymes exist,² some of which carry out substrate non-specific oxidation in order to aid in secretion from a given organism, and others that are substrate specific and are involved in processes such as steroid synthesis.³ For example, 11 β -hydroxylase can catalyze the hydroxylation of 11-deoxycortisol at a single C–H bond among 27 sp^3 C–H bonds

(**Figure 4.1**). Enzymatic reactions accomplish this almost unfathomable selectivity via very large and substrate specific binding pockets which position the substrate such that the C–H bond in question is positioned next to the enzyme active site. While this imparts impressive regio-, chemo-, and stereoselectivity, the reactions are inherently substrate specific. Therefore, chemists have sought to use directed evolution to quickly adapt enzymes for a particular substrate,⁴ to accomplish selective C–H oxidation.⁵

4.1.1.1 Mechanism of Cytochrome P450 C–H oxidation

The mechanism of P450 oxidation begins with substrate association to the enzyme active site displacing a molecule of water (**Figure 4.2, left**).¹ This triggers an electron transfer event from a nearby reductase protein, which reduces Fe^{III} to an Fe^{II} square pyramidal complex. O_2 binding and subsequent reduction and proton transfer steps leads to the formation of the active oxidant, an Fe^{IV} -oxo complex. The existence of this high-valent Fe center has been debated in the literature but has been supported by computational evidence,^{6,7} and was recently characterized for the first

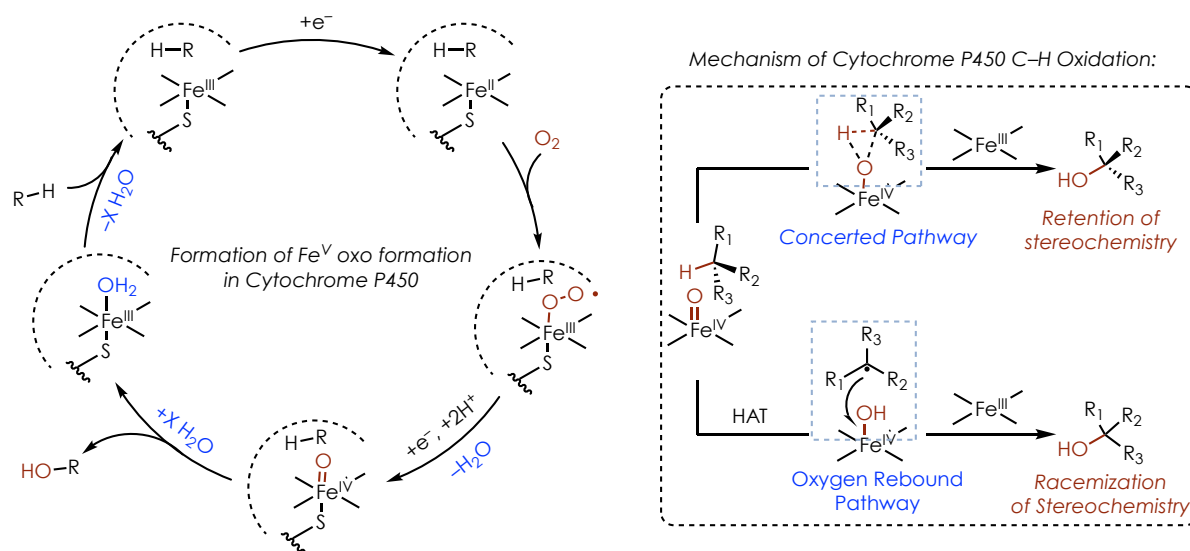


Figure 4.2: Enzymes like cytochrome P450 can routinely catalyze C–H functionalization reactions using molecular oxygen as the terminal oxidant.

time.⁸

There are two predominant mechanistic proposals for the oxidation event (**Figure 4.2, left**):

- 1.) A concerted C–H insertion by the Fe^{IV} -oxo complex results has been proposed based on fast radical clock experiments.^{9,10}
- 2.) A hydrogen atom transfer mechanism followed by “oxygen rebound” has also been proposed to explain the loss of stereochemistry observed in some P450 oxidations. Despite the retention of stereochemistry in some P450 oxidations the general consensus in the literature is that the mechanism more closely resembles the oxygen rebound mechanism which was proposed by the Groves lab in 1976.^{11–13} A breadth of mechanistic evidence has been obtained by the Groves lab and others to support this mechanism including radical clock experiments, showing that the carbon-centered radical intermediates produced have lifetimes in the picosecond regime.¹⁴ Thus, the retention of stereochemistry observed in some cases must be explained by the radical rebound reaction being competitive with inversion of the radical center which would result in racemization.

4.1.2 Traditional sp^3 C–H Bond Oxidation

Chemists have not yet been able to obtain the high levels of regioselectivity obtained by enzymatic systems, however chemical methods for oxidation of organic molecules have been developed based on substrate electronics. Chemists have successfully been able to accomplish

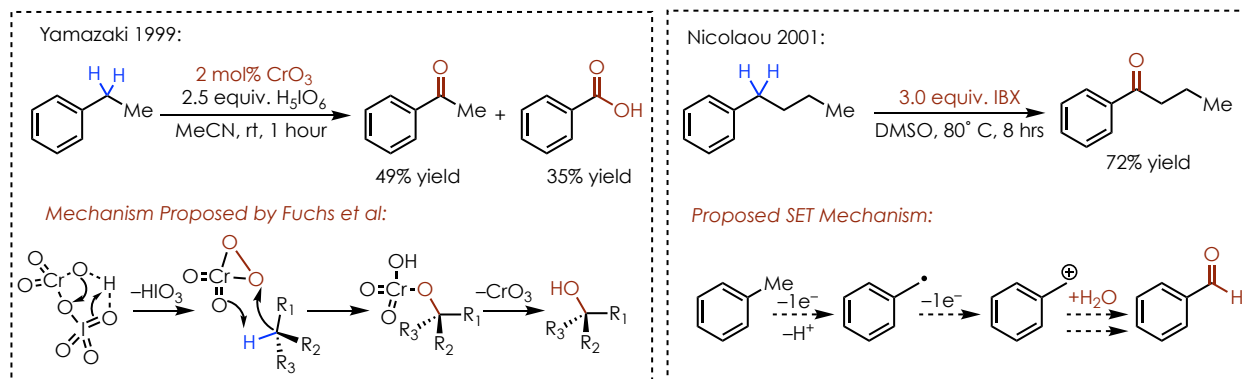


Figure 4.3: Selective Benzylic Oxidation Methods.

functionalization of activated C–H bonds including benzylic, allylic, α -amino, and α -alkoxy. Since there are many examples of C–H functionalizations using stoichiometric reagents, only a few pertinent examples will be discussed below.

Benzylic C–H bonds are some of the most readily functionalized C–H bonds so far, thus unsurprisingly there are many methods for accomplishing these transformations. One of the most common methods for benzylic oxidation is the use of stoichiometric chromium-based oxidants, however Yamazaki has demonstrated that these oxidations can be carried out with catalytic chromium when periodic acid (H_5IO_6) is used as the terminal oxidant (**Figure 4.3**).¹⁵ The Fuchs lab demonstrated that Cr^{VI} mediated oxidations can be very selective for 3° or benzylic C–H bonds.¹⁶ They proposed a mechanism for these transformations in which initial formation of a chromyl periodate leads to decomposition to the active oxidant a chromium peroxy complex. o-Iodoxybenzoic acid (IBX) have also been shown to selectively functionalize benzylic C–H bonds.¹⁷ The mechanism of this oxidation has been proposed to proceed through an SET pathway, in which the arene is oxidized by IBX. Following proton and electron transfer steps, a benzylic cation is proposed to form, which can be trapped with a number of different oxygen sources including DMSO or water.¹⁸

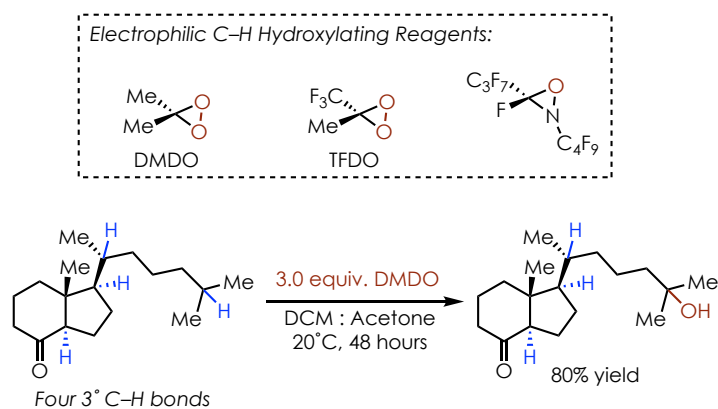


Figure 4.4: Tertiary selective C–H functionalization with DMDO and related reagents.

Other organic based oxidants such as dimethyldioxirane (DMDO)¹⁹ and Methyl(trifluoromethyl)dioxirane (TFDO),²⁰ have been shown to reaction with 3° and 2° C–H bonds and are typically selective for the most electron rich 3° or benzylic bond in the molecule (**Figure 4.4**). TFDO was developed as a more reactive dioxirane, and is 10,000 times more reactive than DMDO.²¹ As seen in Figure 4.4, selective oxidation a remote sites can often be obtained over more sterically crowded 3° C–H bonds.²² Dioxirane reagents must be generated in situⁱ and have to be stored at -20° C to prevent decomposition.²³ For this reason, oxaziridines have also been used to carry out selective 3° C–H oxidations.²⁴ Similarly to enzymatic C–H oxidations, dioxirane and oxaziridine based oxygen transfer reagents can undergo stereospecific oxidation, with the original stereochemistry of the substrate being retained.²⁵

4.1.3 Modern Approaches for Oxidation of sp³ Hybridized C–H Bonds

While stoichiometric metal and organic based oxidants have proven to be very useful for oxidation of electron rich C–H bonds, selective oxidation of less activated C–H bonds requires alternative strategies. Additionally, all of the methods described so far utilize one or more stoichiometric oxidants in order to transfer a single oxygen atom, decreasing the atom economy of the transformations.^{26,27} Therefore, the following sections will focus on modern approaches to accomplish functionalizations of unactivated C–H bonds. Two major strategies have emerged for functionalizing unactivated C–H bonds, which will be discussed below. These sections are not meant to be a comprehensive evaluation of all C–H functionalization methodologies, but rather a survey of some of the more extensively utilized strategies with several supporting examples

ⁱ DMDO is typically produced from the reaction of acetone with oxone under basic conditions.

4.1.3.1 Directed Functionalization of Unactivated C–H Bonds

Directed functionalization is a strategy that utilizes pre-existing functionality in a molecule which can coordinate a metal complex. This has most typically been used to functionalize C–H bonds in a 1,5-relationship to the directing group due to the formation of relatively stable 5-member metallacycles upon insertion.²⁸ The field has evolved from the use of relatively specific directing groups including O-Me oximes,²⁹ oxazoles,³⁰ and pyridines,^{29,31} to the use of very common functional groups such as amides,^{32,33} carboxylic acids,^{34,35} and even alcohols.³⁶

In 2004, the Sanford group published one of the first Pd catalyzed oxidations of unactivated sp³ C–H bonds (**Figure 4.5, top**).²⁹ In this case an O-Me oxime or pyridines were used as the directing group, and functionalization of 1° C–H bonds β-position relative to the directing group

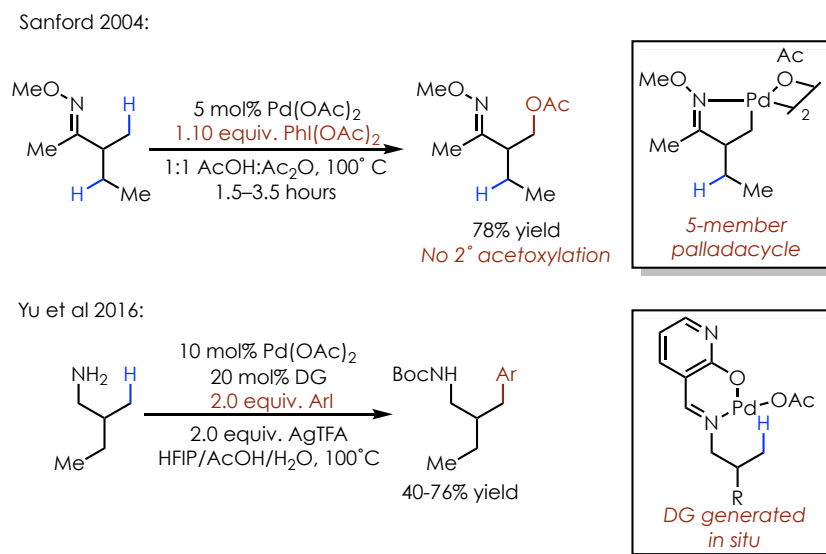


Figure 4.5: Directed C–H insertion enables selective functionalization of traditional inert C–H bonds.

could be acetoxylation. Primary C–H bonds were selectively functionalized, as secondary β-C–H bonds were found to be completely unreactive. Additionally, no functionalization was observed at potential reactive α- or γ-positions. More recently C–H functionalizations have focused on the formation of C–C bonds with common functional groups. In a recent report by the Yu lab, they

show that directing groups can be formed in situ, resulting in the activation of 1° C–H bonds. The directing group is formed by the amine substrate condensing onto an aldehyde directing group, forming a bidentate ligand which complexes with palladium. This positions the metal in close proximity to the γ -nitrogen. After C–H insertion, an aryl iodide can be coupled to give a new C–C bond. While these are only a few of the more recent examples, they give a good representation of the state of the art in directed C–H functionalization of unactivated bonds.

4.1.3.2 Non-Directed C–H Functionalizations

4.1.3.2.1 Iron Catalyzed

There have been many recent efforts to distinguish C–H bonds based on more subtle electronic and steric characteristics than traditional functionalization reactions (See Section 4.1.2). This strategy has largely been based on radical C–H abstraction, and relies on steric and electronic characteristics of the catalyst (or reagent). The White lab has disclosed a biomimetic strategy,

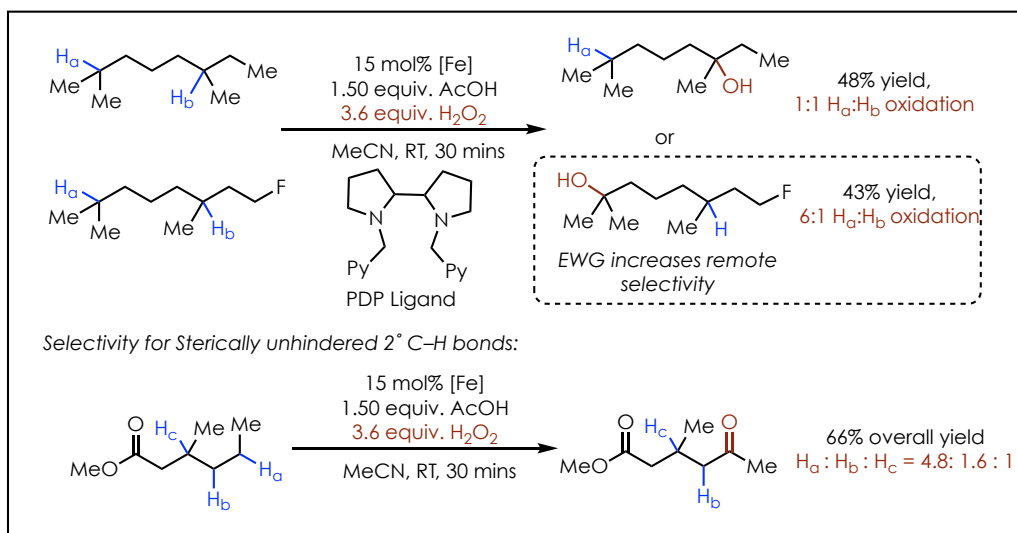


Figure 4.6: Selective functionalization remote from functional groups. [Fe] = [Fe(PDP)MeCN₂](SbF₆)₂. PDP references 2-((S)-2-[(S)-1-(pyridin-2-ylmethyl)pyrrolidin-2-yl]pyrrolidin-1-yl)methylpyridine.

which utilized an iron catalyst using hydrogen peroxide (H_2O_2) as the stoichiometric oxidant (**Figure 4.6, top**).³⁷ Only about three catalyst turnovers were observed for most substrates, with the requirement that three separate additions of catalyst be used. Despite very low catalyst activity, the iron catalysts were shown to be selective for the most electron rich C–H bonds; the authors were able to demonstrate selectivity for sterically similar but electronically differentiated C–H bonds. In a separate report in 2010, the same lab reported that this catalyst could also facilitate oxidation of unactivated 2° C–H bonds, even in the presence of 3° C–H bonds (**Figure 4.6, bottom**).³⁸ This showed that a combination of steric and electronic factors could favor 2° over 3° selectivity. In the example shown at the bottom of Figure 4.6, H_c is in close proximity to the electron withdrawing ester, while also being more sterically crowded than H_a . The reaction was selective for the most remote 2° C–H bond, because it was the most electron rich among the 2° C–H bonds. Models to help predict site selectivity has also been developed as well.³⁹

4.1.3.2.2 Reagent Based C–H oxidation

Stoichiometric reagents have also been developed which can give site selectivity at 2° sites by a radical abstraction mechanism by the Alexanian lab. Chlorination,⁴⁰ bromination,⁴¹ and xanthylation^{42,43} have been so far reported. These reactions proceed via homolysis of an activated amide N–X bond, producing an amidyl radical intermediate, which can selectively react with C–H bonds which are most sterically accessible. Increasing the steric environment around the activated amide,

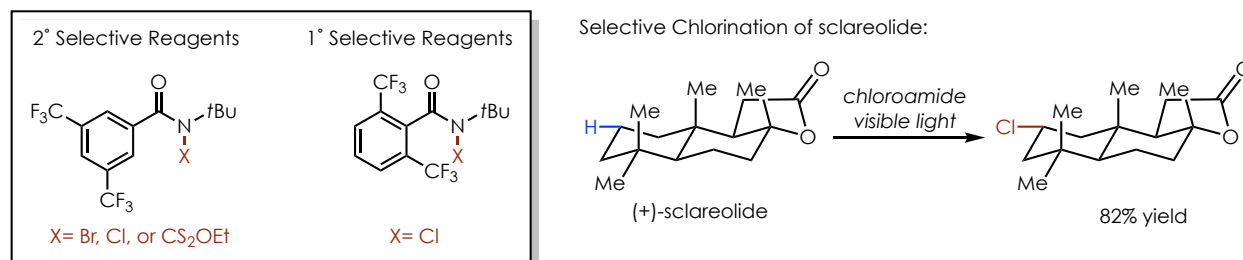


Figure 4.7: Activated amide intermediates developed by the Alexanian lab.

enables 1° C–H, which has been difficult using other radical based methods. They have reported the selective functionalization of complex substrates such as (+)-sclareolide, which enabled the synthesis of (+)-chlorolissoclimide in nine steps.⁴⁰

4.1.3.2.3 Electrochemical C–H Oxidation

The Baran lab has recently disclosed electrochemical methods for oxidation of allylic⁴⁴ and unactivated C–H bonds.⁴⁵ The use of electrochemical mediators, facilitates the oxidation of C–H bonds at relatively low potentials.ⁱⁱ Quinuclidine was chosen as the electrochemical mediator for this reaction, which has also been used in a similar capacity by the Macmillan lab recently to functionalize activated benzylic, α -amino,^{46,47} α -alkoxy,⁴⁸ and aldehyde⁴⁹ C–H bonds.ⁱⁱⁱ

The reaction proceeds by oxidation of the redox mediator; in the case of unactivated C–H bonds, quinuclidine was used (**Figure 4.8**). This generates a 3° amine cation radical, which subsequently abstracts a C–H bond from the substrate. Since a very electron deficient radical is produced, selectivity for the most electron rich position is obtained. The resulting carbon-centered

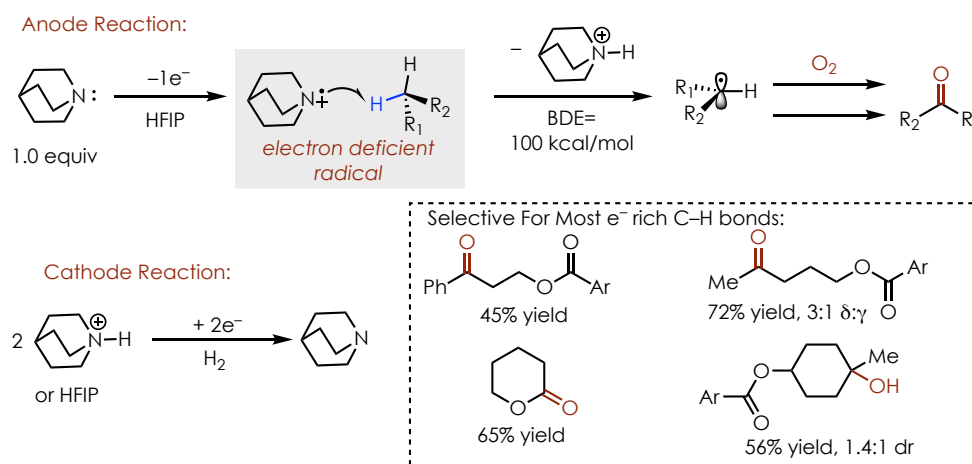


Figure 4.8: Electrochemical oxidation unactivated C–H bonds mediated by quinuclidine

ⁱⁱ Hydrocarbons are typically oxidized at > 2.5 V vs SCE.

ⁱⁱⁱ Related tertiary amine, aceclidine was used rather than quinuclidine in ref. 46.

radical is trapped with O₂ and is subsequently converted to the ketone. Although, quinuclidinium likely gets reduced at the cathode to form H₂ and reform quinuclidine, the mediator was used in stoichiometric quantities. The reactions were carried out in hexafluoroisopropanol (**HFIP**) with tetrabutylammonium tetrafluoroborate as an electrolyte. The authors also propose that HFIP could have some role as a proton donor, to complete the redox cycle. Importantly, this process could be scaled up to 50 g scale without deleterious effect on yield. Another important aspect of this chemistry is that very inexpensive, reticulated vitreous carbon (RVC) electrodes could be used, rather than expensive platinum electrodes used in other electrochemical methods.⁵⁰

The selectivity obtained was similar to the selectivity observed using the iron catalyzed methods discussed above (See Section 4.1.3.2.1). Substrates containing only 2° and 1° C–H were selectively oxidized at the 2° site most distal to electron withdrawing groups. While substrates containing benzylic, allylic, α-alkoxy, or tertiary C–H bonds were preferentially oxidized at those positions. However, there were cases when, similarly to the White chemistry, electronic and steric factors could give selectivity for 2° over 3° oxidation.

4.1.3.3 Summary of Modern C–H Oxidation Strategies

Recently two major strategies have emerged for sp³ C–H functionalization. Directed functionalization, which utilizes preexisting functionality that coordinate transition metals to direct predictable C–H insertion at nearby C–H bonds. Although the number of directing groups which can participate in this chemistry is increasing, this strategy is still limited by the types of substrates that can participate in the reactivity and also in which C–H bonds can be functionalized (Typically C–H at the γ-carbon relative to the coordinated atom are functionalized). Undirected transition metal C–H insertions are typically slow, but can be selective for primary C–H functionalization

due to steric considerations.^{51,52} These methods are also currently limited in both the scope of substrates and reaction type. Therefore, radical based approaches for C–H functionalization have also been developed. These strategies have typically been selective for the most electron rich C–H bonds present, however steric considerations must be considered when multiple C–H bonds of similar substitution are present. Furthermore, selective oxidation of 2° substituted carbon centers over 3° sites, has been accomplished using this strategies. However, none of these strategies are able to selectively oxidize 2° or 1° C–H bonds in the presence of more electron rich benzylic, allylic, or α -heteroatom bonds. Additionally, selecting for intermediary C–H bonds (ie not most electron rich or least sterically crowded) is still an unsolved problem.

4.2 Developing a Strategy for Selective Homobenzylic Oxidation

As discussed in Chapter 3 (Section 3.1.3), our lab has developed a suite of anti-Markovnikov nucleophile addition reactions via the intermediacy of alkene cation-radicals. Recently this chemistry has been applied to net two-electron oxidations of alkenes, through the use of cobaloximes as co-catalysts by Aiwen Lei and coworkers.^{53–55} Of particular interest to us, was the anti-Markovnikov oxidation of styrenes using this system (**Figure 4.9**).⁵³ Similar to hydrofunctionalization reactions developed by the Nicewicz lab, this reaction begins with the single electron oxidation of the styrene substrate in this case by Mes-Acr-Me⁺, forming a reactive cation-radical intermediate. This intermediates undergoes nucleophilic trapping by H₂O, and following deprotonation forming the most stable benzylic radical intermediate.

The authors propose that the radical intermediate then undergoes a second oxidation, by [Co^{III}(dmgH)₂pyCl] potentials ($E_{1/2}^{\text{red}} \text{Co}^{\text{III}} / \text{Co}^{\text{II}} = -0.67 \text{ V vs SCE}$)⁵⁶ to form a benzylic cation

and $[\text{Co}^{\text{II}}(\text{dmgH})_2\text{pyCl}]$. However, the oxidation potential of benzylic radicals has been reported as $E_{p/2}^{\text{ox}} = +0.37 \text{ V}$,⁵⁷ which would make this electron transfer event endothermic by $+1.04 \text{ V}$.^{iv}

Since it seems clear this electron transfer is not feasible, an alternative explanation could be first protonation of the oxime ligand by highly acidic oxonium ion on to make a cationic complex. This complex is likely more easily reduced by either the benzylic radical or Mes-Acr-Me• ($E_{1/2}^{\text{ox}} = -0.57 \text{ V vs SCE}$). A similar process could then occur for the $\text{Co}^{\text{II}}/\text{Co}^{\text{I}}$ redox couple ($E_{1/2}^{\text{red}} \text{ Co}^{\text{II}} / \text{Co}^{\text{I}} = -1.12 \text{ V vs SCE}$), since reduction by Co^{II} is also unfavorable by either Mes-Acr-Me• or the benzylic radical without the proton transfer occurring first. It has been shown that with similar cobaloxime complexes, the position of the cobalt reduction potentials are modified by the addition of acid,⁵⁸ therefore this proposal could be reasonable.

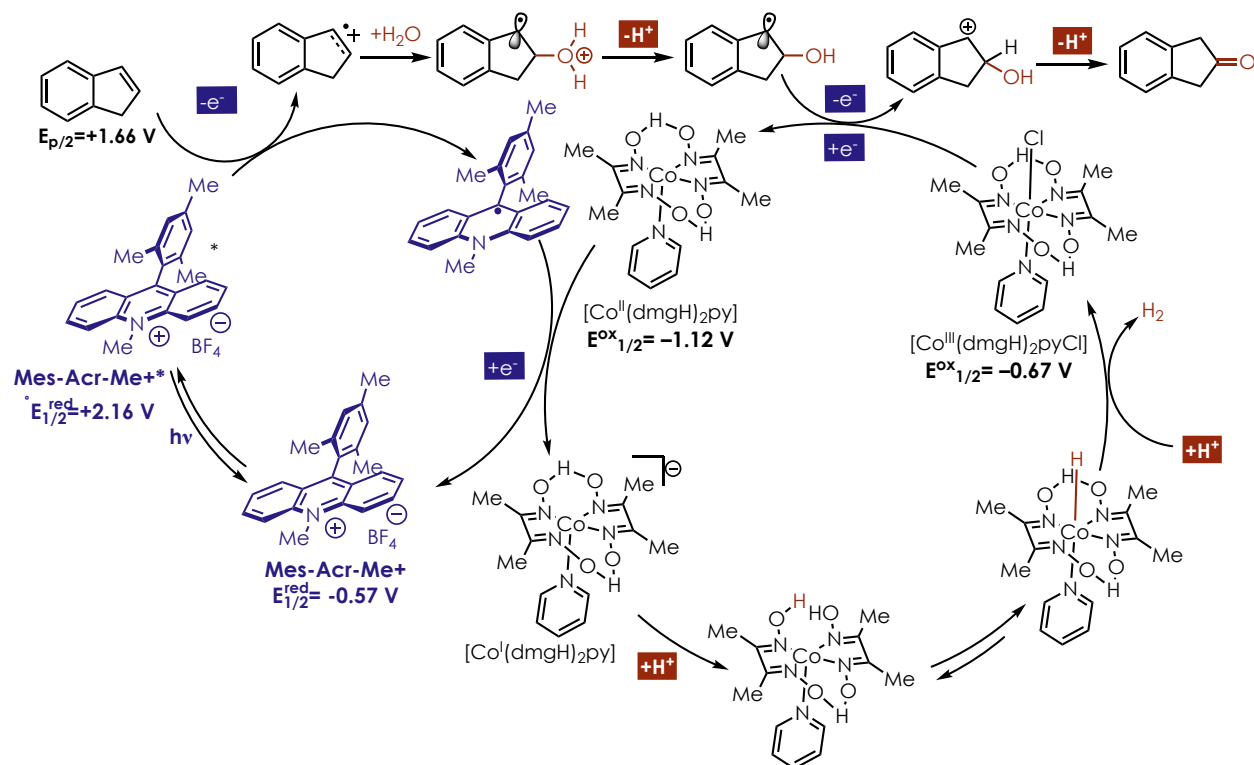


Figure 4.9: Mechanism for anti-Markovnikov styrene oxidation proposed by Aiwen Lei and co-workers. This mechanism is unlikely as the reduction of Co^{II} would be very endergonic.

^{iv} This corresponds to $\sim +24 \text{ kcal/mol}$

Regardless, after formation of the benzylic cation, deprotonation leads to an enol, which quickly tautomerizes to the ketone product. After consecutive proton and electron transfer events, the cobalt catalyst is turned over after releasing H₂. Thus, protons from the substrate and H₂O act as the terminal oxidants, while water is the sole oxygen source.

Around the same time as the publication by the Lei lab, the Kanai lab published a similar reaction in which nitrogen-heterocycles and tetrahydronaphthalene derivatives could be aromatized with release of H₂.⁵⁹ This was accomplished using a three-catalyst system including: Mes-Acr-Me⁺, Pd(BF₄)•4 MeCN, and a thiophosphoramidate catalyst. Early in 2018 they also reported that Ni(NTf₂)₂ X H₂O could be used in place of palladium.⁶⁰ Similar to the redox mediators reported by

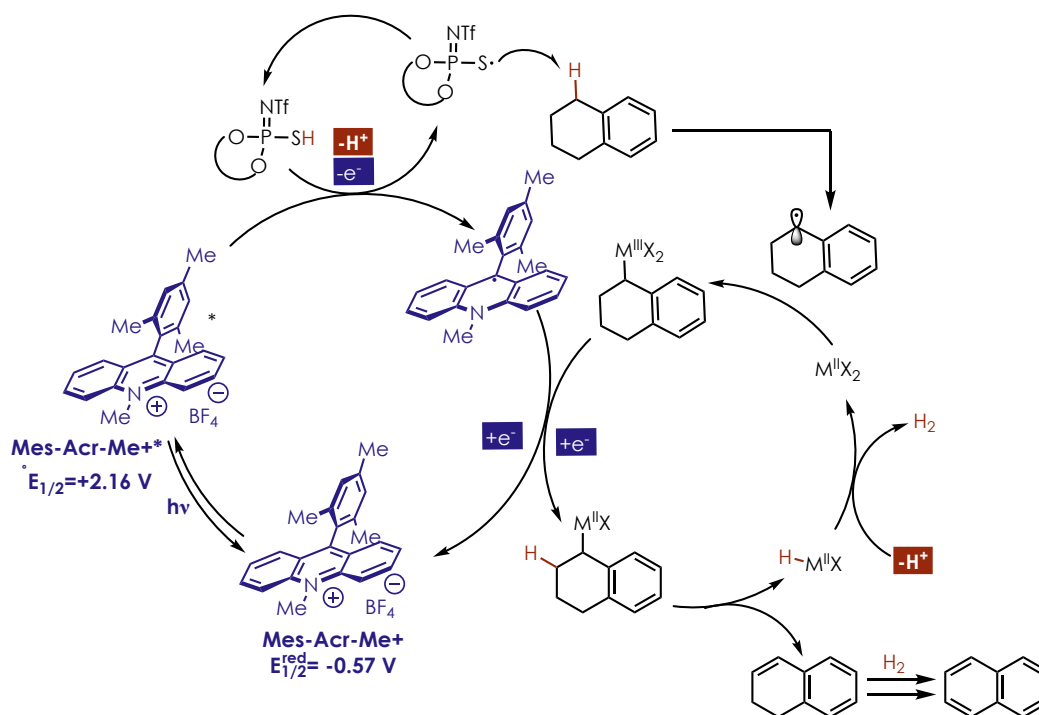


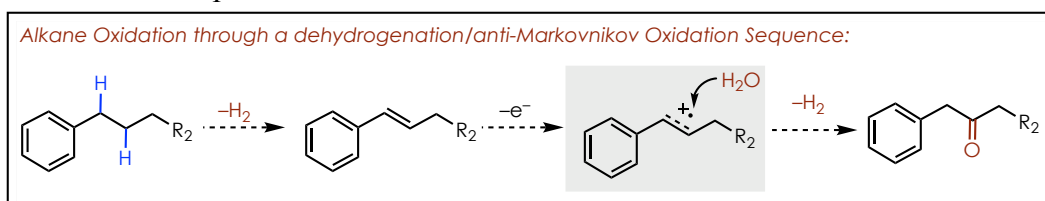
Figure 4.10: Mechanism for dehydrogenation of tetrahydronaphthalene proposed by Kanai and co-workers. BINOL is abbreviated in the thiophosphoramidate structure.

the Baran and MacMillan labs (See Section 4.1.3.2.3), single-electron oxidation of the thiophosphoric acid catalyst followed by proton transfer, enables C–H abstraction of the activated

benzylic C–H bond. After formation of a benzylic radical, either Pd^{II} or Ni^{II} could recombine forming an unstable M^{III} complex, which likely oxidizes Mes-Acr-Me•. β -hydride elimination would result in the formation of a styrene intermediate, which could then undergo the same process a second time ultimately forming the aromatic (e.g. naphthalene, indole, or isoquinoline). The metal-hydride intermediate could be protonated, releasing H₂ and regenerating the catalyst.

Based on these two precedents we thought it would be possible to enact alkane oxidation using a combination of an acridinium photocatalyst, a hydrogen evolution catalyst, and a C–H abstraction agent. Similarly to the work by Kanai and others as mentioned above, initial oxidation of a redox mediator could enable a C–H bond abstraction forming a carbon-centered radical. A second oxidant could then react with the radical, releasing H₂ and forming an alkene intermediate (**Scheme 4.1**). In the presence of a photocatalyst and H₂O this alkene could undergo anti-Markovnikov oxidation based on work from both the Nicewicz and Lei labs. This approach to

Scheme 4.1: General plan for alkane oxidation.



alkane oxidation would mean that unlike other radical based C–H oxidation methods, the site of oxidation does not have to be at the site where the initial C–H abstraction occurs. The radical abstraction is likely to occur at the weakest C–H bond, similar to other radical C–H abstractions. Thus, the alkene could be selectively formed adjacent to the weakest C–H bonds, and because anti-Markovnikov nucleophile additions are well established at this point, this strategy would enable an overall selective oxidation of the C–H bonds beta to the weakest C–H bonds in the molecule.

Some early challenges that were noted before beginning included: 1) dehydrogenation of linear alkanes using a photoredox system had not yet been established 2) identifying both a

photocatalyst and H₂ evolving catalyst that would be sufficiently stable enough to undergo two catalyst turnovers for each substrate molecule 3) identifying a redox mediator (H-atom abstractor) that would be compatible with both catalyst cycles.

4.2.1 Optimization of Tetrahydronaphthalene Oxidation

Initial attempts to reproduce the results from Kanai and coworkers using the Mes-Acr-Me⁺, BINOL based thiophosphoramidate catalyst (**TPA**), and Pd(BF₄)₂•4MeCN system were unsuccessful. (**Table 4.1, Entry 1**). However, they reported utilizing a different LED source (430 nm peak emission) than our typical setups (450 nm peak emission), so it seemed reasonable that this could account for our inability to reproduce this result. However, when using either [Co(dmgh)(dmgh₂)Cl₂] or [Co(dmgh)₂pyCl] as the hydrogen evolution catalyst rather than Pd^{II} resulted in the formation of naphthalene by GC/MS (**Table 4.1, Entries 2 and 3**). Thus, it seemed that cobaloxime catalysts were more efficient in this system, at least qualitatively. [Co(dmgh)₂pyCl] had higher solubility in organic solvents, and was used for further screening.

When reactions were carried out in 9:1 MeCN:H₂O without any other change, the desired oxidation product, 2-tetralone was observed by GC/MS and ¹H NMR in a 15% yield, while benzylic oxidation product 1-tetralone was not observed. Additionally, naphthalene and 1,2-dihydronaphthalene formed in 3% and 6% yields respectively (**Table 4.1, Entry 4**). Other acridinium catalysts were screened because Mes-Acr-Me⁺ has been found to decompose in previous work, particularly in polar solvent systems. Mes-Acr-Ph⁺ did not give any improvement in reactivity (**Table 4.1, Entry 5**), however catalysts with substitution on the acridinium core provided major improvements in reactivity (**Table 4.1, Entries 6 and 7**). Mes-(3,6-*t*Bu-Acr)-Ph⁺ gave the highest

Table 4.1: Optimization of homobenzylic oxidation of tetrahydronaphthalene.

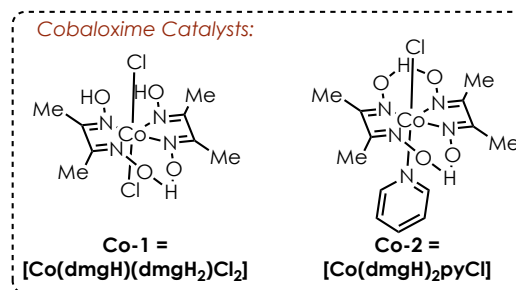
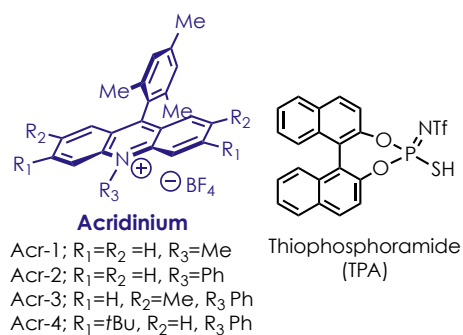
5 mol % Acridinium
H₂-Evolving Catalyst
redox mediator

[0.5 M] DCM or
[0.1 M] 9:1 MeCN:H₂O
16 hours

■ = Site of C-H abstraction

A **B** **C**

Entry	Photocatalyst	H ₂ Evolving Catalyst	Redox Mediator	A% Yield ^v 2-tetralone	B% Yield ^v 1-2 dihydro naphthalene	C% Yield ^v naphthalene
1 ^{vi}	5 mol% Acr-1	2.5 mol% Pd(BF ₄) ₂ ^{vii}	5 mol% TPA	—	—	—
2 ^{vi}	5 mol% Acr-1	3 mol% Co-1	5 mol% TPA	—	—	trace
3 ^{vi}	5 mol% Acr-1	3 mol% Co-2	5 mol% TPA	—	—	trace
4	5 mol% Acr-1	5 mol% Co-2	5 mol% TPA	15%	6%	3%
5	5 mol% Acr-2	5 mol% Co-2	5 mol% TPA	17%	5%	6%
6	5 mol% Acr-3	5 mol% Co-2	5 mol% TPA	40%	5%	6%
7	5 mol% Acr-4	5 mol% Co-2	5 mol% TPA	81%	trace	11%
8	5 mol% Acr-4	5 mol% Co-2	20 mol% LiNO₃	79%	—	13%



^v Yield as determined by ¹H NMR spectroscopic analysis of the crude reaction mixture relative to the internal standard (Me₃Si)₂O.

^{vi} The reaction was carried out without H₂O

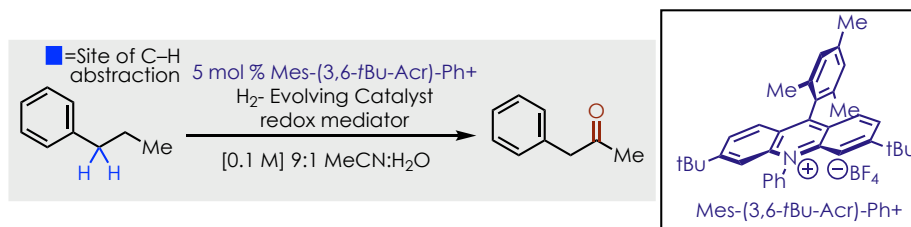
^{vii} Pd(BF₄)₂ was the tetrakisacetonitrile salt.

yield of homobenzylic oxidation product (81%) with only a small amount of naphthalene production. Due to the laborious process of synthesizing the TPA catalyst, as well as its limited number of applicable substrates (See Section 4.2.2), other potential redox-mediators were screened. Ultimately, LiNO_3 was identified as a suitable H-atom abstractor, that was commercially available. When 20% LiNO_3 loading was used nearly identical yields could be obtained (**Table 4.1, Entry 8**).

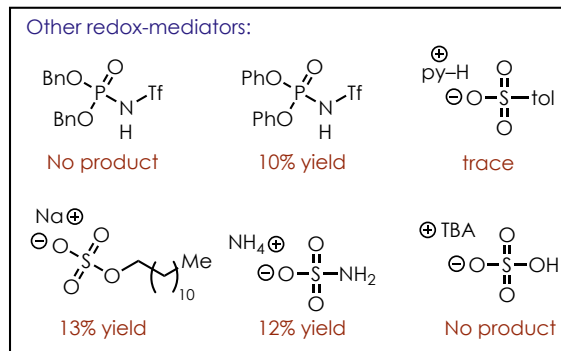
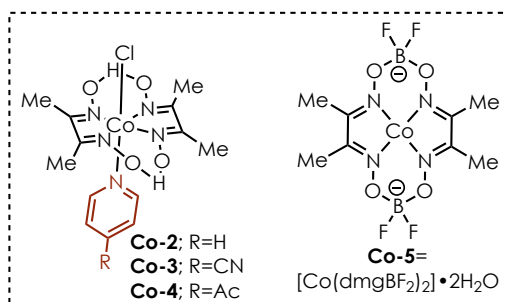
4.2.2 Initial Optimization of Propylbenzene Oxidation

In order to extend this methodology to a much wider array of substrates, linear alkanes were explored. However, as mentioned above dehydrogenation of linear alkane substrates using a photoredox system had not yet been developed. As alluded to in Section 4.2.1, when attempting to use a thiophosphoramidate (TPA) catalyst, almost none of the desired oxidation product could be obtained using a linear alkane substrate like propylbenzene (**Table 4.2, Entry 1**). A report from the König lab showed that LiNO_3 could be oxidized by Mes-Acr-Me^+ , and abstract α -oxy C–H bonds to effect alcohol oxidation.⁶¹ We believed this would be a good fit for our system because nitrate radical abstracts C–H bonds and forms HNO_3 , which should be a strong enough acid to protonate cobaloximes. Additionally, HNO_3 has a BDE of 101 kcal/mol⁶² and should be sufficient to abstract benzylic C–H bonds (BDE ($\text{PhCH}_2\text{--H}$) = 90 kcal/mol).⁶³ When 20 mol% LiNO_3 was used as the redox-mediator a modest yield of the desired oxidation product, 3-phenyl 2-propanone, could be obtained (**Table 4.2, Entry 2**). This could be improved to a yield of 35% or 39%, by the use of 1.0 or 2.0 equivalents of LiNO_3 (**Table 4.2, Entries 3 and 4**). Increasing the reaction time to 40 hours rather than the typical 16 hour reaction time, led to an improvement in the yield (**Table**

Table 4.2: Optimization of propylbenzene oxidation



Entry	H ₂ Evolving Catalyst	Redox Mediator	Reaction Time	% Yield ^{viii} Phenyl 2-propanone
1	5 mol% Co-2	5 mol% TPA ^{ix}	16 h	5%
2	5 mol% Co-2	20 mol% LiNO₃	16 h	14%
3	5 mol% Co-2	1 equiv. LiNO₃	16 h	33%
4	5 mol% Co-2	2 equiv. LiNO₃	16 h	39%
5	5 mol% Co-2	2 equiv. LiNO ₃	40 h	54%
6	5 mol% Co-2	—	16 h	—
7	5 mol% Co-3	1 equiv. LiNO ₃	16 h	33%
8	5 mol% Co-4	1 equiv. LiNO ₃	16 h	36%
9	5 mol% Co-5	1 equiv. LiNO ₃	40 h	58%



^{viii} Yield as determined by ¹H NMR spectroscopic analysis of the crude reaction mixture relative to the internal standard (Me₃Si)₂O.

^{ix} See Table 4.1 for structure of TPA.

4.2, Entry 5). There were also several side products formed in some cases: including benzylic oxidation products, which were likely the result of O₂ getting into the reaction. However, these products were typically only formed in < 5% yield. No products were formed without the use of any redox-mediator (**Table 4.2, Entry 6**).

Since altering other reaction conditions was not found to improve the yields using the LiNO₃, other potential redox-mediators were screened. Most of these proved to be unfruitful, typically giving back completely unreacted starting material. However, in some cases the desired oxidation product could be formed but in low yields.^x Since no improvements could be made by changing the identity of the redox-mediator, the identity of the cobaloxime catalyst was examined. As mentioned previously, it is likely that after initial C–H abstraction at the benzylic position occurs, the cobaloxime catalyst first is protonated by HNO₃ (or H₃O⁺) in situ before SET from the benzylic radical occurs.^{xi} It seemed possible that modifying the pyridine ligand, could potentially alter the redox properties of the cobaloxime catalyst.^{xii} Two cobaloxime derivatives were synthesized; 4-CN-pyridine and 4-Acetyl pyridine respectively. However, these complexes gave almost identical results to [Co(dmgh)₂ pyCl] after 16 hours (**Table 4.2, Entries 7 and 8**). In addition, well known H₂ evolving catalyst [Co(dmghBF₂)₂ (H₂O)₂] was also screened, and gave 58% yield after 40 hours (**Table 4.2, Entry 9**).

^x The reagents of all redox-mediators that produced product and some other related structures are shown at the bottom of Table 4.2.

^{xi} Due to the relevant redox potentials direct oxidation of the benzylic radical is not likely (See Section 4.2).

^{xii} Altering the electronic nature of the pyridine ligand in cobaloxime catalysts has been previously demonstrated in the literature but was not known by us at this point. See ref. 56 for examples.⁵⁶

4.2.3 Evaluating Reaction Irreproducibility

Around this time screening of other standard reaction conditions (catalyst loading, concentration, etc.), began to produce unexpectedly low yields of product. Indeed, attempts to replicate previous results were unsuccessful, resulting in fluxional yields of the expected 2-propanone oxidation product (**Table 4.3, Entry 1**). Initially it seemed plausible that this could be the result of variability in the amount of oxygen present in the reaction. Thus, extensive care was taken to ensure that oxygen was excluded from reactions which seemed to lead to similarly poor results. Next, the ability for O₂ to have a role in production of the product was evaluated, as oxygen could have some role in turning over Mes-(3,6-*t*BuAcr)-Ph• or the reduced cobalt complexes.

Since it was too difficult to control how much oxygen was in the reaction, and large oxygen concentrations led to solely formation of the benzylic oxidation product propiophenone, chemical oxidants were screened to determine if they could restore previous reactivity. Screening chemical oxidants led to the discovery that *t*-butyl peroxy benzoate (**TPB**) when used in stoichiometric quantities restored most of the reactivity, forming the product in a moderate 26% yield after 16 hours (**Table 4.3, Entry 2**). Benzoic acid (or benzoate) was also observed by ¹H NMR indicating that *t*-butylbenzoyl peroxide was indeed acting as an oxidant. However, further screening of other reaction conditions including other peroxide oxidants did not lead to higher conversion. Most other oxidants resulted in benzylic oxidation.

At this point we considered, that oxidative products formed in situ could be potentially catalyzing the reactions. Inconsistency in the reactions could then stem from variable amounts of oxidative products formed in the reactions. Some of the other byproducts formed during the reactions were benzylic oxidation products (propiophenone being the major but benzylic peroxides

and benzaldehyde were also observed), and 4-propylphenol. Particularly interesting was 4-propylphenol, a byproduct that is formed in most of the reactions mentioned above in ~5% yield.

Table 4.3: Optimization of propylbenzene oxidation, continued.

Mes-(3,6-tBu-Acr)-Ph+

Entry	H ₂ Evolving Catalyst	Additive	Reaction Time	% Yield ^{xiii} Phenyl 2-propanone
1 ^{xiv}	5 mol% Co-2	—	16 h	13%
2	5 mol% Co-2	1.0 equiv. TPB	16 h	26%
3	5 mol% Co-2	5 mol% Cu(OTf)₂	16 h	33%
4	5 mol% Co-2	5 mol% Cu₂O	16 h	—
5	5 mol% Co-2	10 mol% HNO ₃	16 h	29%

Co-2 =
[Co(dmgh)₂ pyCl]

Co-5 =
[Co(dmghBF₂)₂]•2H₂O

Surrogates for commonly observed oxidative byproducts:

5 mol%

12% yield

1.0 equiv. HO-OH

benzylic oxidation

5 mol%

15% yield

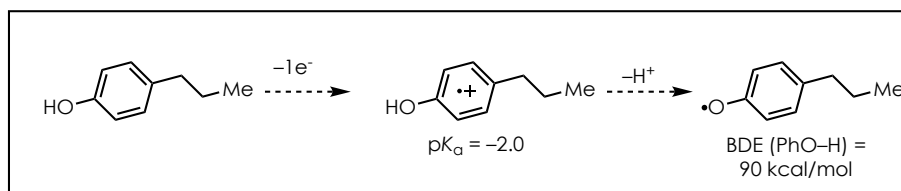
5 mol%

19% yield

^{xiii} Yield as determined by ¹H NMR spectroscopic analysis of the crude reaction mixture relative to the internal standard (Me₃Si)₂O.

^{xiv} Same conditions as Table 4.2, Entry 4.

Scheme 4.2: Phenol could act as a redox-mediator after oxidation by Mes-(3,6-*t*Bu-Acr)-Ph⁺.



We hypothesized that this product could be oxidized by Mes-(3,6-*t*Bu-Acr)-Ph⁺ to form the phenol cation-radical. These intermediates have been shown to have very low pK_a values ($pK_a (PhOH)^+ = -2$).⁶⁴ This could mean that oxidized phenols could be acting as redox-mediators in this reaction, as phenoxy radicals have BDEs similar to that of benzylic radicals ($BDE (PhO-H) = 90 \text{ kcal/mol}$). Regardless, adding cresol (as a surrogate for 4-propylphenol), acetophenone (a surrogate for benzylic ketone products), hydrogen peroxide (a surrogate for peroxides), or benzaldehyde (this was observed in small quantities in most reactions) did not restore the reactivity (See bottom of Table 4.3).

Since no additives seemed to restore reactivity, we began to suspect that inconsistencies in batches of Mes-(3,6-*t*Bu-Acr)-Ph⁺ could be causing difficulty in reproducing results. Trace metal contamination was initially suspected, as one of the final steps in the Mes-(3,6-*t*Bu-Acr)-Ph⁺ synthesis involves Cu catalyzed cross-coupling. Trace metals have been previously found to catalyze ‘metal free’ reactions, so this did not seem out of the realm of possibility.⁶⁵ Contamination of the cobaloxime did not seem likely as multiple Co catalysts had previously given similar results (See Table 4.2). Additionally, reaction irreproducibility began around the time of switching to a new acridinium catalyst batch. Indeed, upon screening several Cu salts, Cu(OTf)₂ was found to restore yields to previously observed levels (33%, **Table 4.3, Entry 3**). It seemed odd that only Cu(OTf)₂ gave any reactivity while all other Cu salts were detrimental to reactivity (**Table 4.3, Entry 4**). This observation also was not consistent with Cu contamination from previous catalyst

batches, as other Cu salts like Cu₂O would likely be closer approximations to any Cu impurities in the catalyst.

Nevertheless, we elected to utilize ICP/MS (Inductively coupled plasma tandem mass spectroscopy), to verify that Cu was not present in abnormally high levels in the very small amount of the original batch of Mes-(3,6-*t*Bu-Acr)-Ph⁺ that was remaining (See Section 4.5.7 for details).^{xv} Mn and Fe were also screened because they have similar molecular weights to Cu, and were used as controls. **Table 4.4** shows the results of the analysis. While detectable levels of Cu were found in the suspect batch of Mes-(3,6-*t*Bu-Acr)-Ph⁺ (A), almost all batches contained Cu. All other catalyst batches included in Table 4.4 had been evaluated for the reactivity and were found to give consistently low yields of product (~10%). Since catalyst batch A contains ppm levels of Cu in intermediate levels relative to other catalyst batches, we took this to indicate that some Cu impurity was not responsible for the increase in catalytic activity with catalyst batch A.

Table 4.4: Analysis of trace-metals using ICP/MS.

Batch of Mes-(3,6- <i>t</i> Bu-Acr)-Ph ⁺	Cu ppm (mg/kg) ^{xvi}	Mn ppm (mg/kg) ^{xvi}	Fe ppm (mg/kg) ^{xvi}
A ^{xvii}	48 ppm	Below LOD	198 ppm
B	Below LOD	Below LOD	Below LOD
C	28 ppm	Below LOD	40 ppm
D	110 ppm	22.5 ppm	487 ppm
E	90 ppm	12.5 ppm	425 ppm

^{xv} For an example of the recent use of this technique to rule out trace metal contamination see: *J. Am. Chem. Soc.*, **2017**, 139 (4), pp 1668–1674⁸²

^{xvi} mg of metal per kg Acridinium catalyst

^{xvii} Batch A was the Mes-(3,6-*t*Bu-Acr)-Ph⁺ which had been used for the optimization reactions found in Tables 4.1 and 4.2.

Furthermore, the concentration of Cu in the reaction mixture would be very low (95 ppb, $\mu\text{g/L}$).

Given that significant trace metal contamination was not found, coupled with the fact that $\text{Cu}(\text{OTf})_2$ was the only successful Cu salt of those screened, it seemed more likely that $\text{Cu}(\text{OTf})_2$ was being hydrolyzed to form Brønsted acid in situ. This could also be consistent with the fact that *t*-butylbenzoyl peroxide was somewhat successful in this reaction, as benzoic acid was observed as a byproduct.^{xviii} When 10 mol% HNO_3 acid was used rather than $\text{Cu}(\text{OTf})_2$ very similar yields were obtained (**Table 4.3, Entry 5**). The fact that Brønsted acid seems to restore reactivity, suggests that slow protonation of one of the cobaloxime intermediates could be problematic. Additionally, this leads us to believe that the first batch of $\text{Mes}-(3,6\text{-}i\text{Bu-Acr})\text{-Ph}^+$ was contaminated with trace acid and was leading to deceptively high yields. This would not be that surprising as the last step in the synthesis of $\text{Mes}-(3,6\text{-}i\text{Bu-Acr})\text{-Ph}^+$ is the addition of $\text{HBF}_4 \cdot \text{Et}_2\text{O}$. Nevertheless, adding 10 mol% HNO_3 to reaction improved reactivity across multiple batches of catalyst.

4.2.4 Kinetic Analysis of Homobenzylic Oxidation

In order to gain further insight into these reactions and potentially expedite the remaining optimization, kinetic analysis was undertaken. Carrying out kinetic analysis before the reaction has been completely optimized could hopefully give us insight into any improvements that could be made without randomly screening and rescreening basic reaction elements.

^{xviii} It is possible that benzoic acid is produced via direct oxidation of a Co–H, which is proposed to form in this reaction. See Schemes 4.3 and 4.4 in Section 4.3.1.

4.2.4.1 Reaction Progress Kinetic Analysis

Reaction progress kinetic analysis has recently been used as a tool for studying reaction kinetics without the necessity of multiple pseudo first order experiments.⁶⁶ Initially React-IR seemed like an ideal method for in-situ monitoring of reaction progress, however due to multiple overlapping IR stretches this was not possible. In situ NMR monitoring is also not possible for this system due to the difficulty in transmitting high intensity light inside the NMR spectrometer, as well as the presence of paramagnetic species like Co^{II} intermediates which could obscure NMR spectra. Instead the concentration of propylbenzene ($[\text{propylbenzene}]_t$) was monitored by GC-FID (See Section 4.5.8). Under standard conditions (Initial concentration = 0.09M propylbenzene) a brief induction period (~20 minutes) was observed, the reaction then proceeds at a relatively fast

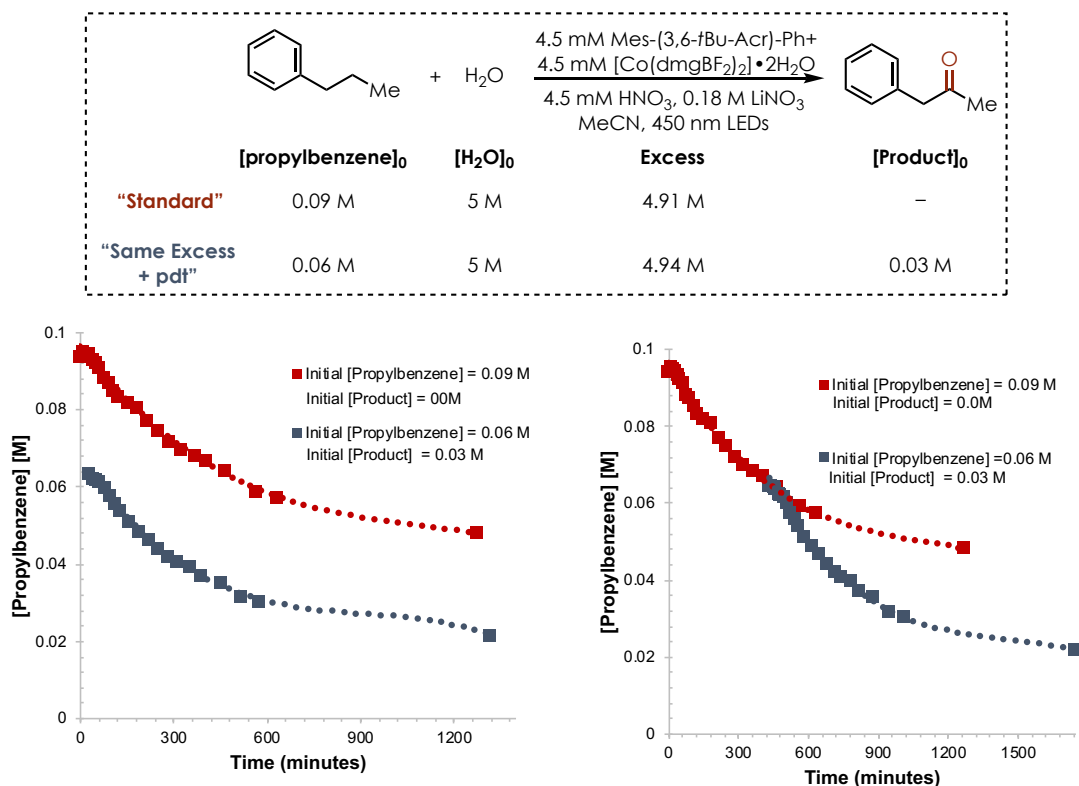


Figure 4.11: (left) Kinetic profile of propylbenzene oxidation under the standard conditions (red line) and the same excess experiment (blue line). **(right)** the same excess experiment was offset on the time axis such that the curves initially overlay at $[\text{propylbenzene}] = 0.06 \text{ M}$ and $[\text{product}] = 0.03 \text{ M}$. From this experiment it is clear that the reaction profiles do not overlay, implicating catalyst decomposition.

rate reaching ~15% conversion after 3 hours (**red line left graph, Figure 4.11**). However, the reaction quickly tails off and only reaches ~40% after 20 hours. A “Same Excess” experiment was run by starting the reaction at a lower concentration of propylbenzene while keeping all other stoichiometric reagents in the same relative concentrations. Since H₂O was already in great excess (55 equivalents relative to propylbenzene) no change was needed to be made with respect to the concentration in the ‘same excess’ experiment (See reaction scheme at the top of **Figure 4.11**).

Even though LiNO₃ is used in stoichiometric quantities, it was treated as a catalyst here because based on our proposed mechanism for this transformation (See Scheme 4.3, Section Section 4.3.1), [LiNO₃] should not change over the course of the reaction. The same excess experiment was run to simulate the reaction at approximately 30% conversion, therefore phenyl 2-propanone was added along with propylbenzene at the beginning of the reaction (**blue line left graph, Figure 4.11**). The ‘same excess’ experiment shows a very similar reaction profile to that of the standard conditions, initially an induction period was observed, then proceeding relatively

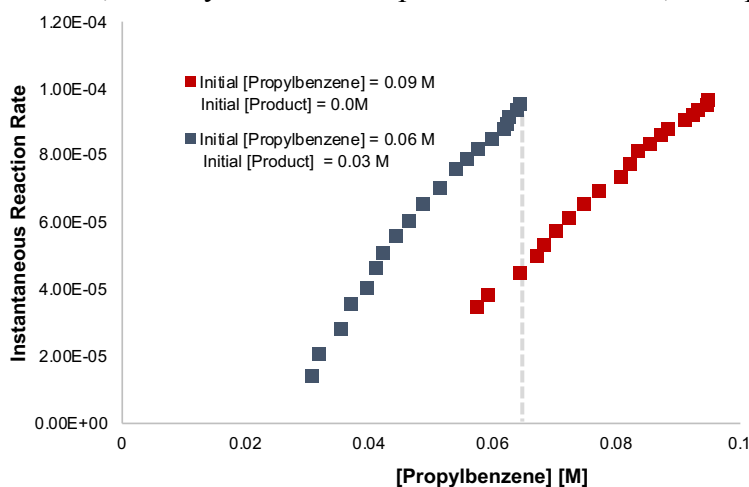


Figure 4.12: Instantaneous reaction rate plotted against [propylbenzene] [M]. From **right to left** this plot shows that the reaction rate decreases markedly at lower substrate concentrations, the fact that the two curves do not overlay is indicative of catalyst decomposition. The gray line intercepts both curves at the same concentration, emphasizing the difference in reaction rates at this concentration. Initial reaction rates for the standard and ‘same excess’ experiments are approximately equal.

fast and tailing off. Interestingly, when offsetting the time axis such that the first point overlays with the standard experiment at the same concentration (0.06 M), the curves do not overlay (**right graph, Figure 4.11**). In catalytic reactions with high fidelity these curves should overlay because all reactant and catalyst concentrations are the same between the two experiments. Since, phenyl 2-propanone should also be present in both reactions at the same concentrations, product inhibition can be ruled out as an explanation for the faster than expected conversion in the ‘same excess’ experiment.

To more clearly visualize the unexpected rate differences the instantaneous rate of reaction (See Section 4.5.8 for more details) can be plotted against concentration of propylbenzene (**Figure 4.12**). Interestingly, this way of plotting the data shows that the first instantaneous rate point for both the standard conditions and the same excess experiment are approximately equal ($1.0 \times 10^{-4} \text{ M}^{-1} \text{ s}^{-1}$).^{xix} This would not be expected for a first order reaction, indicating that the reaction is possibly zero-order with respect to propylbenzene. This is a characteristic feature of light limited reactions but will require further study to confirm that this is the case. Intercepting both curves at 0.06M reveals that the rate is drastically lower than expected for the standard experiment (gray line in **Figure 4.12**). Together these data likely implicate catalyst decomposition. As of yet, we have not determined with certainty which catalyst is decomposing, however we suspected the cobaloxime catalyst because they have been demonstrated in the literature to decompose upon exposure to strong acids.^{58,67}

^{xix} This can also be confirmed by comparing the initial rates measurements of both reactions. The initial rate for the standard conditions reaction was $1.2 \times 10^{-4} \text{ M}^{-1} \text{ min}^{-1}$ whereas the initial rate of the ‘same excess’ reaction was $9.9 \times 10^{-5} \text{ M}^{-1} \text{ min}^{-1}$. These were determined after excluding the induction period, and thus are slightly different from the initial instantaneous rate values in Figure 4.12.

4.2.4.2 Evaluation of other acids

As stated above based on the kinetic profiles of unoptimized reactions, we discovered that catalyst degradation was problematic and believed that $[\text{Co}(\text{dmgBF}_2)_2]$ was most likely the catalyst that was undergoing decomposition. To this end we decided to screen other acids to see if a more suitable acid might alleviate catalyst degradation (**Figure 4.13**). Additionally, $[\text{Co}(\text{dmgBF}_2)_2(\text{H}_2\text{O})_2]$ was used in favor of the less stable $[\text{Co}(\text{dmgH})_2\text{pyCl}]$ which was found to give an improvement in reactivity. Of the acids screened, only dichloroacetic acid (DCA) was found to give significantly better yield of the desired oxidation product. When comparing the reaction profiles (concentration vs time plot, **Figure 4.14**) of the reaction using 5 mol% HNO_3 or DCA, the reaction rates are similar at early reaction times, but the reaction with DCA begins to diverge at ~20% conversion and ultimately reaches higher conversion. The plot of instantaneous reaction rate vs [propylbenzene] plot reveals that the major deviation in rate is in the region between 0.08 and 0.06 M propylbenzene. This indicates that while DCA provides some additional catalyst stability, at higher reaction conversions catalyst decomposition is still likely a problem at this stage. Thus,

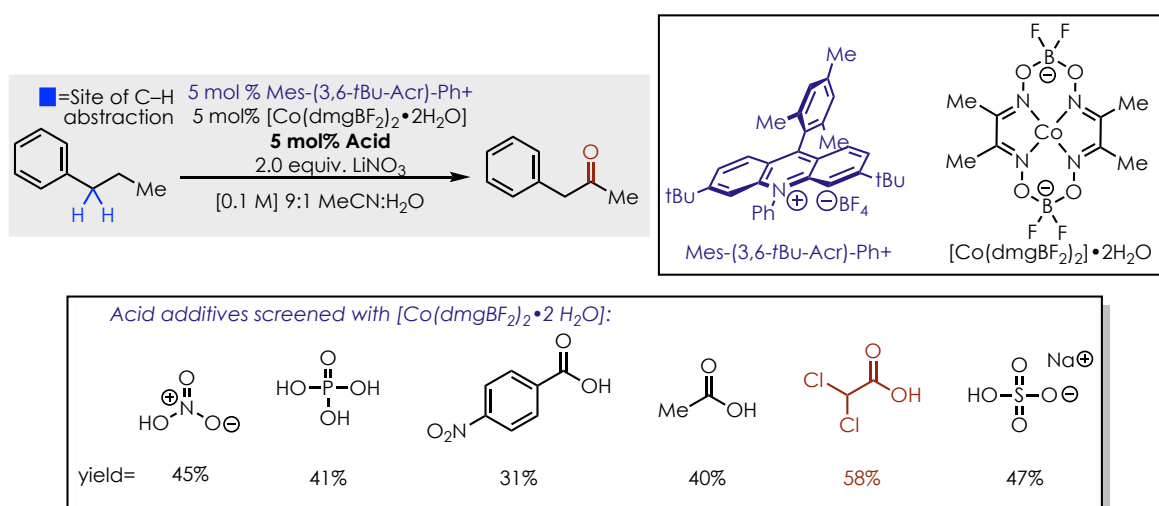


Figure 4.13: Acids having pK_a values in the range of approximately -1–5 were screened as a comparison to nitric acid. All acids were added in 5 mol% loading.

future work will focus on improving catalyst stability by either finding a more stable catalyst or a different acid.

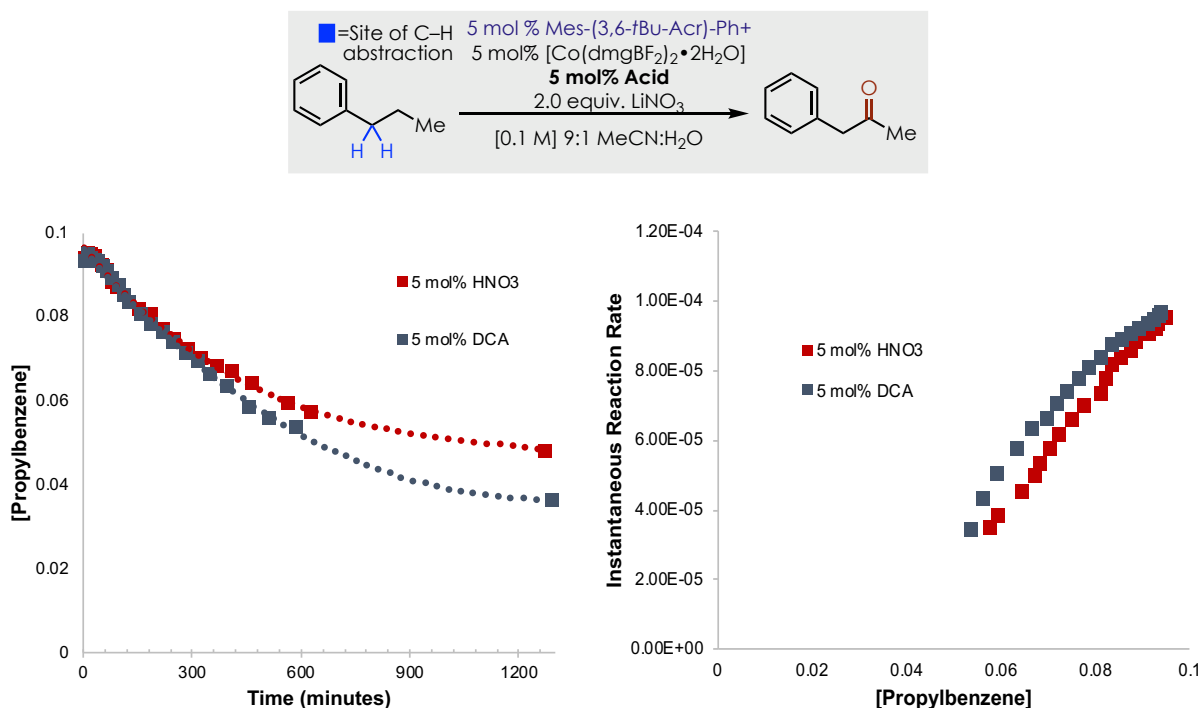
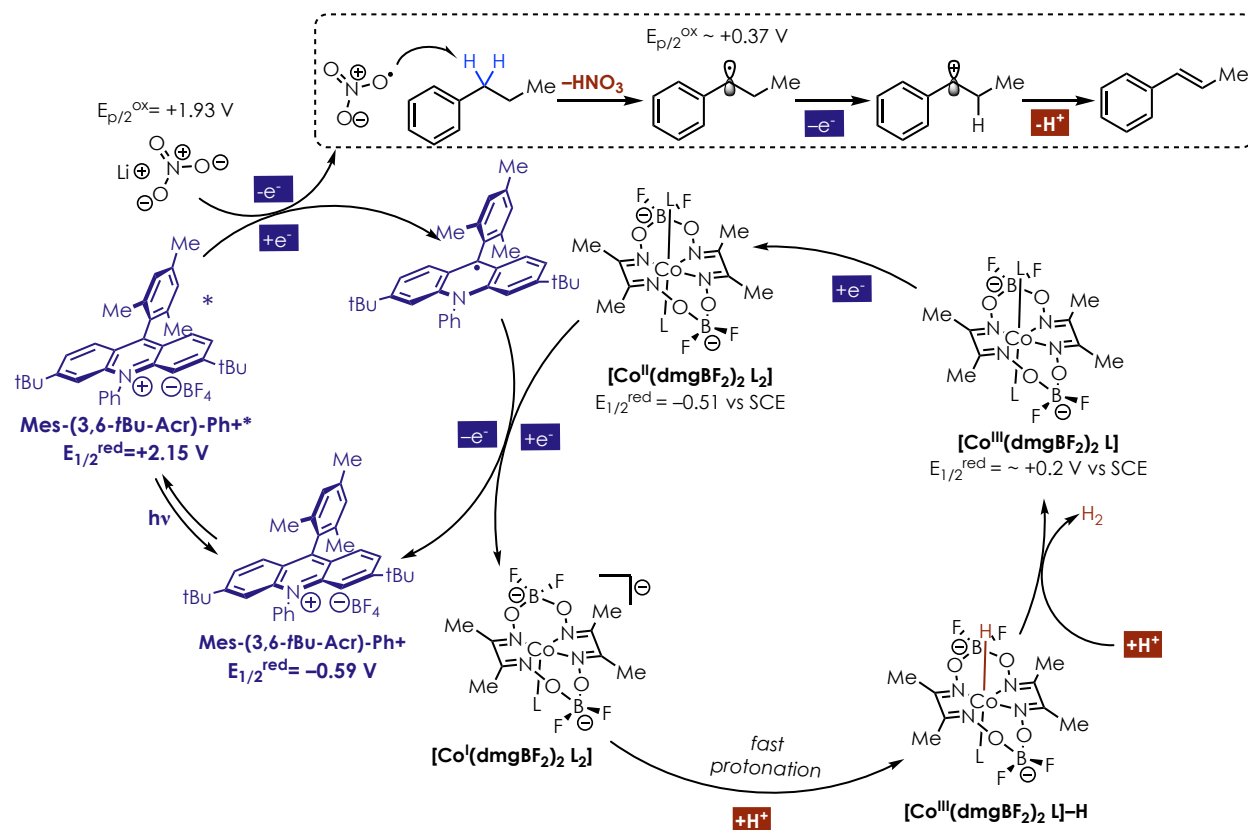


Figure 4.14: (left) Reaction profiles of propylbenzene oxidation when using 5 mol% HNO_3 (red line) or DCA (blue line). (right) Instantaneous reaction rate plotted against propylbenzene concentration. These plots show that at early reaction times the use of DCA leads to higher reaction rates than HNO_3 but ultimately slows to nearly the same rate at about 30% reaction conversion.

4.3 Reaction Mechanism

4.3.1 Initial Mechanistic Proposal

Scheme 4.3: Proposed mechanism of alkane dehydrogenation.



As mentioned previously the reaction likely proceeds through a two stage mechanism. We propose that the reaction proceeds first through the dehydrogenation of the alkane (**Scheme 4.3**). Upon excitation to the singlet excited state with 450 nm light, Mes-(3,6-*t*Bu-Acr)-Ph⁺ (E_{1/2}^{red} = +2.15 V vs SCE)⁶⁸ can undergo SET with LiNO₃ (E_{p/2}^{ox} = +1.93 V vs SCE, See Section 4.5.6 for details). This electrophilic radical then undergoes H-atom abstraction of the alkane substrate at the benzylic position, forming a benzylic radical intermediate along with HNO₃. Mes-(3,6-*t*Bu-Acr)-Ph[•] (E_{1/2}^{ox} = -0.59 V vs SCE)⁶⁹ can feasibly undergo electron transfer with [Co^{II}(dmgBF₂)₂ L₂]

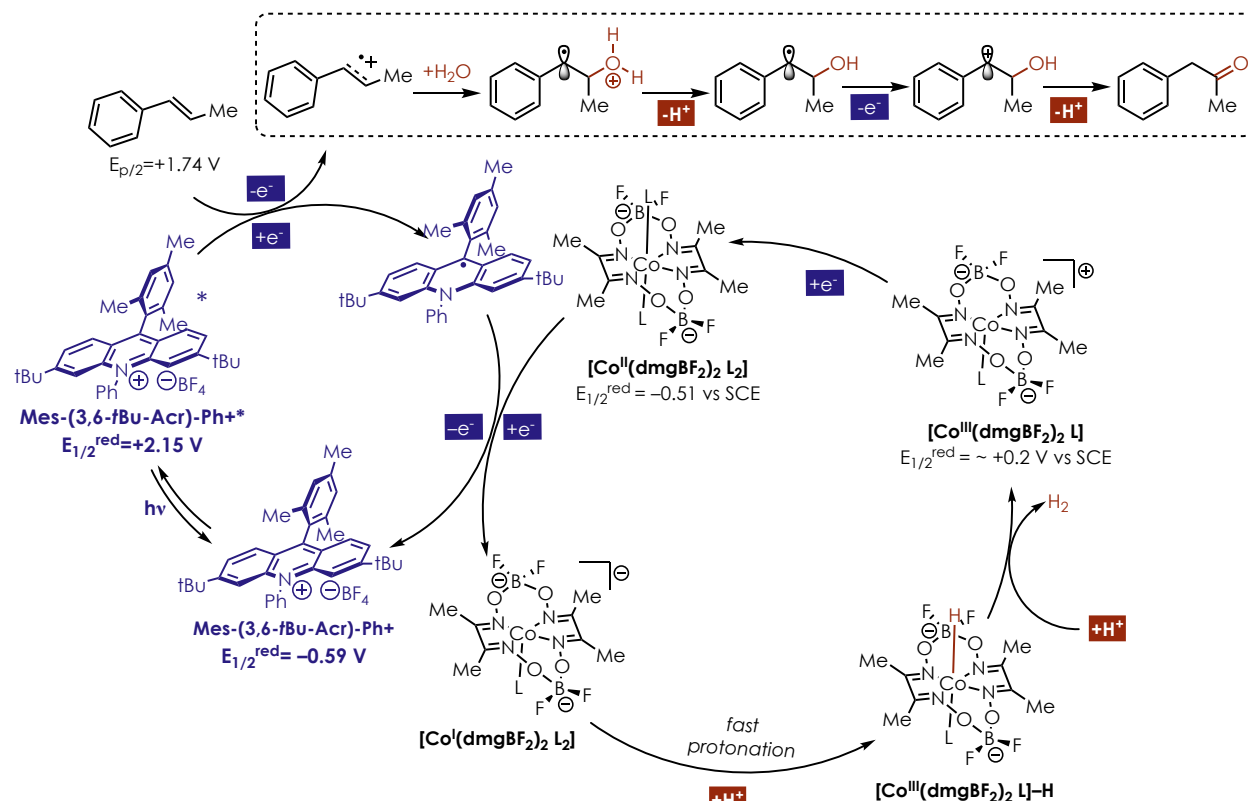
($E_{1/2}^{ox} = -0.51$ V vs SCE)^{56,58xx}. Since this electron transfer has a very low thermodynamic driving force, it seemed it could be slow. Attempts were made to measure a rate constant for this ET using Stopped-Flow rapid mixing with UV/vis monitoring. Upon mixing a solution of Mes-(3,6-*t*Bu-Acr)-Ph• (50 μ M) and [Co^{II}(dmgBF₂)₂ L₂] (50 μ M) new absorbances appeared corresponding to [Co^I(dmgBF₂)₂ L₂]⁻ and Mes-(3,6-*t*Bu-Acr)-Ph⁺ respectively (See 4.5.10 for details). Since the ET occurred within the mixing time (15 ms), a lower limit of $\sim 10^7$ M⁻¹s⁻¹ for the rate constant of this ET can be estimated.

[Co^I(dmgBF₂)₂ L₂]⁻ species have been shown to undergo rapid protonation to form [Co^{III}(dmgBF₂)₂ L₂]-H.⁵⁸ The literature suggests two possible mechanism for turnover of the Co^{III}-H: 1) the first is a heterolytic mechanism in which Co^{III}-H or Co^{II}-H is directly protonated to release H₂ as well as a Co^{III} or Co^{II} species. 2) the second is termed a homolytic mechanism in which two Co^{III}-H species combine to produce H₂ and two Co^{II}. The homolytic mechanism has been shown to be favored in the majority of cases due to the lower associated barrier to reaction.⁷⁰ Recent work by the Dempsey lab has also shown that protonation of a Co^{II}-H is likely H₂ production.⁵⁸ However, in our system the benzylic radical intermediate is not able to reduce Co^{II}. This indicates that either benzylic radical undergoes SET with Mes-(3,6-*t*Bu-Acr)-Ph⁺* or with a Co^{III} intermediate. SET with Mes-(3,6-*t*Bu-Acr)-Ph⁺* would require the benzylic radical to exist in solution for a sufficiently long time to encounter Mes-(3,6-*t*Bu-Acr)-Ph⁺*. As both species are likely to be in solution in very low concentrations, this does not seem likely. Therefore, for our system it seems more likely that direct protonation of Co^{III}-H is occurring, which is also consistent with the necessity of additional acid to be added at the beginning of the reaction. This would form

^{xx} The value for $E_{1/2}^{red}$ of [Co^{II}(dmgBF₂)₂ L₂] varies slightly in the literature, however most sources are between -0.55 and -0.5 V vs SCE.

a cationic Co^{III} ($E_{1/2}^{\text{red}} \sim +0.2 \text{ V}$ vs SCE) which could potentially oxidize the benzylic radical ($E_{p/2}^{\text{ox}} \sim +0.37 \text{ V}$ vs SCE). While this ET is endergonic by about $+0.2 \text{ V}$ (or 4 kcal/mol), rapid deprotonation of the resulting benzylic cation intermediate would render ET irreversible, ultimately producing the styrene intermediate.

Scheme 4.4: Proposed mechanism of styrene oxidation.



Following the formation of styrene the reaction enters the second stage. SET between styrenes and Mes-(3,6-*t*Bu-Acr)-Ph⁺* have been well preceded in the literature to result in anti-Markovnikov attack on the resulting cation-radical intermediate.⁷¹ Following successive deprotonation and oxidation steps results in the formation of the homobenzylic oxidation product (Scheme 4.4). The remaining catalyst turnover steps are described above and are proposed to be identical to the dehydrogenation stage. It should be emphasized that at this stage that this

mechanistic hypothesis is very preliminary. Several mechanistic studies are ongoing to verify some of the elementary steps.

4.3.2 Fluorescence Quenching

Stern-Volmer quenching studies were carried out to ensure that Mes-(3,6-*t*Bu-Acr)-Ph⁺* can undergo SET with LiNO₃ (**Figure 4.15**). Although, reactions between acridinium photooxidants and nitrate have been established the kinetics of this electron transfer have not been studied to best of our knowledge. Additionally, we noted that in most cases styrene was not observed at the end of the reactions; it seemed possible that styrenes were more efficient quenchers of Mes-(3,6-*t*Bu-Acr)-Ph⁺*. To verify this Stern-Volmer analysis was also carried out with β -methyl styrene (**Figure 4.16**).

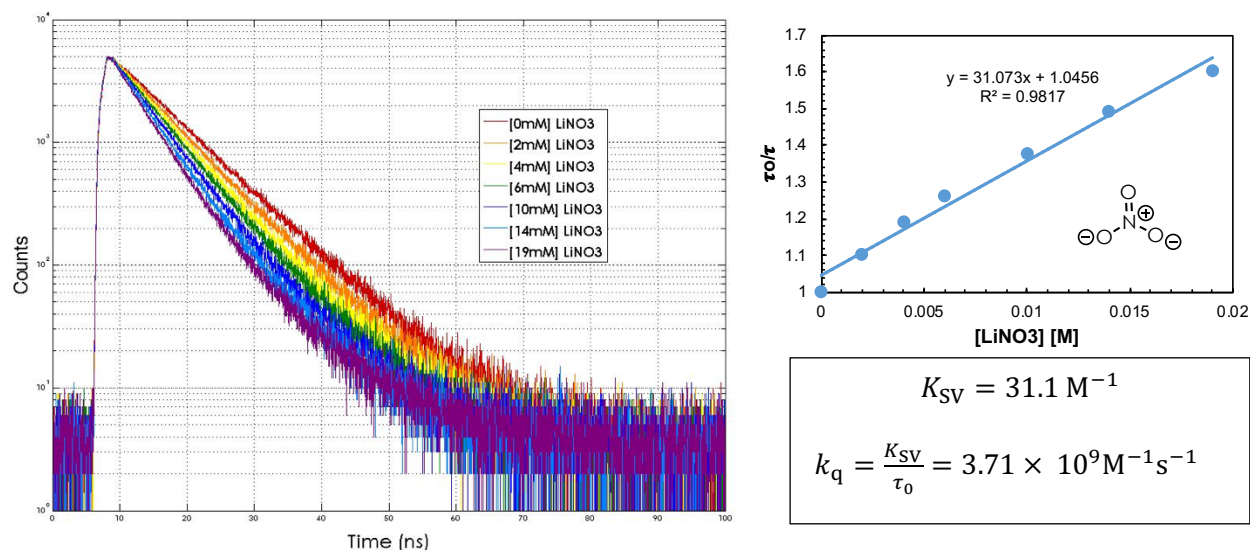


Figure 4.15: (left) Time-resolved fluorescence spectra of Mes-(3,6-*t*Bu-Acr)-Ph⁺ (15 μM) with increasing concentration of LiNO₃ (0-19 mM) quencher run in 9:1 MeCN:H₂O. (right) Stern-Volmer plot of the quenching of Mes-(3,6-*t*Bu-Acr)-Ph⁺ with LiNO₃. The lifetime in the absence of quencher (τ_0) was determined to be 8.37 ns. τ_0 divided by τ at each quencher concentration was plotted against [LiNO₃]. The Stern-Volmer constant (K_{SV}) was determined from the slope of the line.

Figure 4.15 shows the time-resolved fluorescence spectra and Stern-Volmer plot for the quenching of Mes-(3,6-*t*Bu-Acr)-Ph⁺ with LiNO₃. A bimolecular quenching constant of $3.71 \times 10^9 \text{ M}^{-1} \text{ s}^{-1}$ was determined based on the Stern-Volmer plot, indicating that SET is indeed feasible and quite efficient.

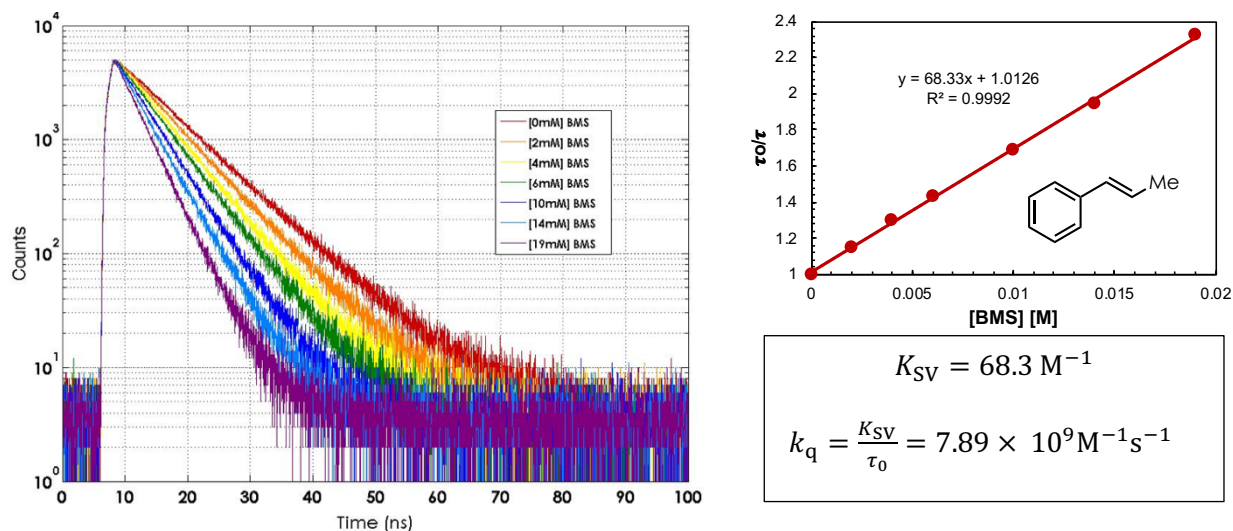


Figure 4.16: (left) Time-resolved fluorescence spectra of Mes-(3,6-*t*Bu-Acr)-Ph⁺ (15 μM) with increasing concentration of BMS (0-19 mM) quencher run in 9:1 MeCN:H₂O. (right) Stern-Volmer plot of the quenching of Mes-(3,6-*t*Bu-Acr)-Ph⁺ with BMS. The lifetime in the absence of quencher (τ_0) was determined to be 8.41 ns. τ_0 divided by τ at each quencher concentration was plotted against [BMS]. The Stern-Volmer constant (K_{SV}) was determined from the slope of the line.

Although k_q has previously been measured for beta-methylstyrene (BMS) with Mes-Acr-Me⁺,⁷² the k_q had not yet been determined for Mes-(3,6-*t*Bu-Acr)-Ph⁺ and BMS. The bimolecular

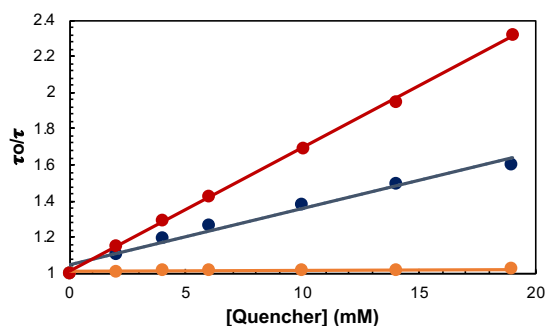


Figure 4.17: Combined Stern-Volmer plots for Mes-(3,6-*t*Bu-Acr)-Ph⁺ singlet excited state quenching. (red line) Quencher = BMS, (blue line) Quencher = LiNO₃ (Orange line) Quencher = propylbenzene.

quenching constant of $7.89 \times 10^9 \text{ M}^{-1}\text{s}^{-1}$ was determined based on the Stern-Volmer plot (**Figure 4.16**). Thus, BMS quenches the excited state of Mes-(3,6-*t*Bu-Acr)-Ph⁺ at roughly twice the rate of LiNO₃. This could potentially be an explanation for the fact that BMS does not build up in high concentrations in the reaction. We find it very likely that pre-association complexes between both the BMS (Charge-transfer) and LiNO₃ are present (Charge-transfer or ion pairing). Further studies will be conducted in order to determine if this is the case.

Finally, in order to demonstrate that propylbenzene ($E_{p/2}^{ox} = +2.27 \text{ V vs SCE}$, See Section 4.5.6) cannot undergo direct oxidation by Mes-(3,6-*t*Bu-Acr)-Ph⁺ the fluorescence lifetime was measured with increasing propylbenzene concentrations. Mes-(3,6-*t*Bu-Acr)-Ph⁺ excited state lifetime was virtually unchanged even with high concentrations of propylbenzene indicating that very little if any electron transfer is taking place. Relative to the other two quenchers in solution propylbenzene oxidation is likely to be insignificant (**Figure 4.17**).

4.4 Conclusions

A method for the homobenzylic oxidation of alkanes is currently being developed. Unlike other methods for C–H oxidation, this method has shown to be selective for unactivated secondary C–H bonds rather than activated benzylic C–H bonds. Rather than try to develop reagents that are selective for the stronger C–H bond, this method instead utilizes the fact that the benzylic C–H bond is the weakest in the molecule and ultimately transfers the radical hybridization through the C–C framework. Mechanistic studies are currently underway. Computational chemistry as well as KIE studies are being used to probe the C–H abstraction step, while other chemical probes will be used to study the fate of the benzylic radical.

4.5 Experimental

4.5.1 General Methods and Materials

General Methods. Proton, carbon, (^1H NMR, ^{13}C NMR) were recorded on a Bruker model DRX 400 or AVANCE III 600 CryoProbe spectrometer (^1H NMR at 400 MHz or 600 MHz, ^{13}C NMR at 100 MHz or 150 MHz respectively). Chemical shifts for proton NMR are reported in parts per million downfield from tetramethylsilane and are referenced to residual CHCl_3 in solution (CHCl_3 set to 7.26 ppm). Chemical shifts for ^{13}C NMR are reported in parts per million downfield from tetramethylsilane and are referenced to the carbon resonances of the solvent (CDCl_3 set to 77.00 ppm). NMR data are represented as follows: chemical shift, multiplicity (s = singlet, br s = broad singlet, d = doublet, dd = doublet of doublet, t = triplet, ddd = doublet of doublet of doublet, q = quartet, m = multiplet, etc.), coupling constants (Hz), and integration. Low Resolution Mass Spectra (**LRMS**) were obtained using GC-MS (Agilent 6850 series GC equipped with Agilent 5973 network Electron Impact-MSD). Inductively Coupled Plasma Mass Spectra (**ICPMS**) were obtained using a Thermo Element XR. Thin layer chromatography (TLC) was performed on SiliaPlate 250 μm thick silica gel plates purchased from Silicycle. Visualization was accomplished using fluorescence quenching, KMnO_4 stain, or ceric ammonium molybdate (CAM) stain followed by heating. Purification of the reaction products was carried out by chromatography using Siliaflash-P60 (40-63 μm) silica gel purchased from Silicycle. All reactions were carried out under an inert atmosphere of nitrogen in flame-dried glassware with magnetic stirring unless otherwise noted. Reactions were carried out in standard borosilicate glass vials purchased from Fisher.

Scientific. Yield refers to isolated yield of analytically pure material unless otherwise noted. NMR yields were determined using hexamethyldisiloxane, $(\text{Me}_3\text{Si})_2\text{O}$, as an internal standard.

Materials. Commercially available reagents were purchased from Sigma Aldrich, Acros, Alfa Aesar, Fisher Scientific, or TCI, and used as received unless otherwise noted. Diethyl ether (Et_2O), dichloromethane (DCM), tetrahydrofuran (THF), toluene (PhMe), and dimethylformamide (DMF) were dried by passing through activated alumina columns under nitrogen prior to use. 1,2-dichloroethane (DCE) was purchased from Fischer and sparged with N_2 before being stored over activated 4Å molecular sieves in a glovebox. Acetonitrile (MeCN) was dried by passing through activated alumina column under nitrogen. MeCN was commonly stored in a glovebox after sparging with N_2 . Other common solvents such as chloroform (CHCl_3) were purified by standard published methods when necessary. Trans- β -methylstyrene was distilled over potassium hydroxide, sparged with N_2 , and stored in a glovebox freezer.

4.5.2 Photoreactor Setup

Photoreactor used for Optimization/small scale reactions:

Reactions were irradiated using a custom built photoreactor which consists of eight reactor wells (Figure 4.18). The reactor was built based on the design of a 4-well reactor conceived by Nathan Romero, where irradiation of the reaction is from the bottom. The casing consists of a 3D printed block, which holds 1 and 2 dram vials. CREE® XT-E Royal Blue LEDs (maximum drive current 1 A) were directly mounted onto a heat sink (with mounted fan) using thermal adhesive and screws. LEDs were wired in series with a driver, which supplies a constant current of 700 mA to each LED. The LEDs were fitted with 60 degree lenses. The casing was then screwed directly down onto the heatsink, holding the LEDs in place. The reactor was cooled with a large cooling fan in order to maintain reaction temperatures close to 30 °C. All components were purchased from Rapid LED.

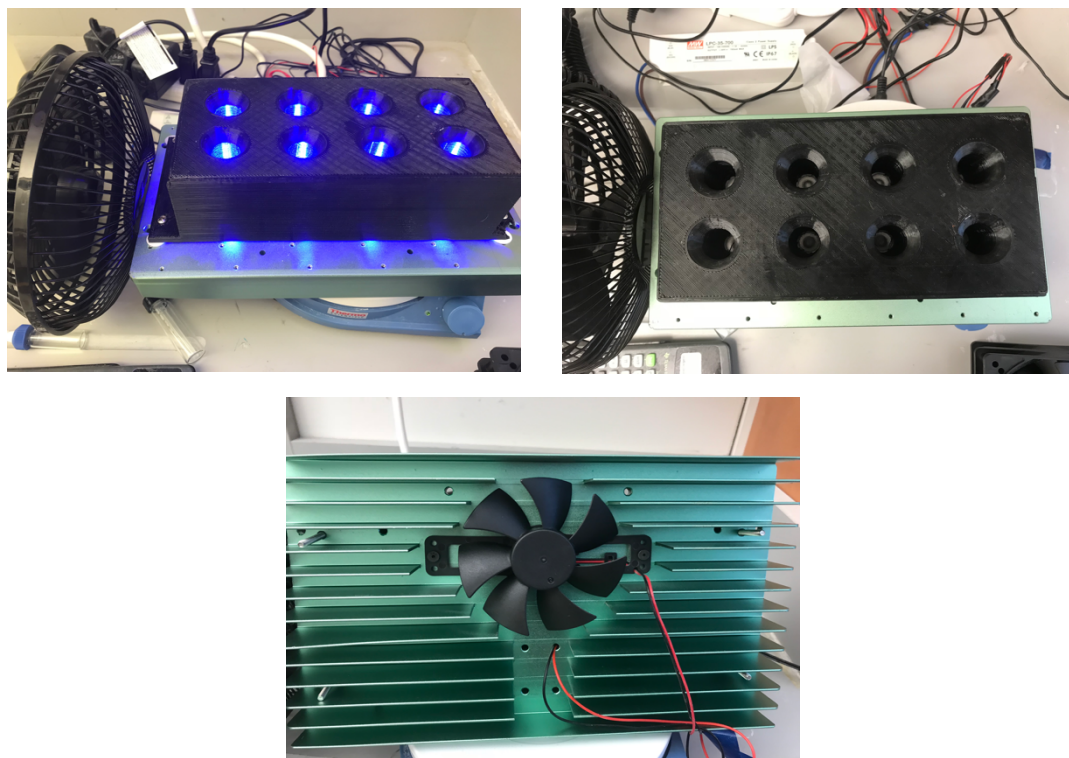


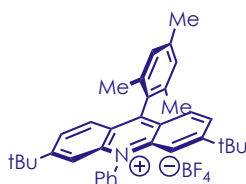
Figure 4.18: Photoreactor setup used for screening small scale reactions.

Photoreactor used for Kinetics and Large Scale Reactions:

A simple photoreactor setup was used for kinetic trials wherein two Kessil® H150 blue LED lamps were positioned such that irradiation occurred from both sides of the reaction vial. The reactions were cooled using a large cooling fan, to ensure reaction temperatures around 30 °C. The lamps were maintained in the same position throughout the trials and between separate trials to ensure consistent photon flux was maintained.

4.5.3 Catalyst Synthesis

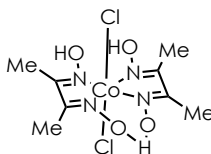
4.5.3.1 Mes-(3,6-*t*Bu-Acr)-Ph⁺ Synthesis



3,6-di-*tert*-butyl-9-mesityl-10-phenylacridin-10-ium tetrafluoroborate was synthesized as previously reported by us in the literature.⁶⁸

4.5.3.2 Cobaloxime Catalyst synthesis

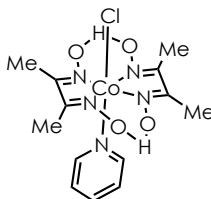
[Co(dmgh)(dmgh₂)Cl₂]:



The procedure was followed from the literature as follows: CoCl₂•6H₂O (2.4 g, 10 mmol) was dissolved in acetone. Dimethylglyoxime was then added (2.44 g, 21 mmol). This solution was

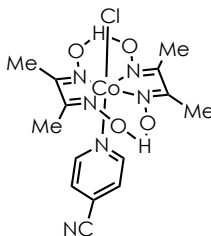
stirred while air was bubbled through. After approximately 3 hours, the blue-green precipitate that formed was filtered and dried in vacuo to give 2.8g, 78% yield of a green solid.⁷³

[Co(dmgh)₂ pyCl]:



Cobaloxime catalysts containing pyridyl ligands were synthesized according to the general procedure described in the literature.⁷³ [Co(dmgh)(dmgh₂)Cl₂] (1.0 g, 2.77 mmol) and pyridine (1.0 g, 2.77 mmol) was first suspended in DCM (10 mL) followed by addition of an aqueous solution of saturated NaHCO₃ (10 mL). This was stirred at room temperature for an hour then diluted with DCM. The organics were washed with H₂O before drying with Na₂SO₄ and evaporating DCM. The compound was obtained as a brown solid. Characterization data matched the reported literature.

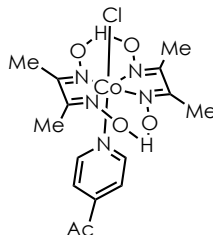
[Co(dmgh)₂ 4-CN-pyCl]:



[Co(dmgh)(dmgh₂)Cl₂] was suspended in methanol. Triethylamine (118 mg, 0.16 mL, 1 Eq, 1.17 mmol) was then added to the flask. After stirring for 5 mins, the suspension turned to a brown/transparent solution. Afterwards, isonicotinonitrile (122 mg, 1 Eq, 1.17 mmol) was added and this was stirred for 1 h to form a brown precipitate. The suspension was filtered and the

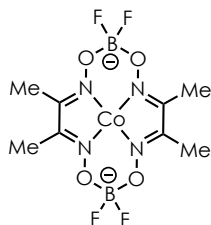
precipitate was washed with water, ethanol, and diethyl ether to afford the cobalt complex. [Co(dmgh)₂ 4-CN-py Cl] (412 mg, 82.4%) of a reddish brown material. ¹H NMR (500 MHz, Chloroform-*d*) δ 8.54 (d, *J* = 6.8 Hz, 2H), 7.48 (d, *J* = 6.8 Hz, 2H), 2.41 (s, 12H).

[Co(dmgh)₂ 4-Ac-pyCl]:



[Co(dmgh)(dmgh₂)Cl₂] (422 mg, 1 Eq, 1.17 mmol) was suspended in methanol. Triethylamine (118 mg, 108 μL, 1 Eq, 1.17 mmol) was then added to the flask. After stirring for 5 mins, the suspension turned to brown/transparent solution. Afterwards, 1-(pyridin-4-yl)ethan-1-one (142 mg, 1 Eq, 1.17 mmol) was added and this was stirred for 1 h to form a brown precipitate. The suspension was filtered and the precipitate was washed with water, ethanol, and diethyl ether to afford the cobalt complexes. [Co(dmgh)₂ 4-Ac-py Cl] (331 mg, 63.5%) of a red-brown material. ¹H NMR (500 MHz, Chloroform-*d*) δ 8.59 – 8.40 (m, 2H), 7.69 – 7.52 (m, 2H), 2.56 (s, 3H), 2.40 (s, 12H).

[Co(dmgbF₂)₂ • 2H₂O]:



Prepared According to the previously reported literature procedure.⁷⁴

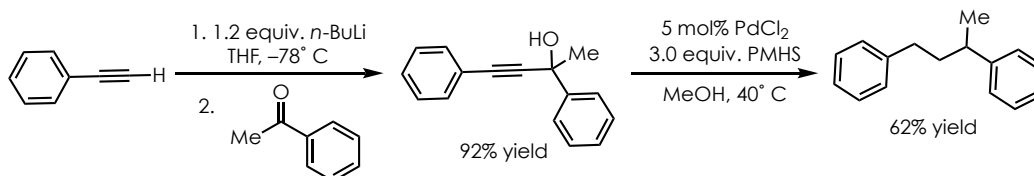
4.5.4 Substrate Synthesis

Additional substrates have been synthesized. Evaluation for suitability in this system is ongoing.

Their synthesis were carried out as follows:

Synthesis of butane-1,3-diyl dibenzene:

Scheme 4.5: Synthesis of butane-1,3-diyl dibenzene



To a flame-dried 250 mL RBF (evacuated twice and back filled with Argon), was added ~75 mL of dry THF. The flask was cooled to -78°C before adding 16.5 mL of *n*-BuLi (1.6 M in hexanes). Next, 2.9 mL of phenyl acetylene was added via the septum and the mixture was allowed to stir for 1 hour. 2.5 mL of acetophenone was then added via syringe via syringe through the septum and the solution was warmed to RT slowly while stirring overnight. The reaction was then carefully quenched with a saturated aqueous solution of NaHCO₃. Most of the THF was removed in vacuo before adding EtOAc and H₂O. The organics were separated and the aqueous layer was extracted once with Et₂O and once with EtOAc. The combined organics were dried over Na₂SO₄ and concentrated in vacuo giving an oily substance. This was purified by chromatography (250 mL

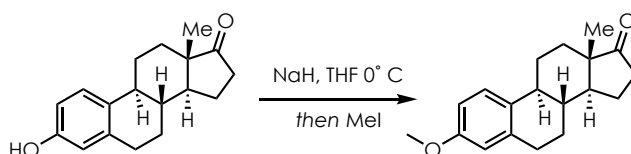
dry silica gel, 4cm column, 1% EtOAc:Hexanes \rightarrow 5% EtOAc:Hexanes \rightarrow 7.5% EtOAc:Hexanes eluent) to give 4.6 g, 92% yield of 2,4-diphenylbut-3-yn-2-ol as a white solid. Characterization matched previously reported spectra⁷⁵:

¹H NMR (400 MHz, Chloroform-*d*) δ 7.74 (d, J = 8.1 Hz, 2H), 7.49 (m, 2H), 7.43 – 7.36 (m, 2H), 7.33 (m, 4H), 2.45 (s, 1H), 1.88 (s, J = 1.0 Hz, 3H).

According to the previously reported literature procedure,⁷⁶ 1.06 g of 2,4-diphenylbut-3-yn-2-ol (from above) was added to a pressure tube. This was followed by 5 mL MeOH, 0.95 mL (3.0 equiv.) polymethylhydrosiloxane (PMHS), and lastly 42 mg of PdCl₂ (5 mol%). The reaction immediately began to evolve gas. Once gas evolution had stopped the vessel was sealed and heated at 40° C overnight. The reaction was then diluted with DCM and passed through a silica plug. TLC and GC/MS revealed complete conversion. Purification was carried by chromatography (20 mL dry silica gel, 2 cm column, 100% hexanes eluent) to give 620 mg, 62% of butane-1,3-diyl dibenzene as a clear oil. Characterization data matched the previous report.⁷⁶

Synthesis of (8*R*,9*S*,13*S*,14*S*)-3-methoxy-13-methyl-6,7,8,9,11,12,13,14,15,16-decahydro-17*H*-cyclopenta[*a*]phenanthren-17-one:

Scheme 4.6: Synthesis of Estrone Methyl-ether



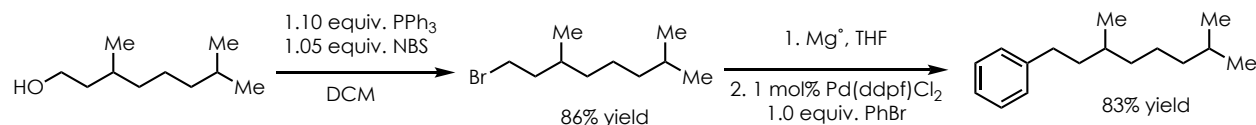
Loosely followed previous literature report.⁷⁷ To a flame-dried 100 mL RBF sodium hydride (0.18 g, 1.2 Eq, 4.44 mmol) (60% by wt) was added. The flask was then evacuated and refilled with

Argon before adding 11 mL of dry THF. The suspension was cooled to 0 °C before adding estrone (1.00 g, 1 Eq, 3.70 mmol) portion-wise. The septum was replaced over the flask and the reaction was allowed to stir until no more H₂ bubbles were observed (~30 mins). iodomethane (4.72 g, 2.07 mL, 9.0 Eq, 33.3 mmol) was then added in a single aliquot and the reaction was allowed to warm to RT and stir overnight. TLC revealed the reaction was complete. Brine was added, followed by EtOAc. The layers were separated and the aqueous was extracted x2 with EtOAc. The combined organics were dried over Na₂SO₄ and concentrated to give an off-white solid that was washed with pentanes to remove trace mineral oil. Result: (8R,9S,13S,14S)-3-methoxy-13-methyl-6,7,8,9,11,12,13,14,15,16-decahydro-17H-cyclopenta[a]phenanthren-17-one (1.02 g, 97.0%) beige to white solid. Characterization data matched the previous report.⁷⁷

¹H NMR (600 MHz, Chloroform-*d*) δ 7.21 (d, *J* = 8.6 Hz, 1H), 6.72 (dd, *J* = 8.6, 2.7 Hz, 1H), 6.65 (d, *J* = 2.7 Hz, 1H), 3.78 (s, 3H), 3.05 – 2.82 (m, 2H), 2.50 (dd, *J* = 19.0, 8.9 Hz, 1H), 2.43 – 2.34 (m, 1H), 2.26 (td, *J* = 10.9, 4.4 Hz, 1H), 2.14 (dt, *J* = 18.7, 8.9 Hz, 1H), 2.09 – 1.98 (m, 2H), 1.98 – 1.91 (m, 1H), 1.71 – 1.38 (m, 7H), 0.91 (s, 3H).

Synthesis of (3,7-dimethyloctyl)benzene:

Scheme 4.7: Synthesis of (3,7-dimethyloctyl)benzene



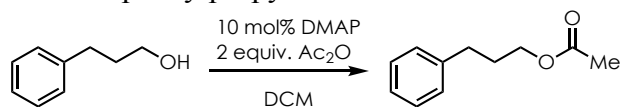
1-Bromo-3,7-dimethyloctane was synthesized according to the previous literature report.⁷⁸ The compound was obtained as an oil that contained a small amount of remaining starting material by ¹H NMR, along with triphenylphosphine oxide. The oil was passed through a plug of silica gel

with pentanes as the eluent and re-concentrated to give a clear oil that was found to be free of impurities by GC/MS and TLC.

Following literature conditions for Kumada coupling.⁷⁹ The Grignard reagent was formed by adding magnesium (707 mg, 3 Eq, 29.1 mmol) that had been ground in a mortar and pedestal into a dried 100 mL RBF. A small amount of I₂ was also added to help activate the Mg. The flask was evacuated and refilled with argon several times. Next, THF (50 mL) dry, was added to the flask followed by 1-Bromo-3,7-dimethyloctane (4.29 g, 2 Eq, 19.4 mmol) carefully. The reaction did not quickly initiate so the flask was gently heated with the heat gun until initiation (flask felt warm without heat). This was allowed to stir at room temperature until the flask felt cool again and then an additional ~30 mins and most of the magnesium had been consumed. In a separate dry 2-neck RBF (250 mL) Pd(dppf)Cl₂ (71.0 mg, 0.01 Eq, 97.0 μmol) was added. The flask was evacuated and refilled with argon several times. When the Grignard reagent was formed it was transferred to the flask containing Pd(dppf)Cl₂ at -78 °C for 1 hour while simultaneously adding bromobenzene (1.52 g, 1.0 mL, 1 Eq, 9.70 mmol) to the solution. The solution was a pale yellow color. The reaction was allowed to warm to 25 °C and stirred for 16 hours. The reaction was quenched carefully with water and then 3 M HCl, then transferred to a separatory funnel and more water was added. Et₂O was then added and the layers were separated and the aqueous layer was back extracted with ether twice. The combined organics were washed with brine and then dried over MgSO₄ and concentrated giving a yellow oil. The solution was re-dissolved in pentanes and passed through a silica plug to remove any polar impurities. After concentration a clear oil was obtained. NMR revealed this material contained a significant amount of 2,6-dimethyloctane but this was the only major impurity. This could mostly be removed on high vacuum while mildly heating. (3,7-dimethyloctyl)benzene (1.76 g, 83.1 %).

Synthesis of 3-phenylpropyl acetate:

Scheme 4.8: Synthesis of 3-phenylpropyl

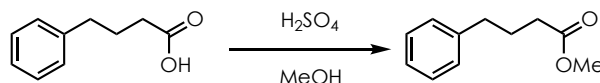


To a flame-dried 100 mL RBF was added N,N-dimethylpyridin-4-amine (343 mg, 0.1 Eq, 2.81 mmol). The flask was evaporated and refilled with argon. Next, of dry DCM (50 mL) was added through the septum followed by 3-phenylpropan-1-ol (3.83 g, 3.82 mL, 1 Eq, 28.1 mmol). Next, acetic anhydride (5.74 g, 5.31 mL, 2 Eq, 56.2 mmol) was added in a single portion and the solution began to feel warm. After about 1 to 2 hours TLC revealed that the reaction had gone to completion. The solution was transferred to a separatory funnel and washed with water once and then a saturated NaHCO₃ solution twice to remove acetic acid and acetic anhydride. The aqueous was back extracted with DCM twice and the combined organics were dried with Na₂SO₄ and concentrated to give a yellow oil. ¹H NMR revealed a significant amount of acetic anhydride remaining. This could be removed under high vacuum while heating. 3-phenylpropyl acetate (4.60 g, 92.0%) was obtained as a yellow liquid. Characterization data matched previously reported.⁸⁰

¹H NMR (600 MHz, Chloroform-*d*) δ 7.29 (t, J = 7.6 Hz, 2H), 7.22 – 7.17 (m, 3H), 4.09 (t, J = 6.6 Hz, 2H), 2.69 (t, J = 8.1, 7.4 Hz, 2H), 2.05 (s, 3H), 2.00 – 1.92 (m, 2H).

Synthesis of methyl 3-phenylpropanoate

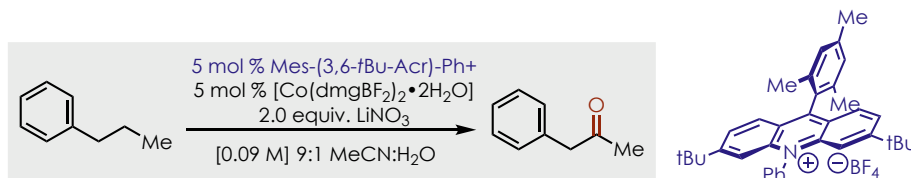
Scheme 4.9: Synthesis of methyl 3-phenylpropanoate



4-phenylbutanoic acid (4.61 g, 1 Eq, 28.1 mmol) was dissolved in ~100 mL of MeOH in a 250 mL RBF. To this was added a small amount of H_2SO_4 . The solution was heated to reflux for 16 hours. The reaction was brought to neutral pH with a saturated aqueous solution of NaHCO_3 . The aqueous layer was then extracted three times with EtOAc. The combined organics were dried with Na_2SO_4 and concentrated to give a clear oil. ^1H NMR revealed the product needed no further purification. 4.77 g, 95% of methyl 4-phenylbutanoate was obtained. Characterization data matched previously reported.

^1H NMR (400 MHz, Chloroform-*d*) δ 7.33 – 7.24 (m, 2H), 7.24 – 7.12 (m, 3H), 3.67 (s, 3H), 2.65 (t, J = 7.6 Hz, 2H), 2.34 (t, J = 7.5 Hz, 2H), 1.96 (p, J = 7.6 Hz, 2H).

4.5.5 Procedure for Homobenzylic Oxidation Reactions



To a flame-dried two dram vial equipped with a magnetic stir bar was added the **Mes-(3,6-tBu-Acr)-Ph⁺** (5 mol%), [Co(dmgBF₂)₂•H₂O] (5 mol%), and LiNO₃ (2.0 equiv). LiNO₃ could also be added as a solution in H₂O. MeCN and H₂O (total concentration with respect to substrate is 0.09 M) are then added and the solution is sparged with N₂ or Ar. For best results liquid substrates can be sparged with N₂ then added via syringe through the septum. The reaction is kept under constant

N₂ pressure to avoid oxidative byproducts. The reaction were irradiated with 450 nm LEDs using one of the photoreactor setups described in Section 4.5.2. Reactions were typically run for approximately 16 hours before removing from the irradiation source. They can be worked up by diluting with DCM, then adding solid Na₂SO₄. The organic solution is then passed through a plug of silica gel to remove any remaining H₂O as well as [Co(dmgbF₂)₂•H₂O] for analysis by ¹H NMR.

4.5.6 Electrochemical Measurements

Cyclic Voltammetry was performed using a Pine Instruments Wavenow potentiostat using a glassy carbon working electrode, Ag/AgCl in 3M NaCl reference electrode, and a platinum counter electrode. Measurements were taken by dissolving 0.05 mmols of sample in about 5 mL of a 0.1 M tetrabutylammonium hexafluorophosphate (TBAPF₆) solution in acetonitrile. The potential range scanned was typically 0.5 V and 2.5 V at a 100 mV/s. A background of the electrolyte solution was subtracted from each voltammogram. *E*_{p/2} is given as the half-wave potential for irreversible oxidation, where the current is equal to one-half the peak current of the oxidation event.

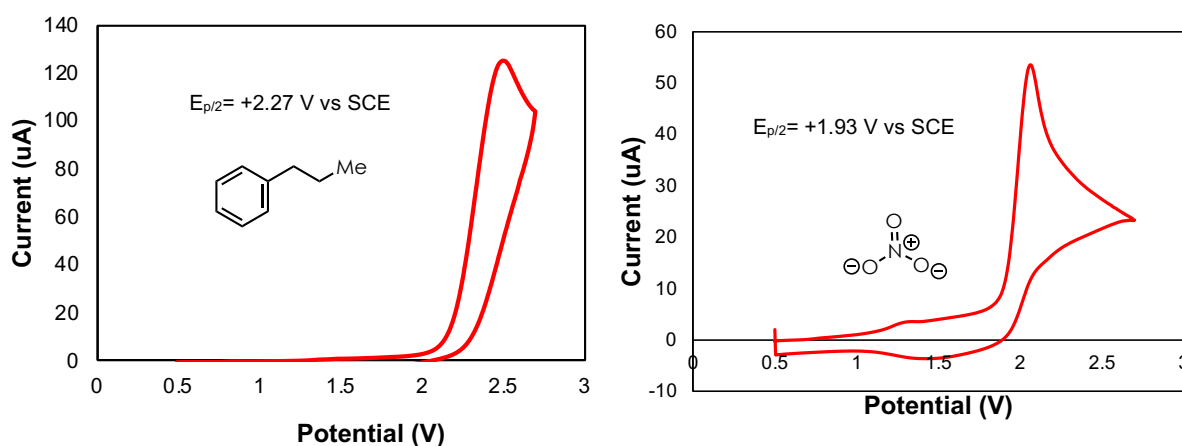


Figure 4.19: Cyclic voltammograms for (left) Propylbenzene (right) Lithium Nitrate.

4.5.7 Inductively Coupled Plasma Mass Spectroscopy (ICP-MS)

ICP-MS experiments were carried out using Thermo Element XR with optional laser ablation source. 2 mg of each batch of Mes-(3,6-*t*Bu-Acr)-Ph⁺ were diluted with 5 mL of 2% HNO₃ in water (Nitric Acid (TraceMetal™ Grade), Fisher Chemical, 18.2 MΩ H₂O). The samples were digested by heating at 50° C for 1 week. The samples were then diluted by 1000 fold and subjected to analysis. Concentrations were determined by calibration against external standards of each of the metals analyzed.

4.5.8 Procedures for Collecting Kinetic Data

To a flame-dried 1-dram vial was added [Co(dmgbF₂)₂ · 2H₂O] (10.5 mg, 0.05 Eq, 25.0 μmol), Mes-(3,6-*t*Bu-Acr)-Ph⁺ (14.3 mg, 0.0500 Eq, 25.0 μmol), and LiNO₃ (68.9 mg, 2.0 Eq, 1.00 mmol). The vial was taken into a N₂ filled glovebox where MeCN (5 mL), propylbenzene (60.1 mg, 69.7 μL, 1.0 Eq, 0.500 mmol)^{xxi}, and 56.5 μL of 1,2 dichlorobenzene (0.5 mmol) as an internal standard was added. The vial was removed from the glovebox, the vial was immediately placed under positive N₂ pressure before adding nitric acid or dichloroacetic acid (1.58 mg, 0.5 mL, 0.05 Eq, 25.0 μmol) as a 0.05 M solution in water (this was sparged with Argon prior to adding to the reaction mixture). The mixture was then stirred until all components were solubilized. A 25 μL aliquot was taken before irradiation began. Irradiation was carried out using the photoreactor setup described in Section 4.5.2. The vial was held in a fixed position in front of the lamps throughout the experiment. A total of 22 time points were taken (25 μL each) over the course of ~21 hours. Approximately 0.1 mL of silica gel was pipetted into a 1 mL syringe fitted

^{xxi} 0.33 mmol of propylbenzene and 0.17 mmol of 1-phenylpropan-2-one was added for the ‘same excess’ experiment.

with syringe filter was used to remove polar impurities, eluting with 400 μL DCM into a GC vial. GC (Agilent 6850 Series II, flame ionization detector) analysis was used to monitor propylbenzene disappearance over time.

Instantaneous reaction rate plots were obtained by fitting the raw concentration vs time data to a multiexponential function. This was an arbitrary function that could be fit in Microsoft Excel. This function was differentiated with respect to time for each of the time points taken to obtain instantaneous rate. This could then be plotted against [propylbenzene] at the corresponding time points in order to obtain the plots shown in Figure 4.11 and 4.13.

4.5.9 Fluorescence Emission Details

Emission lifetime measurements were taken at ambient temperature using a Edinburgh FLS920 spectrometer and fit to a single exponential decay according to the methods previously described by our laboratory.⁷² The respective time constants and fluorescence spectra are given in Section 4.3.2. Stern-Volmer analysis on the quenching of fluorescence lifetime was carried out in 9:1 MeCN:H₂O where the concentration of Mes-(3,6-*t*Bu-Acr)-Ph⁺ was 15 μM . The quenching constant was determined with the quenchers in the range of 0–19 mM. Bimolecular quenching constants, k_q were determined from the corresponding Stern-Volmer constant.⁸¹ UV-Vis spectra of Mes-Acr-Ph⁺ were taken before and after the addition of the quencher to verify the stability of the catalyst.

4.5.10 Stopped-Flow Experiments

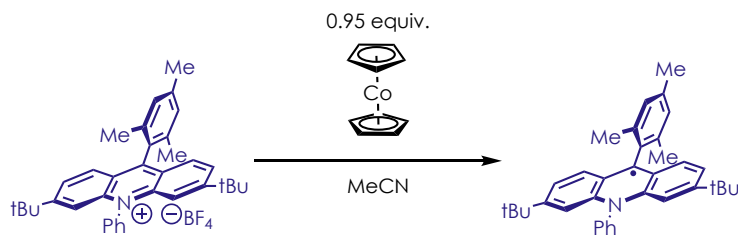


Figure 4.20: Synthesis of Mes-(3,6-*t*Bu-Acr)-Ph[•]

Mes-(3,6-*t*Bu-Acr)-Ph[•] was formed via chemical reduction with cobaltocene under a N₂ atmosphere. In order to ensure that no cobaltocene contaminated the final solution of Mes-(3,6-*t*Bu-Acr)-Ph[•], a slight excess of Mes-(3,6-*t*Bu-Acr)-Ph⁺ was used in the reaction (**Figure 4.20**). The final concentration of Mes-(3,6-*t*Bu-Acr)-Ph[•] was 100 μM in MeCN. A 100 μM solution of [Co(dmgBF₂)₂•2 H₂O] was also made in MeCN. A small H₂O was added to solubilize the complex before diluting to the final concentration. The two solutions were held in separate air tight vessels and were kept under high N₂ pressure throughout the experiment. Initially reference spectra were taken of Mes-(3,6-*t*Bu-Acr)-Ph[•] and [Co(dmgBF₂)₂•2 H₂O] (pink and red traces respectively in **Figure 4.21**). The spectrum of [Co^{II}(dmgBF₂)₂•2 H₂O] matches previously reported,⁷⁰ and the spectrum of Mes-(3,6-*t*Bu-Acr)-Ph[•] matches the expected spectrum based on similar acridine radicals that have been characterized by our lab.⁷² Upon rapid-mixing (with shutter to prevent decomposition caused by constant irradiation) a spectrum was taken after 15 ms (blue trace **Figure 4.21**). The blue spectrum shows that Mes-(3,6-*t*Bu-Acr)-Ph⁺ absorbance had returned as evidenced by a reference spectrum (dashed-yellow trace **Figure 4.21**). Additionally, a characteristic absorbance matching the previously reported spectrum of [Co^I(dmgBF₂)₂•2 H₂O]⁻ appears in the region between ~500 and 750 nm.⁷⁰ This absorbance begins to bleach slowly over time. Since neither Mes-(3,6-*t*Bu-Acr)-Ph⁺ nor [Co^I(dmgBF₂)₂•2 H₂O]⁻ increases after the initial

spectrum taken at 15 ms, the ET was presumed to take place during the mixing time. Therefore, only a lower limit of $\sim 10^7 \text{ M}^{-1}\text{s}^{-1}$ can be estimated as a rate constant for this electron transfer.

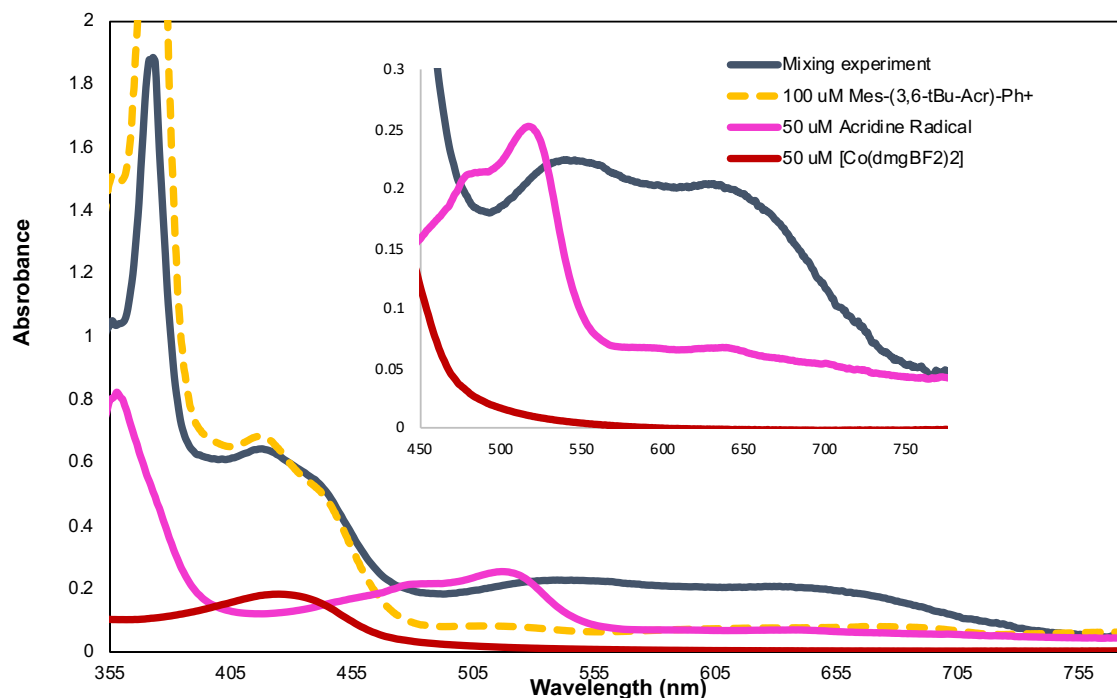


Figure 4.21: UV-vis spectrum of 50 μM $[\text{Co}(\text{dmgbF}_2)_2 \cdot 2\text{L}]$ (red trace) and 50 μM Mes-(3,6-*t*Bu-Acr)-Ph \bullet (pink trace) immediately before the mixing experiment. The two reactants were mixed using stopped-flow method and a spectrum was obtained about 15 ms after the mixing (blue trace). A reference spectrum of Mes-(3,6-*t*Bu-Acr)-Ph $^+$ is included as well (yellow dashed-trace). Concentrations are adjusted for effect of dilution upon mixing when appropriate.

REFERENCES

- (1) Bernard Meunier, ; Samuël P. de Visser, and; Sason Shaik,. *Chem. Rev.* **2004**, *104* (9), 3947–3980.
- (2) Nelson, D. R. *Hum. Genomics* **2009**, *4* (1), 59.
- (3) Nelson, D. L. (David L.; Lehninger, A. L.; Cox, M. M. *Lehninger Principles of Biochemistry*, 5th ed.; W.H. Freeman, 2008.
- (4) Arnold, F. H. *Acc. Chem. Res.* **1998**, *31* (3), 125–131.
- (5) Fasan, R. *ACS Catal.* **2012**, *2* (4), 647–666.
- (6) Roman Davydov, Thomas M. Makris, Victoria Kofman; David E. Werst, Stephen G. Sligar, and; Brian M. Hoffman. *J. Am. Chem. Soc.* **2001**, *123* (7), 1403–1415.
- (7) François Ogliaro; Sam P. de Visser; Shimrit Cohen; Pankaz K. Sharma, and; Shaik, S. *J. Am. Chem. Soc.* **2002**, *124* (11), 2806–2817.
- (8) Rittle, J.; Green, M. T. *Science* **2010**, *330* (6006), 933–937.
- (9) Atkinson, J. K.; Ingold, K. U. *Biochemistry* **1993**, *32* (35), 9209–9214.
- (10) Patrick H. Toy, †; Martin Newcomb, Paul F. Hollenberg. *J. Am. Chem. Soc.* **1998**, *120* (31), 7719–7729.
- (11) Groves, J. T.; McClusky, G. A. *J. Am. Chem. Soc.* **1976**, *98* (3), 859–861.
- (12) Groves, J. T.; Van der Puy, M. *J. Am. Chem. Soc.* **1976**, *98* (17), 5290–5297.
- (13) Groves, J. T.; McClusky, G. A.; White, R. E.; Coon, M. J. *Biochem. Biophys. Res. Commun.* **1978**, *81* (1), 154–160.
- (14) Huang, X.; Groves, J. T. *JBIC J. Biol. Inorg. Chem.* **2017**, *22* (2–3), 185–207.
- (15) Yamazaki, S. *Org. Lett.* **1999**, *1* (13), 2129–2132.
- (16) S. L.; Fuchs, P. L. *J. Am. Chem. Soc.* **2002**, *124* (47), 13978–13979.
- (17) K. C. Nicolaou, ; T. Montagnon; P. S. Baran, and; Zhong, Y.-L. *J. Am. Chem. Soc.* **2002**, *124* (10), 2245–2258.
- (18) K. C. Nicolaou, *; Phil S. Baran, and; Zhong, Y.-L. *J. Am. Chem. Soc.* **2001**, *123* (13), 3183–3185.

- (19) Murray, R. W.; Jeyaraman, R.; Mohan, L. *J. Am. Chem. Soc.* **1986**, *108* (9), 2470–2472.
- (20) Mello, R.; Fiorentino, M.; Fusco, C.; Curci, R. *J. Am. Chem. Soc.* **1989**, *111* (17), 6749–6757.
- (21) Ruggero Curci, Lucia D'Accolti, and; Fusco, C.. *Acc. Chem. Res.* **2005**, *39* (1), 1–9.
- (22) Bovicelli, P.; Lupattelli, P.; Mincione, E.; Prencipe, T.; Curci, R. *J. Org. Chem.* **1992**, *57* (19), 5052–5054.
- (23) Mikula, H.; Svatunek, D.; Lumpi, D.; Glöcklhofer, F.; Hametner, C.; Fröhlich, J. *Org. Process Res. Dev.* **2013**, *17* (2), 313–316.
- (24) Arnone, A.; Cavicchioli, M.; Montanari, V.; Resnati, G. *J. Org. Chem.* **1994**, *59* (19), 5511–5513.
- (25) Alberto Arnone, Stefania Foletto, Pierangelo Metrangolo, Massimo Pregnotato, Giuseppe Resnati. *Org. Lett.* **1999**, *1* (2), 281–284.
- (26) Trost, B. M. *Angew. Chemie Int. Ed. English* **1995**, *34* (3), 259–281.
- (27) Dicks, A. P.; Hent, A. Atom Economy and Reaction Mass Efficiency. In *Green Chemistry Metrics*; Springer, 2015; pp 17–44.
- (28) Lyons, T. W.; Sanford, M. S. *Chem. Rev.* **2010**, *110* (2), 1147–1169.
- (29) Lopa V. Desai; Kami L. Hull, and; Sanford, M. S. *J. Am. Chem. Soc.* **2004**, *126* (31), 9542–9543.
- (30) Giri, R.; Chen, X.; Yu, J.-Q. *Angew. Chemie Int. Ed.* **2005**, *44* (14), 2112–2115.
- (31) Xiao Chen; Charles E. Goodhue, and; Yu, J.-Q. *J. Am. Chem. Soc.* **2006**, *128* (39), 12634–12635.
- (32) B. V. Subba Reddy; Leleti Rajender Reddy, and; Corey, E. J. *Org. Lett.* **2006**, *8* (15), 3391–3394.
- (33) Wasa, M.; Engle, K. M.; Yu, J.-Q. *J. Am. Chem. Soc.* **2009**, *131* (29), 9886–9887.
- (34) Giri, R.; Liang, J.; Lei, J.-G.; Li, J.-J.; Wang, D.-H.; Chen, X.; Naggar, I. C.; Guo, C.; Foxman, B. M.; Yu, J.-Q. *Angew. Chemie Int. Ed.* **2005**, *44* (45), 7420–7424.
- (35) Ramesh Giri; Nathan Mangel; Jiao-Jie Li; Dong-Hui Wang; Steven P. Breazzano; Lindsey B. Saunders, and; Yu, J.-Q. *J. Am. Chem. Soc.* **2007**, *129* (12), 3510–3511.
- (36) Simmons, E. M.; Hartwig, J. F. *Nature* **2012**, *483* (7387), 70–73.

- (37) Chen, M. S.; White, M. C. *A Science* **2007**, *318* (5851), 783–787.
- (38) Chen, M. S.; White, M. C. *Science* **2010**, *327* (5965), 566–571.
- (39) Gormisky, P. E.; White, M. C. *J. Am. Chem. Soc.* **2013**, *135* (38), 14052–14055.
- (40) Quinn, R. K.; Könst, Z. A.; Michalak, S. E.; Schmidt, Y.; Szklarski, A. R.; Flores, A. R.; Nam, S.; Horne, D. A.; Vanderwal, C. D.; Alexanian, E. J. *J. Am. Chem. Soc.* **2016**, *138* (2), 696–702.
- (41) Schmidt, V. A.; Quinn, R. K.; Brusoe, A. T.; Alexanian, E. J. *J. Am. Chem. Soc.* **2014**, *136* (41), 14389–14392.
- (42) Czaplyski, W. L.; Na, C. G.; Alexanian, E. J. *J. Am. Chem. Soc.* **2016**, *138* (42), 13854–13857.
- (43) Williamson, J. B.; Czaplyski, W. L.; Alexanian, E. J.; Leibfarth, F. A. *Angew. Chemie Int. Ed.* **2018**, *57* (21), 6261–6265.
- (44) Horn, E. J.; Rosen, B. R.; Chen, Y.; Tang, J.; Chen, K.; Eastgate, M. D.; Baran, P. S. *Nature* **2016**, *533* (7601), 77–81.
- (45) Kawamata, Y.; Yan, M.; Liu, Z.; Bao, D.-H.; Chen, J.; Starr, J. T.; Baran, P. S. *J. Am. Chem. Soc.* **2017**, *139* (22), 7448–7451.
- (46) Shaw, M. H.; Shurtleff, V. W.; Terrett, J. A.; Cuthbertson, J. D.; MacMillan, D. W. C. *Science* **2016**, *352* (6291), 1304–1308.
- (47) Le, C.; Liang, Y.; Evans, R. W.; Li, X.; MacMillan, D. W. C. *Nature* **2017**, *547* (7661), 79–83.
- (48) Twilton, J.; Christensen, M.; DiRocco, D. A.; Ruck, R. T.; Davies, I. W.; MacMillan, D. W. C. *Angew. Chemie Int. Ed.* **2018**, *57* (19), 5369–5373.
- (49) Zhang, X.; MacMillan, D. W. C. *J. Am. Chem. Soc.* **2017**, *139* (33), 11353–11356.
- (50) Yan, M.; Kawamata, Y.; Baran, P. S. *Chem. Rev.* **2017**, *117* (21), 13230–13319.
- (51) Hartwig, J. F.; Larsen, M. A. *ACS Cent. Sci.* **2016**, *2* (5), 281–292.
- (52) Newhouse, T.; Baran, P. S. *Angew. Chemie Int. Ed.* **2011**, *50* (15), 3362–3374.
- (53) Zhang, G.; Hu, X.; Chiang, C.-W.; Yi, H.; Pei, P.; Singh, A. K.; Lei, A. *J. Am. Chem. Soc.* **2016**, *138* (37), 12037–12040.
- (54) Hu, X.; Zhang, G.; Bu, F.; Lei, A. *Angew. Chemie* **2018**, *130* (5), 1300–1304.

- (55) Hu, X.; Zhang, G.; Bu, F.; Luo, X.; Yi, K.; Zhang, H.; Lei, A. *Chem. Sci.* **2018**, 9 (6), 1521–1526.
- (56) Dempsey, J. L.; Brunschwig, B. S.; Winkler, J. R.; Gray, H. B. Hydrogen Evolution Catalyzed by Cobaloximes. *Acc. Chem. Res.* **2009**, 42 (12), 1995–2004.
- (57) Wayner, D. D. M.; McPhee, D. J.; Griller, D. *J. Am. Chem. Soc.* **1988**, 110 (1), 132–137.
- (58) Rountree, E. S.; Martin, D. J.; McCarthy, B. D.; Dempsey, J. L. *ACS Catal.* **2016**, 6 (5), 3326–3335.
- (59) Kato, S.; Saga, Y.; Kojima, M.; Fuse, H.; Matsunaga, S.; Fukatsu, A.; Kondo, M.; Masaoka, S.; Kanai, M. *J. Am. Chem. Soc.* **2017**, 139 (6), 2204–2207.
- (60) Fuse, H.; Kojima, M.; Mitsunuma, H.; Kanai, M. *Org. Lett.* **2018**, 20 (7), 2042–2045.
- (61) Hering, T.; Slanina, T.; Hancock, A.; Wille, U.; König, B. *Chem. Commun.* **2015**, 51 (30), 6568–6571.
- (62) Dean, J. A. (John A.; Lange, N. A. *Lange's Handbook of Chemistry*; McGraw-Hill, 1973.
- (63) Stephen J. Blanksby, G. Barney Ellison, . *Acc. Chem. Res.* **2003**, 36 (4), 255–263.
- (64) Nicholas, A. M. de P.; Arnold, D. R. *Can. J. Chem.* **1982**, 60 (17), 2165–2179.
- (65) Leadbeater, N. E. *Nat. Chem.* **2010**, 2 (12), 1007–1009.
- (66) Blackmond, D. G. *J. Am. Chem. Soc.* **2015**, 137 (34), 10852–10866.
- (67) Hu, X.; Cossairt, B. M.; Brunschwig, B. S.; Lewis, N. S.; Peters, J. C. *Chem. Commun.* **2005**, 0 (37), 4723.
- (68) Romero, N. A.; Margrey, K. A.; Tay, N. E.; Nicewicz, D. A. *Science* **2015**, 349 (6254), 1326–1330.
- (69) Roth, H.; Romero, N.; Nicewicz, D. *Synlett* **2015**, 27 (5), 714–723.
- (70) Dempsey, J. L.; Winkler, J. R.; Gray, H. B. *J. Am. Chem. Soc.* **2010**, 132 (3), 1060–1065.
- (71) Margrey, K. A.; Nicewicz, D. A. *Acc. Chem. Res.* **2016**, 49 (9), 1997–2006.
- (72) Romero, N. A.; Nicewicz, D. A. *J. Am. Chem. Soc.* **2014**, 136 (49), 17024–17035.
- (73) Hou, S.; Yang, H.; Cheng, B.; Zhai, H.; Li, Y. *Chem. Commun.* **2017**, 53 (51), 6926–6929.
- (74) Bakac, A.; Espenson, J. H. *J. Am. Chem. Soc.* **1984**, 106 (18), 5197–5202.

- (75) Yang, Z.-Z.; Zhao, Y.; Zhang, H.; Yu, B.; Ma, Z.; Ji, G.; Liu, Z. *Chem. Commun.* **2014**, 50 (90), 13910–13913.
- (76) Wang, H.; Li, L.; Bai, X.-F.; Shang, J.-Y.; Yang, K.-F.; Xu, L.-W. *Adv. Synth. Catal.* **2013**, 355, 341–347.
- (77) Rodríguez-Molina, B.; Pérez-Estrada, S.; Garcia-Garibay, M. A. *J. Am. Chem. Soc.* **2013**, 135 (28), 10388–10395.
- (78) Schouten, P. G.; Van Der Pol, J. F.; Zwikker, J. W.; Drenth, W.; Picken, S. J. *Mol. Cryst. Liq. Cryst.* **1991**, 195 (1), 291–305.
- (79) Hayashi, T.; Konishi, M.; Kobori, Y.; Kumada, M.; Higuchi, T.; Hirotsu, K. *J. Am. Chem. Soc.* **1984**, 106 (1), 158–163.
- (80) Akira Sakakura; Kimio Kawajiri; Takuro Ohkubo; Yuji Kosugi, and; Ishihara, K. *J. Am. Chem. Soc.*, **2007**, 129, (47), 14775–14779.
- (81) Lakowicz, J. R. *Principles of Fluorescence Spectroscopy*, 3rd ed.; Lakowicz, J. R., Ed.; Springer US: Boston, MA, 2006.
- (82) Toutov, A. A.; Betz, K. N.; Schuman, D. P.; Liu, W.-B.; Fedorov, A.; Stoltz, B. M.; Grubbs, R. H. *J. Am. Chem. Soc.* **2017**, 139 (4), 1668–1674.